frontiers | Research Topics

Towards an expansion of sustainable global marine aquaculture

Edited by
Yngvar Olsen, Xinxin Wang and
Ida Grong Aursand

Published in
Frontiers in Marine Science

ISSN 1664-8714
ISBN 978-2-8325-7333-4
DOI 10.3389/978-2-8325-7333-4

Generative AI statement
Any alternative text (Alt text) provided alongside figures in the articles in this ebook has been generated by Frontiers with the support of artificial intelligence and reasonable efforts have been made to ensure accuracy, including review by the authors wherever possible. If you identify any issues, please contact us.

About Frontiers

Frontiers is more than just an open access publisher of scholarly articles: it is a pioneering approach to the world of academia, radically improving the way scholarly research is managed. The grand vision of Frontiers is a world where all people have an equal opportunity to seek, share and generate knowledge. Frontiers provides immediate and permanent online open access to all its publications, but this alone is not enough to realize our grand goals.

Frontiers journal series

The Frontiers journal series is a multi-tier and interdisciplinary set of open-access, online journals, promising a paradigm shift from the current review, selection and dissemination processes in academic publishing. All Frontiers journals are driven by researchers for researchers; therefore, they constitute a service to the scholarly community. At the same time, the *Frontiers journal series* operates on a revolutionary invention, the tiered publishing system, initially addressing specific communities of scholars, and gradually climbing up to broader public understanding, thus serving the interests of the lay society, too.

Dedication to quality

Each Frontiers article is a landmark of the highest quality, thanks to genuinely collaborative interactions between authors and review editors, who include some of the world's best academicians. Research must be certified by peers before entering a stream of knowledge that may eventually reach the public - and shape society; therefore, Frontiers only applies the most rigorous and unbiased reviews. Frontiers revolutionizes research publishing by freely delivering the most outstanding research, evaluated with no bias from both the academic and social point of view. By applying the most advanced information technologies, Frontiers is catapulting scholarly publishing into a new generation.

What are Frontiers Research Topics?

Frontiers Research Topics are very popular trademarks of the *Frontiers journals series*: they are collections of at least ten articles, all centered on a particular subject. With their unique mix of varied contributions from Original Research to Review Articles, Frontiers Research Topics unify the most influential researchers, the latest key findings and historical advances in a hot research area.

Find out more on how to host your own Frontiers Research Topic or contribute to one as an author by contacting the Frontiers editorial office: frontiersin.org/about/contact

Towards an expansion of sustainable global marine aquaculture

Topic editors

Yngvar Olsen — Norwegian University of Science and Technology, Norway
Xinxin Wang — Akvaplan niva AS, Norway
Ida Grong Aursand — SINTEF Ocean, Norway

Citation

Olsen, Y., Wang, X., Aursand, I. G., eds. (2026). *Towards an expansion of sustainable global marine aquaculture*. Lausanne: Frontiers Media SA.
doi: 10.3389/978-2-8325-7333-4

Table of contents

05 Editorial: Towards an expansion of sustainable global marine aquaculture
Xinxin Wang, Ida Grong Aursand and Yngvar Olsen

08 Biomass estimations of cultivated kelp using underwater RGB images from a mini-ROV and computer vision approaches
Martin Molberg Overrein, Phil Tinn, David Aldridge, Geir Johnsen and Glaucia M. Fragoso

22 Replacing fishmeal with salmon hydrolysate reduces the expression of intestinal inflammatory markers and modulates the gut microbiota in Atlantic salmon (*Salmo salar*)
Ingrid Schafroth Sandbakken, Hang Su, Louise Johansen, Yupeng Zhang, Einar Ringø, Randi Røsbak, Igor Yakovlev, Kathrine Kjos Five and Rolf Erik Olsen

37 Conceptualization of the Norwegian feed system of farmed Atlantic salmon
Pernille Kristiane Skavang and Andrea Viken Strand

45 Asexual proliferative seedling technology for *Sargassum fusiforme* constructed using tissue culture method
Lina Guo, Guanfeng Pang, Lin Luo, Congquan Gao, Binbin Chen and Zengling Ma

59 Optimum eicosapentaenoic acid + docosahexaenoic acid levels for farmed Atlantic salmon: closing the gap between science and commercial practice
Ian Carr, Ester Santigosa, Tony Chen and John Costantino

67 Adaptation of functional traits in *Gracilaria dura* with the local environment: implications for resource management and exploitation
Vasco M. N. C. S. Vieira, Pankaj S. Dawange, Santlal Jaiswar, José P. Sardinha and Vaibhav A. Mantri

79 Nutritional composition and transcriptome analysis of the newly hatched *Anguilla japonica* from embryo to preleptocephali obtained from artificial reproduction
Kang Li, Yuangu Li, Tiezhu Li, Rongfeng Cui and Liping Liu

91 Monitoring monthly mortality of maricultured Atlantic salmon (*Salmo salar* L.) in Scotland I. Dynamic linear models at production cycle level
Carolina Merca, Annette Simone Boerlage, Anders Ringgaard Kristensen and Dan Børge Jensen

111 ERK1/2 regulates melanin synthesis in fish: a case study on a colourful variety, leopard coral grouper (*Plectropomus leopardus*)
Min Yang, Jie Huang, Decai Zheng, Haizhan Tang, Junchi Liu, Jian Luo and Xin Wen

124 Monitoring monthly mortality of maricultured Atlantic salmon (*Salmo salar* L.) in Scotland II. A hierarchical dynamic linear model
Carolina Merca, Annette Simone Boerlage, Anders Ringgaard Kristensen and Dan Børge Jensen

137 Application of metabolomics approach to investigate the flavor substance differences between triploid and diploid oysters (*Crassostrea angulata*)
Duo Chen, Zewen Zheng, Ziquan Zhou, Yuxin Song, Zhi Chen, Gang Lin and Ting Xue

150 Bridging the protein gap with single-cell protein use in aquafeeds
Louise Buttle, Henk Noorman, Carol Roa Engel and Ester Santigosa

157 From ocean to cage: evaluating the culture feasibility of Black-spotted croaker (*Protonibea diacanthus*)
Shubhadeep Ghosh, Gyanaranjan Dash, Biswajit Dash, Rajesh Kumar Pradhan, Sekar Megarajan, Pralaya Ranjan Behera, Ritesh Ranjan, Swatipriyanka Sen, Madhumita Das, Vettath Raghavan Suresh, Achamveetil Gopalakrishnan and Joykrushna Jena

171 Dynamic motion response of a large-scale steel aquaculture cage during towing
Shuai Niu, Zhi Wang, Lianyi Guo, Lianghao Tang, Tianyu Gu, Can Cui, Dejun Feng, Fukun Gui and Xu Yang

frontiers | Frontiers in Marine Science

TYPE Editorial
PUBLISHED 16 December 2025
DOI 10.3389/fmars.2025.1751441

OPEN ACCESS

EDITED AND REVIEWED BY
Eduardo Luís Cupertino Ballester,
Federal University of Paraná, Brazil

*CORRESPONDENCE
Xinxin Wang
xwa@akvaplan.niva.no

RECEIVED 21 November 2025
REVISED 26 November 2025
ACCEPTED 26 November 2025
PUBLISHED 16 December 2025

CITATION
Wang X, Aursand IG and Olsen Y (2025) Editorial: Towards an expansion of sustainable global marine aquaculture. *Front. Mar. Sci.* 12:1751441. doi: 10.3389/fmars.2025.1751441

Editorial: Towards an expansion of sustainable global marine aquaculture

Xinxin Wang[1]*, Ida Grong Aursand[2] and Yngvar Olsen[3]

[1]Akvaplan-niva, Throndheim, Norway, [2]SINTEF Ocean, Throndheim, Norway, [3]Department of Biology, Norwegian University of Science and Technology, Throndheim, Norway

KEYWORDS

feed ingredients, fish health and welfare, low trophic aquaculture, offshore aquaculture, sustainable marine aquaculture

Editorial on the Research Topic
Towards an expansion of sustainable global marine aquaculture

Aquaculture is the fastest-growing food-producing sector, currently supplying 52 % of the aquatic animals consumed globally by humans (Misund et al., 2024). Yet, it is facing multiple challenges such as environmental impact, disease management, and economic sustainability. Innovative methods, technologies and new production systems are needed to reduce environmental footprints, increase climate resilience, and ensure the long-term viability of aquaculture while providing ecosystem services.

Engineering advances for offshore aquaculture

Nearshore aquaculture areas are facing multiple challenges such as limited water exchange, high parasite risk (e.g., sea lice), and competition with other coastal users. Moving aquaculture to more exposed sites or offshore can mitigate these pressures. However, offshore aquaculture also brings significant challenges and requires carefully designed technological, biological, and regulatory solutions. Niu et al. studies the dynamic motion response of large-scale steel aquaculture cages during towing, an important but underexplored aspect of offshore logistics. The study shows that towing speed, towline length, and towing configuration can significantly affect cage stability and towline tension. Such engineering insights are crucial for ensuring the safe and efficient transport of large aquaculture infrastructure in challenging conditions.

Similarly, Overrein et al. highlights the role of automation and computer vision in kelp aquaculture. By using underwater imaging and computer vision algorithms, the study provides robust, real-time biomass estimation of cultivated kelp. This enables cost-effective monitoring and yield prediction for large scale production. Such automation monitoring tools have the potential to promote the seaweed industry and will be useful for future offshore operations.

Health, welfare, and monitoring

Fish health and welfare remain major challenges to sustainable aquaculture expansion. (Merca et al., a; b) develop dynamic linear models (DLM) for monitoring monthly mortality of Atlantic salmon at multiple levels in Scotland, using open-source salmon production data. This is useful for various stakeholders as part of a monitoring system, offering insights into mortality trends at national, regional, and sites levels that may benefit from strategic resource management.

At the molecular level, Sandbakken et al. investigates the effect of partially replacing fishmeal with salmon protein hydrolysates on the intestinal gene expression and microbiota. Gene expressions of pyloric caeca (PC), midgut (MG) and hindgut (HG) revealed a downregulation of immunological genes involved in inflammation in the intestine of salmon fed with 18% salmon hydrolysate compared to those fed the control diet. Such dietary strategies improve welfare while reducing the reliance on fishmeal. Similarly, (Yang et al.) studies the regulation of melanogenesis in *Plectropomus leopardus*, indicating that ERK1/2 was involved in the regulation of melanogenesis through the regulation of MITF in *P. leopardus*. This provides a new perspective for exploring the variable skin colouration of coral reef fish.

Sustainable feeds

A majority of greenhouse gas emissions from aquaculture is accounted for by feed (Skavang and Strand). Innovation in feed is crucial for sustainable development of aquaculture. Buttle et al. explored the potential of using single-cell proteins (SCP) as feed ingredient, demonstrating high protein digestibility, balanced amino acid profiles, and fish health benefits in rainbow trout. Although cost and scalability remain challenges, SCP shows a promising avenue for sustainable aquafeeds.

Carr et al. explored the optimal levels of eicosapentaenoic acid + docosahexaenoic acid for farmed Atlantic salmon. Through large-scale trials in Chile and big-data analysis in Norway, the study shows that using algal oil-supplemented feed resulted in improved health responses and better fillet quality. The EPA + DHA levels > 8% reduce mortality variability by 21%, improve economic feed conversion ratio by 11%, and increase the likelihood of superior harvests by 27%, demonstrating productivity benefits.

Diversification of aquaculture species and systems

Diversification of aquaculture species and systems is important to meet growing consumer demand while ensuring environmental sustainability, economic viability, and food security.

Portuguese oyster (*Crassostrea angulata*), are highly valued for their nutritional and flavor qualities, making them important in global aquaculture. Chen et al. studies the flavor differences between triploid and diploid oysters, using metabolomics approach. Their findings show significant upregulation of inosine, guanosine, L-aspartic acid, and taurine in triploids which enhanced their flavor. This highlights the advantages of triploid oysters in aquaculture for improved flavor and nutrition, supporting their potential for year-round production.

Ghosh et al. evaluated the potential of the high-value marine fish (*Protonibea diacanthus*) in polyculture with Indian pompano, revealing superior growth of *P. diacanthus* and is a viable candidate species with significant potential for polyculture systems. Li et al. analyzed the nutritional composition of artificially fertilized eggs from Japanese eel (*Anguilla japonica*) and transcriptome of samples from fry to better understand nutrients requirements. Their findings will facilitate future studies on the nutrition of *A. japonica* larvae and other biological traits for reproductive research.

Seaweed aquaculture has gained increasing interest in recent years, especially in Europe. Vieira et al. examined the functional traits of *Gracilaria dura* from two intertidal populations in Gujarat, India, to understand their adaptations and potential for cultivation. The findings suggest that submerged cultivation maximizes biomass yield whereas exposure reduces yield but increases valuable bioactive compounds. Guo et al. developed an asexual tissue culture method for *Sargassum fusiforme* to maintain superior traits. The optimal condition was using holdfasts or stem tips on solid medium with 3 μM uniconazole for 17 days, followed by transfer to liquid medium. This resulted in 100% regeneration with high growth rates and enhanced photosynthesis. The technique enables continuous juvenile production, offering a reliable approach for preserving and expanding algal stocks.

Conclusion

This Research Topic demonstrates the breadth and dynamism of research in shaping the future sustainable marine aquaculture. From offshore aquaculture systems to seaweed genetics, from fish mortality models to alternative feed ingredients, demonstrating that sustainable expansion is possible through innovation, diversification, and systemic integration. Marine aquaculture has the potential to feed the increasing population and support climate-resilient food systems. Achieving this requires innovation, cross-sector collaboration, and global engagement in sustainability.

Author contributions

XW: Writing – original draft, Writing – review & editing. IA: Writing – review & editing. YO: Writing – review & editing.

Conflict of interest

The authors declared that this work was conducted in the absence of any commercial or financial relationships that could be construed as a potential conflict of interest.

The authors YO, XW and IA declared that they were an editorial board member of Frontiers, at the time of submission. This had no impact on the peer review process and the final decision.

Generative AI statement

The author(s) declared that generative AI was not used in the creation of this manuscript.

Any alternative text (alt text) provided alongside figures in this article has been generated by Frontiers with the support of artificial intelligence and reasonable efforts have been made to ensure accuracy, including review by the authors wherever possible. If you identify any issues, please contact us.

Publisher's note

Reference

Misund, A., Thorvaldsen, T., Strand, A. V., Oftebro, T. L., and Dahle, S. W. (2024). Opportunities and challenges in new production systems for salmon farming in Norway—Industry perspective. *Mar. Policy* 170, 106394. doi: 10.1016/j.marpol.2024.106394

frontiers | Frontiers in Marine Science

TYPE Original Research
PUBLISHED 12 March 2024
DOI 10.3389/fmars.2024.1324075

OPEN ACCESS

EDITED BY
Xinxin Wang,
Fisheries and Aquaculture Research (Nofima), Norway

REVIEWED BY
Jessica Knoop,
Ghent University, Belgium
Vasco Manuel Nobre de Carvalho da Silva Vieira,
University of Lisbon, Portugal

*CORRESPONDENCE
Glaucia M. Fragoso
glaucia.m.fragoso@ntnu.no

RECEIVED 18 October 2023
ACCEPTED 21 February 2024
PUBLISHED 12 March 2024

CITATION
Overrein MM, Tinn P, Aldridge D, Johnsen G and Fragoso GM (2024) Biomass estimations of cultivated kelp using underwater RGB images from a mini-ROV and computer vision approaches. *Front. Mar. Sci.* 11:1324075. doi: 10.3389/fmars.2024.1324075

Biomass estimations of cultivated kelp using underwater RGB images from a mini-ROV and computer vision approaches

Martin Molberg Overrein[1], Phil Tinn[2], David Aldridge[3,4], Geir Johnsen[1] and Glaucia M. Fragoso[1]*

[1]Trondheim Biological Station, Department of Biology, Norwegian University of Science and Technology (NTNU), Trondheim, Norway, [2]Department of Software Engineering, Safety and Security, SINTEF Digital, Trondheim, Norway, [3]Seaweed Solutions AS, Trondheim, Norway, [4]Department of Fisheries and New Biomarine Industry, SINTEF Ocean, Trondheim, Norway

Seaweed farming is the fastest-growing aquaculture sector worldwide. As farms continue to expand, automated methods for monitoring growth and biomass become increasingly important. Imaging techniques, such as Computer Vision (CV), which allow automatic object detection and segmentation can be used for rapid estimation of underwater kelp size. Here, we segmented *in situ* underwater RGB images of cultivated *Saccharina latissima* using CV techniques and explored pixel area as a tool for biomass estimations. Sampling consisted of underwater imaging of *S. latissima* hanging vertically from a cultivation line using a mini-ROV. *In situ* chlorophyll *a* concentrations and turbidity (proxies for phytoplankton and particle concentrations) were monitored for water visibility. We first compared manual length estimations of kelp individuals obtained from the images (through manual annotation using ImageJ software). Then, we applied CV methods to segment and calculate kelp area and investigated these measurements as a robust proxy for wet weight biomass. A strong positive linear correlation (r^2 = 0.959) between length estimates from underwater image frames and manual measurements from the harvested kelp was observed. Using unsupervised learning algorithms, such as mean shift clustering, colour segmentation and adaptive thresholding from the OpenCV package in Python, kelp area was segmented and the number of individual pixels in the contour area was counted. A positive power relationship was found between length from manual measurements with CV-derived area (r^2 = 0.808) estimated from underwater images. Likewise, CV-derived area had a positive power relationship with wet weight biomass (r^2 = 0.887). When removing data where visibility was poor due to high turbidity levels (mid-June), the power relationship was stronger between CV-derived area estimates and the field measurements (r^2 = 0.976 for wet weight biomass and r^2 = 0.979 for length). These results show that robust estimates of cultivated kelp biomass *in situ* are possible through kelp colour segmentation. However, we demonstrate that the quality of CV post-processing and accuracy of the model are highly dependent of environmental conditions (e.g. turbidity and chlorophyll a concentrations). The establishment of these technologies has the potential to offer scalability of production, efficient real-time monitoring of sea cultivation and improved yield predictions.

KEYWORDS

kelp farm monitoring, underwater marine robotics, biomass estimation, seaweed production, computer vision

1 Introduction

Cultivated seaweed is the fastest-growing aquaculture sector worldwide (~6% y^{-1}) and a multibillion-dollar industry, comprising half of global mariculture production (Duarte et al., 2021). Seaweed farming has the potential to provide a sustainable, low trophic source of food (and feed) for a world approaching 10 billion by 2050 and can potentially be used as a nature-based solution for climate change mitigation and nutrient remediation (Duarte et al., 2021; van Dijk et al., 2021). The positive impact of seaweed aquaculture can help society to achieve many of the United Nations Sustainable Development Goals (UNSDGs) – from eliminating hunger and climate change mitigation, to economic growth, and improvement of life under water (Duarte et al., 2021; Hossain et al., 2021; Alleway, 2023).

While seaweed aquaculture has a long history in Asia (over a thousand years) (Hwang et al., 2019), which is responsible for 99% of worldwide production, sea cultivation of kelp has only recently become established in Europe (last 5-15 years). Norway, with its long coastline and favourable seaweed growing conditions, has the potential to be a major player as the European industry develops. In Norway alone, the number of licenses for seaweed cultivation has increased from 54 in 2014 to 511 in 2020, revealing the increased interest in seaweed farming (Albrecht, 2023). Predictions suggest the expansion of seaweed cultivation up to 2×10^7 tonnes per year by 2050 (Olafsen et al., 2012; Skjermo et al., 2014; Broch et al., 2017), although there are some discussion about how realistic these projections are (Albrecht, 2023).

Although market demand for seaweed is generally increasing in Europe, Norwegian seaweed aquaculture is not yet profitable. One major reason for this is a lack of automation regarding seedling production, farm operations, monitoring, harvesting and processing of biomass at a large scale. Thus, as seaweed producers scale-up, it is important that they are able to maximise their yields at sea, while minimising production costs. To achieve this goal, a holistic understanding of the environmental conditions influencing macroalgal growth and the onset of biofouling is necessary to achieve biomass of consistent quality and yield. Accurately predicting the total biomass at harvest is also vital for planning the processing of the biomass. To date, kelp biomass measurements, biofouling inspections and environmental monitoring are still largely done by hand, which is time-consuming, labour intensive and cannot easily build up a holistic picture that is representative of the whole farm. Automation of kelp farm monitoring has the potential to revolutionize this aspect of the industry. The more automated and frequent monitoring is, the faster the pace of knowledge acquisition for optimising growth at sea, predicting yield and planning harvest and processing logistics.

Cost-effective monitoring of wild kelp has been performed in pilot studies using Red-Green-Blue (RGB) cameras (Bewley et al., 2012) or hyperspectral imaging by air using aerial drones/airplanes Volent et al. (2007) and from underwater platforms using remotely operated underwater vehicle (ROVs) (Summers et al. (2022). However, very little research has been done using underwater robot monitoring (autonomous underwater vehicles, AUVs, and ROVs) in kelp farms. Biomass growth has been assessed using AUVs with a split-beam acoustic echosounder (Fischell et al., 2019) and a sideward scanner to monitor the macroalgae growth in a kelp farm (Stenius et al., 2022). However, they are more appropriate for seaweed species that possess pneumatocysts (e.g. *Macrocystis pyrifera*), due to enhanced acoustic returns, and not for commercial species from Norway (mostly *Saccharina latissima* and *Alaria esculenta*) (Bell et al., 2020). Visual inspections are still necessary, though, for monitoring the kelp health and for robust estimation of biomass measurements, given that strong currents can underestimate these values by changing the direction of the kelp in the water (Bell et al., 2020). Moreover, AUVs cannot operate everywhere. They are less suited to areas that are heavily populated (near the shore) due to acoustic interference, and have a high collision and entanglement risk, which can lead to damage of the farm. They are also very expensive and require technical personnel for operation. Due to the tight space between kelp lines (maximum of a few meters), small and light underwater robots, such as portable drones (uncrewed surface vehicles, USV) (Zolich et al., 2022) and manually controlled mini-ROVs can offer a low risk assessment of the environmental conditions within the farm. The small, portable, mini-ROV Blueye model X3 (Blueye Robotics, Norway) was chosen in this study because of its user-friendly operability, making it manoeuvrable enough for easy operation in the tight spaces of a kelp farm, while at the same time providing sufficient power to operate in coastal conditions. It is also affordable (~ US$ 12k for the Blueye X3 drone + basic kit), making it an easily available option for seaweed farmers.

The aim of this study was to provide a proof-of-concept for *in situ* biomass estimation of cultivated *S. latissima* derived from underwater RGB imaging and computer vision (CV) techniques. For that, we compared manual length estimations to the ones obtained from images through human supervision, then, we applied CV methods to estimate kelp area and used these measurements as a proxy for wet weight biomass. To our knowledge, this is the first attempt where *in situ* biomass estimations from images are validated against field-measured, harvested biomass data. We show that robust estimates of cultivated kelp biomass *in situ* are possible through lamina colour segmentation, although we demonstrate that the quality of CV post-processing and accuracy of the model are highly dependent of environmental conditions, such as the colour of the water, turbidity, natural illumination and current velocities. The establishment of these technologies will offer scalability of production, efficient real-time monitoring of farm cultivation and improved yield predictions.

2 Methods

2.1 Study area and sampling methods

Fieldwork was carried out at the Seaweed Solutions kelp farm, Måsskjæra, in Frøya, an island located off the coast of mid-Norway (Trøndelag region) (63°44.62'N 8°52.76'E) (Figure 1). Frøya island is a biodiversity-rich area with strong water mixing due to internal waves, strong winds and tidal currents (Fragoso et al., 2021). The hydrography of the region is characterized by two different currents:

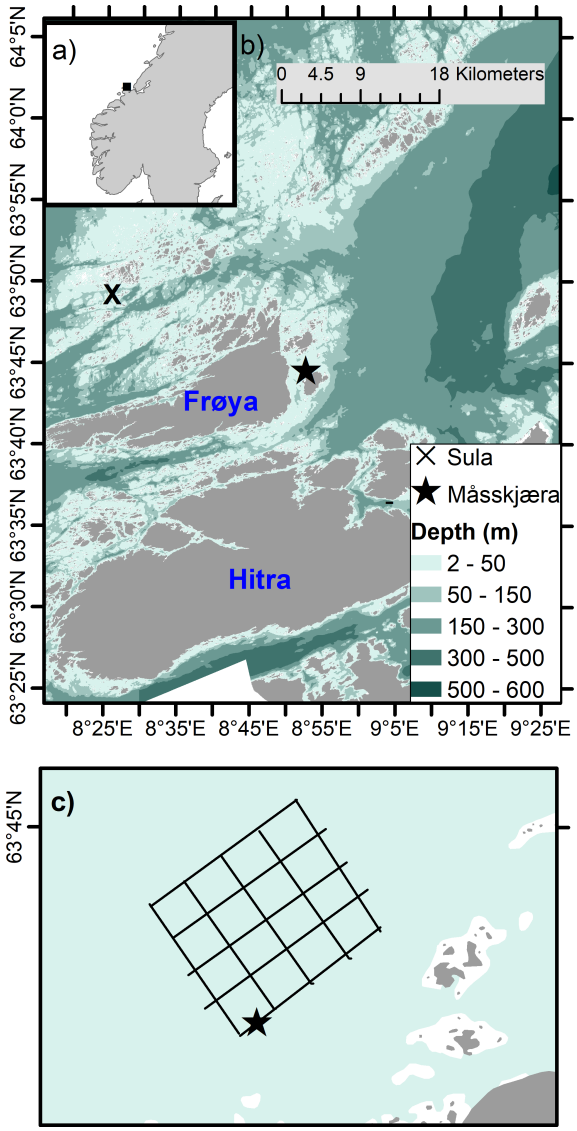

FIGURE 1
Map showing **(A)** Norway, and the coast of Trøndelag (mid-Norway, square) and **(B)** the island of Frøya and the location of Måsskjæra seaweed farm, and Sula meteorological station (where wind data were collected). **(C)** Illustration of the Måsskjæra seaweed farm, showing the collection site (star symbol).

the Norwegian Coastal Current (NCC) located above the Norwegian Atlantic Current (NAC). NCC is a result of freshwater runoff from Norwegian fjords comprising several rivers outflow in each fjord (Skagseth et al., 2011), while the NAC is a warm nutrient-rich water mass located below the NCC that occasionally intrudes to the surface in spring and summer (Skagseth et al., 2011) (Figure 1A). Because of the influence of the NAC, the area is highly productive regarding fisheries and aquaculture activities, with high economical revenue to Norway (Tiller et al., 2015; Ervik et al., 2018).

Måsskjæra is a semi-exposed farm location sheltered from westerly and southerly wind directions and exposed to north-eastly winds (Førde et al., 2016) (Figure 1). Due to the shelter protection provided by the mainland and surrounding islands, wave height does not exceed 2 meters. The depth where the farm is located ranges from 10 - 35 m. The farm size is approximately 400 × 400 m and is based on a horizontal longline system that is divided into approximately 16 cultivation squares. *S. latissima* was cultivated on 100 m long substrate lines (14 mm diameter) that were seeded by wrapping them with cultivation twine (2 mm twisted polyester). The cultivation depth was between 2 and 5 m and was achieved by placing buoyancy in the middle of the 100 m substrate lines. Lines were cultivated with a spacing of approximately 1 m distance.

Sampling consisted of underwater imaging of a single kelp (*S. latissima)* cultivation line (~25 m in length) located at the edge of the farm and at ~ 2-5 m depth (Figures 1B, C). The monitored seaweed line was deployed in November 2021. Sampling occurred every 2 - 4 weeks within the later stages of the main growing season (from March to June 2022, 7 sampling times in total, Table 1). This

allowed imaging and sampling during distinct development stages of *S. latissima*, from young sporophytes in March to 'bushy canopy" in June, to test the method on kelp lines with a range of sizes and growth densities. Sampling was, where possible, carried out at low tide (slack water) to minimise current speeds in order to obtain images of *S. latissima* specimens oriented as vertical as possible. Sampling during high tide could also have been an option but, due to logistical reasons (boat and personnel availability), low tide was chosen in order to maintain consistency. In practice, however, ideal conditions for video recording (low tides) were not possible on all sampling days due to the logistical difficulties of arriving and deploying the ROV during the exact time of slack water (e.g. weather conditions and boat logistics) (Table 1).

Prior to recording underwater video, an aluminium-based hand-made checkerboard plate (30 × 20 cm) was placed at the start of the cultivation line for size reference. The plate was weighted in an attempt to keep it vertical during underwater videos. Additionally, red plastic strips were attached to the same line at 1-meter intervals to mark one meter replicate samples. For each sampling day (total of 7), triplicate 1-meter samples (adjacent to each other) from the cultivation line were selected for image analysis and validation (manual or field-based wet weight biomass and average length estimations collected in the field). Underwater images of marked 1-meter replicates were then captured under natural light conditions by driving the mini-ROV Blueye X3 (Blueye Robotics, Norway) sideways along the cultivation line. To achieve this, the internal camera of the ROV was pointed in the direction of the kelp and at a sufficient distance to ensure that the whole length of the kelp and width of the 1-meter mark was captured in the frame. After video recording, the videos were uploaded for later image post-processing in the lab (Figure 2). The internal camera of the ROV was used as the optical sensor for the image sampling: a digital RGB camera equipped with 30° tilt (up and down), which can collect imagery with Full High-Definition (FHD) resolution (1920 × 1080 25/30 frame per second) and 115° field of view (FOV). For more specifications, see Blueye website (https://support.blueye.no/hc/en-us/articles/4402566916626-X3-technical-specifications)

After video recording, sporophytes of *S. latissima* from each 1 m replicate were sampled for wet weight biomass (presented as field-measured weight per meter) and length measurements (field-measured lamina + stipe + holdfast length, herein referred as lamina length) for validation. For the field-measured weight, the whole wet weight biomass of the 1 m cultivation line was considered. For field-measured length, 10 randomly selected *S. latissima* sporophyte specimens from each 1-meter replicate line were measured for lamina, as well as lamina width at the widest point. Only 10 sporophytes within each 1-meter replicate were chosen because it would be too time consuming to measure the length of each individual specimen (densities can reach many hundreds of individuals per meter). This is also a common methodology used by seaweed farmers when carrying out field monitoring. The same method was repeated on each field day, meaning that the sampling is destructive – the seaweed was permanently removed from the cultivation line for biomass and length measurements.

To investigate the influence of environmental variables, such as particles (phytoplankton and detritus), irradiance and wind speed, on water visibility and image quality for post-processing, additional environmental data were collected. A submersible fluorometer sensor (C3, Turner Designs, USA) was attached at the edge of the farm and placed at 3 m depth (Figure 1C). The sensor measured temperature (°C), chlorophyll *a* fluorescence (calibrated later to concentration [Chl *a*] in mg m^{-3}) and turbidity (Relative Fluorescence Unit - calibrated later to Formazin Turbidity Unit (FTU)) every 10 minutes from mid-February to mid-June. The C3 submersible was also equipped with an antifouling copper plate and a mechanical wiper that rotates and cleans the optical sensor before each measurement (every 10 min). Data on wind speed (m s^{-1}) from February until mid-June was obtained hourly from Sula meteorological station (located west of Frøya, Figure 1) and retrieved from the Norwegian Weather Service Center (https://seklima.met.no/).

2.2 Image processing

2.2.1 ImageJ-derived measurements

To ascertain whether reliable measurements (in this case length) were possible using underwater imaging, preliminary

TABLE 1 Date, local Norwegian time, tidal conditions (cm), average and maximum wind speed (from Sula meteorological station, see methods) and cloud cover (Ørland meteorological station) for each video recording and sampling day at Måsskjæra.

Field day	Date	Local Time (UTC+2)	Tide (cm)	Wind strength (m s^{-1}) (maximum)	Weather
1	22-Mar-22	10:30 - 12:00	103-181 (Rising)	5.0 (6.7)	Partially sunny
2	5-Apr-22	12:30 - 14:00	178-232 (Rising)	1.9 (8.7)	Partially sunny
3	20-Apr-22	07:50 - 09:30	37-39 (Low)	2.4 (3.7)	Sunny
4	4-May-22	08:30 - 09:30	50-63 (Low/rising)	6.1 (8.5)	Cloudy
5	27-May-22	10:20 - 12:10	231-199 (High/receding)	6.7 (8.5)	Partially sunny
6	3-Jun-22	08:40 - 09:20	61-64 (Low)	5.1 (7.9)	Cloudy
7	15-Jun-22	08:40 - 09:50	84-145 (Rising)	7.9 (11.0)	Rainy

Source: www.kartverket.no for tides and www.yr.no for wind and cloud cover conditions.

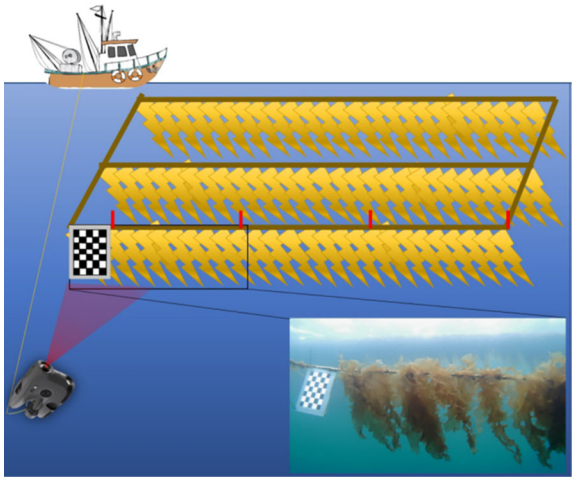

FIGURE 2
Schematic of the image sampling method, where a checkerboard was placed at the edge of the long line and used for size reference. Plastic cable ties indicated 1-meter replicates of kelp samples. A mini-ROV with internal RGB camera was used to collect videos along the longline.

estimates derived from the image frames were compared to the manual measurements obtained from the kelp harvested in the field. For that, comparisons were made between the average length of randomly selected "imaged" fronds (see more below) and the average length of 10 harvested fronds measured in the field (explained in section 2.1). The reason we decided to do this initial step was to ascertain whether, on average, sporophyte length measured manually from an underwater image had comparable results with manual measurements in the field before applying CV (OpenCV package in python) techniques. To achieve this, image frames that included the checkerboard for scaling were selected and uploaded to ImageJ (Image Processing and Analysis in Java) (Figure 3). The checkerboard in the frame was used as a size reference to set a scale for the number of pixels per centimetre (pixels cm^{-1}) for the corresponding frame (Figure 3). Then, 10 kelp specimens in each frame were randomly selected, and their length in centimetres (cm) were measured by drawing a line from the tip to the holdfast of the specimen, using the "line" and "measure" tools in ImageJ (Figure 3). A total of 6 frames for each 1-meter replicate were selected based on checkerboard visibility, and with different distances and positions of the kelp. It was decided that 6 frames were sufficiently representative to capture some variability in the image data, while also being manageable for manual processing. For each frame, 10 sporophyte lengths were measured accounting for a total of 60 measurements per day (10 sporophytes × 6 frames). The pipeline was repeated using image data from each field day (10 sporophytes × 6 frames × 7 sampling days).

2.2.2 Open CV-derived measurements

Kelp area estimates from 1-meter replicates were performed using the Python library OpenCV. The pipeline started with extraction of six frames of the first kelp replicate from the video collected by the mini-ROV camera (Figure 4). The six frames selected were the same frames used for the ImageJ-derived estimates. The region of interest (ROI) in the frame, defined as the width of the 1-meter replicate and height, was cropped from the original frame to sufficiently capture the full length of the kelp within 1-meter replicate (Figure 4).

Before segmenting the kelp from the images, a type of unsupervised learning algorithm known as 'mean shift clustering' was applied to distinguish foreground kelp, background and sea water as separate features. First introduced by Fukunaga and Hostetler (1975) and reintroduced by Comaniciu and Meer (2002) as a general-purpose algorithm for image segmentation and filtering, the algorithm used here deconstructs the original image into several homogeneous, unstructured segments based on the similarity of colour space representation of neighbouring pixels (Figure 4). Colour segmentation was then applied to distinguish the kelp as the object of interest (OOI) from the surrounding background in the frame (Figure 4). Next, adaptive thresholding (Yang et al., 1994) was applied to mask out the OOI from the background, allowing detection of the contour of the OOI (Figure 4). Lastly, the number of individual pixels in the contour area was counted. The pixel count was converted to square decimetres (dm^2 m^{-1}) by using the 1-meter width of the ROI as a scale and is defined herein as CV-derived area per meter. The pipeline was repeated using image data from each field day.

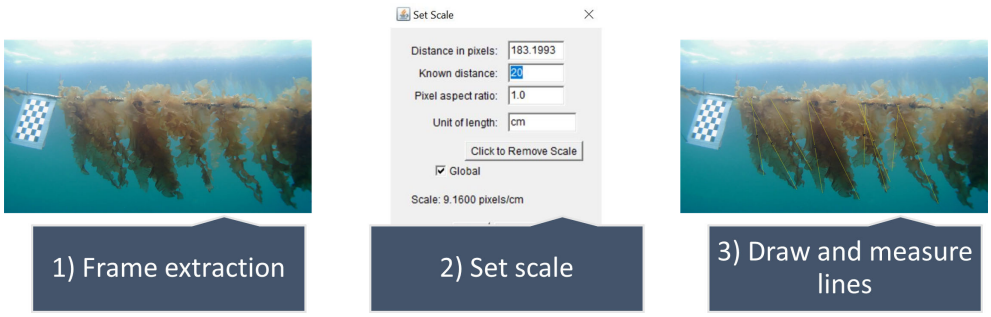

FIGURE 3
Pipeline for manual annotation of length performed using ImageJ. Extraction of image frames from videos. Using a checkerboard to set scale of pixels per centimetre (pixels cm^{-1}). Drawing and measuring length from tip to holdfast (indicated by yellow lines) of ten randomly selected kelp specimens.

10.3389/fmars.2024.1324075

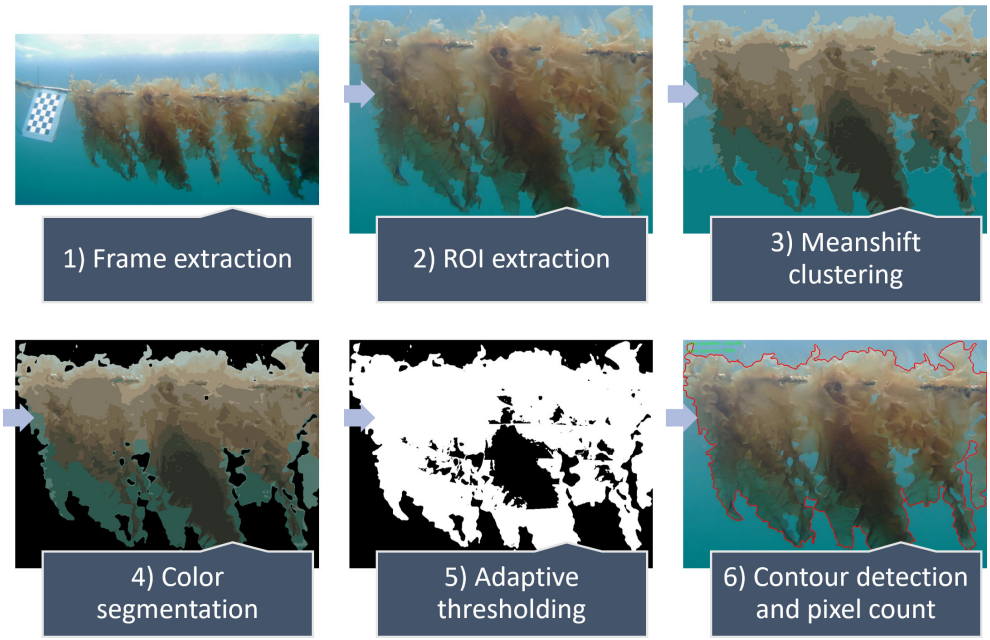

FIGURE 4
Pipeline for the computer vision (CV) area estimation performed with OpenCV. Extraction of frames from image data. Extraction of region of interest (ROI) from frame. Mean shift clustering of pixel values. Segmentation of object of interest (OOI) based on colour. Masking out OOI from the background using adaptive thresholding. Detection of the contour of the OOI and counting of area pixels, converted to square decimetres (dm^2 m^{-1}) using known pixel width and real-world width (one meter) of the frame as size reference, resulting in CV-derived area.

2.3 Statistical analyses

Statistical analyses were performed using NumPy, SciPy, scikit-learn and Matplotlib, libraries for data analysis and visualization in Python and Matlab. Relationships between field-measured length and weight versus ImageJ length and CV-derived area were investigated by applying regressions and evaluated by their coefficient of determination (r^2).

3 Results

3.1 Environmental parameters

Average wind speed varied from February until mid-June, reflecting the dynamic weather in the Frøya region, and was particularly strong (up to 20 m s^{-1}) during March and early April (Figure 5A). Weakening of wind speed (< 10 m s^{-1}) observed from mid- to late April likely contributed to the shoaling of the mixing layer depth and phytoplankton bloom formation. Environmental variables, such as *Chl a* and turbidity levels varied during the field season (Figure 5B). Several peaks in [*Chl a*] were observed from February to June (5b), with a short peak in late March (~2.5 mg m^{-3}), a long peak around mid-April (up to 5.7 mg m^{-3}) and variable values from late May until mid-June (< 4 mg m^{-3}). The overall trend was towards higher concentrations in the second half of the field campaign. The [*Chl a*] served as a proxy for phytoplankton biomass and, thus, indicated when phytoplankton blooms ([*Chl a*] >~ 3 mg m^{-3}) occurred. Turbidity showed significant variability throughout the field season (Figure 5B). A relatively similar trend compared to [*Chl a*] until late May was observed, with a long peak in turbidity levels in mid-to-late April (> 0.2 FTU). A short turbidity peak was observed in mid-June (> 0.2 FTU) (Figure 5B). Seawater temperature showed a gradual increase from February until the end of June, varying from 5.6°C to 9.4°C (Figure 5C).

3.2 Image quality

Differences in the image quality of the videos/frames used for processing were observed between different sampling days (Figure 6). For example, early in the season (22nd March and 5th April), the image quality was very high, indicating good water visibility. During the period of the spring phytoplankton bloom (first peak 20th April, later peaks on May 27th and June 3rd), the observed image quality decreased, indicating bad water visibility due to particles present in the water and the absorption of light from phytoplankton. The visibility of the images slightly improved on May 4th (a period between phytoplankton bloom peaks). On the last sampling day, June 15th, the observed image quality was poor, coinciding with a high concentration of phytoplankton and other particles (indicated by a high peak in *Chl a* and turbidity concentrations Figure 5B). Image quality due to poor visibility decreased towards the end of the cultivation period due to the high abundance of phytoplankton and other particles in the water.

3.3 Calibration and validation

Field-measured verification of kelp length and biomass had a positive power relationship (r^2 = 0.941, biomass = 5.197e-06

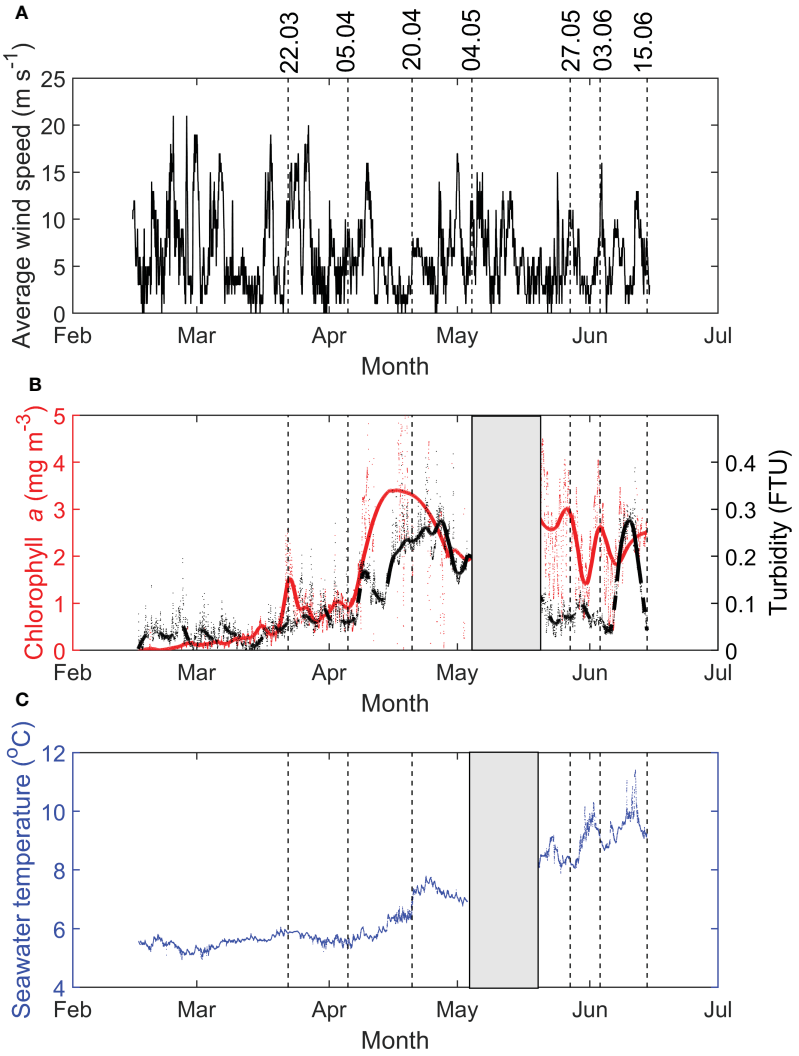

FIGURE 5
(A) Average wind speed (m s^{-1}) at Sula meteorological station, and **(B)** chlorophyll *a* concentrations (red, mg m^{-3}) and turbidity (black, FTU) and **(C)** seawater temperature (°C) at Måsskjæra farm from February 16th to June 15th, 2022. Lines indicate the sampling dates.

length$^{3.037}$, p<0.05) (Figure 7A). On June 15 (latest day in the season), sporophytes were smaller (average= 65.9 cm) than specimens from late May and early June (> 80 cm in May 27th and June 3rd) (Figure 7A). Similarly, imageJ-derived length estimations had a positive strong correlation with field-measured biomass (r^2 = 0.977, biomass = 3.713e-06 ImageJ-length$^{3.083}$, p<0.05) (Supplementary Figure S1, Supplementary Material). The relationship between length (field-measured and derived from ImageJ) and biomass is best approximated by an isometric function (exponent b=3).

ImageJ-derived length (ranging from 33.9 cm to 95.7 cm) had a positive correlation with field-measured length (ranging from 37.4 cm to 93.5 cm) for the 10 randomly selected sporophytes (images and field measurements) (r^2 = 0.959, ImageJ-length = 1.208 field-measured length – 13.817, p < 0.05, Figure 7B). Variability was larger in field-measured length (standard deviation ranged from 12.4 cm to 19.5 cm) compared to variability from ImageJ-derived measurements (standard deviation ranging from 2.8 cm to 14.0 cm) (Figure 7B).

A strong positive power relationship (r^2 = 0.808, CV area = 0.7327 length$^{1.026}$, p < 0.05) was observed between field-measured length and image CV-derived kelp area (Figure 7C). Both CV-derived area and field-measured length showed large variation between sampling timepoints. CV-derived area ranged from 32.2 dm^2 m^{-1} to 79.3 dm^2 m^{-1} (Figure 7C). Measurements from the last sampling day (June 15th) had CV-derived area (35.6 dm^2 m^{-1}) notably below the power trend. When removing the June 15th data from the analysis, an even stronger significant power relationship (r^2 = 0.979, CV area = 0.988 length$^{0.9694}$, p <0.01) was observed (Figure 7D). The area-length relationship with an exponent being equal to 1 indicates a linear relationship between these two variables, where the increase in area is directly proportional to the increase in length.

A wide range in field-measured weight was observed between sampling timepoints, ranging from 0.24 kg to 4.97 kg per meter (Figure 7E). When comparing area measurements (CV-derived) with biomass (wet weight), a strong positive power relationship was

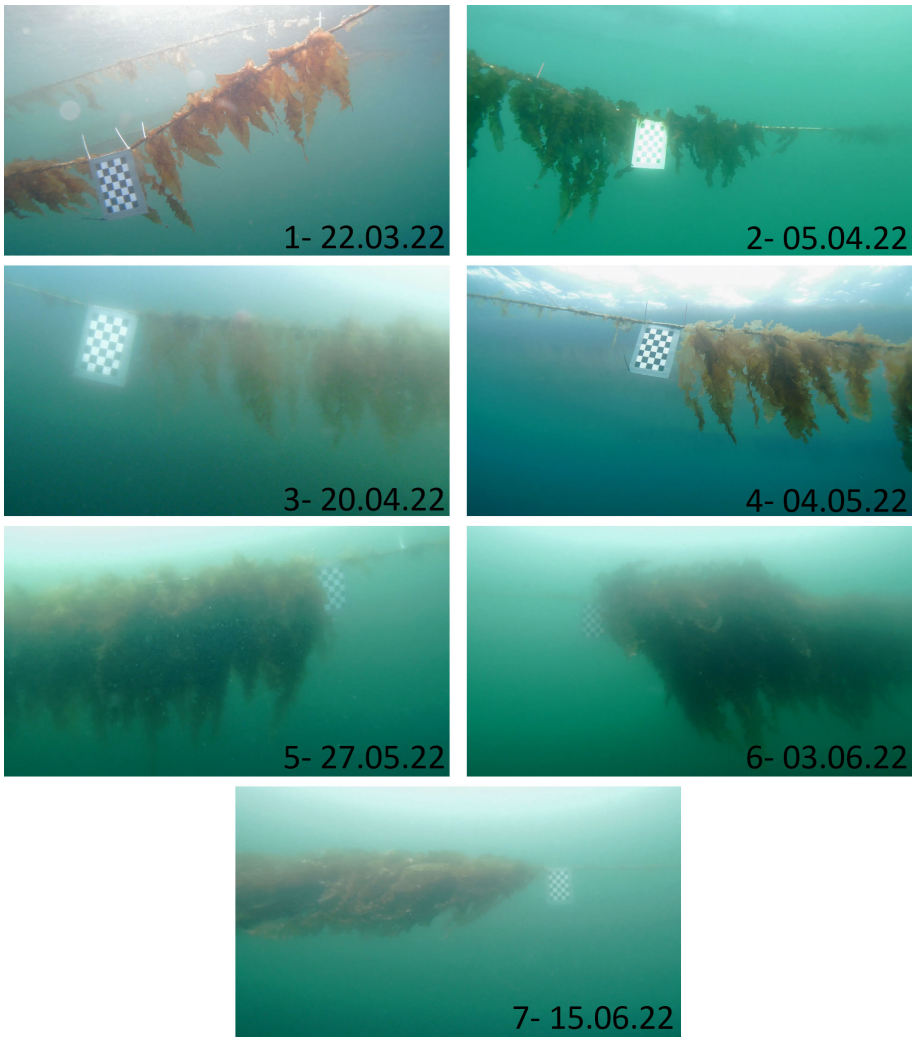

FIGURE 6
Example of image frames collected during each sampling day. Note the variability in water colour, clarity, and the positioning of the kelp (vertical or diagonal) in the cultivation line.

observed (biomass = 2.204e-05 CV area$^{2.81}$, r^2 =0.887) (Figure 7E). Similar to the relationship between CV-derived area and field-measured length, measurements from June 15th had a lower CV-derived area (35.6 dm^2 m^{-1}) compared to the trend, and if removed, the relationship becomes stronger (r^2 = 0.976, biomass = 1.231e-06 CV area$^{3.472}$, $p < 0.01$) (Figure 7F).

4 Discussion

4.1 Effect of environmental factors on image quality

The image quality varied widely in this study as a function of the inherent optical properties (IOPs) of the water, including coloured dissolved organic matter (CDOM) and particle concentrations, such as phytoplankton and detritus. The IOPs, such as phytoplankton cells (light absorption and scattering), non-algal particles (NAP, e.g. detritus and sediments, mainly light scattering) and CDOM (absorbing), will tend to absorb (through pigments) or scatter light through deflection (Werdell et al., 2018), reducing the amount of light reflected from the kelp to the camera. The influence of IOPs varies with the water type and depends on where the seaweed is cultivated, making underwater imaging more suitable for clear, open offshore waters (Broch et al., 2019) and more challenging in turbid and brackish coastal seawater.

Besides IOPs, the apparent optical properties (AOPs) of the water, meaning the angular distribution and intensity of the ambient light-field, can also impact the quality of the images taken under natural light conditions (Johnsen et al., 2009). Measurements of underwater light conditions were not conducted in our study; however, according to our observations, the ambient irradiance impacted water quality image. In this study, incident light would, in some cases, improve water column visibility and detection of kelp from the surrounding water, while in other cases, it could overexpose the images, reducing contrast and corresponding loss of colour information. Kelp self-shading from incident light, which was more prominent as the kelp became bigger, impacted

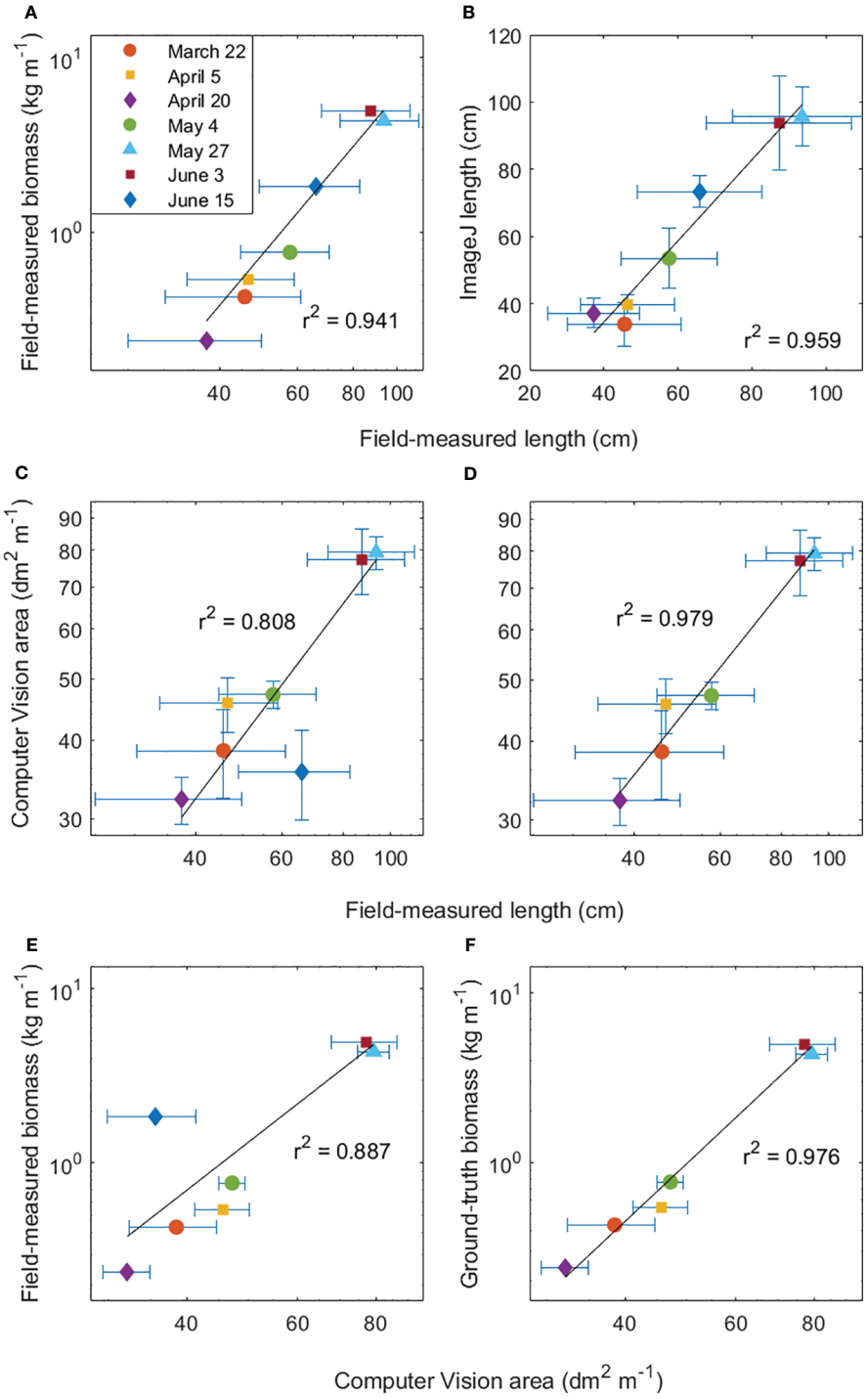

FIGURE 7
Relationships between *S. latissima* **(A)** field-measured lamina length (cm) and field-measured wet weight (kg m^{-1}), **(B)** field-measured length (cm) and ImageJ-derived length (cm), **(C)** field-measured length (cm) and computer vision (CV)-derived area per meter (dm^2 m^{-1}) with and **(D)** without the outlier (June 15th), **(E)** CV-derived area per meter (dm^2 m^{-1}) and field-measured wet weight (kg m^{-1}) with and **(F)** without the outlier (June 15th). Error bars show the standard deviation of ground-truth length (n=10 sporophytes in 1-meter line), ground-truth weight (n=1 in triplicate 1-meter line), ImageJ length (n=6 image frames, 10 sporophyte per frame in 1-meter line).

negatively the algorithms for area detection, particularly towards the later stages of the cultivated kelp (early summer). Kjerstad (2014) showed that light attenuation between the camera and the object limits the range at which pictures of organisms can be taken, since spatial and colour (spectral) resolution becomes distorted in underwater images as the distance to an OOI increases. Artificial light might be a solution, although, in waters with a lot of particles (plankton, sediments and marine snow/detritus), direct light can intensively illuminate those particles, creating bright spots of scattered light and causing image degradation (Boffety and

Galland, 2012). Choice of camera, field of view, spectral resolution and positioning of the external light sources are important pre-image processing factors that should be considered before video recording, in order to optimize post-processing time and image quality.

Waters around Frøya are known to be highly productive, where phytoplankton blooms can start from late March and persist until June-July (Fragoso et al., 2021). Moreover, CDOM concentrations are known to increase from spring and peak in summer as freshwater input from rivers is accumulated in the NCC, the main current along the coastal of Norway (Nima et al., 2016). In this study, CDOM was not measured; however, the other IOPs, such as [*Chl a*] for a proxy of phytoplankton biomass and turbidity, for particle concentration, clearly impacted the quality of the image. The combination of high turbidity and [*Chl a*]- suggesting not only that a bloom is occurring but that it is composed of large cells, colonies and aggregates - makes the water visibility worse, particularly in mid-June. Such conditions become even more detrimental as the kelp gets bigger and the camera needs to move further away to increase the FOV, allowing light to be more attenuated between the camera and the OOI. Chain-forming diatom blooms dominated by the genera *Chaetoceros*, *Skeletonema* and *Thalassiosira* are common during spring in Frøya (Fragoso et al., 2019, Fragoso et al., 2021), as well as many other coastal northern regions (Throndsen et al., 2007), making visibility a challenge for ROV video recording at seaweed farms. Water quality improved on 4th May, after the decline of the first bloom and potentially because of a storm that diluted the particle density throughout the mixed layer depth. Marine snow, as well as zooplankton abundance, which are high in Frøya waters (Fragoso et al., 2019) and other coastal productive regions of Norway, would increase the turbidity signal after bloom conditions, being an additional challenge for water visibility and kelp size inspection.

Underwater imaging enhancement (UIE), such as white balance, dehazing algorithms and histogram equalization are modern tools to improve the contrast of objects from ocean RGB imagery, allowing more accurate segmentation and identification of the OOI (Mathur and Goel, 2022). Mohamed et al. (2020) used the Multi-Scale Retinex (MSR) algorithm for image correction and the YOLO algorithm to enhance fish detection and tracking in tanks, increasing underwater detection of fish specimens by three times. UIE in seaweed and fish farms could be a potential tool to reduce the optical effects of particles in the water, improving the accuracy of our model, particularly for conditions later in the season due to increased turbidity. Another possibility could be to monitor phytoplankton concentrations and turbidity levels using sensors at the kelp farm and adapt the time of video recording to periods with lower turbidity levels and between phytoplankton blooms, in order to collect higher quality imagery.

Strong currents were also another issue that impacted the quality of data. In our studies, slack tides (particularly low tide) were the best periods to video record the kelp lamina hanging vertically from the ropes. This allowed the best positioning of the kelp to be able to better extract area information. According to most of our images, the kelp was aligned vertically from the cultivation rope, except for June 15th, which contributed to the lower rendering of CV-derived area estimations. This suggests that the environmental conditions, possibly obtained from instruments such as acoustic doppler current profilers (ADCPs) and optical instruments for IOPs measurements, need to be taken into consideration before underwater video recording/digital imaging. Awareness of the impact of environmental variables on the reliability of remote sensing results (e.g. seagrass beds, Nahirnick et al. (2019)) has been raised and similar approaches could be implemented for seaweed farms. Pre-analyses of the environmental conditions (irradiance, turbidity and current velocities) from sensors attached to kelp farm infrastructure can help improve decisions about the optimum conditions for underwater farm inspection (Bell et al., 2020).

4.2 Kelp length and area estimations from underwater RGB imagery

Our work indicates that it is possible to detect and derive kelp size from RGB camera images. Through human supervision, length measurements of 10 randomly selected sporophytes extracted from the frames using imageJ (Figure 3) demonstrated strong relationships with measurements done by hand in the field (also 10 randomly selected sporophytes from 1m of cultivation line). Variability in the data is likely related to the fact that these two 1m sections (for image and field measurements) were not the same. Human annotation of traits (length, area, point count, segmentation) is a useful tool in underwater biological image analysis (Gomes-Pereira et al., 2016), which, when combined with CV, has the potential to simplify *in situ* size estimation of underwater organisms.

Automated size estimation, as well as species identification and animal tracking, via CV techniques, are modern tools in ecology. Estimation of individual biomass of marine organism from dimensions derived from images is possible because of the strong isometric/allometric biomass-size relationships expected in many organisms, including macroalgae and seagrasses (Scrosati, 2006; Scrosati et al., 2020). In *S. latissima*, allometric models (where the organism does not maintain its shape as it grows) have been shown to explain a substantial portion of thallus fresh weight (Campbell and Starko, 2021). However, these relationships have previously been studied in individual specimens. In our study, kelp area and biomass estimations were retrieved from a 1-meter line (rather than individuals), while lengths were retrieved from individuals. This makes it complicated to compare our results to these growth models, and it is the reason that we do not observe an isometric/allometric growth function when comparing individual lengths to CV-derived area. Despite this, we observed an isometric relationship between average lamina length and total biomass within 1m line, suggesting that the "canopy" maintains its shape as it grows (conceptually, it can perhaps be thought of as an expanding "cylinder", horizontally oriented in the water column).

Our findings indicate that it is likely possible to derive robust size information about kelp by applying CV techniques to underwater RGB imagery. This technique is commonly applied in agriculture and aquaculture. For example, above ground biomass has been successfully estimated in wheat crops using airborne laser scanning for 3D point cloud reconstruction when comparing

estimated volume and ground-truth biomass (Walter et al., 2018). The plant height of summer barley has also been suggested as a good proxy for fresh and dry biomass using an RGB camera on a small unmanned aerial vehicle (UAV) (Bendig et al., 2015). Comparisons between seaweed biomass and area coverage from intertidal zones derived from UAV multispectral images revealed a positive correlation (r^2 = 0.8, 0.73 and 0.59, respectively for *Ulva pertusa*, *Sargassum thunbergii* and *Sargassum fusiforme*), although accuracy decreased in highly dense beds due to mutual masking of seaweed (Chen et al., 2022). For fish farm applications, CV-derived image area of grey mullet, carp and St. Peter's fish were well correlated to mass (r^2 = 0.954, 0.986, 0.986, respectively) (Zion et al., 1999), while shape and weight exhibited only a 3% error rate in prediction accuracy with machine learning algorithms (Odone et al., 2001). Side view imaging (2D CV) of *Scortum barcoo* showed that shape is a good predictor (r^2 = 0.99) for measuring fish weight outside tanks (Viazzi et al., 2015). The fact that area estimates showed a positive relationship with length and weight in our studies indicates the feasibility of using area as a proxy for biomass under suitable conditions (vertically aligned kelp). Consequently, our results indicate that a model using area estimates as a proxy for biomass can be further developed and eventually applied to accurately predict kelp biomass *in situ* throughout the cultivation season.

These predictions will likely become even more common as machine learning techniques improve and become more mainstream (Weinstein, 2018). During the last decade, machine/deep learning techniques have been increasingly applied to classify distinct functional groups/species in macroalgae and aquatic vegetation (e.g. seagrass beds) from remote sensing imaging derived from drones (Duffy et al., 2018; Chen et al., 2022; Tahara et al., 2022). For seaweed cultivation, however, emerging technologies and methodologies for remote sensing and precision farming, are in their infancy, although they show great promise. Bell et al. (2020), for instance, used underwater colour images from mini-ROVs and side scan sonar of kelp farm longlines, combined with deep learning models, to classify juvenile kelp from the images and acoustic returns before and after pneumatocyst (gas bladders) formation. These acoustic approaches can be a potential way to quantify biomass in species with gas bladders since total gas volume from pneumatocyst increases as kelp laminas grow (Bell et al., 2020). Stenius et al. (2022) also explored the use of side-scan sonar for detection of ropes and buoys at a kelp farm, which could be successfully implemented for biomass estimations of seaweed that possesses pneumatocysts. However, it is unclear whether this methodology would be as successful for other cultivated kelp species that lack pneumatocysts. From RGB imagery, machine learning algorithms successfully classified kelp underwater background, in spite of water motion, although these authors emphasized that water clarity is a requirement for the best visibility and suitability of the model (Bell et al., 2020).

In this study, we showed that a robust relationship between CV-derived area and ground-truth biomass and length. However, post-processing segmentation was time consuming, since we had to manually tune the algorithms for distinct environmental conditions (low versus high turbidity, changes in irradiance, colour hue and contrasts, etc). By combining similar detection algorithms developed by Bell et al. (2020) and others (Duffy et al., 2018; Chen et al., 2022), with the methodology developed in our study, further segmentation for kelp density and automated kelp area estimation for biomass prediction could be feasible. For maintaining the simplicity of this method, density effects (i.e. sporophytes per m) on biomass were not considered and quantified. CV-derived area, by its nature, should capture density more effectively than image derived length. The nature of this relationship (biomass-density) should be explored in detail, however, to verify if cultivation lines with very high densities are likely to have their biomass underestimated due to the inability to capture the third growth dimension (essentially the "thickness" or "bushiness" of the canopy). The relationship between biomass and density, however, is not simplistic as phenomena such as "self-thinning" at high densities, and intra-specific "dynamic thinning" in response to abiotic factors, can occur (see review by Scrosati (2005)).

In order to upscale this method, larger sample datasets can be used as calibration and validation data, as to reduce the statistical uncertainty and provide cross-validation of the results (Bendig et al., 2015). The ultimate goal would be an universally applicable model for different kelp species. However, it is possible that location-specific models will be required. Campbell and Starko (2021) demonstrated that allometric models, for predicting thallus weight from length, were broadly applicable at sites with similar environmental conditions, but suggested the need for region-specific models between substantially different locations. It should be examined if this finding holds true for estimating biomass on cultivation lines from canopy area. If region-specific models need to be constructed, that would still likely be worth the relatively small time invested by the farmer(s) in order to later automate the process of biomass estimation from images.

4.3 Future perspectives for biomass estimation of cultivated kelp

The use of mini-ROVs has been applied in many studies for short-distance inspection and monitoring of several habitats, including benthos (Nevstad, 2022), kelp forests (Summers et al., 2022) and coral reefs (Raoult et al., 2020). In this study we demonstrate that the use of a mini-ROV, equipped with an RGB camera, can reliably estimate kelp biomass using underwater imaging and CV techniques.

Our preliminary results focused on a small section of a farm, which is most likely not representative of the whole farm and has considerable constraints, such as the need for human operation, limited battery time and tether length (Sørensen et al., 2020). Consequently, the use of the ROV can only be applied in sub-sections of the farm to give an idea of how heterogeneously seaweed grow in space and time. In this study we tested our method at the edge of the farm for simplicity (accessibility and so as not to interfere with farm operations). Performing this task inside the farm (e.g. between cultivation lines) is likely to raise issues relating to maneuverability within confined spaces. For further estimations

at a "whole farm" scale, other types of observation platforms equipped with cameras and additional sensors could be used, but this will likely depend on the exact farm design and location (e.g. vertical or horizontal cultivation lines, inshore or offshore, low or high energy environment). As farms scale up in size, there will be an increasing need for kelp farm monitoring at different scales, and combinations of platforms, such as satellites (Jin et al., 2023), UAVs (Bell et al., 2020), AUVs (Stenius et al., 2022) and ROVs.

Here, we anticipate that our concept can be used as the foundation to upscale imagery as a reliable tool for biomass estimation of kelp. For example, Stenius et al. (2022) developed a methodology where they deployed an AUV to monitor a whole kelp-farm autonomously and continuously. In their small-scale scheme, an AUV followed pre-programmed or self-detected sampling patterns based on the outline of the farm and, thus, enabled high resolution monitoring of an entire kelp-farm throughout the cultivation season. Other possibilities could be moving the cameras along strategically structured cables throughout the farm, removing the need for underwater vehicles. Perhaps the cameras do not need to move around at all, but rather placed in fixed positions where they can capture enough image data to build up a representative picture of the total farmed kelp biomass. Ultimately, the goal of the technology and method should be to optimize accuracy of biomass estimation, providing sufficient monitoring, while at the same time minimizing operational risks and costs.

5 Conclusion

Our proof-of-concept results indicate that CV-derived area estimation can serve as a robust proxy for biomass estimation of cultivated kelp. However, accuracy of the data is strongly related to the visibility of the water and current speed. Although there was still a strong relationship when water visibility was reduced, the relationship improved when outliers (with poor water visibility) were removed.

As technology advances and machine learning algorithms for object detection improve, kelp biomass estimation *in situ* with camera systems, perhaps combined with other methods (e.g. acoustics), can be a viable option for large scale farm monitoring. We see this work as an important step towards that goal, where we also envisage autonomous data collection and real-time processing.

Data availability statement

The datasets (source code) presented in this study can be found in the following repository: https://github.com/monitare.

Author contributions

MO: Data curation, Formal analysis, Investigation, Methodology, Validation, Visualization, Writing – original draft, Writing – review & editing. PT: Data curation, Formal analysis, Investigation, Methodology, Software, Supervision, Validation, Visualization, Writing – review & editing. DA: Supervision, Conceptualization, Writing – review & editing. GJ: Resources, Supervision, Writing – review & editing. GF: Conceptualization, Funding acquisition, Project administration, Resources, Supervision, Visualization, Writing – original draft, Writing – review & editing.

Funding

The author(s) declare that financial support was received for the research, authorship, and/or publication of this article. This work was supported by the Research Council of Norway (RCN) through the following project: "Autonomous underwater monitoring of kelp-farm biomass, growth, health and biofouling using optical sensors", MoniTARE (315514). GJ received funding RCN 223254 grant (Center of Excellence, Autonomous Marine Operations and Systems, AMOS).

Acknowledgments

We would like to thank Seaweed Solutions (SES) for providing access to their kelp farm, the irradiance data, in addition to the assistance of SES employees and resources for collection of water samples. Data from this manuscript is part of a NTNU Master's thesis (Overrein, 2023) and is available online (https://ntnuopen.ntnu.no/ntnu-xmlui/handle/11250/3086275). We would also like to thank the journal editor and two reviewers of this paper for their constructive feedback which has strengthened the quality of this manuscript.

Conflict of interest

The authors declare that the research was conducted in the absence of any commercial or financial relationships that could be construed as a potential conflict of interest.

Publisher's note

Supplementary material

The Supplementary Material for this article can be found online at: https://www.frontiersin.org/articles/10.3389/fmars.2024.1324075/full#supplementary-material

References

Albrecht, M. (2023). A Norwegian seaweed utopia? Governmental narratives of coastal communities, upscaling, and the industrial conquering of ocean spaces. *Marit. Stud.* 22, 37. doi: 10.1007/s40152-023-00324-2

Alleway, H. K. (2023). Climate benefits of seaweed farming. *Nat. Sustain.* 6, 356–357. doi: 10.1038/s41893-022-01044-x

Bell, T. W., Nidzieko, N. J., Siegel, D. A., Miller, R. J., Cavanaugh, K. C., Nelson, N. B., et al. (2020). The utility of satellites and autonomous remote sensing platforms for monitoring offshore aquaculture farms: A case study for canopy forming kelps. *Front. Mar. Sci.* 7. doi: 10.3389/fmars.2020.520223

Bendig, J., Yu, K., Aasen, H., Bolten, A., Bennertz, S., Broscheit, J., et al. (2015). Combining UAV-based plant height from crop surface models, visible, and near infrared vegetation indices for biomass monitoring in barley. *Int. J. Appl. Earth Obs. Geoinf.* 39, 79–87. doi: 10.1016/j.jag.2015.02.012

Bewley, M. S., Douillard, B., Nourani-Vatani, N., Friedman, A., Pizarro, O., and Williams, S. B. (2012). Automated species detection: an experimental approach to kelp detection from sea-floor AUV images. In *Proc Australas Conf Rob Autom*. 2012.

Boffety, M., and Galland, F. (2012). Phenomenological marine snow model for optical underwater image simulation: Applications to color restoration. *2012 Oceans - Yeosu (IEEE)* 1–6. doi: 10.1109/OCEANS-Yeosu.2012.6263448

Broch, O. J., Alver, M. O., Bekkby, T., Gundersen, H., Forbord, S., Handå, A., et al. (2019). The kelp cultivation potential in coastal and offshore regions of Norway. *Front. Mar. Sci.* 5. doi: 10.3389/fmars.2018.00529

Broch, O. J., Daae, R. L., Ellingsen, I. H., Nepstad, R., Bendiksen, E.Å., Reed, J. L., et al. (2017). Spatiotemporal dispersal and deposition of fish farm wastes: A model study from central Norway. *Front. Mar. Sci.* 4. doi: 10.3389/fmars.2017.00199

Campbell, J., and Starko, S. (2021). Allometric models effectively predict Saccharina latissima (Laminariales, Phaeophyceae) fresh weight at local scales. *J. Appl. Phycol.* 33, 491–500. doi: 10.1007/s10811-020-02315-w

Chen, J., Li, X., Wang, K., Zhang, S., and Li, J. (2022). Estimation of seaweed biomass based on multispectral UAV in the intertidal zone of Gouqi Island. *Remote Sens.* 14 (9), 2143. doi: 10.3390/rs14092143

Comaniciu, D., and Meer, P. (2002). Mean shift: a robust approach toward feature space analysis. *IEEE Trans. Pattern Anal. Mach. Intell.* 24, 603–619. doi: 10.1109/34.1000236

Duarte, C. M., Bruhn, A., and Krause-Jensen, D. (2021). A seaweed aquaculture imperative to meet global sustainability targets. *Nat. Sustain.* 5, 185–193. doi: 10.1038/s41893-021-00773-9

Duffy, J. P., Pratt, L., Anderson, K., Land, P. E., and Shutler, J. D. (2018). Spatial assessment of intertidal seagrass meadows using optical imaging systems and a lightweight drone. *Estuar. Coast. Shelf Sci.* 200, 169–180. doi: 10.1016/j.ecss.2017.11.001

Ervik, H., Finne, T. E., and Jenssen, B. M. (2018). Toxic and essential elements in seafood from Mausund, Norway. *Environ. Sci. Pollut. Res.* 25, 7409–7417. doi: 10.1007/s11356-017-1000-4

Fischell, E. M., Gomez-ibanez, D., Lavery, A., Stanton, T., and Kukulya, A. (2019). Autonomous underwater vehicle perception of infrastructure and growth for aquaculture. *IEEE ICRA Workshop Underwater Robotic Percept.* 2019, 1–7.

Førde, H., Forbord, S., Handå, A., Fossberg, J., Arff, J., Johnsen, G., et al. (2016). Development of bryozoan fouling on cultivated kelp (Saccharina latissima) in Norway. *J. Appl. Phycol.* 28, 1225–1234. doi: 10.1007/s10811-015-0606-5

Fragoso, G. M., Davies, E. J., Ellingsen, I., Chauton, M. S., Fossum, T., Ludvigsen, M., et al. (2019). Physical controls on phytoplankton size structure, photophysiology and suspended particles in a Norwegian biological hotspot. *Prog. Oceanogr.* 175, 284–299. doi: 10.1016/j.pocean.2019.05.001

Fragoso, G. M., Johnsen, G., Chauton, M. S., Cottier, F., and Ellingsen, I. (2021). Phytoplankton community succession and dynamics using optical approaches. *Cont. Shelf Res.* 213, 104322. doi: 10.1016/j.csr.2020.104322

Fukunaga, K., and Hostetler, L. (1975). The estimation of the gradient of a density function, with applications in pattern recognition. *IEEE Trans. Inf. Theory* 21, 32–40. doi: 10.1109/TIT.1975.1055330

Gomes-Pereira, J. N., Auger, V., Beisiegel, K., Benjamin, R., Bergmann, M., Bowden, D., et al. (2016). Current and future trends in marine image annotation software. *Prog. Oceanogr.* 149, 106–120. doi: 10.1016/j.pocean.2016.07.005

Hossain, M. S., Sharifuzzaman, S. M., Nobi, M. N., Chowdhury, M. S. N., Sarker, S., Alamgir, M., et al. (2021). Seaweeds farming for sustainable development goals and blue economy in Bangladesh. *Mar. Policy* 128, 104469. doi: 10.1016/j.marpol.2021.104469

Hwang, E. K., Yotsukura, N., Pang, S. J., Su, L., and Shan, T. F. (2019). Seaweed breeding programs and progress in eastern Asian countries. *Phycologia* 58, 484–495. doi: 10.1080/00318884.2019.1639436

Jin, R., Ye, Z., Chen, S., Gu, J., He, J., Huang, L., et al. (2023). Accurate mapping of seaweed farms with high-resolution imagery in China. *Geocarto Int.* 38 (1), 2203114. doi: 10.1080/10106049.2023.2203114

Johnsen, G., Volent, Z., Sakshaug, E., Sigernes, F., Pettersson, L. H., and Kovacs, K. (2009). "Remote sensing in the barents sea," in *Ecosystem Barents Sea*, eds. E. Sakshaug, G. Johnsen and K. Kovacs. (Trondheim: Tapir Academic Press), 630.

Kjerstad, I. (2014). Underwater Imaging and the effect of Inherent Optical Properties on image quality. [MSc thesis]. Norwegian University of Science and Technology.

Mathur, M., and Goel, N. (2022). Enhancement algorithm for high visibility of underwater images. *IET Image Process.* 16, 1067–1082. doi: 10.1049/ipr2.12210

Mohamed, H. E.-D., Fadl, A., Anas, O., Wageeh, Y., ElMasry, N., Nabil, A., et al. (2020). MSR-YOLO: Method to enhance fish detection and tracking in fish farms. *Proc. Comput. Sci.* 170, 539–546. doi: 10.1016/j.procs.2020.03.123

Nahirnick, N. K., Reshitnyk, L., Campbell, M., Hessing-Lewis, M., Costa, M., Yakimishyn, J., et al. (2019). Mapping with confidence; delineating seagrass habitats using Unoccupied Aerial Systems (UAS). *Remote Sens. Ecol. Conserv.* 5, 121–135. doi: 10.1002/rse2.98

Nevstad, M. B. (2022). Use of different imaging systems for ROV-based mapping of complex benthic habitats. [MSc thesis]. Norwegian University of Science and Technology.

Nima, C., Frette, Ø., Hamre, B., Erga, S. R., Chen, Y. C., Zhao, L., et al. (2016). Absorption properties of high-latitude Norwegian coastal water: The impact of CDOM and particulate matter. *Estuar. Coast. Shelf Sci.* 178, 158–167. doi: 10.1016/j.ecss.2016.05.012

Odone, F., Trucco, E., and Verri, A. (2001). A trainable system for grading fish from images. *Appl. Artif. Intell.* 15, 735–745. doi: 10.1080/08839510131701857 3

Olafsen, T., Winther, U., Olsen, Y., and Skjermo, J. (2012). "Value Creation Based on Productive Seas in 2050," in Norwegian: Verdiskapning basert på produktive hav i 2050. *Det Kongelige Norske Videnskabers Selskab (DKNVS) and Norges Tekniske Vitenskapsakademi (NTVA).*

Overrein, M. M. (2023). *In situ* biomass estimation of cultivated kelp using RGB imagery. [MSc thesis]. Norwegian University of Science and Technology.

Raoult, V., Tosetto, L., Harvey, C., Nelson, T. M., Reed, J., Parikh, A., et al. (2020). Remotely operated vehicles as alternatives to snorkellers for video-based marine research. *J. Exp. Mar. Bio. Ecol.* 522, 151253. doi: 10.1016/j.jembe.2019.151253

Scrosati, R. (2005). Review of studies on biomass-density relationships (including self-thinning lines) in seaweeds: Main contributions and persisting misconceptions. *Phycol. Res.* 53, 224–233. doi: 10.1111/j.1440-1835.2005.tb00375.x

Scrosati, R. (2006). Length-biomass allometry in primary producers: Predominantly bidimensional seaweeds differ from the "universal" interspecific trend defined by microalgae Vasc. Plants. *Can. J. Bot.* 84, 1159–1166. doi: 10.1139/b06-077

Scrosati, R. A., MacDonald, H. L., Córdova, C. A., and Casas, G. N. (2020). Length and Biomass Data for Atlantic and Pacific Seaweeds From Both Hemispheres. *Front. Mar. Sci.* 7. doi: 10.3389/fmars.2020.592675

Skagseth, Ø., Drinkwater, K. F., and Terrile, E. (2011). Wind- and buoyancy-induced transport of the Norwegian Coastal Current in the Barents Sea. *J. Geophys. Res.* 116, C08007. doi: 10.1029/2011JC006996

Skjermo, J., Aasen, I. M., Arff, J., Broch, O. J., Carvajal, A. K., Hartvig, C. C., et al. (2014). *A new Norwegian bioeconomy based on cultivation and processing of seaweeds: Opportunities and R&D needs*. SINTEF. Available at: https://ntnuopen.ntnu.no/ntnu-xmlui/bitstream/handle/11250/2447684/A25981-++A+new+Norwegian+bioeconomy+based+on+cultivation+and+processing+of+seaweeds+%28ver.2%29-Jorunn+Skjermo.pdf?sequence=1.

Sørensen, A. J., Ludvigsen, M., Norgren, P., Ødegård, Ø., and Cottier, F. (2020). "Sensor-Carrying Platforms." in *POLAR NIGHT Marine Ecology – Life and light in the dead of the night*, eds J. Berge, G. Johnsen and J. Cohen. (Hampton Roads, VA, USA: OCEANS 2022) 380 pp. doi: 10.1007/978-3-030-33208-2

Stenius, I., Folkesson, J., Bhat, S., Sprague, C. I., Ling, L., Özkahraman, Ö., et al. (2022). A system for autonomous seaweed farm inspection with an underwater robot. *Sensors* 22, 1–16. doi: 10.3390/s22135064

Summers, N., Berge, J., Johnsen, G., Mogstad, A., Lovas, H., and Fragoso, G. (2022). Underwater hyperspectral imaging of arctic macroalgal habitats during the polar night using a novel mini-ROV-UHI portable system. *Remote Sens.* 14 (6), 1325. doi: 10.3390/rs14061325

Tahara, S., Sudo, K., Yamakita, T., and Nakaoka, M. (2022). Species level mapping of a seagrass bed using an unmanned aerial vehicle and deep learning technique. *PeerJ* 10, e14017. doi: 10.7717/peerj.14017

Throndsen, J., Hasle, G. R., and Tangen, K. (2007). *Phytoplankton of Norwegian coastal waters.* (Almater Forlag AS).

Tiller, R. G., Hansen, L., Richards, R., and Strand, H. (2015). Work segmentation in the Norwegian salmon industry: The application of segmented labor market theory to work migrants on the island community of Frøya, Norway. *Mar. Policy* 51, 563–572. doi: 10.1016/j.marpol.2014.10.001

van Dijk, M., Morley, T., Rau, M. L., and Saghai, Y. (2021). A meta-analysis of projected global food demand and population at risk of hunger for the period 2010–2050. *Nat. Food* 2, 494–501. doi: 10.1038/s43016-021-00322-9

Viazzi, S., Van Hoestenberghe, S., Goddeeris, B. M., and Berckmans, D. (2015). Automatic mass estimation of Jade perch Scortum barcoo by computer vision. *Aquac. Eng.* 64, 42–48. doi: 10.1016/j.aquaeng.2014.11.003

Volent, Z., Johnsen, G., and Sigernes, F. (2007). Kelp forest mapping by use of airborne hyperspectral imager. *J. Appl. Remote Sens.* 1, 011503. doi: 10.1117/1.2822611

Walter, J., Edwards, J., McDonald, G., and Kuchel, H. (2018). Photogrammetry for the estimation of wheat biomass and harvest index. *F. Crop Res.* 216, 165–174. doi: 10.1016/j.fcr.2017.11.024

Weinstein, B. G. (2018). A computer vision for animal ecology. *J. Anim. Ecol.* 87, 533–545. doi: 10.1111/1365-2656.12780

Werdell, P. J., McKinna, L. I. W., Boss, E., Ackleson, S. G., Craig, S. E., Gregg, W. W., et al. (2018). An overview of approaches and challenges for retrieving marine inherent optical properties from ocean color remote sensing. *Prog. Oceanogr.* 160, 186–212. doi: 10.1016/j.pocean.2018.01.001

Yang, J.-D., Chen, Y.-S., and Hsu, W.-H. (1994). Adaptive thresholding algorithm and its hardware implementation. *Pattern Recognit. Lett.* 15, 141–150. doi: 10.1016/0167-8655(94)90043-4

Zion, B., Shklyar, A., and Karplus, I. (1999). Sorting fish by computer vision. *Comput. Electron. Agric.* 23, 175–187. doi: 10.1016/S0168-1699(99)00030-7

Zolich, A., Faltynkova, A., Johnsen, G., and Johansen, T. A. (2022). *Portable Catamaran Drone – an uncrewed sampling vehicle for micro-plastics and aquaculture research*. (Hampton Roads, VA, USA: OCEANS 2022) 1–6. doi: 10.1109/OCEANS47191.2022.9977294

frontiers | Frontiers in Marine Science

TYPE Original Research
PUBLISHED 22 March 2024
DOI 10.3389/fmars.2024.1376516

OPEN ACCESS

EDITED BY
Ida Grong Aursand,
SINTEF Ocean, Norway

REVIEWED BY
Carlos Alfonso Alvarez-González,
Universidad Juárez Autónoma de Tabasco, Mexico
Erick Perera,
Spanish National Research Council (CSIC), Spain

*CORRESPONDENCE
Ingrid Schafroth Sandbakken
Ingrid.sandbakken@nutrimar.no

RECEIVED 25 January 2024
ACCEPTED 01 March 2024
PUBLISHED 22 March 2024

CITATION
Sandbakken IS, Su H, Johansen L, Zhang Y, Ringø E, Røsbak R, Yakovlev I, Five KK and Olsen RE (2024) Replacing fishmeal with salmon hydrolysate reduces the expression of intestinal inflammatory markers and modulates the gut microbiota in Atlantic salmon (*Salmo salar*). *Front. Mar. Sci.* 11:1376516. doi: 10.3389/fmars.2024.1376516

Replacing fishmeal with salmon hydrolysate reduces the expression of intestinal inflammatory markers and modulates the gut microbiota in Atlantic salmon (*Salmo salar*)

Ingrid Schafroth Sandbakken[1,2]*, Hang Su[3], Louise Johansen[1], Yupeng Zhang[3], Einar Ringø[4], Randi Røsbak[1], Igor Yakovlev[3], Kathrine Kjos Five[1,2] and Rolf Erik Olsen[1]

[1]Department of Biology, Norwegian University of Science and Technology, Trondheim, Norway, [2]Nutrimar AS, Frøya, Norway, [3]Norwegian Institute of Bioeconomy Research, Ås, Norway, [4]Norwegian College of Fishery Science, Faculty of Bioscience, Fisheries, and Economics, UiT the Arctic University of Norway, Tromsø, Norway

The feed legislation allows the use of fish protein hydrolysates in feed for the same species in which it came from, since enzymatic hydrolysis degrades the proteins and eliminates potential prions, which have caused disease in mammals, but not in fish. In this trial, we investigated the effects of partially replacing dietary fishmeal (FM) with salmon protein hydrolysate (FPH) on the intestinal gene expression and microbiota. Atlantic salmon post smolts were either fed a control diet containing 30% fishmeal (FM), a 20% FM diet with 9% salmon hydrolysate (FPH-09) or a 10% FM diet with 18% salmon hydrolysate (FPH-18), until doubling of weight. Gene expression analysis by RNA sequencing of pyloric caeca (PC), midgut (MG) and hindgut (HG) revealed a downregulation of immunological genes involved in inflammation in the intestine of FPH-18 fed salmon compared to salmon fed the FM control. The gene expression of paralogous peptide transporters (PepT) was analyzed by real time quantitative PCR in PC, anterior midgut (AMG), posterior midgut (PMG) and HG of salmon fed all the three diets. The PepT1b paralog had highest relative expression levels in PC and AMG, suggesting that PepT1b is most important for peptide uptake in the anterior intestine. PepT1a was also mainly expressed in the PC and AMG, but at lower levels than PepT1b and PepT2b in the AMG. The PepT2b paralog had high levels of expression in AMG, PMG and HG indicating that it contributed significantly to peptide uptake in the posterior part of the gastrointestinal tract. The gut microbiota in the mucosa and digesta of the MG and HG, were dominated by the phyla Cyanobacteria and Proteobacteria, but also Firmicutes were present. The only dietary effect on the microbiota was the higher prevalence of the phyla Spirochaetes in the mucosa of FPH-18 fed salmon compared to the FM fed salmon. In conclusion, replacing FM with salmon

hydrolysate reduced the expression of inflammatory markers in the Atlantic salmon intestine suggesting improved health benefits. The reduced inflammation may be related to the reduced FM content, potentially bioactive peptides in the hydrolysate and/or the altered gut microbial composition.

KEYWORDS

Atlantic salmon (*Salmo salar*), feed, hydrolysate, gene expression, RNAseq, microbiota, peptide transporters

1 Introduction

The need for novel and sustainable feed ingredients for cultivated fish and land animals is increasing with the growing human population. By-products from marine food production are sustainable alternatives for production of feed ingredients (Rustad et al., 2011; Almås et al., 2020). In Norway a significant biomass of by-products is produced from farmed Atlantic salmon amounting to > 0.5 million tons in 2021 (Myhre et al., 2022). However, the feed legislation prohibits the reuse of proteins from Atlantic salmon into feed of the same species, unless it is hydrolyzed. Complete processing by enzymatic hydrolysis will degrade potential prions and is therefore an exception from the transmissible spongiform encephalopathy (TSE)-legislation (Regulation (EC) No 999/2001; Commission Regulation (EU) No 142/2011; Sandbakken et al., 2023).

Novel feed ingredients should be nutritious, palatable, digestible, and not have any negative impact on the immune response and health of the animal (Glencross, 2020). Protein hydrolysates are mixtures of peptides and free amino acids, which are nutritious, highly digestible and known to be palatable (Kristinsson and Rasco, 2000; Kousoulaki et al., 2013; Khosravi et al., 2015). Hydrolysates may also contain bioactive peptides (Zamora-Sillero et al., 2018; Gao et al., 2021; Siddik et al., 2021). Marine peptides in fish protein hydrolysates (FPH) have shown beneficial effects including antimicrobial, anti-inflammatory and immunomodulatory activities when consumed *in vivo* (Kang et al., 2019). Dietary inclusion of FPH in aquaculture has induced growth performance, digestibility and altered the immune response (Zheng et al., 2014; Siddik et al., 2018).

Optimized diets can improve the general health and immune functions of fish, thereby reduce losses due to diseases, as well as improving recovery after diseases in aquaculture (Waagbø, 1994; Dawood, 2020). Therefore, nutritional status has a major impact on the ability of fish to resist pathogens and cope with stress (Martin et al., 2016). Some feed additives have immunomodulatory properties, which either activates the immune system or downregulates immunological genes. Activating the innate immune system can be beneficial when the fish experiences pathogenic threats, but a general activation can be energy consuming and have negative impact on other processes like growth (Tacchi et al., 2011). A downregulation of genes related to inflammation saves energy for the organism to grow and thrive.

Intestinal protein absorption is performed by different transporters in the brush border membrane of absorptive epithelial cells (Evans and Claiborne, 2006; Kiela and Ghishan, 2016). Peptide transporters (PepT) provide a more efficient uptake mechanism for protein building blocks than amino acid transporters since they transport di- and tripeptides instead of single amino acids (Wang et al., 2017). Due to the whole genome duplication event, Atlantic salmon has at least 4 genes encoding paralogous PepT which are part of the solute carrier 15a (Slc15a) family of transporter molecules. These 4 transporters are *slc15a1a, slc15a1b, slc15a2a* and *slc15a2b*, also known as PepT1a, PepT1b, PepT2a and PepT2b, respectively. PepT1 paralogs are low affinity/high-capacity transporters that serve a key role in peptide absorption, mainly in the proximal part of the intestine (Verri et al., 2003; Rønnestad et al., 2007; Ostaszewska et al., 2010; Wang et al., 2017). Most research available is on the PepT1b paralog, since PepT1a was identified and characterized in Atlantic salmon (*Salmo salar*) quite recently by Gomes et al. (2020). PepT2 paralogs are high affinity/low-capacity transporters which recently were characterized in Atlantic salmon by Vacca et al. (2022). Whereas PepT2b mainly is expressed in the kidney and midgut (MG) to hindgut (HG) (Del Vecchio et al., 2021; Vacca et al., 2022), PepT2a is more abundant in brain and gills, and appears to have a minor role in peptide uptake along the gastrointestinal tract (Del Vecchio et al., 2021). There is however little information on how the expression of peptide transporters is regulated by dietary proteins, and especially available peptides and free amino acids in Atlantic salmon.

Intestinal microbiota composition depends on the diet, environmental factors, and host selection. The microbiota affects the nutrient absorption, immune system, and disease resistance of the host (Luan et al., 2023). Mucosal microbiota is colonizing the mucus layer on the intestinal epithelial cells and is more stable and less affected by diet than the microbiota found in the digesta (feces) (Gajardo et al., 2016). This was clearly shown in Atlantic salmon fed diets with and without insect meal (Li et al., 2021), where the digesta-associated microbiota also showed the highest microbial richness and diversity. Dietary protein can affect the intestinal microbiota composition and function, and interactions between

proteins and microbiota can impact the host health (Bartlett and Kleiner, 2022). Furthermore, if the protein fraction is absorbed much faster than in normal diets, it is possible that remaining bacteria in midgut and hindgut sections will rely more on utilization of feed components reaching there in larger amounts such as fiber and carbohydrates. Such changes in available nutrients for the microbiota can have profound effect on fermentation patterns altering profiles of short chain fatty acids and other products of fermentation (Bartlett and Kleiner, 2022), and on production of inflammatory/anti-inflammatory components.

The current study aimed at assessing the effects of replacing 2/3 of the fishmeal (FM) in a standard diet, with salmon protein hydrolysate (FPH) on intestinal microbiota and health parameters by RNA sequencing analysis. Furthermore, we also report on the response of intestinal peptide transporter expression when the salmon were fed diets with 1/3 and 2/3 of the FM protein replaced with salmon hydrolysate.

2 Materials and methods

2.1 Feed and fish husbandry

A detailed description of the feed composition, experimental design and fish facilities have been reported in Sandbakken et al. (2023). In brief, Atlantic salmon (*Salmo salar*) post smolts were fed one of three diets with spray dried salmon hydrolysate (Nutrimar AS) replacing parts of the fish meal: a control diet with 30% fish meal (FM), a 9% hydrolysate diet with 20% fish meal (FPH-09) and a 18% hydrolysate diet with 10% fish meal (FPH-18) (Supplementary Table 1). The diets were designed to be iso-energetic, iso-nitrogenous, iso-lipidic as well as having the same amount of EPA, DHA and phospholipids. Salmon (mean start weight 141.5 ± 23.6 g (standard deviation)) were PIT-tagged and randomly distributed into 9 tanks (24 fish/tank, ~ 300 L, 10-14 L min^{-1} water flow, > 80% O_2 saturation in the outlet water, 8.2-8.8°C seawater, continuous light) and fed for 2 h twice a day until satiety. After 9 weeks of feeding, the mean salmon weight was 313.8 ± 50 g at sampling. The feeding trial was approved by the Norwegian Food Safety Authority (FOTS ID:23021) and was conducted at NTNU Sealab (Department of Biology, Trondheim, Norway).

2.2 Sampling procedures

Final samples were taken 60 and 62 days after the experimental start, giving RNA samples and microbiota samples, respectively. Before the first sampling day, the fish were not fed for 48 hours to ensure empty intestines for RNA analysis. Five fish from each tank were randomly sampled and euthanized in seawater with Finquel, MS-222 (800 mg/l). Weight, length and PIT-ID was registered before the 5 fish were put on ice and processed immediately. The sampling was performed one tank at a time.

The fish abdomen was opened, and fish were sexed by looking at the gonads. For each fish, 5 intestinal samples were collected for RNA analysis, by cutting ~2 mm of pyloric caeca, 3 segments of the midgut (anterior, mid, and posterior) and a middle segment of the hindgut (HG). Tissue samples for RNA analysis were put in 1 ml cold RNA later (RNA stabilization solution, Ambion Inc.), and stored for 24 h at 4°C before the samples were transferred to -20°C.

The remaining fish (19 per tank) were fed five 2-hour meals over the next 42 hours, before the next sampling two days later. Five random fish from the tanks fed FM control and FPH-18 were euthanized (MS-222) to collect microbiota from midgut (MG) and hindgut (HG) digesta and mucosa. The fish were sexed followed by aseptic removal of the intestine from the abdominal cavity. Sampling equipment was sterilized between each sample by burning 96% ethanol from the metal. The intestine was opened longitudinally with scissors, followed by digesta collection in cryotubes that were snap-frozen on dry ice. The remaining intestine was washed 3 times in cold sterile Phosphate Buffered Saline (PBS, P3813, Sigma-Aldrich) to remove traces of remaining digesta. Some of the intestinal mucosa was scratched off with the backside of a scalpel and snap frozen on dry ice. The same procedure was performed aseptically on both the MG and HG, resulting in four microbiota samples from each fish that were stored at -80°C until analysis.

An overview of analysis performed on the different intestinal segments from fish fed different diets is shown in Table 1.

2.3 RNA extraction and quantification

Intestinal samples were thawed on ice, dried off on a clean piece of paper and weighed (averagely 32 mg) in an Eppendorf tube

TABLE 1 Overview of analysis performed on the different intestinal segments in fish fed different diets: control diet with 30% fish meal (FM), 9% salmon hydrolysate diet with 20% fish meal (FPH-09) and 18% salmon hydrolysate with 10% fish meal (FPH-18).

Intestinal segment		Pyloric caeca (PC)	Anterior midgut (AMG)	Middle of midgut (MG)	Posterior midgut (PMG)	Hindgut (HG)
Analysis	Feed					
RNA seq.	FM FPH-18	X		X		X
RT-qPCR	FM FPH-09 FPH-18	X	X		X	X
Microbiota of digesta and mucosa	FM FPH-18		X			X

(1.5 ml). Samples were added 1 ml of an RLT Lysis buffer (RNeasy Mini kit) mixed with β-mercaptoethanol (1% in RLT) before homogenization using a rotor-stator homogenizator (Polytron Kinematica PT3000) for up to 10 seconds at max speed (28 100 rpm). All samples were kept on ice between homogenization, and frozen at -80°C before further processing. RNA was isolated as described in the RNeasy Mini kit (Qiagen) including a DNase treatment step with RNase-Free DNase set (ID:79256, Qiagen). RNA concentration was measured with Nanodrop 2000c Spectrophotometer (Thermo Scientific) and RNA quality was evaluated by 2100 Bioanalyzer using RNA 6000 Nano Kit (both from Agilent Technologies) following the manufacturer's protocol. All samples with RNA integrity number (RIN) of ≥ 7 were accepted for further use. RNA was kept at -80°C between analysis.

2.4 RNA sequencing and assembly

Extracted RNA samples (6 from each intestinal segment and diet, 36 in total) from pyloric caeca (PC), MG and HG from fish fed FM and FPH-18 diets were sent to The Beijing Genomics Institute (BGI, Beijing, China) for sequencing. RNA quality control, library construction and sequencing were done by BGI, including (i) mRNA enrichment and purification by using Oligo dT beads to enrich mRNA with a polyA tail, (ii) RNA fragment and reverse transcription by random N6-primed reverse transcription, followed by the second-strand cDNA synthesis, (iii) end repair of cDNA fragments, 3' adenylation and adaptor ligation, (iv) PCR amplification to enrich the purified cDNA template, (v) cyclization by heating PCR product, oligos and DNA ligase, (vi) DNA nanoball synthesis, and (vii) sequencing on DNBSeq Technology platform.

Firstly, reads mapped to rRNAs and low-quality reads (where > 20% of the bases had qualities < 10 in base quality score) were removed. Secondly, reads with adaptors and/or with unknown bases (N bases more than 5%) were filtered. Clean reads were mapped onto the reference genome assembly Ssal_v3.1 (GCF_905237065.1), followed by novel gene prediction. After novel transcript detection, coding transcripts were merged with reference transcripts to get complete reference, then clean reads were mapped to it using STAR (Dobin et al., 2013), then gene expression level was calculated for each sample with RSEM (Li and Dewey, 2011). RSEM is a software package for estimating gene and isoform expression levels from RNA-Seq data. Pearson correlation between all samples was calculated using *cor*. Hierarchical clustering between all samples was performed using *hclust*. PCA analysis with all samples was performed using *princomp*, and the diagrams were drawn with *ggplot2* in R. Circos software package (version 1.2.12.) was used to visualize data (Krzywinski et al., 2009). The clustering results were displayed with javaTreeview (Saldanha, 2004) using cluster (Eisen et al., 1998; De Hoon et al., 2004) software to analyze the expression genes and sample scheme at the same time by using the Euclidean distance matrix as the matrix formula.

In order to reflect the gene expression correlation between samples, all the samples were hierarchical clustered by the expression level of all genes, which can directly reflect the relationship between each two samples. Sample variation was visualized by a principal component analysis (PCA) plot (Supplementary Figure 1A), which shows that all samples were divided into three parts according to intestinal segments, indicating the reliability of the sequenced samples. Differentially expression genes (DEGs) were detected between groups based on gene expression levels using DEseq2 algorithms. Summary of DEGs is shown in Supplementary Figure 1B. DEGs were detected including an average of 105 up-regulated genes and on average 61 down-regulated DEGs in the three intestinal segments.

Differentially expressed genes (DEGs) between the FM and FPH-18 group (log fold change ≥ 1 and adjusted p-value ≤ 0.05), were detected based on gene expression levels using DEseq2 algorithms. Clustering analysis and functional annotations including Gene Ontology (GO) (http://www.geneontology.org) and Kyoto Encyclopedia of Genes and Genomes (KEGG) (http://www.genome.jp/kegg/) enrichment were performed. The raw data has been uploaded to NCBI SRA database with BioProject No. PRJNA1072556.

2.5 Reverse transcription and real-time quantitative PCR

Reverse transcription was performed using LunaScript RT SuperMix Kit (New England BioLabs) with 1 µg RNA per 20 µl reaction volume, following the manufacturers protocol. A control without reverse transcriptase (no-RT) was added to each plate (Thermo Scientific, cat. No. AB0600) to evaluate the presence of genomic DNA in a sample. The plate was centrifuged (1 min, 900 rpm, Sigma 2-6 Compact Centrifuge) before incubation in a thermal cycler (Bio-Rad T100) for 2 min at 25°C for primer annealing, followed by cDNA synthesis at 55°C for 10 min and finally heat inactivation at 95°C for 1 min. The cDNA plates were stored at -20°C.

Primers were screened for specificity *in silico* by using BLAST (Ye et al., 2012) and this tool was also used to create new primers when the BLAST results of published primers were insufficient. The primers used for the analysis are listed in Table 2 (Sigma Aldrich). The primer efficiencies were tested by preparing dilution curves of the pooled samples and running a qPCR analysis as described below.

Quantitative real-time PCR (qPCR) was performed by using the LightCycler 480 SYBR Green I Master Kit (Life Science Roche, Cat. No. 04887352001) containing FastStart Taq DNA Polymerase. Primer specific master mixes were made by mixing SYBR Green (10 µl), primers (10 µM, 1 µl each) and nuclease free water (3 µl), multiplying the volumes with sample number and distributing 15 µl per well into 96 well qPCR plates (VWR, Cat. No. 732-1463). Diluted cDNA (1:6, 5 µl) from each sample, no-RT control from the cDNA reaction, no template control (NTC) and pooled cDNA samples of PC, MG and HG (all with the same dilution 1:6) were manually transferred into single wells in a plate and mixed by pipetting. The pooled samples were used as internal calibrators for the reference gene and gene of interest on each plate to facilitate comparisons between different plates. The plate was run in the

TABLE 2 Primers for RT-qPCR analysis of paralogous peptide transporters (PepT1a, -1b, -2a and -2b) and elongation factor 1 alpha (ELF1a).

Gene	GenBank Acc. No.	Primer sequences 5′- 3′	Amplicon (bp)	Efficiency (LinReg)	Source
PepT1a	XM_014172951	F: ATTGCACAGATCGAAGAACA	217	1.791	Own design
		R: CATCTTCATTATGATGGTCTACGAC			
PepT1b	NM_001146682	F: ACGGGCCGGAGAGGAAGAGAGAT	124	1.876	Own design
		R: ACTTCTTGGTTAAGTTGCTCAACAACCGA			
PepT2a	XM_014165384	F: GGGGGACACAACAAGACCAT	198	1.891	(Del Vecchio et al., 2021)
		R: CCGCGTGTTTATGAACCTCA			
PepT2b	XM_014173652	F: AATGTCATTGTGCTGATCGTCGCA	225	1.892	Own design
		R: CTGGTCCATGTGGTATTTCTGGTTC			
ELF1a	NM_001141909	F: CCTGTGGAAGTTTGAGACTGG	173	1.903	(Irachi et al., 2020)
		R: GAGTCTGCCCGTTCTTTGAG			

Lightcycler 480 qPCR instrument (Roche) with these cycling parameters: 1) Preincubation at 95°C for 10 min (1 cycle), 2a) denaturation at 95°C for 15 s, 2b) annealing at 60°C for 15 s, 2c) elongation at 72°C for 15 s (40 cycles of 2a-2c), followed by melt curve 3a) 95°C for 1 min, 3b) 65°C for 30 s, 3c) 97°C for 1 s and finally cooling at 37°C for 30 s.

The ΔCt ($Ct_{gene} - Ct_{ref.}$) values per sample were plotted by diet and intestinal segment in R (version 4.3.1) to reveal outliers, which were removed if they were deviating more than 1.5 interquartile ranges (IQR) above the 75% quartile or below the 25% quartile. After outlier removal, we had 8-15 (averagely 13.6) biological replicates per diet and intestinal segment. The NTC and no-RT controls showed Ct values ranges between 32.03-36.87 and 31.67-35.07, respectively. The choice of elongation factor 1α (ELF1a) as reference gene was based on little variation in Ct values when testing effects of diets and different intestinal segments (Olsvik et al., 2005).

2.6 Bacterial microbiota analysis

DNA of mucosa and feces from MG and HG were extracted using QIAamp Fast DNA Stool Mini Kit (Qiagen, Switzerland). For bacterial microbiota analysis, DNA samples were sequenced at BGI (China), using 16S rRNA gene amplicon sequencing.

DNA template (30 ng) and the 16S rRNA fusion primers (V3-V4 region) were added for PCR. All PCR products were purified by Agencourt AMPure XP beads, dissolved in elution buffer and eventually labeled to finish library construction. Library size and concentration were detected by Agilent 2100 Bioanalyzer. Qualified libraries were sequenced on HiSeq platform according to their insert size.

Raw data were filtered to obtain high-quality clean data, and overlapping clean reads were merged to tags and further clustered to operational taxonomic units (OTU). Taxonomic classifications were assigned to OTU representative sequence using Ribosomal Project Database. Analysis like alpha diversity, beta diversity, differential species analysis, network and model prediction were carried out on the OTU profile table and taxonomic annotation results. Taxonomic analysis of OTU representative sequences was carried out by RDP classifier Bayesian algorithm to identify the composition of microbial structure. Abundances of species on seven levels (Phylum, Class, Order, Family, Genus, Species) was calculated after annotation (Cole et al., 2014). In the present study, only phylum level is presented.

2.7 Statistical analysis

Statistical analysis of RT-qPCR results was performed in R Studio (version R-4.3.1) (R Core Team, 2023). Homogeneity of variance in the residuals after removing outliers was tested using Levene's test. Normal distribution of the residuals was tested by using Q-Q plot and Shapiro-Wilk's normality test. Dietary effects were tested by One-way ANOVA of ΔCt ($Ct_{gene} - Ct_{ref.}$) values for each gene and intestinal segment separately. In cases where ANOVA revealed significant difference of diet, Tukey's Honest Significant Difference (HSD) *post hoc* test was used to find where the differences were. The significance level was set to $p < 0.05$.

3 Results

3.1 Fish performance

The specific growth rate, digestibility and intestinal histology results from this specific trial have been presented elsewhere (Sandbakken et al., 2023). In summary, salmon fed the hydrolysate diets showed significantly higher specific growth rate over the first 25 feeding days, which may indicate feed stimulatory properties of the hydrolysate. The FPH-18 diet had significantly higher protein and amino acid digestibility than the other diets, and the ash digestibility increased linearly with the FPH content, indicating increased mineral uptake from the hydrolysate diets.

Histological analysis of midgut (MG) and hindgut (HG) of the FM and FPH-18 diets did not reveal any significant differences, and the intestines appeared normal and healthy.

3.2 RNA sequencing

Gene expression analysis by RNA sequencing in pyloric caeca (PC), midgut (MG) and hindgut (HG) generally revealed few differentially expressed genes (DEGs) between the salmon fed FM and FPH-18 diets (Supplementary Figure 1B). Gene ontology (GO) enrichments and KEGG (Kyoto Encyclopedia of Genes and Genomes) enriched pathways mostly grouped the downregulated genes, even though more upregulated DEGs (69-129), than downregulated DEGs (44-78) were detected in all intestinal segments of salmon fed FPH-18 compared to FM (Supplementary Figure 1B).

GO biological process enrichment revealed a downregulation of antimicrobial and antiviral immunity in PC, MG and HG of salmon fed the FPH-18 diet compared to the FM diet (Figure 1). In the PC, a downregulation of several immune-related GO biological processes was seen (Figure 1A), like interferon stimulated gene (ISG)15-protein conjugation (GO:0032020), cellular defense response (GO:0006968), positive regulation of T cell cytokine production (GO:0002726) and positive regulation of cytokine production involved in immune response (GO:0002720), which are part of cellular responses to viral and bacterial infections. In the MG, few downregulated GO biological processes were found, and they were linked to triglyceride biosynthetic process (GO:0019432) and superoxide metabolic process (GO:0006801), which are related to lipid metabolism and prevention of oxidative damage (Figure 1B).

In the HG, a downregulation of several GO biological processes related to viral immune response was prominent in salmon fed FPH-18 compared to FM (Figure 1C). The processes ISG15-protein conjugation (GO:0032020), type I interferon-mediated signaling pathway (GO:0060337), cellular response to type I interferon (GO:0071357), viral genome replication (GO:0019079), regulation of defense response to virus (GO:0050688), positive regulation of pattern recognition receptor signaling pathway (GO:0062208),

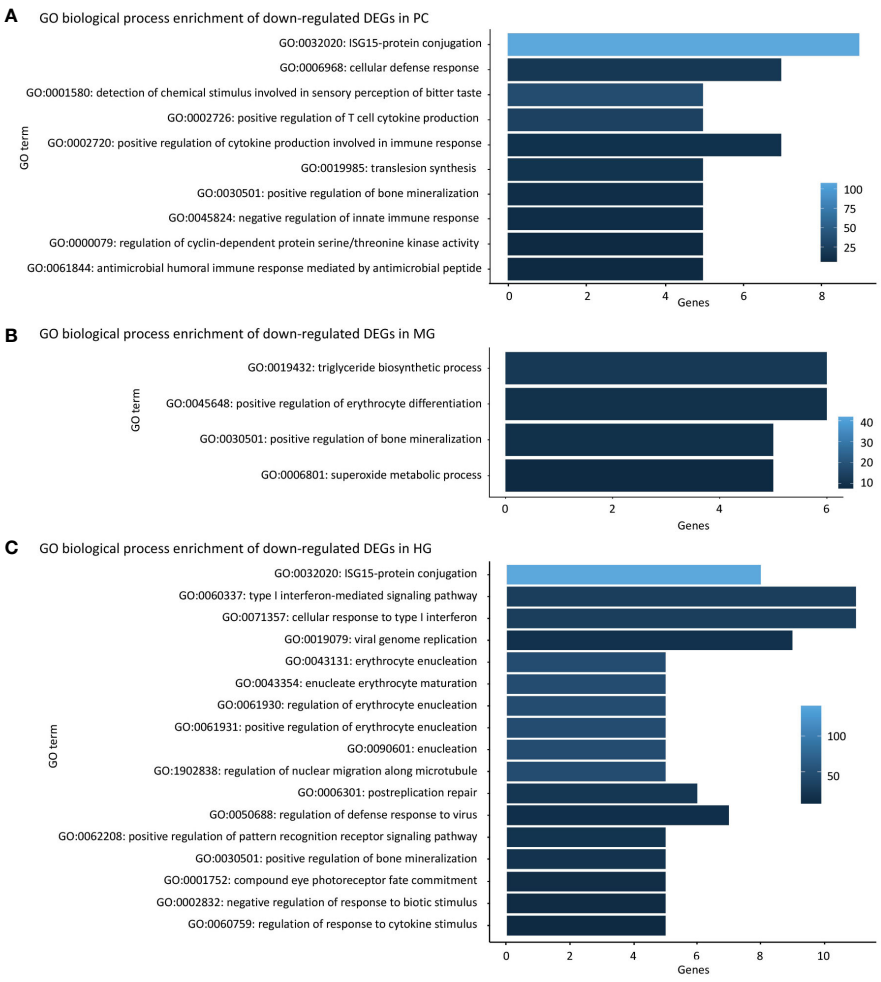

FIGURE 1
FPH-18 reduces inflammatory responses in salmon intestinal segments. Gene ontology (GO) enrichments of differentially expressed genes (DEGs) in 18% salmon protein hydrolysate diet (FPH-18) compared to the fishmeal control diet (FM). GO biological process enrichment of down-regulated DEGs in pyloric caeca (PC), midgut (MG) and hindgut (HG) are shown in **(A–C)** respectively. Only DEGs ≥ 5 genes are displayed, and the color intensity represents fold enrichment.

negative regulation of response to biotic stimulus (GO:0002832) and regulation of response to cytokine stimulus (GO:0060759) are related to pathogen recognition and antimicrobial immunity. This indicates that the immune system did not identify any threats and could therefore downregulate expression of immune-response genes to save energy.

GO molecular function enrichment showed that some downregulated DEGs were related to molecular binding, such as protein tag activity (GO:0031386) in the PC and HG, dynein heavy chain binding (GO:0045504), nuclear androgen receptor binding (GO:0050681) and protein self-association (GO:0043621) in HG (Figure 2). This indicates that the salmon hydrolysate diet (FPH-18) may reduce molecular interactions and protein binding compared to the FM diet.

The comparison between FPH-18 and FM fed salmon had 5 KEGG enriched pathways, where 4 were downregulated and 1 upregulated (Table 3). The downregulated pathways in the PC are related to viral, microbial and pathogen sensing and include the RIG-I-like receptor, NOD-like receptor and toll-like receptor signaling pathways as well as the cytosolic DNA sensing pathway.

3.3 Expression of specifically interesting genes

Some specifically interesting genes were picked for in depth analysis of immune response and ion transport. Heatmap of gene expression in the three intestinal segments related to immune

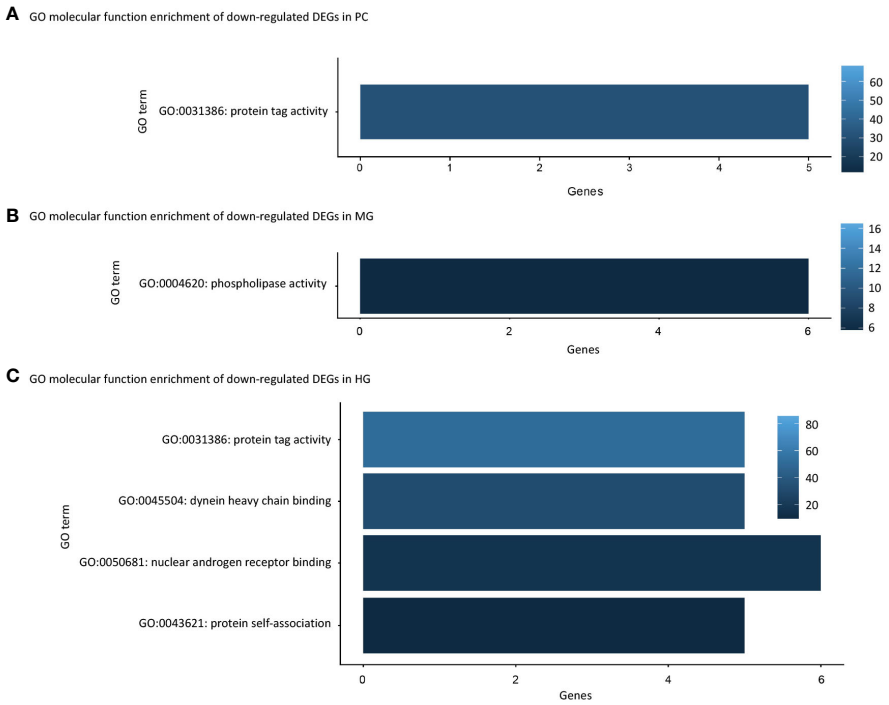

FIGURE 2
Gene ontology (GO) molecular function enrichments of downregulated differentially expressed genes (DEGs) in pyloric caeca (PC), midgut (MG) and hindgut (HG), shown in **(A-C)** respectively. Only DEGs ≥ 5 genes are displayed, and the color intensity represents fold enrichment.

TABLE 3 Results from KEGG enrichment of RNA sequencing data of intestinal samples from salmon fed FPH-18 compared to FM fed salmon.

Enrichment	KEGG ID	Description	DEG ratio*	P value adjusted
PC up-regulated DEGs	sasa04512	ECM-receptor interaction	5/198 (2.53%)	0.01419
PC down-regulated DEGs	sasa04622	RIG-I-like receptor signaling pathway	7/167 (4.19%)	0.00064
	sasa04623	Cytosolic DNA-sensing pathway	6/126 (4.76%)	0.00070
	sasa04620	Toll-like receptor signaling pathway	6/236 (2.54%)	0.01440
	sasa04621	NOD-like receptor signaling pathway	7/380 (1.84%)	0.02543
HG down-regulated DEGs	sasa04622	RIG-I-like receptor signaling pathway	5/167 (2.99%)	0.00349

*DEG ratio, DEG number/total gene number in the signaling pathway.
Differentially expressed genes (DEG) count ≥ 5.

response (Figure 3A) and ion transporters (Figure 3B) shows the differences between the diets by FPKM (Fragments Per Kilobase of transcript per Million mapped reads). Molecules related to immune responses, such as TLR3 (toll-like receptor 3) and Mx (myxovirus resistance protein), seems to have higher expression in the hydrolysate diet (FPH-18), but the variation among the samples were large (Figure 3A). Guanylin is involved in regulating ion transport, and showed highest expression in MG, while the solute carrier 15 (Slc15) family of transporter molecules showed highest expression in PC (Figure 3B). Slc15 is a group of nutrient transporters that mediate the transport of nutrients across the cellular membrane. Peptide transporters (PepT) are in this group (Slc15a), and we looked specifically at 4 paralogous peptide transporters with RT-qPCR.

3.4 Intestinal gene expression by RT-qPCR

Transcriptomic analysis by RT-qPCR was performed on paralogous peptide transporters (PepT, Slc15a) to evaluate the dietary effects in different intestinal segments. Relative expression of the four paralogous peptide transporters PepT1a, PepT1b, PepT2a and PepT2b differed among each other and between intestinal segments. Delta cycle threshold (ΔCt) between the gene of interest and reference gene was plotted for each diet in different intestinal segments to visualize which peptide transporter that mainly contributed to peptide uptake in that specific segment, and how the relative differences change along the gastrointestinal tract (Figure 4).

Generally, there were few dietary effects on PepT expression. The most notable finding was that the PepTs appeared to be differently expressed along the intestinal tract. In PC, PepT1b had the highest mRNA level, followed by PepT1a and PepT2b, which both had about 4 times (2^{-2}) lower mRNA levels. Pept2a generally showed very low expression levels throughout the intestine, with significantly lower expression in fish fed the FPH-18 diet compared to the FM and FPH-09 diets in the anterior midgut (AMG). In the AMG, PepT1b and PepT2b seem to contribute equally to peptide uptake, due to similar relative expressions to the reference gene.

The relative amount of PepT1b mRNA tended to decrease along the intestine, while the opposite was seen for PepT2b mRNA, which contributed the most to peptide uptake from posterior midgut (PMG) to HG. Significantly less PepT2b mRNA was found in the FPH-18 diet compared to FM control in the HG. The relative expression of PepT2b in the HG was 500 times (2^{9}) higher than any of the other paralogous PepT in this intestinal segment.

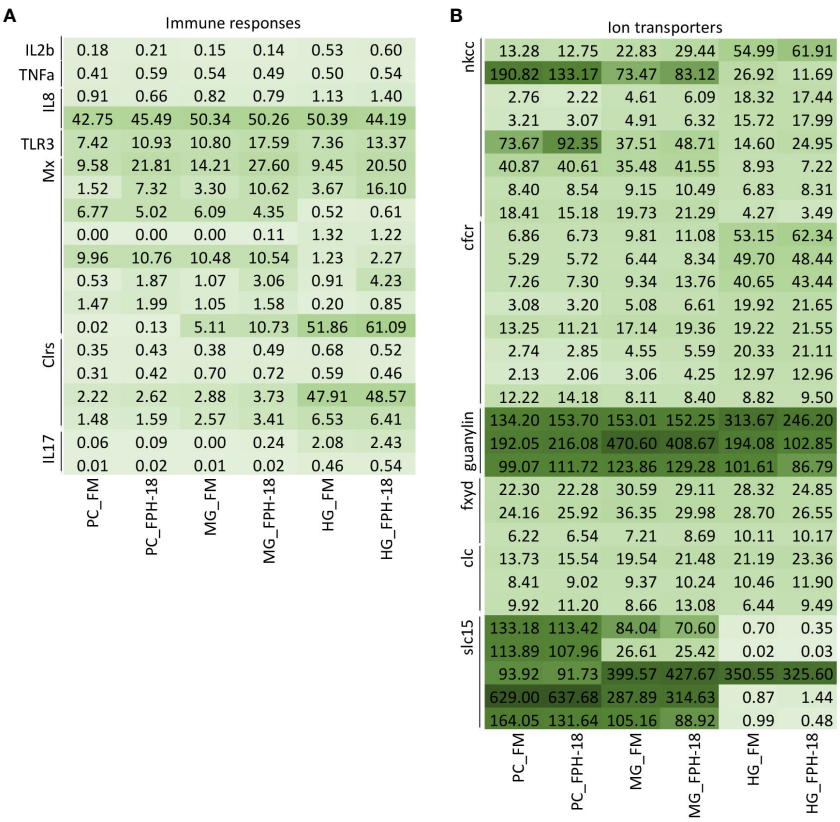

FIGURE 3
Heatmap of gene expression (FPKM) of interesting genes in different intestinal segments: pyloric caeca (PC), midgut (MG) and hindgut (HG) of salmon fed FM or FPH-18 diets. Genes related to immune responses **(A)** (without genes with average FPKM<0.5 in all groups) and ion transporters (without genes with average FPKM<10 in all groups) **(B)**. Darker color shows higher FPKM.

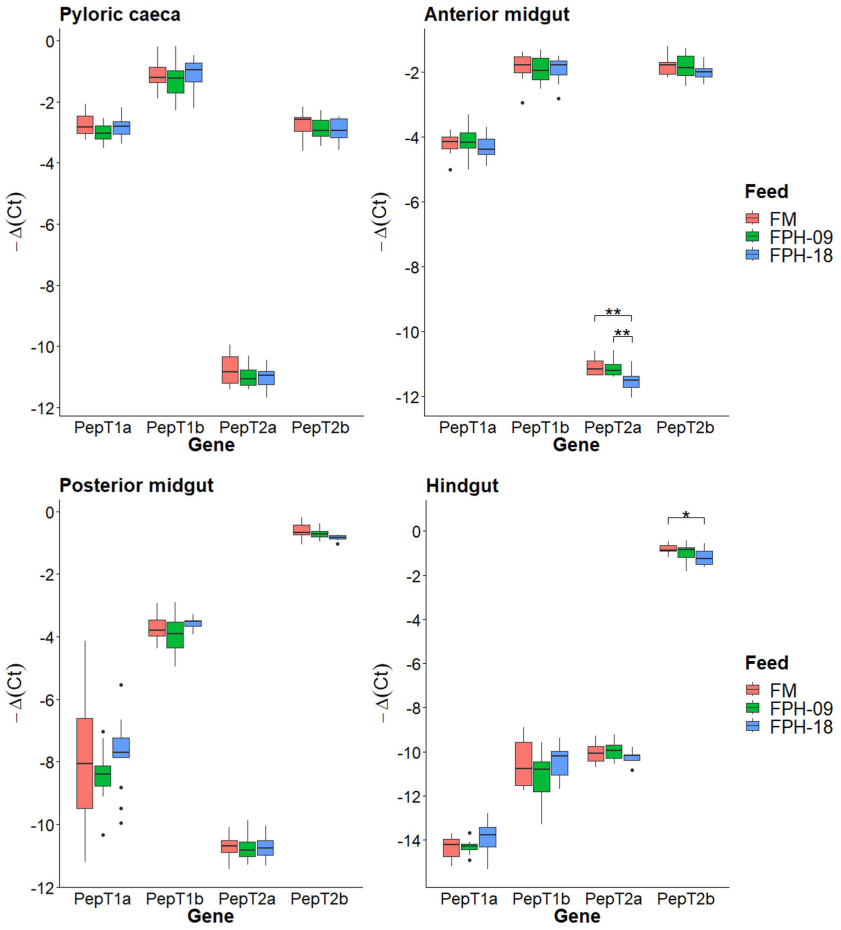

FIGURE 4
Boxplots of relative gene expression ratio as $-\Delta(Ct_{gene} - Ct_{ref})$ for each peptide transporter gene in the different intestinal segments of fish fed fishmeal control diet (FM), 9% and 18% salmon hydrolysate (FPH-09 and FPH-18, respectively). This shows the relative expression levels in the different intestinal segments, comparing which peptide transporters contribute the most to peptide uptake. Significantly different relative expression between diets are marked with *($p < 0.05$) and **($p < 0.01$).

3.5 Bacterial microbiota

In the present study, numerous bacterial phyla were identified. Figure 5 shows the relative abundance of the predominant gut phyla levels in mucosa (A) and digesta (B) from MG and HG of salmon fed a FM or FPH-18 diet. At the phylum level, Cyanobacteria, Proteobacteria, Firmicutes, Spirochaetes and Actinobacteria were predominant in mucosa from MG and HG of salmon fed the two diets, but some dietary effects were noticed (Figure 5A; Supplementary Table 2). The relative abundance of Cyanobacteria, Proteobacteria and Firmicutes in HG mucosa decreased by FPH-18 feeding, in contrast to the relative abundance of Spirochaetes which increased. In the MG, the relative abundance of Cyanobacteria and Spirochaetes increased in the mucosa of salmon fed FPH-18. The relative abundance of Actinobacteria decreased while Firmicutes were unaffected by dietary treatment. The only dietary effect seen in mucosa was the increase in Spirochaetes in the MG and especially the HG of salmon fed FPH-18. Preliminary results on genus level, revealed a high abundance of *Brevinema*, and especially *Brevinema andersonii* on a species level, in mucosa of fed fish FPH-18 in contrast to the FM fed fish.

In the digesta, the relative abundance of phyla was predominated by Cyanobacteria, Proteobacteria, Firmicutes, Spirochaetes, Actinobacteria and Bacteroides (Figure 5B; Supplementary Table 3). The highest relative abundance of Cyanobacteria (43.4%) was noticed in HG digesta from fish fed the FPH-18 diet, and Proteobacteria (44.4%) in MG digesta from fish fed FM. Firmicutes abundance was relatively stable (values between 9.7-15.3%) in digesta samples, while the abundance of Spirochaetes (19.6%) was highest in the digesta from fish fed the FPH-18 diet. The only clear dietary effect in digesta composition was the higher abundance of Spirochaetes in MG of FPH-18 fed salmon.

4 Discussion

4.1 Gene expression by RNA sequencing

The results from GO and KEGG clearly shows that replacing fishmeal with salmon hydrolysate reduced the inflammatory load as viewed by the reduction of pro-inflammatory markers in the

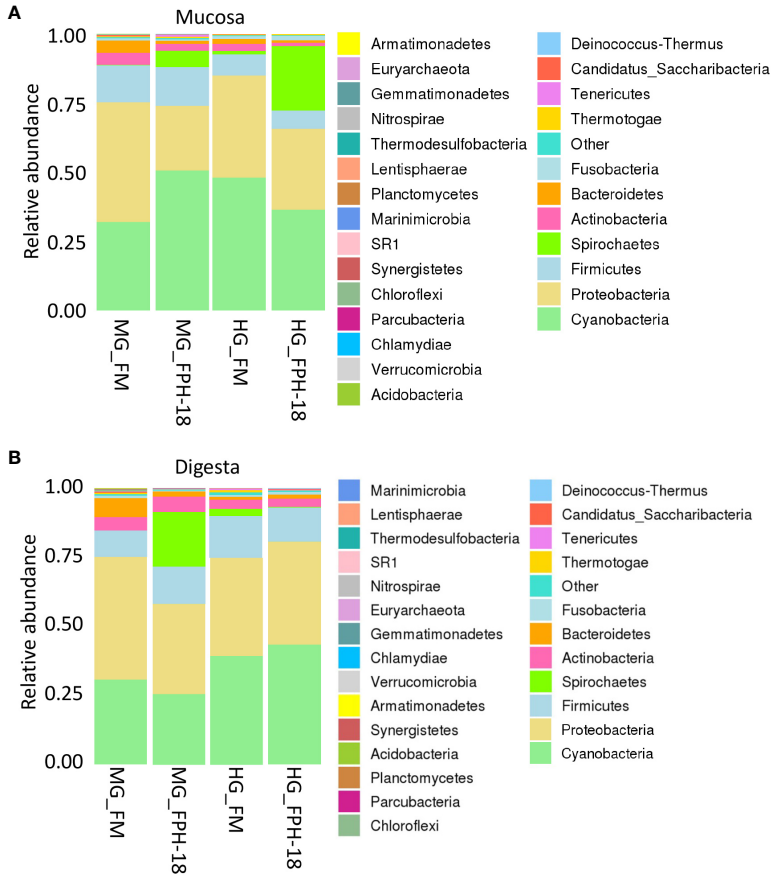

FIGURE 5
The composition of bacterial gut microbiota at phylum level in mucosa **(A)** and digesta **(B)** from midgut (MG) and hindgut (HG) of salmon fed the fishmeal (FM) diets or 18% salmon hydrolysate (FPH-18) diet (n = 6).

intestinal tissue, particularly towards pathogens like viruses. Along with the downregulation of RIG-I-like receptors, NOD-like receptors and toll-like receptors, which are intracellular pattern recognition receptors involved in the recognition of pathogen-associated molecular patterns (PAMPs) by the innate immune system (Barton and Medzhitov, 2003; Kanneganti et al., 2007; Loo and Gale, 2011). It therefore appears likely that the immune system does not sense immediate threats when salmon hydrolysate is partially replaced by FM in the diet. This could suggest that there are components in FM that cause a general upregulation of inflammatory and immune pathways, and that reduction of these would reduce the need to mount a response. Downregulation of genes associated with the immune system has also been seen in the liver of Atlantic salmon that were starved for 28 days. It was also interesting to note that when these fish were challenged with a pathogen, they showed a higher upregulation of immune genes than the non-starved fish (Martin et al., 2010), thus having a potentially better response to a real threat. Downregulation of the immune-related genes is beneficial for saving energy and may still be activated as necessary upon pathogenic threats. It can be speculated that the improved growth response during early phases of the feeding trial these fishes were analyzed from (Sandbakken et al., 2023) can be related to reduced need for energy to mount a continuous low-level inflammatory response.

Another possibility for the downregulation of immune parameters, may lie in a direct effect of protein hydrolysates containing potentially bioactive peptides. Some hydrolysates have been shown to have immunomodulatory functions, which may activate or downregulate the immune system, depending on the hydrolysate source and composition (Kiewiet et al., 2018). Bioactive peptides have been found in salmon protein hydrolysates made by enzymatic hydrolysis of salmon rest raw materials (Opheim et al., 2015). A peptide fraction from salmon hydrolysate showed anti-inflammatory activity *in vitro* by reducing the expression level of pro-inflammatory interleukins in macrophage cells upon lipopolysaccharide (LPS) stimulation (Ahn et al., 2012). Feeding 5% bioactive peptides from farmed Atlantic salmon to European sea bass also downregulated inflammatory responses in the intestine, but the anti-inflammatory effect was not seen at a 10% dietary inclusion level (Parma et al., 2023). Protein hydrolysates from shrimp and tilapia fed to European sea bass also showed a down-regulation of interferon-related genes (Leduc et al., 2018) as seen in this study with salmon hydrolysate. Interferons are signaling molecules produced by immune cells during viral infections, and a down-regulation of these indicate a reduction in viral threats (Ellis, 2001). Furthermore, Leduc et al. (2018) detected positive effects on immune responses and gut health by including 5%

hydrolysate from shrimp, tilapia, or a mix of those to a 5% FM diet, and the European sea bass showed similar growth performance as the positive control fed a 20% FM diet. This indicates that also low inclusion levels of hydrolysates can have beneficial effects in restoring immune function and gut health of fish fed low FM diets, without compromising the growth. In this trial, we only compared the FPH-18 diet with the FM control which had positive effects on growth, digestibility, and gut health (Sandbakken et al., 2023). However, it would be interesting to explore a possible dose-response relationship of salmon hydrolysate to find the optimal inclusion level for maintaining a functional immune system and a good general gut health.

Peptides can also exert immunomodulatory effects by directly stimulating receptors, or by interfering with inflammatory signaling pathways after cellular uptake via a peptide transporter or via endocytosis (Kiewiet et al., 2018). There is also an interesting connection to PepT1 where studies have shown that PepT1 is upregulated in the colon during intestinal inflammation in mammals, and that specific soy peptides transported through PepT1 reduce the inflammatory response *in vitro*. After transport of peptides through PepT1 to the cytosol, some bioactive peptides resist degradation by peptidases and may inhibit the main inflammatory signaling pathways in human intestinal Caco2 cells (Dalmasso et al., 2008; Kovacs-Nolan et al., 2012; Kiewiet et al., 2018).

Some marine peptides have also shown antimicrobial effects (Kang et al., 2019), which may affect the mucosal microbiota. Thus, the immunomodulatory effects of hydrolysates may be due to a direct effect by bioactive peptides, an indirect effect through modulation of the bacterial microbiota or a combination of these.

4.2 Intestinal expression of peptide transporter genes

Based on previous literature from vertebrates (Chen et al., 2005; Gilbert et al., 2008; Bakke et al., 2010), our initial hypothesis was that high dietary peptide content would increase expression of intestinal peptide transporter (PepT) in the anterior part of the intestine, and perhaps reduce the expression in posterior regions since these components are readily absorbed in the anterior part. However, the only significant differences were a slight reduction of PepT2a in the anterior midgut and PepT2b in the hindgut (HG) of FPH-18 fed fish. The difference in the HG could be explained by rapid absorption of the hydrolysate peptides and free amino acids in the proximal part of the intestine, while the FM proteins had to be enzymatically degraded before absorption. The small differences observed may be due to the same protein content in all experimental diets and efficient protein degradation by endogenous enzymes in the digestive tract of Atlantic salmon.

In this trial, the fish were not fed for 48 hours prior to collection of RNA samples. Luminal content can affect PepT expression, but 4 days of fasting had minimal effect on expression of PepT paralogs in intestinal segments of Atlantic salmon (Del Vecchio et al., 2021).

The relative expression of PepT1b was highest in the anterior part of the intestine, followed by a decreasing expression level further down the gastrointestinal tract as previously observed in zebrafish (Verri et al., 2003), Atlantic cod (Rønnestad et al., 2007), European sea bass (Terova et al., 2009) and Atlantic salmon (Gomes et al., 2020). PepT1b had about 4 times (2^{-2}) higher expression levels than PepT1a in PC and AMG, which is in line with what was reported by (Gomes et al., 2020). The relative expression of PepT1b and PepT2b was similar in the anterior midgut (AMG), while PepT2b had the highest mRNA concentration of all paralogs in posterior midgut (PMG) and HG. These results are comparable to previous data on Atlantic salmon (Del Vecchio et al., 2021). Expression of PepT2a was generally negligibly low in all intestinal segments, and 500-1000x lower than PepT2b in PMG and HG, as previously reported (Del Vecchio et al., 2021; Vacca et al., 2022).

In this trial, intestinal expression of PepT paralogs were comparable to previous data in Atlantic salmon, and minimal effects of increased level of dietary peptide were observed. PepT1b showed highest expression levels in the anterior part of the intestine, while PepT2b was most highly expressed in the posterior part of the intestine, thus they both contribute to intestinal peptide absorption in different parts of the gastrointestinal (GI) tract.

4.3 Bacterial microbiota

The present study revealed dietary effect on phyla level of the gut microbiota, an effect well known in fish (Cahill, 1990; Ringø et al., 1995; Egerton et al., 2018; 2020; Kokou et al., 2022; Luan et al., 2023). In addition, the bacterial microbiota in the digesta differed to some extent from the mucosal microbiota (Ringø et al., 2016; Li et al., 2021; Nyholm et al., 2022). The present study investigated the mucosal gut microbiota, but most fish studies have focused only on the digesta microbiota. Since the mucosal microbiota might influence fish health, more focus should be directed towards the mucosal community and furthermore on the importance of the gut microbiota on lipid-, carbohydrate-, protein- and amino acid metabolism of aquatic animals (Ringø et al., 2022).

Different segments of the teleost GI tract must be investigated separately, as the colonization patterns between beneficial bacteria and pathogens may vary along the intestine (Ringø et al., 2003). The difference in colonization of mucosal phyla between MG and HG of Atlantic salmon fed the two diets in the present study was revealed, and the findings are in accordance with the results described in previous studies evaluating the gut microbiota (Ringø et al., 1995; Gajardo et al., 2016). As evaluation of gut microbiota is relatively new, it is important to analyze the different GI tract segments to fully see the relationship between these communities. Furthermore, outcompeting beneficial intestinal microorganisms may lead to dysbiosis and increased gut permeability (Zhang et al., 2020).

The gut microbiota of marine fish of economic interest for aquaculture are being dominated by the phyla Proteobacteria (Egerton et al., 2018) and the results of the present study agrees with the above mentioned studies. Regarding Cyanobacteria, the phyla is seldomly reported as a part of the fish gut microbiota and not at the relative abundance level as revealed in the present study. The reason for this observation is not known, and merits further investigations.

Spirochaetes, Gram negative bacteria with long corkscrew or spiraled morphology are reported to be a part of the intestinal microbiota in several fish species (Egerton et al., 2020; Iwatsuki et al., 2021; Li et al., 2021). A dietary effect was noticed on the relative high abundance of Spirochaetes in mucosa of MG (6%) and HG (23%) of FPH-18 fed Atlantic salmon, while Egerton et al. (2020) revealed significantly lower abundance of intestinal Spirochaetes in Atlantic salmon fed 80% plant protein. The abundance of Spirochaetes in the mucosa of FPH-18 fed salmon were however considerably lower than the 50 and 70% Spirochaetes found in the hindgut mucosa of Atlantic salmon fed a commercial and insect meal diet, respectively (Li et al., 2021). The Spirochaetes detected in this trial were dominated by the genera *Brevinema*, more specifically the species *Brevinema andersonii*, but the prevalence varied between the individual fish. Among the Phyla Spirochaetes, the species *B. andersonii* has been associated with altered expression of pro- and anti-inflammatory genes, and *Spirochaetaceae* with genes related to intestinal barrier function, when found in the hindgut mucosa (Li et al., 2021). High abundance of Spirochaetes including *B. andersonii* has also been detected in the hindgut mucosa of Atlantic salmon fed a prebiotic alginate oligosaccharide derived from brown macroalgae (Gupta et al., 2019). The Spirochaete *B. andersonii* has genes associated with butyrate production, which is favorable for the gut health, since butyrate is one of the main short chain fatty acids (SCFAs) that provide energy for enterocytes and maintain mucosal integrity and immune homeostasis (O'Keefe, 2016). Based on our results, the downregulation of immune responses seen in the present study could be linked to the mucosa associated bacteria, especially Spirochaetes, and their fermentation products. However, as the interactions between immune system and intestinal bacteria are more investigated in mammals than in fish (Maynard et al., 2012; Daniel et al., 2021; Schlechte et al., 2022), so this topic merits further research. It is important to increase the knowledge on how dietary composition influences the immunity and health of farmed aquaculture species.

5 Conclusion

The first paper from this trial (Sandbakken et al., 2023) clearly showed that salmon protein hydrolysate can partially replace fishmeal in diets for Atlantic salmon giving good growth, increased digestibility of protein and ash and good intestinal health as viewed by histology. Intestinal gene expression analysis of the current manuscript showed a downregulation of several inflammatory pathways particularly towards virus and to some extent bacteria when salmon post-smolts were fed 18% salmon hydrolysate compared to a FM control diet. This could reduce energy expenditure by the immune system and free energy available for improved growth. The cause for this downregulation is not known at present but is being studied further. On one hand, it is possible that FM contain molecules that activates the immune system. On the other hand, the salmon hydrolysate with its high load of potentially bioactive peptides may have modulated the immune response through several possible pathways. It is also possible that bacteria selected by salmon hydrolysate could have contributed to reduce the presence of potential pathogens. The gut microbiota in the digesta and mucosa of the MG and HG, were dominated by the phyla Cyanobacteria and Proteobacteria in both diets. However, the phyla Spirochaetes were more prevalent in the mucosa of FPH-18 fed salmon, compared to the FM fed salmon. This dietary difference on mucosal microbiota and the microbial fermentation products may have influenced the inflammatory responses as seen in the gene expression analysis. Further research is needed to fully understand the relationship between fish nutrition, intestinal microbiome, and the immune system. Furthermore, it is well known that dietary manipulation modulates the intestinal microbiota which may improve the resistance towards bacterial infection, this topic must be investigated in future studies when evaluating the effect of salmon protein hydrolysate.

Peptide transporter gene expression was minimally affected by different dietary peptide content, and mostly varied between the intestinal segments. PepT1b contributed most to peptide uptake in the PC, while in AMG PepT1b and PepT2b showed similar relative expression levels. From PMG to HG, PepT2b showed the highest relative expression levels, indicating that PepT2b contributed the most to peptide uptake in the posterior part of the gastrointestinal tract.

Data availability statement

The raw data has been uploaded to NCBI SRA database with BioProject No. PRJNA1072556.

Ethics statement

The animal study was approved by Norwegian Food Safety Authority (FOTS ID:23021). The study was conducted in accordance with the local legislation and institutional requirements.

Author contributions

IS: Writing – original draft, Visualization, Validation, Supervision, Project administration, Investigation, Formal analysis, Data curation, Conceptualization. HS: Writing – original draft, Visualization, Investigation, Formal analysis, Data curation. LJ: Writing – review & editing, Data curation. YZ: Writing – review & editing, Visualization, Formal analysis, Data curation. ER: Writing – original draft. RR: Writing – review & editing, Supervision, Data curation. IY: Writing – review & editing, Formal analysis, Data curation. KF: Writing – review & editing, Data curation. RO: Writing – original draft, Supervision, Conceptualization.

Funding

The author(s) declare financial support was received for the research, authorship, and/or publication of this article. Nutrimar AS, the Norwegian research council [project no: 298839] and project Feed2Food [Grant 319693] funded this research. The

funding sources had no role in study design or data interpretation from this experiment.

Acknowledgments

The authors would like to thank Jihong Liu Clarke (NIBIO) for providing funding for the RNA sequencing and microbiota analysis (Feed2Food project) and for the supervision of HS. We also thank Ralph Kissen (Norwegian University of Science and Technology) for supervision and assistance with RNA testing and RT-qPCR data management.

Conflict of interest

Authors IS and KF were employed by the company Nutrimar AS.

The remaining authors declare that the research was conducted in the absence of any commercial or financial relationships that could be construed as a potential conflict of interest.

The authors declare that this study received funding from Nutrimar AS. The funder was not involved in the study design, collection, analysis, interpretation of data, the writing of this article, or the decision to submit it for publication.

The author(s) declared that they were an editorial board member of Frontiers, at the time of submission. This had no impact on the peer review process and the final decision.

Publisher's note

Supplementary material

The Supplementary Material for this article can be found online at: https://www.frontiersin.org/articles/10.3389/fmars.2024.1376516/full#supplementary-material

References

Ahn, C. B., Jae, Y. J., and Young, S. C. (2012). Antioxidant and anti-inflammatory peptide fraction from salmon byproduct protein hydrolysates by peptic hydrolysis. *Food Res. Int.* 49, 92–985. doi: 10.1016/j.foodres.2012.08.002

Almås, K. A., Josefsen, K. D., Gjøsund, S. H., Skjermo, J., Forbord, S., Jafarzadeh, S., et al. (2020) *Bærekraftig Fôr Til Norsk Laks*. Available online at: https://hdl.handle.net/11250/2758913.

Bakke, S., Jordal, A. E. O., Gómez-Requeni, P., Verri, T., Kousoulaki, K., Aksnes, A., et al. (2010). Dietary protein hydrolysates and free amino acids affect the spatial expression of peptide transporter pepT1 in the digestive tract of atlantic cod (*Gadus morhua*). *Comp. Biochem. Physiol. - B Biochem. Mol. Biol.* 156, 48–555. doi: 10.1016/j.cbpb.2010.02.002

Bartlett, A., and Kleiner, M. (2022). Dietary protein and the intestinal microbiota: an understudied relationship. *IScience*. 25, 105313. doi: 10.1016/j.isci.2022.105313

Barton, G. M., and Medzhitov, R. (2003). Toll-like receptor signaling pathways. *Science* 300, 1524–1525. doi: 10.1126/science.1085536

Cahill, M. M. (1990). Bacterial flora of fishes: A review. *Microbial. Ecol.* 19, 21–41. doi: 10.1007/BF02015051/METRICS

Chen, H., Pan, Y., Wong, E. A., and Webb, K. E. (2005). Nutrient-gene interactions dietary protein level and stage of development affect expression of an intestinal peptide transporter (CPepT1) in chickens 1. *J. Nutr.* 135 (2), 193–198. doi: 10.1016/j.clnu.2016.02.005

Cole, J. R., Wang, Q., Fish, J. A., Chai, B., McGarrell, D. M., Sun, Y., et al. (2014). Ribosomal database project: data and tools for high throughput RRNA analysis. *Nucleic Acids Res.* 42, D633–D642. doi: 10.1093/nar/gkt1244

Commission Regulation (EU) No 142/2011 (2011). *Implementing Regulation (EC) No. 1069/2009 of the European Parliament and of the Council Laying down Health Rules as Regards Animal by-Products and Derived Products Not Intended for Human Consumption and Implementing Council Directive 97/78/EC as Regards Certain Samples and Items Exempt from Veterinary Checks at the Border under That Directive*. Available online at: https://www.fao.org/faolex/results/details/en/c/LEX-FAOC109216/#:~:text=This%20Regulation%20lays%20down%20implementing,by%2Dproducts%20and%20derived%20products.

Dalmasso, G., Charrier-Hisamuddin, L., Thi, H., Nguyen, T., Yan, Y., Sitaraman, S., et al. (2008). PepT1-mediated tripeptide KPV uptake reduces intestinal inflammation. *Gastroenterology* 134, 166–178. doi: 10.1053/j.gastro.2007.10.026

Daniel, N., Lécuyer, E., and Chassaing, B. (2021). Host/microbiota interactions in health and diseases-time for mucosal microbiology! *Mucosal Immunol.* 14, 1006–1016. doi: 10.1038/s41385-021-00383-w

Dawood, M. A. O. (2020). Nutritional immunity of fish intestines: important insights for sustainable aquaculture. *Rev. Aquac.* 13, 642–663. doi: 10.1111/raq.12492

De Hoon, M. J. L., Imoto, S., Nolan, J., and Miyano, S. (2004). Open source clustering software. *Bioinf. Appl. NOTE* 20, 1453–1545. doi: 10.1093/bioinformatics/bth078

Del Vecchio, G., Lai, F., Gomes, A. S., Verri, T., Kalananthan, T., Barca, A., et al. (2021). Effects of short-term fasting on MRNA expression of ghrelin and the peptide transporters pepT1 and 2 in Atlantic salmon (*Salmo salar*). *Front. Physiol.* 12. doi: 10.3389/fphys.2021.666670

Dobin, A., Davis, C. A., Schlesinger, F., Drenkow, J., Zaleski, C., Jha, S., et al. (2013). STAR: ultrafast universal RNA-seq aligner. *Bioinformatics* 29, 15–215. doi: 10.1093/bioinformatics/bts635

Egerton, S., Culloty, S., Whooley, J., Stanton, C., and Ross, R.P. (2018). The gut microbiota of marine fish. *Front. Microbiol.* 9. doi: 10.3389/fmicb.2018.00873

Egerton, S., Wan, A., Murphy, K., Collins, F., Ahern, G., Sugrue, I., et al. (2020). Replacing fishmeal with plant protein in Atlantic salmon (*Salmo salar*) diets by supplementation with fish protein hydrolysate. *Sci. Rep.* 10, 1–16. doi: 10.1038/s41598-020-60325-7

Eisen, M. B., Spellman, P. T., Brown, P. O., and Botstein, D. (1998). Cluster analysis and display of genome-wide expression patterns. *Proc. Natl. Acad. Sci. United States America* 95, 14863–14685. doi: 10.1073/pnas.95.25.14863

Ellis, A. E. (2001). *Innate Host Defense Mechanisms of Fish against Viruses and Bacteria*. Available online at: www.elsevier.com/locate/devcompimm. doi: 10.1016/S0145-305X(01)00038-6

Evans, D. H., and Claiborne, J. B. (2006). *The physiology of fishes. 3rd ed* (Boca Raton: CRC Press). doi: 10.1201/9781420058093

Gajardo, K., Rodiles, A., Kortner, T. M., Krogdahl, Å., Bakke, A. M., Merrifield, D. L., et al. (2016). A high-resolution map of the gut microbiota in Atlantic salmon (*Salmo salar*): A basis for comparative gut microbial research. *Sci. Rep.* 6, 30893. doi: 10.1038/srep30893

Gao, R., Yu, Q., Shen, Y., Chu, Q., Chen, G., Fen, S., et al. (2021). Production, bioactive properties, and potential applications of fish protein hydrolysates: developments and challenges. *Trends Food Sci. Technol.* 110, 687–699. doi: 10.1016/j.tifs.2021.02.031

Gilbert, E. R., Wong, E. A., and Webb, K. E. (2008). Peptide absorption and utilization: implications for animal nutrition and health. *J. Anim. Sci.* 86, 2135–2155. doi: 10.2527/jas.2007-0826

Glencross, B. D. (2020). A feed is still only as good as its ingredients: an update on the nutritional research strategies for the optimal evaluation of ingredients for aquaculture feeds. *Aquacult. Nutr.* 26, 1871–1883. doi: 10.1111/anu.13138

Gomes, A. S., Vacca, F., Cinquetti, R., Murashita, K., Barca, A., Bossi, E., et al. (2020). Identification and characterization of the Atlantic salmon peptide transporter 1a. *Am. J. Physiol. - Cell Physiol.* 318, C191–C204. doi: 10.1152/ajpcell.00360.2019

Gupta, S., Lokesh, J., Abdelhafiz, Y., Siriyappagouder, P., Pierre, R., Sørensen, M., et al. (2019). Macroalga-derived alginate oligosaccharide alters intestinal bacteria of Atlantic salmon. *Front. Microbiol.* 10. doi: 10.3389/fmicb.2019.02037

Irachi, S., Hall, D. J., Fleming, M. S., Maugars, G., Björnsson, B. T., Dufour, S., et al. (2020). Photoperiodic regulation of pituitary thyroid-stimulating hormone and brain deiodinase in Atlantic salmon. *Mol. Cell. Endocrinol.* 519, 111056. doi: 10.1016/j.mce.2020.111056

Iwatsuki, T., Kanazawa, T., Ogasawara, T., Hosotani, K., Tsuchiya, K., Watanabe, S., et al. (2021). 16S RRNA gene amplicon sequencing of gut microbiota in three species of deep-sea fish in suruga bay, Japan. *Microbiol. Resource Announce.* 10, 10:10.1128/mra.01260-20. doi: 10.1128/mra.01260-20

Kang, H. K., Lee, H. H., Seo, C. H., and Park, Y. (2019). Antimicrobial and immunomodulatory properties and applications of marine-derived proteins and peptides. *Mar. Drugs*. 17, 350. doi: 10.3390/md17060350

Kanneganti, T. D., Lamkanfi, M., and Núñez, G. (2007). Intracellular NOD-like receptors in host defense and disease. *Immunity*. 27, 549–559. doi: 10.1016/j.immuni.2007.10.002

Khosravi, S., Bui, H. T. D., Rahimnejad, S., Herault, M., Fournier, V., Kim, S. S., et al. (2015). Dietary supplementation of marine protein hydrolysates in fish-meal based diets for red sea bream (*Pagrus major*) and olive flounder (*Paralichthys olivaceus*). *Aquaculture* 435, 371–376. doi: 10.1016/j.aquaculture.2014.10.019

Kiela, P. R., and Ghishan, F. K. (2016). Physiology of intestinal absorption and secretion. *Best Pract. Res. Clin. Gastroenterol.* 30, 145–595. doi: 10.1016/J.BPG.2016.02.007

Kiewiet, M. B. G., Faas, M. M., and de Vos, P. (2018). Immunomodulatory protein hydrolysates and their application. *Nutrients* 10, 9045. doi: 10.3390/nu10070904

Kokou, F., Gupta, S., and Kumar, V. (2022). Editorial: understanding the interplay between diet, feed ingredients and gut microbiota for sustainable aquaculture. *Front. Mar. Sci.* 9. doi: 10.3389/fmars.2022.853548

Kousoulaki, K., Rønnestad, I., Olsen, H. J., Rathore, R., Campbell, P., Nordrum, S., et al. (2013). Krill hydrolysate free amino acids responsible for feed intake stimulation in Atlantic salmon (*Salmo salar*). *Aquacult. Nutr.* 19, 47–61. doi: 10.1111/anu.2013.19.issue-s1

Kovacs-Nolan, J., Zhang, H., Ibuki, M., Nakamori, T., Yoshiura, K., Turner, P. V., et al. (2012). The pepT1-transportable soy tripeptide VPY reduces intestinal inflammation. *Biochimica et Biophysica Acta – General Subjects* 1820, 1753–1763. doi: 10.1016/j.bbagen.2012.07.007

Kristinsson, H. G., and Rasco, B. A. (2000). Fish protein hydrolysates: production, biochemical, and functional properties. *Crit. Rev. Food Sci. Nutr.* 40, 43–81. doi: 10.1080/10408690091189266

Krzywinski, M., Schein, J., Birol, I., Connors, J., Gascoyne, R., Horsman, D., et al. (2009). Circos: an information aesthetic for comparative genomics. *Genome Res.* 19, 1639–1455. doi: 10.1101/gr.092759.109

Leduc, A., Zatylny-Gaudin, C., Robert, M., Corre, E., Corguille, G. L., Castel, H., et al. (2018). Dietary aquaculture by-product hydrolysates: impact on the transcriptomic response of the intestinal mucosa of European seabass (*Dicentrarchus labrax*) fed low fish meal diets. *BMC Genomics* 19, 396. doi: 10.1186/s12864-018-4780-0

Li, B., and Dewey, C. N. (2011). RSEM: accurate transcript quantification from RNA-seq data with or without a reference genome. *BMC Bioinf.* 12, 1–16. doi: 10.1186/1471-2105-12-323/TABLES/6

Li, Y., Bruni, L., Jaramillo-Torres, A., Gajardo, K., Kortner, T. M., and Krogdahl, Å. (2021). Differential response of digesta- and mucosa-associated intestinal microbiota to dietary insect meal during the seawater phase of Atlantic salmon. *Anim. Microb.* 3, 8. doi: 10.1186/s42523-020-00071-3

Loo, Y.-M., and Gale, M. (2011). Immune Signaling by RIG-I-like Receptors. *Immunity* 34, 680–692. doi: 10.1016/j.immuni.2011.05.003

Luan, Y., Li, M., Zhou, W., Yao, Y., Yang, Y., Zhang, Z., et al. (2023). The fish microbiota: research progress and potential applications. *Engineering*. 29, 137–146. doi: 10.1016/j.eng.2022.12.011

Martin, S. A.M., Dehler, C. E., and Król, E. (2016). Transcriptomic responses in the fish intestine. *Dev. Comp. Immunol.* 64, 103–117. doi: 10.1016/j.dci.2016.03.014

Martin, S. A. M., Douglas, A., Houlihan, D. F., and Secombes., C. J. (2010) Starvation alters the liver transcriptome of the innate immune response in Atlantic salmon (*Salmo salar*). Available online at: http://www.biomedcentral.com/1471-2164/11/418. doi: 10.1186/1471-2164-11-418

Maynard, C. L., Elson, C. O., Hatton, R. D., and Weaver, C. T. (2012). Reciprocal interactions of the intestinal microbiota and immune system. *Nature*. 489, 231–241. doi: 10.1038/nature11551

Myhre, M., Richardsen, R., Nystøyl, R., and Strandheim, G. (2022) *Analyse marint restråstoff 2021*. Available online at: https://hdl.handle.net/11250/3013196.

Nyholm, L., Odriozola, I., Bideguren, G. M., Aizpurua, O., and Alberdi, A. (2022). Gut microbiota differences between paired intestinal wall and digesta samples in three small species of fish. *PeerJ* 10, e12992. doi: 10.7717/peerj.12992

O'Keefe, S. J.D. (2016). Diet, microorganisms and their metabolites, and colon cancer. *Nat. Reviews Gastroenterol. Hepatol.* 13, 697–706. doi: 10.1038/nrgastro.2016.165

Olsvik, P. A., Lie, K. K., Jordal, A. E. O., Nilsen, T. O., and Hordvik, I. (2005). Evaluation of potential reference genes in real-time RT-PCR studies of Atlantic salmon. *BMC Mol. Biol.* 6, 21. doi: 10.1186/1471-2199-6-21

Opheim, M., Šližytė, R., Sterten, H., Provan, F., Larssen, E., and Kjos, N. P. (2015). Hydrolysis of Atlantic salmon (*Salmo salar*) rest raw materials - effect of raw material and processing on composition, nutritional value, and potential bioactive peptides in the hydrolysates. *Process Biochem.* 50, 1247–1575. doi: 10.1016/j.procbio.2015.04.017

Ostaszewska, T., Kamaszewski, M., Grochowski, P., Dabrowski, K., Verri, T., Aksakal, E., et al. (2010). The effect of peptide absorption on pepT1 gene expression and digestive system hormones in rainbow trout (*Oncorhynchus mykiss*). *Comp. Biochem. Physiol. - A Mol. Integr. Physiol.* 155, 107–145. doi: 10.1016/j.cbpa.2009.10.017

Parma, L., Busti, S., Ciulli, S., Volpe, E., Errani, F., Oterhals, Å., et al. (2023). Growth, plasma biochemistry and immune-related gene expression of European sea bass (*Dicentrarchus labrax*) fed bioactive peptides from farmed salmon by-products. *Aquaculture* 563, 738982. doi: 10.1016/j.aquaculture.2022.738982

R Core Team (2023). *R: A language and environment for statistical computing* (Vienna, Austria: R Foundation for Statistical Computing). Available at: https://www.R-project.org/.

Regulation (EC) No 999/2001 (2001). *Laying down Rules for the Prevention, Control and Eradication of Certain Transmissible Spongiform Encephalopathies [2001] OJ L147*. Available online at: https://eur-lex.europa.eu/legal-content/EN/TXT/?uri=celex%3A32001R0999.

Ringø, E., Harikrishnan, R., Soltani, M., and Ghosh, K. (2022). The effect of gut microbiota and probiotics on metabolism in fish and shrimp. *Animals* 12, 30165. doi: 10.3390/ani12213016

Ringø, E., Olsen, R. E., Mayhew, T. M., and Myklebust, R. (2003). Electron microscopy of the intestinal microflora of fish. *Aquaculture*. 227, 395–415. doi: 10.1016/ j.aquaculture.2003.05.00

Ringø, E., Strøm, E., and Tabachek, J.-A. (1995). Intestinal microflora of salmonids: A review. *Aquacult. Res.* 26, 773–895. doi: 10.1111/j.1365-2109.1995.tb00870.x

Ringø, E., Zhou, Z., Vecino, J. L. G., Wadsworth, S., Romero, J., Krogdahl, Å., et al. (2016). Effect of dietary components on the gut microbiota of aquatic animals. A never-ending story? *Aquacult. Nutr.* 22, 219–282. doi: 10.1111/ANU.12346

Rønnestad, I., Gavaia, P. J., Viegas, C. S. B., Verri, T., Romano, A., Nilsen, T. O., et al. (2007). Oligopeptide transporter pepT1 in Atlantic cod (*Gadus morhua*L.): cloning, tissue expression and comparative aspects. *J. Exp. Biol.* 210, 3883–3965. doi: 10.1242/JEB.007898

Rustad, T., Storrø, I., and Slizyte, R. (2011). Possibilities for the utilisation of marine by-products. *Int. J. Food Sci. Technol.* 46, 2001–2145. doi: 10.1111/j.1365-2621.2011.02736.x

Saldanha, A. J. (2004). Java treeview—Extensible visualization of microarray data. *Bioinformatics* 20, 3246–3248. doi: 10.1093/bioinformatics/bth349

Sandbakken, I. S., Five, K. K., Bardal, T., Knapp, J. L., and Olsen, R. E. (2023). Salmon hydrolysate as a protein source for Atlantic salmon; prion content and effects on growth, digestibility and gut health. *Aquaculture*. 576, 739863. doi: 10.1016/j.aquaculture.2023.739863

Schlechte, J., Skalosky, I., Geuking, M. B., and Mcdonald, B. (2022). Long-distance relationships-regulation of systemic host defense against infections by the gut microbiota. *Mucosal Immunol.* 15, 809–818. doi: 10.1038/s41385-022-00539-2

Siddik, M. A. B., Howieson, J., Fotedar, R., and Partridge, G. J. (2021). Enzymatic fish protein hydrolysates in finfish aquaculture: A review. *Rev. Aquacult.* 13, 406–305. doi: 10.1111/raq.12481

Siddik, M. A.B., Howieson, J., Partridge, G. J., Fotedar, R., and Gholipourkanani, H. (2018). Dietary tuna hydrolysate modulates growth performance, immune response, intestinal morphology and resistance to *Streprococcus iniae* in juvenile barramundi, *Lates calcarifer* OPEN. *Nat. - Sci. Rep.* 8, 15942. doi: 10.1038/s41598-018-34182-4

Tacchi, L., Bickerdike, R., Douglas, A., Secombes, C. J., and Martin, S. A. M. (2011). Transcriptomic responses to functional feeds in Atlantic salmon (*Salmo salar*). *Fish Shellf. Immunol.* 31, 704–155. doi: 10.1016/j.fsi.2011.02.023

Terova, G., Corà, S., Verri, T., Rimoldi, S., Bernardini, G., and Saroglia, M. (2009). Impact of feed availability on pepT1 MRNA expression levels in sea bass (*Dicentrarchus labrax*). *Aquaculture* 294, 288–299. doi: 10.1016/j.aquaculture.2009.06.014

Vacca, F., Gomes, A. S., Murashita, K., Cinquetti, R., Roseti, C., Barca, A., et al. (2022). Functional characterization of Atlantic salmon (*Salmo salar* L.) pepT2 transporters. *J. Physiol.* 600, 2377–24005. doi: 10.1113/JP282781

Verri, T., Kottra, G., Romano, A., Tiso, N., Peric, M., Maffia, M., et al. (2003). Molecular and functional characterisation of the zebrafish (*Danio rerio*) PEPT1-type peptide transporter. *FEBS Lett.* 549, 115–122. doi: 10.1016/S0014-5793(03)00759-2

Waagbø, R. (1994). The impact of nutritional factors on the immune system in Atlantic salmon, *Salmo salar* L.: A review. *Aquacult. Res.* 25, 175–197. doi: 10.1111/j.1365-2109.1994.tb00573.x

Wang, J., Yan, X., Lu, R., Meng, X., and Nie, G. (2017). Peptide transporter 1 (PepT1) in fish: A review. *Aquacult. Fish.* 2, 193–206. doi: 10.1016/j.aaf.2017.06.007

Ye, J., Coulouris, G., Zaretskaya, I., Cutcutache, I., Rozen, S., and Madden, T. L. (2012). *Primer-BLAST: A tool to design target-specific primers for polymerase chain reaction*. Available online at: http://www.biomedcentral.com/1471-2105/13/134. doi: 10.1186/1471-2105-13-134

Zamora-Sillero, J., Gharsallaoui, A., and Prentice, C. (2018). Peptides from fish by-product protein hydrolysates and its functional properties: an overview. *Mar. Biotechnol.* 20, 118–130. doi: 10.1007/s10126-018-9799-3

Zhang, H., Ran, C., Teame, T., Ding, Q., Hoseinifar, S. H., Xie, M., et al. (2020). Research progress on gut health of farmers teleost fish: A viewpoint concerning the intestinal mucosal barrier and the impact of its damage. *Rev. Fish Biol. Fish.* 30, 569–586. doi: 10.1007/s11160-020-09614-y

Zheng, K., Xu, T., Qian, C., Liang, M., and Wang, X. (2014). Effect of low molecular weight fish protein hydrolysate on growth performance and IGF-I expression in Japanese flounder (*Paralichthys olivaceus*) fed high plant protein diets. *Aquacult. Nutr.* 20, 372–380. doi: 10.1111/anu.2014.20.issue-4

frontiers | Frontiers in Marine Science

TYPE Brief Research Report
PUBLISHED 04 April 2024
DOI 10.3389/fmars.2024.1378970

OPEN ACCESS

EDITED BY
Xinxin Wang,
Fisheries and Aquaculture Research (Nofima), Norway

REVIEWED BY
Bjørn Eidem,
Institute for Rural and Regional Research (RURALIS), Norway
Malcolm Beveridge,
Retired, Perth, United Kingdom

*CORRESPONDENCE
Pernille Kristiane Skavang
pernille.skavang@sintef.no

RECEIVED 30 January 2024
ACCEPTED 20 March 2024
PUBLISHED 04 April 2024

CITATION
Skavang PK and Strand AV (2024) Conceptualization of the Norwegian feed system of farmed Atlantic salmon. *Front. Mar. Sci.* 11:1378970. doi: 10.3389/fmars.2024.1378970

Conceptualization of the Norwegian feed system of farmed Atlantic salmon

Pernille Kristiane Skavang[1]* and Andrea Viken Strand[2]

[1]Department of Fisheries and New Biomarine Industry, SINTEF Ocean, Trondheim, Norway, [2]Department of Climate and Environment, SINTEF Ocean, Tromsø, Norway

The total production of Norwegian Atlantic salmon is expected to increase considerably in the years to come. A majority of greenhouse gas emissions from aquaculture is accounted for by feed. To investigate and assess the sustainability and robustness of the feed system, a holistic perspective on the system is needed. We aim to conceptualize the current value chains of feed in Norway using the Food Systems Approach, existing literature, and stakeholder inputs. The Sustainable Development Goals include no specific mention of feed. Still, many Norwegian feed and animal producers link their sustainability work to these goals. This paper summarizes the sustainability perspectives of feed and animal producers in the aquaculture sector, as well as relevant background, regulations, and environmental and socio-economic drivers.

KEYWORDS

food systems approach, sustainability, feed value chain, aquaculture, customer characteristics

1 Introduction

Atlantic salmon (*Salmo Salar*) is one of the most important export commodities in Norway, and future growth in the industry is expected (PwC, 2023). A majority of the carbon footprint of the salmon from farm to harvest is accounted for by the feed (Ziegler et al., 2021). Feed for salmon produced in Norway has global and complex supply chains, and in 2020, 92% of the feed ingredients were imported (Aas et al., 2022). These supply chains can be vulnerable to political shifts, epidemics as well as climate change, which has been observed more often in the last years (Free and Hecimovic, 2021). To reduce the dependency of imports and vulnerable supply chains, Norway has developed a goal to increase the self-sufficiency (Regjeringen, 2021), and domestic production of sustainable feed resources for fish feed can contribute to this.

To investigate and assess the sustainability and robustness of the feed system, a holistic perspective on the system is needed. The aim of this work is to conceptualize the current value chain for feed for Norwegian produced salmon. This is performed by creating a conceptual model of the Norwegian feed system following the Food Systems Approach (FSA) (Van Berkum et al., 2018). FSA is a conceptual, interdisciplinary framework based on

systems thinking. This method enables us to have a better understanding of the feed system with focus on salmon aquaculture and identify current challenges and opportunities in a shift towards new and Norwegian produced feed ingredients.

2 Methodology

Based on the FSA framework (Van Berkum et al., 2018), the main elements and drivers of the Norwegian feed system for the grow-out phase for Norwegian salmon aquaculture are identified through existing literature, including journal articles, research reports, company reports and web pages. The components of the Norwegian feed system activities include the supply chain, enabling environment (e.g., regulations, policies etc.), customer characteristics, service industries, environmental and socio-economic drivers and how these interact with each other. A conceptual model was created based on the FSA, shown in Figure 1.

An FSA has several benefits as a framework to assess the food system (Van Berkum et al., 2018). The approach provides a checklist of topics to address when assessing the system that enables the user to identify relationships, root causes and feedback loops in the system. Also, it can help understand and map the environmental and socio-economic impacts as well as determine limiting factors for achieving food security. The framework shows where main interactions and feedback of subsystems are occurring. This can lead to insights on how to use natural resources more efficiently, what potential trade-offs exist, and the implications of the food system on food security, society and environment (United Nations Environment Programme, I. R. P, 2016). Using the FSA also enables comparison between different food systems, such as different types of animal production, or for salmon production in other countries such as Chile, Scotland and Canada, compared to Norway.

Within customer characteristics, the focus is on two links of the supply chain: feed producers and salmon farming companies. To assess this, literature and company reports are reviewed to identify what feed and salmon producers highlight in terms of sustainability. Within enabling environment, the Norwegian regulations regarding feed, and policies are mapped using reviews of document of statutory requirements for feed. Environmental and socio-economic drivers are summarized as examples of relevant impact factors for the relevant value chain. End consumers habits and perception towards consuming seafood are also mapped, based on national surveys and available literature.

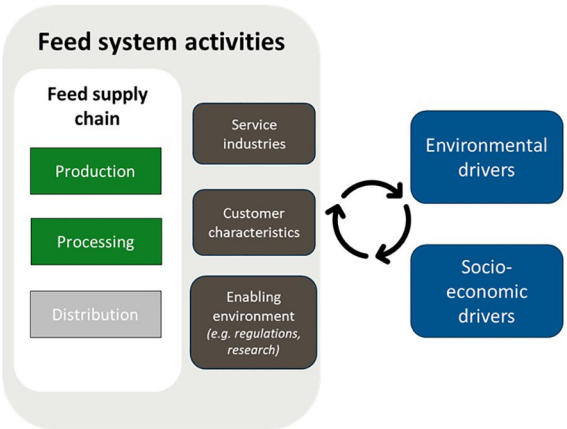

FIGURE 1
A conceptual model of the feed system activities and affecting drivers, based on the food systems approach (Van Berkum et al., 2018).

As part of mapping the supply chain, the material flows of feed for grow-out production of salmon until edible product are quantified for 2020. The feed composition is based on Aas et al. (2022). Total amounts of feed used and production volume are taken from the Directorate of Fisheries (Fiskeridirektoratet 2023c, 2023a). It is estimated that the edible part of salmon is 53% based on round weight (Carvajal et al., 2021). Round weight is approximately 93.7% of the live weight of salmon (Fiskeridirektoratet, 2023b). The round weight is the weight of salmon after it is starved before slaughter and after the blood is removed (Norsk standard, 2012). 47% of the round weight is regarded as rest raw materials (RRM). RRM refer to the parts that do not go to human consumption, such as head, blood, bones, viscera etc (Myhre et al., 2023). However, this is specific for the Norwegian market, as consumers in other countries might have a higher or lower degree of utilization, e.g. in Norway it is not common to eat fish heads, but this is common in other markets. The quantification is visualized with Sankey diagrams using the Plotly package in Python (Plotly Graphing Libraries, n.d).

3 Feed supply chain of salmon aquaculture production in Norway

This section addresses the supply chain of feed in Norway and describes the composition of feed as well as origins of the feed ingredients. We further investigate the production of salmon and shares of edible parts and RRM. The feed use and salmon production has been quantified and is presented in Figure 2.

Total feed used for grow-out fish production was 1.87 million tons in 2020 (Fiskeridirektoratet, 2023a). The feed composition in 2020 consisted of about 22% marine ingredients, 73% plant based and includes 0.4% of insects, microalgae, single cell protein and fermented products (Aas et al., 2022). In total, 92% of the ingredients were imported, including all volumes of plant-based ingredients mainly originating from Europe and Brazil. Only 8% was domestically produced and came from Norwegian fisheries or aquaculture. Another study by Johansen et al. (2022a), report that 38% of the marine oils came from the Northeast Atlantic, 27% from the US, 13% from South America and 0.7% from African sources. 48% of the fish meal sources were also mostly from the Northeast Atlantic. About 30% of fish oils and 33% of fish meal were sourced from off-cuts, while the remaining volume originated from whole fish. Of the plant-based ingredients, soy protein is the dominating ingredient. Johansen et al. (2022a), states that about 81% of the soy protein is sourced from South America, and 19% from Europe and Russia. Rapeseed oil is the most important vegetable oil, with imports from European countries accounting for about 59%,

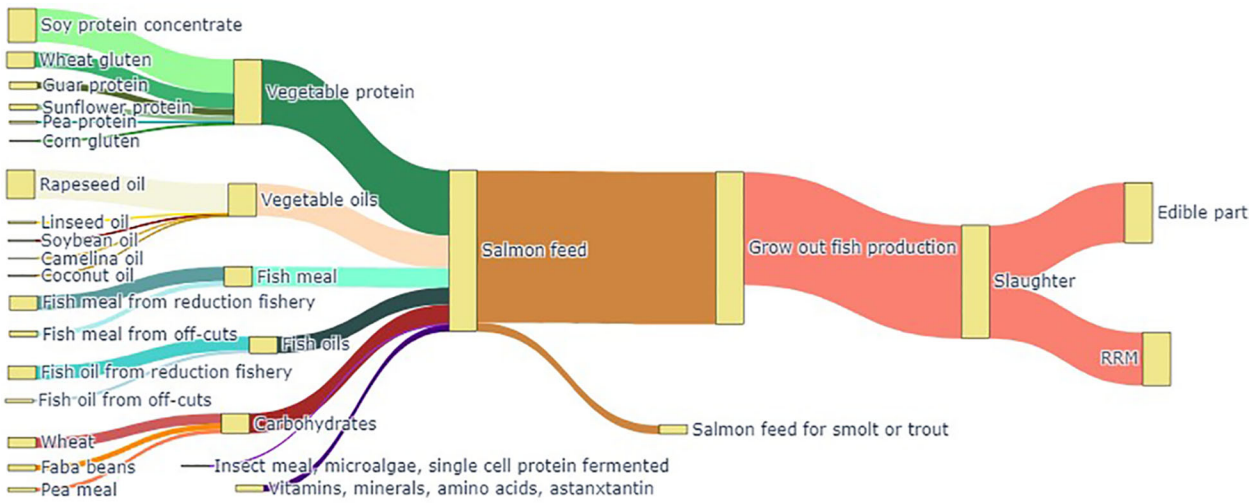

FIGURE 2
Material flows of salmon in 2020, from feed to edible product and rest raw materials (RRM). The figure is based on data extracted from Aas et al. (2022); Fiskeridirektoratet (2023c) and Carvajal et al. (2021). Total feed used for grow-out fish production in 2020 was 1.87 million tons, and 1.39 million tons round weight salmon. This resulted, theoretically, in around 736 000 tons edible product and around 653 000 tons RRM.

followed by about 25% from Russia or Belarus. The composition of salmon feed has changed significantly in the last 30 years from having mostly marine based ingredients to consisting of mainly plant based ingredients (Aas et al., 2019). This is mostly due to decline in the availability of fish oil and meal (Tacon and Metian, 2008; Shepherd and Jackson, 2013; Naylor et al., 2021). The shift to a diet dominated by plant-based oils has also led to a drop in omega-3 content in Norwegian farmed Atlantic salmon (Sissener, 2018).

The marine protein is sourced from wild fish harvested at sea, through extraction of oil at the reduction plant. The remaining mass is dried, milled and processed into fish meal. Off-cuts and by-catch from Norwegian fisheries and aquaculture are also processed into fish meal and oil, commonly used for fish and animal feed. In salmon feed production, the marine and plant-based ingredients are mixed into a company-specific nutritional formula, which varies dependent on the supply of raw materials and the demands of the salmon farmers (Thakur et al., 2020). The feed is then extruded into pellets of a size specific to the development stage of the salmon. According to Thakur et al., 97% of the feed is nationally processed, from ingredients to pellets, and only 3% is imported. Depending on the scale of the customer, the available technology and automation level, the feed is delivered in bulk packaging or pumped in autonomous systems.

In 2022, 1.56 million tons (round weight) of salmon were produced (Fiskeridirektoratet, 2023c). Most of the salmon produced in Norway is being exported as whole fish (head on, gutted). In 2022, about 1.25 million tons of salmon (product weight) were exported, and of this about 995 000 tons were exported as whole, fresh cooled fish (Norwegian Seafood Council, 2023).

In 2022, the amount of available RRM from salmonid aquaculture, including Atlantic salmon and Rainbow trout (*Oncorhynchus mykiss)*, amounted to 546 000 tons (Myhre et al., 2023). This includes heads, blood, viscera, skin, slough, bones etc. A lot of the RRM is not available, since the majority of the fish is exported whole. Except for the blood, which accounts for 2% of the total weight of the salmon, all the available RRM was used for extraction of salmon oil to feed, fish protein hydrolysate, fish meal or fish protein concentrate, according to Myhre et al. (2023). About 67% or 218 000 tons of all utilized and processed RRM from fisheries and aquaculture was used for feed applications, with fish feed accounting for the majority.

4 Enabling environment

Norwegian policies and strategies are set in place for the coming years to implement measures to work towards, and achieve, sustainability goals. Even though the United Nations Sustainable Development Goals (SDGs) do not explicitly include feed, feed is an essential part of sustainable development and implemented measures can contribute to achieving several of the SDGs. As stated by Troell et al. (2023), this can create an iterative feedback process where the contributions made to the SDGs in turn influence decision-making and the conditions of the sector. The focus on feed and sustainability has eminently increased recently. In 2022, the Norwegian government announced two new missions to invest in, one of them being sustainable feed (Forskningsrådet, 2023).

There are several Norwegian regulations concerning requirements for feed, from feed materials to production and import. These regulations greatly impact the feed value chain, as the regulations facilitate or disallow the use of different raw materials, countries of origin or processing methods for use in feed. In particular, animal material for use in feed ingredients is covered by specific regulations such as the legislations regarding the use of by-products not intended for human consumption and export of animal by-products to countries outside the European Economic Area (Landbruks- og matdepartementet and Nærings- og

fiskeridepartementet, 2016; Helse- og omsorgsdepartementet et al., 2020). For instance, by-products from animals are covered by regulations which divide the material into categories based on the risk they pose, and with stricter requirements for food-producing animals. The use of animal material for feed is also limited by the cannibalism ban, which prohibits feeding a species using processed animal protein from the same species. Using fish meal from wild fish to feed farmed fish of the same species is excepted from this ban (Mattilsynet, 2013), and so are hydrolyzed proteins, which may be used as a feed ingredient for fish feed within the same species (Mattilsynet, 2023).

5 Customer characteristics

Sustainability has become increasingly important in businesses along the entire value chain. The Norwegian regulations cover raw materials allowed for different types of feed and import of feed materials. However, no regulations are set regarding sustainability in the choices made for raw materials in feed mixes. Nevertheless, consumers are becoming more aware of the impact of the everyday choices they make, which encourages companies to operate sustainable in order to be competitive. Still, companies differ in their approach when it comes to dissemination of sustainability work and focus externally. To assess this, websites and reports that are available online are reviewed, to identify what feed and salmon producers highlight in terms of sustainability, and to map the information that is available to the general consumer. The information gathered is therefore not based on reportable information, but rather the information the companies themselves have chosen to share in simplified ways and in open reports to reach a different target group - the general consumer who may be interested in the company's sustainability work. However, in the coming years, more companies will be subject to the European Union Corporate Sustainability Reporting Directive, requiring companies to disclose specific information on the impact of their activities (European Commission, n.d). How this will affect the findings below should be explored further in the years to come.

5.1 Feed producers

Feed is the largest emission contributor when it comes to fish farming in Norway. Thus, it is perhaps not surprising that the feed producing companies have the most thorough sustainability information disseminated through their channels. In addition, demands may be set by the aquaculture companies which lead to the feed companies having such a high focus on the sustainability of feed ingredients, and on communicating this. We have looked at six companies producing feed or feed ingredients for farmed fish, where some are large-scale feed producers, and some are small-scale producers of ingredients to be used in the feed. The larger producers are considered first, and the smaller ones in the last paragraph.

Several of the feed producing companies have separate sustainability reports which focus on important matters from a sustainability perspective. The SDGs appear clearly and consistently in all reports, with a thorough explanation of why each of them is important. Several companies list key performance indicators (KPIs) for various topics with the percentage change from previous years as well as what the target is within a given time. The companies also have focus areas with specific sub KPIs that are measurable. Typical KPIs that are reflected among the companies are water use, energy use, greenhouse gas emissions, and waste management, as well as the use of certified soy and palm oil.

The reports are generally perceived as clear and transparent, and it is easy to find the information you are looking for as well as to see overall what the most important goals and the progress of the companies within a number of topics are. There are, however, some companies that have changed the format of their reports over the years, and have removed several good, clear, and informative solutions in the latest reports, making them more difficult to interpret. The companies are all part of greater initiatives, such as SeaBOS (Seafood Business for Ocean Stewardship), Global Salmon Initiative, Sustainable Fisheries Partnership and ProTerra, where sustainability is a main focus. Several of these initiatives are common among the companies.

Some smaller companies producing ingredients for fish feed have also been looked into. These companies do not have reports but simpler websites containing sections about sustainability, what it means to them and why they contribute to sustainable feed. This also shows how important it is, even for smaller companies, to communicate a clear sustainability focus. Regardless of the company size, all feed producing companies we have looked into use the SDGs as indicators, such as SDG 2 Zero hunger, 12 Responsible consumption and production, 14 Life below water and 15 Life on land.

5.2 Aquaculture producers

We have looked at six aquaculture producers. In similarity to the feed producing companies, the aquaculture companies also have a general sustainability focus which is easy to find in websites and reports. Less often than the feed producers do the aquaculture companies have separate sustainability reports. However, the annual reports have sustainability as central and overarching topics. To find specific information, more navigation through websites and reports is required. Some of the websites have many separate web pages with sustainability information of different and overlapping topics, lacking appropriate search options. In these cases, the information is perceived as unavailable to the consumer, as it is hard to get an overview of the given information, and significantly more work is required than searching for what you are looking for in a single report.

There is little difference among the production companies in the information they provide. Some of the information, however, even in the annual reports, is time consuming to locate. The reports are often substantial, and less graphics are used compared to the reports of feed producers. When searching for specific key words, there are not always (relevant) results, and the key words to look up to find relevant information are not always obvious. All companies refer to the SDGs throughout the documentation they provide and elaborate on key focus areas and targets and how these are

achieved. This gives an overview of the available information and a pointer to what topics are considered especially important. Some of the companies also provide specific target values and information of achievement from the last few years for their set indicators, which appears transparent and informative to the reader.

Several KPIs of sustainability work are repeated among the relevant companies, and in particular we have looked at what the companies say regarding sustainable feed. There is a great focus on reducing the environmental footprint from feed. More specifically, the companies aim to do this by introducing new marine ingredients and species, as well as local novel ingredients, in the feed. In addition, increased efficiency of feed consumption and economic feed conversion are mentioned by some as a specific measure to reduce overall footprint of the feed. Despite the goal to source locally, no information was found with any of the individual companies regarding the proportion of Norwegian raw materials in their feed. On the other hand, Aas et al. (2022) reported that the proportion of Norwegian raw material in feed for Norwegian produced salmon in 2020 was only 8%. As the proportion of Norwegian ingredients in the feed is so low, this may be one of the reasons why the companies do not report accurate figures on this in publicly available channels.

5.3 End consumers

The consumption of fish and seafood was between 31-37 kg round weight per person per year between 2003 and 2021 (Helsedirektoratet, 2022). This number includes all species. For fillets, this equals to 13-15 kg per person. The Norwegian Seafood Council has estimated that Norwegians consumed on average 5.63 kg salmon round weight in 2021 (Jensen, 2022).

Most studies on consumer perspectives focus on the end product, the food product consumed, but controversies and critique towards the use of soy in salmon feed and the impact of deforestation of the rain forest in Brazil have been an important factor in making several feed and salmon producers only purchase soy from certified producers (Saue, 2021). Due to both NGOs and consumers becoming more aware of sustainability aspects, it is important to map if consumers will accept novel feed ingredients and even be willing to pay more if they are considered more sustainable. Eidem and Ruud (2022) point out a tendency to eat less of an animal with increased wealth. This means that the RRM ratio increases and less of the animal is used for human consumption, which ultimately reduces the overall resource use efficiency.

Farmed salmon as a source of omega-3 fatty acids has long been an important sales argument (Sprague et al., 2016). As previously noted, the replacement of fish oils to marine oils, has reduced the concentration of omega-3 fatty acids, and increased the levels on omega-6 fatty acids (Sprague et al., 2016; Sissener, 2018), which could overall reduce the health benefits of consuming farmed salmon. On the other hand, a decrease in marine ingredients in the salmon feed has also resulted in lower levels of contaminants such as mercury, arsenic, dioxins, dioxins-like PCBs (Polychlorinated biphenyl) and DDT (Dichlorodiphenyltrichloroethane) in farmed Norwegian salmon between 1999 and 2011 (Nøstbakken et al., 2015). Another study by Lundebye et al. (2017) state that farmed salmon has lower levels of persistent organic pollutants than wild salmon. The levels of omega-3 fatty acids are comparable, but levels of omega-6 fatty acids are higher in farmed salmon. The authors also recommend that the omega-3/omega-6 ratio should not be further decreased as the health benefits of consuming salmon may prevail.

6 Environmental drivers

The FSA divides environmental drivers into six categories, minerals, climate, water, biodiversity, land and soils, and fossil fuels (Van Berkum et al., 2018). These drivers are both impacted by the feed supply chain and vice versa. Life Cycle Assessment has emerged as a common tool to assess the environmental impacts of salmon feed and salmon production (Cashion et al., 2016; Bohnes and Laurent, 2019). Environmental impacts include global warming potential (kg CO_2-eq.), eutrophication potential (kg N or kg P), acidification potential (kg SO_2-eq.). There have been no recent studies assessing all impacts of Norwegian salmon production or salmon feed. However, there has been a series of reports and papers quantifying the carbon footprint of Norwegian salmon (Ziegler et al., 2013; Ziegler et al., 2021; Johansen et al., 2022a).

In 2020, the carbon footprint of salmon at farmgate was approximately 3.8 kg CO_2e/kg live weight (Johansen et al., 2022a). This result includes the impacts from land use change which accounted for 0.8 kg CO_2e/kg live weight salmon. Feed accounted for 75% of the total carbon footprint of the salmon at farmgate including impacts from land use change. The findings of the report state that the use of soy has decreased since 2017 and is sourced from other regions than South America. Soy from Europe and the US have a smaller carbon footprint than soy from South America due to less changes in land use.

Newton and Little (2018) found that for Atlantic Salmon farmed in Scotland in 2018, 90% of all impacts except eutrophication potential was accounted for by the feed, when assessing the impact categories global warming potential, eutrophication potential, ozone depletion potential, acidification potential, water use, land use and photochemical oxidation potential. Eutrophication potential was highest in the farming stage due to nitrogen emissions. Similar results can be expected for salmon produced in Norway, where most of the salmon is farmed in traditional aquaculture production in open net pens, there is usually no collection of sludge, and nutrients and other substances are released directly into the oceans. In 2021 the estimated emissions of phosphorus from aquaculture in Norway was around 15 600 tons (Pandit et al., 2023). A key action to reduce phosphorus emissions from aquaculture is to reduce the phosphorus concentration in the feed using the enzyme phytase, making phosphorus in vegetable sources more digestible for the salmon. The emissions of nitrogen are calculated to be 66 400 tons in 2019 by Broch and Ellingsen (2020). Nitrogen emissions can also be reduced by manipulating the feed composition, and most importantly, avoid feeding the salmon an excess of amino acids (Bureau and Hua, 2010).

7 Socio-economic drivers

The FSA divides socio-economic drivers into five categories, market, policies, science and technology, social organizations and individual factors (Van Berkum et al., 2018). Toussaint et al. (2022) state that social sustainability, in terms of human and labor rights, living conditions and life quality, among other things, are essential to achieve a sustainable food system. Thus, socio-economic drivers can influence, and at the same time be influenced by, the food system as a whole or specific value chains.

The aquaculture sector is economically important in Norway. In 2021, this sector created over 45 000 person-years of employment in the country. Over the last decade, there have been great increases in production value, value creation contribution as well as number of employees in the aquaculture-based supply chain, according to a report from SINTEF (Johansen et al., 2022b).

Resource rent tax on aquaculture has recently been introduced (as of January 1st, 2023) by the government. The tax is on income from the use of natural resources belonging to the state, to ensure the community receives a share of the income created by exploitation of the common resources along the coast. Companies have to pay this as a result of the extra income they get when they are allowed to use a limited resource. This means companies farming salmon, trout, and rainbow trout, and with an income over a certain limit, are taxed at a rate of 40% (Thomassen et al., 2009).

Supply chains and international trade can be vulnerable to global conflicts and events. Sunflower oil and soy are examples of ingredients used salmon feed, and which are imported to Norway (Winther et al., 2020). The soy industry has been reported to cause deforestation, displacement of local peoples and to violate labor rights (Rainforest Foundation Norway and Future in Our Hands, 2018; WWF, n.d). As of September 2023, the ongoing war in Ukraine has greatly affected the world economy. Ukraine and Russia account for 53% of the global production of sunflower oil and seeds. The situation causes reduced trade and increased prices on a number of resources, thus influencing supply chains (Landbruks- og matdepartementet, 2022; Leigland, 2022; NHO, n.d).

8 Conclusion

The Norwegian feed system for aquaculture is a part of a global food system, with significant imports of feed ingredients (92%) and large amounts of exports of salmon. The current feed system and its supply chain are vulnerable to war, conflicts, climate change, extreme weather events and more. Future growth in the industry and reaching the Norwegian government's ambitions to increase the share of Norwegian produced ingredients, will rely on a shift towards new feed ingredients. To ensure the success of new feed ingredients and their sustainability, a thorough understanding of the feed system is required. This paper has highlighted the current status of the feed system, in terms of volumes and composition of feed used, and the produced volumes of salmon. The regulatory environment as well as the characteristics of feed producers, salmon producers and consumers have been mapped.

The composition of salmon feed has undergone great developments from being mostly based on marine ingredients, towards being dominated by plant-based ingredients. This shift has impacted the nutritional composition of the salmon, where levels of omega-3 fatty acids have decreased. This may reduce the overall health benefits of farmed salmon, or at least the reputation of farmed salmon as a source of omega-3 fatty acids. Simultaneously, levels of contaminants have dropped and are currently lower than in wild salmon species.

Differences were observed between the extent of the sustainability focus in producer websites and reports and its attribution among impact categories. Both feed producers and aquaculture companies communicated their sustainability work thoroughly. However, the feed producers were perceived as somewhat more transparent in their dissemination. The research shows that there are variations between the categories along the supply chain when it comes to the sustainability focus. They communicate through websites and reports which are available to the consumer. However, some of the information is not easily accessible and requires extensive searching by the consumer, which could be perceived as less transparent. Nevertheless, there is an increasing focus among companies along the value chains, and many set ambitious goals for the operations going forward, in order to contribute to the mission of increased sustainability. With an increased focus on the topic from regulatory bodies the contributions could be even greater.

Data availability statement

The original contributions presented in the study are included in the article/supplementary material. Further inquiries can be directed to the corresponding author.

Author contributions

PS: Conceptualization, Writing – original draft, Writing – review & editing, Investigation, Methodology. AS: Conceptualization, Writing – original draft, Writing – review & editing, Investigation, Methodology, Visualization.

Funding

The author(s) declare financial support was received for the research, authorship, and/or publication of this article. The performed work is part of the SusFeed project (Sustainable feed production from Norwegian bio-resources for livestock and aquaculture) which is funded by the Research Council of Norway (grant number 326825).

Acknowledgments

The authors would like to thank Maitri Thakur, and the partners in the SusFeed project, in particular project manager Egil

Petter Stræte. The authors acknowledge the financial support from the Research Council of Norway.

Conflict of interest

The authors declare that the research was conducted in the absence of any commercial or financial relationships that could be construed as a potential conflict of interest.

Publisher's note

References

Aas, T. S., Ytrestøyl, T., and Åsgård, T. E. (2019) *Resource utilization of Norwegian salmon farming in 2016*. Available online at: https://www.fhf.no/prosjekter/prosjektbasen/901324.

Aas, T. S., Ytrestøyl, T., and Åsgård, T. E. (2022) *Utnyttelse av fôrressurser i norsk oppdrett av laks og regnbueørret i 2020* (Nofima AS). Available online at: https://nofima.brage.unit.no/nofima-xmlui/handle/11250/2977260 (Accessed April 24, 2023).

Bohnes, F. A., and Laurent, A. (2019). LCA of aquaculture systems: methodological issues and potential improvements. *Int. J. Life Cycle Assess.* 24, 324–337. doi: 10.1007/s11367-018-1517-x

Broch, O. J., and Ellingsen, I. (2020). *Kunnskaps- og erfaringskartlegging om effekter av og muligheter for utnyttelse av utslipp av organisk materiale og næringssalter fra havbruk* (Norway: Delrapport 1 -Kvantifisering av utslipp).

Bureau, D. P., and Hua, K. (2010). Towards effective nutritional management of waste outputs in aquaculture, with particular reference to salmonid aquaculture operations. *Aquaculture Res.* 41, 777–792. doi: 10.1111/are.2010.41.issue-5

Carvajal, A., Myhre, M., Mehta, S., Remme, J., Nystøyl, R., and Strandheim, G. (2021) *Matsvinn i sjømatindustrien 2020*. Available online at: https://www.fhf.no/prosjekter/prosjektbasen/901653/.

Cashion, T., Hornborg, S., Ziegler, F., Hognes, E. S., and Tyedmers, P. (2016). Review and advancement of the marine biotic resource use metric in seafood LCAs: a case study of Norwegian salmon feed. *Int. J. Life Cycle Assess.* 21, 1106–1120. doi: 10.1007/s11367-016-1092-y

Eidem, B., and Ruud, T. (2022). *Fôr- og husdyrbaserte verdikjeder in norsk matproduksjon - nåsituasjon og begreper. Notat 6/22* (Oslo/Trondheim, Norway: Ruralis - Institutt for rural- og regionalforskning). Available at: https://ruralis.no/wp-content/uploads/2022/11/notat-6_22-for-og-husdyrbaserte-verdikjeder-i-norsk-matproduksjon–nasituasjon-og-begreper-b–eidem-og-t–ruud.pdf.

European Commission (n.d) *Corporate sustainability reporting* (European Commission). Available online at: https://finance.ec.europa.eu/capital-markets-union-and-financial-markets/company-reporting-and-auditing/company-reporting/corporate-sustainability-reporting_en (Accessed January 15, 2024).

Fiskeridirektoratet (2023a) *Biomassestatistikk etter produksjonsområde* (Fiskeridirektoratet). Available online at: https://www.fiskeridir.no/Akvakultur/Tall-og-analyse/Biomassestatistikk/Biomassestatistikk-etter-produksjonsomraade (Accessed November 9, 2023).

Fiskeridirektoratet (2023b) *Omregningsfaktorer for produkter av ulike arter som landes* (Fiskeridirektoratet). Available online at: https://www.fiskeridir.no/Yrkesfiske/Tema/Omregningsfaktorer/omregningsfaktorer-for-produkter-av-ulike-arter-som-landes (Accessed October 13, 2023).

Fiskeridirektoratet (2023c) *Salg av laks og regnbueørret* (Fiskeridirektoratet). Available online at: https://www.fiskeridir.no/Akvakultur/Tall-og-analyse/Akvakulturstatistikk-tidsserier/Laks-regnbueoerret-og-oerret/Salg%20av%20laks%20og%20regnbue%C3%B8rret (Accessed January 16, 2023).

Forskningsrådet (2023) *Et samfunnsløft for bærekraftig fôr*. Available online at: https://www.forskningsradet.no/contentassets/ca017d3de07043abbf7f0a2ed1ebe051/et-samfunnsloft-for-barekraftig-for_15nov2023.pdf (Accessed November 16, 2023).

Free, C., and Hecimovic, A. (2021). Global supply chains after COVID-19: the end of the road for the neoliberal globalisation? *Accounting Auditing Accountability J.* 34, 58–84. doi: 10.1108/AAAJ-06-2020-4634

Helsedirektoratet (2022) *Utviklingen i norsk kosthold 2022*. Available online at: https://www.helsedirektoratet.no/rapporter/utviklingen-i-norsk-kosthold/Utviklingen%20i%20norsk%20kosthold%202022%20-%20Fullversjon.pdf?download=false.

Helse- og omsorgsdepartementet, Landbruks- og matdepartementet and Nærings- og fiskeridepartementet (2020) *Forskrift om eksport av næringsmidler, animaliebiprodukter, fôrvarer, levende dyr og avlsprodukter til land utenfor EØS (mateksportforskriften)* (Lovdata). Available online at: https://lovdata.no/dokument/SF/forskrift/2020-06-18-1547?q=f%C3%B4rvarer (Accessed January 9, 2023).

Jensen, B.-A. (2022) *Laksen haler innpå kjøttdeig i popularitet* (IntraFish.no | De siste nyhetene om oppdrettsnæringen). Available online at: https://www.intrafish.no/marked/laksen-haler-innpa-kjottdeig-i-popularitet/2-1-1294008 (Accessed May 10, 2023).

Johansen, U., Myhre, M. S., Young, E., and Richardsen, R. (2022b) *Nasjonal betydning av sjømatnæringen* (SINTEF Ocean). Available online at: https://www.sintef.no/globalassets/sintef-ocean/nasjonal-verdiskapning_sintef_2010-2021_endelig.pdf (Accessed August 31, 2023).

Johansen, U., Nistad, A. A., Ziegler, F., Mehta, S., Langeland, M., Wocken, Y., et al. (2022a). *Greenhouse gas emissions of Norwegian salmon products* (Norway: SINTEF Ocean, RISE and Asplan Viak). Available at: https://www.fhf.no/prosjekter/prosjektbasen/901718/.

Landbruks- og matdepartementet (2022) *Krigens betydning for global matsikkerhet* (Regjeringen.no). Available online at: https://www.regjeringen.no/no/aktuelt/krigens-betydning-for-global-matsikkerhet/id2904682/ (Accessed August 30, 2023).

Landbruks- og matdepartementet and Nærings- og fiskeridepartementet (2016) *Forskrift om animalske biprodukter som ikke er beregnet på konsum (animaliebiproduktforskriften)* (Lovdata). Available online at: https://lovdata.no/dokument/SF/forskrift/2016-09-14-1064 (Accessed March 22, 2023).

Leigland, L. E. (2022) *Slik påvirker Ukraina-krigen internasjonal handel og utvikling* (FN-sambandet). Available online at: https://www.fn.no/nyheter/slik-paavirker-ukraina-krigen-internasjonal-handel-og-utvikling (Accessed August 30, 2023).

Lundebye, A.-K., Lock, E.-J., Rasinger, J. D., Nøstbakken, O. J., Hannisdal, R., Karlsbakk, E., et al. (2017). Lower levels of Persistent Organic Pollutants, metals and the marine omega 3-fatty acid DHA in farmed compared to wild Atlantic salmon (*Salmo salar*). *Environ. Res.* 155, 49–59. doi: 10.1016/j.envres.2017.01.026

Mattilsynet (2013) *Krav til fôr* (Mattilsynet). Available online at: https://www.mattilsynet.no/dyr_og_dyrehold/for/krav_til_for.5567 (Accessed March 22, 2022).

Mattilsynet (2023) *Bearbeiding og omsetning av hydrolysert protein av fisk til fôr* (Mattilsynet). Available online at: https://www.mattilsynet.no/animaliebiprodukter/bearbeiding-og-omsetning-av-hydrolysert-protein-av-fisk-til-for (Accessed January 12, 2024).

Myhre, M., Richardsen, R., Nystøyl, R., and Strandheim, G. (2023). *Analyse marint restråstoff 2022* (Tromsø, Norway: SINTEF Ocean AS and Kontali Analyse AS). Available at: https://www.fhf.no/prosjekter/prosjektbasen/901844/.

Naylor, R. L., Hardy, R. W., Buschmann, A. H., Bush, S. R., Cao, L., Klinger, D. H., et al. (2021). A 20-year retrospective review of global aquaculture. *Nature* 591, 551–563. doi: 10.1038/s41586-021-03308-6

Newton, R. W., and Little, D. C. (2018). Mapping the impacts of farmed Scottish salmon from a life cycle perspective. *Int. J. Life Cycle Assess.* 23, 1018–1029. doi: 10.1007/s11367-017-1386-8

NHO (n.d) *Økonomisk overblikk 1/2022: Krigen i Ukraina og norsk næringsliv - Oppdaterte utsikter 2022-2024* (NHO). Available online at: https://www.nho.no/publikasjoner/kvartdalsrapporter/2022/okonomisk-overblikk-12022-krigen-i-ukraina-og-norsk-naringsliv-oppdaterte-utsikter-2022-2024/ (Accessed August 30, 2023).

Norsk standard (2012). *NS9417:2012. Laks og regnbueørret. Enhetlig terminologi og metode for dokumentasjon av produksjon*. Norway: Standard Norge.

Norwegian Seafood Council (2023) *Årlig eksport fra Norge*. Available online at: https://seafood.no/markedsinnsikt/apen-statistikk/year/ (Accessed September 6, 2023).

Nøstbakken, O. J., Hove, H. T., Duinker, A., Lundebye, A.-K., Berntssen, M. H. G., Hannisdal, R., et al. (2015). Contaminant levels in Norwegian farmed Atlantic salmon (*Salmo salar*) in the 13-year period from 1999 to 2011. *Environ. Int.* 74, 274–280. doi: 10.1016/j.envint.2014.10.008

Pandit, A. V., Dittrich, N., Strand, A. V., Lozach, L., Las Heras Hernández, M., Reitan, K. I., et al. (2023). Circular economy for aquatic food systems: insights from a multiscale phosphorus flow analysis in Norway. *Front. Sustain. Food Syst.* 7. doi: 10.3389/fsufs.2023.1248984

Plotly Graphing Libraries (n.d) *Sankey Diagram in Python*. Available online at: https://plotly.com/python/sankey-diagram/ (Accessed April 28, 2023).

PwC (2023) *PwC Seafood Barometer 2023*. Available online at: https://www.pwc.no/no/publikasjoner/2023-rapport-sjoematbarometeret.pdf (Accessed January 15, 2023).

Rainforest Foundation Norway and Future in Our Hands (2018) *Salmon on soy beans — Deforestation and land conflict in Brazil* (Rainforest Foundation Norway,

Future in Our Hands). Available online at: https://smooth-storage.aptoma.no/users/drp-dn-upload/files/IFM/Salmon-on-soy-beans-deforestation-and-land-conflict-in-Brazil.pdf (Accessed September 1, 2023).

Regjeringen (2021) *Hurdalsplattformen*. Available online at: https://www.regjeringen.no/no/dokumenter/hurdalsplattformen/id2877252/ (Accessed November 23, 2023).

Saue, O. A. (2021) *Nå nekter norske oppdrettere å kjøpe soya fra selskaper som hugger regnskog* (E24). Available online at: https://e24.no/i/PR5Moe (Accessed October 18, 2023).

Shepherd, C. J., and Jackson, A. J. (2013). Global fishmeal and fish-oil supply: inputs, outputs and marketsa. *J. Fish Biol.* 83, 1046–1066. doi: 10.1111/jfb.12224

Sissener, N. H. (2018). Are we what we eat? Changes to the feed fatty acid composition of farmed salmon and its effects through the food chain. *J. Exp. Biol.* 221, jeb161521. doi: 10.1242/jeb.161521

Sprague, M., Dick, J. R., and Tocher, D. R. (2016). Impact of sustainable feeds on omega-3 long-chain fatty acid levels in farmed Atlantic salmon 2006–2015. *Sci. Rep.* 6, 21892. doi: 10.1038/srep21892

Tacon, A. G. J., and Metian, M. (2008). Global overview on the use of fish meal and fish oil in industrially compounded aquafeeds: Trends and future prospects. *Aquaculture* 285, 146–158. doi: 10.1016/j.aquaculture.2008.08.015

Thakur, M., Johansen, U., Jafarzadeh, S., Cechura, L., Rumankova, L., Kroupova, Z. Z., et al. (2020). *Report on Information and Material Flow Analysis for the selected case studies. The VALUMICS project funded by EU Horizon 2020 G.A. No 727243. Deliverable: D4.3* (Trondheim: SINTEF Ocean). doi: 10.5281/zenodo.5105848

Thomassen, E., Semet, T., and Gran, T. (2009) *grunnrente* (Store Norske Leksikon). Available online at: https://snl.no/grunnrente (Accessed August 30, 2023).

Toussaint, M., Cabanelas, P., and Muñoz-Dueñas, P. (2022). Social sustainability in the food value chain: what is and how to adopt an integrative approach? *Qual. Quantity* 56, 2477–2500. doi: 10.1007/s11135-021-01236-1

Troell, M., Costa-Pierce, B., Stead, S., Cottrell, R. S., Brugere, C., Farmery, A. K., et al. (2023). Perspectives on aquaculture's contribution to the Sustainable Development Goals for improved human and planetary health. *J. World Aquaculture Soc.* 54, 251–342. doi: 10.1111/jwas.12946

United Nations Environment Programme, I. R. P (2016) *Food Systems and Natural Resources*. Available online at: https://wedocs.unep.org/20.500.11822/7592.

Van Berkum, S., Dengerink, J., and Ruben, R. (2018). *The food systems approach: sustainable solutions for a sufficient supply of healthy food* (Wageningen: Wageningen University & Research).

Winther, U., Hognes, E., Jafarzadeh, S., and Ziegler, F. (2020) *Greenhouse gas emissions of Norwegian seafood products in 2017* (SINTEF Ocean). Available online at: https://www.sintef.no/contentassets/0ec2594f7dea45b8b1dec0c44a0133b4/report-carbon-footprint-norwegian-seafood-products-2017_final_040620.pdf (Accessed November 14, 2023).

WWF (n.d) *Soy* (WWF). Available online at: https://www.worldwildlife.org/industries/soy (Accessed August 31, 2023).

Ziegler, F., Jafarzadeh, S., Hognes, E., and Winther, U. (2021). Greenhouse gas emissions of Norwegian seafoods: From comprehensive to simplified assessment. *J. Ind. Ecol.* 26, 1908–1919. doi: 10.1111/jiec.13150

Ziegler, F., Winther, U., Hognes, E. S., Emanuelsson, A., Sund, V., and Ellingsen, H. (2013). The carbon footprint of norwegian seafood products on the global seafood market. *J. Ind. Ecol.* 17, 103–116. doi: 10.1111/j.1530-9290.2012.00485.x

frontiers | Frontiers in Marine Science

TYPE Original Research
PUBLISHED 01 May 2024
DOI 10.3389/fmars.2024.1363703

OPEN ACCESS

EDITED BY
Yngvar Olsen,
NTNU, Norway

REVIEWED BY
Leonel Pereira,
University of Coimbra, Portugal
João Cotas,
University of Coimbra, Portugal

*CORRESPONDENCE
Binbin Chen
binbch@163.com
Zengling Ma
mazengling@wzu.edu.cn

RECEIVED 31 December 2023
ACCEPTED 09 April 2024
PUBLISHED 01 May 2024

CITATION
Guo L, Pang G, Luo L, Gao C, Chen B and Ma Z (2024) Asexual proliferative seedling technology for *Sargassum fusiforme* constructed using tissue culture method. *Front. Mar. Sci.* 11:1363703. doi: 10.3389/fmars.2024.1363703

Asexual proliferative seedling technology for *Sargassum fusiforme* constructed using tissue culture method

Lina Guo[1,2], Guanfeng Pang[1,2], Lin Luo[1,2], Congquan Gao[1,2], Binbin Chen[1,2,3]* and Zengling Ma[1,2,3]*

[1]National and Local Joint Engineering Research Center of Ecological Treatment Technology for Urban Water Pollution, Wenzhou University, Wenzhou, China, [2]College of Life and Environmental Science, Wenzhou University, Wenzhou, China, [3]Zhejiang Provincial Key Lab for Subtropical Water Environment and Marine Biological Resources Protection, Wenzhou University, Wenzhou, China

The traditional method of sexual reproduction in *Sargassum fusiforme* can lead to difficulties in maintaining the stable inheritance of superior traits. However, technology for asexual proliferation of seedlings in seaweed tissue culture is not well-developed. Therefore, we established a tissue culture method to study, the effects of different parts of *S. fusiforme*, uniconazole (UIZ) concentrations, and culture methods on the regeneration of tissue-derived juveniles of *S. fusiforme*. The results showed that the optimal culture conditions were solid medium with modified Provassoli's enriched seawater containing 3 μM UIZ for at least 17 days followed by transfer to liquid medium to induce rapid cell proliferation. These optimal conditions resulted in a callus-like/adventitious bud induction rate of 100%, callus-like/adventitious bud number per explant of 27.43 ± 4.57, and relative growth rate of 3.05 ± 0.27. The best plant parts for tissue culture were the filamentous holdfasts followed by the stem tip. In addition, UIZ treatment increased photosynthesis, resulting in soluble sugar and soluble protein contents of 30.47 $mg \cdot g^{-1}$ and 1.39 $mg \cdot g^{-1}$ of in the regenerated juveniles. Based on our results, *S. fusiforme* can be cultured using a tissue culture technique in which UIZ is added to a solid medium, followed by culture in liquid medium for proliferation. *Sargassum fusiforme* juveniles obtained using this technique can be cultured continuously until the next culture season and grow normally, providing a technical reference for indoor preservation and expansion of algal species.

KEYWORDS

***Sargassum fusiforme*, tissue culture, seaweed, hormone, seedling propagation**

1 Introduction

Sargassum fusiforme (Harvey) Okamura (Sargassaceae, Phaeophyta) is a brown macroalga with high economic and nutritional value that grows in warm temperate and subtropical regions (Mantri et al., 2022; Pang et al., 2023). *Sargassum fusiforme* and other seaweeds are widely distributed in eastern China, Korea, and Japan, among other locations, and provide egg-laying and seedling resource sites for various marine organisms (Uji et al., 2015; Hwang et al., 2020; White and White, 2020). This algae is rich in polyunsaturated fatty acids, fucoidans, polysaccharides, and polyphenols, and exerts anti-obesity, anti-inflammatory, antioxidant, anti-tumor, and antiviral properties, making it applicable in the fields of nutraceuticals, pharmaceuticals and cosmetics (Akremi et al., 2017; Garcia-Poza et al., 2020; Kelly et al., 2020; Ali et al., 2021). The global annual production of *S. fusiforme* has increased from 109,597t in 2003 to 303,797 t in 2020; therefore, the seaweed aquaculture industry shows high development prospects (Tian et al., 2023).

Sargassum fusiforme has been traditionally cultivated in two ways; sexual propagation by fertilizing the male and female receptacles to form a zygote, which regenerates the holdfasts, and asexual propagation by artificially retaining the holdfasts of *S. fusiforme* during the harvest of the mature algal mass, followed by culturing the holdfasts in the following year (Xu et al., 2022b). However, the traditional method of seedling cultivation leads to the growth of weed algae, which compete with seedlings for nutrients and space, and it is challenging to control the temperature, pH, and light. Even during sexual reproduction, it is difficult to stabilize the inheritance of some heat- and cold-tolerant strains because of crossbreeding (Chen and Zou, 2014; Chen et al., 2019; Luo et al., 2023). Traditional seedling culture conditions are complicated and time-consuming, and the maintenance and replacement of cultivation equipment during cultivation can cause a serious economic burden (Largo et al., 2020; Collins et al., 2022; Arbaiza et al., 2023). Additionally, cultivation of seaweed in marine areas can alter the ecological structure, abundance, and diversity of phytoplankton, thereby adversely affecting ecosystems, organisms and the surrounding environment (Kelly et al., 2020; Eggertsen and Halling, 2021; Tian et al., 2023). Therefore, improved cultivation methods for *S. fusiforme* must be explored.

Tissue culture is the most common method of cultivation and broadly refers to use of the plant itself, such as isolated organs, tissues, cells, protoplasts, and mutants. This approach has the advantages of simple operation, easy cultivation in large quantities, short cultivation time, easy control of cultivation conditions, and a low mutation rate of cells (Custodio et al., 2022; Yan et al., 2022). Nutritional propagation is an effective means of tissue culture. According to the morphological changes that occur during tissue culture, propagation can be divided into direct regeneration and indirect regeneration (including callus culture and protoplast culture) to generate virus-free and fast-growing resistant algal strains (Avila-Peltroche et al., 2022; Jiksing et al., 2022). However, there are some limitations to tissue culture, such as the lack of development of tissue culture methods for different seaweeds, susceptibility to bacterial contamination during the culture process, uncertainty in the optimal composition of the culture medium, and difficulty in controlling the culture results (Baweja et al., 2009; Yong et al., 2014; Muhamad et al., 2018).

Tissue culture techniques can be used to induce the production of calluses, budding, and plant development by adding plant growth regulators, which are synthetic (or extracted from microorganisms), along with an organic compound similar to natural plant hormones that regulate the growth and development of biological organisms (Rademacher, 2015; Luo et al., 2023). Uniconazole (UIZ), known as a triazole-type cytochrome P450 enzyme inhibitor, is a plant growth regulator. Most studies of UIZ application were conducted in soybean, corn, and wheat to evaluate resistance to high salt, drought and low temperatures, and to induce germination and emergence, and its effects on the photosynthetic characteristics, antioxidant activity, and morphological parameters of plants. However, the application of UIZ to economic seaweeds has not been widely examined (Keshavarz and Khodabin, 2019; de Araújo Amatuzzi et al., 2020; Aghaei et al., 2021; Zhou et al., 2021; Hu et al., 2022).

Tissue culture technology has the advantages of simple operation, easy control of growth conditions, short cultivation time, high yield, and low cost. In this study, we utilized tissue culture technology for seedling propagation of *S. fusiforme* to investigate the effects of different parts, UIZ concentrations and culture methods on juvenile regeneration, growth, development, and nutrient accumulation. We developed a method for juvenile regeneration of *S. fusiforme* tissue, and provide technical support for seedling propagation and expansion of this algae.

2 Materials and methods

2.1 Sample collection and experimental design

Sargassum fusiforme was collected from Dongtou, Zhejiang province, during the harvesting season and brought to the laboratory within 2 h in a 4°C cryopreservation box. The surface of *S. fusiforme* was cleaned with brushes and tweezers to remove attached stray algae and plankton, rinsed with filtered and sterilized natural seawater. Healthy and uniformly sized algal organisms were selected for temporary incubation in a light-illuminated incubator (light incubator, Yanghui, Ningbo, China) for 7 days. The experimental conditions were as follows: temperature was 19°C, light intensity was 90 μmol photons·m^{-2} ·s^{-1}, light:dark photoperiod (L:D) was 12 h:12 h, salinity of the culture solution was 26‰, and the culture medium was supplemented with 200 μmol·L^{-1} $NaNO_3$ and 20 μmol·L^{-1} NaH_2PO_4. The culture solution was aerated continuously using an air pump (ACO-9730, Haili, Guangzhou, China).

After 7 days of domestication, healthy stem tips (2–4 cm in length), the lower end of the stem base (4–5 cm from the base), and

filamentous holdfasts of *S. fusiforme* were selected and rinsed three times in sterile seawater. The seaweed was treated with a solution of 0.38% NaClO and 0.5% KI in a 1:1 volume ratio for 2 min, sterilized with sterile water, and rinsed. The samples were then cut into approximately 1.5 cm segments using a scalpel and cultured on modified Provassoli's enriched seawater (PES) solid medium with different concentrations of UIZ (Macklin, Guangzhou, China). The tissue was cultivated at a temperature of 19°C, with a light intensity of 60 μmol photons·m^{-2} ·s^{-1} and L:D = 12 h:12 h. The solid medium was changed every month to prevent browning of the tissue (Kerrison et al., 2015; Uji et al., 2015; Muhamad et al., 2018; Xu et al., 2022a).

The experiment comprised of two phases. During the first phase, *S. fusiforme* explants were cultured in solid medium containing UIZ. A cross-design was used to divide the culture samples into 12 groups based on the source site of the explants (proximal stem tip, proximal stem base, and filamentous holdfasts) and concentration of UIZ (0, 3, 5, and 7 μM). The culture samples were exposed to a light intensity of 90 μmol photons ·m^{-2} ·s^{-1}. During the second stage of culture, the *S. fusiforme* segments were transferred into modified PES liquid medium on days 14 (first batch), 17 (second batch), 20 (third batch), and 52 (fourth batch) after the first stage of culture. The callus-like/adventitious bud induction rate, callus-like/adventitious bud numbers per explant, relative growth rate (RGR), photosynthetic activity and morphology of *S. fusiforme* tissue culture were recorded. The liquid PES medium was replaced every three days during incubation.

2.2 Morphological changes of *S. fusiforme* under different treatments

Morphological changes in *S. fusiforme* explants were documented using a Sony camera (SONY a6000, Tokyo, Japan) after each medium change. The numbers of callus-like or adventitious buds in each explant segment were recorded. The morphology and cellular structure of the characteristic explants were observed at every 3 days using a stereomicroscope (Leica M80, Wetzlar, Germany) and an orthostatic microscope (Leica DM2700 P, Wetzlar, Germany).

2.3 Determination of callus-like/adventitious bud induction rate, callus-like/adventitious bud numbers per explant

The callus-like/adventitious bud induction rate and callus-like/adventitious bud numbers per explant of *S. fusiforme* were counted every 3 days during the incubation period. The specific formulas were as follows:

$$\text{callus}-\text{like/adventitious buds induction rate}(\%) = \left(\frac{\text{callus}-\text{like/adventitious buds sprouting segments}}{\text{total number of explant segments}}\right) \times 100$$

$$\text{callus}-\text{like/adventitious buds number per explant} = \left(\frac{\text{Total number of callus}-\text{like/adventitious buds sprouting}}{\text{total number of explant segments}}\right)$$

2.4 Determination of relative growth rate

The RGR was calculated by determining the weight of the explants and regenerated juveniles at the time of medium change, using the following formula:

$$\text{RGR}\,(\%\cdot d^{-1}) = [\ln(W_t/W_0)/t] \times 100$$

where W_0 is the initial weight of the explant (g), W_t is the weight of the explant and regenerated juveniles on day t (g), and t is the number of culture (days).

2.5 Determination of photosynthetic activity

The physiological state of regenerating *S. fusiforme* juveniles was determined by measuring their maximum quantum yield (Fv/Fm) and maximum relative electron transfer rate (rETRm) using Junior-Pam (Walz, Effeltrich, Germany). *S. fusiforme* explants together with regenerated juveniles were dark-adapted for 30 min, and the Fv/Fm and rETRm in the range of 0 – 820 μmol photons m^{-2} ·s^{-1} were determined, where $Fv = Fm\text{-}F_0$, Fv is the variable fluorescence, Fm is the maximum fluorescence after dark-adaptation, and F_0 is the minimum fluorescence after dark-adaptation. The rapid light curve was fitted according to the formula described by Platt et al. (1980):

$$\text{rETR}\ (\mu\text{mol electrons}\cdot m^{-2}\cdot s^{-1}) = \text{rETRm}\cdot(1-e^{-\alpha\cdot PAR/\text{rETRm}})\cdot e^{-\beta\cdot PAR/\text{rETRm}}$$

2.6 Determination of soluble carbohydrates, soluble proteins, and mannitol contents

The soluble carbohydrate (SC) content was determined using the anthrone method developed by Ershadi et al. (2015). Approximately 0.1 g of tissue culture from *S. fusiforme* juveniles was crushed in liquid nitrogen; 1 mL of distilled water was added during the crushing process, and then 2 mL of $MgCO_3$ suspension was added. The samples were fixed to 10 mL with distilled water and centrifuged in a freezing centrifuge at 10277×g for 10 min. The supernatant (1 mL) was transferred into a test tube and mixed with 2 mL of distilled water, followed by addition of 10 mL of anthrone reagent. The mixture was shaken continuously until gas escaped and then heated in a boiling water bath at 100°C for 5 min. After the mixture cooled, the absorbance was measured at 620 nm using a UV spectrophotometer with distilled water as a reference. The SC

content was calculated from the standard curve of absorbance values($mg{\cdot}g^{-1}$).

The soluble protein (SP) content was determined using Coomassie Brilliant Blue G-250 dye as described by Bradford (1976). Approximately 0.1 g of *S. fusiforme* juveniles was ground in liquid nitrogen in a mortar, suspended in 10 mL 0.1 mol/L phosphate buffer (pH = 6.8) and centrifuged at 10277×g for 10 min for 10 min at 4°C in an ultra-high-speed freezer centrifuge. The supernatant (1 mL) was collected and mixed with 4 mL of Coomassie Brilliant blue G-250 staining solution. The mixture was allowed stand for 3 min at 25°C and the absorbance measured at 595 nm. For the control group, 1 mL of PBS was mixed with 4 mL of Coomassie Brilliant Blue G-250 staining solution. The mixture was incubated at 25°C for 3 min before absorbance was recorded using a UV spectrophotometer. The SP content was calculated using a bovine serum protein standard curve ($mg{\cdot}g^{-1}$).

The mannitol content was determined as described by Chen et al. (2020). A dried juvenile *S. fusiforme* sample (0.1 g) was collected from a tissue culture source. The sample was milled using liquid nitrogen, and 30mL of HCl with a mass fraction of 1% was added. After the mixture was stirred for 4 min in a 100°C water bath, the supernatant was collected and diluted 100 times. The diluted solution (1 mL) was added to a centrifuge tube. Sodium periodate (1mL) of was then added, mixed well, then it was placed at 25°C for 15 min. 2mL of 0.1% rhamnose was added, mixed thoroughly, and left to wait for 1 min. Nash reagent (4.0 mL) was added and mixed thoroughly. The mixture was heated in a constant temperature water bath at 53°C for 15 min and cooled to room temperature after the mixture changed color. Finally, the absorbance of mannitol was measured at 413 nm using distilled water as a blank. The standard curve of mannitol was drawn using the absorbance a value as the vertical coordinate and the concentration as the horizontal coordinate($mg{\cdot}g^{-1}$).

2.7 Data analysis

All data were preliminarily processed using Excel (Microsoft, Redmond, WA, USA) and subjected to analysis of variance chi-square (F-test), one-way analysis of variance, and two-way analysis of variance using SPSS 25.0 software (SPSS, Inc., Chicago, IL, USA), with the significance level set at $P<0.05$. Graphs were drawn using origin 2023 (OriginLab, Northampton, MA, USA), and experimental results are expressed as the mean ± standard deviation.

3 Results

3.1 Effect of different culture conditions on the morphology of *S. fusiforme*

Figure 1 shows the morphological changes that occurred during the regeneration of different parts of *S. fusiforme* on days 34 and 62 under various batch and UIZ concentration treatments. When using a shorter time to induce callus-like tissues/adventitious buds on solid medium, and higher concentrations of UIZ, *S. fusiforme* was less likely to germinate and sprout compared with low concentration group. In the first bath culture, regenerating buds were induced from *S. fusiforme* filamentous holdfasts, and a few stem tips were produced; production occurred only under conditions of low UIZ content in the medium (0, 3, and 5 UIZ). As the induction time in solid medium was increased, *S. fusiforme* filamentous holdfasts, stem tips and stem bases were induced with

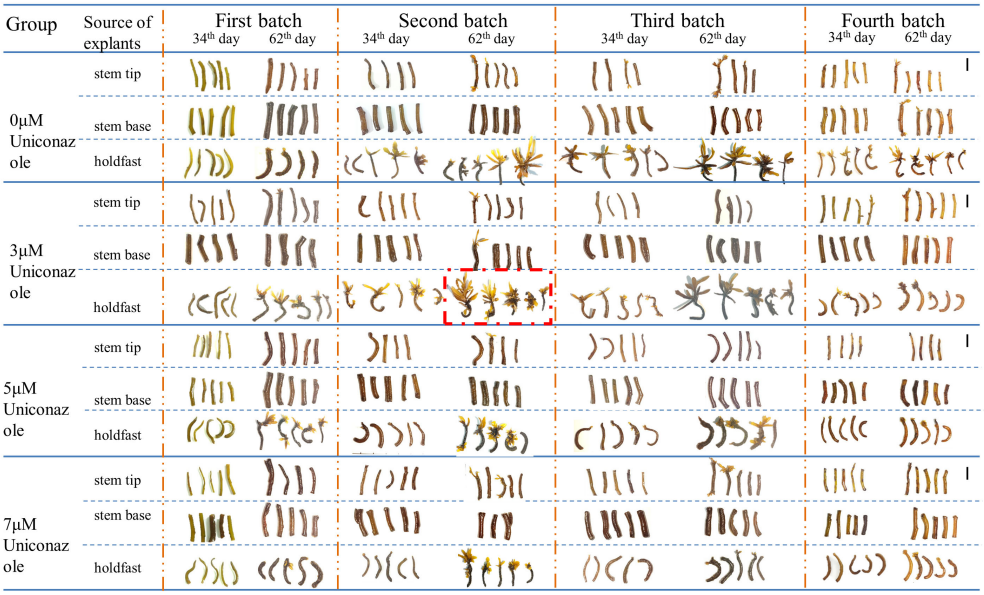

FIGURE 1
Morphological changes in regeneration of various parts of *S. fusiforme* at 34 and 62 days under different batch and UIZ concentration treatments.

different degrees of callus-like tissues or adventitious buds. The most pronounced morphological changes in *S. fusiforme* explants were observed in the 3 μM UIZ-cultured filamentous holdfasts, in which a large number of leaves, cylindrical protuberances and a few holdfasts were induced, whereas only cylindrical protuberances were induced at the stem tip and stem base. Most filamentous holdfasts and a few stem tips appeared as callus-like tissues/adventitious buds in the first stage of culture for approximately 9 days, whereas the stem base appeared after at least 30 days of cultivation in solid medium. Furthermore, in this method, adventitious buds continued to regenerate into gas vesicles or leaves after isolation (Figure 1). After initial morphological optimization screening, we cultured the tissue-derived 3 μM UIZ-activated *S. fusiforme* germlines for a longer period and continued this culture until the next breeding season (Figure 2).

Changes in the explant cells were periodically observed during the culture period using a stereomicroscope and a Leica microscope. Explants treated with UIZ exhibited four distinct morphological structures, whereas regenerating buds formed directly from explants that were not treated with UIZ. The four types involves irregularly structured fragile mulberry embryo-like tissue (Figures 3A–C), hard spherical protuberances (Figures 3D–F), a colorless or light-yellow filamentous texture (Figures 3G–I), and direct regeneration of adventitious buds through the tips or cuts of the *S. fusiforme* filamentous holdfasts (Figures 3J–L). Depending on the site of explant germination and its structure, callus-like tissue can form a hyaline or yellowish bulge or callus through the medullary region at the center of the *S. fusiforme* holdfast (Figure 3C), or regenerative tissue can form through epidermal cells (Figures 3E, F).

The cross-sectional structure of *S. fusiforme* holdfast cells was arranged from outside to inside as follows: epidermis, subepidermis, exodermis, endodermis, and medulla in the middle. The epidermal cells were small, whereas the cortical cells increased in size from the outermost to the innermost layer. Medullary cells were the smallest, and the intercellular boundaries were well-defined (Figure 4). The outer epidermal cells of *S. fusiforme* holdfasts showed a polygonal outline and were darkest in color, as they are rich in pigments and starch grains. The pith, which has denser cells and fewer starch grains than other regions of *S. fusiforme*, exhibited an intermediate morphology. In contrast, the medullary zone of *S. fusiforme* adventitious buds were not necessarily located at the mid-end of the morphology. Morphogenesis was induced in the epidermis and subepidermis of earlier tissues (Figures 4B, D, F). The diameter of the nascent buds cells was smaller than that of the filamentous holdfasts of mature *S. fusiforme* (Figure 4).

3.2 Effect of callus-like/adventitious bud induction rate and callus-like/adventitious bud numbers per explant of *S. fusiforme*

In both stages of culture, the callus-like/adventitious bud induction rate and callus-like/adventitious buds numbers per explant were significantly affected by the UIZ concentration at the *S. fusiforme* explant site ($p < 0.05$, Figure 5). Addition of low

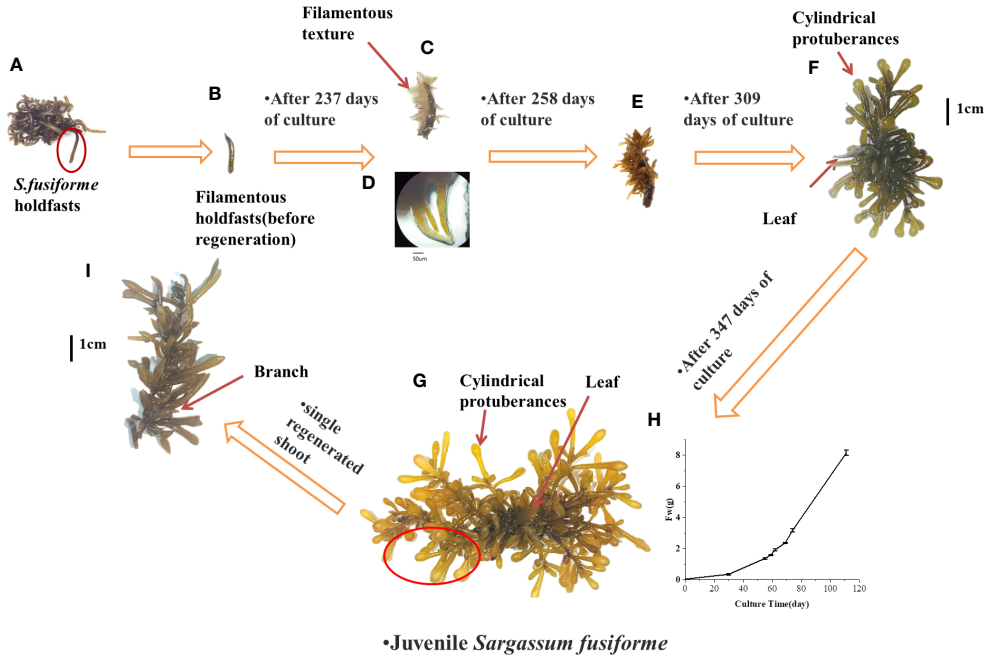

FIGURE 2
Induction of *S. fusiforme* into seedling by prolonged cultivation **(A)** complete holdfast **(B)** filaments holdfasts of *S. fusiforme* before regeneration **(C)** formation of yellowish/transparent filamentous textures; **(D)** morphology of c under the microscope **(E)** filamentous textures begin to diverge for colouring **(F)** formation of cylindrical protuberances and leaf **(G)** formation of *S. fusiforme* juveniles **(H)** change in the fresh weight of *S. fusiforme* seedling in f over time **(I)** growth of single *S. fusiforme* branch into an adult juveniles.

10.3389/fmars.2024.1363703

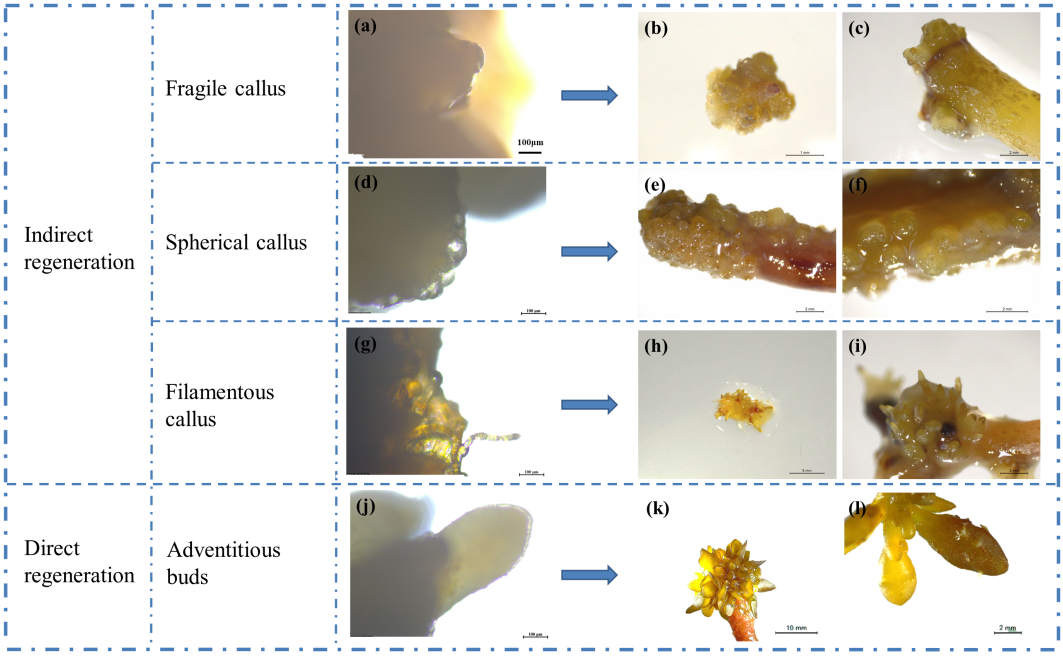

FIGURE 3
Types of regeneration in *S. fusiforme* tissue culture. **(A–C)** friable mulberry-like tissue cells; **(D–F)** hard spherical or cylindrical protuberances; **(G-I)** colorless or transparent filamentous texture; **(J–L)** directly regenerated into leaves.

concentrations of UIZ significantly increased the callus-like/adventitious bud numbers per explant and induction rate of *S. fusiforme* near the stem tips. The induction rate of filamentous holdfasts treated with 3 μM UIZ was 100%. Additionally, 27.43 ± 4.58 callus-like/adventitious buds were produced per explant segment ($p< 0.05$, Figure 5). The number of callus-like or adventitious buds per explant was higher in all parts of the explant under the 3 μM UIZ treatment condition compared to that observed under other UIZ concentrations (Figure 6B). Furthermore, there was a significant difference in the number of callus-like/adventitious bud per explant between the first batch of the earliest liquid medium transfer and the second, third, and fourth batches of the culture($p< 0.05$, Figure 6D).This result suggests that a minimum of 17 days of cultivation in solid medium is necessary.

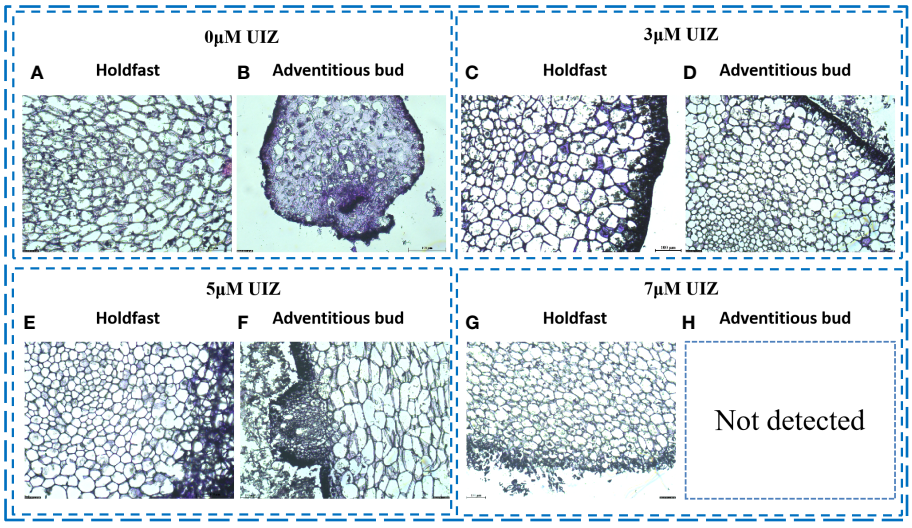

FIGURE 4
Frozen sections of *S. fusiforme* cells at different UIZ concentrations **(A)** cross-sectional view of 0 μM UIZ-treated filamentous holdfasts; **(B)** cross-sectional view of 0 μM UIZ-treated adventitious buds; **(C)** cross-sectional view of 3 μM UIZ-treated filamentous holdfasts; **(D)** cross-sectional view of 3 μM UIZ-treated adventitious buds; **(E)** cross-sectional view of 5 μM UIZ-treated filamentous holdsfasts; **(F)** cross-sectional view of 5 μM UIZ-treated adventitious buds; **(G)** cross-sectional view of 7 μM UIZ-treated filamentous holdfasts. **(H)** not detected.

10.3389/fmars.2024.1363703

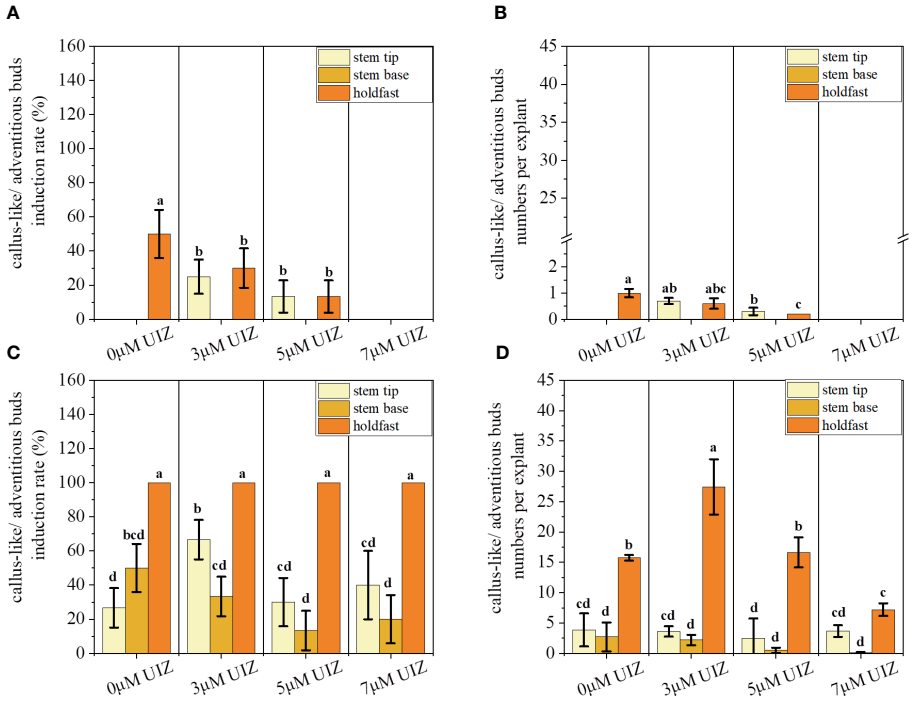

FIGURE 5
Effects of callus-like/adventitious buds induction rate and callus-like/adventitious buds numbers per explant at different culture stages. **(A)** callus-like/adventitious buds induction rate at solid culture stage; **(B)** callus-like/adventitious buds numbers per explant at solid culture stage; **(C)** callus-like/adventitious buds induction rate at batch culture stage; **(D)** callus-like/adventitious buds numbers per explant at batch culture stage. Values are expressed as mean ± standard deviation (n = 3). Different letters indicate significant differences between culture conditions ($p < 0.05$).

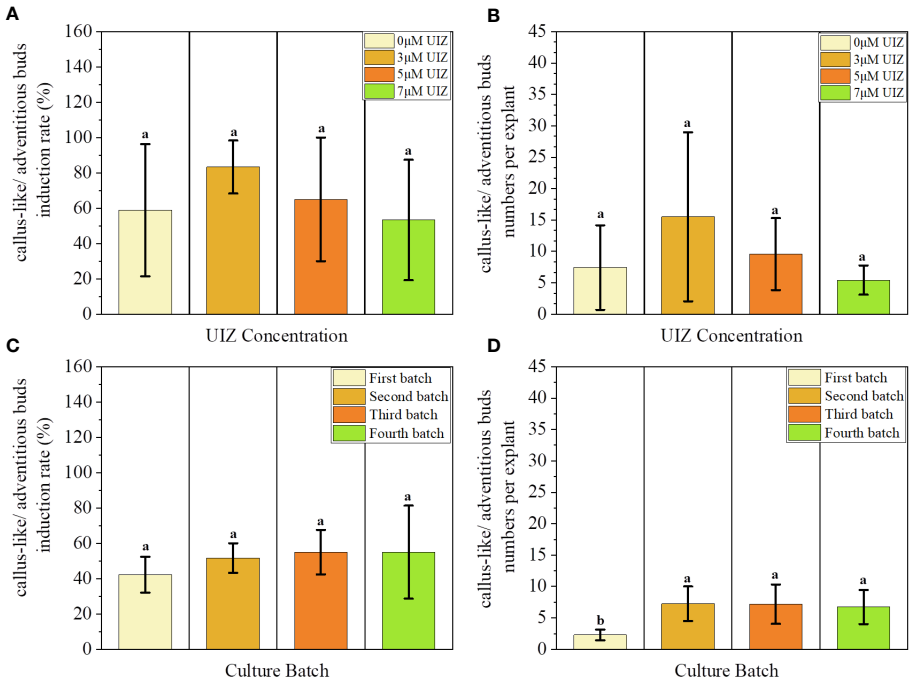

FIGURE 6
Effects of UIZ concentration and culture batch on callus-like/adventitious buds induction rate and callus-like/adventitious buds numbers per explant of *S. fusiforme*. **(A)** callus-like/adventitious buds induction rate of different UIZ concentration treatments; **(B)** callus-like/adventitious buds numbers per explant of different UIZ concentration treatments; **(C)** callus-like/adventitious buds induction rate of different batches of culture; **(D)** callus-like/adventitious buds numbers per explant of different batches of culture. Values are expressed as mean ± standard deviation (n = 3). Different letters indicate significant differences between different culture conditions ($p < 0.05$).

Batch 4 produced 7.19 ± 3.13 adventitious shoots/callus-like tissues per branch segment ($p< 0.05$, Figure 6D). Batch 4 as the group treated with 3 μM UIZ and with the longest solid induction time showed the highest germination rate, indicating that solid medium was beneficial for inducing adventitious buds/callus-like tissues (Figure 6).

3.3 Effect of length and RGR

Changes in the length of *S. fusiforme* were significantly affected by different concentrations of UIZ (Figure 7). The greatest effect was observed at 3 μM UIZ ($p< 0.001$, Figure 7B). The length of regenerated juveniles varied among the different explant sites of *S. fusiforme*. Additionally, changes in *S. fusiforme*'s filamentous holdfasts were greater than those in the stem tips ($p< 0.05$). The 3 μM UIZ treated filamentous holdfasts provided lengths of up to 3.43 ± 0.39 cm ($p< 0.05$).

We observed significant differences in the RGR of *S. fusiforme* based on variations in the culture site, UIZ concentration, and transfer medium ($p< 0.05$, Figure 8). A longer induction time in solid culture resulted in a higher RGR. However, it is necessary to culture the sample in liquid medium for 17days to achieve proliferative culture (Figure 8). Significant variations in the RGR were observed among different parts of *S. fusiforme* explants. Filamentous holdfasts exhibited the highest RGR of approximately 3.05% when cultured in 3μM UIZ ($p< 0.05$). The RGR trend in batch 4 of cultured *S. fusiforme* explants differed from that of the first three batches because the last batch had a long induction time in solid medium and insufficient time for the proliferation of regenerating buds in liquid medium (Figure 9).

3.4 Changes in photochemical activity of *S. fusiforme* under different treatments

Different batches, explant locations, and UIZ concentrations played influenced the Fv/Fm, rETRm and fast light curves of *S. fusiforme* juveniles. The effect of the *S. fusiforme* explant site and UIZ concentration in culture batches 1 and 2 did not significantly affect Fv/Fm ($P > 0.05$, Figure 10A), whereas the effect on rETRm was significant up to a maximum of 39.82 ± 3.86 ($P< 0.05$, Figures 10D, E). The Fv/Fm, rETRm and rapid light curve disparity of *S. fusiforme* varied significantly in batch 4 according to the explant location and UIZ concentration, with the lowest Fv/Fm was 0.356 ± 0.04 and lowest rETRm was 8.98 ± 0.79 at the stem tip of *S. fusiforme* in the presence of UIZ compared to in the absence of UIZ ($P< 0.05$, Figure 10).

3.5 Determination results of SC and SP contents

During the culture process, the concentration of UIZ significantly affected the SC and SP, which increased with increasing UIZ concentrations, The SC contents in the 3, 5 and 7

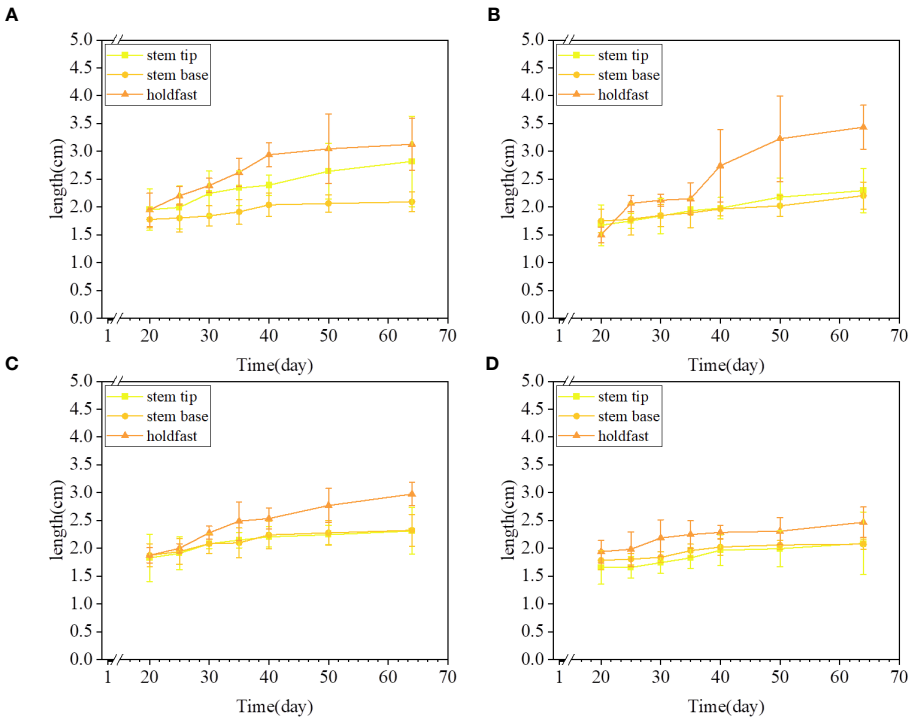

FIGURE 7
Variation in culture length of *S. fusiforme* treated with different concentrations of UIZ. **(A)** length change for 0 μM UIZ treatment; **(B)** length change for 3 μM UIZ treatment; **(C)** length change for 5 μM UIZ treatment; **(D)** length change for 7 μM UIZ treatment. Values are expressed as mean ± standard deviation (n = 3). Different letters indicate significant differences between different culture conditions ($p< 0.05$).

10.3389/fmars.2024.1363703

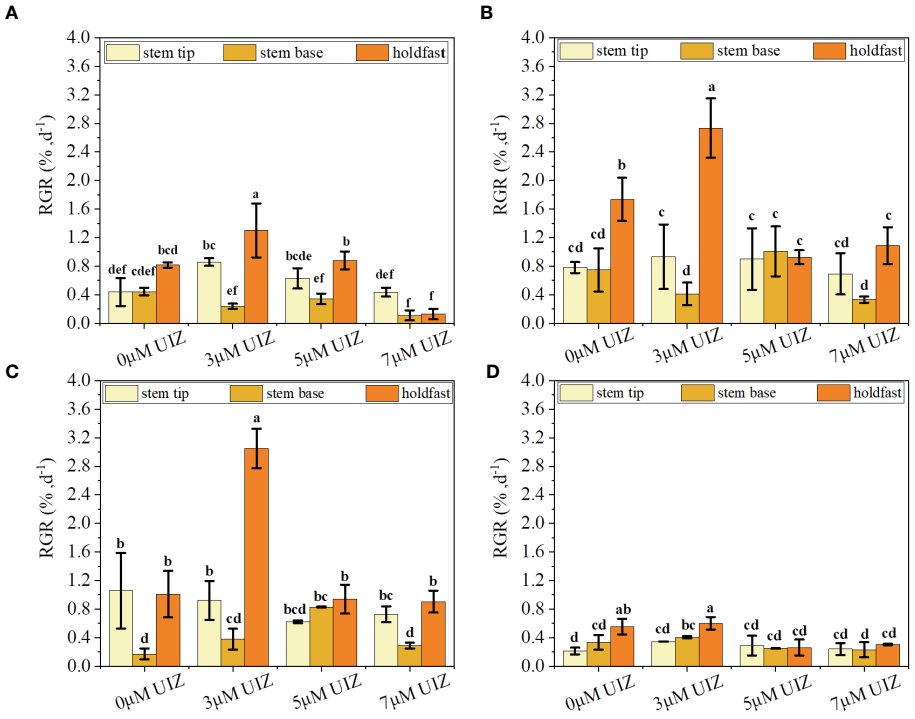

FIGURE 8
Effect of UIZ concentration and *S. fusiforme* parts on RGR of regenerated juveniles under batch culture stage. **(A)** RGR of the first batch of culture; **(B)** RGR of the second batch of culture; **(C)** RGR of the third batch of culture; **(D)** RGR of the fourth batch of culture. values are expressed as mean ± standard deviation (n = 3). Different letters indicate significant differences between different culture conditions ($p < 0.05$).

μM UIZ treatment groups were 105%, 115% and 163% of the control, respectively, with the highest SC content observed in culture containing 7 μM UIZ ($P < 0.05$, Figure 11A). The SP contents in the 3, 5, and 7 μM UIZ groups were 124%, 179%, and 276.2% of the control, respectively. The SP content was significantly affected by 5 and 7 μM UIZ treatment ($P < 0.05$, Figure 11B). As the concentration of UIZ was increased, the mannitol content was 59%, 65%, and 70% of the control. Exogenously added UIZ significantly reduced the mannitol content compared to that in the control group. However, there were no significant differences among the samples treated with different concentrations of UIZ. The most significant change in the mannitol content of *S. fusiforme* tissue culture-derived juveniles was observed under the treatment with 3 μM UIZ ($P < 0.05$, Figure 11C).

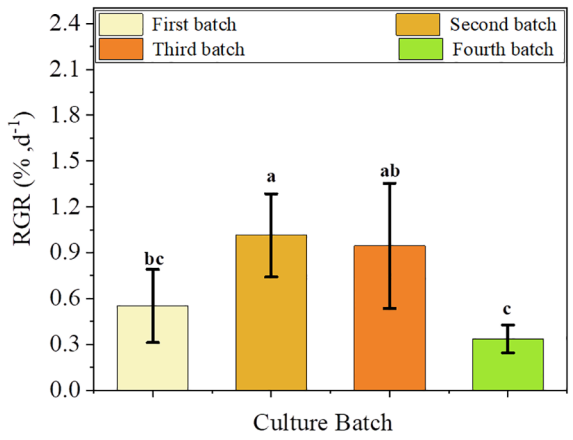

FIGURE 9
Effect of batch culture on changes in RGR of regenerated juveniles of *S. fusiforme*. Values are expressed as mean ± standard deviation (n = 3). Different letters indicate significant differences between different culture conditions ($p < 0.05$).

4 Discussion

We observed that the callus-like/adventitious bud induction rate and number of bud per explant varied widely among explants from different parts of *S. fusiforme* after tissue culture. The holdfasts and stems of *S. fusiforme* can serve as primary materials for tissue culture (Luo et al., 2023). Different parts of the stems were cultivated in groups, with adventitious buds more easily induced near the upper stem tip than near the stem base, possibly because *S. fusiforme* is polarized, similar to other macroalgae. Moreover, the holdfast structures of *S. fusiforme* contain a higher proportion of fibrous components in their cell walls, making them more resilient to high temperatures and nutrient-poor conditions (Endo et al., 2021). Finally, the regenerative capacity of the tissues may be related to their differentiation capacity. Tissues with low differentiation capacity often exhibit a higher regenerative capacity. Recovery from plant trauma may be influenced by key signaling factors involved in this process (Kavale et al., 2021; Liang et al., 2023). Thus, we showed that *S. fusiforme* filamentous holdfasts are the optimal material for

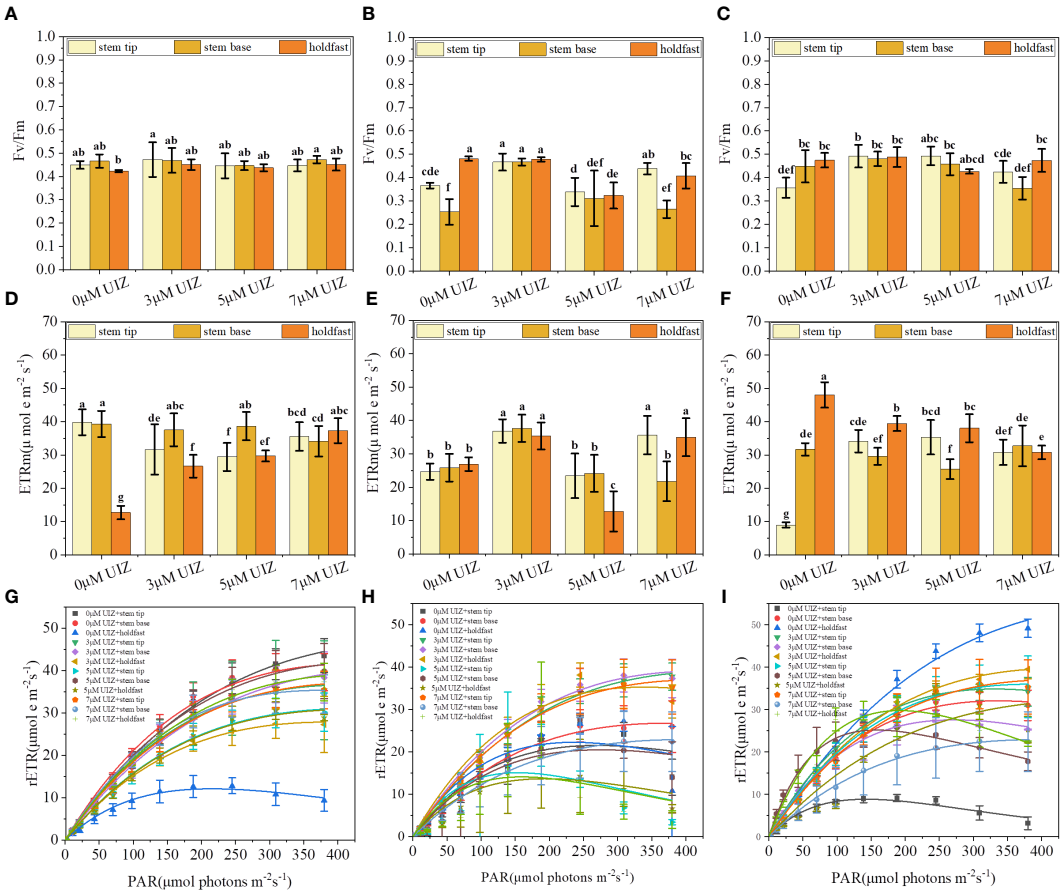

FIGURE 10
Effects of *S. fusiforme* explant parts and UIZ concentration on maximum quantum yield (Fv/Fm) and maximum electron transfer rate (rETRm) of PSII in batch culture. **(A–C)** Fv/Fm of batch 1, 2, and 4 cultures in batch culture; **(D–F)** rETRm of batch 1, 2, and 4 cultures in batch culture; **(G–I)** RLC of batch 1, 2, and 4 cultures in batch culture. Values are expressed as mean ± standard deviation (n = 3). Different letters indicate significant differences between different culture conditions ($p < 0.05$).

asexual propagation and that stem tips have a greater regenerative capacity than do previously grown stem bases.

The regenerating tissues of *S. fusiforme* can form bumps in the epidermal, cortical, and medullary tissue zones. The regeneration process occurs mainly in the outer epidermal pigmentation zone, leading to the growth of adventitious buds and callus-like tissues. Most *S. fusiforme* cell appeared as round or oval in the transverse view, and most cells of the nascent buds were smaller than those of the mature filamentous holdfasts; the medullary tissue area of mature tissues was located in the center, whereas the medullary tissue area of nascent buds regenerated and grew from the side. This may be because of the greater totipotency of plant cells that are more pigmented compared with that of cells that are less pigmented (Kumar et al., 2006; Lin et al., 2021). In addition, after trauma caused by segmentation, trauma-induced wound regeneration may occur when reactive oxygen species induce cellular reconstruction by triggering transduction of wound signals and regulating cell cycle proteins and related genes, leading to the spreading and division of cells inward from the edge of the wound, and finally inducing tissue regeneration (Guan et al., 2022).

We utilized staged culture to induce changes in temperature and culture condition in accordance with different time periods during algae growth state. For instance, *S. fusiforme* was first cultured in nutrient-rich solid medium at low temperature and light intensity to facilitate better germination and generation of adventitious buds. The explants were then transferred to liquid medium to provide sufficient light, space, and nutrient salts for rapid proliferation. During algal growth, the density of the culture and its light intensity influence subsequent growth, photosynthesis, and substance accumulation (Chen et al., 2019; Cao et al., 2022). Kavale et al. (2023) induced bud germination using staged temperature and light controls. Most studies have been limited to laboratory culture conditions or single investigations of large-scale valve cultures, without combining the two factors (Obando et al., 2022; Tirtawijaya et al., 2022). Culturing pre- and post-seedlings at different stages may enhance the efficiency and effectiveness of continuous algal culture.

PES medium was used as the basal medium with regulated components throughout the cultivation process. Solid medium was used to induce the formation of callus-like tissue/adventitious buds, and liquid medium was used to ensure rapid proliferation. The optimal conditions for culture of *S. fusiforme* explants callus-like/adventitious buds led to an induction rate of up to 100%, callus-like/adventitious bud numbers per explant of 27.43 ± 4.58, and RGR of up

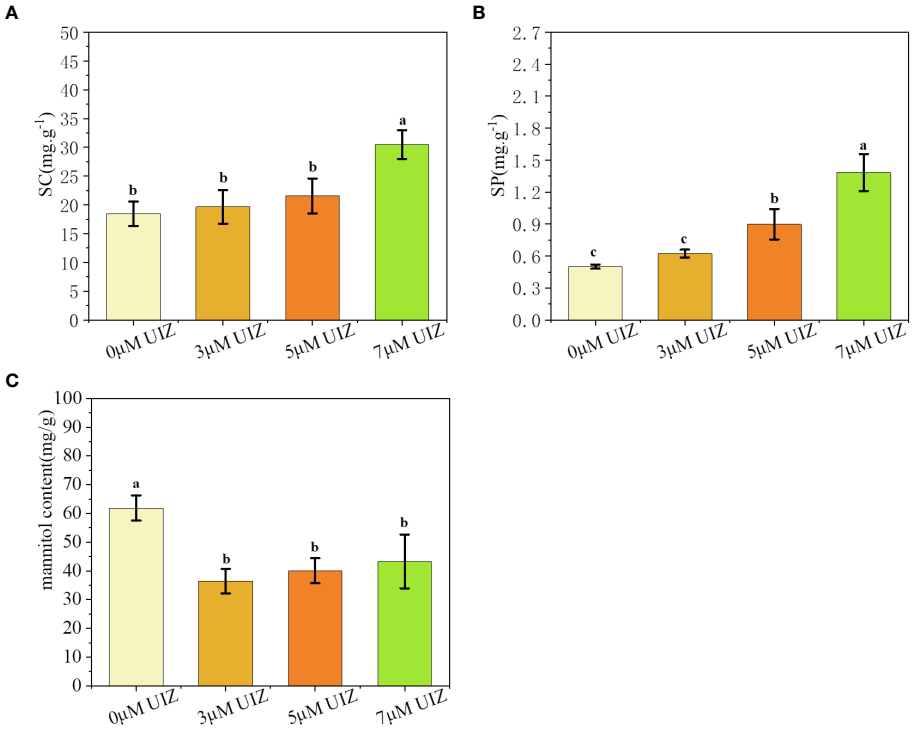

FIGURE 11
Effects of UIZ concentration on the content of soluble carbohydrates, soluble proteins, and mannitol in regenerated juveniles of *S. fusiforme*. **(A)** soluble carbohydrate content; **(B)** soluble protein content; **(C)** mannitol content. Values are expressed as mean ± standard deviation (n = 4). Different letters indicate significant differences between different culture conditions ($p < 0.05$).

to 3.05 ± 0.28. Thus, the concentration of the medium is critical. A nutrient concentration that is too high can lead to the formation of micro-organisms, weed algae, and other unwanted growth factors that compete with the desired algae. However, a nutrient concentration that is too low is not sufficient to support the daily growth and development of algae. Therefore, it is important to adjust the nutrient composition during the cultivation process to meet the needs of algae and promote optimal growth (Sampath-Wiley et al., 2008; Xu et al., 2022b). Previous studies showed that solid medium is more effective in inducing callus tissue formation, whereas liquid PES culture did not result in callus tissue formation (Li et al., 2015).

Endogenous plant hormones undergo dynamic regulation throughout the algal growth stages in response to various stimuli (Pang et al., 2023). External plant growth regulators are essential for achieving the desired effect; however, using regulator concentrations that are too high can be toxic to the plant and affect its future development, whereas concentrations that are too low will not produce the desired effect. UIZ is a plant growth retardant that is commonly used to preserve plant growth (Zhang et al., 2020; Lv et al., 2022). We demonstrated that appropriate concentrations of UIZ were beneficial for determining number of callus-like/adventitious buds per explant and induction rate of callus-like/adventitious buds. The highest induction rate was observed at lower concentrations in the short term. Low concentrations of UIZ had little retardation effect, allowing for rapid germination and sprouting. However, as the culture time increased, the plants adapted to a high concentration of UIZ, resulting in the sprouting and emergence of buds. High concentrations of foreign stimulants can delay or inhibit growth but may induce bud the formation (Carmo et al., 2020). The results demonstrate that explants treated with UIZ produced a significantly higher number of buds than did untreated seaweed. Uji et al. (2015) reported that UIZ treatment promoted germination, likely by regulating healing tissue proliferation and bud differentiation through modulation of endogenous auxin and abscisic acid levels. We found that the most suitable site for tissue culture was the filamentous holdfast, followed by the stem tip and stem base. The number of callus-like buds per explant greatly increased in the batch stage of culture, indicating that solid medium is favorable for inducing the germination of adventitious/adventitious buds and that liquid medium is favorable for the regeneration and proliferation of buds. Callus-like tissues can be induced when the stem tip is transferred to liquid culture conditions for a sufficient number of explants. Therefore, switching to liquid-culture conditions is recommended.

Furthermore, UIZ treatment impacted photosynthesis. Specifically, 3 μM UIZ had a significant effect on rETRm, and varying concentrations of UIZ resulted in an increase or decrease in its relative electron transfer rate. This may be because the UIZ regulates photosynthesis in *S. fusiforme* similarly to its effects in soybean and wheat. Excessive reactive oxygen species can be inhibited by controlling relevant photosynthetic genes, regulating photosynthetic antenna proteins, and enhancing the antioxidant capacity, ultimately leading to increased photosynthesis (Jiang et al., 2021; Hu et al., 2022; Yu et al., 2022).

Our results revealed that the concentration of UIZ was positively correlated with the SC and SP contents of *S. fusiforme*. These effects may be attributed to the ability of UIZ to enhance the antioxidant system and reduce mitochondrial damage, resulting in increased contents of SC and SP (Keshavarz and Khodabin, 2019; Zhou et al., 2021). The mannitol content in the UIZ-treated group was significantly lower than that in the control group. This effect decreased with increasing of UIZ concentrations, possibly because the low concentration of UIZ promoted the production of more adventitious buds, which consumed mannitol stored inside the alga. In contrast, high concentrations of UIZ had a growth slowing effect, which inhibited some regenerating buds. As a result, the mannitol content in the body was higher than that in the low concentration UIZ group.

5 Conclusion

Filamentous holdfasts of *S. fusiforme* can be used as primary sites for tissue culture. The stem tip, stem base and filamentous holdfasts of *S. fusiforme* were cultured in solid PES medium with 60 μmol photons·m^{-2} ·s^{-1} light at 19°C, salinity is 27–28‰, L:D = 12 h:12 h, and 3 μM UIZ added for at least 17 days of induction culture before culture in liquid PES medium with 90 μmol photons·m^{-2} ·s^{-1} light. This method can be used to regenerate *S. fusiforme* juveniles from tissue culture. Tissue cultures of the stem tip of *S. fusiforme* produce fine, dense air vesicles and secondary branches. Finally, UIZ significantly increased the number of callus-like/adventitious buds per explant of regenerated juveniles of *S. fusiforme*, and photosynthesis, SC, and SP. The results showed that this culture method was economical, easy to operate, and did not cause any damage to the ecosystem. Thus, the method can be used for tissue culture and germplasm expansion of *S. fusiforme* in industry.

Data availability statement

The raw data supporting the conclusions of this article will be made available by the authors, without undue reservation.

Author contributions

LG: Writing – original draft, Visualization, Software, Methodology, Investigation, Formal analysis, Data curation. GP: Writing – original draft, Methodology, Investigation. LL: Writing – original draft, Methodology, Investigation. CG: Writing – review & editing, Methodology, Investigation. BC: Writing – review & editing, Writing – original draft, Visualization, Supervision, Resources, Project administration, Methodology, Investigation, Funding acquisition, Conceptualization. ZM: Writing – review & editing, Supervision, Methodology.

Funding

The author(s) declare financial support was received for the research, authorship, and/or publication of this article. This work was supported by the Wenzhou Science and Technology Plan Project (No. N20220005), the National Key R&D Program of China (No. 2018YFD0901503), the Wenzhou Science and Technology Association project (No. kjfw0196), and the National Natural Science Foundation of China (No. 41706147 and 41876124).

Acknowledgments

The authors also would like to appreciate all staffs for their helpful assistance during the materials collection. In addition, we are very grateful to Prof. Mingjiang Wu of Wenzhou University, who had given us great help in the collection of materials, the provision of experimental projects and funding.

Conflict of interest

The authors declare that the research was conducted in the absence of any commercial or financial relationships that could be construed as a potential conflict of interest.

Publisher's note

References

Aghaei, F., Seyed Sharifi, R., and Narimani, H. S. (2021). Effects of uniconazole and biofertilizers application on yield and some biochemical characteristics of wheat under soil salinity stress. *Environ. Stresses. Crop Sci.* 14, 487–499. doi: 10.22077/escs.2020.2810.1730

Akremi, N., Cappoen, D., Anthonissen, R., Verschaeve, L., and Bouraoui, A. (2017). Phytochemical and in *vitro* antimicrobial and genotoxic activity in the brown algae *Dictyopteris membranacea*. *S. Afr. J. Bot.* 108, 308–314. doi: 10.1016/j.sajb.2016.08.009

Ali, O., Ramsubhag, A., and Jayaraman, J. (2021). Biostimulant properties of seaweed extracts in plants: implications towards sustainable crop production. *Plants (Basel)* 10, 531. doi: 10.3390/plants10030531

Arbaiza, S., Avila-Peltroche, J., Castaneda-Franco, M., Mires-Reyes, A., Advincula, O., and Baltazar, P. (2023). Vegetative Propagation of the Commercial Red Seaweed *Chondracanthus chamissoi* in Peru by Secondary Attachment Disc during Indoor Cultivation. *Plants (Basel)* 12, 1940. doi: 10.3390/plants12101940

Avila-Peltroche, J., Won, B. Y., and Cho, T. O. (2022). An improved protocol for protoplast production, culture, and whole plant regeneration of the commercial brown seaweed *Undaria pinnatifida*. *Algal Res.* 67, 102851. doi: 10.1016/j.algal.2022.102851

Baweja, P., Sahoo, D., Garco,/j.algal, P., and Robaina, R. R. (2009). Review: Seaweed tissue culture as applied to biotechnology: Problems, achievements and prospects. *Phycol Res.* 57, 45–58. doi: 10.1111/j.1440-1835.2008.00520.x

Bradford, M. M. (1976). A rapid and sensitive method for the quantitation of microgram quantities of protein utilizing the principle of protein-dye binding. *Anal. Biochem.* 72, 248–254. doi: 10.1016/0003-2697(76)90527-3

Cao, C., Zhang, T., Wu, M., Chen, B., and Ma, Z. (2022). Differential growth and physiological responses of *Sargassum fusiforme* and epiphytic *Ulva lactuca* to culture densities and interspecific competition. *Reg. Stud. Mar. Sci.* 56, 102671. doi: 10.1016/j.rsma.2022.102671

Carmo, L. P., Moura, C. W. N., and Lima-Brito, A. (2020). Red macroalgae extracts affect in *vitro* growth and bud formation in *Comanthera mucugensis* (Giul.) L. R. Parra & Giul., an endemic dry flower species from the Chapada Diamantina (Brazil). *S. Afr. J. Bot.* 135, 29–34. doi: 10.1016/j.sajb.2020.07.033

Chen, B., and Zou, D. (2014). Growth and photosynthetic activity of *Sargassum henslowianum*(Fucales, Phaeophyta) seedlings in responses to different light intensities, temperatures and CO_2 levels under laboratory conditions. *Mar. Biol. Res.* 10, 1019–1026. doi: 10.1080/17451000.2013.872798

Chen, B., Zou, D., Ma, Z., Yu, P., and Wu, M. (2019). Effects of light intensity on the photosynthetic responses of *Sargassum fusiforme* seedlings to future CO_2 rising. *Aquac Res.* 50, 116–125. doi: 10.1111/are.13873

Chen, M., Zhang, W., Wu, H., Guang, C., and Mu, W. (2020). Mannitol: physiological functionalities, determination methods, biotechnological production, and applications. *Appl. Microbiol. Biotechnol.* 104, 6941–6951. doi: 10.1007/s00253-020-10757-y

Collins, N., Kumar Mediboyina, M., Cerca, M., Vance, C., and Murphy, F. (2022). Economic and environmental sustainability analysis of seaweed farming: Monetizing carbon offsets of a brown algae cultivation system in Ireland. *Bioresour Technol.* 346, 126637. doi: 10.1016/j.biortech.2021.126637

Custodio, L., Charles, G., Magne, C., Barba-Espin, G., Piqueras, A., Hernandez, J. A., et al. (2022). Application of *in vitro* plant tissue culture techniques to halophyte species: A review. *Plants (Basel)* 12, 126. doi: 10.3390/plants12010126

de Araújo Amatuzzi, J. C., do Nascimento Vieira, L., Sant'Anna-Santos, B. F., Noseda, M. D., and Pacheco de Freitas Fraga, H. (2020). Improved in *vitro* development of *Epidendrum secundum* (Orchidaceae) by using aqueous extract of the seaweed *Kappaphycus alvarezii* (Rhodophyta, Solieriaceae). *Acta Physiol. Plant* 42, 1–9. doi: 10.1007/s11738-020-03129-6

Eggertsen, M., and Halling, C. (2021). Knowledge gaps and management recommendations for future paths of sustainable seaweed farming in the Western Indian Ocean. *Ambio* 50, 60–73. doi: 10.1007/s13280-020-01319-7

Endo, H., Sugie, T., Yonemori, Y., Nishikido, Y., Moriyama, H., Ito, R., et al. (2021). Vegetative reproduction is more advantageous than sexual reproduction in a canopy-forming clonal macroalga under ocean warming accompanied by oligotrophication and intensive herbivory. *Plants (Basel)* 10, 1522. doi: 10.3390/plants10081522

Ershadi, A., Karimi, R., and Mahdei, K. N. (2015). Freezing tolerance and its relationship with soluble carbohydrates, proline and water content in 12 grapevine cultivars. *Acta Physiol. Plant* 38, 1–10. doi: 10.1007/s11738-015-2021-6

Garcia-Poza, S., Leandro, A., Cotas, C., Cotas, J., Marques, J. C., Pereira, L., et al. (2020). The evolution road of seaweed aquaculture: cultivation technologies and the industry 4.0. *Int. J. Environ. Res. Public Health* 17, 6528. doi: 10.3390/ijerph17186528

Guan, X., Mao, Y., Stiller, J. W., Shu, S., Pang, Y., Qu, W., et al. (2022). Comparative gene expression and physiological analyses reveal molecular mechanisms in wound-induced spore formation in the edible seaweed nori. *Front. Plant Sci.* 13. doi: 10.3389/fpls.2022.840439

Hu, H., Feng, N., Shen, X., Zhao, L., and Zheng, D. (2022). Transcriptomic analysis of *Vigna radiata* in response to chilling stress and uniconazole application. *BMC Genomics* 23, 205. doi: 10.1186/s12864-022-08443-6

Hwang, E. K., Choi, H. G., and Kim, J. K. J. B. M. (2020). Seaweed resources of korea. *Bot. Mar.* 63, 395–405. doi: 10.1515/bot-2020-0007/html

Jiang, Y., Sun, Y., Zheng, D., Han, C., Cao, K., Xu, L., et al. (2021). Physiological and transcriptome analyses for assessing the effects of exogenous uniconazole on drought tolerance in hemp (*Cannabis sativa* L.). *Sci. Rep.* 11, 14476. doi: 10.1038/s41598-021-93820-6

Jiksing, C., Ongkudon, M. M., Thien, V. Y., Rodrigues, K. F., and Yong, W. T. L. (2022). Recent advances in seaweed seedling production: a review of eucheumatoids and other valuable seaweeds. *Algae* 37, 105–121. doi: 10.4490/algae.2022.37.5.11

Kavale, M. G., Alexander, H. J., Malarvizhi, J., Manivannan, M., and Ram, S. (2021). Short note: Preliminary observations on the propagule production of *Sargassum polycystum* C. Agardh from stoloniferous branches. *Aquaculture* 534, 736322. doi: 10.1016/j.aquaculture.2020.736322

Kavale, M. G., Largo, D. B., de la Torre, E. O., Baritugo, A. T., and Azcuna-Montaño, M. (2023). Plantlets directly developed from secondary phyllodes of *Sargassum siliquosum* J. Agardh: Implication for seedling production during the off-reproductive season. *Aquaculture* 563, 738977. doi: 10.1016/j.aquaculture.2022.738977

Kelly, E. L. A., Cannon, A. L., and Smith, J. E. (2020). Environmental impacts and implications of tropical carrageenophyte seaweed farming. *Conserv. Biol.* 34, 326–337. doi: 10.1111/cobi.13462

Kerrison, P. D., Le, H. N., and Hughes, A. D. (2015). Hatchery decontamination of *Sargassum muticum* juveniles and adults using a combination of sodium hypochlorite and potassium iodide. *J. Appl. Phycol* 28, 1169–1180. doi: 10.1007/s10811-015-0672-8

Keshavarz, H., and Khodabin, G. (2019). The role of uniconazole in improving physiological and biochemical attributes of bean (*Phaseolus vulgaris* L.) subjected to drought stress. *J. Crop Sci. Biotechnol.* 22, 161–168. doi: 10.1007/s12892-019-0050-0

Kumar, G. R., Reddy, C. R. K., and Jha, B. (2006). Callus induction and thallus regeneration from callus of phycocolloid yielding seaweeds from the Indian coast. *J. Appl. Phycol* 19, 15–25. doi: 10.1007/s10811-006-9104-0

Largo, D. B., Rance, G. M. S., Diola, A. G., and Aaron-Amper, J. (2020). Method for the mass production of seedlings of the tropical brown seaweed *Sargassum* (Phaeophyceae, Ochrophyta). *MethodsX* 7, 100854. doi: 10.1016/j.mex.2020.100854

Li, H., Liu, J., and pang, T. (2015). Callus induction and morphogenesis of callus in *Kappaphycus alvarezii* (Rhodophyta, Solieriaceae). *Haiyang Xuebao* 37, 52–61. doi: 10.3969/j.issn.0253-4193.2015.04.005

Liang, Y., Heyman, J., Lu, R., and De Veylder, L. (2023). Evolution of wound-activated regeneration pathways in the plant kingdom. *Eur. J. Cell. Biol.* 102, 151291. doi: 10.1016/j.ejcb.2023.151291

Lin, L., Ma, Z., Chen, B., and Wu, M. (2021). Analysis of physiological and ecological functions to mature sporophyte of cultivation *Sargassun fusiforme* based on its organ morphilogical structure. *Oceanol. Limnol. Sin.* 52, 1047–1057. doi: 10.11693/hyhz20210100008

Luo, L., Zuo, X., Guo, L., Pang, G., Ma, Z., Wu, M., et al. (2023). Effects of exogenous hormones on the regeneration of juveniles from *Sargassum fusiforme* holdfasts. *Front. Mar. Sci.* 9. doi: 10.3389/fmars.2022.1072391

Lv, R., Zhang, W., Xie, X., Wang, Q., Gao, K., Zeng, Y., et al. (2022). Foliar application uniconazole enhanced lodging resistance of high-quality indica rice (*Oryza sativa* L.) by altering anatomical traits, cell structure and endogenous hormones. *Field Crop Res.* 277, 108425. doi: 10.1016/j.fcr.2021.108425

Mantri, V. A., Veeragurunthan, V., Sambhwani, K., and Anisoddin Kazi, M. (2022). Concise review of industrially important red seaweed *Gracilaria dura* (C. Agardh) J. Agardh. *J. Appl. Phycol* 34, 1825–1841. doi: 10.1007/s10811-022-02755-6

Muhamad, S. N. S., Ling, A. P.-K., and Wong, C.-L. (2018). Effect of plant growth regulators on direct regeneration and callus induction from *Sargassum polycystum* C. Agardh. *J. Appl. Phycol* 30, 3299–3310. doi: 10.1007/s10811-018-1649-1

Obando, J. M. C., dos Santos, T. C., Martins, R. C. C., Teixeira, V. L., Barbarino, E., and Cavalcanti, D. N. (2022). Current and promising applications of seaweed culture in laboratory conditions. *Aquaculture* 560, 738596. doi: 10.1016/j.aquaculture.2022.738596

Pang, G., Luo, L., Guo, L., Gao, C., Sheng, X., Ma, Z., et al. (2023). Temporal and spatial changes of major endogenous phytohormones during the regeneration of juveniles from *Sargassum fusiforme* holdfasts. *J. Appl. Phycol.* 35, 2995–3006. doi: 10.1007/s10811-023-03113-w

Platt, T., Gallegos, C., and Harrison, W. G. (1980). Photoinhibition of photosynthesis in natural assemblages of marine phytoplankton. *J. Mar. Res.* 38, 687–701. doi: 10.1093/pasj/57.2.341

Rademacher, W. (2015). Plant growth regulators: backgrounds and uses in plant production. *J. Plant Growth Regul.* 34, 845–872. doi: 10.1007/s00344-015-9541-6

Sampath-Wiley, P., Neefus, C. D., and Jahnke, L. S. (2008). Seasonal effects of sun exposure and emersion on intertidal seaweed physiology: Fluctuations in antioxidant contents, photosynthetic pigments and photosynthetic efficiency in the red alga *Porphyra umbilicalis* Kützing (Rhodophyta, Bangiales). *J. Exp. Mar. Biol. Ecol.* 361, 83–91. doi: 10.1016/j.jembe.2008.05.001

Tian, S., Chen, B., Wu, M., Cao, C., Gu, Z., Zheng, T., et al. (2023). Are there environmental benefits derived from coastal aquaculture of *Sargassum fusiforme*? *Aquaculture* 563, 738909. doi: 10.1016/j.aquaculture.2022.738909

Tirtawijaya, G., Negara, B. F. S. P., Lee, J.-H., Cho, M.-G., Kim, H. K., Choi, Y.-S., et al. (2022). The influence of abiotic factors on the induction of seaweed callus. *J. Mar. Sci. Eng.* 10, 513. doi: 10.3390/jmse10040513

Uji, T., Nanaumi, D., Kawagoe, C., Saga, N., and Miyashita, K. (2015). Factors influencing the induction of adventitious bud and callus in the brown alga *Sargassum horneri* (Turner) C. Agardh. *J. Appl. Phycol* 28, 2435–2443. doi: 10.1007/s10811-015-0745-8

White, L. N., and White, W. L. (2020). Seaweed utilisation in New Zealand. *Bot. Mar.* 63, 303–313. doi: 10.1515/bot-2019-0089

Xu, L., Lin, L., Luo, L., Zuo, X., Cao, C., Jin, X., et al. (2022a). Organic acid treatment for removal of epiphytic Ulva L. attached to *Sargassum fusiforme* seedlings. *Aquaculture* 547, 737533. doi: 10.1016/j.aquaculture.2021.737533

Xu, L., Luo, L., Zuo, X., Cao, C., Lin, L., Zheng, H., et al. (2022b). Effects of temperature and irradiance on the regeneration of juveniles from the holdfasts of *Sargassum fusiforme*, a commercial seaweed. *Aquaculture* 557, 738317. doi: 10.1016/j.aquaculture.2022.738317

Yan, K., Du, X., and Mao, B. (2022). Production of virus-free chrysanthemum (*Chrysanthemum morifolium* ramat) by tissue culture techniques. *Methods Mol. Biol.* 2400, 171–186. doi: 10.1007/978-1-0716-1835-6_17

Yong, Y. S., Yong, W. T. L., Thien, V. Y., Ng, S. E., Anton, A., and Yassir, S. (2014). Acclimatization of micropropagated *Kappaphycus alvarezii* (Doty) Doty ex Silva (Rhodophyta, Solieriaceae) in outdoor nursery system. *J. Appl. Phycol* 27, 413–419. doi: 10.1007/s10811-014-0289-3

Yu, M., Huang, L., Feng, N., Zheng, D., and Zhao, J. (2022). Exogenous uniconazole enhances tolerance to chilling stress in mung beans (*Vigna radiata* L.) through cross talk among photosynthesis, antioxidant system, sucrose metabolism, and hormones. *J. Plant Physiol.* 276, 153772. doi: 10.1016/j.jplph.2022.153772

Zhang, M., Yang, J., Pan, H., and Pearson, B. J. (2020). Dwarfing effects of chlormequat chloride and uniconazole on potted baby primrose. *HortTechnology* 30, 536–543. doi: 10.21273/HORTTECH04646-20

Zhou, H., Liang, X., Feng, N., Zheng, D., and Qi, D. (2021). Effect of uniconazole to soybean seed priming treatment under drought stress at VC stage. *Ecotoxicol Environ. Saf.* 224, 112619. doi: 10.1016/j.ecoenv.2021.112619

frontiers | Frontiers in Marine Science

TYPE Brief Research Report
PUBLISHED 10 May 2024
DOI 10.3389/fmars.2024.1379066

OPEN ACCESS

EDITED BY
Yngvar Olsen,
NTNU, Norway

REVIEWED BY
Ye Yuan,
Shantou University, China
Yang Jin,
Johns Hopkins University, United States
Keshuai Li,
BioMar, Norway

*CORRESPONDENCE
Ian Carr
ian.carr@veramaris.com

RECEIVED 30 January 2024
ACCEPTED 26 April 2024
PUBLISHED 10 May 2024

CITATION
Carr I, Santigosa E, Chen T and Costantino J (2024) Optimum eicosapentaenoic acid + docosahexaenoic acid levels for farmed Atlantic salmon: closing the gap between science and commercial practice. *Front. Mar. Sci.* 11:1379066. doi: 10.3389/fmars.2024.1379066

Optimum eicosapentaenoic acid + docosahexaenoic acid levels for farmed Atlantic salmon: closing the gap between science and commercial practice

Ian Carr[1]*, Ester Santigosa[2], Tony Chen[3] and John Costantino[3]

[1]Veramaris V.O.F., Delft, Netherlands, [2]DSM-Firmenich AG, Kaiseraugst, Switzerland, [3]Manolin AS., Bergen, Norway

The shift from fish oil to vegetable oil (VO) sources has lowered eicosapentaenoic acid (EPA) and docosahexaenoic acid (DHA) levels in salmon aquafeeds. VOs are high in omega-6 and low in omega-3 essential fatty acids like EPA and DHA, crucial for fish metabolism and immunity. Algal oil (AO), with high EPA + DHA and lower omega-6 levels supports fish health and growth, but transferring lab-controlled conditions to real-world commercial farming remains a challenge. This study explored the benefits of high dietary EPA + DHA levels through a commercial farm (CF) study in Chile and a Big Data (BD) study in Norway. The CF study, involving 625,000 Atlantic salmon, compared standard feed with AO-supplemented feed. The latter resulted in improved health responses and better fillet quality. The BD study analyzed real data from 232.6 million fish, revealing that EPA + DHA levels > 8% reduce mortality variability by 21%, improve economic feed conversion ratio by 11%, and increase the likelihood of superior harvests by 27%, demonstrating productivity benefits. Both studies emphasize the advantages of feeds with EPA + DHA levels above typical industry practices, enhancing growth, health, and nutritional quality. Importantly, the BD study complements the CF study, bridging the gap between science and aquafarms, and providing evidence that diets with EPA + DHA > 8% offer biological performance benefits for farmers, regardless of farming environments.

KEYWORDS

Atlantic salmon, EPA, DHA, omega-3, commercial trial, big data, quality, health

1 Introduction

The production and market value of aquatic foods have been achieving all-time records driven mainly by the increased demand for such products, which are recognized as essential to global food security and nutrition (FAO, 2022). However, to sustain this growth, operators must encompass changes in farming practices, from feed ingredients' source

selection to management and investment policies, without compromising the farm productivity and business sustainability, which ultimately depend upon fish zootechnical and health performance. For instance, increasing the level of vegetable oils (VOs) in aquafeeds for the partial or total replacement of fish oil (FO) has helped to grow aquaculture production without increasing pressure on marine stocks but has negatively impacted the health and wellbeing of fish by leading to unbalanced essential fatty acid (EFA) profiles (Sprague et al., 2016; Roques et al., 2020). This is because VOs have particularly high content of omega-6 EFAs and relatively low content of omega-3 EFAs, such as eicosapentaenoic acid (EPA) and docosahexaenoic acid (DHA), both playing key metabolic and immune roles in fish (Tocher, 2015).

To tackle this issue, few studies have lately focused on better understanding the EPA and DHA requirements of farmed fish species at the different production stages, to which levels should EPA and DHA be increased, and how to supply nutrients using alternative sources such as genetically modified seed oil, algae biomasses, and algal oil (AO). The latter has received particular attention because it contains a combination of EPA, DHA, and arachidonic acid, low levels of omega-6 EFAs, improved food safety, is easy to incorporate in aquafeed formulations, and supports optimal fish health and growth (Santigosa et al., 2023). Inclusion of AO as a source of omega-3 EFAs also helps reducing the marine footprint of the feed, as indicated by a lower forage fish dependency ratio (FFDR). The added value of AO on providing high levels of EPA + DHA, as well as on maintaining the ratio of these omega-3 EFAs (the *optimum omega nutrition* concept), includes better health and welfare and better fillet quality, which has been extensively documented for Atlantic salmon in scientific lab-scale trials (Santigosa et al., 2018, 2020, 2023). Fillet quality has further repercussions in human health because Atlantic salmon is considered the most valuable source of EPA and DHA for humans (Horn et al., 2019; Carr et al., 2023; Santigosa et al., 2023) and low EPA+DHA levels lead to low fish fillet quality (Oliva-Teles et al., 2015). Indeed, recent studies have shown that the EPA + DHA levels of commercialized Atlantic salmon fillets have been reduced by more than half in recent decades (Sprague et al., 2016, 2020).

However, transferring the science-backed knowledge from the lab to commercial farms has been challenging primarily due to the difficulty in recreating all risks and variables fish are exposed to in the commercial farm environment, although the costs of farm trials and business priorities also play an important role. All these factors hinder farmers' identification of a solid business case for changing EPA + DHA specifications in the feed they provide to their fish, as well as the business case for the feed industry to alter the sources and/or levels of EPA + DHA, particularly if this represents an extra cost. Moreover, commercial-scale studies are often performed on a single farm and using few cages, and significant differences between cages can arise due to many factors, including disease outbreaks. This was the case for a large commercial-scale study on the effects of reducing long-chain fatty acid levels in Atlantic salmon feed, where a pancreatic disease outbreak arose (Sissener et al., 2016) or the 15-month-long study evaluating the effect of increasing dietary levels of EPA + DHA up to 3.5% on the growth, welfare, and fillet quality of Atlantic salmon in sea cages, where a cardiomyopathy syndrome outbreak arose (Lutfi et al., 2022). Such challenges do not allow to attribute the differences found between group growth and health performances, if any, to the levels and ratios of EPA + DHA provided nor the generalization of the results to other farms and/or fish species. Furthermore, results are challenged by farmers as the trial conditions do not match that of their farms.

Big data (BD) is a relatively new approach that retrieves patterns and trend values from large datasets through advanced software programs (Sadiku et al., 2020). The use of BD in research papers on food science has grown by nearly 300% every five years since 2010 (Tao et al., 2021), and it may also help narrow the *lab-to-commercial-scale gap* in aquaculture. By aggregating real production data from many farms and extracting information related to feed composition and fish growth performance, health, and nutritional value, BD can find relationships between these variables that may then be used to confirm the effects observed at lab or single-farm scales.

In the present paper, we aim to highlight how providing below or above-average EPA + DHA levels can impact Atlantic salmon growth, health, and nutritional quality. The results presented here showcase two trials, one performed at a commercial scale and another using the BD approach, to ultimately demonstrate how the aquaculture industry can quantify the benefits of providing optimal levels and ratios of EPA + DHA to farmed Atlantic salmon.

2 Methods

To demonstrate the benefits of adequate EPA + DHA levels in farmed Atlantic salmon, the authors took two approaches. The methods used for each are described below.

2.1 Commercial farm study

For the CF study, a trial was conducted by Veramaris® (Delft, The Netherlands) in collaboration with Skretting (Stavanger, Norway) at a commercial salmon farm site in Chile's Region XII. In this study, 208,000 Atlantic salmon (Control fish; initial body weight, IBW, ~3.0 kg)) were allocated to three cages and fed a Skretting Atlantic salmon feed (crude protein: 38.8 ± 0.14; crude lipid: 36.9 ± 0.28). In addition, 417,000 Atlantic salmon were allocated to six cages and fed a Skretting Atlantic salmon feed supplemented with Veramaris AO [OON fish; IBW, ~3.0 kg; (crude protein: 38.1 ± 0.14; crude lipid: 37.1 ± 0.78)]. Full fatty acid profile of the diets can be found in Supplementary Table 1. Commercial diet formulations cannot be disclosed. All efforts were made to minimize unintended variations between the diets.

Both Control and OON fish were fed for 114 days (June to October). Control and OON diets differed in their EPA+DHA content (6% and 10%, respectively) and EPA: DHA ratio (>1.5:1 and 1:1, respectively), achieved with the inclusion of the AO in the feed formulation.

At the end of the feeding period, biological and economic feed conversion ratios (bFCR and eFCR, respectively) were calculated to

evaluate growth performance. Health and welfare responses, as well as the status of the mucosal barriers of gills, skin, and gut were sampled and determined for Control and OON fish sampled in June and October (n = 90 samples), and processed through an automated software developed by Quantidoc AS (https://www.quantidoc.no; n = 1452 relevant points at the time of analysis) for the stereological image analysis of the mucosa (Veribarr™). For the Quantidoc analysis, all samples of OON fish came from the same cage at the end of the trial. Fillets' nutritional and physical quality were evaluated by calculating the total level of EPA + DHA per 100 grams of fillet (SGS SA, Chile) based on the Official Method 991.39 (AOAC, 2012) and the percentage of fish scoring 24 or above on the SalmoFan™ color measurement scale (dsm-firmenich AG, Kaiseraugst, Switzerland), respectively. The marine footprint was evaluated based on the forage fish dependency ratio for fish oil (FFDRoil), calculated following the ASC Salmon Standard (https://www.asc-aqua.org/).

The experimental unit for all endpoints was the cage. Differences across group means were investigated with a t-stest for pairwise comparisons (JMP 17.0 software; https://www.jmp.com). The accepted significance level was $p < 0.05$. Means in tabulated data are given with standard deviations, SD.

2.2 Big data study

In the BD study, conducted by Veramaris and Manolin AS. (Bergen, Norway), the performance outcomes of utilizing feeds at three different EPA + DHA levels (< 7%, 7%–8%, and > 8%; Table 1) were evaluated based on real production data. The authors focused on mapping the variations in EPA+ DHA levels between categories. Other possible variations in dietary composition have not been taken into consideration and this is a potential limitation of the study. Feed products provided to 232.6 million smolts in 99 active Atlantic salmon farms along the Norwegian coastline between 2013 and 2022 were tagged with their batch-specific median EPA + DHA levels, which were then averaged per generation. This allowed distinguishing the three categories of EPA+DHA inclusion used in the study (Above Average, Average, and Below Average; Table 1) and the number of generations to which they were provided (Table 1). Atlantic salmon mortality (%), eFCR, and superior harvest quality (%) were then calculated for each category.

A One-Way ANOVA test was utilized to see if the differences between the groups were significant. SciPy Statistical Library (https://scipy.org; BD study) was used. Values displayed are group means ± standard deviation (SD).

TABLE 1 The three categories considered in this study, their corresponding EPA + DHA levels, and the total number of generations to which they were provided.

EPA + DHA category	EPA + DHA level	Total generations
Above Average	> 8.0%	79
Average	7.0%–8.0%	110
Below Average	< 7.0%	75

3 Results

3.1 Commercial farm study

Results indicated that fish gained 1.5 kg on average, corresponding to a 50% weight gain irrespective of treatment. This was below the expected 100% weight gain at this production stage, but the feeding period was 114 days (due to operational reasons) instead of the planned 184 days grow-out period. Although bFCR and eFCR were slightly higher for OON fish than for Control fish, the variability within the OON group was much higher than that within the Control group (Figure 1A). This was maybe due to predators on the OON cages, a factor that was not controlled for. Nevertheless, statistical testing revealed no significant differences between the two treatments.

At the beginning of the trial, the gill mucosa of fish in both groups (Figure 1B) were similar but much higher than that of wild adult Atlantic salmon gill cells (marked with X), indicating the activation of an immune response and therefore some degree of activated mucosal protection in the farmed fish. Throughout the trial, a slight improvement in OON fish compared to Control fish was observed, as both the activity and size of mucous cells clearly increased in Control fish throughout the trial but increased only slightly in OON fish. As a result, Control fish distanced more from the common, central zone (green circle) and moved into the red zone (vulnerable or responding), while OON fish remained in the amber zone of the database. This effect was particularly evident in the gills and foregut but not in the skin. In general, skin mucosa has a healthy shield from plentiful mucous cells, whereas gills in healthy circumstances have very few and small mucous cells thus granting easy passage of gasses through the lamellae.

At the beginning of the trial, the EPA + DHA level in 100 g of Atlantic salmon fillet was 0.80 g in Control fish and 0.75 g in OON fish; however, at end of the trial, the nutritional quality of Atlantic salmon fillets was significantly higher in OON fish than in Control fish (Figure 2A) as the EPA + DHA level almost doubled. This increase was even more meaningful as the feeding trial lasted only 114 days instead of the planned 184 days, i.e., the entire grow-out period. Regarding fillet physical quality, 27% more fish scored at least 24 in the SalmoFan color measurement scale in the OON group than in the control group (Figure 2B), indicating an improvement in pigmentation. Notably, these results were obtained using a feed with a higher total level of EPA + DHA (10% in OON vs. 6% in control) but with only a slightly higher FFDRoil (1.75 in OON and 1.68 in control), i.e., without any substantial increase in the marine footprint.

3.2 Big data study

In the BD study, the three EPA + DHA categories (i.e., groups) showed high variability (large SD) in mortality (Figure 3A), eFCR

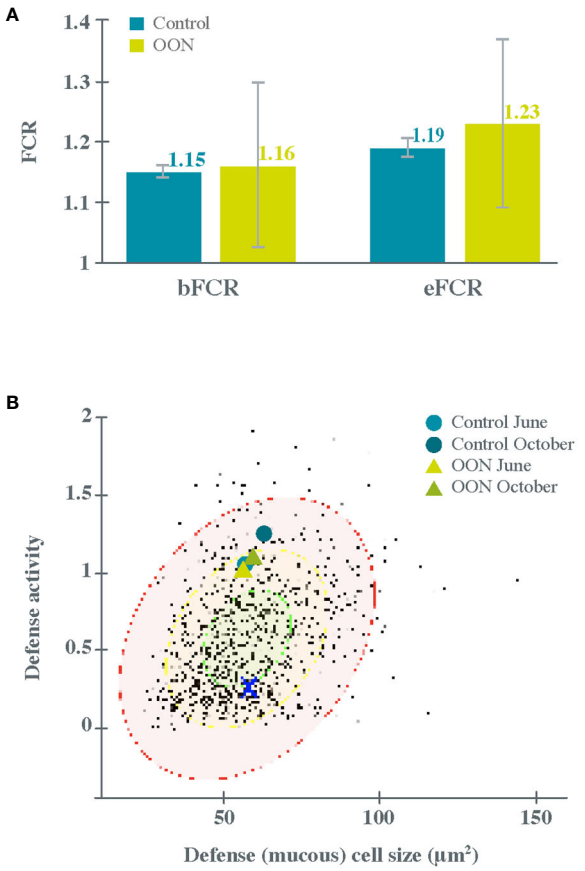

FIGURE 1
Growth **(A)** and health **(B)** performance of Atlantic salmon fed on the control and algal oil-supplemented diets (Control and OON groups, respectively). **(A)** The biological and economic feed conversion ratio (bFCR and eFCR) calculated for fish in both groups at the end of the trial is shown. Values indicated on each bar correspond to group means and the error bars to standard deviation. **(B)** Comparison of Atlantic salmon gill lamellar mucosal measures of mean mucous cell size and mean defense activity (including volumetric density) versus the Quantidoc database of the saltwater subset of salmon gill values in sea-based cages, recirculating water systems, and saltwater flow through systems (n =1452). Triangles = OON diet, circles = Control diet. X = mean for seven wild adult salmon. Green ellipse [30% confidence interval (CI)] is common for farmed salmon, yellow ellipse (70% CI) indicates transition to vulnerability or responding to threat, and red ellipse (95% CI) indicates active response to challenge or exhaustion; white area = 5% CI. Gills of healthy salmon have small and few mucous cells and increases in mucous cell size and abundance indicate a response to stress, water quality, particles, and pathogens.

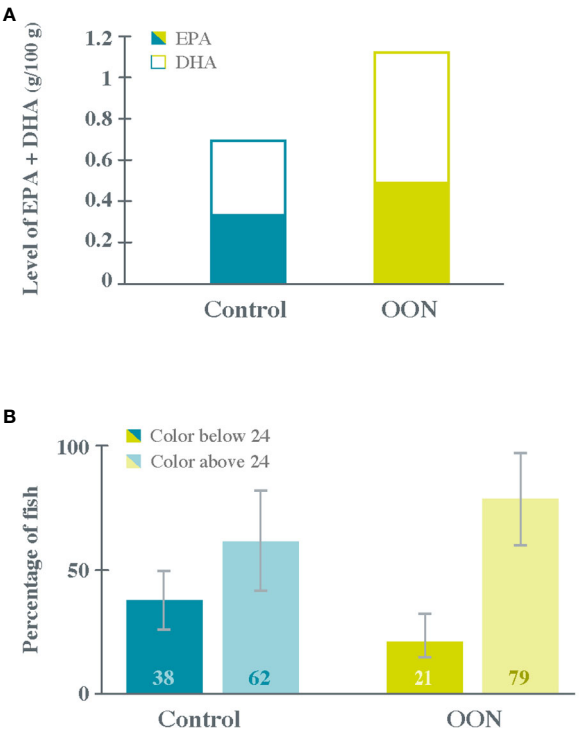

FIGURE 2
Nutritional **(A)** and physical **(B)** quality of Atlantic salmon fillets at the end of the commercial farm trial for fish fed on the control and algal oil-supplemented diets (Control and OON groups, respectively). Nutritional quality was measured as the level of EPA + DHA (g/100 g of fillet) and physical quality as the percentage of fish scoring at least 24 in the SalmoFan™ color measurement scale.

(Figure 3B), and superior harvest quality (Figure 3C). However, this variability was always smaller in the group with Above Average EPA + DHA level. The same trend was found for the interquartile range, indicating a higher predictability of the results obtained when providing EPA + DHA levels > 8%. Furthermore, this group showed the lowest mean mortality and eFCR and the highest mean superior harvest quality. Although the mortality mean was < 20% in all three groups, and no statistical differences were found among them, the interquartile range for the Above Average group was about half of that observed for the Below Average group (Figure 3A). Significant improvements were found in the eFCR and superior harvest quality of the Above Average group, with mean values decreasing to 1.29 and increasing to 90%, respectively (Figures 3B, C).

In summary, the BD study revealed several important insights that can help feed managers to quantify the benefits of higher EPA + DHA levels in farmed Atlantic salmon diets. A key finding was that generations of fish supplied with EPA + DHA levels > 8% showed 21% less variability in the total mortality and an 11% improvement in the eFCR. For farmers, this translated into a 27% higher chance of obtaining a superior harvest quality higher than 90%. Overall, these results allow Atlantic salmon farmers to quantify the benefits of adding higher levels of EPA + DHA to their feed as an improved return on investment (ROI) without a major risk, as the effects observed in this study reflect real data from millions of fish.

4 Discussion

The aquaculture industry is currently facing the important challenge of increasing production, growth rates, and nutritional quality, without compromising fish health and welfare or increasing its environmental impact, thereby ultimately improving the industry's productivity and sustainability. However, salmon feed formulations have changed considerably due to the limited availability of traditionally used marine ingredients, their high costs, and high environmental impact of exploiting such sources. Fish oil in Atlantic salmon feeds has been progressively replaced with vegetable alternatives, mostly rapeseed oil (20.1%) (Aas et al.,

FIGURE 3
Mortality (%, **A**), economic feed conversion ratio (eFCR, **B**), and superior harvest percentage (%, **C**) in the three EPA + DHA categories (groups) examined in the present study, based on data obtained from 291 Atlantic salmon generations between 2013 and 2022 in 99 farms along the Norwegian coast.

2022). This transition had a significant and immediate effect on EPA + DHA levels, which nearly halved in the flesh of Atlantic salmon farmed between 2006 and 2015 (~12% to ~5% of total lipids) (Sprague et al., 2016).

The deleterious effects of low dietary EPA + DHA levels on the growth, survival, health, wellbeing, and nutritional quality have been a concern in the Atlantic salmon industry, and therefore a plethora of studies using different amounts and ratios of EPA + DHA from different sources has been conducted (Katan et al., 2020; Mock et al., 2020; Huyben et al., 2021; Løvmo et al., 2021; Hatlen et al., 2022; Lutfi et al., 2022; Ruyter et al., 2022; Santigosa et al., 2023). Although a recent study found that Atlantic salmon in the freshwater phase can require an EPA + DHA level in feed as low as 3% of TFA because fish at this life stage can bioconvert α-linolenic acid to DHA at ~25% (Qian et al., 2020), EPA + DHA requirements depend on the growing phase and are likely to increase under challenging conditions (Sissener et al., 2016; Bou et al., 2017b; Lutfi et al., 2022). However, results have not always been consistent among studies and this has contributed to delays in the adoption of feeds with higher than required EPA + DHA levels by the farmers as there is no widely recognized model to calculate the ROI for optimum nutrition in aquaculture. Because of this uncertainty, feed producers and farmers currently have differing views on the optimum specifications for EPA + DHA in salmon feed; however, operators are transitioning towards higher specifications in feed as alternative ingredient sources, such as AO, have become commercially available.

Although some of these limitations could be at least partially overcome by collaborations between the feed and supplement industries and fish farms (Mock et al., 2020), to determine the optimal composition of feed for a particular species in a given environment that results in the best ROI and lowest waste, a large volume of diverse datasets need to be collected for the feed, the fish, and the farm (Neethirajan, 2020). However, this is not possible to achieve in commercial-scale trials, which are usually conducted at a single farm during a single production cycle. Furthermore, the few trials performed at commercial-scale and under the farm conditions generally revealed no significant differences in fish growth and bFCR among the groups fed different EPA + DHA levels at least during one production stage (e.g., Hatlen et al., 2022; Lutfi et al., 2022; Ytrestøyl et al., 2023), as was the case of the CF study presented here. However, eFCR results revealed two different and opposing trends in the CF and BD studies. While in the BD study, Atlantic salmon fed diets with EPA + DHA levels > 8% had a

significantly lower and less variable eFCR than those fed EPA + DHA < 8%, in the CF study fish fed the 10% EPA + DHA diet showed a slightly higher eFCR, perhaps due to predator events. This contradiction between the two studies reflects the importance of using large sample sizes (several generations; 10-year dataset) to evaluate the consequences of providing different levels of EPA + DHA on the long term, as pointed out in the scientific literature (Mock et al., 2020; Lutfi et al., 2022). According to the latest data of The Marine Ingredients Organisation (IFFO), the eFCR of salmonids has decreased from 1.54 in 2000 to 1.27 in 2020 (https://www.iffo.com/efcr-data), a level that is in agreement with the 1.29 mean value found for Atlantic salmon fed on diets containing EPA + DHA > 8% in the BD study, suggesting that increased levels of these EFAs lead to better nutrient utilization and thus to improved sustainability. This is corroborated by the FFDRoil values obtained in the CF study, where increasing the level of EPA + DHA in feed by 60% resulted in only a 4% increase in the FFDRoil value.

The results of both studies presented here also support that estimating EPA + DHA requirements based primarily (or solely) on growth and survival is not feasible, in agreement with previous studies (Bou et al., 2017a; Qian et al., 2020; Lutfi et al., 2022), as several fish health and fillet quality impacts are connected with lower EPA + DHA levels. In the CF study, Atlantic salmon fed the diet with 10% EPA + DHA showed defense cells' size and activity much closer to the norm than Atlantic salmon fed the control diet, particularly in the gills. The late stage of life at which this trial was conducted suggests that all the gills have likely been repeatedly exposed to a multitude of challenges. The small but positive effect of the OON diet on gills found in the CF study may be by promoting cell differentiation and cell viability (van Beelen et al., 2007). This improvement of defense mechanisms under challenging conditions, such as those in the farm environment, when consuming higher EPA + DHA levels is in agreement with previous findings (Arnemo et al., 2017; Bou et al., 2017b; Løvmo et al., 2021). Higher levels of EPA + DHA in the feed also resulted in significantly higher levels of these EFAs in the fillet throughout the CF study, indicating high retention of these EFAs in the muscle, as found in previous studies (e.g (Santigosa et al., 2021; Lutfi et al., 2022; Ruyter et al., 2022; Ytrestøyl et al., 2023). In the BD study, results indicate that feeds containing EPA + DHA levels > 8% result in Atlantic salmon fillets of better nutritional quality, which has a positive impact on the value of this species as a source of these omega-3 EFAs for humans. In the CF study, the better nutritional quality of Atlantic salmon fillets when the fish were fed a 10% EPA + DHA diet was accompanied by an improvement in fillet color, as shown by the significantly higher percentage of fillets with a score of at least 24 in the SalmoFan color scale. This positive relationship between EPA + DHA levels and increased SalmoFan scores is in agreement with the recent reported results for Atlantic salmon grown in sea cages in Norway (Lutfi et al., 2022; Ytrestøyl et al., 2023).

Overall, the results presented here indicate that BD can be used to describe, analyze, cluster, segment, score, and predict the effects of nutritional intervention (e.g., new feed ingredients) on improved feed efficiency, fish health, and survival to address the limitations of commercial farm tests, and ultimately help farmers on their decision-making (Roy, 2019). To the best of our knowledge, this paper presents the first approach to using BD to present proof that optimum nutrition, in this case EPA + DHA levels > 8%, leads to improved eFCR, mortality rate, and superior harvest quality. More fish of higher quality and with better feed conversion ability reaching the harvest size will clearly result in an improved biological performance and therefore a better ROI. Although this was demonstrated here for EPA + DHA levels, the BD approach could be utilized for other feed ingredients and functional additives, as well as other zootechnical and wellbeing indices. Moreover, as sensors and smart technologies expand to acquire more data related to the farm environment, feed quality, and productivity, more routes will open to model and forecast patterns related to growth, survival, and FCR, which are the most essential factors in aquaculture (Benjelloun et al., 2022), using BD technology and mathematical models. Such analytical methods based on expanded datasets also have the advantage of profiling and clustering farms according to their unique environmental (site, temperature, location) and operational (feed type and size, animal genetics) features to design the best ROI model. Hence, future BD analysis should integrate data from Atlantic salmon farms not only in Norway but from different world regions (e.g., Chile) that might help strengthen the findings reported here and reveal new patterns.

Both studies show that there are some unique limitations involved with transferring lab-controlled conditions to real-world commercial farming. These include limitations for the transparency of commercial diet formulations, difficulty in separating out potentially confounding factors that may also impact biological performance observations, and the reduced number of replicates to strengthen statistical analysis of data. However whilst recognizing these possible limitations, the results of the studies offer some important insights that can help the salmon farming industry to quantify the benefits of EPA+DHA in farmed Atlantic salmon diets.

In conclusion, the data provided here, are valuable insights to feed managers helping them to formulate a business case for transitioning from least cost formulations to optimum formulations for the fish and for farm productivity, which is based on including higher (> 8%) levels of EPA + DHA in the feed. This is conducive to optimum farm productivity, as demonstrated by reduced fish mortality, better FCR, and improved fish growth and harvest quality. Moreover, if the EPA and DHA originate from a sustainable alternative source and with high bioavailability for fish, as is the case of AO, the sustainability of the industry can be further improved, allowing it to keep on growing to feed the demands of the human population for nutritious and safe food, aligning with the United Nations Sustainable Development Goals 2 (zero hunger), 3 (good health and wellbeing), 12 (responsible consumption and production), 13 (climate action), and 14 (life below water). Although the current example shows the benefits of a sustainable alternative omega-3 oil

source for salmon farming, using a BD approach on real farm data to complement lab-scale and farm trials may therefore be the most upfront pathway to demonstrate the benefits of nutritional interventions for the business, for the people, and for the planet.

Data availability statement

The datasets presented in this article are not readily available because raw data from farmers cannot be shared without prior farmer's permission. Requests to access the datasets should be directed to ian.carr@veramaris.com.

Ethics statement

Ethical approval was not required for the studies involving animals in accordance with the local legislation and institutional requirements because Farm study (Chile) used commercial farm animals grown in a commercial set-up; Big data study (Norway) used only data obtained from salmon farms. Written informed consent was obtained from the owners for the participation of their animals in this study.

Author contributions

IC: Funding acquisition, Conceptualization, Investigation, Methodology, Validation, Visualization, Writing – original draft, Writing – review & editing. ES: Data curation, Formal Analysis, Methodology, Writing – original draft, Writing – review & editing. TC: Data curation, Formal Analysis, Methodology, Writing – review & editing. JC: Data curation, Formal Analysis, Methodology, Writing – review & editing.

Funding

The author(s) declare that financial support was received for the research, authorship, and/or publication of this article. Veramaris® partially funded the CF study and entirely funded the BD study.

Acknowledgments

The authors would like to thank: H. Wellmann, A. Castillo, P. Solis and J. Opitz at Blumar Seafoods for conducting the Commercial farm study; C. Gatica and M. Oyarzun at Skretting Chile for the provision of commercial diets for the Commercial farm study; K. Pittman at Quantidoc, M. Vera Gaedicke at VeHiCe, and F. Strachan at University of Stirling Institute of Aquaculture for their assistance with performing analysis for the Commercial farm study; Y. Le Gal, J. Torres, and F. Almendras at Veramaris for their contribution to the development of concepts explored in both the Commercial farm and Big Data studies and coordination of associated operations; J.F. Marques and M.C. Leal for their support with writing this manuscript.

Conflict of interest

IC is employed by Veramaris; ES is employed by dsm-firmenich; TC and JC are employed by Manolin. This study received funding from Veramaris. The funder had the following involvement with the study: the study design, collection, analysis, interpretation of data, the writing of this article and the decision to submit it for publication.

Publisher's note

Supplementary material

The Supplementary Material for this article can be found online at: https://www.frontiersin.org/articles/10.3389/fmars.2024.1379066/full#supplementary-material

References

Aas, T. S., Åsgård, T., and Ytrestøyl, T. (2022). Utilization of feed resources in the production of Atlantic salmon (Salmo salar) in Norway. *Aquaculture Rep.* 26, 101316. doi: 10.1016/j.aqrep.2022.101316

AOAC (2012). *Official methods of analysis of AOAC international. 19th ed* (Maryland: AOAC International Press), 27–29. Chapter 41.

Arnemo, M., Kavaliauskis, A., Andresen, A. M. S., Bou, M., Berge, G. M., Ruyter, B., et al. (2017). Effects of dietary n-3 fatty acids on Toll-like receptor activation in primary leucocytes from Atlantic salmon (*Salmo salar*). *Fish Physiol. Biochem.* 43, 1065–1080. doi: 10.1007/s10695-017-0353-4

Benjelloun, S., El Aissi, M. E. M., Lakhrissi, Y., and Ali, S. E. H. B. (2022). Big Data technology architecture proposal for smart agriculture for Moroccan fish farming. *WSEAS Trans. Inf. Sci. Appl.* 19, 311–322. doi: 10.37394/23209.2022.19.33

Bou, M., Berge, G. M., Baeverfjord, G., Sigholt, T., Østbye, T.-K., Romarheim, O. H., et al. (2017a). Requirements of n-3 very long-chain PUFA in Atlantic salmon (*Salmo salar* L): effects of different dietary levels of EPA and DHA on fish performance and tissue composition and integrity. *Br. J. Nutr.* 117, 30–47. doi: 10.1017/S0007114516004396

Bou, M., Berge, G. M., Baeverfjord, G., Sigholt, T., Østbye, T.-K., and Ruyter, B. (2017b). Low levels of very-long-chain*n*-3 PUFA in Atlantic salmon (*Salmo salar*) diet reduce fish robustness under challenging conditions in sea cages. *J. Nutr. Sci.* 6. doi: 10.1017/jns.2017.28

Carr, I., Glencross, B., and Santigosa, E. (2023). The importance of essential fatty acids and their ratios in aquafeeds to enhance salmonid production, welfare, and human health. *Front. Anim. Sci.* 4. doi: 10.3389/fanim.2023.1147081

FAO (2022). *The state of world fisheries and aquaculture 2022* (Rome: FAO). doi: 10.4060/cc0461en

Hatlen, B., Larsson, T., Østbye, T.-K., Romarheim, O. H., Rubio, L. M., and Ruyter, B. (2022). Improved fillet quality in harvest-size Atlantic salmon fed high n-3 canola oil as a DHA-source. *Aquaculture* 560, 738555. doi: 10.1016/j.aquaculture.2022.738555

Horn, S. S., Sonesson, A. K., Krasnov, A., Moghadam, H., Hillestad, B., Meuwissen, T. H. E., et al. (2019). Individual differences in EPA and DHA content of Atlantic salmon are associated with gene expression of key metabolic processes. *Sci. Rep.* 9, 3889. doi: 10.1038/s41598–019-40391–2

Huyben, D., Grobler, T., Matthew, C., Bou, M., Ruyter, B., and Glencross, B. (2021). Requirement for omega-3 long-chain polyunsaturated fatty acids by Atlantic salmon is relative to the dietary lipid level. *Aquaculture* 531, 735805. doi: 10.1016/j.aquaculture.2020.735805

Katan, T., Xue, X., Caballero-Solares, A., Taylor, R. G., Rise, M. L., and Parrish, C. C. (2020). Influence of dietary long-chain polyunsaturated fatty acids and ω6 to ω3 ratios on head kidney lipid composition and expression of fatty acid and eicosanoid metabolism genes in atlantic salmon (*Salmo salar*). *Front. Mol. Biosci.* 7. doi: 10.3389/fmolb.2020.602587

Løvmo, S. D., Whatmore, P., Sundh, H., Sigholt, T., Madaro, A., Bardal, T., et al. (2021). Effects of Atlantic salmon (*Salmo salar*) fed low- and high HUFA diets on growth and midgut intestinal health. *Aquaculture* 539, 736653. doi: 10.1016/j.aquaculture.2021.736653

Lutfi, E., Berge, G., Baeverfjord, G., Sigholt, T., Bou, M., Larsson, T., et al. (2022). Increasing dietary levels of the omega-3 long-chain polyunsaturated fatty acids, EPA and DHA, improves the growth, welfare, robustness, and fillet quality of Atlantic salmon in sea cages. *Br. J. Nutr.* doi: 10.1017/S0007114522000642

Mock, T. S., Francis, D. S., Drumm, D. W., Versace, V. L., Glencross, B. D., Smullen, R. P., et al. (2020). A systematic review and analysis of long-term growth trials on the effect of diet on omega-3 fatty acid levels in the fillet tissue of post-smolt Atlantic salmon. *Aquaculture* 516, 734643. doi: 10.1016/j.aquaculture.2019.734643

Neethirajan, S. (2020). The role of sensors, big data and machine learning in modern animal farming. *Sens. BioSensing Res.* 29, 100367. doi: 10.1016/j.sbsr.2020.100367

Oliva-Teles, A., Enes, P., and Peres, H. (2015). "Replacing fishmeal and fish oil in industrial aquafeeds for carnivorous fish," in *Feed and feeding practices in aquaculture* (Elsevier), 203–233. doi: 10.1016/b978–0-08–100506–4.00008–8

Qian, C., Hart, B., and Colombo, S. M. (2020). Re-evaluating the dietary requirement of EPA and DHA for Atlantic salmon in freshwater. *Aquaculture* 518, 734870. doi: 10.1016/j.aquaculture.2019.734870

Roques, S., Deborde, C., Richard, N., Skiba-Cassy, S., Moing, A., and Fauconneau, B. (2020). Metabolomics and fish nutrition: a review in the context of sustainable feed development. *Rev. Aquac.* 12, 261–282. doi: 10.1111/raq.12316

Roy, A. K. (2019). Big data analytics to fight challenges of fisheries and aquaculture sector. *J. Inland fisheries Soc. India* 51, 30–36. doi: 10.13140/RG.2.2.36654.66884

Ruyter, B., Bou, M., Berge, G. M., Mørkøre, T., Sissener, N. H., Sanden, M., et al. (2022). A dose-response study with omega-3 rich canola oil as a novel source of docosahexaenoic acid (DHA) in feed for Atlantic salmon (*Salmo salar*) in seawater; effects on performance, tissue fatty acid composition, and fillet quality. *Aquaculture* 561, 738733. doi: 10.1016/j.aquaculture.2022.738733

Sadiku, M. N. O., Ashaolu, T. J., Ajayi-Majebi, A., and Musa, S. M. (2020). Big data in food industry. *Int. J. Sci. Adv.* 1. doi: 10.51542/ijscia.v1i3.5

Santigosa, E., Brambilla, F., and Milanese, L. (2021). Microalgae oil as an effective alternative source of EPA and DHA for gilthead seabream (*Sparus aurata*) aquaculture. *Anim. (Basel)* 11. doi: 10.3390/ani11040971

Santigosa, E., Constant, D., Prudence, D., Wahli, T., and Verlhac-Trichet, V. (2020). A novel marine algal oil containing both EPA and DHA is an effective source of omega-3 fatty acids for rainbow trout (*Oncorhynchus mykiss*). *J. World Aquac. Soc* 51, 649–665. doi: 10.1111/jwas.12699

Santigosa, E., Olsen, R. E., Madaro, A., Trichet, V. V., and Carr, I. (2023). Algal oil gives control of long-chain omega-3 levels in full-cycle production of Atlantic salmon, without detriment to zootechnical performance and sensory characteristics. *J. World Aquac. Soc* 54, 861–881. doi: 10.1111/jwas.12947

Santigosa, E., Verlhac-Trichet, V., Olsen, R. E., and Figuereido-Silva, C. (2018). "A microalgal oil containing EPA+DHA can be an effective source of omega 3 for Atlantic salmon post- smolts," in *Proceedings of the 18th International Symposium on Fish Nutrition & Feeding (ISFNF)*. 3–20.

Sissener, N. H., Waagbø, R., Rosenlund, G., Tvenning, L., Susort, S., Lea, T. B., et al. (2016). Reduced n-3 long chain fatty acid levels in feed for Atlantic salmon (*Salmo salar* L.) do not reduce growth, robustness or product quality through an entire full scale commercial production cycle in seawater. *Aquaculture* 464, 236–245. doi: 10.1016/j.aquaculture.2016.06.034

Sprague, M., Dick, J. R., and Tocher, D. R. (2016). Impact of sustainable feeds on omega-3 long-chain fatty acid levels in farmed Atlantic salmon 2006–2015. *Sci. Rep.* 6, 1–9. doi: 10.1038/srep21892

Sprague, M., Fawcett, S., Betancor, M. B., Struthers, W., and Tocher, D. R. (2020). Variation in the nutritional composition of farmed Atlantic salmon (*Salmo salar* L.) fillets with emphasis on EPA and DHA contents. *J. Food Compost. Anal.* 94, 103618. doi: 10.1016/j.jfca.2020.103618

Tao, Q., Ding, H., Wang, H., and Cui, X. (2021). Application research: Big data in food industry. *Foods* 10, 2203. doi: 10.3390/foods10092203

Tocher, D. R. (2015). Omega-3 long-chain polyunsaturated fatty acids and aquaculture in perspective. *Aquaculture* 449, 94–107. doi: 10.1016/j.aquaculture.2015.01.010

van Beelen, V. A., Roeleveld, J., Mooibroek, H., Sijtsma, L., Bino, R. J., Bosch, D., et al. (2007). A comparative study on the effect of algal and fish oil on viability and cell proliferation of Caco-2 cells. *Food Chem. Toxicol.* 45, 716–724. doi: 10.1016/j.fct.2006.10.017

Ytrestøyl, T., Bou, M., Dimitriou, C., Berge, G. M., Østbye, T.-K., and Ruyter, B. (2023). Dietary level of the omega-3 fatty acids EPA and DHA influence the flesh pigmentation in Atlantic salmon. *Aquac. Nutr.* 2023, 1–14. doi: 10.1155/2023/5528942

frontiers | Frontiers in Marine Science

TYPE Original Research
PUBLISHED 26 June 2024
DOI 10.3389/fmars.2024.1397379

OPEN ACCESS

EDITED BY
Xinxin Wang,
Fisheries and Aquaculture Research (Nofima), Norway

REVIEWED BY
Sasi Nayar,
South Australian Research and Development Institute, Australia
Veeragurunathan Veeraprakasam,
Central Salt & Marine Chemicals Research Institute (CSIR), India

*CORRESPONDENCE
Vaibhav A. Mantri
vaibhav@csmcri.res.in
Vasco M. N. C. S. Vieira
vasco.vieira@tecnico.ulisboa.pt
Santlal Jaiswar
santlal@csmcri.res.in

RECEIVED 07 March 2024
ACCEPTED 04 June 2024
PUBLISHED 26 June 2024

CITATION
Vieira VMNCS, Dawange PS, Jaiswar S, Sardinha JP and Mantri VA (2024) Adaptation of functional traits in *Gracilaria dura* with the local environment: implications for resource management and exploitation.
Front. Mar. Sci. 11:1397379.
doi: 10.3389/fmars.2024.1397379

Adaptation of functional traits in *Gracilaria dura* with the local environment: implications for resource management and exploitation

Vasco M. N. C. S. Vieira[1,2*], Pankaj S. Dawange[3,4], Santlal Jaiswar[3,4*], José P. Sardinha[5] and Vaibhav A. Mantri[3,4*]

[1]Marine Environment and Technology Center (MARETEC), Instituto Superior Tecnico, Universidade Tecnica de Lisboa, Lisbon, Portugal, [2]Marine and Environmental Sciences Centre, Universidade Nova de Lisboa, Caparica, Portugal, [3]Applied Phycology and Biotechnology Division, CSIR- Central Salt & Marine Chemicals Research Institute, Bhavnagar, India, [4]Academy of Scientific and Innovative Research (AcSIR), Ghaziabad, India, [5]Departamento de Engenharia e Ciências Nucleares (DECN) and Centro de Recursos Naturais e Ambiente (CERENA), Instituto Superior Técnico, Universidade de Lisboa, Lisboa, Portugal

Seaweed functional traits provide insights on natural populations, their adaptations to the local environment, which can be utilized for commercial exploitation. Here, we analyzed the functional traits of *Gracilaria dura* from two intertidal populations in Veraval and Adri, from the coast of Gujarat, India, over a period of three months. Functional traits were measured by analyzing growth rates, respiration, primary production, antioxidant activity and the content of plant growth hormones. The weight-to-length allometric exponent ≈3 indicated that *G. dura* grew almost isometrically. Furthermore, frond shape was not significantly different. Fronds in Veraval, resting submerged, grew faster than the fronds in Adri, which, lay exposed in the flat bare rock during low tide. Accordingly, the simultaneous increase in antioxidant activity, O_2 production and chlorophyll content in fronds from Adri suggests that stress from desiccation and UV led to the detrimental accumulation of Reactive Oxygen Species, leading to decreased growth and decreased production of growth hormones. The increased Chl-a may indicate enhanced non-photochemical quenching (NPQ) for the dissipation of excess absorbed light. These results aid in establishing the best practices for maximizing biomass yield or the yield of specific molecules. For maximized biomass yield, fronds should not be subject to emersion nor cultivated on the sea-surface. On the other hand, fronds grown subject to emersion or at the sea-surface yield less biomass but more content on molecules such as antioxidants (flavonoids, phenolics, enzymes), that fight stress from desiccation high temperatures and UV. In this case, stress should still be avoided during the initial growth, at the onset of the growth season, in order to not disrupt the production of growth hormones. The increased O_2 production at Adri was initially mistakenly perceived as enhanced Net Primary Production. Only a posterior holistic perspective over the whole data allowed to conclude that it was likely the stress-induced detrimental accumulation of

Reactive Oxygen Species. More robust experiments are required to establish if the differences observed between locations have led to the evolution of genetic strains specific to each habitat that may show different performances and yields when cultivated in similar environments.

KEYWORDS

aquaculture, functional traits, plant growth hormones, morphology, Rhodophyta

1 Introduction

Seaweeds are the most efficient primary producers on the planet, surpassing plants in their ability to concentrate biomass per unit area (Creed et al., 2019). Therefore, seaweed farming has great potential to contribute to the ever-increasing human demand for food and raw materials. Seaweed applications are no novelty, and society has long cultivated seaweeds using traditional methods (McHugh, 2003; Valero et al., 2017; Cai et al., 2021). Red algae are the most harvested seaweeds, both from natural and farmed populations, for uses other than as a food source (McHugh, 2003; Cai et al., 2021). Their major uses are the extraction of agar and carrageenans, mostly from Gelidiales and Gracilariales. Harvesting of wild Gelidiales severely declined in Europe during the latter decades, mainly due to over exploitation. Gracilariales, yielding better-quality agarose, became its predominant source (McHugh, 2003). Most of the Gracilariales production is harvested in Asia, although there is also a fair amount of harvesting in South America (McHugh, 2003; Alemañ et al., 2019). For the extraction of hydrocolloids, there is no natural alternative to the cultivation of red seaweeds yielding agarose and carrageenans, given that the cultivation of brown seaweeds is too expensive and inefficient for the industrial production of alginate (McHugh, 2003). Hence, worldwide, Gracilariales play a pivotal role in supplying feedstock to local agarose production units. Time is due to optimize cultivation practices for Gracilariales as well as adapt them according to local needs and constraints.

Domestic agar (including agarose) demand in India is 400 ton·year^{-1}, of which only 10–20% has been supplied through the indigenous supply chain. *Gracilaria dura* from India has been found to produce commercial-grade agarose. The technique employed for this process was a specially-developed surfactant-induced coagulation technology (Meena et al., 2014). Further commercially lucrative products from *G. dura* such as pigments, lipids, agar, agriculturally important nutrient-rich liquids, and energy-dense cellulose have been produced through a green processing route (Reddy et al., 2018). The farming of this species has thus been initiated at two coastal villages, namely Simar and Rajpara, along the north-west coast of India (Shah et al., 2022). About 10–12 tons of fresh biomass have been produced in pre-commercial trials at these locations.

Gracilaria dura (C. Agardh) J. Agardh is an intertidal red alga present in the Mediterranean, Arabian Sea and Indian Ocean. Along the north-west coast of India, the growth season goes from January to March. During this period (slightly extending from December to April) both gametophytic and sporophytic thalli coexist. Beyond this season, we never observed *G. dura* thalli, leading us to assume that bare holdfasts and dormant spores are most likely the only remnants, lying on the rocky surface until the next growth season arrives. This strong seasonality and scarcity of biomass in the wild (Mantri et al., 2009) drove the research and development of farming methods, namely, the floating bamboo raft, polypropylene net, net bag, hanging rope, monoline, net pouch and tube net (Veeragurunathan et al., 2015; Mantri et al., 2020; Shah et al., 2021). Among these, the floating bamboo raft, monoline and tube net methods have been used by commercial seaweed farmers (Kavale et al., 2021).

The seasonal occurrence of *G. dura* and the limited availability of natural biomass, even during the favorable season, were initially perceived as impediments to large-scale commercial aquaculture. However, new knowledge and improved practices enabled a year-round seedling production (see Saminathan et al., 2015; Vignesh et al., 2020; Shah et al., 2022). Commercial exploitation for aquaculture purposes has only been undertaken with the germplasm collected from Veraval, in the province of Gujarat, India. A tight control of the germplasm is fundamental for selecting and preserving the best strains for specific purposes or environments (Valero et al., 2017). However, for the *G. dura* in Gujarat, continuous and repeated farming from the same germplasm has resulted in declining growth rates due to aging or senescence. For most domesticated algal species, the best practice is to select and preserve strains through asexual cultivation (Valero et al., 2017). Whether from spores or through vegetative propagation, *G. dura* cultivation in Gujarat still requires determining which strains are the best to cultivate. This leads to the urgent need for a greater and more in-depth understanding of the variation in functional traits such as morphology, growth, pigments, antioxidant activity, plant growth regulators and net productivity. These traits have been demonstrated essential in the determination of growth, survival and production of molecules of commercial relevance (Gupta et al., 2015; Sambhwani et al., 2020, 2022; Dawange et al., 2023a, b).

Farmed species have evolved specific functional traits related to reproduction, growth and survival. Consequently, highly specific local aquaculture practices have led to the involuntary selection of

traits with economic importance (Valero et al., 2017; Usandizaga et al., 2019; Sambhwani et al., 2020, 2022). In natural populations of *G. dura*, such traits also showed considerable seasonal variation (Sambhwani et al., 2020, 2022). Here, we analyzed functional traits, namely morphology, growth, pigments, antioxidant activity, plant growth regulators, productivity and respiration, for *G. dura* sampled during the growth season from two locations with distinct environmental conditions. The present study provides practical and novel information for the optimization of the commercial cultivation of *G. dura* selecting specimens retrieved from natural populations. To the best of our knowledge, this is the first study investigating spatial and temporal patterns of variation in six different functional traits crucial for the growth and survival of *G. dura*.

2 Material and methods

2.1 Gracilaria dura in Gujarat

Gracilaria dura is an intertidal red alga with the isomorphic byphasic life cycle typical of rhodophytes - also known as the haploid-diploid life cycle - alternating isomorphic free living tetrasporophytes (diploid) and gametophytes (haploid) (Guillemin et al., 2014; Vieira et al., 2018a, b, 2021, 2022). Individuals are fixed to the rocky bottom by a holdfast. Along the north-west coast of India, *G. dura* has only been reported in Adri, Okha, and Veraval (Jha et al., 2009), where it is found occasionally in a few restricted locations (Mantri et al., 2009). In Veraval, fronds can be found permanently submerged within intertidal rockpools, whereas in Adri, fronds lie on the flat bare rock exposed to desiccation during low tide. The environmental conditions observed at Adri and Veraval during the growth season are presented in Table 1.

2.2 Sampling

Healthy vegetative thalli of *Gracilaria dura* were collected from the coasts at Veraval (20.910404°N, 70.351273°E) and Adri (20.961213°N, 70.277051°E). Because reproductive fronds were not collected and biochemical tracers of the ploidy phase were not tested, it is not known whether each thallus was a male or female gametophyte (haploid) or a tetrasporophyte (diploid). Ecological differences have been reported between phases and sexes in various *Gracilaria* species, e.g., *G. gracilis* (Engel et al., 2001), *G. tenuistipitata* (Skriptsova and Nabivailo, 2009), *Gracilaria caudata* (Faria et al., 2017) and *G. chilense* [former *Agarophyton chilensis*] (Vieira et al., 2022). Here, we assumed that whatever the proportions among life-cycle phases, these were not significantly different among treatments of the experimental design (i.e., the Adri and Veraval populations and the three months) and thus did not bias the analysis. In this case, the different proportions of life-cycle phases would be accounted for by the homoscedastic within-group variances and would not affect the results relative to sites and seasons. Three sampling episodes took place, namely in January, February and March of 2021. This is the natural growth season for *G. dura* in India. Samples were collected during low tide at distances of 50, 100, 150, 200, and 250 m from the high tide limit. Based on these distances, samples were named V50, V100, V150, V200, and V250, and A50, A100, A150, A200, and A250, respectively, for Veraval and Adri. Each sample consisted of 5 *G. dura* thalli (having 5 – 10 fronds, but no discs) with lengths of 5–18 cm. Samples were placed in seawater and cool conditions, and immediately transported to the CSIR-CSMCRI laboratory, where they were cleaned with filtered seawater to remove calcareous and extraneous adhering detritus materials. To estimate daily growth rate (DGR), respiration and productivity, 5 fronds (one from each thallus) were selected from each sample and acclimatized in the laboratory for 5 days in filtered seawater at 12:12 h photoperiod, 25°C, 35 ppt salinity and 40 µmol photons m^{-2} s^{-1} light. To estimate the fresh weight (FW) to dry weight (DW) calibration, 15 frond fragments of various sizes were randomly collected. Dry weights were determined after 48 h at 60°C. For analyzing pigments, antioxidant capacity and plant growth hormones, the remaining thalli were surface dried with blotting paper to remove extra seawater, frozen in liquid N_2 and stored at -80°C. Later, 5 fragments were taken from each site × month × distance combination and subjected to the procedures described below for the estimation of each variable. The final reading was the average of the five fragments. Sampling for the morphological analysis followed a different protocol described below.

TABLE 1 Environmental conditions in Veraval and Adri during the growth season.

Parameter	Veraval	Adri
Atmospheric temp. (°C)	28.26 ± 0.19	28.46 ± 0.12
Surface water temp. (°C)	25.3 ± 0.17	25.7 ± 0.16
Salinity (PSU)	31.42 ± 0.31	31.37 ± 0.28
pH	7.94 ± 0.05	8.26 ± 0.14
Dissolved oxygen ($mg{\cdot}L^{-1}$)	10.47 ± 0.33	11.47 ± 0.65
Nitrite ($mg{\cdot}L^{-1}$)	0.030 ± 0.01	0.039 ± 0.01
Phosphate ($mg{\cdot}L^{-1}$)	0.1 ± 0.03	0.11 ± 0.07
Depth during high tide (m)	1–5	1–5

2.3 Morphology

The morphological characterization of *G. dura* relied on total length (L), diameter (D), fresh weight (W) and count of primary branches (B) measured on 50 single fronds collected each month (January, February and March of 2021) from the coasts of Veraval and Adri. The weight-to-length allometric exponent was estimated. In isometric growth, individuals grow proportionally in all 3 spatial dimensions, thus keeping their shape. Consequently, biomass = $a{\times}L^3$.

2.4 Growth rate

Five fronds (= 5 replicates) were selected from each site at each census. For each replicate, 10 fragments approx. 2 cm in length were

excised and placed in a 500-ml flask containing Erdschreiber seawater (ESS) culture medium (Suto, 1959) with 35 ppt salinity, at 25°C, 7.8 pH, 40 µmol photons m^{-2} s^{-1} light and a 12:12 h photoperiod. Media was replenished every 5 days and fragments were cleaned with a soft brush to reduce fouling. After 15 days, all fragments were weighed and the daily growth rate (DGR) was estimated using the formula DGR (day^{-1}) = ln [(W_2/W_1)/t], where W_1 is the initial weight, W_2 is the final weight and t is the number of days (see Dawes et al., 1993).

2.5 Antioxidant capacity

To prepare the extract, 100 mg of frozen algal material was ground to powder in the pre-chilled mortar and pestle using liquid nitrogen. Sequential extraction was performed in two steps: first, to the crushed sample was added 1 ml of distilled water, incubated overnight at 4°C and thereafter centrifuged at 11384*g* (Eppendorf Centrifuge – 5424-R, Germany) for 15 min at 4°C. Then, the supernatant was collected and stored to be mixed later with the second extract, 1 ml of 70% methanol was added to the pellet, and the mix was incubated overnight at 4°C followed by centrifugation at 11384*g* for 15 min at 4°C. Both supernatants were pooled and the extract was used for the analysis of total antioxidant capacity (TAC) and CUPric Reducing Antioxidant Capacity (CUPRAC).

A TAC assay was implemented according to the method of Prieto et al. (1999). Briefly, 100 µl of the above extract were mixed with 1 ml of mixed reagent (28 mM sodium phosphate, 4 mM ammonium molybdate and 0.6 M sulfuric acid) and incubated for 1 h at 100°C. After cooling to room temperature, absorbance was recorded at 695 nm (detection limits 200–999nm) using a UV-Vis spectrophotometer (EPOCH/2 Biotek). Using a calibration curve, TAC ($mg{\cdot}g^{-1}$) was standardized to the ascorbic acid equivalent antioxidant capacity (AAEAC) (Gonzales et al., 2021).

The CUPRAC spectrophotometric method was used for determining antioxidant capacity (Apak et al., 2004). To 100 µl of the extract mentioned above were added 50 µl of 10 mM copper chloride, 50 µl of ammonium acetate buffer (pH 7) and 50 ml of 7.5 mM neocuproine, followed by 1 h incubation at room temperature. Absorbance was recorded at 450 nm (detection limits 200–999nm). Using a calibration curve, CUPRAC ($mg{\cdot}g^{-1}$) was standardized to the ascorbic acid equivalent antioxidant capacity (AAEAC) (Gonzales et al., 2021).

2.6 Photosynthetic pigments

A 100-mg sample of each of the 5 fragments was taken and crushed to powder, and homogenized in a mortar and pestle using liquid nitrogen. To determine R-Phycoerythrin (PE) and R-Phycocyanin (PC) content, 0.8 ml of 0.1 M phosphate buffer (6.8 pH) was added to the homogenate and incubated overnight at 4°C. Samples were then vortexed and centrifuged at 15900g for 10 min at 4°C (Eppendorf Centrifuge – 5424-R, Germany). The supernatant was collected and 0.2 ml of phosphate buffer was added to the pellet for re-extraction. The chemicals used in the experiments were all analytical grade (Sigma Aldrich Pvt. Ltd.). The absorbances at 564 nm (A_{564}), 618 nm (A_{618}) and 730 nm (A_{730}) were recorded on a dual beam UV-Vis spectrophotometer (EPOCH BIOTEK) with detection limits 200–999nm (Sampath-Wiley and Neefus, 2007). A similar process was implemented for the extraction of Chlorophyll-a (Chl-a) using 90%acetone as a solvent and absorbance was recorded at 664 nm (A_{664}) and 647 nm (A_{647}) (Jeffrey and Humphrey, 1975). The R-PE ($\mu g{\cdot}g^{-1}$) and R-PC ($\mu g{\cdot}g^{-1}$) content was estimated from Equations 1, 2, respectively:

$$\mathrm{R-PE}\ (\mathrm{mg}\cdot\mathrm{ml}^{-1}) = 0.1247[(A_{564}-A_{730})-0.4583(A_{618}-A_{730})] \quad (1)$$

$$\mathrm{R-PC}\ (\mathrm{mg}\cdot\mathrm{ml}^{-1}) = 0.154(A_{618}-A_{730}) \quad (2)$$

Chl-a ($\mu g{\cdot}g^{-1}$) content was estimated following Equation 3:

$$\text{Chlorophyll a}\ (\mu\mathrm{g}\cdot\mathrm{ml}^{-1}) = 11.93(A_{664})-1.93(A_{647}) \quad (3)$$

2.7 Primary production and respiration

Net primary productivity (NPP) (mg $O_2{\cdot}gDW^{-1}{\cdot}h^{-1}$) and respiration (R) (mg $O_2{\cdot}gDW^{-1}{\cdot}h^{-1}$) were measured using the light and dark bottle method (Guillemin et al., 2014). Five frond fragments of approximately 0.3 g were placed in 100-ml glass bottles filled with autoclaved filtered seawater (salinity 35) and kept at 25°C, 40 µmole photons m^{-2} s^{-1} light for 12 h (the "Light" bottles). Another 5 frond fragments of approximately 0.3 g were placed in 100-ml glass bottles filled with autoclaved filtered seawater (salinity 35), kept at 25°C and covered with black plastic sheets (the "Dark" bottles). The 12-h time intervals mimicked the diel pattern as well as the 5-day acclimatization photoperiod. Initial and final dissolved oxygen (O_2) concentrations were recorded using a HACH HQ30D DO probe, USA. As established in previous studies, there was no O_2 saturation after 12 h (Sambhwani et al., 2022). Respiration (R), net primary productivity (NPP), and gross primary productivity (GPP) were calculated by using Equations 4–6 respectively.

$$\mathrm{R}(\mathrm{mg\ O_2\ \ gDW^{-1}h^{-1}}) = \text{Initial DO}_{(\mathrm{Dark})} - \text{Final DO}_{(\mathrm{Dark})} \quad (4)$$

$$\mathrm{NPP}(\mathrm{mg\ O_2\ gDW^{-1}h^{-1}}) = \text{Final DO}_{(\mathrm{Light})} - \text{Initial DO}_{(\mathrm{Light})} \quad (5)$$

$$\mathrm{GPP}(\mathrm{mg\ O_2 gDW^{-1}h^{-1}}) = \text{Respiration} + \text{Net primary productivity} \quad (6)$$

2.8 Extraction of plant growth hormones

The extractions were implemented separately for auxin ($\mu g{\cdot}g^{-1}$), cytokinin ($\mu g{\cdot}g^{-1}$) and gibberellic acid ($\mu g{\cdot}g^{-1}$). Each frond fragment (1 g) was homogenized in a mortar and pestle and collected in a 50-ml tube. Distilled water (5 ml) was added and stirred overnight on

the tabletop stirrer. The supernatant was collected upon centrifugation at 7500g for 15 min at 4°C (Eppendorf Centrifuge – 5430-R, Germany). Auxin, cytokinin and gibberellic acid were extracted using diethyl ether (DEE), n-butanol and ethyl acetate (EA), respectively (Prasad et al., 2010; Sambhwani et al., 2022).

2.8.1 Extraction of auxin

For estimating auxin ($\mu g \cdot g^{-1}$), the pH of the above extract was adjusted to 3 with 1N hydrochloric acid (HCl). Extraction was implemented with equal volumes of di-ethyl ether (DEE) and repeated thrice. Equal volumes of 5% sodium bicarbonate were added to the DEE layer. The bicarbonate layer was then collected in another fresh tube and its pH was adjusted to 3.0 by dropwise addition of 1N HCl. This was extracted with equal volumes of DEE and repeated thrice for maximum extraction. Both the DEE layers were pooled and washed with distilled water. The solvents were then evaporated and the residue was dissolved in 1 ml of HPLC-grade methanol.

2.8.2 Extraction of cytokinin

To estimate cytokinin ($\mu g \cdot g^{-1}$), the pH of the extract from Section 2.8 was adjusted to pH 3 by dropwise addition of 1N HCl. Equal volumes of dichloromethane (DCM) were used thrice for extraction and collected in a separate tube. The pH of the aqueous layer was adjusted to 8 with 1N NaOH. For the second extraction, equal volumes of n-butanol were used thrice. Both DCM and n-butanol layers were pooled and then evaporated. The residue was dissolved in 1 ml of HPLC-grade methanol.

2.8.3 Extraction of gibberellic acid

To estimate gibberellic acid ($\mu g\ g^{-1}$), the pH of the extract from Section 2.8 was adjusted to 2.5 by 3.2 N HCl, followed by extraction with equal volumes of ethyl acetate (EA) three times. The pH of the aqueous layer was adjusted to 11.0 with 3.75 M NaOH. This was hydrolyzed at 60°C for 1 h in a water bath. The pH was then readjusted to 2.5, followed by re-extraction with EA. Both the EA layers were combined and an equal volume of $NaHCO_3$ was added. The combined EA layer was transferred to a fresh tube. The pH of the $NaHCO_3$ layer was adjusted to 2.5. For maximum extraction, the EA extraction was repeated and all EA samples were pooled. The solvent was evaporated and the residue was dissolved in 1 ml of HPLC-grade methanol.

2.8.4 HPLC analysis and quantification of plant growth hormones

The growth hormone content was quantified by High Performance Liquid Chromatography (HPLC). First, the extracted residue (see explanation above) was dissolved in methanol and passed through a 0.22-µm syringe filter. Standards of 25 ppm were prepared for all three growth hormones as follows: for auxin — indole-3-acetic acid Batch No: 2283040 of Sisco Research Laboratories; for cytokinin — zeatin Batch:0000008065 of Sigma Aldrich, and for gibberellins — gibberellic acid (GA3) Batch No:8962367 of Sisco Research Laboratories. Samples were analyzed in HPLC for the estimation of concentration with respect to the standards. The retention times were 14.7, 12.8 and 3.6 min for the standard IAA, GA_3 and *trans*-zeatin, respectively. Prominence model of M/s. Shimadzu, Japan, including a Rheodyne injector, was used for HPLC analysis. The C18 stainless steel column of M/s. Thermo Scientific with specifications of 250 mm x 4.6 mm (i.d.) Nucleosil (5 µm particle size, 300 A° pore size) was used at a constant temperature of 37°C. The binary elution system of separation was carried out using mobile phases A (water with 0.1% formic acid) and B (methanol with 0.1% formic acid). A constant flow rate of 1 ml min^{-1} was maintained. Further, UV detection was attempted at 254 nm. The detector was an SPD M20A with wavelength range from 190 nm to 900 nm and operated at 25° C. The elution was achieved through a linear gradient as follows: 70% A and 30% B at 0 min, 70% A and 30% B (2 min), 0% A and 100% B (20 min), 0% A and 100% B (22 min), 70% A and 30% B (25 min) and 70% A and 30% B (30 min). The detection of the eluted plant growth regulators was performed at 254 nm and the identification of different PGRs measured against standards was based on HPLC peak areas.

2.9 Statistical analysis

The morphological growth dynamic (isometric vs. allometric) of *G. dura* fronds was inferred from the $\log_{10}$DW-to-$\log_{10}$L fit. Several model I and model II regression methods were tested, including Ordinary Least Squares (OLS), Reduced Major Axis (RMA) Principal Components Analysis (PCA), Quantile Regression (QR), among others. Differences in morphological growth between fronds from Adri or Veraval were tested by ANCOVA. The significance of these differences was estimated by permutation tests (Vieira and Creed, 2013a, b).

The morphometry data set, comprising 300 sampling units (2 sites × 3 months × 50 thalli), was subject to a Principal Components Analysis (PCA) to search for consistent associations between variables. The PCA was performed on the correlation matrix. The significances of the associations (described by the principal components – pc) and of the variables contributing to them (described by the respective loadings) were estimated by permutation tests following the protocol and software by Vieira (2012). Meaningful pcs replaced the original variables significantly contributing to them. Hence, each sampling unit had the original measurements replaced by the z-score estimated from the corresponding pc. To test for significant differences among sites (fixed effects) and/or months (fixed effects), 2-way permutation tests (also known as Permanova) were implemented using either the z-scores or uncorrelated original variables as the dependent variable.

The hormones, pigments, respiration and primary production data set comprising 30 sampling units (2 sites × 3 months × 5 distances from shore) were subject to a Principal Components Analysis (PCA) performed on the correlation matrix, as above. To test for significant differences among sites (fixed effects), months (fixed effects) or distances from shore (random effects), 3-way permutation tests were implemented using either the z-scores or uncorrelated original variables as the dependent variable.

3 Results

The best $\log_{10}$DW fit to $\log_{10}$L (Figure 1) was obtained by Reduced Major Axis (RMA, a model II linear regression), leading to the allometric relation $DW=0.0003 \cdot L^{2.87}$. The allometric exponent close to 3 indicates that *G. dura* growth is almost isometric. This almost isometric growth was not significantly different between *G. dura* fronds from Veraval and from Adri (p=0.08), as determined by an ANCOVA procedure.

The PCA upon all the morphometric variables was meaningful (p<0.0001). Only the first (largest) principal component (pc1) extracted was meaningful (p<0.0001). This component was a weighted average of all morphometric variables under the form $z_i=0.54 \cdot \log_{10}L_i+0.57 \cdot \log_{10}DW_i+0.42 \cdot D_i+0.44 \cdot B_i$, where the subscript i stands for the i^{th} frond. When selecting the variables significantly contributing to this component, the IL metric (see Vieira, 2012) selected all variables, in which case the pc represents 55.9% of the total normalized variation. On the other hand, the Correlation Index (see Vieira, 2012) selected only $\log_{10}$L and $\log_{10}$DW, in which case pc1 represents 34,8% of the total normalized variation. We chose the latter pc1 version with only the L and DW association as the subsequent analysis provided a clearer picture of the morphometric growth dynamics (Figure 2). Frond size, as represented by pc1, was significantly different among sites (p<0.0001) as well as among months (p<0.0001). At the start of the monitoring experiment, *G. dura* fronds were already larger at Veraval than at Adri and, as the growth season progressed, this pattern enhanced, leading *G. dura* fronds to end the growth season on average 2.3 times larger in Veraval than in Adri (Figure 2A). The larger divergence in the morphological growth dynamics occurred from February to March, when fronds enhanced growth in Veraval but stopped growing in Adri. During the monitoring experiment, *G. dura* fronds did not increase their diameter (Figure 2B), as shown by the non-significant differences among months (p=0.129). Nevertheless, *G. dura* branches were consistently thicker at Veraval than at Adri (p<0.0001) (Figure 2B). During the monitoring experiment, *G. dura* fronds slightly increased their number of primary branches (Figure 2C), as shown by the significant differences among months (p<0.0005). Furthermore, *G. dura* fronds were bushier at Veraval than at Adri (p=0.0114) (Figure 2C).

The PCA of the molecular, respiration and primary production data set generated a significant result (p<0.0001). However, each of the variables respiration, NPP, GPP, cytokinin and chlorophyll was uncorrelated with any other variable. Hence, a new PCA was performed with only the remaining correlated variables, namely DGR, TAC, CUPRAC, PE, PC, auxin and gibberellins. The two largest principal components extracted were significant (p<0.0001 for pc1 and p<0.0001 for pc2). Pc1 was a weighted contrast between growth and antioxidant activity given by $z1_i=0.53 \cdot DGR_i-0.56 \cdot TAC_i-0.53 \cdot CUPRAC_i$ (Supplementary Figure S1), and explaining 31.9% of the total normalized variation. The 3-way Permanova was applied using z1 as the response (dependent) variable (Figure 3). Differences between months (fixed factor) were significant (p=0.0037), but only January and March were significantly different from each other (p<0.0137). Differences between sites (fixed factor) were significant (p=0.0008). Differences between distances from shore (random factor) were not significant (p=0.9241). There were no interactions (always p>0.7994). Pc2 was a weighted average of PE and growth hormones, given by $z2_i=0.42 \cdot PE_i+0.44 \cdot PC_i+0.5 \cdot Auxin_i+0.52 \cdot Gibberelins_i$ (Supplementary Figure S2), and explaining 27.8% of the total normalized variation. The 3-way Permanova was applied using z2 as the response (dependent) variable (Figure 3). Differences between months (fixed factor) were not significant (p=0.1895), as were differences between sites (fixed factor; p=0.2448), and differences between distances from shore (random factor; p=0.8775). There were interactions between month and site (p<0.0408), with z2 being significantly larger at Veraval during January.

Since the remaining variables Chlorophyll-a (Chl-a), Cytokinin, Respiration, Gross Primary Production (GPP) and Net Primary Production (NPP) were not significantly correlated among themselves or with any other variable, they were analyzed separately (Figure 4). The 3-way Permanova using Chl-a as

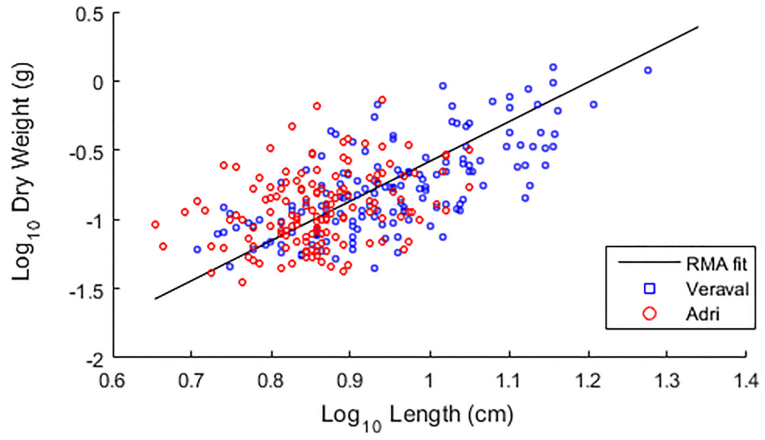

FIGURE 1
Scatter plot of length vs weight of fronds of *Gracilaria dura* from Adri and Veraval. The morphometric relation between frond length and dry weight was tested by Reduced Major Axis (RMA) for *G. dura* collected from Adri and Veraval coasts. An ANCOVA showed that this relation was isometric and not significantly different between fronds from the two sites.

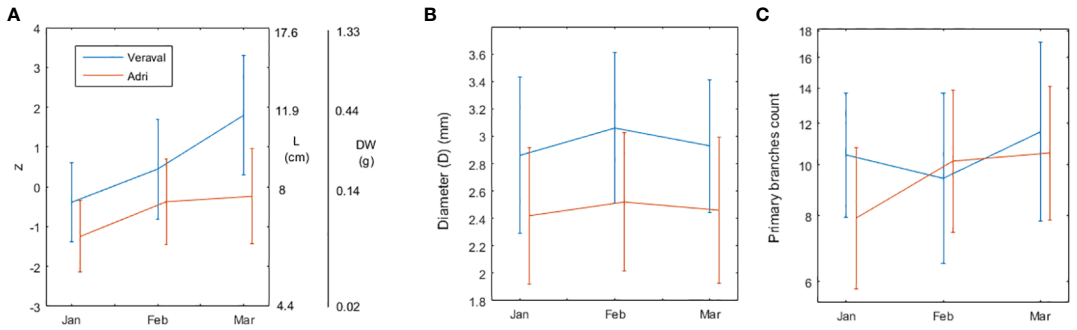

FIGURE 2
Gracilaria dura morphometry (length, dry weight, diameter and number of primary branches) during the growth season. **(A)** Principal component 1 (z in the left vertical axis) combining Length (L in cm, in the right vertical axis) and Dry Weight (DW in g, in the right vertical axis) into $z=0.54 \cdot \log_{10}L + 0.57 \cdot \log_{10}DW$. PCA was performed using the correlation matrix, which implied that $\log_{10}L$ and $\log_{10}DW$ were normalized to zero mean and unit variance. **(B)** Diameter (D in mm) of the primary branches. **(C)** Number of primary branches in each frond. This data was log transformed for statistical inference. Error bars are standard deviations (n=50).

response variable yielded significant differences between sites ($p<0.0001$). Fronds from Adri had significantly more Chl-a than fronds from Veraval. Differences between months and between distances from shore were not significant ($p=0.643$ and 0.622, respectively), and there were no interactions (always $p>0.508$). In a similar manner, the 3-way Permanova using NPP as response variable yield significant differences between sites ($p=0.0019$). Because NPP was measured by the O_2 method, this meant that fronds from Adri produced significantly more O_2 than fronds from Veraval. Differences between months were significant ($p=0.037$), with February showing significantly less NPP than January ($p=0.044$). Differences between distances from shore were not significant ($p=0.5439$). There were no interactions (always $p>0.455$). This pattern is close to the pattern above described by pc1. In fact, the PCA results yield Chl-a and NPP almost significantly associated with (or contributing to) pc1. The reason they were not so well correlated with growth, TAC and CUPRAC is because they do not match the time series evolution. While the association between growth, TAC and CUPRAC evolves consistently with time (Figure 3), Chl-a and NPP do not evolve consistently with time (Figure 4). Nevertheless, the key finding is the differentiation between sites shared by all these variables. The 3-way Permanova using Cytokinin as a response variable yields non-significant differences between sites ($p=0.718$). Differences between months were not significant ($p=0.108$). However, differences between distances from shore were significant ($p=0.0008$), with fronds collected 100m away having significantly more Cytokinin than the fronds collected anywhere else. We question whether this was simply a coincidence. There were no interactions (always $p>0.242$). The 3-way Permanova using respiration (R) as response variable yield non-significant differences between sites ($p=0.643$). Differences between months were significant ($p=00025$). Respiration was significantly less during January than during February ($p=0.0003$) or during March ($p=0.0025$). Differences

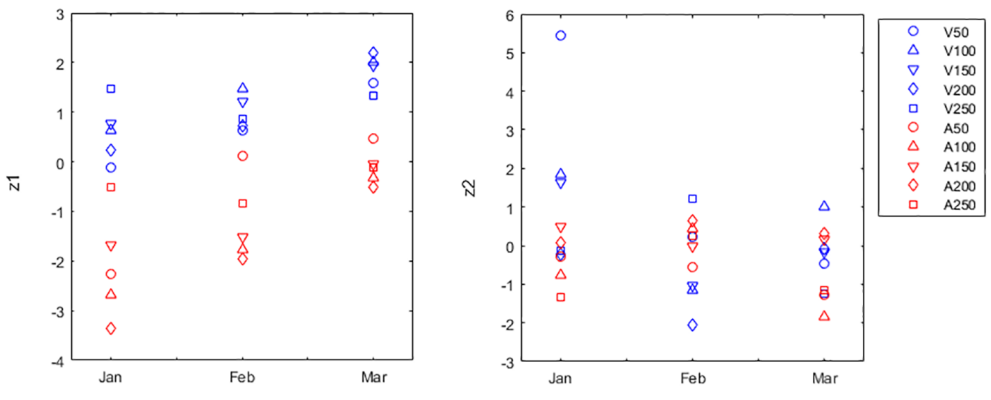

FIGURE 3
Principal Components Analysis (PCA) of the growth, molecular composition, respiration and primary production data set of *Gracilaria dura*. The largest principal component (z1 in the left panel vertical axis) corresponds to $z1_i=0.53 \cdot Growth_i - 0.56 \cdot TAC_i - 0.53 \cdot CUPRAC_i$. The second largest principal component (z2 in the right panel vertical axis) corresponds to $z2_i=0.42 \cdot PE_i + 0.0.44 \cdot PC_i + 0.5 \cdot Auxin_i + 0.52 \cdot Gibberelins_i$. Both z1 and z2 were tested for their relation with month, site, and distance from shoreline. Months were January (Jan), February (Feb) and March (Mar). Sites were Adri (A) and Veraval (V). Distances from shoreline were 50, 100, 150, 200 and 250m. Markers identify sampling locations (A50) Adri, 50m, (A100) Adri, 100m, (A150) Adri, 150m, (A200) Adri, 200m, (A250) Adri, 250m, (V50) Veraval, 50m, (V100) Veraval, 100m, (V150) Veraval, 150m, (V200) Veraval, 200m and (V250) Veraval, 250m. PCA calculated using correlation matrix in which original variables were normalized to zero mean and unit variance.

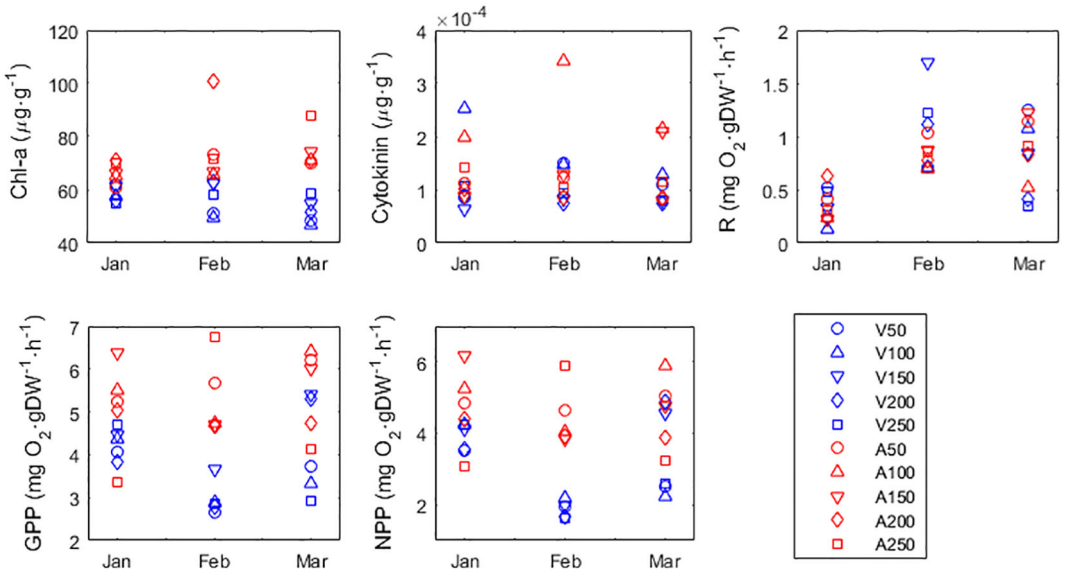

FIGURE 4
Chlorophyll-a (Chl a), cytokinin, respiration, gross primary production (GPP) and net primary production (NPP) of *Gracilaria dura* in different months, sites (A, Adri; V, Veraval), and distances from the shoreline (m). Distances from shoreline were 50, 100, 150, 200 and 250m. Markers identify sampling locations (A50) Adri, 50m, (A100) Adri, 100m, (A150) Adri, 150m, (A200) Adri, 200m, (A250) Adri, 250m, (V50) Veraval, 50m, (V100) Veraval, 100m, (V150) Veraval, 150m, (V200) Veraval, 200m and (V250) Veraval, 250m.

between distances from shore were not significant (p=0.654). There were no interactions (always p>0.187). The 3-way Permanova using Gross Primary Production (GPP) as response variable yield significant differences between sites (p=0.001). Fronds from Adri had significantly more GPP than fronds from Veraval. Differences between months were not significant (p=0.217). Differences between distances from shore were not significant (p=0.729). There were no interactions (always p>0.24).

4 Discussion

The weight-to-length exponent indicates whether or not individuals preserve their shape while growing. Fronds that do preserve their shape (i.e., isometric growth) have exponents ≈ 3. Fronds that do not preserve their shape (i.e., allometric growth) have exponents smaller than 3. Exponents larger than 3 indicate that something more happened besides fronds elongating along the three spatial dimensions; which could be increased branching or branch thickness. Scrosati et al. (2020) present examples of seaweeds corresponding to all these cases. The *G. dura* weight-to-length allometric exponent of 2.87 indicates that it grows almost isometrically (i.e., equally along the three spatial dimensions) (Figure 1). Thus, the fronds grew preserving their shape. However, while growing, *G. dura* barely increased the number of its primary branches (Figure 2C) or thickened them (Figure 2B), which goes in accordance with the isometric exponent ≈ 3. In conclusion, *G. dura* growth is basically a process of frond elongation along the three spatial dimensions. The same happens with the Kelp *Saccharina latissima* cultivated in longlines in Norway, showing an isometric exponent = 3.03 (r^2 = 0.941) (Overrein et al., 2024). Despite *G. dura* growth being basically a process of frond elongation along the three spatial dimensions, fronds where bushier and branches were thicker at Veraval than at Adri, which also contributed to the larger biomass yield in Veraval. This differentiation was present and constant since the beginning of the growing season, and not something that evolved with time; raising the question about whether this was strictly forced by the environment or is there a genetic differentiation between Veraval and Adri strains. Supporting a strictly environmental justification, the environment should have been particularly stressful at Adri, leading to the reduced production of growth hormones at the onset of the growing season (Figure 3.right panel – z1) and the reduced growth coupled with the enhanced antioxidant activity during the entire growth season (Figure 3.left panel – z2). Notice that the major differentiation between Veraval and Adri for frond branching was during January, at the onset of the growing season (Figure 2C), which exactly matched the Veraval and Adri differentiation in growth hormones (Figure 3.right panel).

Gracilaria dura grew much larger at Veraval than at Adri. This was demonstrated both by the morphometric data (Figures 1, 2) and by the growth rate data (pc1\z1 in Figure 3). The principal component contrasting growth with antioxidant activity (pc1) suggested the reason for this differentiation between Veraval and Adri was growth inhibition by stress. The cause of stress was desiccation during low tide, which is debated in detail in a paragraph below. Presently, we highlight that stress from UV, excessive temperature and excessive light leads photoautotrophs (plants and seaweeds) to the detrimental uncontrolled accumulation of reactive oxygen species (ROS) that negatively impact metabolism, deter growth, oxidize tissue, and ultimately lead to cell death (Cruces et al., 2018; Savchenko and Tikhonov, 2021). To avoid such effects, photoautotrophs evolved countermeasures including increased antioxidative activity (Kusvuran et al., 2016; Cruces et al.,

2018; Khaleghi et al., 2019; Kowalczewski et al., 2020; Savchenko and Tikhonov, 2021), here demonstrated by increased TAC and CUPRAC. Corroborating the hypothesis that ROS stress played an important part in the decreased frond growth and size observed in Adri, were the concomitant increases in O_2 production and Chl-a content. Oxidative stress in photoautotrophs commonly results from the saturation of the photosynthetic electron transport chain, leading to the increased production of ROS, including O_2 (Tietz et al., 2017; Savchenko and Tikhonov, 2021). This may explain the increased O_2 production by fronds from Adri, which was initially mistakenly perceived as an increase in NPP. The saturation of the photosynthetic electron transport chain is promoted by excessive illumination or a reduced rate of CO_2 fixation (Savchenko and Tikhonov, 2021). The increased Chl-a content may represent an adaptation to the saturating light environment by enhancing the Non-photochemical quenching (NPQ). This is a process for the harmless dissipation of excess absorbed light energy, most often as heat, although other forms of energy dissipation are possible (Demmig-Adams et al., 2014; Ruban, 2016; Tietz et al., 2017). NPQ prevents the harmful build-up of excess energy that could damage the antenna, the pigments and ultimately lead to cell death. This process (and molecular adaptation), taking place in the antenna and requiring photosynthetic pigments for energy transfers, is considered the most efficient and fastest response of the photosynthetic membrane to excess light (Demmig-Adams et al., 2014; Ruban, 2016; Tietz et al., 2017). Chl-a has a fundamental role in NPQ (Papageorgiou and Govindjee, 2014).

Fighting stress - from desiccation as well as other sources - demands allocating significant amounts of resources (nutrients and energy) that become unavailable for growth. In the case of antioxidant activity, this is generally performed by phenolic compounds (Cruces et al., 2018; Marinho et al., 2019; Kowalczewski et al., 2020), flavonoid compounds (Marinho et al., 2019) and enzymes (Kusvuran et al., 2016; Khaleghi et al., 2019). Furthermore, seaweeds also produce other costly metabolites to protect themselves directly from UV radiation (Gómez et al., 2005; Jiang et al., 2008; Kumar et al., 2011; Cruces et al., 2018). For fronds in Adri, the direct detrimental effects of desiccation and ROS stress may have been added to the cost of allocating resources to fight them, with these resources having become unavailable for growth. The strongest evidence suggesting that such was the case came from the content of costly metabolites (namely, R-phycoerythrin, R-phycocyanin, auxin and gibberellic acid) being lower in Adri than in Veraval (pc2\z2 in Figure 3). Auxins and gibberellins in particular have been found responsible for the induction of frond elongation, apical dominance, and tissue differentiation (Tarakhovskaya et al., 2007; Sambhwani et al., 2022). These hormones were found in much higher quantities in the fronds from Veraval than in the fronds from Adri, as demonstrated by pc2. However, this only occurred during the early growth season (i.e., during January, when growth hormones peaked at Veraval) and for the remaining monitorization, these hormones remained similarly lower at both sites. This suggests that the environment was so stressful at Adri at the onset of the growth season, demanding so much resource allocation for antioxidant activity, that the fronds in there lacked resources to produce growth hormones and photosynthetic pigments in larger quantities. Later on, during February and March, either the environment became more favorable and this bias tended to dissipate, or the posterior reduction in the content of growth hormones is a natural process in the biology of *G. dura*. Either way, growth had already been triggered in January with the discrepancies between Veraval and Adri.

The different stress levels experienced by *G. dura* fronds growing at Veraval or Adri likely resulted from the type of substrate. In both cases, the locations were intertidal. However, while fronds in Veraval occupied rockpools enabling them to stay submerged during low tide, fronds in Adri laid in the flat bare rocks, thus desiccating during low tide. This was exactly the same that happened to *Gracilaria chilensis* (also named *Agarophyton chilensis*) fronds in the Valdivia River estuary. In this case, the fronds occupying Niebla intertidal rock pools outperformed the fronds laying (and desiccating) in the Corral intertidal flat bare rocks. This outperformance was evident in adult survival (Vieira et al., 2018a), growth (Vieira et al., 2021), fertility and sporeling survival (Vieira et al., 2018b), ultimately leading to more vigorous and productive sub-populations that occupied the niche more efficiently (Vieira et al., 2022). Intertidal seaweed stands subject to desiccation and excessive light due to emersion during low tide suffer from decreased photosynthesis and growth, bleaching and mortality (Figueroa and Gómez, 2001; Hays, 2007; Zheng and Gao, 2009; Miller et al., 2011; Mueller et al., 2015). For algae occupying these habitats, forming denser turfs mitigates these stresses and their consequences, while also decreasing the energetic costs of copping with them (Hay, 1981; Scrosati and Dewreede, 1998; Kamiya et al., 2021).

The first conclusion that can be drawn is that *G. dura* fronds cultivated permanently submerged could grow faster and larger. Thus, this should be the protocol to maximize biomass production. However, for the specific production of antioxidative molecules of commercial interest, it is better to cultivate fronds with some degree of stress from emersion, provided that this stress is initially avoided (i.e., avoided for *G. dura* germlings and young fronds). Hence, the optimization of *G. dura* production on floating structures (as described in the methods) requires that these are always submerged, and thus never placed in intertidal locations. Furthermore, the fronds placed on top (i.e., closer to, or even on, the sea-surface) will be richer in antioxidative compounds. On the other hand, the optimized exploration of natural *G. dura* stands in Gujarat should harvest in Veraval for maximum biomass yield and in Adri for antioxidative compounds. Furthermore, for the specific objective of producing antioxidative compounds, after the onset of the growth season, some *G. dura* fronds in rockpools may be relocated to more exposed substrates. These relocated fronds shall not lack for biomass production as, according to the sell-thinning theory (see Creed et al., 2019 and references therein), competition in crowded rockpools would induce mortality in some of these fronds, anyway (Vieira et al., 2018a, 2022). Then, it becomes a matter of determining how crowded the rockpools get and how many fronds may be relocated without impacting biomass yield.

Gracilaria spp. from the Indo-Pacific are commonly adapted to high temperatures and irradiances (Raikar et al., 2001), and such is also the case for *G. dura*. A previous study suggests that marked phenotypical differentiation should not be expected in *G. dura* in

Gujarat (Dawange et al., 2023b). Still, the differentiation between Veraval and Adri in the light environment, temperature and desiccation led *G. dura* individuals from either location to show marked differences in ecophysiology, metabolism and growth. Subject to more stress, *G. dura* in Adri clearly underperformed. This is common in rhodophytes (see, as examples, Duarte and Ferreira, 1995; Mueller et al., 2015; Vieira et al., 2018a, b, 2021, 2022). The question arose about whether the differences between environmental conditions observed in Veraval and Adri led to the evolution of genetic strains specific to either habitat that may show different performances and yields when cultivated in similar environments. A marked phenotypical differentiation, whether of a genetic origin or acquired during development (photo-acclimatation), in response to these stressors can be observed at spatial resolution as thin as among individuals occupying different bands (i.e., heights) of the same intertidal population or among individuals occupying the same habitat during different seasons (Smith and Berry, 1986; Matta and Chapman, 1991; Britting and Chapman, 1993; Figueroa and Gómez, 2001; Wright et al., 2004; Williams and Dethier, 2005; Hays, 2007; Miller et al., 2011). For these differences to be driven from genetics, they need to be observed among individuals cultivated for a long time in similar conditions. However, in our study some variables were measured from fronds subject to only 5-day acclimatization while other variables were measured from fronds subject to no acclimatization at all. Therefore, our work does not allow us to determine whether the observed phenotypic differences resulted from genetic differentiation or acquired memory of recent ecological history (i.e., preserved adaptations to recent ecological conditions).

A word of caution about the estimation of NPP and GPP for intertidal photoautotrophs. We think that the results of enhanced NPP were false and that the likeliest explanation is the application of the O_2 method in situations where stress from desiccation, excess temperature and excess light lead photoautotrophs to an uncontrolled accumulation of reactive oxygen species (ROS), including O_2. Because the estimation of GPP depends on the NPP input (GPP=R–NPP), we also have no confidence in the GPP readings. Respiration seems not to have been affected by the challenging environmental conditions at Veraval.

5 Conclusions

The differences between the two locations studied, namely Veraval and Adri, were preserved even when the frond fragments were acclimatized and grown under the same conditions. Therefore, we infer that either there is a genetic differentiation or G. dura fronds preserve a phenotypic memory of their recent ecological past. Veraval is better for biomass production, although it is uncertain whether this is exclusively due to the environmental conditions of the site or a site-specific strain has also evolved. On the other hand, the intertidal fronds of G. dura desiccating in Adri's flat bare rock during low tide, despite growing less (possibly due to the stress from the detrimental uncontrolled accumulation of Reactive Oxygen Species), still have commercial value as they show increased accumulation of antioxidants.

Data availability statement

The raw data supporting the conclusions of this article will be made available by the authors, without undue reservation.

Author contributions

VV: Data curation, Formal analysis, Investigation, Methodology, Software, Validation, Visualization, Writing – original draft, Writing – review & editing. PD: Data curation, Formal analysis, Writing – original draft. SJ: Data curation, Formal analysis, Funding acquisition, Project administration, Writing – original draft, Writing – review & editing. JS: Funding acquisition, Project administration, Writing – review & editing. VM: Conceptualization, Funding acquisition, Methodology, Project administration, Supervision, Writing – review & editing.

Funding

The author(s) declare financial support was received for the research, authorship, and/or publication of this article. PD and SJ were funded by the Science and Engineering Research Board (SERB), New Delhi (India) under the project EEQ/2018/000562. VM received funding from the Council of Scientific and Industrial Research, New Delhi (India) under the project MLP 0051. JS received funding from the Mar2020 program (Portugal) under project PhycosPT (MAR02.01.01-FEAMP-0039). PD received funding through a research fellowship from MAR2020 program (Portugal). VV was supported by FCT/MCTES (PIDDAC) through project LARSyS - FCT Pluriannual funding 2020-2023 (UIDB/EEA/50009/2020).

Acknowledgments

The authors would like to thank the Director, CSIR-Central Salt and Marine Chemicals Research Institute, Bhavnagar for providing facilities. This communication has CSMCRI PRIS approval number 38/2023.

Conflict of interest

The authors declare that the research was conducted in the absence of any commercial or financial relationships that could be construed as a potential conflict of interest.

Publisher's note

Supplementary material

The Supplementary Material for this article can be found online at: https://www.frontiersin.org/articles/10.3389/fmars.2024.1397379/full#supplementary-material

SUPPLEMENTARY FIGURE 1
Association between z1 and its contributing variables Daily Growth Rates (DGR), CUPRAC and TAC of *Gracilaria dura*.

SUPPLEMENTARY FIGURE 2
Association between z2 and its contributing variables R-Phycoerythrin (PE) and R-Phycocyanin (PC), Auxin and Gibberellic acid of *Gracilaria dura*.

References

Alemañ, A. E., Robledo, D., and Hayashi, L. (2019). Development of seaweed cultivation in Latin America: current trends and future prospects. *Phycologia* 58, 462–471. doi: 10.1080/00318884.2019.1640996

Apak, R., Güçlü, K., Özyürek, M., and Karademir, S. E. (2004). Novel total antioxidant capacity index for dietary polyphenols and vitamins C and E, using their cupric ion reducing capability in the presence of neocuproine: CUPRAC method. *J. Agric. Food. Chem.* 52, 7970–7981. doi: 10.1021/jf048741x

Britting, S., and Chapman, D. (1993). Physiological comparison of the isomorphic life history phases of the high intertidal alga Endocladia muricata (Rhodophyta). *J. Phycol. - J. Phycol.* 29, 739–745. doi: 10.1111/j.0022-3646.1993.00739.x

Cai, J., Lovatelli, A., Aguilar-Manjarrez, J., Cornish, L., Dabbadie, L., Desrochers, A., et al. (2021). Seaweeds and microalgae: an overview for unlocking their potential in global aquaculture development. *FAO Fisheries and Aquaculture Circular No. 1229*. (Rome: FAO). doi: 10.4060/cb5670en

Creed, J., Vieira, V.M.N.C.S., Norton, T. A., and Caetano, D. (2019). A meta-analysis shows that seaweeds surpass plants, setting life-on-Earth's limit for biomass packing. *BMC Ecol.* 19, 1–11. doi: 10.1186/s12898-019-0218-z

Cruces, E., Flores-Molina, M. R., Dıaz, M. J., Huovinen, P., and Gómez, I. (2018). Phenolics as photoprotective mechanism against combined action of UV radiation and temperature in the red alga *Gracilaria Chilensis*? *J. Appl. Phycol.* 30, 1247–1257. doi: 10.1007/s10811-017-1304-2

Dawange, P., Mantri, V. A., and Jaiswar, S. (2023a). Selection and development of superior strains through functional trait- based approach in agarophytic red alga *Gracilaria dura* (Rhodophyta). *J. Envin. Biol.* 44, 795–803. doi: 10.22438/jeb/

Dawange, P. S., Vieira, V.M.N.C.S., Sardinha, J. P., Jaiswar, S., and Mantri, V. A. (2023b). Resource-limited Gracilaria dura partitions resources between growth and survival: Knowledge base for optimizing production. *J. Appl. Phycol.* 35, 2985–2994. doi: 10.1007/s10811-023-03101-0

Dawes, C. J., Trono, G. C., and Lluisma, A. O. (1993). Clonal propagation of *Eucheuma denticulatum* and *Kappaphycus alvarezii* for Philippine seaweed farms. *Hydrobiologia* 260, 379–383. doi: 10.1007/BF00049044

Demmig-Adams, B., Garab, G., Adams, W. III, and Govindgee, (2014). *Non-photochemical quenching and energy dissipation in plants, algae and cyanobacteria, Advances in Photosynthesis and Respiration 40* (Dordrecht: Springer). doi: 10.1007/978-94-017-9032-1

Duarte, P., and Ferreira, J. G. (1995). Seasonal adaptation and short-term metabolic responses of *Gelidium sesquipedale* to varying light and temperature. *Mar. Ecol. Prog. Ser.* 121, 289–300. doi: 10.3354/meps121289

Engel, C., Åberg, P., Gaggiotti, O. E., Destombe, C., and Valero, M. (2001). Population dynamics and stage structure in a haploid-diploid red seaweed, *Gracilaria gracilis*. *J. Ecol.* 89, 436–450. doi: 10.1046/j.1365-2745.2001.00567.x

Faria, A. V. F., Bonomi-Barufi, J., and Plastino, E. M. (2017). Ecotypes of *Gracilaria caudata* (Gracilariales, Rhodophyta): physiological and morphological approaches considering life history phases. *J. Appl. Phycol.* 29, 707–719. doi: 10.1007/s10811-016-1018-x

Figueroa, F. L., and Gómez, I. (2001). Photosynthetic acclimation to solar UV radiation of marine red algae from the warm-temperate coast of southern Spain: A review. *J. Appl. Phycol.* 13, 233–245. doi: 10.1023/A:1011126007656

Gómez, I., Figueroa, F. L., Huovinen, P., Ulloa, N., and Morales, V. (2005). Photosynthesis of the red alga *Gracilaria Chilensis* under natural solar radiation in an estuary in southern Chile. *Aquaculture* 244, 369–382. doi: 10.1016/j.aquaculture.2004.11.037

Gonzales, M., Villena, G. K., and Kitazono, A. A. (2021). Evaluation of the antioxidant activities of aqueous extracts from seven wild plants from the Andes using an in *vivo* yeast assay. *Results. Chem.* 3, 100098. doi: 10.1016/j.rechem.2021.100098

Guillemin, M. L., Valenzuela, P., Gaitán-Espitia, J. D., and Destombe, C. (2014). Evidence of reproductive cost in the triphasic life history of the red alga *Gracilaria Chilensis* (Gracilariales, Rhodophyta). *J. Appl. Phycol.* 26, 569–575. doi: 10.1007/s10811-013-0072-x

Gupta, V., Kumari, P., and Reddy, C. (2015). Development and Characterization of Somatic Hybrids of Ulva reticulata Forsskål (×) Monostroma oxyspermum (Kutz.) Doty. *Front. Plant Sci.* 6. doi: 10.3389/fpls.2015.00003

Hay, M. E. (1981). The functional morphology of turf-forming seaweeds: persistence in stressful marine habitats. *Ecology* 62, 739–750. doi: 10.2307/1937742

Hays, C. G. (2007). Adaptive phenotypic differentiation across the intertidal gradient in the alga *Silvetia compressa*. *Ecology* 88, 149–157. doi: 10.1890/0012-9658(2007)88[149:APDATI]2.0.CO;2

Jeffrey, S. T., and Humphrey, G. F. (1975). New spectrophotometric equations for determining chlorophylls a, b, c1 and c2 in higher plants, algae and natural phytoplankton. *Biochem. Physiol. Pflanz.* 167, 191–194. doi: 10.1016/S0015-3796(17)30778-3

Jha, B., Reddy, C. R. K., Thakur, M. C., and Rao, M. U. (2009). *Seaweeds of India: the diversity and distribution of seaweeds of Gujarat coast* (Dordrecht, The Netherland: Springer), 215 pp.

Jiang, H., Gao, K., and Helbling, E. W. (2008). UV-absorbing compounds in *Porphyra haitanensis* (Rhodophyta) with special reference to effects of desiccation. *J. Appl. Phycol.* 20, 387–395. doi: 10.1007/s10811-007-9268-2

Kamiya, M., Inoue, N., Suzuki, C., and Abe, S. (2021). Ecological, physiological, and biomechanical differences between gametophytes and sporophytes of *Chondrus ocellatus* (Gigartinales, Rhodophyta). *J. Phycol.* 57, 1590–1603. doi: 10.1111/jpy.13193

Kavale, M. G., Yadav, A., and Mantri, V. A. (2021). Initial comparison between monoline and tube net method of farming in red agarophyte Gracilaria dura: Evidence from hydrodynamic CFD simulations. *Aquaculture* 536, 736485. doi: 10.1016/j.aquaculture.2021.736485

Khaleghi, A., Naderi, R., Brunetti, C., Maserti, B. E., Salami, S. A., and Babalar, M. (2019). Morphological, physiochemical and antioxidant responses of *Maclura pomifera* to drought stress. *Sci. Rep.* 9, 19250. doi: 10.1038/s41598-019-55889-y

Kowalczewski, P.Ł., Radzikowska, D., Ivanišová, E., Szwengiel, A., Kačániová, M., and Sawinska, Z. (2020). Influence of abiotic stress factors on the antioxidant properties and polyphenols profile composition of green barley (*Hordeum vulgare* L.). *Int. J. Mol. Sci.* 21, 397. doi: 10.3390/ijms21020397

Kumar, M., Gupta, V., Trivedi, N., Kumari, P., Bijo, A. J., Reddy, C. R. K., et al. (2011). Desiccation induced oxidative stress and its biochemical responses in intertidal red alga *Gracilaria corticata* (Gracilariales, Rhodophyta). *Environ. Exp. Bot.* 72, 194–201. doi: 10.1016/j.envexpbot.2011.03.007

Kusvuran, S., Kiran, S., and Ellialtioglu, S. S. (2016). "Antioxidant Enzyme Activities and Abiotic Stress Tolerance Relationship in Vegetable Crops," in *Abiotic and Biotic Stress in Plants*. Eds. A. K. Shanker and C. Shanker (IntechOpen). doi: 10.5772/60477

Mantri, V. A., Shah, Y., and Thiruppathi, S. (2020). Feasibility of farming the agarose-yielding red alga Gracilaria dura using tube-net cultivation in the open sea along the Gujarat coast of NW India. *Appl. Phycol.* 1, 12–19. doi: 10.1080/26388081.2019.1648181

Mantri, V. A., Thakur, M. C., Kumar, M., Reddy, C. R. K., and Jha, B. (2009). The carpospore culture of industrially important red alga *Gracilaria dura* (Gracilariales, Rhodophyta). *Aquaculture* 297, 85–90. doi: 10.1016/j.aquaculture.2009.09.004

Marinho, G. S., Sørensen, A. D. M., Safafar, H., Pedersen, A. H., and Holdt, S. L. (2019). Antioxidant content and activity of the seaweed *Saccharina latissima*: A seasonal perspective. *J. Appl. Phycol.* 31, 1343–1354. doi: 10.1007/s10811-018-1650-8

Matta, J., and Chapman, D. (1991). Photosynthetic responses and daily carbon balance ofColpomenia peregrina: Seasonal variations and differences between intertidal and subtidal populations. *Mar. Biol.* 108, 303–313. doi: 10.1007/BF01344345

McHugh, D. J. (2003). *A guide to the seaweed industry. FAO Fisheries Technical Paper. No. 441* (Rome: FAO), 105p.

Meena, R., Chaudhary, J. P., Agarwal, P. K., Maiti, P., Chatterjee, S., Raval, H. D., et al. (2014). Surfactant-induced coagulation of agarose from aqueous extract of *Gracilaria dura* seaweed as an energy-efficient alternative to the conventional freeze–thaw process. *RSC. Adv.* 4, 28093–28098. doi: 10.1039/C4RA04476B

Miller, S. M., Hurd, C. L., and Wing, S. R. (2011). Variations in growth, erosion, productivity, and morphology of *Ecklonia radiata* (Alariaceae; Laminariales) along a fjord in southern New Zealand. *J. Phycol.* 47, 505–516. doi: 10.1111/jpy.2011.47.issue-3

Mueller, R., Fischer, A. M., Bolch, C. J., and Wright, J. T. (2015). Environmental correlates of phenotypic variation: do variable tidal regimes influence morphology in intertidal seaweeds? *J. Phycol.* 51, 859–871. doi: 10.1111/jpy.12329

Overrein, M. M., Tinn, P., Aldridge, D., Johnsen, G., and Fragoso, G. M. (2024). Biomass estimations of cultivated kelp using underwater RGB images from a mini-

ROV and computer vision approaches. *Front. Mar. Sci.* 11. doi: 10.3389/fmars.2024.1324075

Papageorgiou, G. C., and Govindjee, (2014). "The Non-Photochemical Quenching of the Electronically Excited State of Chlorophyll a in Plants: Definitions, Timelines, Viewpoints, Open Questions," in *Non-Photochemical Quenching and Energy Dissipation in Plants, Algae and Cyanobacteria. Advances in Photosynthesis and Respiration*, vol. 40 . Eds. B. Demmig-Adams, G. Garab, W. Adams III and Govindjee, (Dordrecht, Springer). doi: 10.1007/978-94-017-9032-1_1

Prasad, K., Das, A. K., Oza, M. D., Brahmbhatt, H., Siddhanta, A. K., Meena, R., et al. (2010). Detection and quantification of some plant growth regulators in a seaweed-based foliar spray employing a mass spectrometric technique sans chromatographic separation. *J. Agric. Food Che.* 58, 4594–4601. doi: 10.1021/jf904500e

Prieto, P., Pineda, M., and Aguilar, M. (1999). Spectrophotometric quantitation of antioxidant capacity through the formation of a phosphomolybdenum complex: specific application to the determination of vitamin E. *Anal. Biochem.* 269, 337–341. doi: 10.1006/abio.1999.4019

Raikar, S. V., Iima, M., and Fujita, Y. (2001). Effect of temperature, salinity and light intensity on the growth of Gracilaria spp. (Gracilariales, Rhodophyta) from Japan, Malaysia and India. *Indian. J. Mar. Sci.* 30, 98–104.

Reddy, C. R. K., Baghel, R. S., Trivedi, N., Kumari, P., Gupta, V., Prasad, K., et al. (2018). *U.S. Patent No. 10,000,579* (Washington, DC: U.S. Patent and Trademark Office).

Ruban, A. V. (2016). Nonphotochemical Chlorophyll fluorescence quenching: mechanism and effectiveness in protecting plants from photodamage. *Plant Physiol.* 170, 1903–1916. doi: 10.1104/pp.15.01935

Sambhwani, K., Mathukiya, G., Dawange, P., Sequeira, R. A., Prasad, K., and Mantri, V. A. (2022). Analysis of functional traits in Gracilaria dura (Rhodophyta: Gracilariacae) reveals variation in wild and farmed populations. *J. Appl. Phycol.* 34, 1017–1031. doi: 10.1007/s10811-022-02697-z

Sambhwani, K., Modi, J., Singhala, A., Bramhabatt, H., Mishra, A., and Mantri, V. A. (2020). Analysis of functional traits in female gametophytic and tetrasporophytic life phases of industrially important red alga *Gracilaria dura* (Rhodophyta: Gracilariacae). *J. Appl. Phycol.* 32, 1961–1969. doi: 10.1007/s10811-020-02116-1

Saminathan, K. R., Ashok, K. S., Veeragurunathan, V., and Mantri, V. A. (2015). Seedling production in the industrially important agarophyte *Gracilaria dura* (Gracilariales, Rhodophyta). *J. Appl. Phycol.* 27, 1541–1548. doi: 10.1007/s10811-014-0450-z

Sampath-Wiley, P., and Neefus, C. D. (2007). An improved method for estimating R-phycoerythrin and R-phycocyanin contents from crude aqueous extracts of *Porphyra* (Bangiales, Rhodophyta). *J. Appl. Phycol.* 19, 123–129. doi: 10.1007/s10811-006-9118-7

Savchenko, T., and Tikhonov, K. (2021). Oxidative stress-induced alteration of plant central metabolism. *Life (Basel).* 11, 304. doi: 10.3390/life11040304

Scrosati, R., and Dewreede, R. E. (1998). The impact of frond crowding on frond bleaching in the clonal intertidal alga *Mazzaella cornucopiae* (Rhodophyta, Gigartinaceae) from British Columbia, Canada. *J. Phycol.* 34, 228–232. doi: 10.1046/j.1529-8817.1998.340228.x

Scrosati, R. A., MacDonald, H. L., Córdova, C. A., and Casas, G. N. (2020). Length and biomass data for Atlantic and Pacific seaweeds from both hemispheres. *Front. Mar. Sci.* 7, 592675. doi: 10.3389/fmars.2020.592675

Shah, Y., Rathod, M., Kavale, M. G., Jaiswar, S., and Mantri, V. A. (2022). Socio-demographic profiling and asset indicators of *Gracilaria dura* farmers from northern west coast of India useful for longitudinal analysis. *Aquacult. Int.* 30, 273–287. doi: 10.1007/s10499-021-00797-0

Shah, Y., Yadav, A., Kumar, M. A., Kavale, M. G., Prasad, K., and Mantri, V. A. (2021). 'Proof of concept' of how tube-net diameter affects growth and agar content in industrially important farmed red seaweed *Gracilaria dura*. *J. Appl. Phycol.* 33, 2349–2358. doi: 10.1007/s10811-021-02443-x

Skriptsova, A. V., and Nabivailo, Y. V. (2009). Comparison of three gracilarioids: growth rate, agar content and quality. *J. Appl. Phycol.* 21, 443–450. doi: 10.1007/s10811-008-9389-2

Smith, C., and Berry, J. (1986). Recovery of photosynthesis after exposure of intertidal algae to osmotic and temperature stresses: comparative studies of species with differing distributional limits. *Oecologia* 70, 6–12. doi: 10.1007/BF00377105

Suto, S. (1959). Skeletonema no tame no jinkou baiyoueki. *Suisan. Zoushoku.* 7, 17–19.

Tarakhovskaya, E. R., Maslov, Y. I., and Shishova, M. F. (2007). Phytohormones in algae. *Russ. J. Plant Physiol.* 54, 163–170. doi: 10.1134/S1021443707020021

Tietz, S., Hall, C. C., Cruz, J. A., and Kramer, D. M. (2017). NPQ(T): a chlorophyll fluorescence parameter for rapid estimation and imaging of non-photochemical quenching of excitons in photosystem-II-associated antenna complexes. *Plant Cell Environ.* 40, 1243–1255. doi: 10.1111/pce.12924

Usandizaga, S., Camus, C., Kappes, J. L., Guillemin, M. L., and Buschmann, A. H. (2019). Effect of temperature variation in *Agarophyton Chilensis*: Contrasting the response of natural and farmed populations. *J. Appl. Phycol.* 31, 2709–2717. doi: 10.1007/s10811-019-1757-6

Valero, M., Guillemin, M. L., Destombe, C., Jacquemin, B., Gachon, C. M., Badis, Y., et al. (2017). Perspectives on domestication research for sustainable seaweed aquaculture. *Perspect. Phycol.* 4, 33–46. doi: 10.1127/pip/2017/0066

Veeragurunathan, V., Eswaran, K., Saminathan, K. R., Mantri, V. A., Ajay, G., and Jha, B. (2015). Feasibility of *Gracilaria dura* cultivation in the open sea on the South-eastern coast of India. *Aquaculture* 438, 68–74. doi: 10.1016/j.aquaculture.2015.01.009

Vieira, V.M.N.C.S. (2012). Permutation tests to estimate significances on Principal Components Analysis. *Comput. Ecol. Software.* 2, 103–123.

Vieira, V.M.N.C.S., and Creed, J. (2013a). Estimating significances of differences between slopes: A new methodology and software. *Comput. Ecol. Software.* 3, 44–52.

Vieira, V.M.N.C.S., and Creed, J. (2013b). Significances of differences between slopes: An upgrade for replicated time series. *Comput. Ecol. Software.* 3, 102–109.

Vieira, V.M.N.C.S., Engelen, A. H., Huanel, O. R., and Guillemin, M. L. (2018a). Haploid females in the isomorphic biphasic life-cycle of *Gracilaria Chilensis* excel in survival. *BMC Evol. Biol.* 18, 174. doi: 10.1186/s12862-018-1285-z

Vieira, V.M.N.C.S., Engelen, A. H., Huanel, O. R., and Guillemin, M. L. (2018b). Differentiation of haploid and diploid fertilities in *Gracilaria Chilensis* affect ploidy ratio. *BMC Evol. Biol.* 18, 183. doi: 10.1186/s12862-018-1287-x

Vieira, V.M.N.C.S., Engelen, A. H., Huanel, O. R., and Guillemin, M.-L. (2021). Differential frond growth in the isomorphic haploid-diploid red seaweed *Agarophyton Chilense* by long-term in *situ* monitoring. *J. Phycol.* 57, 592–605. doi: 10.1111/jpy.13110

Vieira, V.M.N.C.S., Engelen, A. H., Huanel, O. R., and Guillemin, M.-L. (2022). An individual-based model of the red alga *agarophyton Chilense* unravels the complex demography of its intertidal stands. *Front. Ecol. Evol.* 10, 797350. doi: 10.3389/fevo.2022.797350

Vignesh, M., Kazi, M. A., Rathore, M. S., Kavale, M. G., Dineshkumar, R., and Mantri, V. A. (2020). Artificial neural network modelling for seedling regeneration in *Gracilaria dura* (Rhodophyta) under different physiochemical conditions. *Plant Cell Tissue Organ Cult. (PCTOC).* 143, 583–591.

Williams, S., and Dethier, M. (2005). High and dry: Variation in net photosynthesis of the intertidal seaweed Fucus gardneri. *Ecology* 86, 2373–2379. doi: 10.1890/04-1569

Wright, J., Williams, S., and Dethier, M. (2004). No zone is always greener: Variation in the performance of Fucus gardneri embryos, juveniles and adults across tidal zone and season. *Mar. Biol.* 145, 1061–1073. doi: 10.1007/s00227-004-1399-2

Zheng, Y., and Gao, K. (2009). Impacts of solar UV radiation on the photosynthesis, growth, and UV-absorbing compounds in *Gracilaria lemaneiformis* (rhodophyta) grown at different nitrate concentrations. *J. Appl. Phycol.* 45, 314–323. doi: 10.1111/j.1529-8817.2009.00654.x

frontiers | Frontiers in Marine Science

TYPE Original Research
PUBLISHED 24 July 2024
DOI 10.3389/fmars.2024.1424999

OPEN ACCESS

EDITED BY
Yngvar Olsen,
NTNU, Norway

REVIEWED BY
Chunyan Zhao,
Qingdao Agricultural University, China
Yun Wang,
Chinese Academy of Fishery Sciences (CAFS), China

*CORRESPONDENCE
Liping Liu
lp-liu@shou.edu.cn

†These authors have contributed equally to this work

RECEIVED 29 April 2024
ACCEPTED 17 June 2024
PUBLISHED 24 July 2024

CITATION
Li K, Li Y, Li T, Cui R and Liu L (2024) Nutritional composition and transcriptome analysis of the newly hatched *Anguilla japonica* from embryo to preleptocephali obtained from artificial reproduction. *Front. Mar. Sci.* 11:1424999. doi: 10.3389/fmars.2024.1424999

Nutritional composition and transcriptome analysis of the newly hatched *Anguilla japonica* from embryo to preleptocephali obtained from artificial reproduction

Kang Li[1,2,3†], Yuangu Li[1†], Tiezhu Li[1], Rongfeng Cui[4] and Liping Liu[1,2,3*]

[1]Key Laboratory of Exploration and Utilization of Aquatic Genetic Resources, Ministry of Education, Shanghai Ocean University, Shanghai, China, [2]National Demonstration Center for Experimental Fisheries Science Education, Shanghai Ocean University, Shanghai, China, [3]Shanghai Engineering Research Center of Aquaculture, Shanghai Ocean University, Shanghai, China, [4]School of Ecology, Sun Yat-sen University, Guangzhou, China

The starter diet for Japanese eel (*Anguilla japonica*) has always been a difficult problem for the realization of total artificial reproduction. Therefore, this research analyzed the nutritional composition of artificially fertilized eggs, and transcriptome of samples from early hatchlings of fry to better understand nutrients requirements. The composition of crude lipid and crude protein in fertilized eggs was 7.24% ± 0.32% and 10.56% ± 0.41%, respectively. Seven kinds of essential amino acids (EAA) were detected but took a comparable lower content (3.19%) than other marine fish eggs. We randomly assembled 265.74 million clean reads and identified 1751 differentially expressed genes (DEGs) ($P < 0.01$) from pre-leptocephalus larvae. A total of 23 KEGG pathways related to the digestive and metabolic system were detected. Genes related to the secretion pathway of saliva, pancreatic juice and other digestive juices were significantly changed. Transcriptome analysis showed that as larvae aged, glycolytic metabolism and the transcription level of hexokinase (HK) increased significantly (day 0 to 12). This study will facilitate future studies on the nutrition of *A. japonica* larvae and other biological traits to reproductive research.

KEYWORDS

***Anguilla japonica*, embryo, larvae, transcriptome analysis, nutritional components**

1 Introduction

Japanese eel (*Anguilla japonica*) is an important cultured species in East Asia with a mysterious life cycle that involving spawning in the ocean and migrating to freshwater (Tsukamoto, 1992; Tanaka, 2015; Kuan-Mei et al., 2018). However, its populations have suffered a severe reduction due to overfishing, habitat loss, and environmental deterioration (Matsushige et al., 2019; Pike et al., 2020). Eel farming, which relies on wild-caught glass eels, is also experiencing a sharp decrease in annual harvests (Dekker and Casselman, 2014; Koh et al., 2017; Feunteun and Prouzet, 2020). Although the complete life cycle of *A. japonica* was firstly closed in the lab in 2010 (Tanaka et al., 2001; Masuda et al., 2012), commercialization remains challenging due to the low survival rate of pre-leptocephalus larvae (Okamura et al., 2014).

The low survival rate of newly hatched larvae in lab is likely due to nutritional deficiencies in their artificial diets. Despite efforts to include shark egg yolk, Antarctic krill, and rotifer paste, additional nutritional improvements are still necessary (Tanaka et al., 2003; Okamura et al., 2013; Liu et al., 2017; Okamura et al., 2019). Pousão-Ferreira et al. (1999) successfully used gilthead seabream (*Sparus aurata*) eggs to feed *S. aurata* larvae, determining nutritional requirements during the larval rearing based on egg composition. Mourente and Rosa (1996) confirmed the fatty acids levels for unfed Senegal sole (*Solea senegalensis*) larvae. Ohkubo et al. (2008) highlighted the importance of understanding egg nutritional composition for developing starter diets by describing nutrient changes from fertilized eggs to yolk-sac larvae of *A. japonica*.

The digestive system function in fish larvae depends on both genetically pre-programmed and extrinsically influenced factors (Politis et al., 2018). The expression of several selected pancreatic enzyme genes indicated that *A. japonica* larvae acquire full function by the onset of exogenous feeding at 8-12 dph (Okamura et al., 2019). However, other digestive enzyme genes and nutrient transporters in *A. japonica* are not well studied, and few studies address food digestion and nutrient absorption during the preleptocephali stage. The advent of next-generation sequencing technology has advanced genome and transcriptome analysis in aquatic organisms, providing insight into gene expression during developmental stages (Kleppe et al., 2014). Changes in the quantity and quality of transcriptome data can reflect the expression status of related genes in specific circumstances, which can effectively improve the quality of basic research. RNA-Seq, in partic3ular, is a powerful tool for profiling and quantifying RNA transcripts, enhancing the quality of basic research (Wang et al., 2010). It provides fundamental insights into biological processes and applications such as gene expression levels in developmental stages, combining advantages of high throughput, low background noise and high sensitivity (Ozsolak and Milos, 2010; Churcher et al., 2015; Hsu et al., 2015).

With the aim to explore the dietary requirements for the preleptocephali of *A. japonica* during the critical early life history stage, the nutritional composition of eggs was determined and the RNA of both embryos and preleptocephali was sequenced. It is hope to reveal the molecular events that affect the nutrient digestion and absorption, and to provide a basis for the future research on nutrient requirements of artificially *A. japonica* hatchlings.

2 Materials and methods

2.1 Artificial reproduction and sampling

The wild-caught broodstock *A. japonica* were cultured in the experimental facility of the Marine and Fisheries Research Institute of Ningbo (China), where they were kept in 8 m × 4 m × 1.7 m pond and the natural seawater was maintained at 20 ± 4°C and adjusted to 31 ± 5 psu salinity using Red Sea® Salts. Fish were not fed during the experiment and around 75% of the pond area was shaded by the black net. At the onset of experiments, all experimental broodstock *A. japonica* were anaesthetized (MS-222) and then tagged with a passive integrated transponder.

The *A. japonica* were artificially induced to mature using the method detailed in Jiang et al. (2012). Five female broodstocks were euthanized after stripping to collect eggs, which were pooled at equal ratios before being stored at -80°C until nutritional analyses. Natural spawning happened around 12 h after the remaining females and males were put together, then fertilized eggs were collected and reared at 24°C in seawater (31 psu) in darkness. Hence, 50 fertilized eggs were collected as 0 d sample, and 30 pre-leptocephalus samples were taken every three days after hatching until the 12th day. All samples were preserved by RNA*later* (Tiangen Biotech, Beijing, China) and then stored at -80°C until RNA extraction.

2.2 Nutritional analysis of eggs

The proximate composition analysis of eggs was performed using official methods of analysis of AOAC (1996). Moisture content was determined by drying 0.2g eggs' sample in an oven at 110°C to a constant weight. Ash content of eggs was determined by heating 0.2g eggs' sample in a muffle furnace for about 10-12 h at 550°C and weighting it after cooling. Crude protein content was measured by the Kjeldahl method (N content × 6.25) using a Kjeltech system (Kjeltec 2300, Foss, Sweden). The extraction of lipids from 0.2g eggs' sample was carried out with a mixture of chloroform and methanol (2:1, v/v) containing 0.01% BHT and determination of crude lipids was performed according to Folch et al. (1957).

Fatty acid methyl esters (FAMEs) were esterified with 14% BF_3 in methanol and the FAMEs extracted with hexane (Morrison and Smith, 1964). FAMEs were separated and detected by an Agilent 7890 gas chromatograph (Agilent Technologies, CA, USA) equipped with a flame ionization detector instrument. The 37-FAME Mix (Supelco, Bellefonte, PA, USA) was used to identify the FAMEs, and the fatty acid C19:0 (nonadecanoic acid, Sigma) was used as an internal standard for fatty acid quantification. All measurements were performed in triplicates, the fatty acids content was expressed as the percentage of each FA to the total FAs. The amino acid composition of the freeze-dried eggs digested

with hydrochloric acid was determined with a HITACHI L-8900 amino acid automatic analyzer (Hitachi Limited, Tokyo, Japan), and the peak areas were recorded (Gilani and Peace, 2005). Standard curves were plotted with amino acid peak area as the ordinate and amino acid concentration as the abscissa.

2.3 Calculation of the theoretical demand of nutrients in the starter diets of larvae *A. japonica*

The theoretical demand of each nutrient was calculated according to previous research (Pousão-Ferreira et al., 1999; Li et al., 2016). The crude lipid and crude protein contents of the fresh weight base were converted into dry weight base, which was the theoretical requirement for fat and protein of larvae eels. The requirement of each amino acid can be converted according to the content of crude protein on the basis of dry weight. Since the amino acids in this study were tested on the basis of dry weight, the detected value is the theoretical requirement of amino acids in the feed of larvae eels. Similarly, according to the crude fat content based on dry weight, the theoretical requirement of fatty acids in the feed can be calculated.

2.4 RNA extraction, library construction and sequencing

The total RNA of the whole fish was extracted using TRIzol® reagent (Invitrogen, California, USA) according to the manufacturer's instructions. Purified RNA was quantified by Agilent 2100 Bioanalyzer (Agilent Technologies, CA, USA). From each pooled sample, 5μg mRNA was isolated from total RNA using oligo (dT) magnetic beads (Invitrogen). Then five sequencing libraries, one for each time point, were constructed using Truseq™ RNA sample prep Kit (Illumina, San Diego, USA) according to the instruction. The mRNA was interrupted into~200 bp short fragments using the fragmentation buffer. It was then transcribed into the first-strand cDNA using reverse transcriptase and random hexamer primers, followed by second-strand cDNA synthesis. The double-stranded cDNA was subjected to end repair, phosphorylation, a-tailed and indexed adapters were ligated. Suitable fragments were selected and enriched by PCR to create the final cDNA library. The paired-end cDNA library was sequenced on an Illumina HiSeq™ 4000 platform (Majorbio Biotech Co., Ltd., Shanghai, China).

2.5 *De novo* assembly and functional annotation

The raw RNA-seq data were processed to discard the dirty reads that include reads with adaptors, reads with more than 10% Q<20 bases. The low complexity reads were removed by Seqprep and Sickle program. Clean and high-quality reads from the five samples were then assembled using the Trinity program, meanwhile, the counts of transcripts and the N50 were calculated. The assembled unigenes of five samples were used for BlastX search and annotation against the NR, Swissprot, COG (Clusters of Orthologous Groups of proteins), KEGG (Kyoto Encyclopedia of Genes and Genomes) and GO (Gene Ontology) databases with a cut-off E-value < 10^{-5}. Based on Nr-matched unigenes, the annotation of GO was obtained by Web Gene Ontology Annotation Plot (WEGO; http://wego.genomics.org.cn/) program. The transcripts were also blasted against the Pfam database to identify specific protein domains and acquire GO annotations.

2.6 Comparative expression analysis

All clean sequence reads from each of the five libraries (0, 3, 6, 9, 12 days) were mapped to reference sequences (unigenes from the assembled transcriptome data) using Bowtie2 software with default setting (Langmead, 2012). Subsequently, RSEM (http://deweylab.biostat.wisc.edu/rsem/) was used to calculate the FPKM (Fragments per kilobase of transcripts per million fragments mapped values) of the assembled transcripts (Li and Dewey, 2011). Identifying differentially expressed genes (DEGs) among five groups was performed using the R package WGCNA (Robinson et al., 2010). Because we have a single sample from each time point, pair-wise comparisons between time points are not feasible. We decided to examine time-dependent transcriptional changes using a linear model where time points are the independent variable and expression levels are the dependent variable. The false discovery rate (FDR) method was introduced to determine the threshold *P*-value in multiple tests. If FDR was smaller than 0.05 and FPKM values showing at least twofold difference two groups, this unigene was considered as significant time-dependent DEGs. DEGs among the samples were further annotated by GO and KEGG pathway analysis.

2.7 Statistical analysis

In the experiment, the data of each group were presented as mean ± standard deviation (SD) and analyzed by Excel 2010 statistical software and SPSS version 17 (Michigan Avenue, Chicago, IL, USA). The original transcriptomic data were analyzed by a linear model implemented in the WGCNA package. With day-age as the independent variable and gene expression as the dependent variable, genes significantly changed with day-age were identified. We applied a WGCNA module significance filter of $P< 0.01$ and DEG FDR < 0.05 for the final DEG gene set.

3 Results

3.1 Nutrition composition of eggs

The published fatty acid composition of different marine fish eggs was summarized in Table 1. Proximate composition of unfertilized eggs is shown in Figure 1. The composition of crude

TABLE 1 Analysis of fatty acid composition of different marine fish eggs (% total fatty acid).

Marine fish species	C 16:0	C 18:0	C 16:1	C 18:1n9c	C 18:3n3	C 20:5n3 (EPA)	C 22:6n3 (DHA)	SFA	MUFA	PUFA	n-3PUFA	n-6PUFA	References
Gadus macrocephalus	24.29	1.84	np	18	0.29	10.48	31.15	30.26	24.99	44.75	np	np	(Chen et al., 2016)
Hemitripterus villosus	16.74	7.1	0.56	0.67	np	16.41	24.1	24.73	23.86	50.29	41.92	7.43	(Yang et al., 2014)
Pseudosciaena crocea	12.79	7.31	9.01	1.04	1.13	11.31	22.38	23.69	26.56	40.24	34.84	5.42	(Zheng et al., 2020)
Osmerus eperlanus dentex Steindachner	14.23	2.04	10.77	np	1.31	22.02	21.76	19.86	31.7	47.67	45.09	2.58	
Lophiiformes	15.19	6.44	4.64	np	0.49	14.18	24.49	25.38	26.87	47.71	39.16	8.55	
Katsuwonus pelamis	26.66	20.9	0.87	6.04	0.12	10.45	23.34	51.56	11.28	37.16	36.19	0.97	(Wang et al., 2020)
Alosa sapidissima	22.39	6.75	1.32	27.13	1.14	0.73	11.29	30.43	28.45	41.04	13.16	26.11	(Shi et al., 2020)
Salmon solar	12.61	9.32	4.59	np	np	21.91	20.68	26.35	24.63	47.77	np	np	(Ma et al., 2019)
Exocoetidae cypselurus	14.99	8.64	8.57	np	np	13.77	26.05	25.83	26.41	46.77	np	np	
Pseudosciaena crocea	17.78	12.13	4.47	np	np	17.13	18.64	35.41	21.39	41.84	np	np	
Acipenser gueldenstaedti	18.66	9.86	2.85	np	np	0.03	20.03	29.96	25.66	43.72	np	np	
Scophthalmus maximus	18.97	3.79	np	np	0.53	6.03	20.4	26.58	33.26	36.42	27.15	5.18	(Tong et al., 2016)
Sardina pilchardus	47.03	4.37	np	1.93	np	4.52	10.39	58.19	26.63	15.2	14.91	0.29	(Guedes et al., 2020)
Alosa sapidissima	24.41	8.87	np	19.47	0.39	3.51	20.98	35.02	np	37.73	26.15	np	(Liu et al., 2018)
Centropomus undecimalis	20.7	5.26	6.43	14.82	0.67	2.38	13.73	34.46	31.48	34.86	23.81	9.45	(Yanes-Roca et al., 2009)
Latris lineata	17.8	2.9	3.8	18.6	np	6.8	20.5	23.7	32.2	36	np	np	(Bransden et al.,2007)
Gadus morhua L.	18.35	1.64	2.25	np	0.43	13.96	30.52	22.03	5.32	49.56	47.42	2.09	(Lanes et al., 2012)

SFA, Saturated fatty acid; MUFA, Monounsaturated fatty acids; PUFA, Polyunsaturated fatty acids; np, not published.

10.3389/fmars.2024.1424999

10.3389/fmars.2024.1424999

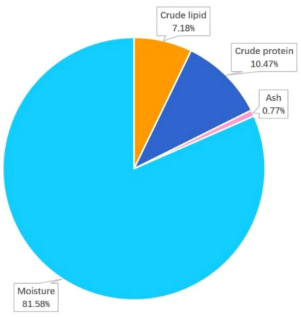

SFA	Content (%)	MUFA	Content (%)	PUFA	Content (%)
C14:0	1.60±0.13	C14:1	0.02±0.01	C18:2n6c	0.84±0.10
C15:0	0.40±0.04	C15:1	0.07±0.01	C18:3n3	3.07±0.20
C16:0	29.39±2.52	C16:1	8.25±0.14	C18:3n6	0.64±0.07
C18:0	6.32±0.48	C17:1	0.42±0.03	C20:2	0.87±0.08
C20:0	0.65±0.06	C18:1n9c	6.23±0.36	C20:3n3	0.69±0.07
C21:0	0.44±0.06	C20:1	1.77±0.08	C20:3n6	0.72±0.09
C22:0	0.56±0.07	C22:1n9	0.72±0.07	C20:4n6	2.83±0.23
C23:0	0.65±0.08	C24:1	0.71±0.08	C20:5n3 (EPA)	4.27±0.24
C24:0	0.73±0.09			C22:2	0.74±0.10
				C22:6n3 (DHA)	25.98±0.49
Sum	41.14±1.61		18.19±0.69		40.69±1.11
HUFA	36.14±1.01				
n-3 PUFA	34.03±0.50				
n-6 PUFA	5.04±0.48				
n-3/n-6	6.79±0.57				

FIGURE 1
The proximate composition (% wet weight basis) and fatty acid composition (% total FA) in unfertilized eggs of *Anguilla japonica*.

lipid and crude protein was 7.24% ± 0.32% and 10.56% ± 0.41%, respectively. A total of nine saturated fatty acids (SFA) were detected in the eggs, together with 8 monounsaturated fatty acids (MUFA), and 10 polyunsaturated fatty acids (PUFA), which took 41.14% ± 1.61%, 18.19% ± 0.69%, and 40.69% ± 1.11% of total fatty acids. The n-3 PUFA takes up about 34.03% ± 0.50% of total fatty acids, while the n-6 PUFA took around 5.04% ± 0.48% in total. The EPA (C20:5n3) and DHA (C22:6n3) accounted for 4.27% ± 0.24% and 25.98% ± 0.49% of total fatty acids, respectively, in which EPA was lower than most marine fish, and DHA was higher than most marine fish (Figure 1 and Table 1). Moreover, the total EPA and DHA content is 30.25% is medium level, comparing to other marine fish. The SFA of *A. japonica* eggs accounted for 41.14% ± 1.61% of the total fatty acids, which was higher than most marine fishes listed in Table 1, among which the content of C16:0 was the highest. Simultaneously, compared to the contents of fatty acids in other marine fish eggs, it was found that eel eggs were rich in fatty acids, which provided a good foundation for the development of eel larvae (Table 1 and Figure 1). The theoretical fat demand of starter diet was 40.86% in the current study, that the demand of C16:0 and DHA was the highest (Table 2).

A total of 17 amino acids were detected, including 7 kinds of essential amino acids (EAA) and 10 nonessential amino acids (NEAA, Figure 2). Leucine (0.69%) took a higher percentage compare to other EAAs, and the glutamic acid was the highest (0.98%) among NEAAs. The ratio of EAA/NEAA was 65.37%, and the EAA made up about 39.53% of the total amino acids (Figure 2). Compared with other amino acids, the contents of glutamic acid (0.98%), alanine (0.82%), leucine (0.69%), and lysine (0.63%) in artificial breeding eel eggs are higher, and glutamate is the highest, which is similar to most marine fish. Still, the content of each amino acid is far lower than that of other marine fish eggs (Table 3). The theoretical demand for protein in the diet of the larvae was 59.59%, the theoretical demand for glutamate was the highest, and the theoretical demand for cysteine was the lowest (Table 2).

TABLE 2 Theoretical requirements of nutrients of *Anguilla japonica* larvae (%, dry weight).

Items	Theoretical requirement	Items	Theoretical requirement
Protein	59.59	Fat	40.86
Glutamate	0.98	C16: 0	12.89
Cysteine	0.16	C20: 4n6	1.24
Leucine	0.69	C20: 5n3	1.87
Lysine	0.63	C22: 6n3	11.39
Alanine	0.82	n-3 PUFA	14.91
Valine	0.42	n-6 PUFA	2.21

3.2 Processing of sequencing data and *de novo* assembly

The RNA sequencing generated a total of 271,423,952 raw reads, and 265,743,784 (97.9%) clean reads were obtained after removing SeqPrep adapter and low-quality reads (Table 4). Thereafter, we got a total of 102941 unigenes with a Q20 percentage over 98%. The contig N50 was 1398 bps. The average length of it was 856.6 bps (Table 5). For the functional annotation, the unigenes were aligned with sequences from major databases including Pfam, Swiss-Prot, KEGG, GO and Nr. The statistics of overall functional annotations were shown in Table 6.

3.3 Identification and analysis of the differently expressed genes

A summary of unigenes classified to each term at GO level 2 is shown in Figure 3. A total of 1664 terms in the biological process category were produced, the most dominant subcategories were cellular process (17087; 21.14%), single-organism process (12101; 14.97%), metabolic process (11794; 14.59%), biological regulation (7441; 9.21%), and regulation of biological process (6915; 8.56%). In cellular component functions, we got 774 terms. And there were 15712 (19.89%) of unigenes that were assigned to the cell, followed by cell part 15469 (19.58%), membrane 11852 (15.00%), organelle

10.3389/fmars.2024.1424999

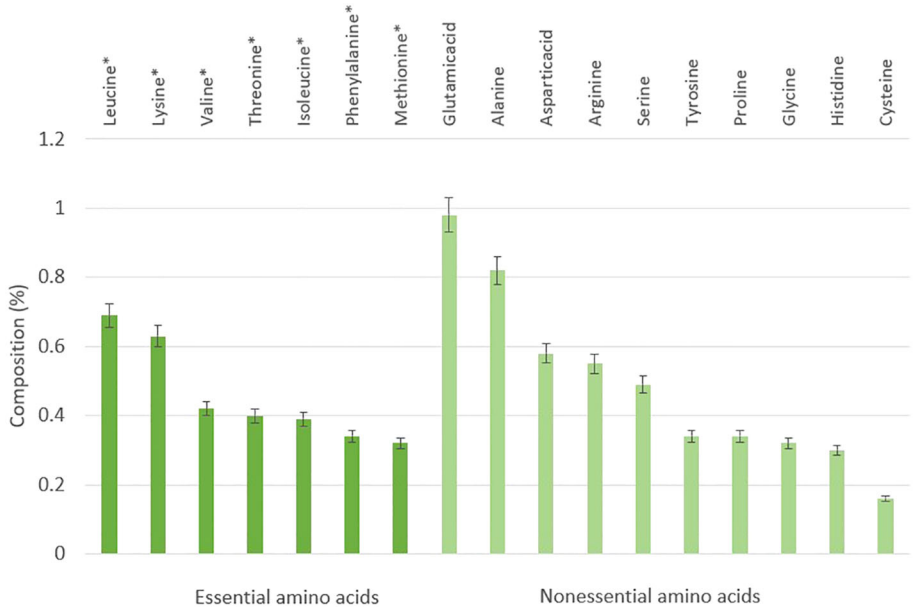

FIGURE 2
Composition of essential amino acids and nonessential amino acids in unfertilized eggs of *Anguilla japonica*. * This means essential amino acid.

9858 (12.48%), and macromolecular complex 5782 (7.32%). In the molecular function category, 422 terms were produced, and the five most dominant subcategories were binding (20754; 43.91%), catalytic activity (15442; 32.67%), transporter activity (2474; 5.23%), signal transducer activity (2054; 4.35%) and structural molecule activity (1971; 4.17%).

By running the WGCMA to perform a linear regression of time-dependent gene expression on the original transcriptome data,

TABLE 3 Analysis of amino acid composition of different marine fish eggs (% dry weight basis).

Marine fish species	Glutamate	Alanine	Leucine	Lysine	Cysteine	TAA	EAA	NEAA	DAA	References
Gadus macrocephalus	9.36	5.14	6.25	4.93	np	65.51	28.25	37.26	25.2	(Chen et al., 2016)
Hemitripterus villosus	10.2	4.03	7.46	5.49	np	78.77	33.24	38.95	30.24	(Yang et al., 2014)
Pseudosciaena crocea	6.64	3.72	6.08	5.23	np	61.71	29.36	32.35	16.78	(Zheng et al., 2020)
Osmerus eperlanus dentex Steindachner	3.9	6.04	4.93	5.33	np	52.3	20.36	31.94	16.02	
Lophiiformes	5.97	6.78	7.7	6.48	np	79.48	29.31	50.17	25.53	
Katsuwonus pelamis	8.34	4.33	5.52	5.15	0.95	65.65	26.37	32.77	np	(Wang et al., 2020)
Alosa sapidissima	7.96	6	6.28	4.1	0.66	61.41	27.05	30.54	21.12	(Shi et al., 2020)
Salmon solar	3.62	1.98	2.47	2.06	np	26.23	11.47	12.56	8.7	(Ma et al., 2019)
Exocoetidae cypselurus	2.26	0.87	1.34	0.98	np	13.67	5.89	6.64	4.51	
Pseudosciaena crocea	3.19	1.92	2.37	1.99	np	24.79	10.88	11.58	7.89	
Acipenser gueldenstaedti	4.05	1.82	2.45	2.29	np	27.67	11.44	13.51	9.31	
Rachycentron canadum	6.6	4.22	4.41	3.6	np	49.45	24.02	25.43	np	(Faulk et al., 2008)
Lates calcarifer	3.9	4.01	4.15	3.65	0.52	41.94	24.23	17.7	np	(Dayal et al., 2003)
Gadus morhua L.	7.88	5.21	5.38	4.47	0.53	57.4	28.82	28.52	np	(Lanes et al., 2012)

EAA, essential amino acids; NEAA: nonessential amino acids; TAA, total amino acids; DAA, delicious amino acids; np, not published.

10.3389/fmars.2024.1424999

TABLE 4 Read data of *Anguilla japonica* before and after processing.

Day-age	Number of raw read pairs	Number of cleaned read pairs
0	49,215,850	48,233,440 (98.0%)
3	54,441,304	53,379,346 (98.0%)
6	58,638,172	57,402,690 (97.9%)
9	51,574,270	50,400,978 (97.7%)
12	57,554,356	56,327,330 (97.9%)

TABLE 5 Statistics of assembly of *Anguilla japonica*.

Type	Unigene
Total sequence number	102,941
Total sequence base	88,179,496
Percent GC	54.92%
Largest length	26610 bp
Smallest length	201 bp
Average length	856.6 bp
N50	1398 bp

TABLE 6 Statistics of unigene functional annotation.

Database	Annotated unigenes	Percentage
Pfam	30993	30.11%
KEGG	33072	32.13%
GO	25245	24.52%
Swiss-prot	45067	43.78%
Nr	56574	54.96%

genes significantly changed with day-age were identified. A total of 1,751 genes were selected that changed significantly with age, contained in WGCNA module with $P < 0.01$ and gene DEG FDR < 0.05. By comparing and analyzing the screened genes with KEGG database, 23 pathways related to the digestive and metabolic system were detected. With the change of age, 120 genes showed a significant increase in gene expression, and 18 genes showed a significant decrease in gene expression. Among them, genes related to the secretion pathway of saliva, pancreatic juice and other digestive juices were significantly changed. The genes of carbohydrate metabolism, glycerolipid metabolism, glycerophospholipid metabolism, and other metabolic pathways were up-regulated significantly with age (Table 7).

Statistical overrepresentation test was performed for genes whose gene expression significantly increased with age after screening. A total of 20 significantly enriched Go-slim molecular function pathways were detected. Through analysis, it is found that among the genes enriched in the transmembrane transporter activity pathway, the TRPC1 gene and CFTR gene are related to the secretion and transport of digestive enzymes such as saliva, pancreatic juice, and bile (Table 8).

4 Discussion

Studies have demonstrated that the knowledge of nutrient composition of fish eggs will not only provide key insights into requirements of nutrient, but also support formulating the starter diet (Pousão-Ferreira et al., 1999; Yang et al., 2014). Meanwhile, the transcriptomic analysis could reveal the changes of food digestion and nutrient absorption during the preleptocephali stage to eliminating the hurdle to complete full artificial reproduction.

Protein is essential for cell and tissues function, crucial for growth and life maintenance. The protein content data from eel eggs emphasize the nutritional requirements for first larval feeding (Pousão-Ferreira et al., 1999). The theoretical protein demand of starter diet of *A. japonica* was 59.59% that calculated depending on the crude protein composition (10.56%) of eel eggs in present study, aligning with previous findings (Xiong et al., 1996; de Souza Romaneli et al., 2021). However, the EAA content (3.19%) was significantly lower compared to other marine fish, potentially leading to malnutrition and high mortality before feeding.

Lysine, the first restrictive amino acid, enhances the utilization of other EAAs, prevents nitrogen loss, and promotes growth (Zhou et al., 2008). Therefore, a higher lysine content in fish egg is beneficial to both fish growth and survival. Although the content of lysine (0.69%) was one of the highest amino acid in the eel eggs of this study, a comparable lower rate to other marine fish eggs still implies that a limited lysine content could be another cause for the mass death in the artificial reproduction. Fatty acids are one of the main energy sources for fish (Cejas et al., 2004; Bennett et al., 2007). The analysis shows that the SFA of *A. japonica* eggs accounts for 41.14% of the total fatty acids, among which the content of C16:0 was the richest that is similar to *Alosa sapidissima* (Yanes-Roca et al., 2009), *Sardina pilchardus* (Liu et al., 2018), and *Centropomus undecimalis* (Guedes et al., 2020). PUFA has been proved to have a significant effect in promoting fish growth and development, as well as the fish immunity and survival rate (Xu et al., 2010). A 40.69% of the total fatty acids' PUFA was detected in this study, and a similar high proportion was found in other marine fish eggs as well (Liu et al., 2018; Tang et al., 2020; Zheng et al., 2020).

In this study, the transcription levels of various digestive enzymes and carbohydrate metabolism in the larvae were comparably high with the changes of the larvae's age. The metabolic capability for low molecular carbohydrate, especially in galactose, fructose, and sucrose metabolism pathways, showed increasing with the day-age growing. The hyaluronic acid, a disaccharide substance, is found to be the main body composition of leptocephali, highlights the importance of carbohydrates for growth (Pfeiler, 1999). The marine snow, a most likely starter diet of *A. japonica*, happens to be a collection of different carbohydrates also supports the demands of low molecular carbohydrate during the early life (Pfeiler, 1999). Okamura et al. (2020) found that dietary supplementation with chitin hydrolysates including mono-, di- and trimers of N-acetylglucosamine, supporting the growth and

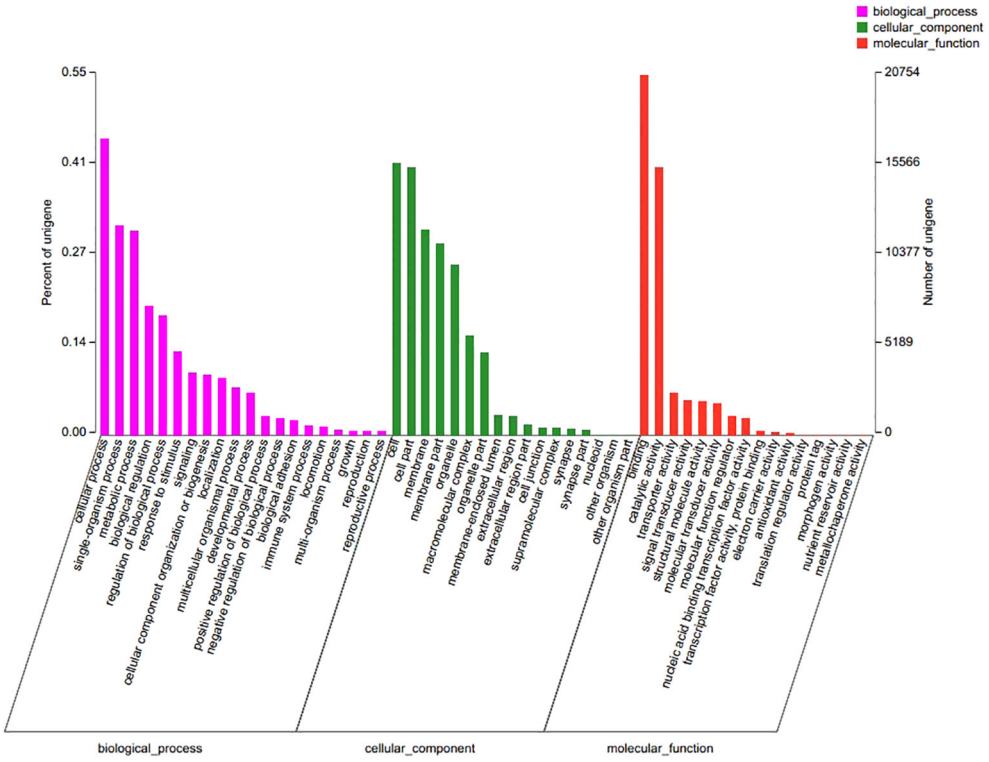

FIGURE 3
Functional annotation of assembled contigs associated with GO terms.

TABLE 7 Digestive and metabolism-related pathways in KEGG term.

Pathway id	Pathway	Up No.	Down No.	Total No.
Map04972	Pancreatic secretion	12	1	13
Map04970	Salivary secretion	13	1	14
Map04971	Gastric acid secretion	10	1	11
Map04976	Bile secretion	4	1	5
Map04973	Carbohydrate digestion and absorption	7	0	7
Map04974	Protein digestion and absorption	4	0	4
Map04975	Fat digestion and absorption	2	0	2
Map04978	Mineral absorption	1	0	1
Map04977	Vitamin digestion and absorption	0	0	0
Map00310	Lysine degradation	6	3	9
Map00250	Alanine, aspartate and glutamate metabolism	1	2	3
Map00380	Tryptophan metabolism	2	0	2
Map00350	Tyrosine metabolism	2	0	2
Map00270	Cysteine and methionine metabolism	0	1	1
Map00600	Sphingolipid metabolism	5	1	6
Map01040	Biosynthesis of unsaturated fatty acids	2	0	2

(Continued)

TABLE 7 Continued

Pathway id	Pathway	Up No.	Down No.	Total No.
Map00561	Glycerolipid metabolism	11	1	12
Map00564	Glycerophospholipid metabolism	13	1	14
Map00562	Inositol phosphate metabolism	9	3	12
Map00051	Fructose and mannose metabolism	5	1	6
Map00052	Galactose metabolism	4	1	5
Map00500	Starch and sucrose metabolism	5	0	5
Map00010	Glycolysis/Gluconeogenesis	3	0	3

survival of eel larvae. It demonstrates that feeding low-molecular bait such as glucose sugar and maltose to larvae eel is beneficial to improve the survival time of larvae (Skoog et al., 2008; Jang et al., 2022), which is consistent with our experimental results. During the early stage of post-hatching, the larvae consume endogenous yolk protein to supply the growth needs (Nobuyuki et al., 2008). It implies that the consumption of yolk nutrient continued after the larvae hatch, and the body carbohydrates kept strengthen in order to meet the energy demand for its growth. Our previous study indicated that the teeth began to form on the 6th day of membrane emergence, and the oil globule completely disappeared from the day 8, which marked the transition from endogenous nutrition to exogenous nutrition of larvae eel (Liu et al., 2017).

Amino acids play essential role in fish metabolism. They act as signal molecules for physiological regulation and can be oxidized to provide energy through gluconeogenesis during hunger or malnutrition (Aragão et al., 2004; Hamidoghli et al., 2019). Transcriptome analysis revealed that lysine metabolism increased steadily with age. The relatively high lysine content in fish eggs supports early larval growth. As a key ketogenic amino acid, lysine

TABLE 8 Enrichment of genes significantly different with age in GO term.

Pathway id	Pathway	Number of matched GO	+/-	FDR
GO:0005262	calcium channel activity	7	+	0.016900
GO:0015085	calcium ion transmembrane transporter activity	7	+	0.015700
GO:0046873	metal ion transmembrane transporter activity	19	+	0.000202
GO:0022890	inorganic cation transmembrane transporter activity	19	+	0.000737
GO:0008324	cation transmembrane transporter activity	22	+	0.000092
GO:0015075	ion transmembrane transporter activity	26	+	0.000103
GO:0022857	transmembrane transporter activity	31	+	0.000032
GO:0005215	transporter activity	33	+	0.000031
GO:0015318	inorganic molecular entity transmembrane transporter activity	25	+	0.000128
GO:0005261	cation channel activity	13	+	0.007660
GO:0005216	ion channel activity	16	+	0.001290
GO:0015267	channel activity	17	+	0.000836
GO:0022803	passive transmembrane transporter activity	17	+	0.000940
GO:0015081	sodium ion transmembrane transporter activity	8	+	0.008010
GO:0015077	monovalent inorganic cation transmembrane transporter activity	14	+	0.001780
GO:0015079	potassium ion transmembrane transporter activity	10	+	0.019700
GO:0008509	anion transmembrane transporter activity	11	+	0.025100
GO:0004930	G protein-coupled receptor activity	11	+	0.040200
GO:0004888	transmembrane signaling receptor activity	16	+	0.028700
GO:0038023	signaling receptor activity	18	+	0.027100

contributes to ketone body and glucose metabolism, serving as a vital energy source when other energy supplies are insufficient (Huang et al., 2021).

Transcriptome analysis showed a significant increase in glycolytic metabolism in larvae as they aged, particularly in the transcription level of hexokinase (HK), a key enzyme in glycolysis (Table 7). This suggests that larvae convert glucose and other sugars into energy to meet their growth needs. Additionally, the transcription level of gluconeogenesis and the metabolism of glycerides and glycerophospholipids increased with age. The metabolism and transcription levels of glyceride and glycerophospholipid were enhanced. This indicates that larvae may convert non-carbohydrate substances into glucose or glycogen to supplement their energy requirements due to insufficient carbohydrate reserves.

A previous study presented that the growth rate of the farmed leptocephali (which feeds on shark eggs) is lower than that of the wild leptocephali (Ishikawa et al., 2001). As one of the commonly used artificial starter diet components, the *Acanthias* shark egg-based diet are composed with protein (26.3%), lipids (17.5%), carbohydrates (0.1%) and moisture (54.4%) (Okamura et al., 2014). Our results demonstrate an age-dependent increase in carbohydrate conversion in larvae, suggesting a potential correlation between the sluggish growth of cultured preleptocephali larvae and insufficient carbohydrate supplementation in the bait. Okamura et al. (2020) presented that dietary supplementation with high sugar content such as N-acetylglucosamine, glucose and maltose could significantly improve the growth rate of larvae. Furthermore, our study suggests that the egg itself provides sufficient fatty acids to meet the nutritional requirements of the preleptocephali stage. Consequently, optimizing the carbohydrate content and supplementing essential amino acids like lysine in the diet of artificially bred *A. japonica* larvae may enhance growth, although the specific mechanisms of digestion and metabolism necessitate further experimental validation. Notably, our analysis of significantly enriched GO-Slim pathways indicates a predominance of pathways associated with ion transport, suggesting potential implications for early nutrient metabolism and transport, possibly influenced by water salinity, warranting deeper investigation.

5 Conclusions

In present study, we examined the nutritional composition and transcriptome of the artificially fertilized eggs and pre-leptocephalus larvae of *A. japonica*. Seven kinds of essential amino acids (EAA) were detected, with *A. japonica* exhibiting lower levels compared to other marine fish eggs. Through random assembly of 265.74 million clean reads, we identified 1751 differentially expressed genes. Notably, genes associated with carbohydrate metabolism, glycerolipid metabolism and glycerophospholipid metabolism showed significant up-regulation with larval growth. These findings lay a foundation for future studies into the nutrient requirements and digestive functions of newly hatched *A. japonica*, thereby advancing the field of artificial reproduction of eels.

Data availability statement

The original contributions presented in the study are deposited in the NCBI repository, accession number: PRJNA1133914.

Ethics statement

The animal study was approved by Animal Care and Use Ethics Committee of the Shanghai Ocean University. The study was conducted in accordance with the local legislation and institutional requirements.

Author contributions

KL: Conceptualization, Data curation, Investigation, Methodology, Writing – original draft, Writing – review & editing. YL: Conceptualization, Data curation, Investigation, Methodology, Writing – original draft, Writing – review & editing. TL: Data curation, Investigation, Methodology, Writing – original draft. RC: Methodology, Writing – review & editing. LL: Conceptualization, Funding acquisition, Supervision, Writing – original draft, Writing – review & editing.

Funding

The author(s) declare financial support was received for the research, authorship, and/or publication of this article. This study was supported by the National Natural Science Foundation of China (No: 32072994); the Shanghai Agriculture Applied Technology Development Program, China (2020-02-08-00-10-F01471); and Startup Foundation for Young Teachers of Shanghai Ocean University.

Conflict of interest

The authors declare that the research was conducted in the absence of any commercial or financial relationships that could be construed as a potential conflict of interest.

The author(s) declared that they were an editorial board member of Frontiers, at the time of submission. This had no impact on the peer review process and the final decision.

Publisher's note

References

AOAC (1996). *Official methods of analysis of the association of official analytical Chemists* (Arlington (U.S.A: Association of Official Analytical Chemists).

Aragão, C., Conceição, L. E., Dinis, M. T., and Fyhn, H. J. (2004). Amino acid pools of rotifers and Artemia under different conditions: nutritional implications for fish larvae. *Aquaculture* 234, 429–445. doi: 10.1016/j.aquaculture.2004.01.025

Bennett, P. M., Weber, L. P., and Janz, D. M. (2007). Comparison of chloroform–methanol-extracted and solvent-free triglyceride determinations in four fish species. *J. Aquat. Anim. Health* 19, 179–185. doi: 10.1577/H06-044.1

Bransden, M. P., Battaglene, S. C., Goldsmid, R. M., Dunstan, G. A., and Nichols, P. D. (2007). Broodstock condition, egg morphology and lipid content and composition during the spawning season of captive striped trumpeter, *Latris lineata*. *Aquaculture* 268 (1–4), 2–12.

Cejas, J. R., Almansa, E., Jérez, S., Bolaños, A., Felipe, B., and Lorenzo, A. (2004). Changes in lipid class and fatty acid composition during development in white seabream (*Diplodus sargus*) eggs and larvae. *Comp. Biochem. Physiol. Part B: Biochem. Mol. Biol.* 139, 209–216. doi: 10.1016/j.cbpc.2004.07.010

Chen, J. M., Liu, X. F., Leng, K. L., Gao, H., Miao, J. K., and Wang, S. (2016). Analysis and evaluation of nutritional components of *Gadus macrocephalus* roe. *Journal of Qingdao University (National science edition)* 29 (2), 57–62. (in Chinese).

Churcher, A. M., Hubbard, P. C., Marques, J. P., Canario, A. V., and Huertas, M. (2015). Deep sequencing of the olfactory epithelium reveals specific chemosensory receptors are expressed at sexual maturity in the European eel *Anguilla Anguilla*. *Mol. Ecol.* 24, 822–834. doi: 10.1111/mec.13065

Dayal, J. S., Ali, S. A., Thirunavukkarasu, A. R., Kailasam, M., and Subburaj, R. (2003). Nutrient and amino acid profiles of egg and larvae of Asian seabass, *Lates calcarifer* (Bloch). *Fish Physiology and Biochemistry* 29, 141–147.

Dekker, W., and Casselman, J. M. (2014). The 2003 Québec declaration of concern about eel declines-11 years later: are eels climbing back up the slippery slope? *Fisheries* 39, 613–614. doi: 10.1080/03632415.2014.979342

de Souza Romaneli, R., do Nascimento, T. M. T., Gous, R. M., de Paula Reis, M., Mansano, C. F. M., Khan, K. U., et al. (2021). Response of Nile tilapia (*Oreochromis niloticus*) to lysine: Performance, body composition, maintenance and efficiency of utilization. *Aquaculture* 538, 736522. doi: 10.1016/j.aquaculture.2021.736522

Faulk, C. K., and Holt, G. J. (2008). Biochemical composition and quality of captive-spawned cobia *Rachycentron canadum* eggs. *Aquaculture* 279, 70–76.

Feunteun, E., and Prouzet, P. (2020). "Forty years of decline and 10 years of management plan: Are European eels (*Anguilla Anguilla*) recovering?," in *Coast bordeaux symposium and of the 17th french-Japanese oceanography symposium* (Cham, Switzerland: Springer International Publishing), 269–295.

Folch, J., Lees, M., and Sloane Stanley, G. H. (1957). A simple method for the isolation and purification of total lipides from animal tissues. *J. Biol. Chem.* 226, 497–509. doi: 10.1016/S0021-9258(18)64849-5

Gilani, G. S., and Peace, R. W. (2005). Chromatographic determination of amino acids in foods. *J. AOAC Int.* 88, 877–887. doi: 10.1093/jaoac/88.3.877

Guedes, M., Costa-Pinto, A. R., Gonçalves, V. M., Moreira-Silva, J., Tiritan, M. E., Reis, R. L., et al. (2020). Sardine roe as a source of lipids to produce liposomes. *ACS Biomaterials Sci. Eng.* 6, 1017–1029. doi: 10.1021/acsbiomaterials.9b01462

Hamidoghli, A., Bae, J., Won, S., Lee, S., Kim, D. J., and Bai, S. C. (2019). A review on Japanese eel (*Anguilla japonica*) aquaculture, with special emphasis on nutrition. *Rev. Fisheries Sci. Aquaculture* 27, 226–241. doi: 10.1080/23308249.2019.1583165

Hsu, H. Y., Chen, S. H., Cha, Y. R., Tsukamoto, K., Lin, C. Y., and Han, Y. S. (2015). *De novo* assembly of the whole transcriptome of the wild embryo, preleptocephalus, leptocephalus, and glass eel of *Anguilla japonica* and deciphering the digestive and absorptive capacities during early development. *PloS One* 10, e0139105. doi: 10.1371/journal.pone.0139105

Huang, D., Liang, H., Ren, M., Ge, X., Ji, K., Yu, H., et al. (2021). Effects of dietary lysine levels on growth performance, whole body composition and gene expression related to glycometabolism and lipid metabolism in grass carp, *Ctenopharyngodon idellus* fry. *Aquaculture* 530, 735806. doi: 10.1016/j.aquaculture.2020.735806

Ishikawa, S., Suzuki, K., Inagaki, T., Watanabe, S., Kimura, Y., Okamura, A., et al. (2001). Spawning time and place of the Japanese eel *Anguilla japonica* in the North Equatorial Current of the western North Pacific Ocean. *Fisheries Sci.* 67, 1097–1103. doi: 10.1046/j.1444-2906.2001.00366.x

Jang, W. J., Kim, S. K., Lee, S. J., Kim, H., Ryu, Y. W., Shin, M. G., et al. (2022). Effect of Bacillus sp. supplementation diet on survival rate and microbiota composition in artificially produced eel larvae (*Anguilla japonica*). *Front. Microbiol.* 13, 891070. doi: 10.3389/fmicb.2022.891070

Jiang, T. B., Liu, L. P., Gao, X. Y., Chen, W. Y., and Wu, J. M. (2012). The changes of serum biochemical components during carp pituitary extract and HCG induced maturation of the female Japanese eel *(Anguilla japonica)* (in Chinese). *J. Fisheries China* 36, 893–899. doi: 10.3724/SP.J.1231.2012.27821

Kleppe, L., Edvardsen, R. B., Furmanek, T., Taranger, G. L., and Wargelius, A. (2014). Global transcriptome analysis identifies regulated transcripts and pathways activated during oogenesis and early embryogenesis in Atlantic cod. *Mol. Reprod. Dev.* 81, 619–635. doi: 10.1002/mrd.22328

Koh, I. C. C., Hamada, D., Tsuji, Y., Okuda, D., Nomura, K., Tanaka, H., et al. (2017). Sperm cryopreservation of Japanese eel, *Anguilla japonica*. *Aquaculture* 473, 487–492. doi: 10.1016/j.aquaculture.2017.03.011

Kuan-Mei, H., Shingo, K., Yu-San, H., Aigo, T., Yoshiyuki, I., and Caroline, D. (2018). Effect of ENSO events on larval and juvenile duration and transport of Japanese eel (*Anguilla japonica*). *PloS One* 13, e0195544. doi: 10.1371/journal.pone.0195544

Lanes, C. F. C., Bizuayehu, T. T., Bolla, S., Martins, C., de Oliveira Fernandes, J. M., Bianchini, A., et al. (2012). Biochemical composition and performance of Atlantic cod (*Gadus morhua L.*) eggs and larvae obtained from farmed and wild broodstocks. *Aquaculture* 324, 267–275.

Langmead, B. (2012). Fast gapped-read alignment with bowtie 2. *Nat. Methods* 9, 357–359. doi: 10.1038/nmeth.1923

Li, C., Cheng, X. F., Hong, B., Chen, X. Y., Wu, Y. N., and Li, H. (2016). Nutritional analysis and evaluation on eggs of *Spinibarbus caldwelli*. *Chin. J. Anim. Nutr.* 28, 2204–2212. Available at: http://www.chinajan.com/CN/abstract/html/20160726.htm.

Li, B., and Dewey, C. N. (2011). RSEM: accurate transcript quantification from RNA-seq data with or without a reference genome. *BMC Bioinf.* 12, 1–16. doi: 10.1186/1471-2105-12-323

Liu, Z. F., Gao, X. Q., Yu, J. X., Wang, Y. H., and Guo, Z. L. (2018). Changes of protein and lipid contents, amino acid and fatty acid compositions in eggs and yolk-sac larvae of American shad (*Alosa sapidissima*). *J. Ocean Univ. China* 17, 209–215. doi: 10.1007/s11802-018-3403-3

Liu, L. P., Liu, D. P., Pu, J. C., Du, L., Chen, T. Y., Chen, W. Y., et al. (2017). Effects of different initial diets on the survival and behavior characteristics of the larvae of Japanese eel (*Anguilla japonica*) (in Chinese). *J. Fisheries China* 41, 703–710. doi: 10.11964/jfc.20160910542

Ma, S., Hao, S. X., Li, L. H., Yang, X. Q., Huang, Y., Wei, Y., et al. (2019). Comparative analysis of nutritional components of several roes. *South China Fisheries Science* 15 (4), 113–121.

Masuda, Y., Imaizumi, H., Usuki, H., Oda, K., Hashimoto, H., and Teruya, K. (2012). Artificial completion of the Japanese eel, *Anguilla japonica*, life cycle: challenge to mass production. *Bull. Fisheries Res. Agency* 35, 111–117.

Matsushige, K., Yasutake, Y., and Mochioka, N. (2019). Spatial distribution and habitat preferences of the Japanese eel, *Anguilla japonica*, at the reach and channel-unit scales in four rivers of Kagoshima Prefecture, Japan. *Ichthyological Res.* 67, 68–80. doi: 10.1007/s10228-019-00704-x

Morrison, W. R., and Smith, L. M. (1964). Preparation of fatty acid methyl esters and dimethylacetals from lipids with boron fluoride-methanol. *J. Lipid Res.* 5, 600–608. doi: 10.1016/S0022-2275(20)40190-7

Mourente, G., and Rosa, V. (1996). Changes in the content of total lipid, lipid classes and their fatty acids of developing eggs and unfed larvae of the Senegal sole, *Solea Senegalensis* kaup. *Fish Physiol. Biochem.* 15, 221–235. doi: 10.1007/BF01875573

Ohkubo, N., Sawaguchi, S., Nomura, K., Tanaka, H., and Matsubara, T. (2008). Utilization of free amino acids, yolk protein and lipids in developing eggs and yolk-sac larvae of Japanese eel *Anguilla japonica*. *Aquaculture* 282, 130–137. doi: 10.1016/j.aquaculture.2008.06.017

Okamura, A., Horie, N., Mikawa, N., Yamada, Y., and Tsukamoto, K. (2014). Recent advances in artificial production of glass eels for conservation of anguillid eel populations. *Ecol. Freshw. Fish* 23, 95–110. doi: 10.1111/eff.12086

Okamura, A., Yamada, Y., Horie, N., Mikawa, N., Tanaka, S., Kobayashi, H., et al. (2013). Hen egg yolk and skinned krill as possible foods for rearing leptocephalus larvae of *Anguilla japonica* Temminck & Schlegel. *Aquaculture Res.* 44, 1531–1538. doi: 10.1111/are.2013.44.issue-10

Okamura, A., Yamada, Y., Horie, N., Mikawa, N., and Tsukamoto, K. (2019). Long-term rearing of Japanese eel larvae using a liquid-type diet: food intake, survival and growth. *Fisheries Sci.* 85, 687–694. doi: 10.1007/s12562-019-01316-0

Okamura, A., Yamada, Y., Mikawa, N., Horie, N., and Tsukamoto, K. (2020). Dietary supplementation with chitin hydrolysates for *Anguilla japonica* leptocephali. *Fisheries Sci.* 86, 685–692. doi: 10.1007/s12562-020-01440-2

Ozsolak, F., and Milos, P. M. (2010). RNA sequencing: advances, challenges and opportunities. *Nat. Rev. Genet.* 12, 87–98. doi: 10.1038/nrg2934

Pfeiler, E. (1999). Developmental physiology of elopomorph leptocephali. *Comp. Biochem. Physiol. Part A Mol. Integr. Physiol.* 123, 113–128. doi: 10.1016/S1095-6433(99)00028-8

Pike, C., Crook, V., and Gollock, M. (2020). Anguilla Anguilla (The IUCN Red List of Threatened Species). Available online at: https://dx.doi.org/10.2305/IUCN.UK.2020-2.RLTS.T60344A152845178.en (Accessed 2024 12 June). 2020.

Politis, S. N., Sørensen, S. R., Mazurais, D., Servili, A., Zambonino-Infante, J. L., Miest, J. J., et al. (2018). Molecular ontogeny of first-feeding European eel larvae. *Front. Physiol.* 9. doi: 10.3389/fphys.2018.01477

Pousão-Ferreira, P., Morais, S., Dores, E., and Narciso, L. (1999). Eggs of gilthead seabream *Sparus aurata* L. as a potential enrichment product of Brachionus sp. in the larval rearing of gilthead seabream *Sparus aurata* L. *Aquaculture Res.* 30, 751–758. doi: 10.1046/j.1365-2109.1999.00394.x

Robinson, M. D., Mccarthy, D. J., and Smyth, G. K. (2010). EdgeR: a Bioconductor package for differential expression analysis of digital gene expression data. *Bioinformatics* 26, 139–140. doi: 10.1093/bioinformatics/btp616

Shi, Y. H., Xu, J. B., Xie, Y. D., Liu, Y. S., Shui, C., Lu, G. H., et al. (2020). Nutritional composition analysis and evaluation of eggs in American Shad Alosa sapidissima. *Fisheries Science* 39 (3), 407–413. (in Chinese).

Skoog, A., Alldredge, A., Passow, U., Dunne, J., and Murray, J. (2008). Neutral aldoses as source indicators for marine snow. *Mar. Chem.* 108, 195–206. doi: 10.1016/j.marchem.2007.11.008

Tanaka, H. (2015). Progression in artificial seedling production of Japanese eel *Anguilla japonica*. *Fisheries Sci.* 81, 11–19. doi: 10.1007/s12562-014-0821-z

Tanaka, H., Kagawa, H., and Ohta, H. (2001). Production of leptocephali of Japanese eel (*Anguilla japonica*) in captivity. *Aquaculture* 201, 51–60. doi: 10.1016/S0044-8486(01)00553-1

Tanaka, H., Kagawa, H., Ohta, H., Unuma, T., and Nomura, K. (2003). The first production of glass eel in captivity: fish reproductive physiology facilitates great progress in aquaculture. *Fish Physiol. Biochem.* 28, 493–497. doi: 10.1023/B:FISH.0000030638.56031.ed

Tang, L., Xiao, X., Shi, H., Chen, J., Han, C., Huang, H., et al. (2020). Induction of oocyte maturation and changes in the biochemical composition, physiology and molecular biology of oocytes during maturation and hydration in the orange-spotted grouper (*Epinephelus coioides*). *Aquaculture* 522, 735115. doi: 10.1016/j.aquaculture.2020.735115

Tong, X. H., Tang, X. H., Bao, C. M., Yang, X. L., and Chen, Q. (2016). Relationship between embryonic growth and nucleic acids of *Scophthalmus maximus*. *Acta Agri. Zhejiangensis.* 28 (3), 428–434. (in Chinese).

Tsukamoto, K. (1992). Discovery of the spawning area for Japanese eel. *Nature* 356, 789–791. doi: 10.1038/356789a0

Wang, B., Wu, H. W., and Li, L. Y. (2020). Analysis and evaluation of the nutritional compositions of skipjack tuna (Katsuwonus pelamis) roes. *Journal of Guangdong Ocean University* 40 (2), 111–116. (in Chinese).

Wang, Z., Gerstein, M., and Snyder, M. (2010). RNA-Seq: a revolutionary tool for transcriptomics. *Nat. Rev. Genet.* 10, 57–63. doi: 10.1038/nrg2484

Xiong, B. X., Long, L. Q., Su, X., and Chang, Q. (1996). Crude protein and essential amino acid countens among eel feeds made in China (in Chinese). *J. Huazhong Agric. Univ.* 15, 60–63.

Xu, Y., Li, W., and Ding, Z. (2010). Effects of polyunsaturated fatty acids on immunity and survival of fish and their mechanisms (in Chinese). *Chin. J. Anim. Nutr.* 23, 551–556.

Yanes-Roca, C., Rhody, N., Nystrom, M., and Main, K. L. (2009). Effects of fatty acid composition and spawning season patterns on egg quality and larval survival in common snook (*Centropomus undecimalis*). *Aquaculture* 287, 335–340. doi: 10.1016/j.aquaculture.2008.10.043

Yang, J. J., Jiang, Z. Q., Zuo, R. T., Wang, S. Y., Wen, S. H., and Sun, H. (2014). Nutritional analysis and evaluation on eggs of *Hemitripterus villosus* (in Chinese). *Chin. J. Anim. Nutr.* 26, 1103–1110.

Zheng, T. T., Zhou, J., Weng, X., Chen, L. J., Cheng, W. J., Pang, J., et al. (2020). Analysis and evaluation of nutritional components of four types of marine aquatic roes. *Food Fermentation Industries* 46, 244–249. doi: 10.13995/j.cnki.11-1802/ts.023891

Zhou, X. Q., Zhao, C. R., Jiang, J., Feng, L., and Liu, Y. (2008). Dietary lysine requirement of juvenile Jian carp (*Cyprinus carpiovar* var. Jian). *Aquaculture Nutr.* 14, 381–386. doi: 10.1111/anu.2008.14.issue-5

frontiers | Frontiers in Marine Science

TYPE Original Research
PUBLISHED 03 September 2024
DOI 10.3389/fmars.2024.1436755

OPEN ACCESS

EDITED BY
Yngvar Olsen,
NTNU, Norway

REVIEWED BY
Morten Omholt Alver,
NTNU, Norway
Marcos Godoy,
San Sebastián University, Chile

*CORRESPONDENCE
Carolina Merca
cmgm@sund.ku.dk

RECEIVED 22 May 2024
ACCEPTED 01 August 2024
PUBLISHED 03 September 2024

CITATION
Merca C, Boerlage AS, Kristensen AR and Jensen DB (2024) Monitoring monthly mortality of maricultured Atlantic salmon (*Salmo salar* L.) in Scotland I. Dynamic linear models at production cycle level. *Front. Mar. Sci.* 11:1436755. doi: 10.3389/fmars.2024.1436755

Monitoring monthly mortality of maricultured Atlantic salmon (*Salmo salar* L.) in Scotland I. Dynamic linear models at production cycle level

Carolina Merca[1]*, Annette Simone Boerlage[2], Anders Ringgaard Kristensen[1] and Dan Børge Jensen[1]

[1]Department of Veterinary and Animal Sciences, Faculty of Health and Medical Sciences, University of Copenhagen, Frederiksberg, Denmark, [2]Center for Epidemiology and Planetary Health (CEPH), SRUC School of Veterinary Medicine, Inverness, United Kingdom

The mortality of Atlantic salmon is one of the main challenges to achieving its sustainable production. This sector benefits from generating many data, some of which are collated in a standardized way, on a monthly basis at site level, and are accessible to the public. This continuously updated resource might provide opportunities to monitor mortality and prompt producers and inspectors to further investigate when mortality is higher than expected. This study aimed to use the available open-source data to develop production cycle level dynamic linear models (DLMs) for monitoring monthly mortality of maricultured Atlantic salmon in Scotland. To achieve this, several production cycle level DLMs were created: one univariate DLM that includes just mortality; and various multivariate DLMs that include mortality and different combinations of environmental variables. While environmental information is not collated in a standardized way across all sites, open-source remote-sensed satellite resources provide continuous, standardized estimates. By combining environmental and mortality data, we seek to investigate whether adding environmental variables enhanced the estimates of mortality, and if so, which variables were most informative in this respect. The multivariate model performed better than the univariate DLM (P = .004), with salinity as the only significant contributor out of 12 environmental variables. Both models exhibited uncertainty related to the mortality estimates. Warnings were generated when any observation fell above the 95% credible interval. Approximately 30% of production cycles and more than 50% of sites experienced at least one warning between 2015 and 2020. Occurrences of these warnings were non-uniformly distributed across space and time, with the majority happening in the summer and autumn months. Recommendations for model improvement include employing shorter time periods for data aggregation, such as weekly instead of on a monthly basis. Furthermore, developing a model that takes hierarchical relationships into account could offer a promising approach.

KEYWORDS

salmon, mortality, dynamic linear models, aquaculture, open-source data, environmental data, state-space models, warnings

1 Introduction

Over the past few decades, farmed Atlantic salmon has been a major contributor to the growth of international trade in fisheries and aquaculture products. It is an important global food source with a key role to play in food security and nutrition (FAO, 2022). Scotland is the third largest farmed salmon producer in the world with a production share of 7.6%, behind Norway (55.3%) and Chile (25.4%) (Iversen et al., 2020). Scottish salmon is amongst the top food export products of the UK (Department for Environment, Food & Rural Affairs, 2023), and the industry generates income in remote areas with few other opportunities (Murray et al., 2021).

The production of farmed salmon consists of two distinct phases: freshwater and seawater. To transition between these phases, salmon undergo a process called smoltification, during which they develop the ability to move from freshwater to seawater, becoming smolts (FAO, 2004). In this study, only the seawater phase was considered. Initially, salmon are raised in large tanks of freshwater for about 10 to 16 months and then moved to open net pens in seawater for about 14 to 22 months (Walde et al., 2023). There has been a tendency to keep smolts as long as possible in freshwater, where they face fewer challenges (Bjørndal and Tusvik, 2018; Hilmarsen et al., 2018). The farms in the open sea are usually referred to as sites and contain one generation of fish at a time, with the time between stocking and harvesting being one production cycle. A production cycle refers to a site-level period in which at least one pen on a site is occupied consecutively (Boerlage et al., 2017). It is recommended to fallow a site (entire site has no fish) for a minimum of 4 weeks before a new generation of salmon is introduced again (Scottish Salmon Producers Organisation, 2014). In 2022, around 55.2 million smolts were put to sea in Scotland, resulting in a total annual production of 169,194 tons (Munro, 2023).

Mortality rates are one of the main constraints to the sustainability of the industry. In Scotland, the mortality rates in the marine phase were approximately 24% in 2020, 26% in 2019 and 23% in 2018 (Munro, 2023). Mortality represents a significant economic loss to the producers and is considered an indicator of suboptimal fish welfare (Noble et al., 2018). Due to the open net-pen structures in which salmon are cultured, salmon are exposed to the natural environment that directly impacts their well-being. Salmon mortality can be influenced by several factors, including infectious and non-infectious agents. Examples of the most important infectious contributors are sea lice and sea lice treatments (Boerlage et al., 2024), and gill disease and cardiomyopathies (Mowi, 2022). Non-infectious agents are algal blooms, predators and the natural environmental conditions of the water (Sommerset et al., 2022). Optimal ranges have been determined for environmental variables, such as sea surface temperature, salinity, pH and dissolved oxygen requirements (Noble et al., 2018). Outside of these ranges, health and welfare of salmon may be impacted, resulting in increased mortalities.

Salmon aquaculture has become one of the most technologically advanced industries (FAO, 2022), with an increasing accumulation of data collected. Most producers have sensors that monitor the environment continuously. Additionally, all companies collect and store mortality data in their management programs. Some governments, such as in Scotland, collect and collate monthly mortality data from all aquaculture producers of all sites, in a standardized way, which is subsequently made publicly accessible. This valuable, continuously updated resource might provide an opportunity to develop an industry-wide monitoring model for mortality that does not require additional administrative complexities. Such a monitoring model could help identify events where mortality is higher than expected and prompt producers and inspectors to investigate the event further. Including environmental information into the monitoring model could enhance the predictions. Although salmon sites monitor and record many environmental variables, such information is not collated in a standardized way. A promising solution emerges from the widespread availability of open-source environmental data derived from satellites, which are standardized and publicly available (Thakur et al., 2018).

Using open-source databases collected by governments to model mortality of maricultured salmon has been done before. Recent studies have used different modelling methods, each with a different approach regarding the relevant variables to include. Moriarty et al. (2020) included only sea temperature and fish biomass, while others, such as Oliveira et al. (2021) and Tvete et al. (2022) included a wider range of variables such as sea temperature, sea salinity, fish weight at stocking, sea lice information or the occurrence of pancreas disease. These studies found sea temperature and salinity to be key drivers of farmed salmon mortality. However, these models assumed a fixed relationship between the response variable and the predictors, which may not hold over time as the underlying process changes.

Dynamic linear models (DLMs), a special case of state-space models, allow for time-varying parameters, which enables the model to adjust to changes in the underlying processes that generate the data over time (West and Harrison, 1997). DLMs can easily incorporate exogenous variables and it is possible to include terms to model trends and seasonality to improve the predictions. In addition, DLMs utilize a Bayesian framework where historical knowledge is combined with current data to detect changes within an observed process. This approach enables a more comprehensive understanding of the situation, facilitating well-informed decision-making (Kristensen et al., 2010). Thus, the use of DLMs is a promising approach to monitor farmed salmon mortality. In other farmed animal species, DLMs have been applied and proven effective in monitoring animal production (Dominiak et al., 2019a, 2019b; Jensen et al., 2016, 2017; Skjølstrup et al., 2022). To the farmed salmon industry, they have been applied only to a limited extent. One example of using such models for salmon aquaculture modelling is by Elghafghuf et al. (2020) who compared different state-space models in estimating the sea lice infestation pressure in salmon sites. Furthermore, a state-space monitoring model for salmon mortality and movement has been developed for wild Pacific salmon (Newman, 1998).

The purpose of this study was to use the available open-source mortality and environmental data to develop production cycle level DLMs for monitoring monthly mortality of maricultured Atlantic

salmon in Scotland. We intended to assess if these already existing resources can give valuable information to be used in the surveillance of mortality for Scottish salmon aquaculture, by triggering warnings when mortality is higher than expected. This can inform producers, veterinarians and inspectors, alerting them to further investigate. More specifically, we had four objectives: (1) to create a univariate production cycle level DLM using mortality data from salmon sites in Scotland; (2) to create multivariate production cycle level DLMs combining both mortality and environmental data. With this combination, we investigated if adding environmental data improved the estimates of mortality; (3) to compare the univariate and multivariate models and select the best model for monitoring salmon mortality; (4) to create warnings when observed mortality exceeded the expected levels.

2 Materials and methods

Data cleaning, manipulation and modelling were performed using the statistical programming environment R (R Core Team, 2022) and RStudio (Posit team, 2022). The time-series analysis workflow is freely accessible (https://doi.org/10.5281/zenodo.10617901).

2.1 Data sources

We used two different types of data: salmon production data and environmental data.

Scotland's Aquaculture website (https://aquaculture.scotland.gov.uk/; last accessed 9 February 2023) hosts an open access database containing various datasets with information on the aquaculture industry of Scotland. This study utilizes data from the "Fish Farm Monthly Biomass and Treatments" dataset owned by the Scottish Environment Protection Agency (SEPA). This dataset contains information about all fish species produced in Scotland and is submitted by all producers on a monthly basis. The salmon production data used in this study consists exclusively of data of Atlantic salmon (*Salmo salar* L.) from the period between 2002 and 2020 (entire period available at the time of extraction).

The environmental data used in this study is remotely sensed data from satellites. The environmental variables included were: temperature, salinity, concentration of phytoplankton, chlorophyll, dissolved oxygen, precipitation, concentration of dinoflagellates, diatoms, nanophytoplankton, picophytoplankton, pH and concentration of nitrate. Precipitation data (Huffman et al., 2019) was obtained from NASA's Earthdata platform (https://urs.earthdata.nasa.gov; last accessed on 9 February 2023). The other variables were obtained from E.U. Copernicus Marine Service Information (Tonani et al., 2022a, 2022b) and downloaded through Copernicus Marine Environment Monitoring Service (https://marine.copernicus.eu/services-portfolio/access-to-products/; last accessed on 9 February 2023). All environmental data are open-source and reported daily. To match the production data, the time period downloaded was from 2002 to 2020.

2.2 Data cleaning and data manipulation

The descriptive statistics of the variables used throughout the study are shown in Table 1.

2.2.1 Production data

All active marine salmon sites in Scotland between 2002 and 2020 were part of the dataset. Not all sites were active during the entire study period, either because they started production after the beginning of the study period, or because they discontinued it during the study period. Therefore, some sites made a first appearance in the study after 2002 and others disappeared before 2020. It resulted in a total of 402 sites and 2138 production cycles.

Scotland is geographically divided into six regions: Highland, Argyll & Bute, Shetland Islands, Eilean Siar, Orkney Islands, and North Ayrshire (Figure 1). The region North Ayrshire only has one site, therefore, we grouped it with the nearest region (Argyll & Bute) and only the remaining five regions were considered.

During the data cleaning process, some sites and production cycles were excluded from the study. First, production cycles for which it could not be guaranteed that they were in the dataset from stocking to harvesting were removed from the study. Production cycles with persistently missing or zero values for mortality (kg) or biomass (kg) throughout the entire production cycle were also excluded (92 production cycles). Records that did not meet the standard production cycle for commercial purposes, which we defined as between 6 and 36 months, were dropped (224 production cycles). Sites with less than 2 years of reported data (24 months) in the study period were also removed (24 sites). Finally, incoherent production cycles where information from some months was not reported were excluded from the study (33 production cycles).

The mortality reported corresponded to the number of kilograms of dead salmon per month per site (Table 1). We converted mortality to a proportion to take the production size into account, using the reported biomasses. Estimating biomasses at fish farming sites is based on management program algorithms and food intake data, typically periodically adjusted through sampling to determine the average fish weight. This average weight is then multiplied by the number of existing fish on the site, calculated as the initial number of fish put into the sea minus the countable dead fish (Costa et al., 2006). Mortality values for analysis were calculated as:

$$Mortality = \frac{Dead\ \ salmon\ \ (kg)}{Biomass\ \ (kg)}. \quad (1)$$

We regarded some mortality proportions as unrealistic. Reasons possibly included data entry mistakes; or stocking, harvesting or moving fish between sites in the middle of a month, which timing and quantity of fish moved were not available to us. This absence of movement data introduced a source of error in our proportion estimates, as the reported biomasses were a snapshot of the biomasses at the end of the month, while mortality accounts for the cumulative mortalities throughout the month. Moving fish from a site during the month leads to lower biomasses reported at the end of a month relative to the mortalities observed during the month,

10.3389/fmars.2024.1436755

TABLE 1 Descriptive statistics of the variables used in the study.

Variable	Type	Unit/Calculation	Missing	Median [iqr]
Mortality (dead salmon)	quantitative, continuous (monthly)	Kg	147 (0.46%)	1885 [610.0, 5671.25]
Biomass	quantitative, continuous (monthly)	Kg	0 (0%)	69000 [0, 520000]
Feed intake	quantitative, continuous (monthly)	Kg	0 (0%)	78800 [33000, 153351.5]
Realistic biomass	quantitative, continuous (monthly)	Kg	5115 (16.13%)	24000 [0, 519000]
Mortality (proportion)	quantitative, continuous (monthly)	$\frac{Dead\ \ salmon\ \ (kg)}{\text{Realistic biomass (kg)}}$	5253 (16.56%)	0.004 [0.002, 0.011]
Temperature	quantitative, continuous (daily)	°C	596840 (7.22%)	9.836 [7.774, 12.225]
Salinity	quantitative, continuous (daily)	ppt	596840 (7.22%)	34.638 [34.191, 35.213]
Phytoplankton	quantitative, continuous (daily)	mmol m-3	596840 (7.22%)	2.955 [0.620, 5.505]
Chlorophyll	quantitative, continuous (daily)	mg m-3	596840 (7.22%)	0.584 [0.166, 0.990]
Dissolved oxygen	quantitative, continuous (daily)	mmol m-3	596840 (7.22%)	266.59 [251.01, 276.85]
Precipitation	quantitative, continuous (daily)	mm	20247 (0.73%)	1.117 [0.240, 4.736]
Dinoflagellates	quantitative, continuous (daily)	mg m-3	596840 (7.22%)	0.012 [0.004, 0.023]
Diatoms	quantitative, continuous (daily)	mg m-3	597945 (7.23%)	0.34 [0.101, 0.600]
Nanophytoplankton	quantitative, continuous (daily)	mg m-3	596840 (7.22%)	0.124 [0.034, 0.198]
Picophytoplankton	quantitative, continuous (daily)	mg m-3	596840 (7.22%)	0.091 [0.020, 0.149]
pH	quantitative, continuous (daily)	–	596840 (7.22%)	8.121 [8.101, 8.156]
Nitrate	quantitative, continuous (daily)	mmol m-3	596840 (7.22%)	4.16 [2.144, 6.103]

iqr: Interquartile range.

whereas introducing fish to a site during the month leads to higher reported biomasses relative to the observed mortalities. To reduce this source of error as much as possible, we identified unrealistic mortality proportions and we made them missing. For that, we defined biomasses lower than realistic as:

$$Low\ \ biomass_t \ \leq \ Biomass\ \ (kg)_{t-1} - Mortality\ \ (kg)_{t-1} - 0.2 \times Biomass\ \ (kg)_{t-1}, \quad (2)$$

and biomasses higher than realistic as:

$$High\ \ biomass_t \ \geq \ 1.2 \times Biomass\ \ (kg)_{t-1} + Feed\ \ intake\ \ (kg)_t \ \times 0.77, \quad (3)$$

where t corresponds to the current month and $t-1$ to the previous month. As shown in Equations 2 and 3, we set limits of 20% deviation from expected biomasses, below and above which biomasses were considered abnormal. In Equation 3, additionally we used the feed intake reports to foresee how much the salmon where expected to grow in each month. Although the feed conversion ratio (FCR) for salmon fluctuates throughout a production cycle, for the sake of simplification, we adopted a reported FCR of 1.3 for salmon in the United Kingdom (Torrissen et al., 2011), meaning that 77% of feed intake is transformed in weight gain. Equations 2 and 3 were applied to all reported biomasses on the dataset. When the biomasses were considered lower or higher than realistic, these observations were replaced by missing values. Therefore, we restricted the analysis to only realistic biomasses, which were used to calculate mortality as defined in Equation 1.

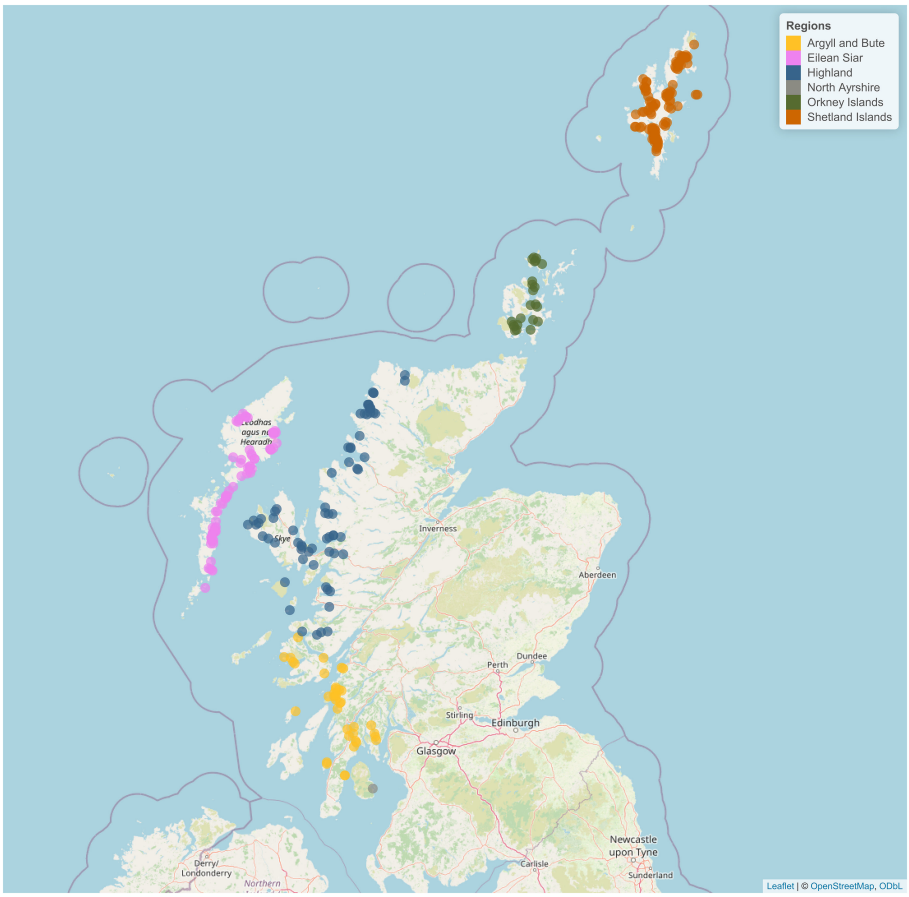

FIGURE 1
Salmon sites distributed across the six regions of Scotland. Created using the *leaflet* R package (Cheng et al., 2024).

2.2.2 Environmental data

The environmental data (2002-2020) have three dimensions: spatial, temporal and depth. These data were transformed into observations of 20 km around a site (spatial), monthly (temporal) and averaged of 0, 3, and 10 meters below the surface (depth; precipitation only at 0 meters). These transformations were accomplished using the R packages: *tidyverse* (Wickham et al., 2019), *janitor* (Firke et al., 2023), *lubridate* (Grolemund and Wickham, 2011), *ncdf4* (Pierce, 2023), *raster* (Hijmans et al., 2023), *sp* (Pebesma et al., 2018) and *sf* (Pebesma et al., 2022).

Spatial coverage of environmental data from satellite images was not available for around 65% of the exact site locations for all environmental variables except for precipitation which was available for 100% of the locations. Because aquaculture sites are often next to the shore or in sea lochs, estimates for this data at the aquaculture site location are often missing. Reasons are the compromised pixel edge lengths and coastal effects, dissolved organic compounds of terrestrial origin, and weather patterns (Thakur et al., 2018). Dropping these sites would bias our study towards offshore sites and leave the study with too few observations. Therefore, we used buffer zones of 20 km around the aquaculture sites and averaged the values within that buffer as a proxy for site location. For 24 sites we could not obtain environmental data even with the 20 km buffer, as they were situated too close to the shore or far inside sea lochs. As a result, these sites were not part of the study.

Temporal coverage meant that daily environmental data obtained were aggregated into monthly data to have the same dimensions as the mortality data (Table 1). We aggregate the environmental data with the intention of looking at both extremes and variation. For extremes, we aggregated into monthly data by using the 1st and 9th deciles to best capture the amount of abnormal days with more extreme environmental factors needed to cause salmon mortality (Table 2). For the environmental variables where both increases and decreases can lead to salmon mortality, we used both deciles, while for variables where only increases were of interest, we applied only the 9th decile. The only exception is for precipitation, where we used the 9th decile even though only decreases might affect mortality. The reason is that relying solely on the 1st decile would often result in a value of 0, which would lose the impact of precipitation. Thus, we looked at its negative effect, when the 9th decile is lower than normal should lead to salmon mortality. To investigate the effect of relatively quick changes in environmental variables, *i.e.* their variation, we designed variables that portrayed the maximum daily variation out of a month for the variables where variability may affect mortality (Table 2). This was not the case for precipitation, nor for the phytoplankton and chlorophyll type variables (Phytoplankton, Chlorophyll, Dinoflagellates, Diatoms, Nanophytoplankton,

10.3389/fmars.2024.1436755

TABLE 2 Variables used as inputs on the DLMs.

Variable groups	Transformation	Aggregated by month	Variable names
Temperature	–	1st decile	d1.temp
		9th decile	d9.temp
	log (*x*)	max (|*daily range*|)	log.max.daily.range.temp
Salinity	log (*x*)	1st decile	log.d1.sal
		9th decile	log.d9.sal
		max (|*daily range*|)	log.max.daily.range.sal
Phytoplankton	log (*x* + 1)	9th decile	log.d9.phyc
Chlorophyll	log (*x*)	9th decile	log.d9.chl
Dissolved oxygen	log (*x*)	1st decile	log.d1.do
		9th decile	log.d9.do
		max (|*daily range*|)	log.max.daily.range.do
Precipitation	log (*x*)	9th decile	log.d9.prep
Dinoflagellates	log (*x*)	9th decile	log.d9.dino
Diatoms	log (*x*)	9th decile	log.d9.diato
Nanophytoplankton	log (*x*)	9th decile	log.d9.nano
Picophytoplankton	log (*x*)	9th decile	log.d9.pico
pH	–	1st decile	d1.ph
		9th decile	d9.ph
		max (|*daily range*|)	max.daily.range.ph
Nitrate	log (*x*)	9th decile	log.d9.no3
		max (|*daily range*|)	log.max.daily.range.no3
Mortality	log (*x* + 0.00005)	Already monthly data	log.mortality

Picophytoplankton) because they usually appear as blooms (a sudden increase of the concentration in seawater) (Brown et al., 2020). Therefore, the maximum daily variation on a month would be similar to what is given by the 9th decile.

For depth coverage, we determined the depth level to be an average of values at 0, 3 and 10 meters depth. Salmon swim vertically to the depth that better meets their physiological needs, *e.g.* fish swim to deeper depths in the summer than in the winter to avoid the stronger surface light (Oppedal et al., 2007). Thus, using only one of the reported depths would not be an accurate measure of what salmon were exposed to.

After cleaning both environmental and mortality data, they were combined into one dataset. Our study population was reduced to 293 seawater Scottish salmon sites, corresponding to 1610 production cycles distributed in five regions of Scotland.

2.2.3 Transformation and standardization

The residuals of a DLM should follow a normal distribution (West and Harrison, 1997). To assess if this assumption was met, a univariate DLM was run for each input variable individually. For some variables, a logarithmic transformation was needed (Table 2). Two variables that were subject to logarithmic transformation included zeros. On those cases, the logarithmic transformation was conducted as: $\log(x+\alpha)$, where $\alpha \in]0,1]$.

The variances of the different variables were adjusted to a similar scale by standardizing each variable individually. It was accomplished by subtracting the sample mean of the variable from all observations and then dividing them by the sample standard deviation.

2.3 Learning and test sets

The available data were split into a learning set (145 sites, distributed by five regions of Scotland, and 784 production cycles) for estimating parameters for the DLMs and a test set (the same 145 sites and 353 other production cycles) for validating the models.

This division was done by chronologically dividing the dataset into two parts, where the first three quarters of the data were used as a learning set, while the remaining quarter was used as the test set. A division at a specific date would cut production cycles, having parts of some production cycles in the learning set and other parts of the same production cycles in the test set. Instead, we used different cut-off dates at each site as close to the three quarters reference as

possible, ensuring that production cycles would remain intact. Sites with less than two production cycles on the learning set were excluded.

For the expectation maximization (EM) algorithm, which was used in the training phase of the model, the learning set was again divided into a training set and validation set with a three quarters-one quarter split, in the same way described above. Sites where all mortality or environmental information was missing on the EM algorithm training set were excluded.

Only the sites which were present in all four sets - EM training set, EM validation set, DLM learning set and DLM test set - were included in this study. Therefore, all sets include the same sites.

2.4 Dynamic linear models

Dynamic linear models (DLMs) are generally used to estimate the true state of a given variable at each time t, by filtering the random noise. DLMs use a Bayesian framework to base their estimates on observed data, while incorporating any prior knowledge available prior to a given observation. Besides, DLMs do not follow the assumption that the estimates remain constant over time, allowing them to have systematic fluctuations and changes as time passes (West and Harrison, 1997).

A DLM is represented by a combination of two equations, namely the observation equation (Equation 4) and the system equation (Equation 5).

$$Y_t = F_t{}' \theta_t + \nu_t, \qquad \nu_t \sim N(0, V_t), \tag{4}$$

$$\theta_t = G_t \ \theta_{t-1} + w_t, \qquad w_t \sim N(0, W_t). \tag{5}$$

The observation equation (Equation 4) describes how the values of an observation vector (Y_t) depend on underlying (unobservable) parameters (θ_t). The transposed design matrix ($F_t{}'$) extracts the expected values of the observable variables from the parameter vector the system equation (Equation 5) is what makes the DLMs dynamic since it updates the values from time $t-1$ to time t, through the system matrix (G_t). The observational variance-covariance matrix (V_t) is where the uncertainty about the observations is depicted. The systematic variance-covariance matrix (W_t) represents how uncertain we are about how much each element of the system will randomly change from one time step to another and how changes in one element affect changes in all other elements, and vice versa.

For a complete specification of the DLM, the matrices F_t, G_t, V_t and W_t must be given together with the initial distribution of $(\theta_0 | D_0) \sim N(m_0, C_0)$. The prior information/belief at time 0 (before any observations are made) is presented as D_0, which consists of the initial mean (m_0) and a variance-covariance matrix (C_0).

In this study, the systematic variance-covariance matrix (W_t) was assumed constant, so that $W_t = W$. The dimensions of the observational variance-covariance matrix (V_t) and the transposed design matrix ($F_t{}'$) changed over time according to which variables had missing observations at a given time t. Thus, the missing observations at any given time step were ignored. The system matrix (G_t) was not constant for the variables that do not have a seasonal pattern. In those cases, G_t was updated at each month t.

Two types of production cycle level DLMs (univariate and multivariate) were created and are explained in detail in the following subsections. The term "production cycle level" indicates that the predictions will be made individually per production cycle based on prior information given at country level. Therefore, these models do not account for the potential relationships within the same sites or regions.

2.4.1 Univariate DLM

A univariate production cycle level DLM (West and Harrison, 1997) was used to monitor salmon mortality on a monthly basis (mortality defined as explained in Table 2).

In this case, Y_t consisted of only one value (the observed mortality for month t). The parameter vector (θ_t) contained the level and a trend factor for the variable mortality at time t. The initial level of m_0 was calculated by fitting a spline function to the mortality data available in the learning set (all sites), which was then used to predict the mortality value for $t = 0$ (initial level). The spline function was created using the default settings of the *smooth.spline* function available in *stats* R package (R Core Team, 2022). It was decided to use the default settings, as the role of the spline's exact shape is less important here than in classical static models due to the dynamic model's inherent capability to adapt over time. The trend factor was initially set to 1, indicating that before any observations are made, we expected the system to evolve exactly in accordance with the estimated spline function. A trend component greater than 1 would then correspond to a trend (positive or negative) being faster than the average, while a trend component less than 1 would correspond to a trend which is slower than the average.

The prior variance (C_0) was determined by computing the covariance between the differences amid all two consecutive mortality observations for the first six observed mortality values of each production cycle on the learning set and the first six original observed mortality values.

The $F_t{}'$ matrix was represented in the univariate case as:

$$F_t{}' = [\,1 \ 0\,].$$

This structure serves to separate the level and the trend of θ_t, when $F_t{}'$ is multiplied by θ_t on the observation equation (Equation 4). The result was the predicted mortality value at each time t.

The G_t matrix for the univariate case was defined as:

$$G_t = \begin{bmatrix} 1 & \delta_t \\ 0 & 1 \end{bmatrix},$$

with

$$\delta_t = \hat{m}_t - \hat{m}_{t-1}$$

where $\hat{m}_t$ and $\hat{m}_{t-1}$ being the expected log-transformed mortality at times t and $t-1$, respectively, given by the spline function. Thus δ_t is the expected rate of change in log-transformed mortality values from time $t-1$ to time t.

The observational variance-covariance matrix (V) expressed the uncertainty about the mortality observations. To make an initial estimate for V, which in the univariate case was a scalar (only one value), we calculated a two-sided moving average with a moving

window equal to five months to each production cycle on the learning set individually. Then, the residuals between the observed and estimated values of each production cycle were combined. The variance of the combined residuals corresponds to the initial estimate for V.

Finally, W matrix was defined as:

$$W = \begin{bmatrix} W_{1,1} & W_{1,1d} \\ W_{1d,1} & W_{1d,1d} \end{bmatrix},$$

where $W_{1,1}$ expresses how uncertain we were about the evolution of the mortality level, $W_{1d,1d}$ expresses how uncertain we were about the evolution of the trend factor, and the off-diagonal elements $W_{1,1d}$ & $W_{1d,1}$ are equal and represent the systematic covariance between the evolution of mortality level and the evolution of the trend factor. The systematic variance-covariance matrix (W) was initially estimated by diving the prior variance, C_0 by 10.

Afterwards, we optimized the values in V and W using the expectation maximization (EM) algorithm, as described in subsection 2.4.3.

2.4.2 Multivariate DLM

In multivariate models, more than one variable is modelled simultaneously. Here, all environmental variables (21) and mortality (all represented in Table 2) were given as inputs. Thus, the multivariate DLM forecasted the 22 variables expected values for each month. The hypothesis was that this multivariate model would learn from previous mortality and environmental data and work on associations between the variables to give an accurate prediction of mortality considering the environmental factors of that month.

Most environmental variables had a clear seasonal pattern (see for example Figure 2). This knowledge was included in the DLMs to improve the predictions by using a linear combination of trigonometric functions (sine and cosine, also known as *harmonic waves*), called the Fourier form representation (West and Harrison, 1997). For each variable, we assessed the sum of harmonic waves that better reflected its seasonality. To do so, we used a linear regression to get the relationship between the observations of each variable on the learning set and a trigonometric function representing a sum of a specific number of harmonic waves. Each of the harmonic waves has its own frequency ranging from 1 cycle per year to 6 cycles per year (the Nyquist harmonic). The Nyquist harmonic corresponds to the maximum number of waves allowed for a given period (West and Harrison, 1997). In this study, the Nyquist harmonic corresponded to the 6th harmonic wave ($\frac{12\ months}{2}$). The harmonic with the lowest frequency represents the main annual pattern, whereas those with higher frequencies account for deviations from the overall pattern. For a graphical illustration of the method, reference is made to (Dominiak et al 2019a, Figure 7).

Next, we measured the fit of the trigonometric function to the data using the adjusted Coefficient of determination (R^2). We successively tested several sums of harmonic waves and when the adjusted R^2 stopped improving, the number of harmonic waves that had the highest adjusted R^2 was selected as the optimal for that variable. The best number of harmonic waves for each variable is presented in Table 3. For some variables the best number of harmonic waves is 0, meaning that those variables did not have a seasonal pattern.

In Supplementary Figure S1 is illustrated the expected patterns for each variable modelled with the respective sum of harmonic waves or with spline functions (for the variables without seasonal pattern). The data points shown are from one arbitrary site, but the waves and the splines were defined based on data from all sites. The x-axis for the variables with seasonal pattern correspond to the calendar months, whereas for the variables that did not show any seasonality correspond to the months of the production cycle since stocking.

The process of creating a multivariate DLM involves combining the univariate models required to represent each variable individually, as exemplified previously with mortality, while also considering the interdependencies between those variables.

Here, the Y_t consisted on a vector with all observed values in month t for the 22 variables. Also, θ_t was a vector containing the underlying parameters for all variables in month t. A linear

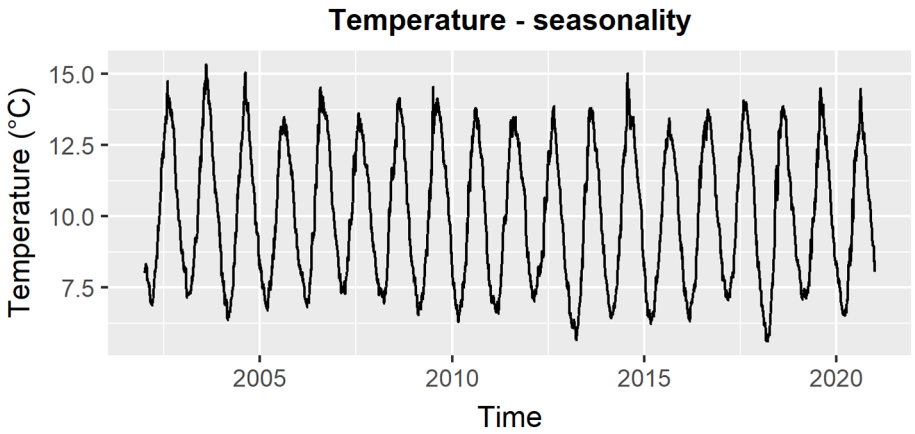

FIGURE 2
Seasonal pattern in daily temperature data from 2002 to 2020, utilizing a 20 km buffer and averaging across the three depths and all sites.

10.3389/fmars.2024.1436755

regression based on the best number of harmonic waves (Table 3) for a period of 12 months was created as previously explained for each seasonal variable individually, and its coefficient estimates were used in m_0. The coefficient estimates values corresponded to the intercept and one sine and cosine wave for each harmonic wave needed. For example, for the variable *d1.temp* the best number of harmonic waves was 2 (Table 3) thus, 5 coefficient estimates were allocated to m_0. For the variables that used all waves possible (including the Nyquist harmonic) the last sine wave could not be calculated. In those cases, only the available information (12 coefficient estimates) was added to m_0. For the variables that did not show seasonal patterns, *i.e.* the variables related to mortality and salinity (Table 3), the levels were calculated with spline functions as explained on the univariate case and the trend factors were again defined as 1. Therefore, the unobservable parameter vector $\theta_t = (\theta_{t,1}, \ldots, \theta_{t,137})$ had 137 elements.

To compute the prior variance (C_0), firstly the *vcov* function available on *stats* R package (R Core Team, 2022) was applied to each linear regression previously created for each seasonal variable. This function returned a variance-covariance matrix of the main parameters of each regression model. For all the variables that do not have seasonality, the variance-covariance matrices were calculated as explained in the univariate model. Then, the final variance-covariance matrix (C_0) was a combination of each variable individual variance-covariance matrix.

In the multivariate case, the system matrix (G_t) was also a combination of each variable's individual G matrix. A system submatrix describing a single harmonic wave is defined as:

$$G = \begin{bmatrix} cos(a\omega) & sin(a\omega) \\ -sin(a\omega) & cos(a\omega) \end{bmatrix},$$

where $\omega = \frac{2\times\pi}{12}$ and a defines the frequency. If $a = 1$, the frequency is 1 full cycle per year. If $a = 2$, the frequency is 2 cycles per year, etc. The case $a = 6$ corresponds to 6 cycles per year (the Nyquist harmonic), which is a special case represented as:

$$G = (-1).$$

For the variables without cyclical patterns, the G matrix was defined as explained for the univariate case. Therefore, the system matrix for the multivariate corresponded to a 137 × 137 matrix and was defined as:

$$G_t = \begin{bmatrix}
1 & 0 & 0 & 0 & 0 & \cdots & 0 & 0 & 0 & 0 & 0 & \cdots & 0 & \cdots & 0 & 0 \\
0 & cos(\omega) & sin(\omega) & 0 & 0 & \cdots & 0 & 0 & 0 & 0 & 0 & \cdots & 0 & \cdots & 0 & 0 \\
0 & -sin(\omega) & cos(\omega) & 0 & 0 & \cdots & 0 & 0 & 0 & 0 & 0 & \cdots & 0 & \cdots & 0 & 0 \\
0 & 0 & 0 & cos(2\omega) & sin(2\omega) & \cdots & 0 & 0 & 0 & 0 & 0 & \cdots & 0 & \cdots & 0 & 0 \\
0 & 0 & 0 & -sin(2\omega) & cos(2\omega) & \cdots & 0 & 0 & 0 & 0 & 0 & \cdots & 0 & \cdots & 0 & 0 \\
\vdots & \vdots & \vdots & \vdots & \vdots & \ddots & \vdots & \vdots & \vdots & \vdots & \vdots & \cdots & \vdots & \cdots & \vdots & \vdots \\
0 & 0 & 0 & 0 & 0 & \cdots & 1 & 0 & 0 & 0 & 0 & \cdots & 0 & \cdots & 0 & 0 \\
0 & 0 & 0 & 0 & 0 & \cdots & 0 & cos(\omega) & sin(\omega) & 0 & 0 & \cdots & 0 & \cdots & 0 & 0 \\
0 & 0 & 0 & 0 & 0 & \cdots & 0 & -sin(\omega) & cos(\omega) & 0 & 0 & \cdots & 0 & \cdots & 0 & 0 \\
0 & 0 & 0 & 0 & 0 & \cdots & 0 & 0 & 0 & cos(2\omega) & sin(2\omega) & \cdots & 0 & \cdots & 0 & 0 \\
0 & 0 & 0 & 0 & 0 & \cdots & 0 & 0 & 0 & -sin(2\omega) & cos(2\omega) & \cdots & 0 & \cdots & 0 & 0 \\
\vdots & \vdots & \vdots & \vdots & \vdots & \cdots & \vdots & \vdots & \vdots & \vdots & \vdots & \ddots & \vdots & \cdots & \vdots & \vdots \\
0 & 0 & 0 & 0 & 0 & \cdots & 0 & 0 & 0 & 0 & 0 & \cdots & -1 & \cdots & 0 & 0 \\
\vdots & \vdots & \vdots & \vdots & \vdots & \cdots & \vdots & \vdots & \vdots & \vdots & \vdots & \cdots & \vdots & \ddots & \vdots & \vdots \\
0 & 0 & 0 & 0 & 0 & \cdots & 0 & 0 & 0 & 0 & 0 & \cdots & 0 & \cdots & 1 & \delta_t \\
0 & 0 & 0 & 0 & 0 & \cdots & 0 & 0 & 0 & 0 & 0 & \cdots & 0 & \cdots & 0 & 1
\end{bmatrix}$$

where $\delta_t = \hat{m}_t - \hat{m}_{t-1}$ (being $\hat{m}$ the expected log-transformed mortality given by the spline function). Due to space constraints, it was not possible to present the complete G_t matrix. Thus, we decided to show the three different designs present in G_t: the system matrix with 2 harmonic waves for the variable *d1.temp* (upper left corner block), the Nyquist harmonic for *log.d9.pico* (middle block) and the system matrix for *log.mortality* (lower right corner block).

In the multivariate DLMs the transposed design matrix (F_t') has the same aim as in the univariate case: separate the observable values from the trend factor or harmonic waves (depending on the variable). Therefore, the $F_t{}'$ had repeated structures according to the number and the type of variables used (with or without seasonal patterns). The transposed design matrix in the multivariate case, when no observation was missing in month t, corresponded to a 22 × 137 matrix depicted as:

TABLE 3 Number of harmonic waves used to model the seasonality of each variable.

Variable names	Number of harmonic waves	Variable names	Number of harmonic waves
d1.temp	2	log.d9.prep	3
d9.temp	2	log.d9.dino	4
log.max.daily.range.temp	2	log.d9.diato	4
log.d1.sal	0	log.d9.nano	5
log.d9.sal	0	log.d9.pico	6
log.max.daily.range.sal	0	d1.ph	2
log.d9.phyc	3	d9.ph	3
log.d9.chl	5	max.daily.range.ph	3
log.d1.do	2	log.d9.no3	3
log.d9.do	2	log.max.daily.range.no3	3
log.max.daily.range.do	2	log.mortality	0

Key to variable names: d1, 1st decile; d9, 9th decile; max.daily.range, maximum daily variation; log, logarithmic transformation; temp, temperature; sal, salinity; phyc, phytoplankton; chl, chlorophyll; do, dissolved oxygen; prep, precipitation; dino, dinoflagellates; diato, diatoms; nano, nanophytoplankton; pico, picophytoplankton; ph, pH; no3, nitrate.

$$F_t' = \begin{bmatrix} \mathbf{1} & \mathbf{1} & \mathbf{0} & \mathbf{1} & \mathbf{0} & \cdots & 0 & 0 & 0 & 0 & 0 & 0 & 0 & 0 & 0 & 0 & 0 & \cdots & 0 & 0 \\ \vdots & \vdots & \vdots & \vdots & \vdots & \ddots & \vdots & \vdots & \vdots & \vdots & \vdots & \vdots & \vdots & \vdots & \vdots & \vdots & \vdots & \cdots & \vdots & \vdots \\ 0 & 0 & 0 & 0 & 0 & \cdots & \mathbf{1} & \mathbf{1} & \mathbf{0} & \mathbf{1} & \mathbf{0} & \mathbf{1} & \mathbf{0} & \mathbf{1} & \mathbf{0} & \mathbf{1} & \mathbf{0} & \cdots & 0 & 0 \\ \vdots & \vdots & \vdots & \vdots & \vdots & \cdots & \vdots & \vdots & \vdots & \vdots & \vdots & \vdots & \vdots & \vdots & \vdots & \vdots & \vdots & \ddots & \vdots & \vdots \\ 0 & 0 & 0 & 0 & 0 & \cdots & 0 & 0 & 0 & 0 & 0 & 0 & 0 & 0 & 0 & 0 & 0 & \cdots & \mathbf{1} & \mathbf{0} \end{bmatrix},$$

Again, it was not possible to show the complete F_t' matrix due to space restrictions. Thus, we presented the designs corresponding to the same three variables shown on Gt: *d1.temp* (upper left corner block), *log.d9.pico* (middle block) and *log.mortality* (lower right corner block). When there was a missing observation for some variable in month t, the row corresponding to that variable on the F_t' matrix was excluded.

The observational variance-covariance matrix (V_t) was a quadratic matrix with the number of rows and columns being equal to the number of variables without missing observations in month t, being defined as:

$$V_t = \begin{bmatrix} V_{1,1} & \cdots & V_{1,n} \\ \vdots & \ddots & \vdots \\ V_{n,1} & \cdots & V_{n,n} \end{bmatrix},$$

where the maximum value of n was 22 (total number of variables). If *d1.temp* is considered variable number 1 and *log.mortality* variable number 22, $V_{1,1}$ is the observational variance of *d1.temp*, $V_{22,22}$ is the observational variance of *log.mortality*, and $V_{1,22}$ and $V_{22,1}$ correspond to the observational covariance between *d1.temp* and *log.mortality*. An initial estimate of V was created by placing the individual observational variances of each variable along the diagonal, while the off-diagonal values were set to 0. The observational variances of the variables without seasonality were calculated as explained in the univariate DLM, while the observational variances for the variables with seasonal patterns were defined by computing the variance of each linear regression residuals formerly created.

The systematic variance-covariance matrix was initially determined by dividing the prior variance by 10 (as in the univariate case), being a 137 × 137 matrix.

As in the univariate case, the initial estimates of V_t and W were optimized using the EM algorithm as described in sub-section 2.4.3. The values located in the off-diagonal areas of V_t and W contribute with the additional information about how the different variables mutually affect each other.

2.4.2.1 Variables selection methodology

We initially developed a multivariate production cycle level DLM incorporating all available variables (21 environmental variables and mortality), as previously explained in subsection 2.4.2. However, our subsequent analysis revealed that utilizing all this information might not be the most efficient strategy. Some of the environmental variables may not influence mortality and including them could result in a more complex and computationally demanding model than required. Nevertheless, we have provided a thorough explanation of the most intricate model, thus creating other models with fewer variables is a simple matter of excluding from the initial specifications the irrelevant variables.

A systematic approach would entail the construction of individual multivariate production cycle DLMs for all possible variable combinations. This would result in over 2 million possibilities. Instead, we made a DLM per variable group, and then applied the stepwise forward selection method.

In the first step, seven multivariate production cycle level DLMs were created, each one using the variables included in each environmental variable group (Temperature, Salinity, Phytoplankton and Chlorophyll, Dissolved oxygen, Precipitation, Nitrate, pH) plus the variable mortality. To compare the performance of the seven multivariate DLMs, it was necessary to evaluate how different the mortality observations were from the predictions, represented as forecast errors. This evaluation was conducted by calculating the Root Mean Squared Error (RMSE) for the collective set of mortality forecast errors across all production cycles within each DLM. A lower RMSE signifies a higher level of model precision, allowing the comparative analysis of the models. Considering our aim of investigating if adding environmental variables improves the predictions of mortality, the RMSEs from the seven multivariate models were compared against the RMSE of the univariate model. If those RMSEs were lower than the RMSE of the univariate model, it was considered to improve the mortality predictions.

The second step was to build six multivariate DLMs each one with the variables that provided the best DLM on the first step and one other environmental variable group per model. In this way, we could understand if adding any other environmental group improved the estimates of mortality. The RMSEs were compared against the RMSE of the best performing multivariate DLM from the first step.

In the third step, we wanted to assess if all variables present on the best DLM from the second step were relevant to the model. In that sense, several multivariate DLMs consisting of all possible variables combinations were created. The RMSEs were compared against the RMSE of the best model from the second step.

To see if we could improve the best DLM so far, the fourth step involved employing the stepwise forward selection method. It consisted of building a multivariate DLM with the most promising selection of variables identified thus far and adding all other variables, one at a time. The model with the lowest RMSE was designated as the best.

2.4.3 Optimizing DLM variance components

The expectation maximization (EM) algorithm (West and Harrison, 1997) was used to optimize the systematic variance-covariance matrix (W) and the full version of the observational variance-covariance matrix (V) for both the univariate and the multivariate versions of the DLM.

The EM algorithm is a mathematical method that estimates unknown parameters by finding the most likely outcome based on observed data. It involves a series of iterations, which implies calculating the likelihood of the data given previous estimates, and then refining those estimates based on the new information (Dethlefsen, 2001).

Running the EM algorithm is usually computationally demanding, especially if working with large datasets or using several variables simultaneously. To tackle this challenge we ran the EM algorithm using an early stopping technique. For that, we started by dividing the learning set into a training set, consisting of the first three quarters of the data and a validation set, consisting of the last quarter, as previously explain in section 2.3. After each iteration of the EM algorithm, the DLM with the most recent set of variance components (W and V) was applied to the validation set, and the root mean squared error (RMSE) of the forecast errors was calculated. When the RMSE (rounded to 4 decimal places) stopped decreasing, the EM algorithm was terminated and the variance components which minimized the RMSE were returned.

2.4.4 Filtering and smoothing

Since the initial specifications needed were already calculated (m_0, C_0 F_t, G_t, V_t and W) the next step was to update the models. The updating procedure for the DLMs was computed by utilizing the Kalman filter updating equations (filtering) as described by West and Harrison (1997). The values were forecast at each time step, relying on the current estimate of the mean and prior information about error and variance around both the system and the data. These values were subsequently "corrected" according to the new observation, where the predicted values by the model and the actual observed values were compared, and the forecast errors were used to improve the estimated value of the next time step. As a result of the Kalman filter, we got the monthly expected values (filtered mean and variance) and the forecasts for each variable (mortality in the univariate DLM and all 22 variables in the full multivariate DLM).

The parameter vectors θ_t are autocorrelated to each other through the system equation. In the Kalman filter, we only used the previous information to obtain the best estimate of θ_t. However, owing to the autocorrelation present between the parameter vectors, the subsequent observations have as much useful information to estimate the true values of θ_t as the past observations. Therefore, a retrospective analysis called smoothing can be employed, where data are analyzed from the latest update and working backwards to the initial point, as outlined by West and Harrison (1997). This retrospective analysis is useful because we obtain the best possible estimates for each variable, which are important since they can provide better knowledge about the effects of specific events, like disease outbreaks (Kristensen et al., 2010).

2.5 Generating warnings

Warnings were generated when the observed mortality values fell above the 95% credible intervals (CI). The 95% CI were calculated using the forecasted values (f_t) produced by the Kalman filter, along with its respective variance Q_t:

$$95\ \%\ CI = f_t \pm 1.96 \times \sigma_t,$$

where $\sigma_t = \sqrt{Q_t}$. Whenever a warning was triggered, it indicated that the mortality was higher than expected for that time step on that production cycle and further investigation is required.

3 Results

The following results were obtained by applying the DLMs to the test set while using the initial specifications calculated based on the learning set. Every production cycle in the test set (a total of 353 production cycles across 145 sites) was subjected to both univariate and multivariate DLMs individually.

3.1 Univariate DLM

The outcomes of the univariate DLM for production cycle number 614 are illustrated in Figure 3. This production cycle was chosen because it has almost no missing data and no warnings were detected. Specifically, these outcomes are the filtered mean estimated by the prospective Kalman filter and the smoothed mean estimated by the retrospective smoothing (Figure 3A), and the forecasted values produced at each time step in the Kalman filter (Figure 3B). All outcomes are presented with their corresponding 95% credible interval, based on their respective variance components. The filtered mean can be interpreted as the best possible estimate of the true underlying mortality level given all previous information at each time step, while the smoothed mean can be interpreted as the best possible estimate of the true underlying mortality level given all available information prior to and after a given time step. Both means (filtered and smoothed) demonstrated a consistent alignment with the observations (Figure 3A). The 95% credible interval for the mortality forecasts (Figure 3B) was wider than the 95% credible intervals of both filtered and smoothed means (Figure 3A). This suggests that there is a higher level of uncertainty in the predictions (Figure 3B), with a RMSE value of 0.86028.

Even though errors associated with the predictions existed, it was possible to detect warnings in several production cycles. Figure 4 illustrates the mortality forecasts for production cycle number 466 and it shows that the observations exceed the predictions 95% credible interval at month 11 after stocking.

Between 2015 and 2020, 109 out of the 353 production cycles exhibited at least one warning. Among these 109 cycles, 77% experienced a single warning during the cycle, 20% had two warnings, and 3% encountered three.

Out of the 145 sites, 86 experienced warnings, affecting all five regions. The region of Eilean Siar had the highest occurrence rate with 28 production cycles with at least one warning out of 63 production cycles (44%) and 36 warnings in total. The region Orkney Islands showed the lowest number of warnings, having 6 production cycles with at least one warning out of 55 production cycles (11%) and 8 warnings in total, as depicted in Table 4.

Concerning the months of the year with more warnings (Table 4), the upward trend commenced in April with 12 warnings in 490 production cycle-months that took place during April (2.4%). July (3.7%), August (6.8%), September (5.1%), and October (4.3%) stood out as the months with the highest occurrences of warnings.

The year 2016 had the highest frequency of warnings with 42 occurrences within 903 production cycle-months (4.7%), followed by

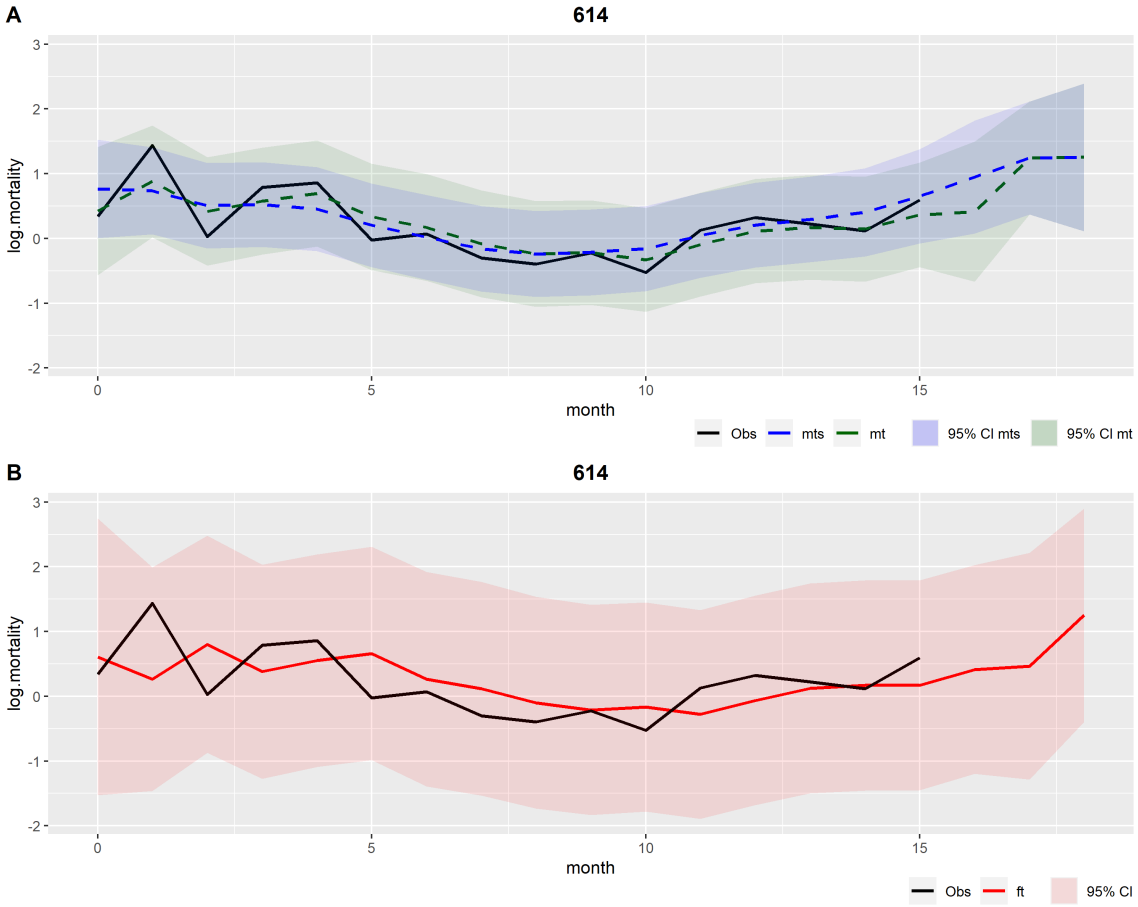

FIGURE 3
Outcomes from the univariate DLM applied to production cycle number 614. Observations (obs) in black. **(A)** In green: Filtered mean (mt) and the respective 95% credible interval (CI); In blue: Smoothed mean (mts) and the respective 95% credible interval (CI). **(B)** In red: Forecasts (ft) and the respective 95% credible interval (CI).

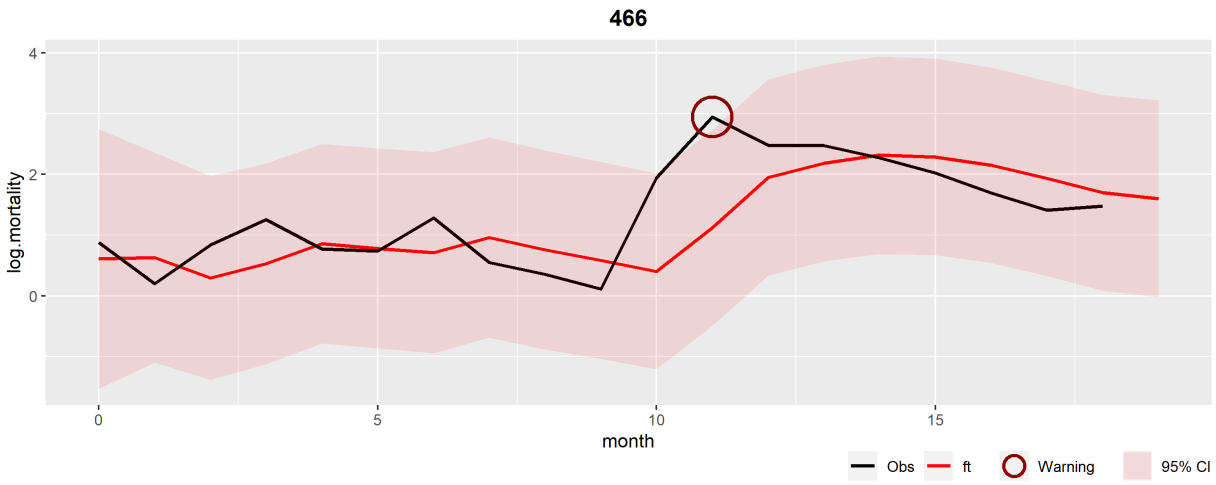

FIGURE 4
Outcomes from the univariate DLM applied to production cycle number 466. Observations (obs) in black and the forecasts (ft) and the respective 95% credible interval (CI) in red; Circle: warning.

10.3389/fmars.2024.1436755

2017 (2.9%) and 2018 (2.2%) (Table 4). In 2015, only three months of data were available, making direct comparisons not applicable.

3.2 Multivariate DLM

In the process of selecting the most relevant variables to be used on the multivariate production cycle level DLM, the first step was to create seven multivariate DLMs each one using the variables included in one environmental variable group, in addition to the mortality variable (Table 5). The RMSEs from the models were compared against the RMSE of the univariate model (0.86028). As shown in Table 5, the model including the salinity variables had a better performance (lowered the RMSE).

For the second step, six multivariate DLMs were built, each one with the variables that provided the best DLM thus far (salinity related variables and mortality) and one other environmental variable group per model. The RMSEs were compared against the RMSE of the multivariate DLM that used the salinity variables and mortality (0.85862). Supplementary Table S1 shows that the models' performances did not improve by adding any of the other environmental groups.

For the third step, we generated seven DLMs consisting of all possible combinations using the salinity variables (Table 6). Two combinations improved the performances when compared to using all salinity variables. The best DLM used the variables *log.d9.sal, log.max.daily.range.sal* and *log.mortality* (lower RMSE).

The fourth and last step consisted of applying the stepwise forward selection method. The results are illustrated in Supplementary Table S2, and demonstrate that the inclusion of additional variables did not lead to improved performances. Therefore, the best multivariate DLM in predicting the mortality estimates was the DLM that included the variables *log.d9.sal, log.max.daily.range.sal* and *log.mortality*, with a RMSE of 0.85860.

The best multivariate DLM had a smaller RMSE than the univariate DLM (0.85860 and 0.86028, respectively). To determine whether this very small difference is statistically significant or not, a paired t-test was applied to the squared forecast errors of the univariate and best multivariate DLMs. T-tests are known to be useful in studies with large sample sizes and are robust even for skewed data (Fagerland, 2012). We intend to compare the variances; therefore, it is natural to square the forecast errors. The resulting p-value was 0.003714, which indicated that both models are significantly different from each other. We concluded that the best multivariate DLM performed better than the univariate DLM.

The subsequent results are based on the best and final multivariate DLM, which is henceforth referred to simply as multivariate DLM. Figures 5–7 show the outcomes of the multivariate DLM for production cycle 614 (the same presented in the univariate DLM results section). Figures 5 and 6 illustrate the filtered and the smoothed mean (A), and the forecasts (B) for the logarithmic transformation of the 9th decile of salinity (*log.d9.sal*) and for the maximum daily range of salinity (*log.max.daily.range.sal*), respectively.

TABLE 4 Warnings identified in the univariate and multivariate DLMs between 2015 and 2020: per region, month of the year and year.

Univariate												
Warnings per region	**Highland**		**Argyll and B.**			**Shetland Isl.**		**Orkney Isl.**			**Eilean Siar**	
	34/101 (34%)		21/59 (36%)			20/75 (27%)		6/55 (11%)			28/63 (44%)	
	45		27			21		8			36	
Warnings per month of the year (%)	**Jan**	**Feb**	**Mar**	**Apr**	**May**	**Jun**	**Jul**	**Aug**	**Sep**	**Oct**	**Nov**	**Dec**
	0.7	0.7	0.9	2.4	2.3	1.5	3.7	6.8	5.1	4.3	0.6	0.7
Warnings per year (%)	**2015**		**2016**		**2017**		**2018**		**2019**		**2020**	
	0.0		4.7		2.9		2.2		1.5		1.6	
Multivariate												
Warnings per region	**Highland**		**Argyll and B.**			**Shetland Isl.**		**Orkney Isl.**			**Eilean Siar**	
	31/101 (31%)		18/59 (31%)			19/75 (25%)		6/55 (11%)			25/63 (40%)	
	41		22			19		8			32	
Warnings per month of the year (%)	**Jan**	**Feb**	**Mar**	**Apr**	**May**	**Jun**	**Jul**	**Aug**	**Sep**	**Oct**	**Nov**	**Dec**
	0.7	0.7	0.9	2.4	2.0	1.3	3.7	5.5	4.6	3.4	0.4	0.7
Warnings per year (%)	**2015**		**2016**		**2017**		**2018**		**2019**		**2020**	
	0.0		4.0		2.5		2.0		1.5		1.4	

For the "Warnings per region", the first row corresponds to the number of production cycles that triggered at least one warning out of the total number of production cycles in that region; the second row shows the total number of warnings triggered in each region. For the "Warnings per month of the year (%)" and "Warnings per year (%)", the percentages correspond to the division between the total number of warnings generated on that month or year and the corresponding number of production cycle-months, multiplied by 100.
Isl., Islands; B., Bute; Jan, January; Feb, February; Mar, March; Apr, April; Jun, June; Jul, July; Aug, August, Sep, September; Oct, October; Nov, November; Dec, December.

TABLE 5 First step - Information about the multivariate DLMs created per variable group, in addition to the mortality variable.

Variable groups used in DLM	Variables names	RMSE	Improved[a]
Temperature + Mortality	d1.temp; d9.temp; log.max.daily.range.temp; log.mortality	0.86319	False
Salinity + Mortality	log.d1.sal; log.d9.sal; log.max.daily.range.sal; log.mortality	0.85862	True
Phytoplankton and Chlorophyll type + Mortality	log.d9.phyc; log.d9.chl; log.d9.dino; log.d9.diato; log.d9.nano; log.d9.pico; log.mortality	0.86955	False
Dissolved oxygen + Mortality	log.d1.do; log.d9.do; log.max.daily.range.do; log.mortality	0.86340	False
Precipitation + Mortality	log.d9.prep; log.mortality	0.86982	False
pH + Mortality	d1.ph; d9.ph; max.daily.range.ph; log.mortality	0.86965	False
Nitrate + Mortality	log.d9.no3; log.max.daily.range.no3; log.mortality	0.86889	False
Mortality (Univariate DLM)	log.mortality	0.86028	—

[a]Compared to the univariate model of mortality alone.

Concerning the logarithmic transformation of mortality (*log.mortality*), Figure 7A shows that once again the filtered and smoothed means demonstrated a consistent alignment with the observations. The 95% credible interval of the forecasts (Figure 7B) was also wider than the 95% credible intervals of both filtered and smoothed means (Figure 7A). This shows that the uncertainty in the predictions on mortality continued after adding the environmental variables considered most relevant. The multivariate DLM was also capable of giving warnings in production cycle 466, as shown in Supplementary Figure S2.

TABLE 6 Third step - Information about the multivariate DLMs created with all possible combinations using salinity variables, and mortality.

Variables names	RMSE	Improved[a]
log.d1.sal; log.mortality	0.85982	False
log.d9.sal; log.mortality	0.85981	False
log.max.daily.range.sal; log.mortality	0.86331	False
log.d1.sal; log.d9.sal; log.mortality	0.85985	False
log.d1.sal; log.max.daily.range.sal; log.mortality	0.85861	True
log.d9.sal; log.max.daily.range.sal; log.mortality	0.85860	True
log.d1.sal; log.d9.sal; log.max.daily.range.sal; log.mortality	0.85862	—

[a]Compared to the multivariate model using mortality and all salinity variables.

Between 2015 and 2020, 99 out of 353 production cycles experienced at least one warning from the multivariate model. All these 99 production cycles also generated warnings in the univariate model. In line with the univariate DLM, 79% of the 99 production cycles had one warning, 19% had two warnings, and 2% had three.

Among the 145 sites, 79 generated warnings, all of which were also identified when using the univariate model. All regions generated warnings (Table 4). The region of Eilean Siar recorded the highest occurrence rate (40%) and the Orkney Islands the lowest (11%), consistent with what we found in the univariate DLM.

Regarding the seasonality of the warnings produced by the multivariate model, an increase was seen in April (2.4%), with July (3.7%), August (5.5%), September (4.6%) and October (3.4%) having the highest occurrence of warnings (Table 4), similar to the pattern seen with the univariate model.

In accordance with the univariate DLM, warnings occurred most frequently in the year 2016 (4.0%), followed by 2017 at 2.5% and 2018 at 2.0%, as seen in Table 4. Once again, the year 2015 is not applicable for comparisons due to the limited availability of data.

4 Discussion

One univariate and various multivariate production cycle level DLMs were developed using open-source data. The main goal was to investigate the value of these already collected data for monitoring monthly mortality of maricultured Atlantic salmon in Scotland. The best DLM consisted of mortality and salinity related variables. Both the univariate and the final multivariate DLMs exhibited a degree of uncertainty in the mortality predictions. Nevertheless, both models were capable of giving warnings about unexpected increases in mortality. If implemented in a near real-time surveillance system, these warnings can be used by stakeholders such as salmon producers to further investigate the observation and possibly detect (emerging) diseases. Therefore, we demonstrated that, despite the underlying data being of low resolution, the open-source data sources can be successfully used as part of a monitoring system. This has the potential to provide stakeholders with valuable information without requiring additional efforts such as more data collection or developing more data sharing agreements.

The uncertainty associated with the forecasts of mortality in both models led to wide 95% credible intervals. Many different factors have likely contributed to the uncertainty observed in the predictions of mortality. First, salmon mortality can be influenced by various factors that were not considered in this study. For example, an increase in mortality can be caused by non-infectious and infectious health challenges such as pathogens like sea lice (Noble et al., 2018), and a decrease can be caused by the mitigation measures carried out by health managers. Information on cause-specific high mortality is openly available and can be found in Salmon Scotland's monthly mortality reports (https://www.salmonscotland.co.uk/reports; last accessed 5 January 2024), but these were unavailable during most of our study period. Incorporating these unaddressed factors into our models might have decreased the uncertainties about the predictions of mortality, but there are concerns that suboptimal validity of the cause-specific salmon mortality can lead to selection

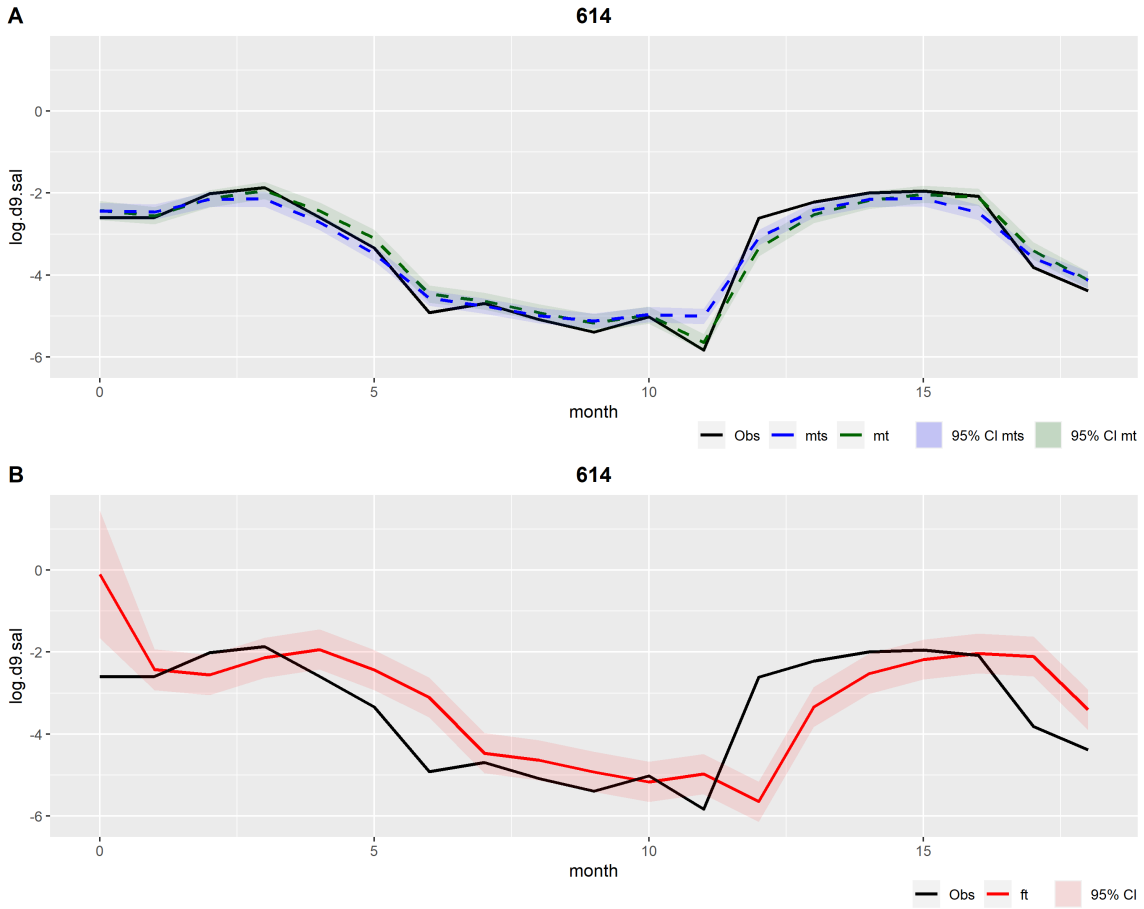

FIGURE 5
Outcomes related to the variable *log.d9.sal* from the multivariate DLM applied to production cycle number 614. Observations (obs) in black. **(A)** In green: Filtered mean (mt) and the respective 95% credible interval (CI); In blue: Smoothed mean (mts) and the respective 95% credible interval (CI). **(B)** In red: Forecasts (ft) and the respective 95% credible interval (CI).

and misclassification bias when using this information to model mortality (Aunsmo et al., 2008). Second, the absence of movement data and, consequently, the indirect method used to detect the movements most likely did not capture all movements of fish. Therefore, the calculated mortality has itself associated uncertainty. Third, it would have been optimal to train the models with data where the mortality was known to be "normal" to ensure that the models learned the "normal" patterns, as was done by Jensen et al. (2016). The lack of health and welfare information about fish populations in the database made it impossible to determine what normal mortality was, and thus it was not possible to separate production cycles with only normal mortality for the learning set from those with abnormal mortality. That being said, other studies have successfully developed DLMs for monitoring purposes in the past without knowing the normal state of the animals (Bono et al., 2012, 2013, 2014; Dominiak et al., 2019a, 2019b).

Favorable environmental conditions are of paramount importance for the survival of salmon (Noble et al., 2018; Murray et al., 2022). Therefore, several multivariate DLMs including different environmental variables were made to better understand which environmental factors influence salmon mortality in Scotland. Our study demonstrated that including salinity related variables is relevant for predicting salmon mortality in Scotland. This is similar to the findings of Oliveira et al. (2021) and Tvete et al. (2022) who also described salinity as an important environmental factor. Temperature is commonly described as having significant influence in salmon mortality (Elliott and Elliott, 2010; Moriarty et al., 2020), but including it did not improve the mortality predictions further.

Uncertainty was also embedded in the environmental variables. We used buffer zones of 20 km around the aquaculture sites and averaged the environmental values within that buffer as a proxy for site location, to optimally use the satellite data. As a result, the values used did not exactly represent the environmental factors experienced by the salmon. Furthermore, we used the daily mean of three depths (0, 3, and 10 meters) to aggregate data on a monthly basis, rather than incorporating each depth in the models. While this approach saved computational time, the resulting values used in the models do not precisely correspond to the environmental conditions that salmon experienced. Despite exploration of many different types of aggregation of the environmental variables per month (*e.g.* different quartile levels), extremes that are known to be outside of comfort levels for salmon would always be under detected if durations were brief (less than 3 days using the 1st and 9th deciles). Moreover, suboptimal conditions may have no effect when salmon are healthy, but may affect health and

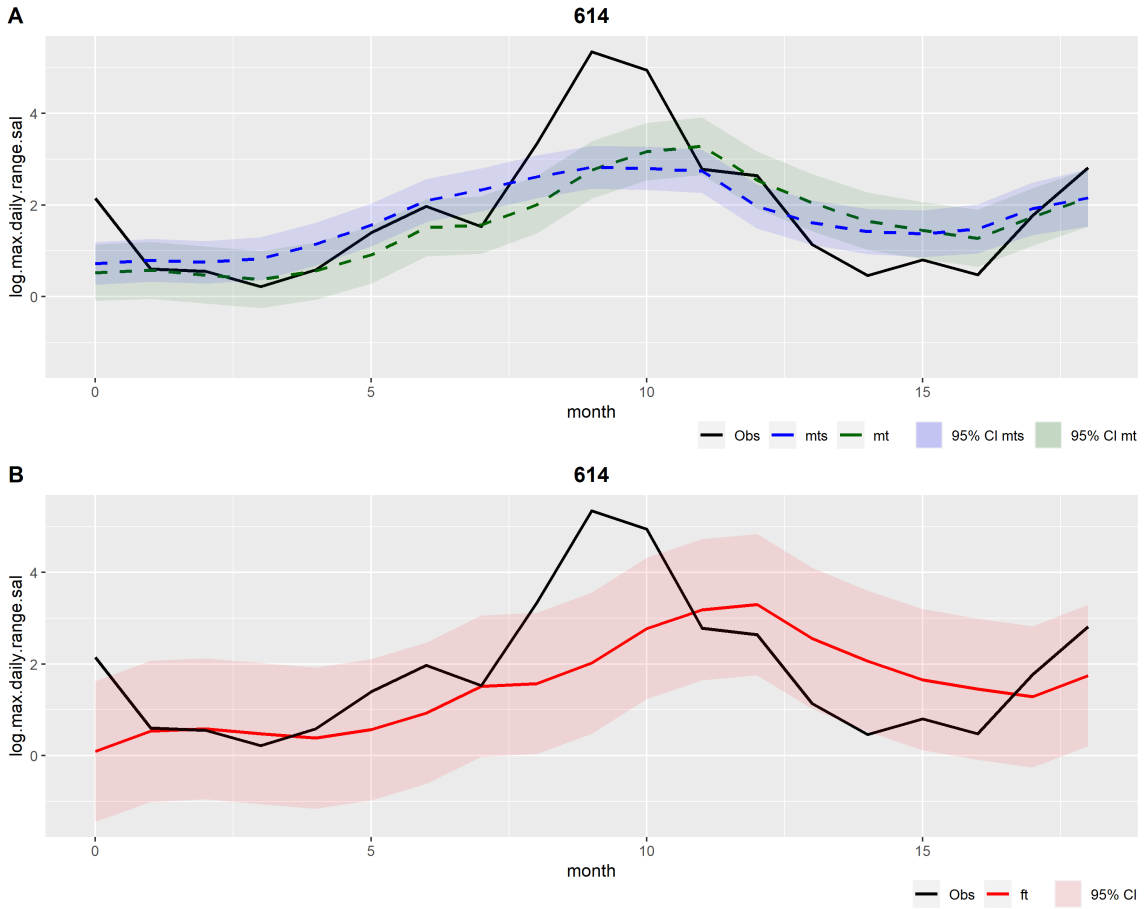

FIGURE 6
Outcomes related to the variable *log.max.daily.range.sal* from the multivariate DLM applied to production cycle number 614. Observations (obs) in black. **(A)** In green: Filtered mean (mt) and the respective 95% credible interval (CI); In blue: Smoothed mean (mts) and the respective 95% credible interval (CI). **(B)** In red: Forecasts (ft) and the respective 95% credible interval (CI).

welfare if salmon are stressed or have underlying conditions (Noble et al., 2018). Therefore, some important information may have been lost in the aggregations. These simplifications, such as buffer, depth and monthly aggregations could have contributed to the uncertainty seen in the mortality predictions, and could be the reason for the environmental variables considered most relevant in the literature had little effect on the predictions of mortality in this study.

Salmon farming sites monitor and record many environmental factors using sensors, which are typically more accurate and have greater resolution than satellite data (Thakur et al., 2018). However, there is a lack of standardization across all sites. Not all relevant environmental factors are measured at every site, protocols vary between sites (*e.g.* depths) and the data are not collected centrally from all sites at near real-time, as it is done for mortality data. Therefore, it is more suitable to use satellite data when creating models considering different sites. Sharing data between companies requires data-sharing agreements, which can be difficult. Using both satellite data and the open-source mortality dataset provided a chance to develop models without adding administrative complexities.

This study provided insights into the occurrence and distribution of warnings in Scotland. A warning indicated that salmon mortality was higher than expected. Access to raw mortality data alone does not clarify whether increased mortality is normal for the phase of the production cycle or merely a result of natural variation. With the warnings generated (using credible intervals), stakeholders are alerted to instances of increased mortality that are beyond natural variation and are higher than expected for the specific phase of the production cycle. When comparing the warnings generated by the univariate and multivariate models, it is noteworthy that both models exhibit similar results. However, the univariate model generated a greater number of warnings overall. Approximately 30% of the production cycles and more than 50% of the sites experienced at least one warning between 2015 and 2020. Considering the wide 95% credible interval of the models, the real values might be higher. Geographically, the generated warnings exhibited a non-uniform distribution across Scotland. The region of Eilean Siar had the highest warning rate and the Orkney Islands had the lowest. These findings were different from a previous study that applied a specific threshold to mortality events in Scotland between 2002 and 2009, and found that more warnings were generated on the Northern Islands (Orkney Islands and Shetland Islands) (Salama et al., 2016). In our study, most warnings happened between July and October, which is when the water temperature is higher. As temperature increases, salmon's metabolic activity also rises, leading to a greater demand for oxygen. In addition, the amount of dissolved

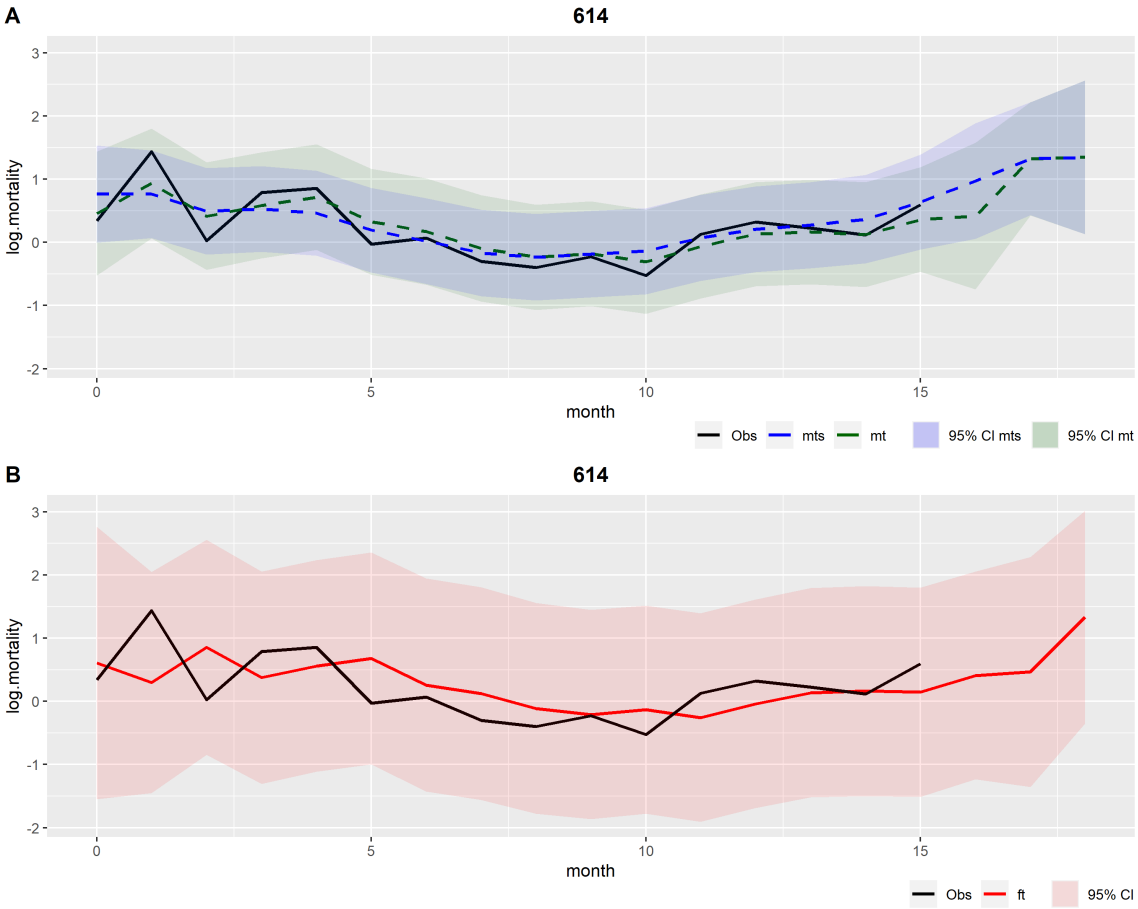

FIGURE 7
Outcomes related to the variable *log.mortality* from the multivariate DLM applied to production cycle number 614. Observations (obs) in black. **(A)** In green: Filtered mean (mt) and the respective 95% credible interval (CI); In blue: Smoothed mean (mts) and the respective 95% credible interval (CI). **(B)** In red: Forecasts (ft) and the respective 95% credible interval (CI).

oxygen in the water decreases as the water temperature increases (Noble et al., 2018). Also, infectious agents, such as *Neoparamoeba perurans*, the causative agent of Amoebic Gill Disease (AGD), and sea lice proliferate at higher rates in warmer waters (Oldham et al., 2016; Brooker et al., 2018; Murray et al., 2022). Studies have shown that salmon mortality due to Pancreas disease is also higher in the summer months (Kilburn et al., 2012). Therefore, an increase in warnings during this period may be the result of a higher incidence of disease outbreaks and unfavorable conditions. Another interesting finding was the declining trend in the frequency of warnings from 2016 to 2020. The year 2016 had the highest prevalence of warnings in our study, while the year 2017 was reported as the one with highest total mortality between 2015 and 2020 (Munro, 2023). However, it should be noticed that the warnings generated by these models are related to unexpected changes in mortality, not necessarily to total mortality. It is unclear to us why the frequency of warnings decreased after 2016, although one of the reasons may be the establishment of gill disease that changed from emerging disease to being a consistent (and thus expected) constraint. Many other reasons could have contributed to this observation.

The warnings generated in this study were defined as any observation falling above the 95% credible interval. Nevertheless, other methods could have been used to generate warnings using the DLMs outputs. Examples of other methods include the Tabular Cumulative Sums and the V-mask (Antunes et al., 2017).

We utilized DLMs despite encountering non-normally distributed residuals in some of the original variables. To address this issue, we applied a logarithmic transformation to these variables prior to analysis and assessed whether the assumption of normality was satisfied. The practice of transforming data is frequently employed to conform to Gaussian assumptions, see for example Larsen et al. (2019). The selection of the DLM was based on its computational ease of use, allowing a more seamless execution on computer systems compared to other more complex models. The logarithmic transformation can be easily transformed back to the original values, ensuring that the interpretation of results can be conducted in terms of the original data scale.

With the available open-source data it was possible to design a monitoring model for mortality with a certain level of uncertainty. Suggestions for improvements of the models that may reduce uncertainty include using shorter time periods when aggregating the mortality data (*e.g.* weekly). Another approach might be to develop a novel structure that would integrate the monthly mortality data and the daily environmental data into a framework that could be utilized in the multivariate DLM. Furthermore,

including reasons for mortality and movement data may improve the monitoring process. Some of these improvements require additional data collection efforts as they are not currently being collected from all producers.

The next step of this project is to develop a hierarchical DLM that will use the same mortality data used in this study. It is a more complex model in which the mutual interconnectedness between all sites in all regions are taken into account, with the sites in the same region being assumed to be more closely correlated than sites in different regions. Such a hierarchical framework has the potential to enhance the monitoring of salmon mortality, offering a more comprehensive and insightful perspective on the complex factors influencing salmon mortality.

5 Conclusion

The open-source Scottish salmon data can be used to monitor salmon mortality, allowing stakeholders to be informed when mortality is higher than expected. One key advantage of this dataset is that it has already been collated and does not require data sharing agreements. Nevertheless, a degree of uncertainty was found in the mortality predictions in both univariate and multivariate DLMs. This uncertainty may be reduced if mortality data collected on a shorter time period (such as weekly), additional data on relevant factors that influence salmon mortality and movement data are made publicly available in the future and are included in the models. Moreover, using salinity information from open-source environmental data improved the mortality predictions, even with the monthly aggregations carried out. This study presents a systematic and extensive framework for constructing univariate and multivariate DLMs, and the codes used are freely accessible. Future research will focus on creating a hierarchical DLM that considers site, regional, and country levels.

Data availability statement

Publicly available datasets were analyzed in this study. This data can be found here: https://aquaculture.scotland.gov.uk, https://urs.earthdata.nasa.gov, https://data.marine.copernicus.eu.

Author contributions

CM: Conceptualization, Data curation, Formal analysis, Investigation, Methodology, Software, Visualization, Writing – original draft. AB: Conceptualization, Methodology, Resources, Supervision, Writing – review & editing. AK: Conceptualization, Formal analysis, Funding acquisition, Methodology, Resources, Software, Supervision, Writing – review & editing. DJ: Conceptualization, Formal analysis, Funding acquisition, Methodology, Resources, Software, Supervision, Writing – review & editing.

Funding

The author(s) declare financial support was received for the research, authorship, and/or publication of this article. This work has received funding from the European Union's Horizon 2020 research and innovation program under grant agreement No. 101000494 (DECIDE).

Conflict of interest

The authors declare that the research was conducted in the absence of any commercial or financial relationships that could be construed as a potential conflict of interest.

The author(s) declared that they were an editorial board member of Frontiers, at the time of submission. This had no impact on the peer review process and the final decision.

Publisher's note

Author disclaimer

Supplementary material

The Supplementary Material for this article can be found online at: https://www.frontiersin.org/articles/10.3389/fmars.2024.1436755/full#supplementary-material

References

Antunes, A. C. L., Jensen, D., Halasa, T., and Toft, N. (2017). A simulation study to evaluate the performance of five statistical monitoring methods when applied to different timeseries components in the context of control programs for endemic diseases. *PloS One* 12, e0173099. doi: 10.1371/journal.pone.0173099

Aunsmo, A., Bruheim, T., Sandberg, M., Skjerve, E., Romstad, S., and Larssen, R. B. (2008). Methods for investigating patterns of mortality and quantifying cause-specific mortality in sea-farmed Atlantic salmon *Salmo salar*. *Dis. Aquat. Organ* 81, 99–107. doi: 10.3354/dao01954

Bjørndal, T., and Tusvik, A. (2018). *Økonomisk analyze av alternative produksjonsfomer innan oppdrett (in Norwegian: An economic analysis of alternative production technologies in aquaculture)*. SNF-prosjekt nr. 5730. Bergen, Norway.

Boerlage, A. S., Shrestha, S., Leinonen, I., Jansen, M. D., Revie, C. W., Reeves, A., et al. (2024). Sea lice management measures for farmed Atlantic salmon (*Salmo salar*) in Scotland: Costs and effectiveness. *Aquaculture* 580, 740274. doi: 10.1016/j.aquaculture.2023.740274

Boerlage, A. S., Stryhn, H., Sanchez, J., and Hammell, K. L. (2017). Case definition for clinical and subclinical bacterial kidney disease (BKD) in Atlantic Salmon (*Salmo salar* L.) in New Brunswick, Canada. *J. Fish Dis.* 40, 395–409. doi: 10.1111/jfd.12521

Bono, C., Cornou, C., and Kristensen, A. R. (2012). Dynamic production monitoring in pig herds I: Modeling and monitoring litter size at herd and sow level. *Livestock Sci.* 149, 289–300. doi: 10.1016/j.livsci.2012.07.023

Bono, C., Cornou, C., Lundbye-Christensen, S., and Ringgaard Kristensen, A. (2013). Dynamic production monitoring in pig herds II. Modeling and monitoring farrowing rate at herd level. *Livestock Sci.* 155, 92–102. doi: 10.1016/j.livsci.2013.03.026

Bono, C., Cornou, C., Lundbye-Christensen, S., and Ringgaard Kristensen, A. (2014). Dynamic production monitoring in pig herds III. Modeling and monitoring mortality rate at herd level. *Livestock Sci.* 168, 128–138. doi: 10.1016/j.livsci.2014.08.003

Brooker, A. J., Skern-Mauritzen, R., and Bron, J. E. (2018). Production, mortality, and infectivity of planktonic larval sea lice, *Lepeophtheirus salmonis* (Kroyer 1837): Current knowledge and implications for epidemiological modelling. *ICES J. Mar. Sci.* 75, 1214–1234. doi: 10.1093/icesjms/fsy015

Brown, A. R., Lilley, M., Shutler, J., Lowe, C., Artioli, Y., Torres, R., et al. (2020). Assessing risks and mitigating impacts of harmful algal blooms on mariculture and marine fisheries. *Rev. Aquac.* 12, 1663–1688. doi: 10.1111/raq.12403

Cheng, J., Schloerke, B., Karambelkar, B., and Xie, Y. (2024). *leaflet: Create Interactive Web Maps with the JavaScript 'Leaflet'*. R package version 2.2.2. Available online at: https://CRAN.R-project.org/package=leaflet. (Accessed July 25, 2024).

Costa, C., Loy, A., Cataudella, S., Davis, D., and Scardi, M. (2006). Extracting fish size using dual underwater cameras. *Aquac. Eng.* 35, 218–227. doi: 10.1016/j.aquaeng.2006.02.003

Department for Environment, Food & Rural Affairs. (2023). *National statistics: Agriculture in the United Kingdom 2022. Chapter 13: Overseas trade*. Available online at: https://www.gov.uk/government/statistics/agriculture-in-the-united-kingdom-2022/chapter-13-overseas-trade. (Accessed March 1, 2024).

Dethlefsen, C. (2001). Space Time Problems and Applications. Aalborg, Denmark: Aalborg University. [PhD dissertation].

Dominiak, K. N., Hindsborg, J., Pedersen, L. J., and Kristensen, A. R. (2019a). Spatial modeling of pigs' drinking patterns as an alarm reducing method II. Application of a multivariate dynamic linear model. *Comput. Electron. Agric.* 161, 92–103. doi: 10.1016/j.compag.2018.10.037

Dominiak, K. N., Pedersen, L. J., and Kristensen, A. R. (2019b). Spatial modeling of pigs' drinking patterns as an alarm reducing method I. Developing a multivariate dynamic linear model. *Comput. Electron. Agric.* 161, 79–91. doi: 10.1016/j.compag.2018.06.032

Elghafghuf, A., Vanderstichel, R., Hammell, L., and Stryhn, H. (2020). Estimating sea lice infestation pressure on salmon farms: Comparing different methods using multivariate state-space models. *Epidemics* 31, 100394. doi: 10.1016/j.epidem.2020.100394

Elliott, J. M., and Elliott, J. A. (2010). Temperature requirements of Atlantic salmon *Salmo salar*, brown trout Salmo trutta and Arctic charr Salvelinus alpinus: Predicting the effects of climate change. *J. Fish Biol.* 77, 1793–1817. doi: 10.1111/j.1095-8649.2010.02762.x

Fagerland, M. W. (2012). t-tests, non-parametric tests, and large studies-a paradox of statistical practice? *BMC Med. Res. Methodol.* 12. doi: 10.1186/1471-2288-12-78

FAO. (2004). *Cultured Aquatic Species Information Program* - Salmo salar. Available online at: https://www.fao.org/fishery/en/culturedspecies/salmo_salar/en (Accessed February 7, 2023).

FAO. (2022). *The State of World Fisheries and Aquaculture 2022. Towards Blue Transformation* (Rome: FAO). doi: 10.4060/cc0461en

Firke, S., Denney, B., Haid, C., Knight, R., Grosser, M., and Zadra, J. (2023). *Package "janitor"*. Available online at: https://github.com/sfirke/janitorhttps://sfirke.github.io/janitor/ (Accessed February 15, 2023).

Grolemund, G., and Wickham, H. (2011). Dates and Times Made Easy with lubridate. *J. Stat. Softw.* 40. Available at: http://www.jstatsoft.org/.

Hijmans, R. J., van Etten, J., Sumner, M., Cheng, J., Baston, D., Bevan, A., et al. (2023). *Package "raster"*. Available online at: https://rspatial.org/raster (Accessed February 15, 2023).

Hilmarsen, Ø., Holte, E. A., Brendeløkken, H., Høyli, R., and Hognes, E. S. (2018). *Konsekvensanalyse av landbasert oppdrett av laks – matfisk og post-smolt (in Norwegian: Consequenses of land-bases salmon farming)*. Rapport nr. OC2018 A-033, prosjekt nr. 302003741. Trondheim, Norway.

Huffman, G. J., Stocker, E. F., Bolvin, D. T., Nelkin, E. J., and Tan, J. (2019). *GPM IMERG Late Precipitation L3 1 day 0.1 degree x 0.1 degree V06 (Goddard Earth Sciences Data and Information Services Center - GES DISC)*. NASA, Washington DC, USA. Available at: https://disc.gsfc.nasa.gov/datasets/GPM_3IMERGDL_06/summary.

Iversen, A., Asche, F., Hermansen, Ø., and Nystøyl, R. (2020). Production cost and competitiveness in major salmon farming countries 2003–2018. *Aquaculture* 522, 735089. doi: 10.1016/j.aquaculture.2020.735089

Jensen, D. B., Hogeveen, H., and De Vries, A. (2016). Bayesian integration of sensor information and a multivariate dynamic linear model for prediction of dairy cow mastitis. *J. Dairy Sci.* 99, 7344–7361. doi: 10.3168/jds.2015-10060

Jensen, D. B., Toft, N., and Kristensen, A. R. (2017). A multivariate dynamic linear model for early warnings of diarrhea and pen fouling in slaughter pigs. *Comput. Electron. Agric.* 135, 51–62. doi: 10.1016/j.compag.2016.12.018

Kilburn, R., Murray, A. G., Hall, M., Bruno, D. W., Cockerill, D., and Raynard, R. S. (2012). Analysis of a company's production data to describe the epidemiology and persistence of pancreas disease in Atlantic salmon (*Salmo salar* L.) farms off Western Scotland. *Aquaculture* 368-369, 89–94. doi: 10.1016/j.aquaculture.2012.09.004

Kristensen, A. R., Jørgensen, E., and Toft, N. (2010). *Herd Management Science II. Advanced topics* (*2010 Edition*), pp. 75–144.

Larsen, M. L. V., Pedersen, L. J., and Jensen, D. B. (2019). Prediction of tail biting events in finisher pigs from automatically recorded sensor data. *Animals* 9, 458. doi: 10.3390/ani9070458

Moriarty, M., Murray, A. G., Berx, B., Christie, A. J., Munro, L. A., and Wallace, I. S. (2020). Modelling temperature and fish biomass data to predict annual Scottish farmed salmon, *Salmo salar* L., losses: Development of an early warning tool. *Prev. Vet. Med.* 178, 104985. doi: 10.1016/j.prevetmed.2020.104985

Mowi. (2022). *Mowi Integrated Annual Report 2022*. Bergen, Norway.

Munro, L. A. (2023). *Scottish fish farm production survey 2022* (Edinburgh: Scottish Government). Available online at: https://www.gov.scot/publications/scottish-fish-farm-production-survey-2022/pages/5/ (Accessed February 5, 2024).

Murray, A., Falconer, L., Clarke, D., and Kennerley, A. (2022). Climate change impacts on marine aquaculture relevant to the UK and Ireland. *MCCIP Science Review* 2022, 18. doi: 10.14465/2022.reu01.aqu

Murray, A. G., Ives, S. C., Smith, R. J., and Moriarty, M. (2021). A preliminary assessment of indirect impacts on aquaculture species health and welfare in Scotland during COVID-19 lockdown. *Vet. Anim. Sci.* 11, 100167. doi: 10.1016/j.vas.2021.100167

Newman, K. B. (1998). State-Space Modeling of Animal Movement and Mortality with Application to Salmon. *Biometrics* 54, 1290–1314. https://www.jstor.org/stable/2533659.

Noble, C., Gismervik, K., Iversen, M. H., Kolarevic, J., Nilsson, J., Stien, L. H., et al. (2018). *Welfare Indicators for farmed Atlantic salmon: tools for assessing fish welfare*. Available online at: www.nofima.no/fishwell/english (Accessed February 24, 2023).

Oldham, T., Rodger, H., and Nowak, B. F. (2016). Incidence and distribution of amoebic gill disease (AGD) - An epidemiological review. *Aquaculture* 457, 35–42. doi: 10.1016/j.aquaculture.2016.02.013

Oliveira, V. H. S., Dean, K. R., Qviller, L., Kirkeby, C., and Bang Jensen, B. (2021). Factors associated with baseline mortality in Norwegian Atlantic salmon farming. *Sci. Rep.* 11, 14702. doi: 10.1038/s41598-021-93874-6

Oppedal, F., Juell, J. E., and Johansson, D. (2007). Thermo- and photoregulatory swimming behavior of caged Atlantic salmon: Implications for photoperiod management and fish welfare. *Aquaculture* 265, 70–81. doi: 10.1016/j.aquaculture.2007.01.050

Pebesma, E., Bivand, R., Racine, E., Sumner, M., Cook, I., Keitt, T., et al. (2022). *Package "sf."*. Available online at: https://r-spatial.github.io/sf/ (Accessed February 15, 2023).

Pebesma, E., Bivand, R., Rowlingson, B., Gomez-Rubio, V., Hijmans, R., Sumner, M., et al. (2018). *Package "sp."*. Available online at: https://github.com/edzer/sp/https://edzer.github.io/sp/ (Accessed February 15, 2023).

Pierce, D. (2023). *Package "ncdf4."*. Available online at: https://cirrus.ucsd.edu/~pierce/ncdf/ (Accessed February 15, 2023).

Posit team. (2022). *RStudio: Integrated Development Environment for R*. RStudio, PBC, Boston, MA. http://www.rstudio.com/.

R Core Team. (2022). *R: A language and environment for statistical computing*. R Foundation for Statistical Computing, Vienna, Austria. https://www.R-project.org/.

Salama, N. K. G., Murray, A. G., Christie, A. J., and Wallace, I. S. (2016). Using fish mortality data to assess reporting thresholds as a tool for detection of potential disease concerns in the Scottish farmed salmon industry. *Aquaculture* 450, 283–288. doi: 10.1016/j.aquaculture.2015.07.023

Scottish Salmon Producers Organization (2014). *Scottish Salmon farming code of good practice. Growing a sustainable industry*. Durn, Isla Road, Perth.

Skjølstrup, N. K., Lastein, D. B., de Knegt, L. V., and Kristensen, A. R. (2022). Using state space models to monitor and estimate the effects of interventions on treatment risk and milk yield in dairy farms. *J. Dairy Sci.* 105, 5870–5892. doi: 10.3168/jds.2021-21408

Sommerset, I., Walde, C. S., Bang Jensen, B., Wiik-Nielsen, J., Bornø, G., Oliveira, V. H. S., et al. (2022). *Fiskehelserapporten 2021. Veterinærinstituttet rapportserie nr 2a/2022*. Available online at: www.vetinst.no (Accessed September 14, 2023).

Thakur, K. K., Vanderstichel, R., Barrell, J., Stryhn, H., Patanasatienkul, T., and Revie, C. W. (2018). Comparison of remotely-sensed sea surface temperature and

salinity products with in *situ* measurements from British Columbia, Canada. *Front. Mar. Sci.* 5. doi: 10.3389/fmars.2018.00121

Tonani, M., Ascione, I., and Saulter, A. (2022a). *Product user manual (Ocean Physical and Biogeochemical reanalysis) NWSHELF_MULTIYEAR_BGC_004_011*. EU Copernicus Marine Service. doi: 10.48670/moi-00058

Tonani, M., Ascione, I., and Saulter, A. (2022b). *Product user manual (Ocean Physical and Biogeochemical reanalysis) NWSHELF_MULTIYEAR_PHY_004_009*. EU Copernicus Marine Service. doi: 10.48670/moi-00059

Torrissen, O., Olsen, R. E., Toresen, R., Hemre, G. I., Tacon, A. G. J., Asche, F., et al. (2011). Atlantic salmon (*Salmo salar*): the "Super-chicken" of the sea? *Rev. Fisheries Sci.* 19, 257–278. doi: 10.1080/10641262.2011.597890

Tvete, I. F., Aldrin, M., and Jensen, B. B. (2022). Towards better survival: Modelling drivers for daily mortality in Norwegian Atlantic salmon farming. *Prev. Vet. Med.* 210, 105798. doi: 10.1016/j.prevetmed.2022.105798

Walde, C. S., Bang Jensen, B., Stormoen, M., Asche, F., Misund, B., and Pettersen, J. M. (2023). The economic impact of decreased mortality and increased growth associated with preventing, replacing or improving current methods for delousing farmed Atlantic salmon in Norway. *Prev. Vet. Med.* 221, 106062. doi: 10.1016/j.prevetmed.2023.106062

West, M., and Harrison, J. (1997). *Bayesian Forecasting and Dynamic Models. 2nd Edn* (New York: Springer).

Wickham, H., Averick, M., Bryan, J., Chang, W., McGowan, L., François, R., et al. (2019). Welcome to the tidyverse. *J. Open Source Softw.* 4, 1686. doi: 10.21105/joss.01686

frontiers | Frontiers in Marine Science

TYPE Original Research
PUBLISHED 26 September 2024
DOI 10.3389/fmars.2024.1441589

OPEN ACCESS

EDITED BY
Ida Grong Aursand,
SINTEF Ocean, Norway

REVIEWED BY
Liang Guo,
Hunan Normal University, China
Yin Zhang,
Shantou University, China
Yang Jin,
Johns Hopkins University, United States

*CORRESPONDENCE
Xin Wen
wenxinfish@163.com

RECEIVED 31 May 2024
ACCEPTED 28 August 2024
PUBLISHED 26 September 2024

CITATION
Yang M, Huang J, Zheng D, Tang H, Liu J, Luo J and Wen X (2024) ERK1/2 regulates melanin synthesis in fish: a case study on a colourful variety, leopard coral grouper (*Plectropomus leopardus*). *Front. Mar. Sci.* 11:1441589. doi: 10.3389/fmars.2024.1441589

ERK1/2 regulates melanin synthesis in fish: a case study on a colourful variety, leopard coral grouper (*Plectropomus leopardus*)

Min Yang, Jie Huang, Decai Zheng, Haizhan Tang, Junchi Liu, Jian Luo and Xin Wen*

Sanya Nanfan Research Institute of Hainan University, Hainan Aquaculture Breeding Engineering Research Centre, Hainan Academician Team Innovation Centre, Hainan University, Haikou, China

Understanding the molecular mechanism of melanogenesis in *Plectropomus leopardus* is important for exploring the pattern of skin colour variation in grouper. The research team conducted a combined transcriptomic and proteomic analysis of *P. leopardus* skin tissues in red-skinned and black-skinned fish and found that the common differences were reflected in the melanogenesis pathway. Therefore, to further investigate the molecular mechanism of melanogenesis in *P. leopardus*, the full-length sequences of the *erk1/2* and *mitf* genes were obtained in this study using the RACE technique. Through structure-function analysis and differential expression in different red-skinned and black-skinned *P. leopardus* tissues, it was found that the MAPK signalling pathway may be involved in skin colour changes in *P. leopardus*, and when *erk1/2* expression was decreased in *P. leopardus*, *mitf* expression increased accordingly. On the one hand, through short-term *in vivo* injection of *erk1/2*-dsRNA, the optimal interference primer for experimented fish was found to be group D: F2R1(F2: TAATACGACTCACTATAGGGATCAACGACATTCTCAGGGC; R1: TAATACGACTCACTATAGGGTCCATGGAGAAAGTGAAGGG), the optimal injection site was the tail vein, the optimal interference concentration was 5 μg/g, and the duration of the interference effect was 5 days. The results of long-term interference showed that when *erk1/2* expression was decreased in *P. leopardus*, the skin colour of the treats fish then darkened, which indicated that ERK1/2 was involved in the regulation of melanogenesis. On the other hand, *in vitro* Co-Immunoprecipitation (Co-IP) results showed that there was a direct or indirect interaction between MITF and ERK1/2 proteins. In conclusion, this is the first time that an interaction between ERK1/2 and MITF, which indicated that ERK1/2 was involved in the regulation of melanogenesis through the regulation of MITF in *P. leopardus*. These results further enrich our understanding of the theoretical basis of the changing pattern of skin colour in *P. leopardus* and provides a new perspective for exploring the variable skin colouration of coral reef fish.

KEYWORDS

***Plectropomus leopardus*, ERK1/2, skin colour, MITF, melanogenesis**

1 Introduction

Plectropomus leopardus, belonging to Perciformes, Epinephelinae (Sugianti and Mujiyanto, 2016), mainly lives in the tropical waters of the Pacific and Indian Oceans, and a small number of them also exist in the east coast and southern waters of Hainan (Yoseda et al., 2008). Because of its rich nutrition and bright colour, *P. leopardus* is popular among consumers and has broad market prospects (Wang et al., 2011; Sun et al., 2015). However, environmental factors such as changes in light intensity and human activities during artificial culture produced a stress response in *P. leopardus*, resulting in the gradual darkening or blackening of the skin colour, which directly affects the ornamental and economic value of *P. leopardus* (Zhao et al., 2016). Recent studies in wild *P. leopardus* have found the presence of melanomas (Sweet et al., 2012), indicating that *P. leopardus* can be used as a good model to study the molecular mechanism of melanin metabolic diseases in fish (Lerebours et al., 2016). Exploring the process of melanogenesis can not only enrich our basic understanding of *P. leopardus* and skin colour research but also has certain scientific value in ecological conservation applications.

The MAPK signalling pathway is involved in the metabolic activities of organisms and plays a crucial role in cell growth and development, migration, differentiation, and apoptosis (Wang et al., 2017). There are three main highly conserved signalling pathways in the MAPK family, namely, ERK1/2, JNK1, and p38MAPK, which function through a tertiary kinase cascade and are inactive in the nonphosphorylated state; the MAPK signalling pathway stays quiescent and is activated upon stimulation by stepwise phosphorylation of MAPK (Zheng et al., 2009). In addition, MITF (microphthalmia-associated transcription factor) is a tissue-specific MAPK substrate found in melanocytes (Wellbrock and Arozarena, 2015) and the level of MAPK pathway activation is critical for MITF abundance and function in melanocytes (Molina et al., 2005). Recently, the MAPK pathway was found to be involved in the biological activities of pigment cells during skin colour formation in fish. By comparing the transcriptome and microbiome of *Carassius auratus* and *Oreochromis mossambicus*, researchers found that the MAPK signalling pathway is one of the key pathways involved in the regulation of skin colour formation (Zhu et al., 2016). These transcriptional level and epigenetic studies have provided good insights, but the specific mechanism through which signalling pathways and skin colour variation are related has not been fully elucidated. In particular, the skin colour of *P. leopardus* is very sensitive to changes in environmental factors, and MAPK signalling may be closely related to the regulation of environmental stress (Jalmi and Sinha, 2015).

The MAPK signalling pathway has been extensively studied in mammalian melanin synthesis, which is involved in the regulation of survival of many pigmented mammalian cells. For example, lipopolysaccharide (LPS) induces melanin production in human melanocytes through activation of the p38MAPK signalling pathway. Meanwhile, it was demonstrated that p38MAPK activation mediated the expression of the *mitf* and tyrosinase (*tyr)* genes (Zhou et al., 2021), which in turn induced melanin production, after negative regulation by p38MAPK inhibitors (Ahn et al., 2008). The same results were confirmed in mouse studies, where inhibition of p38MAPK resulted in reduced melanin secretion by melanocytes (Kim et al., 2007). JNK1 was revealed to be primarily involved in the regulation of melanocyte resistance to adversity. Minocycline reduces cell death in cutaneous melanocytes by activating the JNK1 pathway against the threat posed by H_2O_2 (Song et al., 2008); similarly, endothelin-1 plays a role in protecting human cutaneous melanocytes from UV-induced DNA damage by activating the JNK1 and p38MAPK signalling pathways (von Koschembahr et al., 2015). Interestingly, in contrast to p38MAPK and JNK1, activation of ERK1/2 inhibits melanocyte melanin synthesis. Inhibition of ERK1/2 activity stimulates melanin synthesis (Kim et al., 2002). Abundant evidence suggests that ERK1/2 is closely linked to the vital activities of melanocytes and plays an important role in the melanogenic pathway in mammals, and that this role is closely linked to *mitf*, a key gene for melanogenesis. Some studies have confirmed that ERK1/2 can directly bind to Ser73, the phosphorylation site of MITF, phosphorylate MITF and thus regulate melanin synthesis (Figure 1) (Wu et al., 2000).

Fish skin colour studies, using the comparative transcriptome approach, in red crucian carp (Zhang et al., 2017), *Oreochromis mossambicus* (Zhu et al., 2016; Wang et al., 2018)and *P. leopardus* (Dai et al., 2015) have identified the MAPK signalling pathway as potentially being involved in the regulation of skin colour in fishes. However, the molecular mechanism through which the MAPK signalling pathway regulates melanin synthesis in fish is still not elucidated. The research team conducted a combined transcriptomic and proteomic analysis of skin tissues from red-skinned and black-skinned *P. leopardus* and found that the differences were reflected in the melanogenesis pathway, which was closely related to the MAPK signalling pathway, and the activation levels of ERK1/2, which differed the most among experimental fish with different skin colours (Wen et al., 2022). Previous pre-experimental results showed that some fish turned black after 24h after RNAi interfered with *erk1/2*, This study will take these data as an entry point to explore the connection between ERK1/2, MITF and melanocyte differentiation and skin colour changes in *P. leopardus* by combining *in vivo* RNAi and *in vitro* Co-IP experiments as well as integrating these results with those of morphological observations, molecular biology, cell culture, *in vivo* injection, and protein interactions in our research. These results will open new perspectives for us to investigate the regulatory mechanism of skin colour change in *P. leopardus* and provide basic information for the in-depth understanding of how skin colour change occurs in coral reef fishes.

2 Materials and methods

2.1 Animals

The *Plectropomus leopardus* used in this experiment were placed in a recirculating aerated bucket of water at 28°C in a

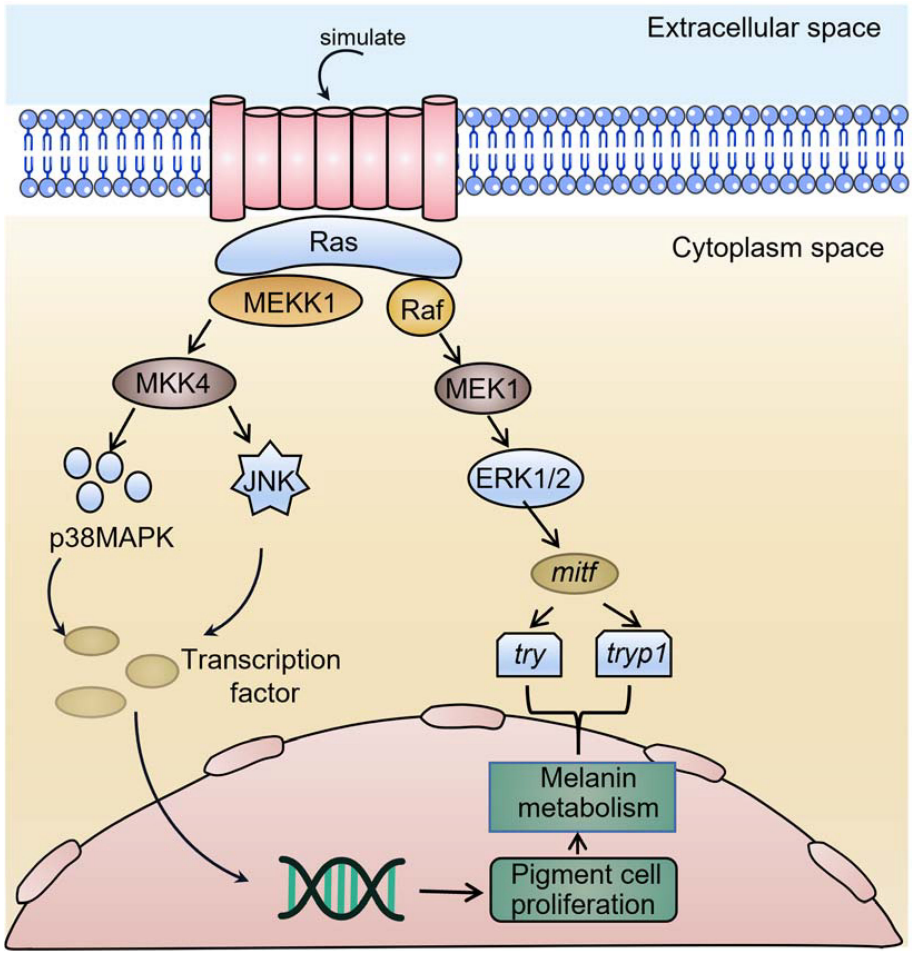

FIGURE 1
A schematic model of *mitf*-mediated regulation of melanogenesis by *erk1/2*.

culture room with a controlled 12:12 h light:dark cycle. A Motic SMZ-168 body vision system was used to differentiate between individuals with different skin colours in the culture population (Wen et al., 2022). We also screened 300 red-coloured and 300 black-coloured individuals, each with a body length of 11 ± 0.5 cm and a body weight of 32 ± 0.5 g, from cultured fish with large variations in skin colour. All the sampling procedures were conducted according the standards and ethical guidelines established by the Animal Ethical Review Committee of Hainan University, Haikou, China.

2.2 Nucleic acid preparation and first-strand cDNA synthesis

The transcriptome data were searched for *erk1/2* and *mitf* candidate sequences (Wen et al., 2022). To clone the intermediate fragments of these two genes, PCR primers for *erk1/2* and *mitf* were designed (Supplementary Table S1), total RNA was extracted from *P. leopardus* skin tissue using TRIzol reagent (Invitrogen, Carlsbad, CA, USA), and genomic DNA was removed using a PrimeScriptTM RT kit (Takara, Japan) with gDNA Eraser. An RNA purification kit (Qiagen, Valencia, CA) was used to purify RNA. RNA was tested for integrity and concentration using agarose gel electrophoresis and a Thermo Scientific NanoDrop instrument (Thermo Scientific, USA), respectively. One microgram of total RNA was reverse transcribed into cDNA using the HiScript III RT SµperMix for qPCR kit (Vazyme, Nanjing, China), and the intermediate fragments of the two genes were amplified by polymerase chain reaction (PCR).

2.3 Rapid amplification of cDNA ends

To obtain the full-length cDNA sequences of *erk1/2* and *mitf*, 3' and 5'-RACE-ready cDNAs were prepared according to the instructions in the SMARTer® RACE 5'/3' Kit (Clontech, USA). cDNA was prepared according to the SMARTer® RACE 5'/3' Kit (Clontech, USA) instructions, and two pairs of RACE primers (Supplementary Table S1) were designed for nested PCR amplification. cDNAs were separated and purified by agarose gel electrophoresis, ligated into vectors, transformed and sequenced. After splicing the sequences, a pair of gene-specific primers (Supplementary Table S1) was designed based on the terminal sequence of the cDNA for full-length cDNA amplification, and

the products were sequenced again to confirm the nucleotide sequence. Finally, the full-length cDNA sequences of *erk1/2* and *mitf* were verified with high-fidelity PrimerSTAR HS DNA polymerase reagent (Takara, Japan).

2.4 Multiple sequence alignment and phylogenetic analysis

We retrieved ERK1/2 and MITF protein sequences of different species from GenBank and phylogenetically compared them with those of *P. leopardus* and aligned them multiple times using ClustalW2. We constructed a bootstrap neighbour-joining (NJ) phylogenetic tree using MEGA 5.0 software and tested branching reliability using bootstrap resampling with 1000 pseudoreplicates.

2.5 RT-qPCR analysis

Total RNA was extracted from skin tissues of red-coloured and black-coloured fish using TRIzol (Invitrogen, 15,596-025) according to the manufacturer's instructions. Reverse transcription PCR was performed using HiScript® III RT SuperMix for qPCR (+gDNA wiper) (Vazyme™, R123-01). RT-qPCR was performed on a Roche LightCycler 384 real-time PCR system (Applied Roche, Basel, Switzerland) using ChamQ SYBR Color qPCR Master Mix (Vazyme Biotech Co., Piscataway, NJ, China) with the following steps: 40 cycles of initial denaturation at 95°C for 30 s, followed by 95°C for 5 s, 55°C for 30 s, 72°C for 30 s, and a 95°C to 65°C cycle. All reactions were performed in triplicate in a final reaction volume of 10 µL. RT-qPCR primers designed with Primer Express® software Primer5.0 are shown in Supplementary Table S2.

2.6 RNA interference

dsRNA for *erk1/2* was synthesized *in vitro* using the TranscriptAid T7 High Yield Transcription Kit (Thermo Scientific, USA) according to the manufacturer's instructions. We prepared templates for *erk1/2* synthesis by amplifying skin tissue in *P. leopardus* cDNA with the design of four pairs of RNAi primers (Supplementary Tables S3, S4). We measured the concentration of dsRNA at 260 nm using a Thermo Scientific NanoDrop, dsRNA purity and integrity were detected by 1% agarose gel electrophoresis and then stored at -80°C for use.

Preliminary experiments showed that the interference effect was greatest with the group D (F2R1) interfering agent, a dose of 5 µg/g of body weight, and the injection site was tail vein injection. By taking samples on days 1, 2, 3, 4, 5, 6, 7, 9, 11, 13, and 15 after injection and then detecting *erk1/2* mRNA expression, it was found that the interference effect was greatest on day 5 after injection. In this study, we randomly divided juvenile experimental fish with an initial body weight of 32 ± 0.5 g into eight groups with eight fish in each group for one, two, three, and four consecutive rounds of RNA interference and injected *erk1/2*-dsRNA into the tail vein at dose of 5 µg/g of body weight. The control group was injected with an equal volume (300 µL) of DEPC H_2O. Twelve tissues were taken (dorsal skin (BSK), abdominal skin (ASK), liver (L), kidney (K), spleen (SP), gill (G), heart (H), intestine (I), eye (E), muscle (M), and brain (BR), and two samples were taken from each group. Microscopic observation of skin tissue was performed before sampling. After sampling, the samples were rapidly frozen in liquid nitrogen and stored at -80°C until use. One sample was used for RT-qPCR analysis of mRNA expression using the primers shown in Supplementary Table S5; the other biological sample was used for the related enzyme activity assay.

2.7 Enzyme activity assay

BSK and ASK skin tissues obtained from fish in the experiment were homogenized with PBS and then centrifuged at 2500 rpm/min for 10 min to obtain the supernatant. A fish tyrosinase (TYR) enzyme immunoassay kit (Abimat PharmaTech Shanghai Co., Ltd., AB-10122A) and a fish melanin (ML) content immunosorbent assay kit (Shanghai Enzymotec Biotech Co., Ltd., ml025778-96T) were used to determine to tyrosinase activity and the concentration of melanin in the samples, respectively. The tyrosinase activity and melanin content of the samples were calculated from the standard curve.

2.8 Microscopic observation of skin

The BSK of the experimented fish was observed microscopically with a Tipscope microscope (Kenwickis (Wuhan) Technology Co., Ltd., China), and five identical positions were selected at the observation interface for melanocyte counting. This observation occurred after anaesthesia with MS222 and before tissue sampling.

2.9 Coimmunoprecipitation

In this study, proteins interacting with ERK1/2 were identified by Co-IP. HEK 293T cells transfected with empty vector were used as the control group, while the ERK1/2 plasmid was transfected into the experimental group. Cells were lysed 24 h after transfection, and Western blotting was performed both before and after Co-IP. The differences in bound proteins in the experimental and control groups were later compared by silver staining. Specific binding was considered to have occurred if a protein-stained band appeared at the same position in the experimental group but not in the control group, while a band at the same position in the treated group and the control group was considered nonspecific binding. The input group was set up for electrophoresis and immunoblotting to determine whether the transfected plasmid was expressed in the cells. FLAG antibody detection before IP (MITF target protein size: 41.5 kD; DIAAN:2064); HIS antibody detection before IP (ERK1/2 target protein size 43.1 kD; CUSABIO: CSB-MA000159); GAPDH antibody detection (GAPDH target protein size 36kD; proteintech:60004-1-Ig).

2.10 Statistical analysis

The *erk1/2* and *mitf* mRNA expression levels were calculated using the comparative CT ($2^{-\Delta\Delta Ct}$) method (Livak and Schmittgen, 2001). All results are expressed as the mean ± standard error of three replicate experiments. The means and standard deviations of three replicate experiments were calculated to confirm homogeneity of variance, and comparisons between means were made using one-way ANOVA. Each data set was analysed using GraphPad Prism 5.0 software (GraphPad software Inc., CA, USA). Multiple comparisons between groups were performed using Tukey B and Duncan's test, with $p < 0.05$ being considered a statistically significant difference. SPSS 17 (Chicago, IL, USA) was used for all statistical analyses.

3 Results

3.1 *erk1/2* and *mitf* cDNA cloning and sequence analysis

The study results showed that the full-length sequence of *P. leopardus erk1/2* was 1449 bp, and the ORF of *erk1/2* was 1176 bp, encoding a protein molecule containing 391 amino acids. The length of the obtained 3' RACE product was 105 bp, containing a typical polyA tail; the length of the obtained 5' RACE product was 168 bp. The intermediate fragment of the *P. leopardus erk1/2* gene, the 3' RACE and the 5' RACE base sequences were spliced together using DNAStar software (Supplementary Figure S1A). The gene sequence was uploaded to NCBI (ID: OM831230). DNAMAN multiple sequence comparison analysis revealed that ERK1/2 is a serine/threonine protein kinase that his highly conserved among various different species, and sequence comparison showed that *P. leopardus* and *Epinephelus lanceoletus* have up to 93.62% similarity (Supplementary Figure S2A).

The full-length sequence of *P. leopardus mitf* was 1802 bp, and the ORF of *mitf* was 1134 bp, encoding a protein molecule containing 377 amino acids. The length of the obtained 3' RACE product was 560 bp, containing a typical polyA tail; the length of the obtained 5' RACE product was 108 bp. The base sequences of the intermediate fragment of the *P. leopardus mitf* gene, the 3' RACE and the 5' RACE base sequences were spliced together using DNAStar software (Supplementary Figure S1B), and the gene sequences were uploaded to NCBI (ID: OM914601). DNAMAN multiple sequence comparison analysis revealed that the MITF proteins of *P. leopardus* and *Epinephelus lanceoletus* had up to 88.89% similarity (Supplementary Figure S2B).

3.2 Phylogenetic analysis of *erk1/2* and *mitf*

Phylogenetic analysis of ERK1/2 from representative fish and mammals yielded an NJ phylogenetic tree indicating that ERK1/2 from *P. leopardus* was highly homologous to that from *Epinephelus coioides* and *Siniperca chuatsi* (Supplementary Figure S3A). Analysis of the ERK1/2 amino acid sequence using the signalP4.1 website revealed no signal peptide and indicated that the ERK1/2 protein may be intracellular. Additional analysis using the Compute pl/Mw website revealed that the isoelectric point of ERK1/2 was pH 6.19, and the predicted molecular weight was 44.304 kDa. The hydrophobicity of the ERK1/2 protein was analysed by using ProtScale online software, and the results showed that ERK1/2 is hydrophilic and is a soluble protein.

The NJ phylogenetic tree showed that the MITF of *P. leopardus* is highly homologous to that of *E. lanceoletus* (Supplementary Figure S3B). Analysis of the MITF amino acid sequence using the signalP4.1 website revealed no signal peptide and indicated that the MITF protein was probably intracellular. Additional analysis using the Compute pl/Mw website showed that the isoelectric point of MITF was pH 5.92, and the predicted molecular was 41.796 kDa. In addition, MITF protein has relatively good hydrophilicity and is considered to be a soluble protein.

3.3 Expression analysis of *erk1/2* and *mitf* in tissues of *P. leopardus* with different skin colours

The expression of *erk1/2* and *mitf* in 10 tissues of *P. leopardus* (skin, liver, spleen, head kidney, intestine, heart, fin, eye, muscle, brain) was examined using RT-qPCR, and the primers are shown in Table S2. Quantitative relative expression was plotted using real-time fluorescence as shown in Figure 2. The results showed that the *erk1/2* and *mitf* genes were constitutively expressed in the skin, liver, spleen, head kidney, intestine, heart, fin, eye, muscle, and brain. The highest level of *erk1/2* expression was observed in the fins of *P. leopardus* and the lowest expression was observed in the heart. *mitf* genes were most highly expressed in the eyes and the lowest expression was observed in the kidney.

3.4 Determination of optimal injection conditions for *P. leopardus*

3.4.1 Determination of optimal primers

Whether the synthesized dsRNA can have a significant interference effect is determined by the quality of the primers. In this study, four pairs of specific primers were designed, and the T7 promoter was added to the primers. All four pairs of primers can synthesize dsRNA *in vitro*. As seen from the experimental results shown in Supplementary Figure S4, 24 hours after the injection of *erk1/2*-dsRNA, the four primer pairs have different degrees of *erk1/2* RNA interference in all tissues of *P. leopardus*. Comparing the differences in *erk1/2* mRNA expression in each tissue after injection, the primer pair in group D *erk1/2*-iF2R1 (743 bp) was selected for subsequent experiments.

3.4.2 Determination of optimal injection site

The injection site directly affects the interference efficiency of *erk1/2*-dsRNA. The sites at which fish underwent *in vivo* injections included the abdominal cavity, dorsal muscle and tail vein. From the experimental results shown in Supplementary Figure S5, it can

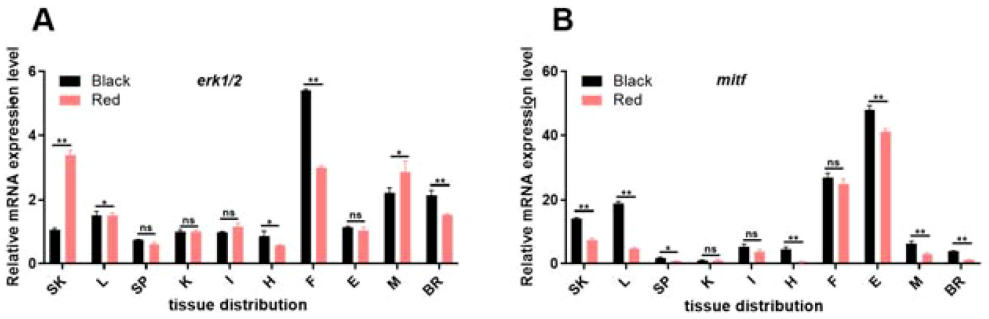

FIGURE 2
Relative expression of *erk1/2* **(A)** and *mitf* **(B)** in tissue species in red-skin and black-skin *P. leopardus*. **, Indicates significant differences in the gene of tissues with red-skin and black-skin individuals. SK, skin; L, liver; SP, spleen; K, kidney; I, intestines; H, heart; F, fin; E, eye; G, gills; M, musle; BR, brain. Different letters indicate significant differences in gene expression between different experimental groups.

be seen that the interference effect of abdominal cavity and dorsal muscle injection fluctuated greatly, while the interference effect was most obvious after tail vein injection, so this site was chosen for the subsequent experiments.

3.4.3 Determination of optimal injection dose

Based on the results of previous studies, five dose groups, 0, 1, 5, 10, and 15 μg/g, were designed. Among them, 0 μg/g was the control group, and animals in this group were injected with an equal volume(300μL) of DEPC water. The results shown in Figure 3 reveal that there was no death of experimental fish 24 h after injection, and analysis of *erk1/2* mRNA expression in each tissue revealed that the 5 μg/g dose group had the greatest RNA interference effect. Therefore, 5 μg/g was chosen as the subsequent interference dose.

3.4.4 Determination of the duration of the interference effect

After *P. leopardus* was injected with *erk1/2*-dsRNA at a dose of 5 μg/g, *erk1/2* mRNA expression decreased in all tissues of the experimental group by varying degrees from days 1 to 15, which indicated that the RNA interference was successful. The results of this experiment are shown in Figure 4. The expression of *erk1/2* mRNA reached its lowest level on day 5 after injection of *erk1/2*-dsRNA. Therefore, in the subsequent long-term interference experiment, the injection was performed every 5 days for a total of 20 days.

3.5 Long-term disturbance of *P. leopardus erk1/2*

3.5.1 Differential expression of related genes after RNAi in *P. leopardus*

The experimental results in Figure 5A show that four consecutive injections of *erk1/2*-dsRNA resulted in changes in *erk1/2* mRNA expression in all *P. leopardus* tissues, with an overall decreasing trend, suggesting successful interference with the expression of *erk1/2* mRNA. In addition, Figure 5B shows that the expression of *mitf* and *kitα* mRNA (Nassar and Tan, 2020) (The mutational landscape of mucosal melanoma), which are related to melanogenesis, was elevated, while the expression of dopachrome tautomerase *(dct)* mRNA was decreased (Zhou et al., 2021) (Epigenetic regulation of melanogenesis).

3.5.2 Differential enzyme activity after RNAi in *P. leopardus*

The tyrosinase (TYR) activity and melanin content of the BSK and ASK of *P. leopardus* were increased after four consecutive injections of *erk1/2*-dsRNA, but the difference was not significant (Supplementary Figure S7). However, elevated TYR activity inclines the organism to the true melanogenesis pathway (Hoekstra et al., 2006; Ito and Wakamatsu, 2003). which is consistent with these findings.

3.5.3 Phenotypic differences in skin tissues after RNAi in *P. leopardus*

The experimental results show that observation of *P. leopardus* 24 h after the injection of *erk1/2*-dsRNA, reveals a significant change in the local skin colour at the injection site (Wen et al., 2022); Phenotypic observation of experimental fish after long-term RNAi revealed that the skin colour of treated fish was darker than control fish (Figure 6A), and the number of melanocytes in the experimental group was significantly higher than that in the control group under the same viewing angle (Figure 6B).

3.6 ERK1/2 and MITF protein interaction analysis

After silver staining the gel scanning map results showed that the target proteins were labelled according to their positional size (Figure 7). Before Co-IP, Figure 7A shows that the FLAG antibody could detect the MITF signal after normal type exposure for 2 min; the His antibody could detect the ERK1/2 target signal after ultrasensitive type exposure for 20 min; and the GADPH antibody could detect the internal reference signal, indicating that the MITF, ERK1/2, and GAPDH proteins can be normally expressed in HEK

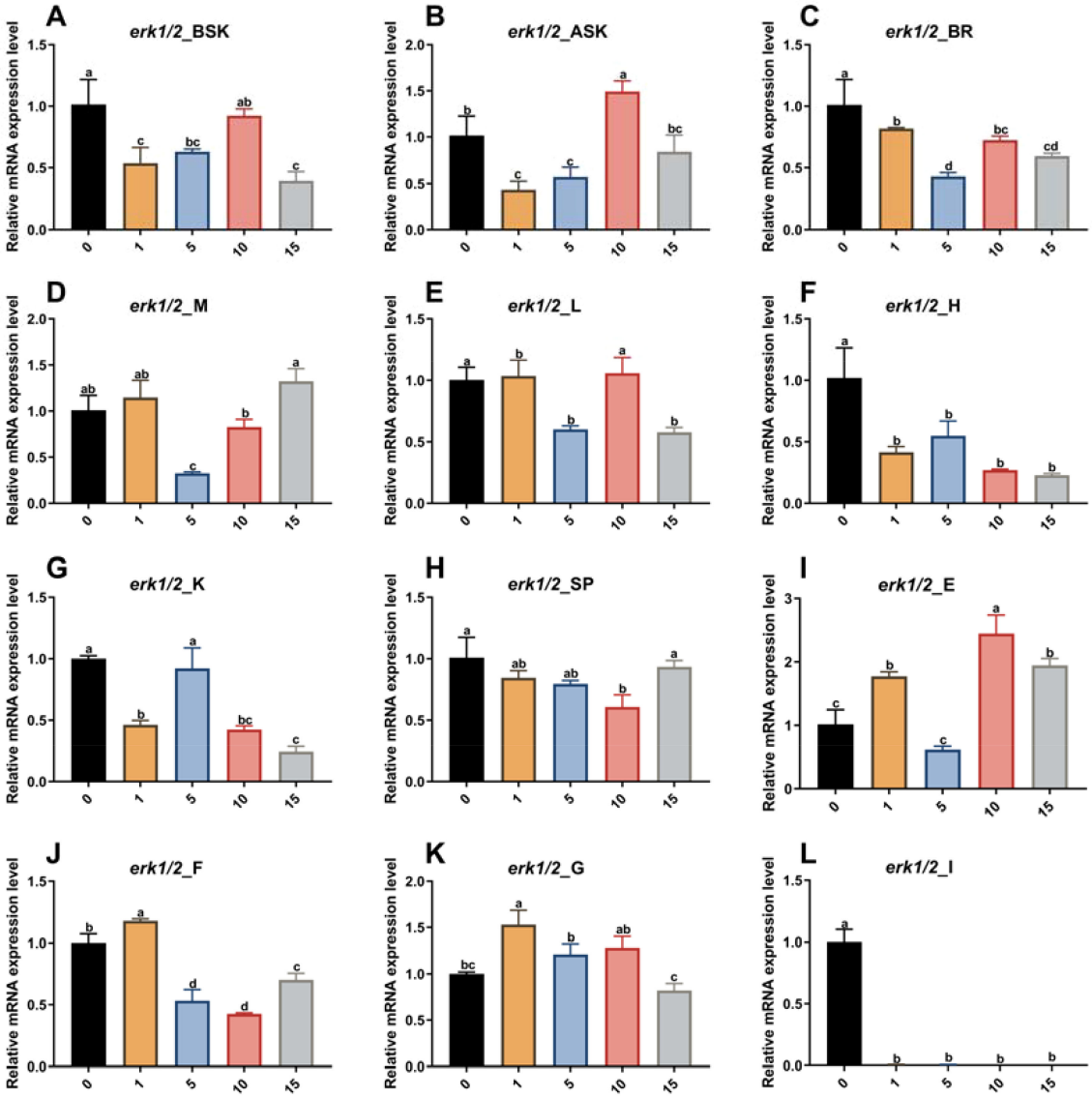

FIGURE 3
Effect of different doses of *erk1/2*-dsRNA injected into the tail vein on the relative expression of the *erk1/2* gene in various *P. leopardus* tissues (n=8). 0, 1, 5, 10 and 15 indicate *erk1/2* injection concentrations of 0 μg/g (DEPC water), 1 μg/g, 5 μg/g, 10 μg/g and 15 μg/g, respectively. BSK, back skin; ASK, abdominal; BR, brain; M, muscle; L, liver; H, heart; K, kidney; SP, spleen; E, eye; F, fin; G, gills I, intestines. Different letters indicate significant differences in gene expression between different experimental groups.

293T cells. After Co-IP, Figure 7B shows that the MITF target signal was detected in the Co-IP group after exposure to FLAG antibody, and the ERK1/2 target signal was detected in the Co-IP group after exposure to HIS antibody for 10 min. The two target proteins were still detectable after Co-IP, which indicates that MITF and ERK1/2 have a mutual binding relationship in *P. leopardus*.

4 Discussion

The relationship between the MAPK signalling pathway and colour has been abundantly studied in mammals and fish, but the mechanism of regulation in fish is not clear. In this study, the full-length *P. leopardus erk1/2* gene sequence was cloned, and the *erk1/2* gene does not exist as an isoform in this species. The complete cDNAs of *erk1* and *erk2* were cloned in the early 1990s (Boulton et al., 1990, 1991). After comparison, it was found that the ERK1 and ERK2 proteins share approximately 83% amino acid homology (Supplementary Figures SI, S2) (Boulton et al., 1990). The phylogenetic tree suggests that in *P. leopardus* ERK1/2 is a MAPK3 (Supplementary Figure S3), which has important implications for our understanding of the ERK pathway. RT-qPCR was used to investigate the differences in the tissue distribution of *P. leopardus erk1/2* in red-skinned and black-skinned fish, and the results showed that *erk1/2* showed a constitutive distribution in all of the examined tissues in all experimental fishes, with higher expression observed in skin, fins, muscle, and brain (Figure 2), and when *erk1/2* expression was

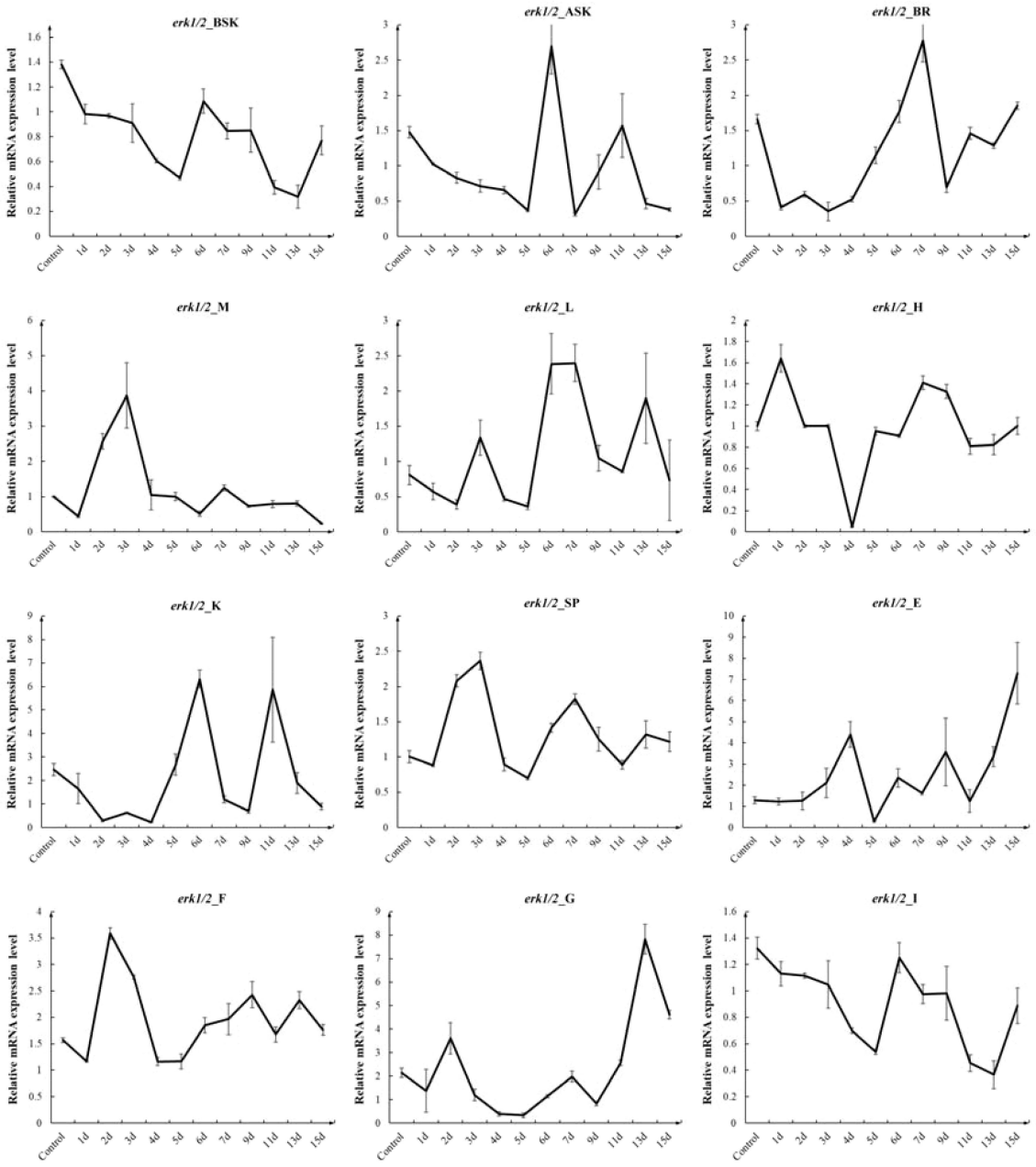

FIGURE 4
Effect of injection of *erk1/2*-dsRNA from the tail vein at 5 μg/g for different times on the relative expression of the *erk1/2* gene in various tissues of *P. leopardus* (n=8). 1d, 2d, 3d, 4d, 5d, 6d, 7d, 9d, 11d, 13d, 15d denote 1, 2, 3, 4, 5, 6, 7, 9, 11, 13, 15 days after injection. BSK, back skin; ASK, abdominal; BR, brain; M, muscle; L, liver; H, heart; K, kidney; SP, spleen; E, eye; F, fin; G, gills I, intestines.

decreased in *P. leopardus*, *mitf* expression increased accordingly. This result is similar to the *erk1/2* expression pattern in other vertebrates, but there is a significant difference in expression in other species, which is similar to the distribution of *erk1/2* in mammals (Boulton et al., 1990), suggesting that *erk1/2* may be widely involved in a variety of essential processes in organisms (Schmitt et al., 2019). ERK1/2 expression in skin tissues was significantly lower in experimental fish with black skin than that in fish with red skin. Related studies in mammals have confirmed that ERK1/2 directly binds to Ser73, the phosphorylation site of MITF, phosphorylates MITF and thus regulates melanin synthesis (Wu et al., 2000). In mammals, the ERK signalling pathway is one of the major regulators of a variety of biological activities, including cell differentiation and proliferation (Yang, 2020). The results of this study suggest that the ERK1/2 protein is a very conserved serine/threonine protein kinase, and the *erk1/2* gene of *P. leopardus* may have a direct or indirect regulatory role in skin colour, which is a critical life process in pigment cells and ultimately exerts a role in the regulation of the number, migration, morphology, and function of pigment cells.

In addition, pigment cells in fish skin tissues develop by differentiation from pigmentoblasts in the neural crest, which are

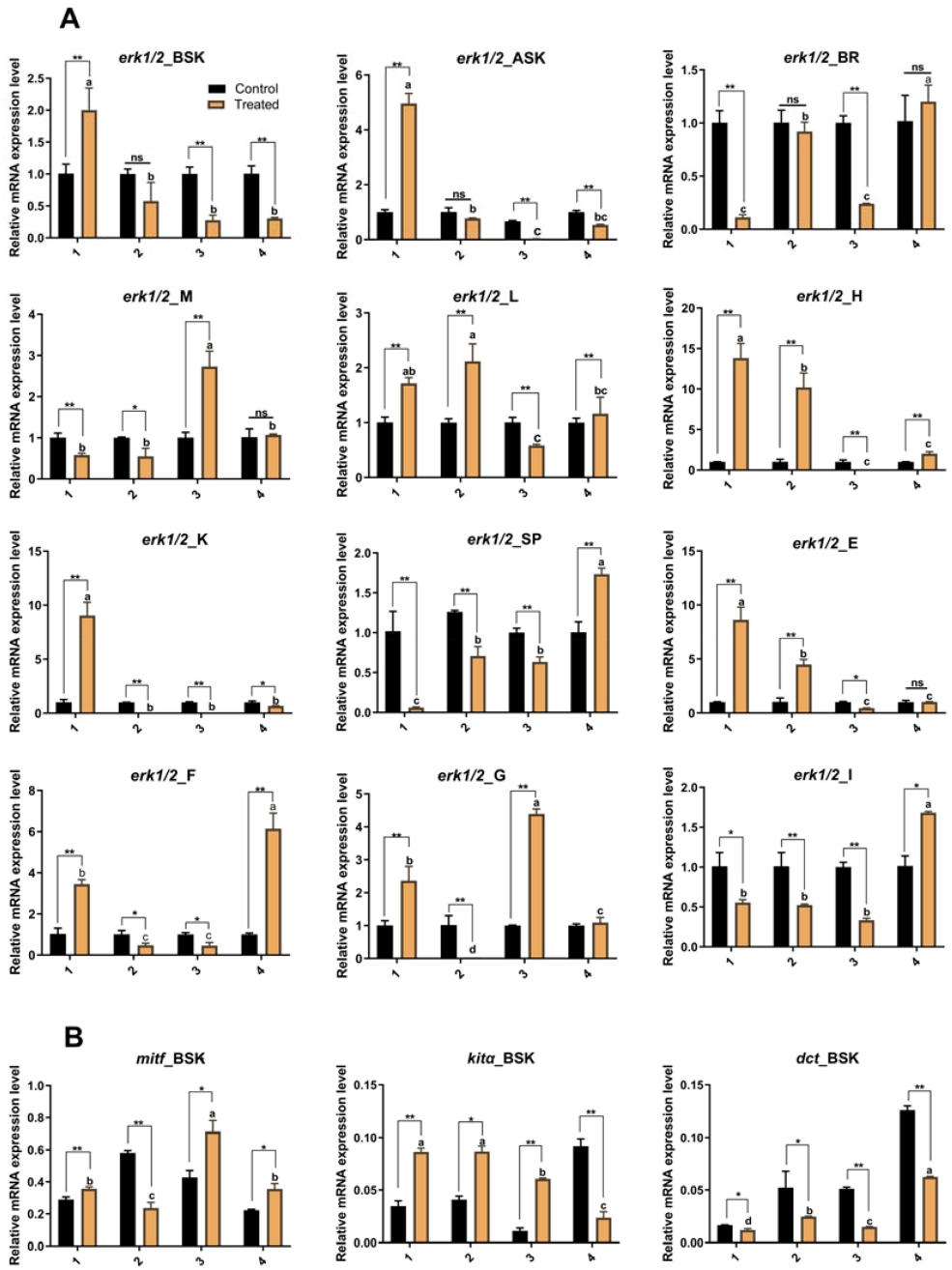

FIGURE 5
Effect of continuous injection of *erk1/2*-dsRNA on gene expression in *P. leopardus*. **(A)** The effect of continuous *erk1/2*-dsRNA injection on the *erk1/2* gene in various tissues of *P. leopardus*; **(B)** The effect of continuous erk1/2-dsRNA injection on the expression of mitf, kitα, and dct genes in the dorsal skin of *P. leopardus*. 1, 2, 3, and 4 indicate the number of injections. BSK, back skin; ASK, abdominal; BR, brain; M, muscle; L, liver; H, heart; K, kidney; SP, spleen; E, eye; F, fin; G, gills I, intestines. **, Indicates significant differences in gene expression between different control and experimental groups. Different letters indicate significant differences in gene expression between different experimental groups.

devoid of pigment precursors, and the role of the *mitf* gene in this process should not be underestimated; *mitf* is not only a prominent marker gene for melanin stem cells and is mainly involved in the regulation of melanocyte differentiation but also plays a role in regulating the differentiation of nonmelanocyte cells (Johnson et al., 2011). The current study shows that the expression of the *mitf* gene is relatively high in tissues with an abundant number of melanocytes. For example, Zhang et al. found that the skin colour of *Carassius auratus* was able to change from grey to red, and *mitf* mRNA expression was reduced accordingly (Zhang et al., 2017). Expression of the *mitf* gene was also significantly higher in skin tissues in black-white *Cyprinus carpio* than in golden, tricolour, and red-white *Cyprinus carpio* (Liu et al., 2015). This phenomenon is not unique to fish, and similar results have been observed in terrestrial vertebrates (Xin et al., 2018; Zhang et al., 2016). In the present study, the expression of the *mitf* gene in various tissues of *P.*

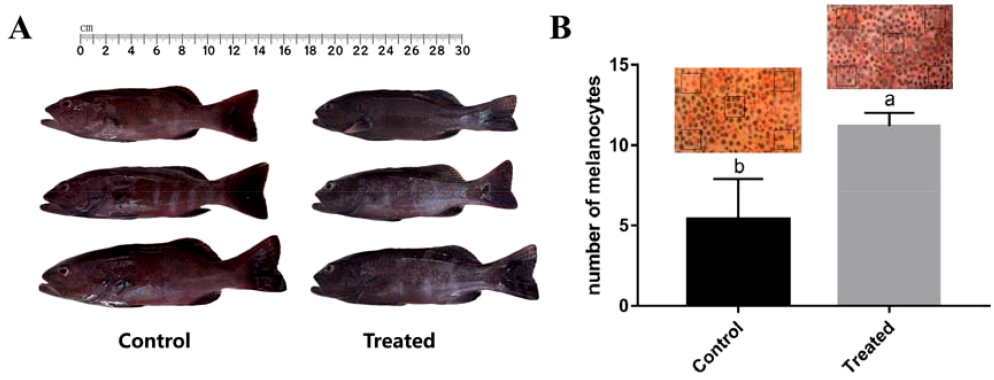

FIGURE 6
Effects of continuous *erk1/2*-dsRNA injection on phenotypes in *P. leopardus* (n=8). **(A)** Observation of variation in skin-colour after long-term RNAi; **(B)** Microscopic observation and statistics of variation in body-colour at the same viewing angle. The statistical area is the boxed portion of the figure, with 5 tails for each of the experimental and control groups counted separately. Different letters indicate significant differences in number of melanocytes between different experimental groups.

leopardus was similar to the above findings. The *mitf* gene was highly expressed in the dorsal skin, eye and fin tissues of *P. leopardus* (Figure 2), and this result verifies that the *mitf* gene regulates melanin synthesis in the organism. When the *mitf* gene is expressed at high levels in an organism, it will favour melanin production in that individual (Steunou et al., 2013); if the gene is expressed at a low levels, it will inhibit or reduce melanin production in the organism (Wu et al., 2021). Combining the *erk1/2* results from this study and those from related studies in mammals, we hypothesize that in *P. leopardus, erk1/2* may be involved in the regulation of melanogenesis through the regulation of *mitf*.

The *erk1/2* gene plays an important role in the formation of skin colour in mammals and fish (Luo et al., 2013), but there are still few studies on *erk1/2* loss-of-function in fish. In RNAi experiments, the dsRNAs synthesized with different primer sequences had different in effects. In this study, group D (*erk1/2*iF2R1, 743 bp) had the best RNA interference effect (Supplementary Figure S4), indicating that the nucleic acid sequence of *erk1/2*-dsRNA (group D) was an efficient RNAi target, which was consistent with the findings of the researchers (Wang et al., 2013). Then, equal doses of *erk1/2*-dsRNA were injected into three different sites, namely, the abdominal cavity, the back muscle, and the tail vein, and analysis of *erk1/2* mRNA expression in each tissue of the experimental fish showed that tail vein

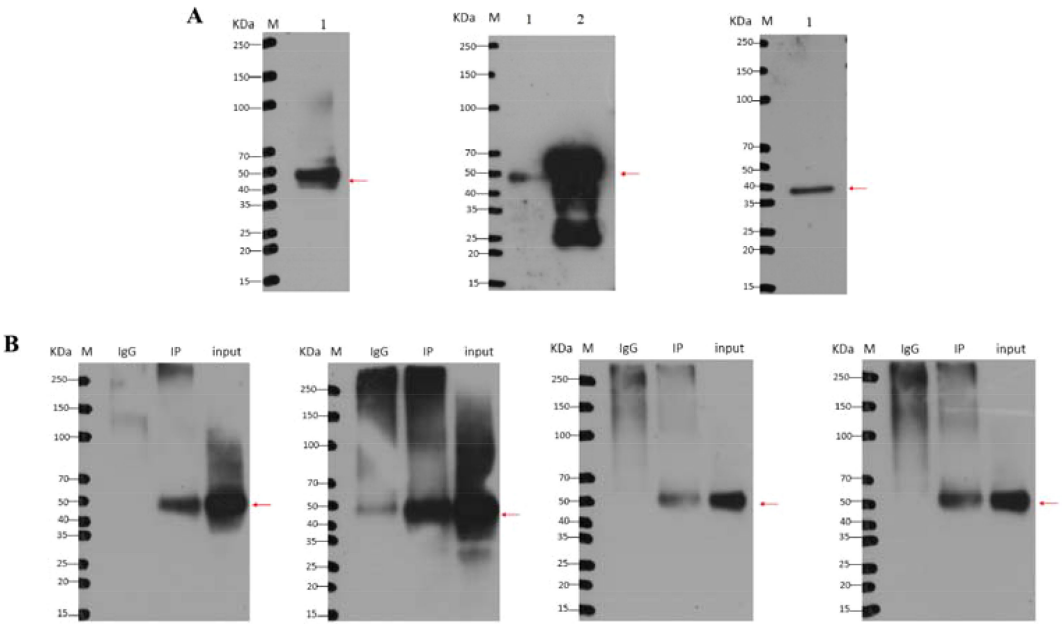

FIGURE 7
Western blot detection before and after Co-IP. **(A)** Western blot detection before Co-IP; **(B)** Western blot detection after Co-IP. M, marker; 1, 293T cotransfected cells; 2, positive control. The target proteins are labelled according to their position and size in the figure.

injection had the best interference effect (Supplementary Figure S5). This is likely because it is possible to transport the injected interference sequence throughout the body through the fish blood circulation system allowing the sequence to produce its full RNA interfering effect (Bu, 2019). Therefore, based on the results of this experiment and the specifications of the experimented fish, tail vein injection is proposed for subsequent experiments. In addition to the specific dsRNA sequence used, and the injection site both directly affecting the efficacy of RNAi, the dsRNA injection dose also has an effect (Ge et al., 2020; Tan et al., 2020). The results of this study showed that the experimental fish injected with 5 μg/g dsRNA had the best interference effect (Figure 3), and the *erk1/2* RNA interference effect was not completely positively correlated with the dsRNA injection dose. In recent years, an interference dose of 4-5 μg/g has mostly been used for RNAi in crustaceans, and the interference effect is obvious at this dose. After one injection of *erk1/2*-dsRNA (5 μg/g), the expression of e*rk1/2* mRNA decreased and reached the lowest level 5 days post-injection in most tissues, and the interference effect was most stable at this time point (Figure 4). In addition, fish skin colour is coregulated by many genes, and some researchers found that the mRNA expression of the *slc7a11* gene was decreased after siRNA treatment, resulting in a significant downregulation of the expression of genes related to melanin formation, such as *mitf* in rabbit skin fibroblasts (Yang et al., 2018). In this study, we found that the expression level of *erk1/2* mRNA in experimental fish could be significantly reduced by injecting *erk1/2*-dsRNA after long-term interference was completed, and the expression levels of *mitf* and *kitα* mRNA in dorsal skin tissues were significantly increased following *erk1/2* interference (Figure 6), suggesting that *erk1/2* has a negative regulatory effect on *mitf* and other genes related to skin colour formation in fish. Previous findings suggest that *erk1/2* has a regulatory role in fish melanogenesis, which is possibly related to the synthesis of tyrosine proteases. In melanosomes, tyrosinase acts as a catalyst in the first two stages of the melanogenesis mechanism, and overexpression of tyrosinase leads to overproduction of melanin and pathological disorders such as hyperpigmentation (Hearing and Jiménez, 1987). Measurements of tyrosinase activity and melanin content in the DSK and ASK of *P. leopardus* in this study showed that *erk1/2* expression was suppressed, and melanin content increased along with the TYR activity involved in melanin synthesis (Supplementary Figure S6), which promoted melanogenesis (Chung et al., 2019). It has also been shown that long-term RNA interference can lead to significant phenotypic changes in tissues or organs (Tan et al., 2020; Ventura et al., 2009), and it is clear that fewer injections can reduce the damage caused to experimental fish. In the present study, the number of melanocytes in the skin of *P. leopardus* increased significantly after several consecutive injections, and the fish skin darkened significantly (Figure 7). In conclusion, the results of gene expression, enzyme activity and phenotypic observation suggest that ERK1/2 may be involved in melanogenesis in *P. leopardus* through the regulation of MITF, but the specific mechanism through which these proteins interact still needs further study.

Studies in vertebrates suggest that ERK1/2 may interact with MITF, and activation of MITF promotes melanogenesis by increasing the expression of melanin-related enzymes (Jimenez-Cervantes et al., 1994; Tsukamoto et al., 1992). Studies have shown that MAPK family proteins, including p38MAPK, ERK1/2, and JNK1, are activated by numerous extracellular stimuli and play key roles in melanin synthesis (Peng et al., 2014). For example, phosphorylated ERK inhibits MITF expression and thus reduces melanin synthesis, while phosphorylation of p38MAPK and JNK1 can increase melanin synthesis by activating MITF (Kang et al., 2015). Kim et al. found that UV-B induced apoptosis in human melanocytes, which correspondingly increased the phosphorylation levels of JNK1 and p38MAPK but transiently inactivated ERK1/2 kinases (Kim et al., 2007). These studies suggest that the three members of the MAPK pathway, JNK1, p38MAPK, and ERK1/2, are mediated through the regulation of key genes for melanin synthesis, which in turn participate in the life process of melanocytes, ultimately exerting regulatory effects on melanocyte number, migration, morphology, and function. The results of the preliminary study showed that e*rk1/2* was significantly expressed in the brains of *P. leopardus* with different skin colours, suggesting that *erk1/2* may have a direct or indirect regulatory role in skin colour, participate in the life process of pigment cells, and ultimately play a role in the regulation of the number, migration, morphology, and function of pigment cells. Currently, the mechanism of interaction between the different proteins in the process of pigment cell formation is poorly understood and needs to be investigated more fully. In this study, the results of immunoprecipitation indicate that *P. leopardus* ERK1/2 and MITF proteins are normally expressed in HEK 293T cells (Figure 7A). Moreover, MITF and ERK1/2 target proteins could still be detected after Co-IP (Figure 7B), indicating that the two proteins can bind to each other in *P. leopardus*. Wu et al. found that ERK1/2 can bind to Ser73, the phosphorylation site of MITF, which phosphorylates MITF and then regulates melanin synthesis (Wu et al., 2000), which is consistent with the results of this study, suggesting that MITF and ERK1/2 bind to each other and are involved in the regulation of melanogenesis in *P. leopardus* (Figure 1). In addition, the reciprocal relationship between ERK1/2 and MITF was confirmed for the first time in coral reef fishes, which provides technical and theoretical support for more in-depth investigation of the mechanism of skin colour formation in fishes, but further studies are still needed to reveal the reasons for the variation in skin colour in fishes.

5 Conclusion

In summary, the full-length *erk1/2* and *mitf* genes were cloned and it was found that these genes were differentially expressed in with red-skinned and black-skinned *P. leopardus* fish, suggesting that *erk1/2* and *mitf* may be involved in melanogenesis. Injection *in vivo* experiments revealed that ERK1/2 can be involved in regulating melanogenesis in *P. leopardus*. Co-IP *in vitro* shows that there was a direct or indirect interaction between MITF and ERK1/2 proteins. Therefore, this study the study demonstrates that ERK1/2 regulates melanogenesis through the mediation of MITF in *P. leopardus*. Which is the first study showing that ERK1/2 interacts with MITF to regulate melanin synthesis in coral reef fishes. The results of this study further enrich our understanding of the changing pattern of

skin colour in *P. leopardus* and provide a new perspective for exploring the variable skin colour of coral reef fishes.

Data availability statement

The datasets presented in this study can be found in online repositories. The names of the repository/repositories and accession number(s) can be found in the article/Supplementary Material.

Ethics statement

The animal studies were approved by a Sanya Nanfan Research Institute of Hainan University, Hainan Aquaculture Breeding Engineering Research Center, Hainan Academician Team Innovation Center, Hainan University, Haikou 570228, China. The studies were conducted in accordance with the local legislation and institutional requirements. Written informed consent was obtained from the owners for the participation of their animals in this study.

Author contributions

MY: Conceptualization, Writing – original draft. JH: Investigation, Writing – review & editing. DZ: Software, Writing – review & editing. HT: Methodology, Software, Writing – review & editing. JCL: Methodology, Writing – review & editing. JL: Supervision, Writing – review & editing. XW: Supervision, Writing – original draft, Writing – review & editing.

Funding

The author(s) declare financial support was received for the research, authorship, and/or publication of this article. This work was supported by the National Natural Science Foundation of China (32202901); Key R&D Project in Hainan (ZDYF2023XDNY046); The Innovation Center of Hainan University (XTCX2022NYC16).

Conflict of interest

The authors declare that the research was conducted in the absence of any commercial or financial relationships that could be construed as a potential conflict of interest.

Publisher's note

All claims expressed in this article are solely those of the authors and do not necessarily represent those of their affiliated organizations, or those of the publisher, the editors and the reviewers. Any product that may be evaluated in this article, or claim that may be made by its manufacturer, is not guaranteed or endorsed by the publisher.

Supplementary material

The Supplementary Material for this article can be found online at: https://www.frontiersin.org/articles/10.3389/fmars.2024.1441589/full#supplementary-material

References

Ahn, J. H., Jin, S. H., and Kang, H. Y. (2008). LPS induces melanogenesis through p38 MAPK activation in human melanocytes. *Arch. Dermatol. Res.* 300, 325–329. doi: 10.1007/s00403-008-0863-0

Boulton, T. G., Nye, S. H., Robbins, D. J., Ip, N. Y., Radzlejewska, E., Morgenbesser, S. D., et al. (1991). ERKs: a family of protein-serine/threonine kinases that are activated and tyrosine phosphorylated in response to insulin and NGF. *Cell* 65, 663–675. doi: 10.1016/0092-8674(91)90098-J

Boulton, T. G., Yancopoulos, G. D., Gregory, J. S., Slaughter, C., Moomaw, C., Hsu, J., et al. (1990). An insulin-stimulated protein kinase similar to yeast kinases involved in cell cycle control. *Science* 249, 64–67. doi: 10.1126/science.2164259

Bu, H. (2019). *Study on the RNA innterference of* slc7a11 *Gene in Red Tilapia* (Nanjing: Nanjing Agricultural University).

Chung, Y. C., Kim, M.-J., Kang, E. Y., Kim, Y. B., Kim, B. S., Park, S.-M., et al. (2019). Anti-melanogenic effects of hydroxyectoine via mitf inhibition by jnk, p38, and akt pathways in b16f10 melanoma cells. *Natural Product. Commun.* 14, 1934578X19858523. doi: 10.1177/1934578X19858523

Dai, P., Huan, P., Wang, H., Lu, X., and Liu, B. (2015). Characterization of a long-chain fatty acid-CoA ligase 1 gene and association between its SNPs and growth traits in the clam Meretrix meretrix. *Gene* 566, 194–200. doi: 10.1016/j.gene.2015.04.047

Ge, H.-L., Tan, K., Shi, L.-L., Sun, R., Wang, W.-M., and Li, Y.-H. (2020). Comparison of effects of dsRNA and siRNA RNA interference on insulin-like androgenic gland gene (IAG) in red swamp crayfish Procambarus clarkii. *Gene* 752, 144783. doi: 10.1016/j.gene.2020.144783

Hearing, V. J., and Jiménez, M. (1987). Mammalian tyrosinase-the critical regulatory control point in melanocyte pigmentation. *Int. J. Biochem.* 19, 1141–1147. doi: 10.1016/0020-711X(87)90095-4

Hoekstra, R., Fekkes, D., Pepplinkhuizen, L., Loonen, A. J. M., Tuinier, S., and Verhoeven, W. M. A. (2006). Nitric oxide and neopterin in bipolar affective disorder. *Neuropsychobiology* 54, 75–81. doi: 10.1159/000096042

Ito, S., and Wakamatsu, K. (2003). Quantitative analysis of eumelanin and pheomelanin in humans, mice, and other animals: a comparative review. *Pigment. Cell Res.* 16, 523–531. doi: 10.1034/j.1600-0749.2003.00072.x

Jalmi, S. K., and Sinha, A. K. (2015). ROS mediated MAPK signaling in abiotic and biotic stress-striking similarities and differences. *Front. Plant Sci.* 6. doi: 10.3389/fpls.2015.00769

Jimenez-Cervantes, C., Solano, F., Kobayashi, T., Urabe, K., Hearing, V. J., Lozano, J. A., et al. (1994). A new enzymatic function in the melanogenic pathway. The 5, 6-dihydroxyindole-2-carboxylic acid oxidase activity of tyrosinase-related protein-1 (*TRP1*). *J. Biol. Chem.* 269, 17993–18000. doi: 10.1007/BF00006249

Johnson, S. L., Nguyen, A. N., and Lister, J. A. (2011). Mitfa is required at multiple stages of melanocyte differentiation but not to establish the melanocyte stem cell. *Dev. Biol.* 350, 405–413. doi: 10.1016/j.ydbio.2010.12.004

Kang, S. J., Choi, B. R., Lee, E. K., Kim, S. H., Yi, H. Y., Park, H. R., et al. (2015). Inhibitory effect of dried pomegranate concentration powder on melanogenesis in B16F10 melanoma cells; involvement of p38 and PKA signaling pathways. *Int. J. Mol. Sci.* 16, 24219–24242. doi: 10.3390/ijms161024219

Kim, D. S., Kim, S. Y., Chung, J. H., Kim, K. H., Eun, H. C., and Park, K. C. (2002). Delayed ERK activation by ceramide reduces melanin synthesis in human melanocytes. *Cell. Signalling.* 14, 779–785. doi: 10.1016/S0898-6568(02)00024-4

Kim, D.-S., Park, S.-H., Kwon, S.-B., Na, J.-I., Huh, C.-H., and Park, K.-C. (2007). Additive effects of heat and p38 mapk inhibitor treatment on melanin synthesis. *Arch. Pharmacal. Res.* 30, 581–586. doi: 10.1007/BF02977652

Lerebours, A., Chapman, E. C., Sweet, M. J., Heupel, M. R., and Rotchell, J. M. (2016). Molecular changes in skin pigmented lesions of the coral trout *Plectropomus leopardus*. *Mar. Environ. Res.* 120, 130–135. doi: 10.1016/j.marenvres.2016.07.009

Liu, J. H., Wen, S., Luo, C., Zhang, Y. Q., Tao, M., Wang, D. W., et al. (2015). Involvement of the mitfa gene in the development of pigment cell in Japanese ornamental (Koi) carp (*Cyprinus carpio L.*). *Genet. Mol. Res.* 14, 2775–2784. doi: 10.4238/2015.March.31.7

Livak, K. J., and Schmittgen, T. D. (2001). Analysis of relative gene expression data using real-time quantitative PCR and the 2– ΔΔCT method. *methods* 25, 402–408. doi: 10.1006/meth.2001.1262

Luo, z., Jiang, m., Zhou, y., Wen, s., Wang, m., Liu, s., et al. (2013). The expression of erk1/2 in tissues and embryos of the Triploid fish. *Life Sci. Res.* 17, 11–13 + 42. doi: 10.16605/j.cnki.1007-7847.2013.01.002

Molina, D. M., Grewal, S., and Bardwell, L. (2005). Characterization of an ERK-binding domain in microphthalmia-associated transcription factor and differential inhibition of ERK2-mediated substrate phosphorylation. *J. Biol. Chem.* 280, 42051–42060. doi: 10.1074/jbc.M510590200

Nassar, K. W., and Tan, A. C. (2020). The mutational landscape of mucosal melanoma. *Semin. Cancer Biol.* 61, 139–148. doi: 10.1016/j.semcancer.2019.09.013

Peng, H.-Y., Lin, C.-C., Wang, H.-Y., Shih, Y., and Chou, S.-T. (2014). The melanogenesis alteration effects of *Achillea millefolium L.* essential oil and linalyl acetate: involvement of oxidative stress and the JNK and ERK signaling pathways in melanoma cells. *PloS One* 9, e95186. doi: 10.1371/journal.pone.0095186

Schmitt, M., Sinnberg, T., Nalpas, N. C., Maass, A., Schittek, B., and Macek, B. (2019). Quantitative proteomics links the intermediate filament nestin to resistance to targeted BRAF inhibition in melanoma cells. *Mol. Cell. Proteomics* 18, 1096–1109. doi: 10.1074/mcp.RA119.001302

Song, X., Xu, A., Pan, W., Wallin, B., Kivlin, R., Lu, S., et al. (2008). Minocycline protects melanocytes against H_2O_2-inducedcell death via JNK and p38 MAPK pathways. *Int. J. Mol. Med.* 22, 9–16. doi: 10.3892/ijmm.22.1.9

Steunou, A.-L., Ducoux-Petit, M., Lazar, I., Monsarrat, B., Erard, M., Muller, C., et al. (2013). Identification of the hypoxia-inducible factor 2α Nuclear interactome in melanoma cells reveals master proteins involved in melanoma development. *Mol. Cell. Proteomics* 12, 736–748. doi: 10.1074/mcp.M112.020727

Sugianti, Y., and Mujiyanto, M. (2016). Biodiversitas hayati ikan karang di perairan Taman Nasional Karimunjawa Jepara. *BAWAL. Widya. Riset. Perikanan. Tangkap.* 5, 23–31. doi: 10.15578/bawal.5.1.2013.23-31

Sun, Z., Xia, S., Feng, S., Zhang, Z., Rahman, M. M., Rajkumar, M., et al. (2015). Effects of water temperature on survival, growth, digestive enzyme activities, and body composition of the leopard coral grouper Plectropomus leopardus. *Fisheries. ence.* 1, 107–112. doi: 10.1007/s12562-014-0832-9

Sweet, M., Kirkham, N., Bendall, M., Currey, L., Bythell, J., and Heupel, M. (2012). Evidence of melanoma in wild marine fish populations. 7(8):e41989. doi: 10.1371/journal.pone.0041989

Tan, K., Li, Y., Zhou, M., and Wang, W. (2020). siRNA knockdown of MrIR induces sex reversal in *Macrobrachium rosenbergii*. *Aquaculture* 523, 735172. doi: 10.1016/j.aquaculture.2020.735172

Tsukamoto, K., Jackson, I. J., Urabe, K., Montague, P. M., and Hearing, V. J. (1992). A second tyrosinase-related protein, TRP-2, is a melanogenic enzyme termed DOPAchrome tautomerase. *EMBO J.* 11, 519–526. doi: 10.1002/j.1460-2075.1992.tb05082.x

Ventura, T., Manor, R., Aflalo, E. D., Weil, S., Raviv, S., Glazer, L., et al. (2009). Temporal silencing of an androgenic gland-specific insulin-like gene affecting phenotypical gender differences and spermatogenesis. *Endocrinology* 150, 1278–1286. Available at: https://doi.org/2020071612270331300.

von Koschembahr, A. M., Swope, V. B., Starner, R. J., and Abdel-Malek, Z. A. (2015). Endothelin-1 protects human melanocytes from UV-induced DNA damage by activating JNK and p38 signalling pathways. *Exp. Dermatol.* 24, 269–274. doi: 10.1111/exd.12638

Wang, R., Qi, Z., Zhang, X., Wang, F., Wang, Y., Fu, S., et al. (2011). Biological characteristics and Artificial Cultivation Techniques of Plectropomus leopardus. *China Fisheries.* 2011(4), 33–34. CNKI: SUN : SICA.0.2011-04-020.. doi: 10.3969/j.issn.1002-6681.2011.04.017

Wang, T., Wen, H., Yang, J., Yin, H., Liao, J., He, Y., et al. (2017). Research progress on the relationship between osteoarthritis and MAPK signaling pathway. *Chin. J. Ethnomed. Ethnopharmacy.* 26, 27–29 + 33. CNKI: SUN : MZMJ.0.2017-19-010. doi: CNKI:SUN:MZMJ.0.2017-19-010

Wang, J., Wu, M., Wang, B., and Han, Z. (2013). Comparison of the RNA interference effects triggered by dsRNA and siRNA in Tribolium castaneum. *Pest Manage. Sci.* 69, 781–786. doi: 10.1002/ps.3432

Wang, L., Zhu, W., Dong, Z., Song, F., Dong, J., and Fu, J. (2018). Comparative microRNA-seq analysis depicts candidate miRNAs involved in skin color differentiation in red tilapia. *Int. J. Mol. Sci.* 19, 1209. doi: 10.3390/ijms19041209

Wellbrock, C., and Arozarena, I. (2015). Microphthalmia-associated transcription factor in melanoma development and MAP-kinase pathway targeted therapy. *Pigment. Cell Melanoma. Res.* 28, 390–406. doi: 10.1111/pcmr.12370

Wen, X., Yang, M., Zhou, K., Huang, J., Fan, X., Zhang, W., et al. (2022). Transcriptomic and proteomic analyses reveal the common and unique pathway (s) underlying different skin colors of leopard coral grouper (*Plectropomus leopardus*). *J. Proteomics* 266, 104671. doi: 10.1016/J.JPROT.2022.104671

Wu, M., Hemesath, T. J., Takemoto, C. M., Horstmann, M. A., Wells, A. G., Price, E. R., et al. (2000). c-Kit triggers dual phosphorylations, which couple activation and degradation of the essential melanocyte factor Mi. *Genes Dev.* 14, 301–312. doi: 10.1101/gad.14.3.301

Wu, S., Huang, J., Li, Y., Zhang, Q., Pan, Y., and Wang, X. (2021). Cloning and expression analysis of body colour-related gene mitfa in Rainbow Trout (Oncorhynchus mykiss). *J. Agric. Biotechnol.* 29, 753–763. doi: 10.3969/j.issn.1674-7968.2021.04.013

Xin, Q., Li, L., Miao, Z., Zhang, L., Liu, Y., Zhu, Z., et al. (2018). Expression of MITF gene in Putian Black Duck (Anas anas domesticus) and its association with melanin deposition. *J. Agric. Biotechnol.* 26, 1928–1937. doi: 10.3969/j.issn.1674-7968.2018.11.012

Yang, M. (2020). *Molecular cloning and characterization of a cDNA encoding extracellular signal-regulated kinase (ERK) from blood clam Tegillarca granosa* (Xiamen: Third Institute Of Oceanography,Ministry of Natural Resources).

Yang, N., Mu, L. I. N., Zhao, B., Wang, M., Hu, S., Zhao, B. I. N., et al. (2018). RNAi-mediated *SLC7A11* knockdown inhibits melanogenesis-related genes expression in rabbit skin fibroblasts. *J. Genet.* 97, 463–468. doi: 10.1007/s12041-018-0945-5

Yoseda, K., Yamamoto, K., Asami, K., Chimura, M., Hashimoto, K., and Kosaka, S. (2008). Influence of light intensity on feeding, growth, and early survival of leopard coral grouper (*Plectropomus leopardus*) larvae under mass-scale rearing conditions. *Aquaculture* 279, 55–62. doi: 10.1016/j.aquaculture.2008.04.002

Zhang, Y., Liu, J., Fu, W., Xu, W., Zhang, H., Chen, S., et al. (2017). Comparative Transcriptome and DNA methylation analyses of the molecular mechanisms underlying skin color variations in Crucian carp (*Carassius carassius L.*). *BMC Genet.* 18, 1–12. doi: 10.1186/s12863-017-0564-9

Zhang, H., Xu, C., Song, X., Zhou, N., Zhang, L., Xing, X., et al. (2016). Progress in melanocyte regulation of microphthalmia-associated transcription factors. *Anim. Husbandry. Vet. Med.* 48, 113–117. CNKI: SUN : XMYS.0.2016-08-030. doi: CNKI:SUN:XMYS.0.2016-08-030

Zhao, N., Zhou, B., Li, Y., Zhang, J., Ma, J., and Yu, X. (2016). Effects of light color on growth, skin color, and physiological indices of juvenile Plectropomus leopardus in a recirculating aquaculture system. *J. Fishery. Sci. China* 23, 976–984. doi: 10.3724/SP.J.1118.2016.15438

Zheng, S., Zheping, H., Zhang, D. D., and Edward, M. R. (2009). Phosphorylation of nrf2 at multiple sites by MAP kinases has a limited contribution in modulating the nrf2-dependent antioxidant response. *PloS One* 4, e6588–. doi: 10.1371/journal.pone.0006588

Zhou, S., Zeng, H., Huang, J., Lei, L., Tong, X., Li, S., et al. (2021). Epigenetic regulation of melanogenesis. *Ageing Res. Rev.* 69, 101349. doi: 10.1016/j.arr.2021.101349

Zhu, W., Wang, L., Dong, Z., Chen, X., Song, F., Liu, N., et al. (2016). Comparative transcriptome analysis identifies candidate genes related to skin color differentiation in red tilapia. *Sci. Rep.* 6, 31347. doi: 10.1038/srep31347

frontiers | Frontiers in Marine Science

TYPE Original Research
PUBLISHED 30 October 2024
DOI 10.3389/fmars.2024.1483796

OPEN ACCESS

EDITED BY
Yngvar Olsen,
NTNU, Norway

REVIEWED BY
Ioannis A. Giantsis,
Aristotle University of Thessaloniki, Greece
Shengjie Ren,
Queensland University of Technology, Australia

*CORRESPONDENCE
Carolina Merca
cmgm@sund.ku.dk

RECEIVED 20 August 2024
ACCEPTED 27 September 2024
PUBLISHED 30 October 2024

CITATION
Merca C, Boerlage AS, Kristensen AR and Jensen DB (2024) Monitoring monthly mortality of maricultured Atlantic salmon (*Salmo salar* L.) in Scotland II. A hierarchical dynamic linear model.
Front. Mar. Sci. 11:1483796.
doi: 10.3389/fmars.2024.1483796

Monitoring monthly mortality of maricultured Atlantic salmon (*Salmo salar* L.) in Scotland II. A hierarchical dynamic linear model

Carolina Merca[1]*, Annette Simone Boerlage[2], Anders Ringgaard Kristensen[1] and Dan Børge Jensen[1]

[1]Department of Veterinary and Animal Sciences, Faculty of Health and Medical Sciences, University of Copenhagen, Frederiksberg, Denmark, [2]Centre for Epidemiology and Planetary Health (CEPH), SRUC School of Veterinary Medicine, Inverness, United Kingdom

The sustainability of the salmon farming industry is being challenged by increased mortality rates. Scotland's open-source salmon production data provides the possibility of developing an industry-wide mortality monitoring model, valuable for identifying and addressing unexpected increases in mortality without needing data sharing agreements across different companies. This study aimed to utilize these data to develop a hierarchical dynamic linear model (DLM) for monitoring monthly mortality of maricultured Atlantic salmon in Scotland. We evaluated whether considering the hierarchical structure present in the data (country, region, and site) would improve mortality predictions when compared to the production cycle level DLMs developed in a previous study. Our findings demonstrated that the hierarchical DLM outperformed the production cycle level DLMs, confirming the value of this more complex modelling approach. Nevertheless, the hierarchical model, like the production cycle level DLMs, exhibited some uncertainty in the mortality predictions. When mortality is higher than expected, site level warnings are generated, which can encourage producers and inspectors to further investigate the cause. Between 2015 and 2020, approximately 25% of the production cycles and 50% of the sites encountered at least one warning, with most warnings happening in the summer and autumn months. Additionally, the hierarchical model enabled monitoring mortality at multiple levels. This information is useful for various stakeholders as part of a monitoring system, offering insights into mortality trends at national, regional, and sites levels that may benefit from strategic resource management. Recommendations for model improvements include utilizing shorter data aggregation periods, such as weekly, which are not currently available as open-source data.

KEYWORDS

salmon, mortality, multi-level model, hierarchical model, dynamic linear models, aquaculture, open-source data, warnings

1 Introduction

Farmed salmon are a significant contributor to the aquaculture trade, playing an increasingly important role in providing food and nourishment worldwide (FAO, 2022). Scotland stands as the third-largest producer of farmed salmon globally (Iversen et al., 2020). Within the UK, farmed salmon is one of the top food exports (Department for Environment, Food & Rural Affairs, 2023). Despite these achievements, the industry faces sustainability concerns particularly with mortality rates exceeding 20% of the production in the last years in Scotland (Munro, 2023), a trend also observed in Norway (Sommerset et al., 2024). This mortality translates into economic losses and suboptimal fish welfare and is one of the main challenges to the industry's sustainable growth (Noble et al., 2018).

Salmon aquaculture is a highly technologically advanced industry (FAO, 2022), which collects an increasing amount of data. In Scotland, the government systematically collects and collates monthly mortality data from all producers, making it publicly accessible in a standardized format across all sites. This continuously updated resource holds the potential for the development of an industry-wide mortality monitoring model, eliminating the need for complex data sharing agreements.

In a previous study, these Scottish open-source mortality data were used to create dynamic linear models (DLMs) at production cycle level (Merca et al., 2024). A univariate production cycle level DLM was created using exclusively mortality data. Additionally, several multivariate production cycle level DLMs were developed using mortality data with different combinations of environmental variables. The best multivariate model was the one that incorporated mortality and salinity related variables. Despite the presence of uncertainty in mortality predictions, the Scottish open-source mortality data enabled monitoring salmon mortality. Indeed, it was possible to trigger warnings when mortality was higher than expected, enabling further investigation of the cases if implemented in real-time. Nevertheless, the authors hypothesized that a hierarchical framework, where multiple units (in this case: sites, regions, and country) organized in a stratified structure are monitored simultaneously, could potentially improve the monitoring of salmon mortality. For instance, the hierarchical model can take into account that the sites within the same region are more closely correlated than sites in different regions (Dohoo et al., 2014). Besides, hierarchical modelling would enable monitoring mortality at multiple levels. Such information can be valuable for different stakeholders, by providing insights about mortality trends at regional and national levels, and by allowing comparisons of mortality across different regions.

In animal production, hierarchical DLMs are proven effective in capturing complex relationships and dynamics across multiple organizational levels, facilitating informed decision-making. For instance, in pig production, a hierarchical DLM was successfully employed to analyze drinking patterns across pen, section, and herd levels (Dominiak et al., 2019b, a). In another study in pig herds, conducted by Bono et al. (2012), DLMs were employed for monitoring litter sizes at both herd and sow levels. In dairy cows, DLMs have been implemented to estimate the effects of interventions at herd level, while also considering the cow effect (Stygar et al., 2017; Skjølstrup et al., 2022; Rustas et al., 2024). For aquatic animals, fewer examples of hierarchical modelling exist. In trout, hierarchical modelling has been used to study trout growth in locations such as Lake Superior, North America (Stebbins et al., 2024), and in Neste d'Oueil, Pyrénéss, France (Lecomte and Laplanche, 2012). For salmon, examples include Hubley and Gibson (2011) who developed a Bayesian hierarchical model to estimate the annual mortality of wild Atlantic salmon in Nova Scotia, Canada. Another example is Scheuerell et al. (2015), who used a hierarchical time-series model to investigate the effects of large-scale hatchery supplementation on the density of wild Pacific salmon adults.

The purpose of this study was to use the same open-source mortality data as in Merca et al. (2024) to develop a hierarchical DLM for monitoring monthly mortality of maricultured Atlantic salmon in Scotland. We assessed whether this more complex modelling approach that takes the hierarchical structure of the data into account improved the predictions of mortality when compared to the production cycle level DLMs previously developed. Besides, the hierarchical model can generate estimates for salmon mortality at site, region, and country levels, allowing stakeholders to monitor mortality at different levels. Additionally, the hierarchical DLM created was designed to trigger warnings when the observed mortality exceeds the expected levels. These warnings can inform producers, veterinarians, and inspectors, alerting them to further investigate. More specifically, we had four objectives: (1) to create a hierarchical DLM using mortality data from salmon sites in Scotland; (2) to compare the production cycle level DLMs with the hierarchical model and select the best model for monitoring salmon mortality; (3) to monitor salmon mortality at multiple levels (4) to create warnings at site level when observed mortality exceeded the expected levels.

2 Materials and methods

The present study involved data cleaning, manipulation, and modelling utilizing the statistical programming environment R (R Core Team, 2022) and RStudio (Posit team, 2022). The time-series analysis workflow is freely available (https://doi.org/10.5281/zenodo.13881599).

2.1 Data source

The data used in this study consisted of the same production data previously utilized in Merca et al. (2024), obtained from the Scotland's Aquaculture website (http://aquaculture.scotland.gov.uk/; last accessed 9 February 2023). The data were extracted from a dataset called "Fish Farm Monthly Biomass and Treatments", which consists of monthly data submitted by all active producers of all fish species produced in Scotland. Specifically, this study focuses on production data of seawater Atlantic salmon (*Salmo salar* L.), covering the period from 2002 to 2020.

2.2 Data cleaning and data manipulation

The data cleaning and manipulation procedures conducted in this study followed the framework outlined in Merca et al. (2024), as the same mortality data were utilized in both studies. For a more extensive description of these procedures, refer to Merca et al. (2024).

All marine salmon sites operating in Scotland from 2002 to 2020 were included in the original dataset, totaling 402 sites (open sea farms) and 2138 production cycles (period between stocking and harvesting). Those sites were spread across the six regions of Scotland: Highland, Argyll & Bute, Shetland Islands, Eilean Siar, Orkney Islands, and North Ayrshire (see Merca et al., 2024, Figure 1). Since North Ayrshire region only has one site, it was grouped with the nearest region, *i.e.* Argyll & Bute. Only the resulting five regions were considered.

The dataset used contained monthly mortality data reported as kilograms of dead salmon, per month and per site. In order to account for variations in production size, we converted mortality into proportions by utilizing the biomass data also available:

$$Mortality = \frac{Dead\ \ salmon\ \ (kg)}{Biomass\ \ (kg)}. \tag{1}$$

Upon analyzing the mortality proportions, we identified some as unrealistic, such as instances of negative mortality proportions. The unrealistic values are potentially due to fish movements between sites during the month, for which timing and quantities were unavailable. The reported biomasses represent a snapshot of the biomasses at the end of the month, while mortality accounts for cumulative mortalities throughout the month. Therefore, when fish are moved from one location to another within a given month, the site from where the fish left will report biomasses at the end of the month that are lower relative to the mortalities recorded within that same month. On the other hand, when fish are introduced to a site during the month, the reported biomasses are higher compared to the mortalities observed. To mitigate this error, we tried to capture these movements by defining biomasses considered lower than realistic as

$$Low\ \ biomass_t \leq \tag{2}$$
$$Biomass\ \ (kg)_{t-1} - Mortality\ \ (kg)_{t-1} - 0.2 \times Biomass\ \ (kg)_{t-1},$$

and biomasses higher than realistic as:

$$High\ \ biomass_t \geq \tag{3}$$
$$1.2 \times Biomass\ \ (kg)_{t-1} + Feed\ \ intake\ \ (kg)_t \times 0.77,$$

where t corresponds to the current month and $t-1$ to the previous month. For both cases we established limits of 20% deviation from expected biomasses, and any biomasses falling below or above were deemed abnormal (Equations 2 and 3). Additionally in Equation 3, we relied on feed intake reports (available in the dataset) to foresee how much the salmon where expected to grow in each month. We used a reported feed conversion ratio (FCR) of 1.3 for salmon in the United Kingdom (Torrissen et al., 2011), meaning that 77% of feed intake is transformed into weight gain. Equations 2 and 3 were applied to all reported biomasses in the dataset, and any considered lower or higher than realistic were replaced with missing values. The remaining realistic biomasses were then used to calculate mortality according to Equation 1.

Additionally as part of the data cleaning process, some sites and production cycles were excluded from the study. This was done for various reasons such as missing data and records that did not meet the standard production cycle for commercial purposes, as detailed in Merca et al. (2024).

After data cleaning and manipulation, our study population was reduced to 293 seawater Scottish salmon sites, corresponding to 1610 production cycles distributed in five regions of Scotland.

2.2.1 Transformation and standardization

According to West and Harrison (1997), the residuals of a DLM are expected to follow a normal distribution, as long as the system does not deviate from the expected behavior. In order to achieve this, mortality values underwent a logarithmic transformation: $log\ \ (x + 0.00005)$. As some of these mortality values were zero, we added a small constant before applying the logarithmic transformation. The data were then standardized by subtracting the sample mean from all observations and dividing them by the sample standard deviation.

2.3 Learning and test sets

The available data (293 sites and 1610 production cycles) were utilized to create the learning and test sets, employing the same methodology as described in Merca et al. (2024). By using the same learning and test sets in both studies, a direct and comprehensive comparison of the results can be achieved. The learning set consisted of 145 sites and 784 production cycles, which were utilized to estimate the parameters for the DLM. The test set comprised the same 145 sites and 353 additional production cycles used to validate the models.

2.4 Hierarchical dynamic linear model

Dynamic linear models (DLMs) represent a specific type of time series models. DLMs rely on a Bayesian framework to infer the underlying parameter vector from observed data, while incorporating any relevant prior information available before the observations are made. Each time step involves forecasting values accommodating measurement errors and allowing systematic fluctuations (West and Harrison, 1997).

Hierarchical models (also referred to as multi-level models) are convenient when dealing with data that have an inherent stratified structure. In this case, a dataset comprising a country with different regions, each containing various sites, is an example of a dataset that might benefit from hierarchical modelling. This approach is likely to be advantageous because different geographical locations likely result in greater similarity within the same region, such as similar water temperatures or currents. Hierarchical modelling captures

those correlations between different units, thereby potentially explaining more variation than would be explained without taking the structure into account. Moreover, it enabled simultaneous monitoring of mortality at multiple levels.

An extensive framework for constructing production cycle level DLMs (non-hierarchical) using the same mortality data is described in Merca et al. (2024). Hierarchical DLMs are defined within the usual framework of a DLM with an observation equation and a system equation. The hierarchical architecture of the model is only reflected in the structure of the matrices present in those equations.

In this study, we created a hierarchical DLM using site level monthly mortality data (logarithmically transformed). The model created had all three levels (country, region, and site) directly represented. Consider Y_{rit} as the observed value (mortality) in month t for site i within region r. A straightforward approach of modelling the hierarchy (country/region/site) is through the following model:

$$Y_{rit} = \mu_t + \alpha_{rt} + \beta_{rit} + \nu_{rit}, \quad \nu_{rit} \sim N(0, \sigma^2), \tag{4}$$

where μ_t is a dynamic country level, α_{rt} is a dynamic region level, β_{rit} is a dynamic site level, and ν_{rit} is a random observation error. Therefore, each component contributes to explaining a specific aspect of the observed mortality. This framework allows for changes over time across all levels – country, region, and site.

2.4.1 Harmonic waves and trend factors

After running the simplest type of a hierarchical DLM where no time trends were assumed, we noticed a seasonal pattern in the country level mortality estimates. Thus, we incorporated that seasonality into our model by using the Fourier form representation (West and Harrison, 1997), which involves a linear combination of trigonometric functions (sine and cosine, also known as *harmonic waves*). We tested four approaches: including solely one harmonic wave, the sum of two harmonic waves, the sum of three harmonic waves, and not including any harmonic wave. To compare the performance of these four approaches, we calculated the Root Mean Squared forecast Error (RMSE) for the forecast errors across all sites. The forecast errors consist of the difference between the observed mortality and the forecasted mortality values. Smaller RMSE values indicate greater model precision. We found that the sum of two harmonic waves provided the best fit for the data.

Each harmonic wave is represented by two parameters, in addition to a mean level element. Using the sum of two harmonic waves, 5 parameters were needed: λ_t, h_{11t}, h_{12t}, h_{21t}, h_{22t}. Thus, the country level was defined as follows:

$$\mu_t = \begin{bmatrix} 1 & 1 & 0 & 1 & 0 \end{bmatrix} \begin{bmatrix} \lambda_t \\ h_{11t} \\ h_{12t} \\ h_{21t} \\ h_{22t} \end{bmatrix},$$

where λ_t corresponds to the intercept, h_{11t} and h_{12t} represent the parameters of the first harmonic wave and h_{21t} and h_{22t} represent the parameters of the second harmonic wave.

For the regional levels, we did not consider any time trend. However, we assumed a trend for the site levels, as they may change according to the stage of the production cycle (*i.e.* the age of the fish at the site). To model this trend, we use a spline function created using the *smooth.spline* function available in *stats* R package (R Core Team, 2022). One spline function was developed for each site, which provided the desired shape to reflect the mortality of the corresponding site's production cycles. The magnitude of the trend was dynamically estimated as a *trend factor* (ϱ).

2.4.2 Observation equation

The observation equation (Equation 5) can be written in matrix notation as

$$Y_t = F_t{}' \theta_t + \nu_t, \qquad \nu_t \sim N(0, V_t), \tag{5}$$

and describes how the values of an observation vector (Y_t) depend on underlying (unobservable) parameters (θ_t), through a transposed design matrix ($F_t{}'$). Observation errors are also considered (ν_t). Here, Y_t corresponds to a vector with the observed mortalities of all sites in month t. The parameter vector was defined as

$$\theta_t = (\lambda_t, h_{11t}, h_{12t}, h_{21t}, h_{22t}, \alpha_{At}, \alpha_{Bt}, \alpha_{Ct}, \alpha_{Dt}, \alpha_{Et},$$

$$\beta_{A1t}, \varrho_{A1t}, \ldots, \beta_{B1t}, \varrho_{B1t}, \ldots, \beta_{C1t}, \varrho_{C1t}, \ldots, \beta_{D1t}, \varrho_{D1t}, \ldots, \beta_{E1t}, \varrho_{E1t}, \ldots,$$
$$\beta_{ENt}, \varrho_{ENt})',$$

where indexes A, B, C, D, and E represent the five regions, ϱ_{rit} denotes the trend factor for site i in region r at month t and N corresponds to the total number of sites in region E. The parameter vector (θ_t) consisted of 300 elements.

The transposed design matrix is where the structure of the model is represented, allowing the integration of information from all three levels. The number of rows in $F_t{}'$ is equal to the number of sites and the number of columns corresponds to the size of θ_t. Thus, when no observations were missing in month t, it corresponded to a 145 × 300 matrix:

$$F_t' = \begin{bmatrix} 1 & 1 & 0 & 1 & 0 & 1 & 0 & 0 & 0 & 0 & 1 & 0 & \cdots & 0 & 0 & \cdots & 0 & 0 & \cdots & 0 & 0 & \cdots & 0 & 0 \\ \vdots & \vdots & \vdots & \vdots & \vdots & \vdots & \vdots & \vdots & \vdots & \vdots & \vdots & \vdots & \ddots & \vdots & \vdots & \ddots & \vdots & \vdots & \ddots & \vdots & \vdots & \ddots & \vdots & \vdots \\ 1 & 1 & 0 & 1 & 0 & 0 & 1 & 0 & 0 & 0 & 0 & 0 & \cdots & 1 & 0 & \cdots & 0 & 0 & \cdots & 0 & 0 & \cdots & 0 & 0 \\ \vdots & \vdots & \vdots & \vdots & \vdots & \vdots & \vdots & \vdots & \vdots & \vdots & \vdots & \vdots & \ddots & \vdots & \vdots & \ddots & \vdots & \vdots & \ddots & \vdots & \vdots & \ddots & \vdots & \vdots \\ 1 & 1 & 0 & 1 & 0 & 0 & 0 & 1 & 0 & 0 & 0 & 0 & \cdots & 0 & 0 & \cdots & 1 & 0 & \cdots & 0 & 0 & \ldots & 0 & 0 \\ \vdots & \vdots & \vdots & \vdots & \vdots & \vdots & \vdots & \vdots & \vdots & \vdots & \vdots & \vdots & \ddots & \vdots & \vdots & \ddots & \vdots & \vdots & \ddots & \vdots & \vdots & \ddots & \vdots & \vdots \\ 1 & 1 & 0 & 1 & 0 & 0 & 0 & 0 & 1 & 0 & 0 & 0 & \cdots & 0 & 0 & \cdots & 0 & 0 & \cdots & 1 & 0 & \cdots & 0 & 0 \\ \vdots & \vdots & \vdots & \vdots & \vdots & \vdots & \vdots & \vdots & \vdots & \vdots & \vdots & \vdots & \ddots & \vdots & \vdots & \ddots & \vdots & \vdots & \ddots & \vdots & \vdots & \ddots & \vdots & \vdots \\ 1 & 1 & 0 & 1 & 0 & 0 & 0 & 0 & 0 & 1 & 0 & 0 & \cdots & 0 & 0 & \cdots & 0 & 0 & \cdots & 0 & 0 & \cdots & 1 & 0 \end{bmatrix}.$$

Each row corresponded to a site (here five sites are represented, each belonging to a different region). The first five columns corresponded to the country level, followed by other five columns representing the regions levels. The remaining 290 columns corresponded to the sites levels and trend factors. When there was a missing observation for some site in month t, the row corresponding to that site on the $F_t{}'$ matrix was excluded.

This model already takes the hierarchy into account by seeing each observation as a result of effects at all three levels. Furthermore, it may be reasonable to assume that the error terms within each

level (v_{rit}) are correlated with each other. This can be accomplished if the individual error term is seen as the sum of three underlying independent errors at the country (c), region (r), and site (i) levels

$$v_{rit} = v_{ct} + v_{rt} + v_{it}, \quad v_{ct} \sim N(0, \sigma_C^2), \quad v_{rt} \sim N(0, \sigma_R^2), \quad v_{it} \sim N(0, \sigma_I^2).$$

Thus, the variance-covariance matrix V_t of v_t, when no observations were missing in month t, corresponded to a 145 × 145 matrix, represented as:

$$V_t = \begin{bmatrix} \sigma_C^2 + \sigma_R^2 + \sigma_I^2 & \sigma_C^2 + \sigma_R^2 & \cdots & \sigma_C^2 & \sigma_C^2 \\ \sigma_C^2 + \sigma_R^2 & \sigma_C^2 + \sigma_R^2 + \sigma_I^2 & \cdots & \sigma_C^2 & \sigma_C^2 \\ \vdots & \vdots & \ddots & \vdots & \vdots \\ \sigma_C^2 & \sigma_C^2 & \cdots & \sigma_C^2 + \sigma_R^2 + \sigma_I^2 & \sigma_C^2 + \sigma_R^2 \\ \sigma_C^2 & \sigma_C^2 & \cdots & \sigma_C^2 + \sigma_R^2 & \sigma_C^2 + \sigma_R^2 + \sigma_I^2 \end{bmatrix},$$

considering that the sites represented in the first two columns (and rows) are situated within the same region (region A), while the sites represented in the last two columns (and rows) are both part of a common region which is different from the initial one (region E).

2.4.3 System equation

The system equation (Equation 6) is represented as

$$\theta_t = G_t \ \theta_{t-1} + w_t, \qquad w_t \sim N(0, W_t), \qquad (6)$$

where G_t is called the system matrix and serves to update the parameter vector, and w_t represents the system errors. The system matrix is a quadratic matrix with the same size as θ_t:

$$G_t = \begin{bmatrix} 1 & 0 & 0 & 0 & 0 & 0 & 0 & 0 & 0 & 0 & 0 & \cdots & 0 & 0 \\ 0 & \cos(\omega) & \sin(\omega) & 0 & 0 & 0 & 0 & 0 & 0 & 0 & 0 & \cdots & 0 & 0 \\ 0 & -\sin(\omega) & \cos(\omega) & 0 & 0 & 0 & 0 & 0 & 0 & 0 & 0 & \cdots & 0 & 0 \\ 0 & 0 & 0 & \cos(2\omega) & sin(2\omega) & 0 & 0 & 0 & 0 & 0 & 0 & \cdots & 0 & 0 \\ 0 & 0 & 0 & -\sin(2\omega) & cos(2\omega) & 0 & 0 & 0 & 0 & 0 & 0 & \cdots & 0 & 0 \\ 0 & 0 & 0 & 0 & 0 & 1 & 0 & 0 & 0 & 0 & 0 & \cdots & 0 & 0 \\ 0 & 0 & 0 & 0 & 0 & 0 & 1 & 0 & 0 & 0 & 0 & \cdots & 0 & 0 \\ 0 & 0 & 0 & 0 & 0 & 0 & 0 & 1 & 0 & 0 & 0 & \cdots & 0 & 0 \\ 0 & 0 & 0 & 0 & 0 & 0 & 0 & 0 & 1 & 0 & 0 & \cdots & 0 & 0 \\ 0 & 0 & 0 & 0 & 0 & 0 & 0 & 0 & 0 & 1 & 0 & \cdots & 0 & 0 \\ 0 & 0 & 0 & 0 & 0 & 0 & 0 & 0 & 0 & 0 & \delta_{A1t} & \cdots & 0 & 0 \\ \vdots & \vdots & \vdots & \vdots & \vdots & \vdots & \vdots & \vdots & \vdots & \vdots & \vdots & \ddots & \vdots & \vdots \\ 0 & 0 & 0 & 0 & 0 & 0 & 0 & 0 & 0 & 0 & 0 & \cdots & 1 & \delta_{ENt} \\ 0 & 0 & 0 & 0 & 0 & 0 & 0 & 0 & 0 & 0 & 0 & \cdots & 0 & 1 \end{bmatrix},$$

where $\omega = \frac{2\times\pi}{12}$, $\delta_{rit} = \hat{m}_{rit} - \hat{m}_{ri,t-1}$ (being $\hat{m}$ the expected log-transformed mortality at times t and $t-1$ for site i in region r, given by the spline function), and N corresponds to the total number of sites in region E. The two harmonic waves for the country level are represented in the first five rows and columns. The expected rate of change in log-transformed mortality (δ_{rit}) are shown in the corresponding rows and columns of each site, being utilized to update the site levels.

The systematic variance-covariance matrix W_t of w_t describes how much each element of the system is likely to randomly change from one time step to the next, and was calculated using a component discounting approach described by West and Harrison (1997). A discount factor is a numeric value that falls within the range of 0 to 1. Discount factors that are closer to 0 reflect large system variance, while those closer to 1 indicate a small variance. This approach is referred to as component discounting, as it allows each level (component) to have its own discount factor. Therefore, the model can change at a different rate for each level, offering more modelling flexibility. In this case, three discount factors were included: one for country (ρ_C), one for region (ρ_R), and one for site (ρ_I). The resulting variance-covariance matrix W_t is a block-diagonal matrix with a dimension of 300 × 300.

2.4.4 Initialization

In order to fully describe a DLM, it is necessary to provide the initial distribution $(\theta_0 | D_0) \sim N(m_0, C_0)$ of the parameter vector θ_0, before any observations are made (D_0). We achieved this my defining an initial mean m_0 and the initial variance-covariance matrix C_0.

The initial mean m_0 followed the same structure of θ_t, first having the country elements, then the regions, followed by the sites. For the season-dependent country level two harmonic waves were introduced, representing 5 elements. We created a linear regression to determine the relationship between the observations of mortality (on the learning set) and a trigonometric function representing a sum of two harmonic waves, for a period of 12 months. The resulting coefficients estimates were used in m_0. The coefficient estimates corresponded to the intercept and one sine and cosine wave for each harmonic wave used, resulting in 5 elements. For the regions' levels, we calculated the average of mortality for each region using the learning set. We then subtracted the five elements calculated for the country level, and added the results to m_0. Finally, for the sites' elements, each site had a level and a trend factor. For all sites, the level and the trend factor were set to 0 and 1, respectively. A trend factor of 1 indicates that, prior to any observations, we expected the system to evolve according to the estimated spline function.

The initial variance-covariance matrix C_0 corresponded to a quadratic matrix with the same size as θ_t, also having the country, regions, and sites elements. For the country part, we applied the *vcov* function available on *stats* R package (R Core Team, 2022) to the linear regression previously created for m_0. This function returned a 5 × 5 variance-covariance matrix of the main parameters of the regression model. For the regions' elements, we used the learning set to calculate the average of mortality in each region, for the first 7 months of the production cycles. Therefore, for each region we had 7 values, one for each of the 7 months. From each of those values, we subtracted the five elements calculated for the country level in m_0. Then, we computed the covariance of those subsequent 7 elements, resulting in one value per region. For the sites, we also calculated the average of mortality in each site, for the first 7 months of the production cycles. To each of those 7 elements, we subtracted the corresponding region mean and the five elements calculated for the country level in m_0. Then, on the 7 resulting values, we calculated the differences between each two consecutive elements. Finally, we computed the covariance between the differences and the 7 mortality averages already discounting the country and region parts. The final variance-covariance matrix C_0 was accomplished by diagonally combining the country individual

variance-covariance matrix, the regions variances and the sites variance-covariance matrices.

It is worth mentioning that the initial values of m_0 and C_0 were of minor importance. As soon as the DLM was applied to the data, it automatically adapted over time.

2.4.4.1 When a new production cycle starts

Every time a new production cycle started, the site needed to be reinitialized to ensure it did not incorporate information from previous production cycles when predicting the new one.

The system equation (Equation 6) updates the parameter vector from θ_{t-1} to θ_t. Whenever a new production cycle started, we wanted to reset the corresponding site to its initial state. Therefore, we changed the level and the trend factor for the specific site in θ_{t-1} to 0 and 1, respectively (as in m_0). Moreover, in G_t, we inserted zeros in the rows and columns of the site that had a new production cycle starting in order to "break the connection" between cycles. Finally, we added some additional variance (C_0) to the elements of W_t for the specific site that was initiating a new production cycle. Hence, we increased the adaptability of the model.

2.4.5 Optimizing DLM variance components

For a full specification of the variance components of this hierarchical model, six parameters were needed: three observational variances $\sigma_C^2, \sigma_R^2, \sigma_I^2$ (used in V_t) and three discount factors ρ_C, ρ_R, ρ_I (used in W_t).

These six parameters were estimated from the learning set, through numerical optimization. The values selected were the ones that minimized the Root Mean Squared forecast Error (RMSE). This estimation was performed using the *optim* function in R (R Core Team, 2022), with the Nelder-Mead optimization algorithm. The resulting observational variances were $\sigma_C^2 = 0.02883$, $\sigma_R^2 = 0.01053$ and $\sigma_I^2 = 0.45801$, and the discount factors were $\rho_C = 0.77978$, $\rho_R = 0.97855$ and $\rho_I = 0.78199$.

2.4.6 Filtering and smoothing

The DLM incorporated the Kalman filter technique, which produces estimates updated according to new observations (West and Harrison, 1997). Given the information available at time t (D_t), the conditional probability of the parameter vector (θ_t) is denoted as $(\theta_t \mid D_t) \sim N(m_t, C_t)$, where m_t is the filtered mean and C_t the variance-covariance matrix. The Kalman filter allowed us to obtain monthly expected values (filtered mean and variance) and forecasts for mortality at site level. Additionally, it gave us expected mortality values for the country as a whole and for each of the five regions.

The parameter vectors θ_t are autocorrelated. The Kalman filter estimates the θ_t based on previous information only. However, due to this autocorrelation, the future observations also contain valuable information for estimating θ_t. Therefore, a retrospective analysis called smoothing can be employed (West and Harrison, 1997). This method takes into account all the available observations, including past and future ones, providing the best possible estimates.

2.5 Monitoring at country and region levels

As stated in Equation 4, the observed mortalities at a site consisted of the sum of the dynamic country, region, and site levels. However, obtaining mortality estimates at the country and regional levels required additional calculations.

To obtain the mortality estimates at regional level, we defined a vector that could extract the regional estimates from the estimated means (filtered and smoothed). For each region and at each time step, a different vector was created. For example, the vector for region A at time t was defined as

$$z_{At} = \left(1,1,0,1,0,1,0,0,0,0,\frac{1}{M_{At}},0,\ldots,\frac{1}{M_{At}},0,\ldots,0,0,\ldots,0,0,\ldots,0,0,\ldots,0,0\right),$$

where M_{At} corresponds to the number of sites belonging to region A with observations at time t. This vector had the same structure as θ_t, where the first five elements correspond to the country level, the following five values represent the different regions (with the number 1 in the position of region A), and the remaining elements correspond to the sites levels and trends. In the positions of the sites levels belonging to region A with observations at time t, we assigned $\frac{1}{M_{At}}$ to equally capture each site's influence on the region. The same logic was employed to create the vectors for all five regions. Then, to extract the mortality estimates at regional level, we multiplied the previously described vector by the filtered mean (m_t). To extract the mortality estimates at regional level estimated by the retrospective smoothening, the same methodology was used: the same previously explained vector was multiplied by the smoothed mean.

For the country level, we also created a vector to extract the mortality estimates:

$$z_{ct} = (1,1,0,1,0,\frac{1}{5},\frac{1}{5},\frac{1}{5},\frac{1}{5},\frac{1}{5},$$
$$\frac{1}{5\times M_{At}},0,\ldots,\frac{1}{5\times M_{At}},0,\ldots,\frac{1}{5\times M_{Bt}},0,\ldots,0,0,\ldots,$$
$$\frac{1}{5\times M_{Ct}},0,\ldots,\frac{1}{5\times M_{Dt}},0,\ldots,\frac{1}{5\times M_{Et}},0),$$

where the M_{At}, M_{Bt}, M_{Ct}, M_{Dt}, and M_{Et} correspond to the number of sites belonging to regions A, B, C, D, and E, respectively, with observations at time t. The logic behind the structure of this vector was the same as that used in creating the vectors for the regions: the first five elements represent the country level, the next five values correspond to the regions, and the following represent the sites levels and trends. In all region positions, we assigned $\frac{1}{5}$, where 5 represents the number of regions, to equally reflect the impact for each of the five regions on the country. The same rationale was employed for the site levels, where we divided 1 by the product of 5 (number of regions) and the number of sites with observations at time t within each region. Positions corresponding to sites where no observations existed at time t were set as 0. Subsequently, to extract the mortality estimates at country level, both filtered and smoothed, we multiplied the country vector by the filtered mean (m_t) and by the smoothed counterpart, respectively.

Finally, we also needed to extract the variance of the smoothed and filtered levels for region (C_{rt}) and for country (C_{ct}). The same previously defined vectors were again used. At regional level the variance was extract as

$$C_{rt} = z_{rt} \times C_t \times z_{rt}',$$

where $r \in \{A, B, C, D, E\}$, and at country level

$$C_{ct} = z_{ct} \times C_t \times z_{ct}',$$

where the C_t corresponds to the variances of the filtered or smoothed levels, depending on which variance we are extracting, at time t.

2.6 Generating warnings

Warnings were generated at site level. A warning was defined as any observation of mortality falling above the 95% credible intervals (CI). The 95% CI were determined using the forecasted values f_t (and their respective variance Q_t) produced by the Kalman filter, as:

$$95\ \%\ \ CI = f_t \pm 1.96 \times \sigma_t, \tag{7}$$

where $\sigma_t = \sqrt{Q_t}$. The warnings were generated using the same methodology as in the previous study (Merca et al., 2024).

3 Results

The results presented were achieved by applying the hierarchical DLM to the test set using initial specifications derived from the learning set.

3.1 Comparison of hierarchical and production cycle level DLMs

After developing the hierarchical DLM (objective 1), the second objective was to compare the performances of the univariate production cycle level DLM (which used only mortality data) and the best multivariate production cycle level DLM (which incorporated both mortality and salinity related variables) created in a previous study (Merca et al., 2024), with the newly developed hierarchical DLM. These comparisons involved assessing the discrepancies between the mortality observations and the models predictions, represented as forecast errors. The RMSEs were calculated for the collective set of mortality forecast errors across all production cycles for the production cycle level DLMs and across all sites for the hierarchical DLM.

The RMSEs of the three models are shown in Table 1. The smaller RMSE for the hierarchical DLM suggest better precision. To determine the statistical significance of these differences, a paired t-test was performed on the squared forecast errors of the models being compared. T-tests are recognized for their utility in studies characterized by large sample sizes and are noted for their robustness, even when dealing with skewed data (Fagerland, 2012). Since we aimed to compare variances, squaring the forecast errors was appropriate. The p-value computed between the univariate production cycle level DLM and the hierarchical DLM was 6.14×10^{-5}, and 2.44×10^{-4} between the multivariate production cycle level DLM and the hierarchical DLM. Thus, we can conclude that the hierarchical DLM performed significantly better than both production cycle level DLMs.

3.2 Monitoring mortality at multiple levels

The hierarchical DLM provided estimates of mortality at country, region, and site levels (objective 3). At country level (Figure 1), we can see the filtered mean estimated by the prospective Kalman filter (in green) and the smoothed mean (in blue) estimated by the retrospective smoothening. Both estimates are accompanied by their corresponding 95% credible intervals (CI), derived from their respective variance components. The filtered mean (in green) provides the most accurate estimates of the true underlying mortality level at each time step, incorporating all prior information. Meanwhile, the smoothed mean (in blue) offers the best possible estimates of mortality at country level by considering all available information both before and after each time step. At country level, mortality exhibits a consistent pattern with clear seasonal variations, showing higher mortality in the summer months (Figure 1).

At region level (Figure 2), the filtered mean (in green) and the smoothed mean (in blue) are illustrated for each of the five regions included in this study. At the region levels it is also possible to see the seasonality in the estimates, with increased mortality during the summer. Each region displayed distinct mortality trends that can be analyzed individually. The region Highland experienced an upward trajectory in mortality from 2016 to 2018, while being stable in subsequent years. Argyll & Bute showed a notable decrease in mortality in 2018 compared to the other years. The Shetland Islands exhibited a decrease in mortality in the last months of 2020. In the Orkney Islands it is possible to see a declining trend in mortality over the years. Eilean Siar showed an increase in mortality in the last six months of 2020.

Here, we explain the site level using two sites as examples: Site X (Figures 3A, B) and Site Y (Figures 4A, B). Starting with Site X, the DLM provided estimates (filtered and smoothed means - Figure 3A) but also the forecasted values produced at each time step in the Kalman filter (Figure 3B). The two darker grey shaded areas represent the two production cycles present in Site X during the analyzed timeframe, interrupted by a fallow period in which no fish were present in the site. Figure 3A illustrates that the means (filtered and smoothed) demonstrated a consistent alignment with the observations. It is worth noticing that the DLM continued to provide estimates even in the absence of observations, based on information from other sites (for instance in the last months of 2017 and beginning of 2018). Additionally, it is evident that during the periods without observations (between the production cycles), the 95% confidence intervals widened, reflecting increased uncertainty about the true mortality values due to the lack of mortality data. In Figure 3B, the forecasts are depicted along with the corresponding 95% CI. The 95% CI are wide, implying a degree of uncertainty in

TABLE 1 Root mean squared errors (RMSEs) for the univariate and best multivariate production cycle level DLMs (Merca et al., 2024), and the hierarchical DLM.

DLMs	RMSEs
Univariate production cycle level	0.86028
(Best) multivariate production cycle level	0.85860
Hierarchical	0.82840

the forecasts. In Site X the mortality is considered to be as expected, since the observations do not exceed the 95% CI.

Figure 4 illustrates the filtered and smoothed means (Figure 4A) and the forecasted values (Figure 4B), for Site Y. The observations exceeded the forecasts 95% CI in May and August 2016, March 2017 and October 2020, therefore these observations gave rise to warnings (Figure 4B).

At all levels - country, region and site - the estimates at the initial time steps should be interpreted with caution, given that the DLM was still adapting to the data, and the accuracy of these estimates may be limited during this initial phase.

3.3 Warnings

The fourth and last objective of this study was to generate warnings at site level when the observed mortality exceeded the expected levels. To ensure comparability with the warnings generated using the non-hierarchical models created in Merca et al. (2024), the warnings here were also assessed per production cycle. However, it is important to clarify that in this study the warnings were generated at site level. We could then identify the corresponding production cycle for each warning generated.

Between 2015 and 2020, 84 of the 353 production cycles experienced at least one warning. Of these 84 cycles, 70% had only one warning, 21% encountered two warnings, and 9% experienced three.

Of the 145 sites, 71 exhibited warnings, spanning all five regions. The region of Argyll and Bute had the highest occurrence, with 19 of 59 production cycles (32%) experiencing at least one warning, with a total of 28 warnings (Table 2). This was followed by the Highland region with 29% and Eilean Siar with 27%. The Orkney Islands region had the lowest number of warnings, with 5 production cycles each recording one warning out of 55 production cycles (9%), resulting in 5 total warnings, as shown in Table 2.

Regarding the months of the year (Table 2), there was an increase in March with 9 warnings out of 462 production cycle-months (1.9%). Similarly, April had a 2.0% occurrence rate. The months with the highest warning occurrences were July (3.5%), August (4.4%), September (2.9%), and October (4.5%).

Concerning the years (Table 2), 2016 had the highest rate with 42 warnings over 903 production cycle-months (4.7%). This was followed by 2017 with a 2.7% warning rate, 2015 with 2.1%, and 2018 with 1.6%. However, in 2015 only three months of data were available, making direct comparisons inapplicable.

4 Discussion

A hierarchical DLM was developed to monitor salmon mortality using open-source Scottish salmon data. The main goal was to evaluate whether this more complex modelling approach, which leverages the hierarchical data structure, offers better model precision compared to the simpler production cycle level DLMs (non-hierarchical) described in a previous study (Merca et al., 2024). Indeed, the hierarchical model outperformed the production cycle level DLMs, demonstrating that the additional modelling effort of accounting for the structure of the data confers a significant advantage. Similarly to the production cycle level models, the hierarchical DLM also exhibited a degree of uncertainty in the mortality predictions. Nevertheless, it was possible to trigger warnings at site level when the observed mortality exceeded the expected levels. An additional benefit of the hierarchical model was

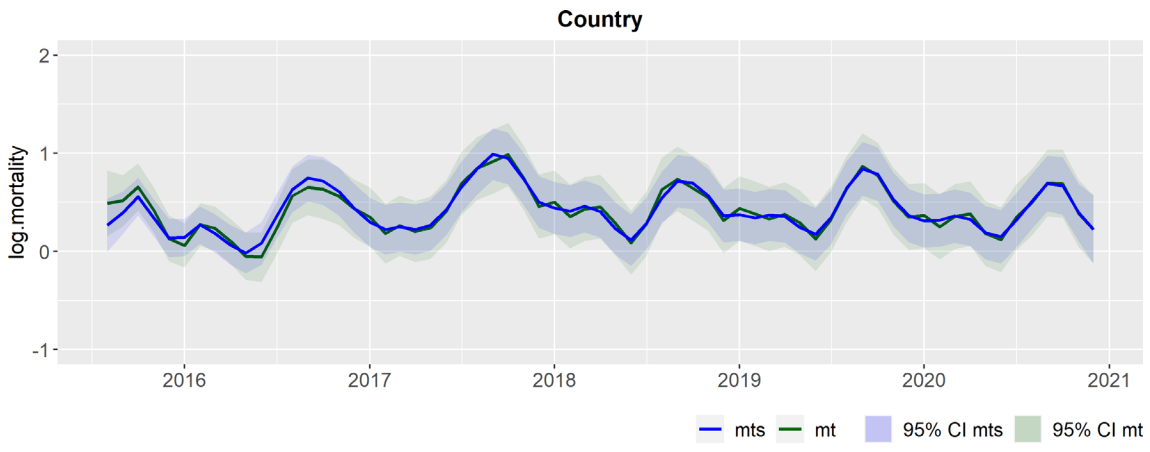

FIGURE 1
Outcomes from the hierarchical DLM at country level. In green: Filtered mean for the country level (mt) and the respective 95% credible interval (CI); In blue: Smoothed mean for the country level (mts) and the respective 95% credible interval (CI).

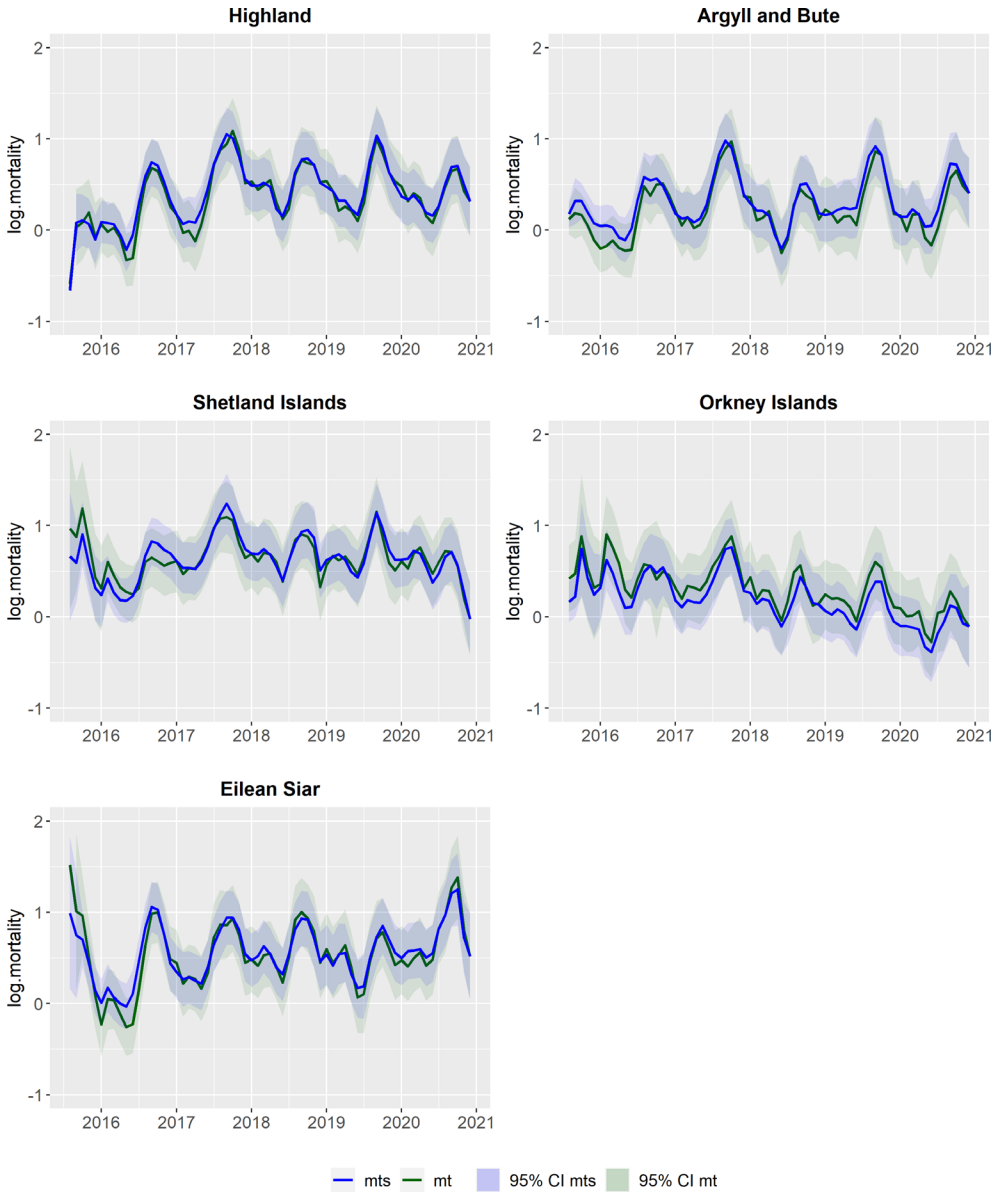

FIGURE 2
Outcomes from the hierarchical DLM at region level, for each of the five regions. In green: Filtered means for the regional levels (mt) and the respective 95% credible intervals (CI); In blue: Smoothed means for the regional levels (mts) and the respective 95% credible intervals (CI).

its ability to monitor mortality at country, region, and site levels. This information provided by the hierarchical model can be particularly valuable for various stakeholders as part of a monitoring system, offering insights into mortality trends at multiple levels, while also providing warnings at site level when mortality is higher than expected.

Using open-source data offers numerous advantages, particularly in the context of hierarchical modelling. Monitoring production at higher levels, such as a country or region, typically involves aggregating information from various companies operating in different locations. Openly available datasets simplify the creation of comprehensive models by facilitating data integration across these entities. Open-source datasets eliminate the need for complicated and time-consuming data sharing agreements between companies, thereby reducing administrative complexities and fostering a more efficient process. This accessibility not only accelerates innovation but also ensures transparency and reproducibility of the methods.

The idea behind creating a hierarchical DLM aimed to reflect the inherent hierarchical structure present in the data. It is typically anticipated that a relationship among the responses of observations within a group exists, as the shared feature tends to make the outcomes more similar than they would be otherwise (Dohoo et al., 2014). In a previous study, we developed production cycle level DLMs (Merca et al., 2024), which modelled each production cycle individually, without considering correlations between production cycles within the same site or region. In the current study, we incorporated the data hierarchy, encompassing a country level, grouped into five different regions, with each

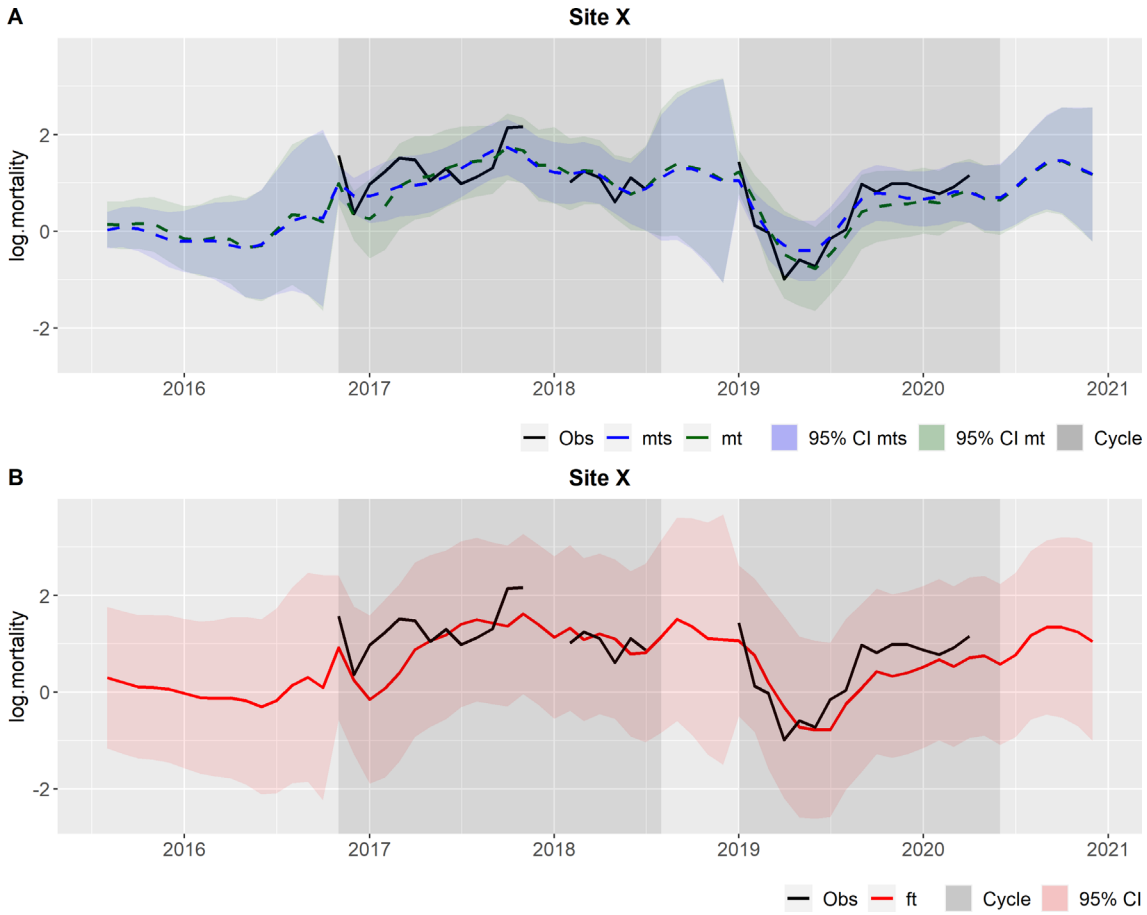

FIGURE 3
Outcomes from the hierarchical DLM at site level, for Site X. Observations (obs) in black and the production cycles are represented by the grey shaded areas. **(A)** In green: Filtered mean (mt) and the respective 95% credible interval (CI); In blue: Smoothed mean (mts) and the respective 95% credible interval (CI). **(B)** In red: Forecasts (ft) and the respective 95% credible interval (CI).

region containing several sites. Accounting for this hierarchy has proven beneficial in monitoring salmon mortality, justifying the development of this more complex modelling approach.

The hierarchical DLM provided valuable outcomes: (1) it enabled the monitoring of mortality at various levels, and (2) it triggered site level warnings when mortality exceeded the expected levels. Regarding the first outcome, we were able to calculate estimates for country, region, and site levels over time (using data collected at site level) offering critical insights into mortality trends. This information can be valuable for various stakeholders, including health authorities, in understanding trends that may benefit from strategic resource management practices at regional or national levels. Two types of estimates were generated at country, regional, and site levels: filtered and smoothed values. It should be noted that the smoothed values, obtained through retrospective analysis, are not suitable for real-time monitoring and are therefore only relevant for retrospective assessments. In turn, filtered values are best suited for real-time analysis, and could be implemented as an industry-wide mortality monitoring model. Concerning the second outcome, triggering warnings when observed mortality significantly exceeds the expected levels is an important feature of monitoring systems. These warnings can alert stakeholders, such as salmon producers or authorities, to investigate the causes of excessive mortality. The models are based on monthly mortality that is collated by a government body. Therefore, the outputs are at least one or two months behind real-time observations, and thus results of our model are too late to be of use for immediate mitigative actions. However, increasing warnings, or unexplained warnings, can point at a need for health management issues or emerging diseases that may have been otherwise left unnoticed for longer. This could save the industry time, money and resources, and improve its sustainability.

Warnings were generated at site level when the observed mortalities exceeded the 95% CI of the forecasts, calculated as shown in Equation 7. A warning indicates that mortality on that site was significantly higher than expected for that particular time step. The application of the hierarchical model revealed that approximately 25% of the production cycles and 50% of the sites encountered at least one warning between 2015 and 2020. When compared to the production cycle level DLMs (Merca et al., 2024), the hierarchical DLM produced fewer warnings overall but the warnings were coherent across models. This can be beneficial because stakeholders in the agricultural sector emphasize the necessity for reliability and

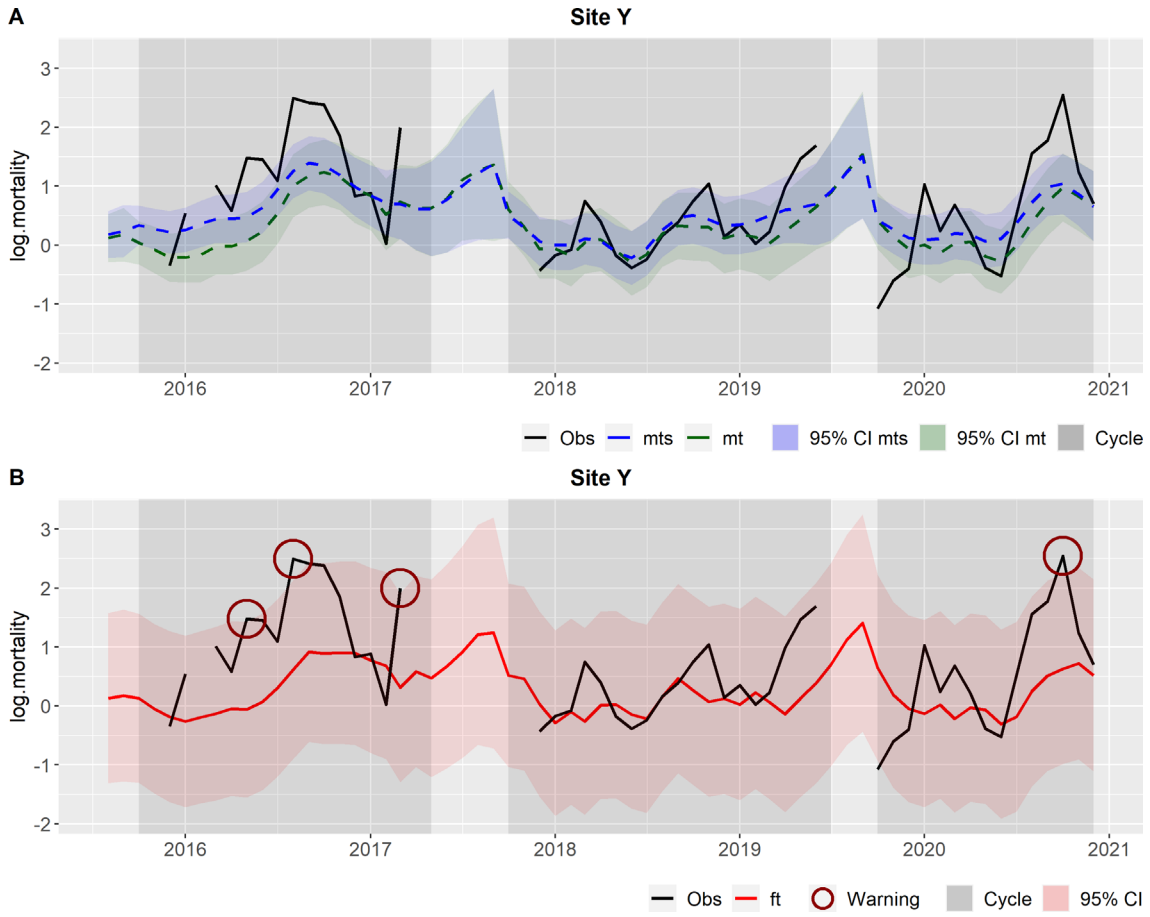

FIGURE 4
Outcomes from the hierarchical DLM at site level, for Site Y. Observations (obs) in black and the production cycles are represented by the grey shaded areas. **(A)** In green: Filtered mean (mt) and the respective 95% credible interval (CI); In blue: Smoothed mean (mts) and the respective 95% credible interval (CI). **(B)** In red: Forecasts (ft) and the respective 95% credible interval (CI); Circles: warnings.

robustness to justify the utilization of the models and mitigate distrust in technology (Kaler and Ruston, 2019; Kopler et al., 2023).

Geographically, the region of Argyll and Bute experienced the highest warning rate (32%), followed by Highland (29%), Eilean Siar (27%), Shetland Islands (19%) and Orkney Islands (9%). In both univariate and multivariate production cycle level DLMs developed in the previous study, the region of Orkney Islands also had the lowest warning rate (11% on both cases), but Eilean Siar had the highest (44% and 40%, respectively). This difference might be due to the consideration of the region each site belongs to,

TABLE 2 Warnings identified in the hierarchical DLM between 2015 and 2020: per region, month of the year and year.

Hierarchical DLM												
Warnings per region	**Highland**		**Argyll and B.**		**Shetland Isl.**			**Orkney Isl.**		**Eilean Siar**		
	29/101 (29%)		19/59 (32%)		14/75 (19%)			5/55 (9%)		17/63 (27%)		
	42		28		17			5		24		
Warnings per month of the year (%)	**Jan**	**Feb**	**Mar**	**Apr**	**May**	**Jun**	**Jul**	**Aug**	**Sep**	**Oct**	**Nov**	**Dec**
	1.0	0.9	1.9	2.0	1.2	0.8	3.5	4.4	2.9	4.5	1.1	0.9
Warnings per year (%)	**2015**		**2016**		**2017**		**2018**		**2019**		**2020**	
	2.1		4.7		2.7		1.6		0.9		0.9	

For the "Warnings per region", the first row corresponds to the number of production cycles that triggered at least one warning out of the total number of production cycles in that region; the second row shows the total number of warnings triggered in each region. For the "Warnings per month of the year (%)" and "Warnings per year (%)", the percentages correspond to the division between the total number of warnings generated on that month or year and the corresponding number of production cycle-months, multiplied by 100.
Isl., Islands; B., Bute; Jan, January; Feb, February; Mar, March; Apr, April; Jun, June; Jul, July; Aug, August; Sep, September; Oct, October; Nov, November; Dec, December.

which influenced the expected mortality, and therefore the warnings generated. By accounting for the region associated with each site, the hierarchical DLM can better estimate the expected mortalities, reflecting the regional variations.

In terms of seasonality, most warnings triggered by the hierarchical DLM occurred during the summer and autumn months. This is in accordance with what was found in the production cycle level DLMs. During summer, rising water temperatures increase salmon metabolic rates, escalating oxygen demand. Simultaneously, warmer water temperatures lead to diminishing dissolved oxygen levels in water (Noble et al., 2018). Additionally, warm water fosters the proliferation of most of the currently relevant infectious agents and parasites such as amoebic gill disease and sea lice (Oldham et al., 2016; Brooker et al., 2018; Murray et al., 2022), and non-infectious harmful agents such as micro jellyfish and phytoplankton (Boerlage et al., 2020). No open-source data about the cause(s) of excessive mortalities were available during the full study period, limiting our ability to incorporate these factors into the models. During the summer, the model already expects higher mortalities due to the incorporation of a seasonal pattern at country level within the hierarchical framework, which prevents the generation of warnings for these already expected increases. However, the model indicates that the instances of higher-than-expected mortalities, which do trigger warnings, are also more frequent during this period.

The distribution of warnings from 2015 to 2020 was also similar between the hierarchical DLM and the production cycle level models. For all models (since the same mortality data were used) the year 2015 only had three months of data available, making direct comparisons not applicable. The year 2016 continued as the one with the highest warning rate, followed by a declining trend until 2020. The reasons for the declining trend are unclear; however, it is plausible that they may be attributed to potentially less precise mortality estimates during the initial time steps of the modelling process, leading to overestimations of warnings in 2016. Such an effect would not occur in later years when the model has been running for longer.

In all three models here compared (hierarchical, univariate production cycle level, and multivariate production cycle level DLMs), the warnings were defined as any observation exceeding the 95% credible interval. The method chosen was applied to all three types of DLMs to ensure comparability of warnings across different models. Alternative methods for generating warnings from DLM outputs could have been used, as discussed in Merca et al. (2024).

The residuals of a DLM should follow a normal distribution, as long as the system remains as expected (West and Harrison, 1997). The original mortality data resulted in non-normally distributed residuals. Thus, we applied a logarithmic transformation to meet normality assumptions. The results can still be interpreted on the original data scale. The decision of using DLMs was previously discussed in Merca et al. (2024). To ensure methodological consistency, all models compared utilized the same logarithmically transformed mortality data.

Similarly to the production cycle level DLMs developed in the previous study (Merca et al., 2024), the mortality forecasts derived from the hierarchical model also exhibited wide 95% credible intervals. This may be attributed to the absence of health, management, and fish movement data. Ideally, models should be trained with data representing "normal" mortality to establish baseline patterns, as conducted by Jensen et al. (2016). However, the absence of health and management related information in the mortality dataset made it impossible to distinguish normal from abnormal mortality. Salmon producers collect these data internally, but they only report it to government and to the salmon producers' organization (Salmon Scotland) when mortality reaches a specific threshold. These data have only become openly available recently, and therefore could not be incorporated in the entire timeframe of our study. Additionally, the movement of fish among sites, a common practice among producers, may have not been entirely captured in our analysis, despite our attempts detailed in section 2.2. For a more detailed exploration of potential sources of uncertainty, refer to Merca et al. (2024).

To address these uncertainties, future models could incorporate data on the reasons for mortality and salmon movements. However, salmon movements' data are not openly available. Additionally, including mortality data over shorter time periods, such as weekly intervals, would likely improve the monitoring process.

5 Conclusion

Accounting for the hierarchical structure of the data (country, region, and site) is beneficial in monitoring salmon mortality, outperforming the production cycle level DLMs developed in a previous study. This hierarchical approach enabled us to monitor mortality at country, region, and site levels, providing additional valuable insights into the mortality trends. Moreover, we could provide warnings at site level when the observed mortality exceeded the expected levels, which can contribute to the detection of management issues or emerging diseases. However, some uncertainty was found in the mortality predictions. Our exclusive reliance on open-source data has enabled the development of an industry-wide mortality monitoring model, providing additional value to already existing data, and eliminating the need for complex data sharing agreements.

Data availability statement

Publicly available datasets were analyzed in this study. This data can be found here: https://aquaculture.scotland.gov.uk/.

Author contributions

CM: Writing – original draft, Visualization, Software, Methodology, Investigation, Formal analysis, Data curation, Conceptualization. AB: Writing – review & editing, Supervision, Resources, Methodology, Conceptualization. AK: Writing – review & editing, Supervision, Software, Resources, Methodology, Funding acquisition, Formal analysis, Conceptualization. DJ: Writing – review & editing, Supervision, Software, Resources, Methodology, Funding acquisition, Formal analysis, Conceptualization.

Funding

The author(s) declare financial support was received for the research, authorship, and/or publication of this article. This work has received funding from the European Union's Horizon 2020 research and innovation programme under grant agreement No. 101000494 (DECIDE).

Conflict of interest

The authors declare that the research was conducted in the absence of any commercial or financial relationships that could be construed as a potential conflict of interest.

The author(s) declared that they were an editorial board member of Frontiers, at the time of submission. This had no impact on the peer review process and the final decision.

Publisher's note

Author disclaimer

References

Boerlage, A. S., Ashby, A., Herrero, A., Reeves, A., Gunn, G. J., and Rodger, H. D. (2020). Epidemiology of marine gill diseases in Atlantic salmon (*Salmo salar*) aquaculture: a review. *Rev. Aquac.* 12, 2140–2159. doi: 10.1111/raq.12426

Bono, C., Cornou, C., and Kristensen, A. R. (2012). Dynamic production monitoring in pig herds I: Modeling and monitoring litter size at herd and sow level. *Livestock Sci.* 149, 289–300. doi: 10.1016/j.livsci.2012.07.023

Brooker, A. J., Skern-Mauritzen, R., and Bron, J. E. (2018). Production, mortality, and infectivity of planktonic larval sea lice, *Lepeophtheirus salmonis* (Kroye): Current knowledge and implications for epidemiological modelling. *ICES J. Mar. Sci.* 75, 1214–1234. doi: 10.1093/icesjms/fsy015

Department for Environment, Food & Rural Affairs (2023).Chapter 13: Overseas trade. In: *National statistics: Agriculture in the United Kingdom 2022*. Available online at: https://www.gov.uk/government/statistics/agriculture-in-the-united-kingdom-2022/chapter-13-overseas-trade (Accessed March 1, 2024).

Dohoo, I., Martin, W., and Stryhn, H. (2014). *Veterinary Epidemiologic Research. 2nd Edn* (Charlottetown, Prince Edward Island, Canada: VER). Available at: www.upei.ca/ver.

Dominiak, K. N., Hindsborg, J., Pedersen, L. J., and Kristensen, A. R. (2019a). Spatial modeling of pigs' drinking patterns as an alarm reducing method II. Application of a multivariate dynamic linear model. *Comput. Electron. Agric.* 161, 92–103. doi: 10.1016/j.compag.2018.10.037

Dominiak, K. N., Pedersen, L. J., and Kristensen, A. R. (2019b). Spatial modeling of pigs' drinking patterns as an alarm reducing method I. Developing a multivariate dynamic linear model. *Comput. Electron. Agric.* 161, 79–91. doi: 10.1016/j.compag.2018.06.032

Fagerland, M. W. (2012). t-tests, non-parametric tests, and large studies-a paradox of statistical practice? *BMC Med. Res. Methodol.* 12:78. doi: 10.1186/1471-2288-12-78

FAO (2022). *The State of World Fisheries and Aquaculture 2022. Towards Blue Transformation* (Rome: FAO). doi: 10.4060/cc0461en

Hubley, P. B., and Gibson, A. J. F. (2011). A model for estimating mortality of Atlantic salmon, *Salmo salar*, between spawning events. *Can. J. Fish. Aquat. Sci.* 68, 1635–1650. doi: 10.1139/f2011-074

Iversen, A., Asche, F., Hermansen, Ø., and Nystøyl, R. (2020). Production cost and competitiveness in major salmon farming countries 2003–2018. *Aquaculture* 522, 735089. doi: 10.1016/j.aquaculture.2020.735089

Jensen, D. B., Hogeveen, H., and De Vries, A. (2016). Bayesian integration of sensor information and a multivariate dynamic linear model for prediction of dairy cow mastitis. *J. Dairy Sci.* 99, 7344–7361. doi: 10.3168/jds.2015-10060

Kaler, J., and Ruston, A. (2019). Technology adoption on farms: Using Normalisation Process Theory to understand sheep farmers' attitudes and behaviours in relation to using precision technology in flock management. *Prev. Vet. Med.* 170, 104715. doi: 10.1016/j.prevetmed.2019.104715

Kopler, I., Marchaim, U., Tikász, I. E., Opaliński, S., Kokin, E., Mallinger, K., et al. (2023). Farmers' Perspectives of the benefits and risks in precision livestock farming in the EU pig and poultry sectors. *Animals* 13, 2868. doi: 10.3390/ani13182868

Lecomte, J. B., and Laplanche, C. (2012). A length-based hierarchical model of brown trout (*Salmo trutta fario*) growth and production. *Biom. J.* 54, 108–126. doi: 10.1002/bimj.201100083

Merca, C., Boerlage, A. S., Kristensen, A. R., and Jensen, D. B. (2024). Monitoring monthly mortality of maricultured Atlantic salmon (*Salmo salar* L.) in Scotland I. Dynamic linear models at production cycle level. *Front. Mar. Sci.* 11. doi: 10.3389/fmars.2024.1436755

Munro, L. A. (2023). *Scottish fish farm production survey 2022* (Edinburgh: Scottish Government). Available online at: https://www.gov.scot/publications/scottish-fish-farm-production-survey-2022/pages/5/ (Accessed February 5, 2024).

Murray, A., Falconer, L., Clarke, D., and Kennerley, A. (2022). Climate change impacts on marine aquaculture relevant to the UK and Ireland. *MCCIP Sci. Rev.* 2022, 18. doi: 10.14465/2022.reu01.aqu

Noble, C., Gismervik, K., Iversen, M. H., Kolarevic, J., Nilsson, J., Stien, L. H., et al. (2018). *Welfare Indicators for farmed Atlantic salmon: tools for assessing fish welfare*. Available online at: www.nofima.no/fishwell/english (Accessed February 24, 2023).

Oldham, T., Rodger, H., and Nowak, B. F. (2016). Incidence and distribution of amoebic gill disease (AGD) - An epidemiological review. *Aquaculture* 457, 35–42. doi: 10.1016/j.aquaculture.2016.02.013

Posit team (2022). *RStudio: Integrated Development for R* (Boston, MA: RStudio, PBC). Available at: http://www.rstudio.com/.

R Core Team (2022). *R: A language and environment for statistical computing* (Vienna, Austria: R Foundation for Statistical Computing). Available at: https://www.R-project.org/.

Rustas, B. O., Persson, Y., Ternman, E., Kristensen, A. R., Stygar, A. H., and Emanuelson, U. (2024). The evolutionary operation framework as a tool for herd-specific control of mastitis in dairy cows. *Livestock Sci.* 279, 105390. doi: 10.1016/j.livsci.2023.105390

Scheuerell, M. D., Buhle, E. R., Semmens, B. X., Ford, M. J., Cooney, T., and Carmichael, R. W. (2015). Analyzing large-scale conservation interventions with Bayesian hierarchical models: A case study of supplementing threatened Pacific salmon. *Ecol. Evol.* 5, 2115–2125. doi: 10.1002/ece3.1509

Skjølstrup, N. K., Lastein, D. B., de Knegt, L. V., and Kristensen, A. R. (2022). Using state space models to monitor and estimate the effects of interventions on treatment risk and milk yield in dairy farms. *J. Dairy Sci.* 105, 5870–5892. doi: 10.3168/jds.2021-21408

Sommerset, I., Wiik-Nielsen, J., Moldal, T., Henrique Silva de Oliveira, V., Christine Svendsen, J., Haukaas, A., et al. (2024). Fiskehelserapporten 2023. Available online at: https://www.vetinst.no/rapporter-og-publikasjoner/rapporter/2024/fiskehelserapporten-2023 (Accessed May 27, 2024). Veterinærinstituttet rapportserie nr 8a/2024.

Stebbins, E., Bence, J. R., Brenden, T. O., and Hansen, M. J. (2024). A hierarchical model of persistent and transient growth variation applied to Lake Superior lake trout. *Fish. Res.* 278, 107081. doi: 10.1016/j.fishres.2024.107081

Stygar, A. H., Krogh, M. A., Kristensen, T., Østergaard, S., and Kristensen, A. R. (2017). Multivariate dynamic linear models for estimating the effect of experimental interventions in an evolutionary operations setup in dairy herds. *J. Dairy Sci.* 100, 5758–5773. doi: 10.3168/jds.2016-12251

Torrissen, O., Olsen, R. E., Toresen, R., Hemre, G. I., Tacon, A. G. J., Asche, F., et al. (2011). Atlantic salmon (*Salmo salar*): the "Super-chicken" of the sea? *Rev. Fisheries Sci.* 19, 257–278. doi: 10.1080/10641262.2011.597890

West, M., and Harrison, J. (1997). *Bayesian Forecasting and Dynamic Models. 2nd Edn* (New York: Springer).

frontiers | Frontiers in Marine Science

TYPE Original Research
PUBLISHED 04 November 2024
DOI 10.3389/fmars.2024.1481047

OPEN ACCESS

EDITED BY
Ida Grong Aursand,
SINTEF Ocean, Norway

REVIEWED BY
Zhangli Hu,
Shenzhen University, China
Huan Wang,
Ningbo University, China

*CORRESPONDENCE
Ting Xue
xueting@fjnu.edu.cn
Gang Lin
lgffz@fjnu.edu.cn

†These authors have contributed equally to this work

RECEIVED 15 August 2024
ACCEPTED 07 October 2024
PUBLISHED 04 November 2024

CITATION
Chen D, Zheng Z, Zhou Z, Song Y, Chen Z, Lin G and Xue T (2024) Application of metabolomics approach to investigate the flavor substance differences between triploid and diploid oysters (*Crassostrea angulata*). *Front. Mar. Sci.* 11:1481047. doi: 10.3389/fmars.2024.1481047

Application of metabolomics approach to investigate the flavor substance differences between triploid and diploid oysters (*Crassostrea angulata*)

Duo Chen[1†], Zewen Zheng[1†], Ziquan Zhou[1], Yuxin Song[1], Zhi Chen[2], Gang Lin[1*] and Ting Xue[1*]

[1]Fujian Key Laboratory of Special Marine Bioresource Sustainable Utilization, The Public Service Platform for Industrialization Development Technology of Marine Biological Medicine and Products of the Department of Natural Resources, Fujian Normal University, Fuzhou, China, [2]Aquatic Animal Nutrition Research Laboratory, Fujian Institute of Freshwater Fisheries, Freshwater Fisheries Research Institute of Fujian, Fuzhou, China

Oysters, particularly Portuguese oyster (*Crassostrea angulata*), are highly valued for their nutritional and flavor qualities, making them important in global aquaculture. Triploid oysters have gained attention for maintaining higher meat quality year-round compared to diploids, but there is limited research on how ploidy affects their biochemical and flavor profiles. This study uses a non-targeted metabolomics approach, including gas chromatography-mass spectrometry (GC-MS) and liquid chromatography-mass spectrometry (LC-MS), to investigate flavor substance differences between triploid and diploid *C. angulata*. A total of 13 volatile compounds were identified in diploid oysters, while 28 were found in triploids. Significant upregulation of inosine, guanosine, L-aspartic acid, and taurine in triploids contributes to their enhanced flavor profile. Additionally, triploids showed higher nicotinamide concentrations, while diploids had increased 25-hydroxycholesterol. These findings highlight the advantages of triploid oysters in aquaculture for improved flavor and nutrition, supporting their potential for year-round production.

KEYWORDS

***Crassostrea angulata*, flavor substance, triploid, diploid, metabolomics**

1 Introduction

Oysters (*Mollusca, Bivalve*), are the most extensively cultured marine shellfish globally (Teng et al., 2022). Renowned for their superb nutritional value and distinctive flavor, they are highly prized by consumers and are often referred to as the "milk of the ocean" (Yuasa et al., 2018). In Europe, there is a well-known adage: "Avoid oysters in months without an 'R'."

This saying stems from the seasonal nature of diploid oysters' reproduction. From May to August each year, these oysters spawn, leading to a decrease in meat quality and flavor due to the release of gametes, which can diminish the consumer's eating experience. To address this issue, the aquaculture industry has begun introducing triploid oysters. These oysters, being sterile, do not undergo gonad development, thus conserving energy that would otherwise be expended during this process. This energy conservation results in enhanced meat quality, offering a promising solution to maintaining year-round oyster consumption without compromising taste (Villanueva-Fonseca et al., 2017; Qin et al., 2018).

In recent years, a significant amount of research has focused on the crossbreeding of oysters, resulting in the production of triploid oysters that exhibit superior traits. These studies have explored both intraspecific and interspecific hybridizations, such as the crossbreeding of *C.gigas* with diploid oysters and the combination of tetraploid *C. gigas* with diploid *C.ariakensis* and *C.angulate* (Que and Allen, 2002; Jiang et al., 2022; Li et al., 2022a). The resultant triploid offspring display characteristics inherited from both parent strains. Additionally, triploid oysters offer several advantages including rapid growth, larger size, lower mortality rates during the breeding season, and greater meat yield. For instance, triploid oysters grew 88% to 190% faster than their diploid counterparts (Guo et al., 2008). Similarly, the soft tissue weight (TWR) and condition index (CI) were significantly higher in triploid oysters (Park and Choi, 2022). The edible components of oysters typically include the gonadal gland, hepatopancreas, gills, and adductor muscle. Based on our unpublished data, there are notable differences in the proportions of these tissues between different ploidies; for example, the gonadal gland, hepatopancreas, gills, and adductor muscle make up 28.08%, 4.34%, 11.05%, and 10.43% of triploid oysters respectively, compared to 31.94%, 12.98%, 10.29%, and 8.24% in diploids. These variations in tissue structure and nutritional composition are especially pronounced in the gonads. Triploid oysters also show distinct differences in cellular and tissue morphology compared to diploids. For instance, the internal structure of gill filaments, mitochondrial diameter, and muscle fibers are more developed in triploids (Kong et al., 2003; Dong et al., 2023). Studies of the gonads have revealed that triploid oysters possess smaller follicles and more abundant connective tissues, and their gonads do not undergo significant changes during the breeding season, remaining in a state of diapause (Wang et al., 2021). These structural and nutritional differences likely contribute to the varied flavors between triploid and diploid oysters, underscoring the importance of differentiating the taste profiles of various oyster tissues to better understand the underlying causes of flavor discrepancies in oysters of different ploidies.

In the quest to evaluate the quality of oysters varying in ploidy, the triploid Hong Kong oysters exhibit significantly higher levels of glycogen and n-3/n-6 polyunsaturated fatty acids (PUFAs) compared to their diploid counterparts (Qin et al., 2018). Beyond these nutrients, flavor compounds also play an important role in the sensory and quality characteristics of oysters. Fresh oysters have a unique taste and aroma, which greatly influence consumer choices. Therefore, studying the flavor characteristics of oysters is of great significance for the development of the oyster industry. Flavor is a comprehensive concept that encompasses multiple sensory experiences, including taste and aroma. Taste is caused by non-volatile compounds (Khan et al., 2015), such as free amino acids, which are important taste substances and can produce flavors such as umami, sweetness, and bitterness (Meng et al., 2022). Aroma, on the other hand, is closely related to volatile compounds. In meat products, most of these are non-contributory or low-contributory aroma compounds, with only a small portion of volatile compounds affecting the overall aroma of the meat, known as key aroma compounds (Sohail et al., 2022). These flavor substances are produced through various chemical reactions, such as lipid oxidation, Strecker degradation, and the Maillard reaction, and include free amino acids, 5'-nucleotides, aldehydes, alcohols, and ketones (Wu et al., 2022). It has been reported that the free amino acids present in oysters directly influence taste; for example, Glu is crucial for umami, while Gly and Ala affect sweetness (Liu et al., 2021). 5'-nucleotides like AMP, GMP, and IMP are the most important components that contribute to umami (Liu et al., 2022). In terms of aroma, aldehydes, ketones, and alcohols are the most prominent volatile flavor compounds in oysters (Liu et al., 2023). Currently, the majority of flavor research focuses on how different strains, cultivation regions, and harvesting seasons affect the volatile profiles of oysters (Huang et al., 2019; Chen et al., 2024). Although there have been investigations into the flavor components of oysters with different ploidies, these studies have generally concentrated on the whole meat (Fu et al., 2023; Sun et al., 2023). However, the nutrient distribution in oysters varies not only by ploidy but also across different body parts (Li et al., 2022b), suggesting that volatile flavor compounds may also be distributed unevenly within the oyster's tissues.

In recent years, with the continuous development of metabolomics, metabolomic tools have been widely used in the identification and analysis of key substances in food (Utpott et al., 2022). By comprehensively analyzing the metabolites in food, these tools can accurately identify and quantify important biomolecules, helping to reveal critical information about the nutritional value, flavor components, and safety of the food. Headspace Solid-Phase Microextraction combined with Gas Chromatography-Mass Spectrometry (HS-SPME-GC-MS) is a precise method for enriching and analyzing volatile or semi-volatile compounds in food (Jeleń et al., 2012). This technique not only allows for the identification, qualitative, and quantitative analysis of complex mixtures, but it also offers advantages such as speed and high accuracy. LC-MS technology is widely applied in food flavor analysis (Zhong et al., 2022). It can accurately separate and identify flavor compounds within complex matrices, particularly those that are non-volatile, highly polar, and thermally unstable. Both of these techniques are powerful means for exploring food flavors. For example, techniques such as HS-SPME-GC-MS and LC-MS have been used to characterize the structure, flavor, and texture of grass carp fed with broad beans (Fu et al., 2024). HS-SPME-GC-MS and metabolomics analysis methods have been employed to explore the flavor compounds related to odor deterioration in tilapia during refrigeration (Cheng et al., 2023). Therefore, metabolomic analysis are powerful tools for the comprehensive study of both non-volatile and volatile compounds in meat products. However, to our knowledge,

few studies have used metabolomics to investigate the differences in flavor components between different ploidy levels of oysters and among their different tissues.

This study compares and evaluates the flavor profiles of different tissues in diploid and triploid oysters, based on metabolomics technology using LC-ESI-MS/MS and volatile analysis using HS-SPME-GC-MS. The findings are expected to provide fresh insights into the flavor characteristics of oysters based on ploidy and tissue type, which will be valuable for the future development and sustainability of oyster products.

2 Materials and methods

2.1 Formation of the triploid oyster

The triploid samples used in the experiment were collected from the raft-cultured population in Fuqing Sea. This population's seedlings were purchased from Qingdao Frontier Marine Seed Industry Co., Ltd. The triploids were bred by crossing tetraploid male *C. angulata* with diploid female *C. angulata*. The tetraploid male *C. angulata* parents originated from the sea area of Xiuyu District, Putian City, and were part of a tetraploid self-breeding population derived from diploid *C. angulata* through seed production. The diploid female *C. angulata* were sourced from the same sea area's cultured population. The diploid samples used in the experiment were also collected from the raft-cultured population in Fuqing Sea, where both diploid and triploid *C. angulata* are cultured.

2.2 Sample preparation and extraction

Samples of *C. angulata* were collected from the Fuqing Sea (119.5797346 E, 25.3601630 N) (Figure 1). The collection took place on April 7, 2023. The oyster soft parts were cleaned with sterilized seawater after removing the right shell by using a dissecting knife close to the inner surface of the shell and severing the adductor muscle. The cleaned oysters were placed on an ice box, the mantle was lifted and the gills were removed first, then the mantle tissue (the mantle-gonadal junction portion) was carefully peeled off to remove the white gonad, followed by the darker hepatopancreas, and lastly the adductor muscle. From both the triploid and diploid oysters, samples of four different tissues were obtained: the adductor muscle (AM), gonadal gland (GG), hepatopancreas (H), and gills (G). These samples were immediately frozen in liquid nitrogen at the collection site and subsequently stored at -80°C for preservation. (n=3) Samples were freeze-dried, and metabolite content was calculated by unit dry weight. Samples were then finely ground in the presence of liquid nitrogen to preserve integrity. Subsequently, a 400 µL mixture of methanol and water in a 7:3 volume ratio, containing an internal standard, was added to approximately 20 mg of the ground sample. The mixture was vigorously shaken at 1000×*g* for 5 min to ensure thorough mixing. After shaking, the sample was allowed to cool on ice for 15 min to stabilize before being centrifuged at 4800×*g* for 10 min at a temperature of 4°C. Take 300 µL of the clear supernatant and store it at -20°C for 30 min to further concentrate the volatile compounds. Following this brief storage, the sample underwent a second centrifugation under the same conditions (4800×*g* at 4°C) but for a shorter period of 3 min. From this, 200 µL aliquots of the supernatant were carefully extracted and prepared for subsequent liquid chromatography-mass spectrometry (LC-MS) analysis, facilitating detailed biochemical profiling.

2.3 Metabolomic analysis

Samples were freeze-dried, and metabolite content was calculated by unit dry weight. The samples were packed into a

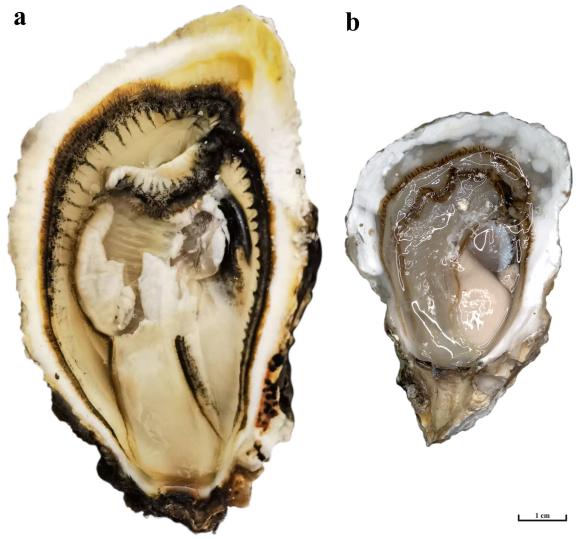

FIGURE 1
Triploid and Diploid of *C. angulata*. **(A)** Triploid of *C. angulata;* **(B)** Diploid of *C. angulata*.

solid-phase microextraction headspace bottle and extracted by magnetic stirring for 30 min. After the extraction was completed, the extraction head was quickly inserted into the sample inlet and thermal desorption was performed at 250°C for 4 min. The volatile flavor components were analyzed by GC-MS, and the relative content of flavor components in oyster tissues was calculated by peak area normalization method. Combined with the sensory thresholds of each volatile flavor substance in water, rOAV method was used to evaluate the contribution of each compound to the main tissue flavor of Portuguese oyster. All volatile flavor substances should meet $0 \leq rOAV \leq 100$, and the greater the rOAV, the greater the contribution of the substance to flavor (Bi et al., 2022; Su et al., 2022).

The sample extracts were analyzed using a sophisticated LC-ESI-MS/MS setup under the following conditions: Ultra-Performance Liquid Chromatography (UPLC) was carried out using a Waters ACQUITY UPLC HSS T3 C18 column (1.8 μm, 2.1 mm x 100 mm), maintained at a column temperature of 40°C. The flow rate was set at 0.4 mL/min with an injection volume of 2μL. The solvent system comprised water and acetonitrile, both containing 0.1% formic acid, applied in a gradient as follows: starting at 95:5 (v/v) at 0 min, shifting to 10:90 (v/v) from 11.0 min to 12.0 min, returning to 95:5 (v/v) at 12.1 min and holding until 14.0 min. Mass spectrometric analysis was performed on a QTRAP® LC-MS/MS System equipped with a triple quadrupole-linear ion trap (QTRAP) and an ESI Turbo Ion-Spray interface. This system operated in both positive and negative ion modes. Throughout the analysis, specific Multiple Reaction Monitoring (MRM) transitions were closely monitored to track the metabolites as they eluted.

2.4 Data processing and statistical analysis

Principal Component Analysis (PCA) and Hierarchical Cluster Analysis (HCA) were conducted using R (version 4.2.0). For PCA, data was scaled to unit variance using the prcomp function, while HCA results, alongside Pearson Correlation Coefficients (PCC) between samples, were visualized as heatmaps (with dendrograms for HCA) using the ComplexHeatmap package. Differential metabolites for two-group comparisons were identified using Variable Importance in Projection (VIP) scores and P-values (VIP > 1 and P-value < 0.05 from Student's t-test), derived from Orthogonal Projections to Latent Structures-Discriminant Analysis (OPLS-DA). The OPLS-DA, which included score plots and permutation plots to prevent overfitting (200 permutations), was performed after log transformation and mean centering of data using the MetaboAnalystR package. Metabolite annotation and pathway enrichment were executed through the KEGG databases. Identified metabolites were annotated using the KEGG Compound database and mapped onto the KEGG Pathway database. Significant pathways were analyzed using Metabolite Set Enrichment Analysis (MSEA), with significance assessed by hypergeometric test's p-values.

3 Results

3.1 Principal component analysis of the metabolites in oysters

PCA revealed clear metabolomic differentiation between triploid and diploid oysters. The PCA score chart demonstrated distinct clusters, indicating significant differences in metabolite profiles between the two groups (Figures 2B, C).

3.2 Cluster analysis of the metabolites in oysters

Hierarchical clustering was performed to analyze differences in metabolite expression between triploid and diploid oysters. The resulting heatmap highlighted significant metabolite expression differences across tissues, particularly in the gonadal gland and hepatopancreas (Figures 2D, 3).

3.3 Orthogonal projections of latent structures-discriminant analysis

The S-plot from the OPLS-DA analysis uses the horizontal axis to represent the covariance and the vertical axis to show the correlation between principal components and metabolites (Figure 3). Metabolites positioned near the upper right and lower left corners of the plot are indicative of more significant differences (Figures 3A–D).

3.4 Identification of the volatile metabolites in oysters by GC-MS

A total of 13 volatile compounds, including aldehydes (5), ketones (4), alcohols (2) and others (2) were identified in 4 tissues of diploid Portuguese oysters, while 28 volatile compounds, including aldehydes (11), ketones (5), alcohols (3) and others (9) were identified in 4 tissues of triploid Portuguese oysters (Figure 4; Supplementary Table 1). Compared with the diploid oysters, the number of volatile substances in the 4 tissues of triploid oysters was significantly increased, especially the number of aldehydes in the adductor muscle and gills of diploid and triploid Portuguese oysters was significantly different. Therefore, changes in oyster ploidy also lead to changes in the composition of volatile components. The main volatile components in the gills and gonads of diploid and triploid Portuguese oysters are aldehydes, while the main volatile components in the hepatopancreas are alcohols (Figure 2). The main volatile components in the closed shell muscle of diploid Portuguese oysters were alcohols, while those in the closed shell muscle of triploid Portuguese oysters were aldehydes. In addition, the levels of other classes in the closed shell muscle of triploid oysters were higher than that of diploid oysters, the levels of ketones and

10.3389/fmars.2024.1481047

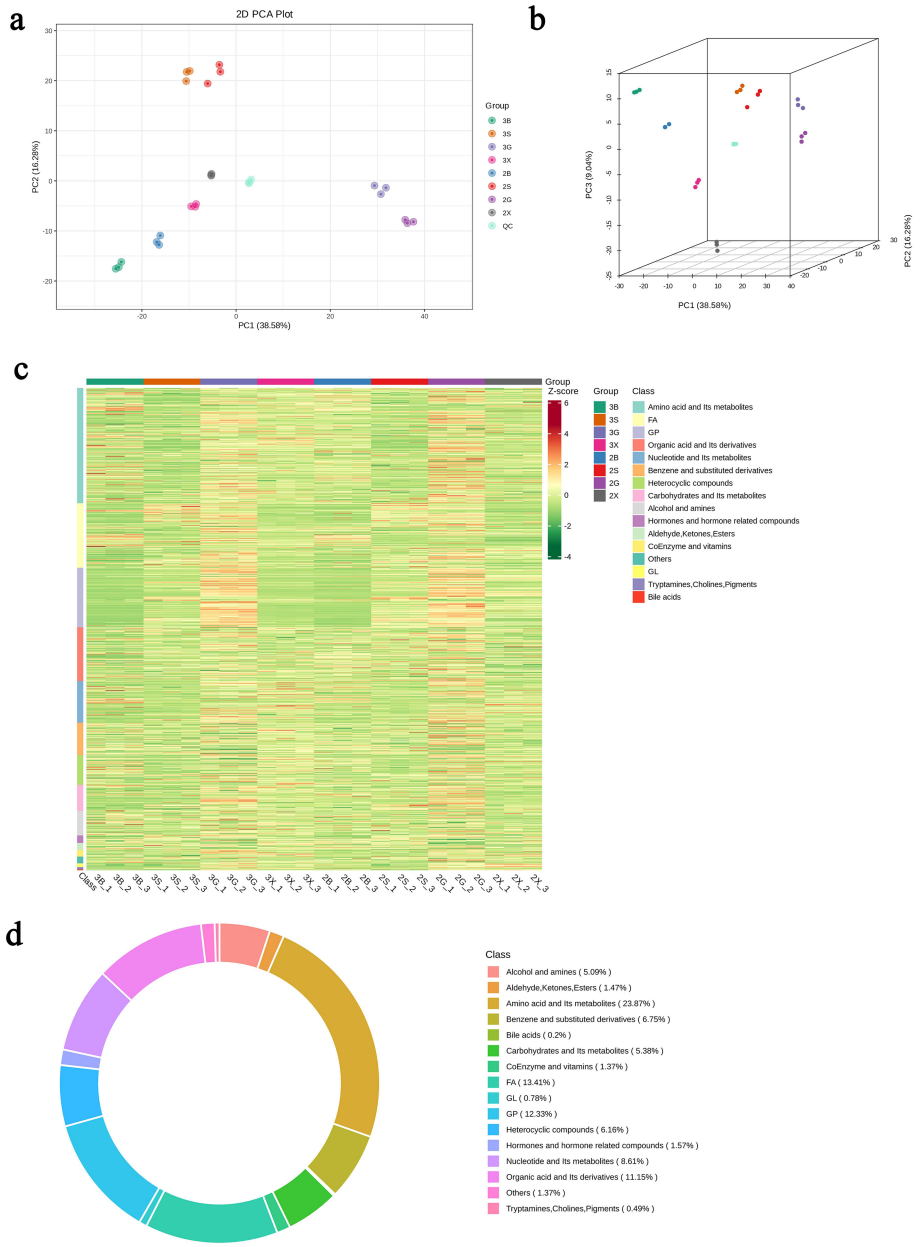

FIGURE 2
Identification of metabolites in triploid and diploid *C. angulata*. **(A)** Principal Component Analysis (PCA) plot in 2D showing clear metabolomic differentiation; **(B)** PCA plot in 3D showing separation of metabolites; **(C)** Heatmap visualization of all metabolite classes; **(D)** Circular graph representing the proportions of different metabolite classes.

alcohols in the gills of triploid oysters were also higher than that of diploid oysters, and the levels of other classes in the gonads of diploid oysters were higher than that of diploid oysters. These results indicated that the tissue flavor distribution of oysters with different ploidy levels was different.

3.5 Identifies key volatile metabolites in oysters by rOAV

rOAV represents the contribution of a compound to the overall odor, and compounds with rOAV> 1 are generally considered as odorant-active compounds, and the greater the rOAV, the greater the contribution of the substance to flavor. According to the results of GC-MS analysis, the most important odor compounds are aldehydes (10), ketones (5), and alcohols (2). 1-Octen-3-ol and (E,Z)-2, 6-nonadienal contribute major odors to the cleistor muscles of diploid and triploid oysters, respectively. 1-Octen-3-ol contributes the main odor in diploid and triploid oyster hepatopancreas. Interestingly, we found that ketones are important volatile components in diploid and triploid oyster hepatopancreas, which may be related to the special function of oyster hepatopancreas. (E,Z)-2, 6-nonadienal contributes major odors in the gills and gonads of diploid and triploid oysters. In addition, it was found that Octanal identified in the gills of triploid

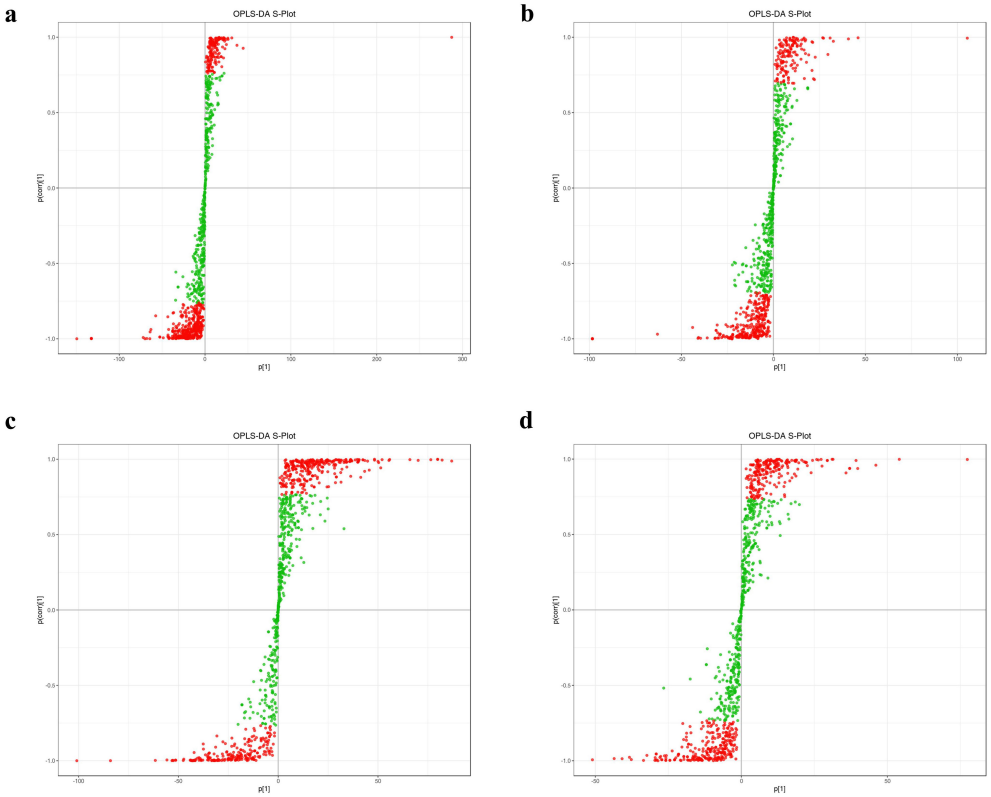

FIGURE 3
S-plot from the OPLS-DA analysis for triploid and diploid *C. angulata*. **(A)** S-plot for 3AM vs. 2AM; **(B)** S-plot for 3H vs. 2H; **(C)** S-plot for 3G vs. 2G; **(D)** S-plot for 3GG vs. 2GG.;

oysters had a higher rOVA. These volatile compounds made the triploid oysters more pleasant odor, thereby improving the quality. The adductor muscle, gills and gonads of triploid Portuguese oysters showed more obvious pleasant aroma than those of diploid oysters. Among them, the green, fruit and cucumber fragrance can be described as the aroma characteristics of triploid oysters, which leads to triploid oysters having a stronger aroma than diploid oysters (Table 1).

3.6 Identification of the metabolites in oysters by LC-ESI-MS/MS

Using a local metabolic database, metabolites in the samples were analyzed both qualitatively and quantitatively through mass spectrometry. In total, 1022 metabolites were identified, encompassing a diverse array of biochemical classes: 244 types of amino acid and its metabolites, 69 types of benzene and substituted derivatives, 52 types of alcohol and amines, 2 types of bile acids, 14 types of coEnzyme and vitamins, 126 types of glycerophospholipids, 8 types of glycerolipid, 88 types of nucleotide and Its metabolites, 16 types of hormones and hormone related compounds, 15 types of aldehyde, ketones and esters, 5 types of tryptamines, cholines, and pigments, 55 types of carbohydrates and Its metabolites, 114 types of organic acid and its derivatives (Figure 2A).

3.7 Screening and correlation of differential metabolites

Our findings showed key upregulations and downregulations across tissues. For instance, in comparisons such as 3GG to 3H, 3GG to 3AM, and 3GG to 3G, 160, 416, and 330 metabolites were upregulated, while downregulations reached 430, 144, and 182. Notably, nucleotides and amino acids, crucial for flavor enhancement, were predominantly upregulated in the GG tissue (Supplementary Tables 2–6). Additionally, relationships among these differential metabolites across groups were visualized using a Venn diagram (Figure 3), illustrating both common and unique metabolites in each group. The total number of distinct metabolites identified across all groups was 111. We also generated a heatmap to illustrate the differences in metabolite levels between triploid and diploid oysters, particularly in the GG tissue (Figure 5). This visualization highlights significant differences in metabolite regulation between the groups. For instance, in the comparison 3GG vs. 2GG, while the GP metabolite in 2GG shows up-regulation, most other metabolites are up-regulated in 3GG. Pearson correlation analysis was conducted to assess the relationships between these metabolites (Figure 6). In the figure, the intensity of the color correlates with the magnitude of the correlation coefficient, as detailed in the legend. This comprehensive mapping includes all identified differential metabolites, but for

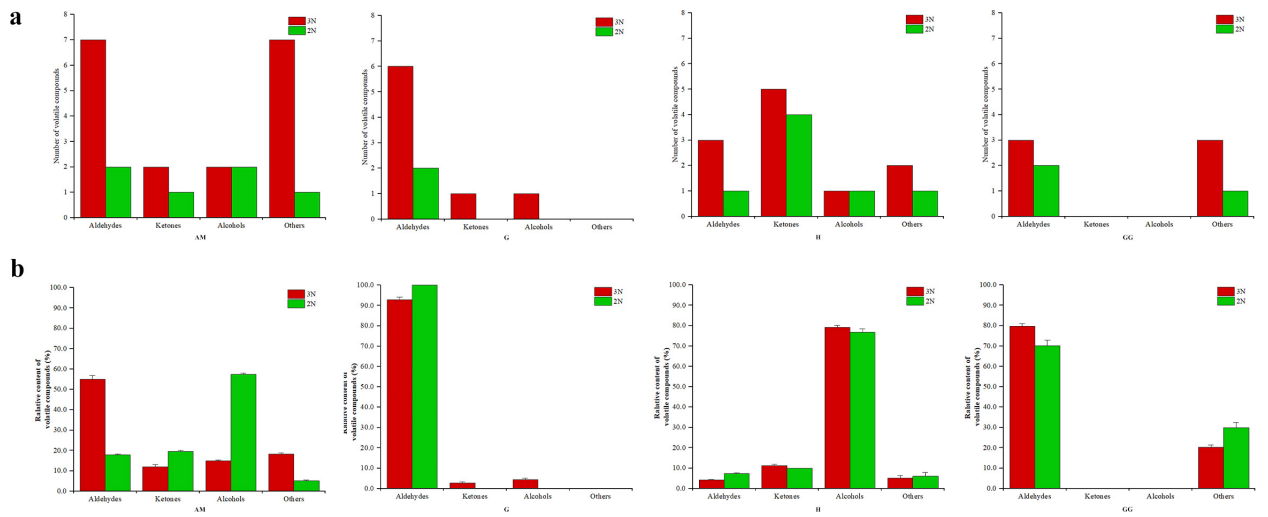

FIGURE 4
Number and relative content of volatile compounds in triploid (3N) and diploid (2N) *C. angulata* across different tissues. **(A)** Number of volatile compounds in each tissue; **(B)** Relative content of volatile compounds (percentage) in each tissue.

TABLE 1 rOAV for volatile aroma compounds in different tissues of *C. angulata*.

Compound	T_i (mg/kg)[A]	rOAV								Odor Description[B]
		AM		G		H		GG		
		3N	2N	3N	2N	3N	2N	3N	2N	
Hexanal	0.21	–	–	<0.1	–	–	–	–	–	green, grass, fruity
Heptanal	0.005	0.36	–	–	–	–	–	–	–	fatty, green, heavy, oily, planty green, putty
Octanal	0.0001	–	–	23.26	–	–	–	–	–	orange, green, herbal
Benzeneacetaldehyde	0.009	–	–	–	–	–	7.49	–	–	sweet, honey, floral
(E)-2-Octenal	0.061	–	–	<0.1	<0.1	–	–	<0.1	<0.1	green, herbal, banana
Nonanal	0.0035	2.29	55.17	0.2	–	4.22	–	–	–	citrus, fatty, floral, green,soapy
(E,Z)-2,6-Nonadienal	0.0001	100	–	100	100	–	–	100	100	cucumber, green, cucumber peel
(E)- 2-Nonenal	0.0001	–	–	–	–	–	–	54.21	–	cucumber, fatty, green
Decanal	0.007	1.31	43.68	–	–	2.02	–	–	–	fatty, floral, orange peel, soapy, wax
(E)-2-Decenal	0.001	1.21	–	0.67	–	8.84	–	–	–	fatty, green
2-Nonanone	0.05	–	–	–	–	0.51	–	–	–	blue cheese, fatty, fruity, green, ketone, musty
2-Undecanone	0.01	0.43	54.20	<0.1	–	1.74	2.18	–	–	dusty, floral, fruity, rose,green, ketone, musty
α-Ionone	0.02	–	–	–	–	1.40	1.29	–	–	wood, violet
Geranyl acetone	0.01	0.37	–	–	–	0.83	1.91	–	–	rose, floral, green, fruity
β-Ionone	0.005	–	–	–	–	4.12	4.70	–	–	woody, floral, sweet, fruity
1-Octen-3-ol	0.007	1.08	100	–	–	100	100	–	–	fatty, fruity, grass, mushroom, perfumy, sweet
(E,Z)-3,6-Nonadien-1-ol	0.01	–	–	<0.1	–	–	–	–	–	cucumber, melon rind

[A]T*i*, odor threshold: the data from compilations of odor threshold values in air, water, and other media (second enlarged and revised edition). Beijing: Science Press. 2018.
[B]Odor descriptions adapted from (Ma et al., 2021).

visual clarity, only the top 50 metabolites with the highest VIP values are shown.

3.8 The differential metabolites on the taste and nutritional content of diploid and triploid oysters

3.8.1 Lipids and their derivatives

We identified a comprehensive array of lipids and their derivatives, encompassing 281 total lipids, 137 distinct lipid types, 126 glycerophospholipids, and 8 glycerolipids (Supplementary Table 3). Our analysis revealed significant upregulation in differential metabolites between triploid and diploid oysters, with notable increases in 3GG to 2GG, 3H to 2H, 3AM to 2AM, and 3G to 2G by 23, 62, 23, and 17 units respectively (Supplementary Tables 4–7). A key compound identified was N-Arachidonoyl-L-Alanine, an endocannabinoid analogue known for its potential anti-cancer properties. Compared with diploid oysters, triploid oysters had significantly higher content of N-Arachidonoyl-L-Alanine in 4 parts. It is highly present in the gonadal gland, gill and hepatopancreas of the triploid oyster and almost absent in the gonadal gland of the diploid oyster, which had a good effect on flavor and nutrition (Figure 7A). oxidized lipids such as (±)5-HETE, Prostaglandin F2α, and acylcarnitines like Carnitine C7-OH and LPC (O-20:3) were detected at higher levels in triploid oysters (Figures 7B–G)

3.8.2 Nucleosides and their derivatives

We identified 88 types of nucleosides, nucleotides, and their derivatives. Notable changes were observed when the fold change (FC) was either ≥ 1.5 or ≤ 0.50, with significant up-regulation noted in comparisons between triploid and diploid groups (3GG to 2GG, 3H to 2H, 3AM to 2AM, and 3G to 2G) with increases of 10, 8, 8, and 5 respectively. Among these, notable metabolites included

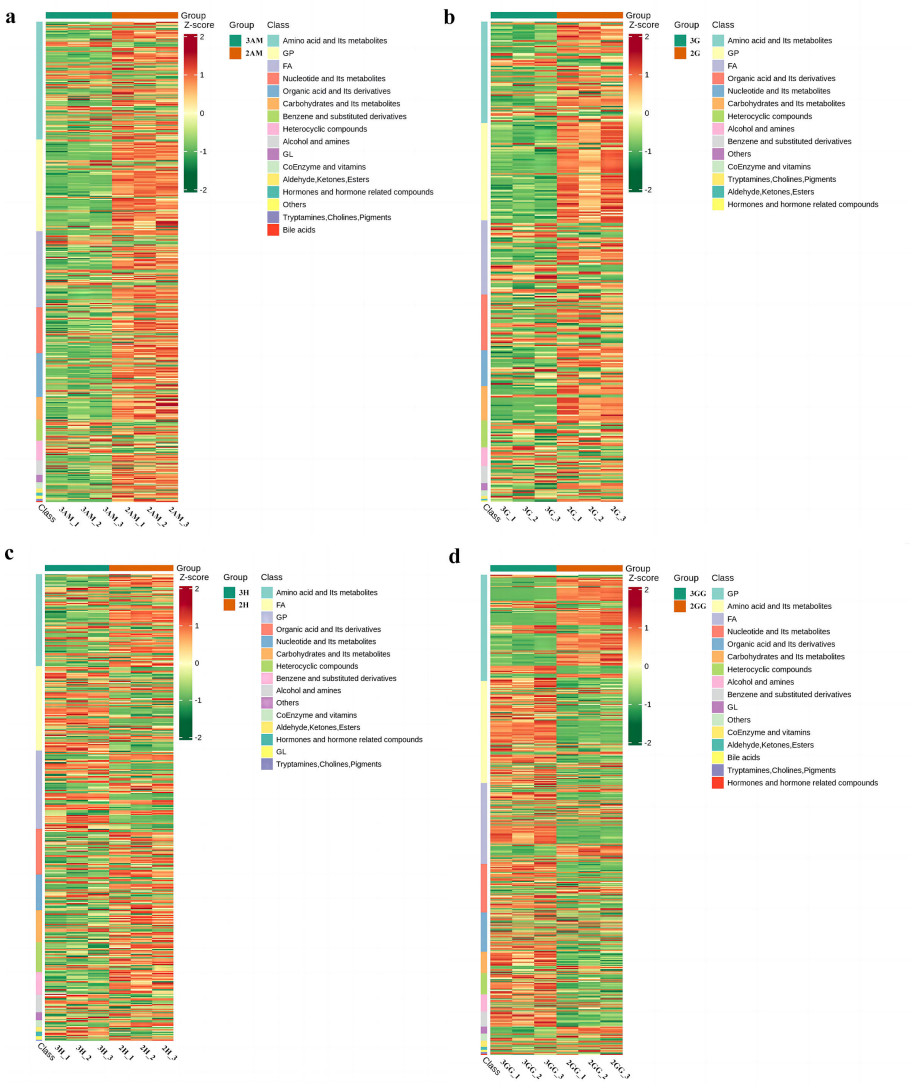

FIGURE 5
Heat map visualization of the metabolites of Triploid and Diploid of *C. angulata* samples in different parts. **(A)** Heat map visualization of The 3AM_vs_2AM; **(B)** Heat map visualization of The 3G_vs_2G; **(C)** Heat map visualization of 3H_vs_2H; **(D)** Heat map visualization of 3GG_vs_2GG.

10.3389/fmars.2024.1481047

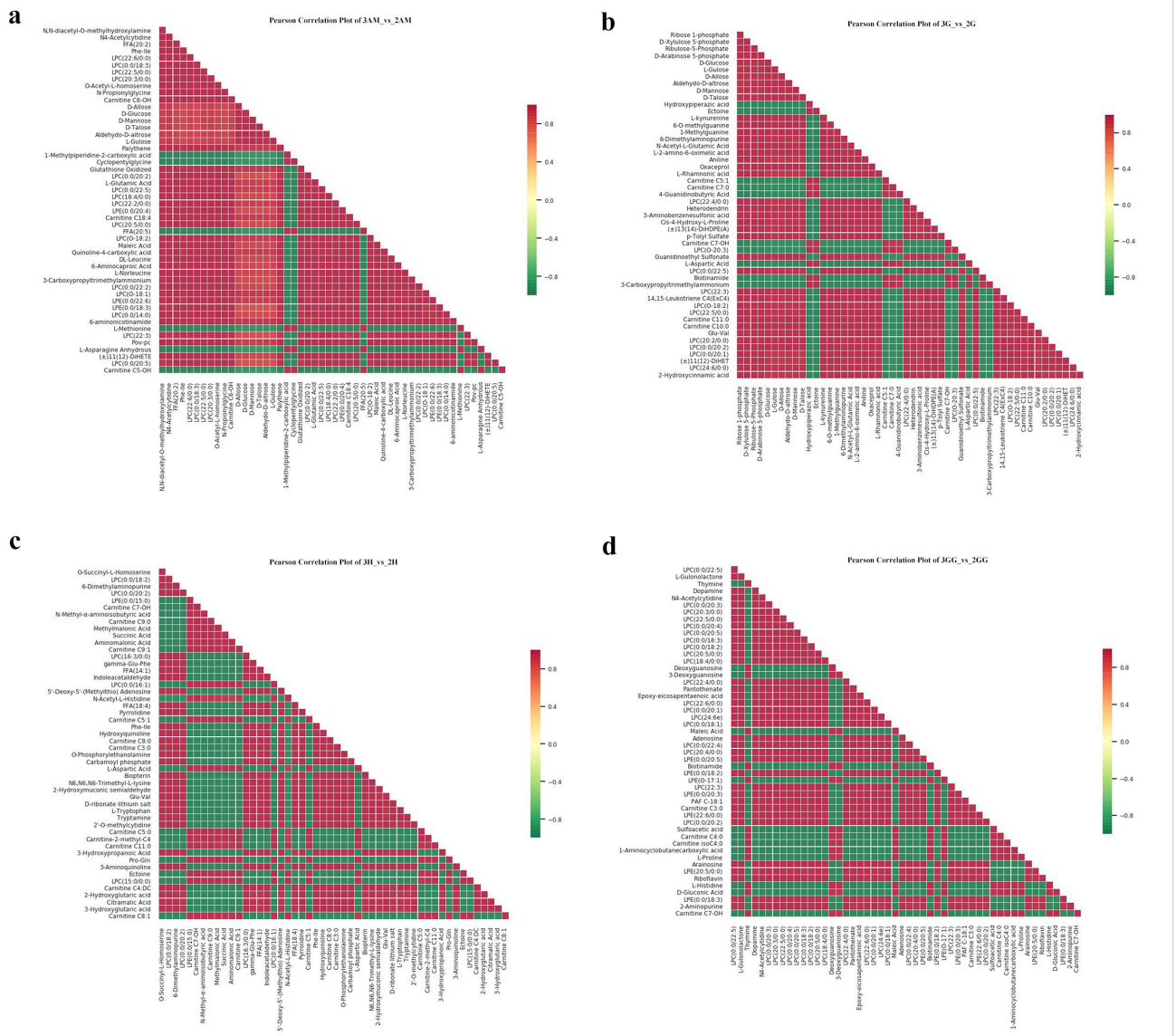

FIGURE 6
Correlation map of the metabolites for Triploid and Diploid *C. angulata* in different parts. **(A)** The 3AM_vs_2AM; **(B)** The 3G_vs_2G; **(C)** The 3H_vs_2H; **(D)**The 3GG_vs_2GG.

Deoxyguanosine, Methylguanosine, Methyluridine, Methylguanine, Thymine, Adenosine, and Inosine diphosphate (Supplementary Tables 4–7). Among these compounds, the relative contents of inosine (Figure 7H), guanosine (Figure 7I) inosine diphosphate (Figure 7K) deoxyguanosine (Figure 7L) and methylguanosine (Figure 7M) screened in the triploid group were significantly increased. The relative contents of adenosine (Figure 7J) and methylguanine (Figure 7N) screened in the driploid group were significantly increased.

3.8.3 Amino acids and their derivatives

We identified a diverse range of metabolites, including 244 types of amino acids and their derivatives. Significant variations were observed when the fold change (FC) was either greater than 1.5 or less than 0.5 Specifically, the increases in metabolite levels from triploid to diploid oysters were as follows: 3GG to 2GG by 11, 3H to 2H by 16, 3AM to 2AM by 29, and 3G to 2G by 16. These metabolites included a variety of amino acids such as L-Asparagine Anhydrous, L-Proline, Glutaconic acid (Supplementary Tables 4–7). The relative contents of glutaconic acid (Figure 7O), L-aspartic acid (Figure 7P), L-proline (Figure 7Q),L-serine (Figure 7R), L-threonine (Figure 7S), taurine (Figure 7T), 3-p-(pyrazol-1-yl)-L-alanine (Figure 7U) and cyclopentylglycine (Figure 7V) increased significantly in the most parts of triploid group.

3.8.4 Other small molecule substances

These represented 69 types of benzene and substituted derivatives, 52 types of alcohols and amines, 2 types of bile acids, 14 types of coenzymes and vitamins, 16 types of hormones and hormone-related compounds, 15 types of aldehydes, ketones, and esters, 5 types of tryptamines, cholines, and pigments, 55 types of

10.3389/fmars.2024.1481047

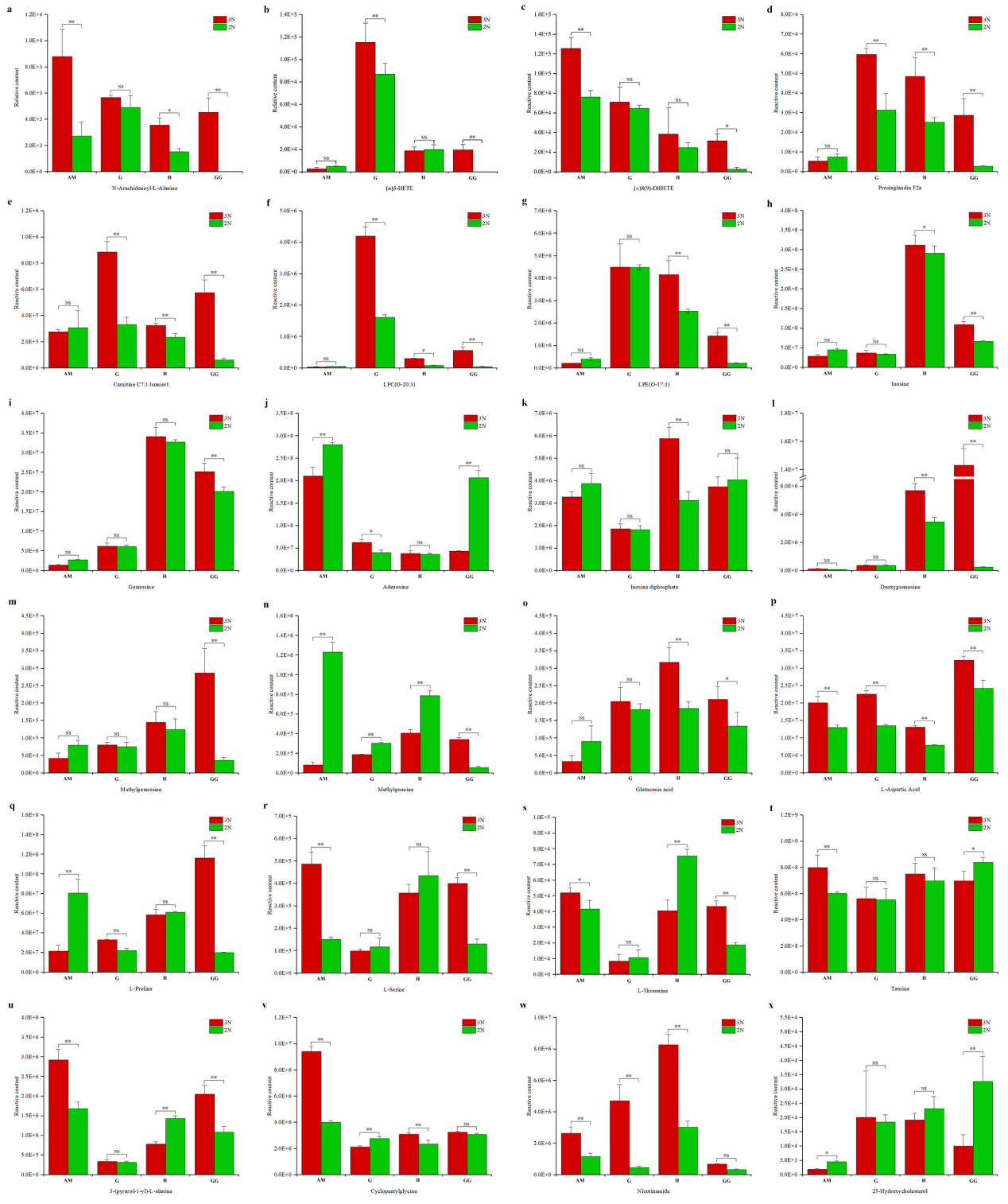

FIGURE 7
Comparison of metabolite concentrations between triploid (3N) and diploid (2N) oysters across various tissues (B: adductor muscle, G: gills, H: hepatopancreas, GG: gonadal gland). Significant differences in metabolite levels are marked with asterisks (*p < 0.05, **p < 0.01), and "NS" stands for "Not Significant". The compounds measured include **(A)** N-Arachidonoyl-L-Alanine, **(B)** (±)5-HETE, **(C)** Carnitine C7: OH, **(D)** Prostaglandin F2α, **(E)** Carnitine C7: Isooctyl, **(F)** LPC (O-20:3), **(G)** LPC (O-18:1), **(H)** Inosine, **(I)** Guanosine, **(J)** Adenosine, **(K)** Inosine diphosphate, **(L)** Deoxyguanosine, **(M)** Methylguanosine, **(N)** Methylguanine, **(O)** Glutaconic acid, **(P)** L-Aspartic acid, **(Q)** L-Proline, **(R)** L-Serine, **(S)** L-Threonine, **(T)** Taurine, **(U)** 3-p-(pyrazol-1-yl)-L-alanine, **(V)** Cyclopentylglycine, **(W)** Nicotinamide, and **(X)** 25-Hydroxycholesterol.

carbohydrates and their metabolites, 114 types of organic acids and their derivatives, 63 types of heterocyclic compounds, and 14 other substances (Supplementary Tables 3–6). Notably, the concentration of Nicotinamide was significantly higher in triploid oysters compared to diploid ones (Figure 7W). The relative contents of 25-Hydroxycholesterol increased significantly in the most parts of diploid group (Figure 7X). This compound is an intermediate in the primary bile acid biosynthesis pathway, where bile acids-steroid carboxylic acids are synthesized from cholesterol in vertebrates.

4 Discussion

Meat aroma is an important indicator of quality and influences consumer acceptance. Oysters can produce volatile compounds during the growth process that give them their own characteristic aroma. Therefore, different types of volatile compounds and their amounts result in food products carrying different aromas. In this study, the amount of volatile compounds in all four tissues of triploid oysters was higher than that of diploids. Aldehydes and alcohols are important volatile odors in volatile organic compounds, and the threshold of aldehydes is relatively low, which has a significant effect on the flavor of oysters (Zhang et al., 2009). Aldehydes are usually produced by oxidative degradation of polyunsaturated fatty acids. Short-chain aldehydes often have a "fresh, grass, green" smell, and as carbon atoms increase, they may give a strong "greasy and fatty" impression (Liu et al., 2023). The enaldehydes and dienaldehydes produced by the degradation of hydroperoxides of linoleate and linolenic acid esters usually have pleasant aromas, such as the creamy, cucumber and fatty aromas that give oyster characteristics (Aruna and Baskaran, 2010). The quantity and relative content of enal and dienal in the 4 tissues of triploid Portuguese oysters were more than those of diploid oysters. (E)-2-Decenal identified in the adductor muscle, hepatopancreas and gill of triploid oysters could produce grassy odor, while (E)-2-Nonenal unique in the gonads of triploid oysters could produce citrus and cucumber-like taste. In contrast, the threshold for alcohol compounds was relatively high, which did not significantly contribute to oyster flavor (Zhang et al., 2019). However, the threshold for unsaturated alcohols is relatively low, and these compounds contribute significantly to oyster flavor. Alcohols usually produce aromatic and vegetative aromas (Ma et al., 2021). Among them, 1-Octen-3-ol identified in both diploid and triploid oysters can produce a unique earthy and mushroom taste, while (E,Z)-3, 6-nonadien-1-ol identified separately in triploid oyster gills can produce a cucumber-like aroma.

Our study provides valuable insights into the distinct metabolic profiles of diploid and triploid oysters, focusing on lipids, nucleosides, amino acids, and other small molecules. One of the key findings was the significantly higher concentration of lipids and their derivatives in triploid oysters. We identified 281 lipids, including 126 glycerophospholipids, and observed that specific compounds such as N-Arachidonoyl-L-Alanine were notably upregulated in triploids, particularly in the gonadal gland, gill, and hepatopancreas. This compound, known for its potential anti-cancer properties, likely enhances both the nutritional value and flavor of triploid oysters. Phospholipids, in particular, are critical for flavor development during cooking (Sohail et al., 2022), and the elevated presence of oxidized lipids like (±) 5-HETE and Prostaglandin F2α in triploid oysters supports their role in generating volatile flavor compounds. These findings align with previous studies, which highlight the importance of lipid oxidation in seafood flavor formation, particularly through interactions with Maillard reaction products (Sohail et al., 2022), potentially explaining the richer taste of triploid oysters.

Regarding nucleosides, we identified 88 types, with significant increases in inosine, guanosine, and inosine diphosphate in triploid oysters. These nucleosides play key roles in nucleic acid synthesis, energy metabolism, and physiological regulation (Bucci, 2020). The elevated levels of inosine and its derivatives in triploids enhance umami taste and provide additional health benefits, such as improved liver function and immune system support (Koito et al., 2010). Our results are consistent with previous research demonstrating the importance of nucleosides in food for both flavor and nutritional enhancement (Kasumyan, 2016). In triploid oysters, the higher concentration of these compounds contributes to their superior flavor profile and their potential for greater health benefits compared to diploid oysters.

The amino acid profile also revealed significant differences between diploid and triploid oysters. We detected 244 amino acids and their derivatives, with particularly high levels of glutamate and aspartate, which are known for enhancing umami flavor, in triploid oysters. These amino acids are essential for the savory, rich taste associated with seafood, and their abundance in triploids supports the notion that these oysters offer a more complex and desirable flavor (Kasumyan, 2016). Additionally, the presence of free amino acids such as glycine, alanine, and proline, which are linked to sweet flavors, was significantly higher in triploid oysters. This is consistent with other studies that show these amino acids play a crucial role in flavor development during cooking or food processing (Zhang et al., 2023b). Moreover, the higher levels of taurine in triploid oysters, an amino acid known for its antioxidant properties and cardiovascular health benefits, further highlight the enhanced nutritional value of triploids (Koito et al., 2010).

Several small molecules, including vitamins and coenzymes, were more abundant in triploid oysters. Notably, Nicotinamide (vitamin B3) was significantly higher in triploids, suggesting enhanced metabolic benefits (Mehmel et al., 2020). Nicotinamide is essential for energy metabolism and redox reactions, and its presence highlights the potential health advantages of consuming triploid oysters. In contrast, diploid oysters showed higher levels of 25-Hydroxycholesterol, a compound involved in bile acid biosynthesis, which indicates distinct metabolic pathways between diploid and triploid oysters (Zhang et al., 2023a). These differences open avenues for further research, particularly regarding how these metabolites influence flavor and health outcomes in human diets.

Our research demonstrates that triploid oysters have a more complex and beneficial metabolic profile than diploid oysters, with significant enhancements in lipids, nucleosides, amino acids, and small molecules that contribute to both superior flavor and nutritional value. These results advance our understanding of

oyster metabolomics and provide a foundation for future research aimed at optimizing the cultivation of triploid oysters to improve both taste and health benefits. Further studies could explore the environmental and genetic factors influencing these metabolic differences, as well as the bioavailability and long-term health impacts of these enriched metabolites in human diets.

5 Conclusions

This study used a metabolomics approach to distinguish the flavor profiles of diploid and triploid oysters, revealing significant biochemical differences. Our findings demonstrate that triploid oysters exhibit a more complex array of metabolites and higher concentrations of compounds that enhance both flavor and nutritional value. Notably, triploid oysters contain elevated levels of essential amino acids, nucleotides, and taurine, contributing to their richer taste and potential health benefits. The adductor muscle, gills, and gonads of triploid Portuguese oysters showed more pronounced pleasant aromas compared to diploids, characterized by green, fruit, and cucumber-like fragrances, giving triploids a stronger aroma, while the ketones in the diploid oyster hepatopancreas had a stronger floral and fruity taste than in triploids. The differential metabolic profiles, including higher levels of umami-enhancing nucleotides and sweet-tasting amino acids in triploids, suggest these oysters may offer a superior culinary experience along with enhanced nutritional benefits. The presence of bioactive peptides with potential health-promoting properties further highlights the value of triploid oysters in a balanced diet. Additionally, this research provides key insights into the metabolic pathways influenced by oyster ploidy, with important implications for aquaculture and food science. Understanding these pathways will help optimize breeding programs to enhance flavor and health qualities, contributing to the sustainable development of the oyster aquaculture industry. This study lays a foundational framework for selecting flavor phenotypes in triploid oysters, aiming to enhance consumer satisfaction and health outcomes through targeted breeding and cultivation practices, with future research needed to explore the long-term health impacts of consuming triploid oysters and further investigate the metabolic mechanisms behind the observed differences in taste and nutritional content.

Data availability statement

The original contributions presented in the study are included in the article/supplementary material, further inquiries can be directed to the corresponding authors.

Author contributions

TX: Conceptualization, Formal analysis, Funding acquisition, Methodology, Project administration, Writing – original draft, Writing – review & editing, Supervision. DC: Conceptualization, Formal analysis, Investigation, Methodology, Software, Supervision, Writing – original draft, Writing – review & editing, Data curation. ZWZ: Data curation, Formal analysis, Investigation, Resources, Validation, Writing – original draft. ZQZ: Data curation, Formal analysis, Investigation, Methodology, Resources, Software, Validation, Visualization, Writing – review & editing. YS: Data curation, Formal analysis, Investigation, Resources, Software, Writing – original draft. ZC: Conceptualization, Investigation, Methodology, Resources, Supervision, Writing – original draft. GL: Conceptualization, Resources, Supervision, Writing – original draft, Writing – review & editing.

Funding

The author(s) declare financial support was received for the research, authorship, and/or publication of this article. This work was supported by Science and Technology Project of Fuzhou Institute of Oceanography, China (2022F03).

Conflict of interest

The authors declare that the research was conducted in the absence of any commercial or financial relationships that could be construed as a potential conflict of interest.

Publisher's note

Supplementary material

The Supplementary Material for this article can be found online at: https://www.frontiersin.org/articles/10.3389/fmars.2024.1481047/full#supplementary-material

References

Aruna, G., and Baskaran, V. (2010). Comparative study on the levels of carotenoids lutein, zeaxanthin and β-carotene in Indian spices of nutritional and medicinal importance. *Food Chem.* 123, 404–409. doi: 10.1016/j.foodchem.2010.04.056

Bi, J., Li, Y., Yang, Z., Lin, Z., Chen, F., Liu, S., et al. (2022). Effect of different cooking times on the fat flavor compounds of pork belly. *J. Food Biochem.* 46, e14184. doi: 10.1111/jfbc.14184

Bucci, L. R. (2020). *Nutrients as Ergogenic Aids for Sports and Exercise* (Boca Raton: CRC Press). doi: 10.1201/9781003068051

Chen, L., Teng, X., Liu, Y., Shi, H., Li, Z., and Xue, C. (2024). The dynamic change of flavor characteristics in Pacific oyster (*Crassostrea gigas*) during depuration uncovered by mass spectrometry-based metabolomics combined with gas chromatography-ion mobility spectrometry (GC-IMS). *Food Chem.* 434, 137277. doi: 10.1016/j.foodchem.2023.137277

Cheng, H., Mei, J., and Xie, J. (2023). The odor deterioration of tilapia (*Oreochromis mossambicus*) fillets during cold storage revealed by LC-MS based metabolomics and HS-SPME-GC-MS analysis. *Food Chem.* 427, 136699. doi: 10.1016/j.foodchem.2023.136699

Dong, L., Zhao, L., Zhang, E., Li, Z., Wang, W., and Yang, J. (2023). Histological and ultrastructural observation of adductor and sperm of *Crassostrea gigas* with different ploidy. *J. Fishery Sci. China* 30, 433–446. doi: 10.12264/JFSC2022-0398

Fu, J., Sun, Y., Cui, M., Zhang, E., Dong, L., Wang, Y., et al. (2023). Analysis of volatile compounds and flavor fingerprint using gas chromatography-ion mobility spectrometry (GC-IMS) on *crassostrea gigas* with different ploidy and gender. *Molecules* 28, 4475. doi: 10.3390/molecules28114475

Fu, B., Zheng, M., Yang, H., Zhang, J., Li, Y., Wang, G., et al. (2024). The effect of broad bean diet on structure, flavor and taste of fresh grass carp: A comprehensive study using E-nose, E-tongue, TPA, HS-SPME-GC-MS and LC-MS. *Food Chem.* 436, 137690. doi: 10.1016/j.foodchem.2023.137690

Guo, X., Wang, Y., DeBrosse, G., Bushek, D., and Ford, S. E. (2008). Building a superior oyster for aquaculture. *Jersey Shorel* 25, 7–9.

Huang, Y., Yang, F., Qin, X., Zhang, C., and Lin, H. (2019). Chemical composition and characteristic odorans of oyster (*Crassostrea hongkongensis*) from different culture areas. *Food Sci.* 40, 236–242. doi: 10.7506/spkx1002-6630-20180822-239

Jeleń, H. H., Majcher, M., and Dziadas, M. (2012). Microextraction techniques in the analysis of food flavor compounds: A review. *Analytica Chimica Acta* 738, 13–26. doi: 10.1016/j.aca.2012.06.006

Jiang, G., Li, Q., and Xu, C. (2022). Growth, survival and gonad development of two new types of reciprocal triploid hybrids between *Crassostrea gigas* and *C. angulata*. *Aquaculture* 559, 738451. doi: 10.1016/j.aquaculture.2022.738451

Kasumyan, A. O. (2016). Taste attractiveness of free amino acids and their physicochemical and biological properties (as exemplified by fishes). *J. Evol. Biochem. Phys.* 52, 271–281. doi: 10.1134/S0022093016040013

Khan, M. I., Jo, C., and Tariq, M. R. (2015). Meat flavor precursors and factors influencing flavor precursors–A systematic review. *Meat Sci.* 110, 278–284. doi: 10.1016/j.meatsci.2015.08.002

Koito, T., Nakamura-Kusakabe, I., Yoshida, T., Maruyama, T., Omata, T., Miyazaki, N., et al. (2010). Effect of long-term exposure to sulfides on taurine transporter gene expression in the gill of the deep-sea mussel Bathymodiolus platifrons, which harbors a methanotrophic symbiont. *Fish Sci.* 76, 381–388. doi: 10.1007/s12562-010-0219-5

Kong, L., Wang, Z., Yu, R., and Wang, R. (2003). Comparative observation of the gills of diploid and triploid Pacific oyster using scanning electron microscopy. *Chin. J. Zoology* 384, 2–4. doi: 10.13859/j.cjz.2003.04.001

Li, W., Du, R., Majura, J. J., Chen, Z., Cao, W., Zhang, C., et al. (2022b). The spatial distribution patterns, physicochemical properties, and structural characterization of proteins in oysters (*Crassostrea hongkongensis*). *Foods* 11, 2820. doi: 10.3390/foods11182820

Li, H., Yu, R., Li, Q., and Ma, P. (2022a). Evaluation of advantages in the growth, survival and reproductive aspects of triploid hybrids derived from *Crassostrea gigas* tetraploids and *C. ariakensis* diploids in northern China. *Aquaculture* 548, 737675. doi: 10.1016/j.aquaculture.2021.737675

Liu, C., Gu, Z., Lin, X., Wang, Y., Wang, A., Sun, Y., et al. (2022). Effects of high hydrostatic pressure (HHP) and storage temperature on bacterial counts, color change, fatty acids and non-volatile taste active compounds of oysters (*Crassostrea ariakensis*). *Food Chem.* 372, 131247. doi: 10.1016/j.foodchem.2021.131247

Liu, C., Ji, W., Jiang, H., Shi, Y., He, L., Gu, Z., et al. (2021). Comparison of biochemical composition and non-volatile taste active compounds in raw, high hydrostatic pressure-treated and steamed oysters *Crassostrea hongkongensis*. *Food Chem.* 344, 128632. doi: 10.1016/j.foodchem.2020.128632

Liu, L., Zhao, Y., Lu, S., Liu, Y., Xu, X., and Zeng, M. (2023). Metabolomics investigation on the volatile and non-volatile composition in enzymatic hydrolysates of Pacific oyster (*Crassostrea gigas*). *Food Chem. X* 17, 100569. doi: 10.1016/j.fochx.2023.100569

Ma, Y., Wang, R., Zhang, T., Xu, Y., Jiang, S., and Zhao, Y. (2021). High hydrostatic pressure treatment of oysters (*Crassostrea gigas*)—Impact on physicochemical properties, texture parameters, and volatile flavor compounds. *Molecules* 26, 5731. doi: 10.3390/molecules26195731

Mehmel, M., Jovanović, N., and Spitz, U. (2020). Nicotinamide riboside—The current state of research and therapeutic uses. *Nutrients* 12, 1616. doi: 10.3390/nu12061616

Meng, Q., Zhou, J., Gao, D., Xu, E., Guo, M., and Liu, D. (2022). Desorption of nutrients and flavor compounds formation during the cooking of bone soup. *Food Control* 132, 108408. doi: 10.1016/j.foodcont.2021.108408

Park, S. J., and Choi, Y. H. (2022). Relationship between condition index values and expression levels of gene and protein in the adductor muscle of diploid and triploid oysters *crassostrea gigas*. *Dev. Reprod.* 26, 165–174. doi: 10.12717/DR.2022.26.4.165

Qin, Y., Zhang, Y., Ma, H., Wu, X., Xiao, S., Li, J., et al. (2018). Comparison of the biochemical composition and nutritional quality between diploid and triploid Hong Kong oysters, *crassostrea hongkongensis*. *Front. Physiol.* 9. doi: 10.3389/fphys.2018.01674

Que, H., and Allen, S. (2002). Hybridization of tetraploid and diploid *crassostrea gigas* (Thunberg) with diploid *C-ariakensis* (Fujita). *J. Of Shellfish Res.* 21, 137–143.

Sohail, A., Al-Dalali, S., Wang, J., Xie, J., Shakoor, A., Asimi, S., et al. (2022). Aroma compounds identified in cooked meat: A review. *Food Res. Int.* 157, 111385. doi: 10.1016/j.foodres.2022.111385

Su, D., He, J., Zhou, Y., Li, Y., and Zhou, H. (2022). Aroma effects of key volatile compounds in Keemun black tea at different grades: HS-SPME-GC-MS, sensory evaluation, and chemometrics. *Food Chem.* 373, 131587. doi: 10.1016/j.foodchem.2021.131587

Sun, Y., Fu, J., Zhang, E., Dong, L., Cui, X., Sun, Y., et al. (2023). Fingerprint Analysis of Volatile Flavor Compounds in *Crassostrea gigas* of Different Ploidy and Gender under High-Temperature Incubation. *Molecules* 28, 6857. doi: 10.3390/molecules28196857

Teng, X., Cong, X., Chen, L., Wang, Q., Xue, C., and Li, Z. (2022). Effect of repeated freeze-thawing on the storage quality of pacific oyster (*Crassostrea gigas*). *Food Measure* 16, 4641–4649. doi: 10.1007/s11694-022-01537-5

Utpott, M., Rodrigues, E., Rios, A., de, O., Mercali, G. D., and Flôres, S. H. (2022). Metabolomics: An analytical technique for food processing evaluation. *Food Chem.* 366, 130685. doi: 10.1016/j.foodchem.2021.130685

Villanueva-Fonseca, B. P., Góngora-Gómez, A. M., Muñoz-Sevilla, N. P., Domínguez-Orozco, A. L., Hernández-Sepúlveda, J. A., García-Ulloa, M., et al. (2017). Growth and economic performance of diploid and triploid Pacific oysters *Crassostrea gigas* cultivated in three lagoons of the Gulf of California. *Latin Am. J. Aquat. Res.* 45, 466–480. doi: 10.3856/vol45-issue2-fulltext-21

Wang, S., Xue, M., Yang, Q., Yu, H., and Li, Q. (2021). Comparison of nutritional components of different fertility triploid Pacific oyster (*Crassostrea gigas*) during gonadal development. *J. Fisheries China* 45, 88–97. doi: 10.11964/jfc.20200412244

Wu, T., Wang, M., Wang, P., Tian, H., and Zhan, P. (2022). Advances in the formation and control methods of undesirable flavors in fish. *Foods* 11, 2504. doi: 10.3390/foods11162504

Yuasa, M., Kawabeta, K., Eguchi, A., Abe, H., Yamashita, E., Koba, K., et al. (2018). Characterization of taste and micronutrient content of rock oysters (*Crassostrea nippona*) and Pacific oysters (*Crassostrea gigas*) in Japan. *Int. J. Gastronomy Food Sci.* 13, 52–57. doi: 10.1016/j.ijgfs.2018.06.001

Zhang, J., Cao, J., Pei, Z., Wei, P., Xiang, D., Cao, X., et al. (2019). Volatile flavour components and the mechanisms underlying their production in golden pompano (*Trachinotus blochii*) fillets subjected to different drying methods: A comparative study using an electronic nose, an electronic tongue and SDE-GC-MS. *Food Res. Int.* 123, 217–225. doi: 10.1016/j.foodres.2019.04.069

Zhang, Y., Guo, Y., and Song, X. (2023b). Comprehensive insight into an amino acid metabolic network in postharvest horticultural products: a review. *J. Sci. Food Agric.* 103, 5667–5676. doi: 10.1002/jsfa.12638

Zhang, Z., Li, T., Wang, D., Zhang, L., and Chen, G. (2009). Study on the volatile profile characteristics of oyster *Crassostrea gigas* during storage by a combination sampling method coupled with GC/MS. *Food Chem.* 115, 1150–1157. doi: 10.1016/j.foodchem.2008.12.099

Zhang, J., Zhu, Y., Wang, X., and Wang, J. (2023a). 25-hydroxycholesterol: an integrator of antiviral ability and signaling. *Front. Immunol.* 14. doi: 10.3389/fimmu.2023.1268104

Zhong, P., Wei, X., Li, X., Wei, X., Wu, S., Huang, W., et al. (2022). Untargeted metabolomics by liquid chromatography-mass spectrometry for food authentication: A review. *Compr. Rev. Food Sci. Food Saf.* 21, 2455–2488. doi: 10.1111/1541-4337.12938

frontiers | Frontiers in Marine Science

TYPE Perspective
PUBLISHED 23 December 2024
DOI 10.3389/fmars.2024.1384083

OPEN ACCESS

EDITED BY
Xinxin Wang,
Akvaplan niva AS, Norway

REVIEWED BY
Pavan Kumar,
Guru Angad Dev Veterinary and Animal Sciences University, India

*CORRESPONDENCE
Louise Buttle
louise.buttle@dsm-firmenich.com

RECEIVED 08 February 2024
ACCEPTED 03 December 2024
PUBLISHED 23 December 2024

CITATION
Buttle L, Noorman H, Roa Engel C and Santigosa E (2024) Bridging the protein gap with single-cell protein use in aquafeeds. *Front. Mar. Sci.* 11:1384083. doi: 10.3389/fmars.2024.1384083

Bridging the protein gap with single-cell protein use in aquafeeds

Louise Buttle[1]*, Henk Noorman[2], Carol Roa Engel[2] and Ester Santigosa[1]

[1]Animal Nutrition & Health, dsm-firmenich Nutritional Products AG, Kaiseraugst, Switzerland, [2]dsm-firmenich, Centre of Biotech Innovation, Delft, Netherlands

Blue foods from aquaculture are essential in bridging the protein gap to feed the human population in the future. However, for aquaculture production to be sustainable, production must be within planetary boundaries, and sourcing of sustainable raw materials is a key driver in sustainable production. This article explores the role of single-cell proteins (SCPs) derived from microorganisms in aquafeeds. Three main aspects are discussed: sustainability, scalability of fermentation technology, and fish performance. In addition, and through a comprehensive proof-of-concept trial with rainbow trout (*Oncorhynchus mykiss*), this article demonstrates SCP's efficacy in replacing traditional feed ingredients without compromising fish growth and health. The trial's findings demonstrate a high protein digestibility and a balanced amino acid profile, as well as health benefits measured through oxidative burst response. To date, commercial adoption of SCP has been hindered by high production costs and the need for substantial investments to scale fermentation technologies. However, the sustainability landscape is changing as large industry players openly commit to sustainability targets and realize that longer-term and investment thinking into the future is needed. In conclusion, SCP emerges as a promising avenue for sustainable aquafeeds, offering a solution to the protein supply challenge within planetary boundaries. In addition, in terms of environmental benefit, SCP shows clear advantages regarding land use, carbon emissions, biodiversity impact, and water consumption. Ultimately, the successful integration of SCP into aquafeeds could significantly contribute to the industry's sustainability goals and play an essential role in securing the future supply of raw material proteins.

KEYWORDS

novel, bacteria, yeast, fungi, protein, salmonids, digestibility, aquaculture

Introduction

Aquaculture has become the fastest-growing animal protein industry, and it has been identified as one of the main blue food industries that play a critical role to meet the protein gap of 100 million (dry) MTs annually estimated by 2050 for our growing human population (FAO, 2022). However, this food production must be delivered within planetary boundaries, and one of the drivers of sustainable aquaculture is the use of sustainable raw materials. For many years, the aquaculture industry has been searching for novel or alternative protein-rich raw materials to complement a raw material basket of marine ingredients, animal by-products, and plant ingredients. In addition, heightened prices and supply shortages in plant proteins have been recorded since 2022 due to natural and geopolitical events, which further motivates a drive for alternative protein sources (Aas et al., 2022). Alternative or novel protein candidates include insects, macroalgae, and single-cell organisms or single-cell proteins (SCPs) (Colombo et al., 2023).

SCP products are derived from the fermentation of microorganisms, such as bacteria, yeast, fungi, or microalgae using renewable feedstocks, and provide a readily available protein-rich microbial biomass. While SCP is not a new concept, having been used for human and animal nutrition since the 1960s, biotechnological advances have enabled more efficient and cost-effective production processes (Glencross et al., 2020b; Jones et al., 2020; Sharif et al., 2021). Fermentation technologies are used today to produce food and feed ingredients and additives such as yeast extracts, organic acids, enzymes, and vitamins. Some famous examples of food fermentation products are *Spirulina* used by NASA for astronaut foods (Soni et al., 2021) and the meat replacement Quorn, which was launched in the 1980s (Gastaldello et al., 2022). However, the industry is still judged with mixed opinions, partly related to the use of synthetic biology concerns and the lack of full understanding related to the environmental, climate, and nature-based benefits of these technologies.

The potentially high protein content (70% or higher) of these microorganisms combined with high growth rates, a balanced amino acid profile that meets the nutritional requirements of various aquaculture species, and the ability to convert a diverse array of platform molecules into protein makes SCP a frontrunner when it comes extending the raw material basket beyond fish meal and plant protein currently used. However, SCP still represents a very low inclusion of protein sources in commercial aquafeeds (Aas et al., 2022). To increase the commercial use of SCP, it is important that production costs decrease, and this requires a substantial increase in investment to produce large volumes in bioreactors located close to aquaculture farming facilities (Sarker, 2023). In this view, investors need reliable and thorough scientific evidence to support decision-making. This article summarizes the landscape for SCP across the three critical levers of (i) sustainability, (ii) scalability and advances in fermentation technology, and (iii) fish nutrition and performance, and presents a recent proof-of-concept trial.

Sustainable aquaculture and single-cell proteins

Modern aquafeeds currently rely on relatively high levels of terrestrial plant materials, such as soy protein concentrate, which have their limitations, including high water and land use, pesticide use, biodiversity loss, deforestation risk, greenhouse gas (GHG) emissions, and price volatility (Fry et al., 2016; Glencross et al., 2020a). Despite the fact that the aquaculture industry has become more efficient with improved feed conversion (Glencross et al., 2023a), while also improving its environmental footprint, and reduced dependency on marine proteins from capture fisheries (Aas et al., 2022; Naylor et al., 2021), a large proportion of the environmental or carbon footprint is defined by feed and raw materials (Boyd and McNevin, 2024). In consequence, investing in SCP technologies and optimizing them for aquafeed can help create a more resource-efficient model for aquaculture, promoting a sustainable seafood supply chain that meets growing global demand. The adoption of this alternative needs an extra validation step to show that food and feed safety will not be compromised (Glencross et al., 2020a; Jones et al., 2020).

Figure 1 shows a potential schematic for the process of SCP production. The sustainability of SCPs lies in their ability to address several environmental and resource challenges that potentially enables a near-zero carbon footprint. For example, traditionally fermentation technologies have used sugars as the carbon feedstock, but producing the feedstock molecules from carbon capture and the electrolysis of water to produce hydrogen and oxygen are an emerging possibility. Given that the energy required for electrolysis of water is renewable, then resource use (and GHG emissions) can be minimized when compared to soy protein without land use change (1.8 kg CO_2e/kg), Norwegian fish meal (2–3 kg CO_2e/kg), and krill (2.8 kg CO_2e/kg) and massively reduced with regard to soy protein with land use change (5–7 kg CO_2e/kg) (Ulf et al., 2022; Skretting Sustainability report, 2022). In addition, the feedstock production requires very little or no water and land use, compared to proteins derived from agriculture. This feedstock source also limits any reputational and environmental sustainability risks related to deforestation, biodiversity loss, and the protection of marine stocks and biomass. Together with the availability of renewable energy, the choice of microorganism and the management of waste streams can impact the environmental footprint of SCP production. Ongoing research and development are focused on optimizing these processes to enhance sustainability further and full LCA studies are needed to fully understand the impact.

This is of great importance in the current context, where many companies, including large aquaculture companies, have signed up to science-based targets (https://sciencebasedtargets.org/). Targets for Scope 3 emission reductions by 2030, compared to baselines before 2020, start at 30% and higher. To support these targets, SCPs offer a promising avenue for sustainable feed ingredient production. Their lower footprint, potential to reduce land use, carbon

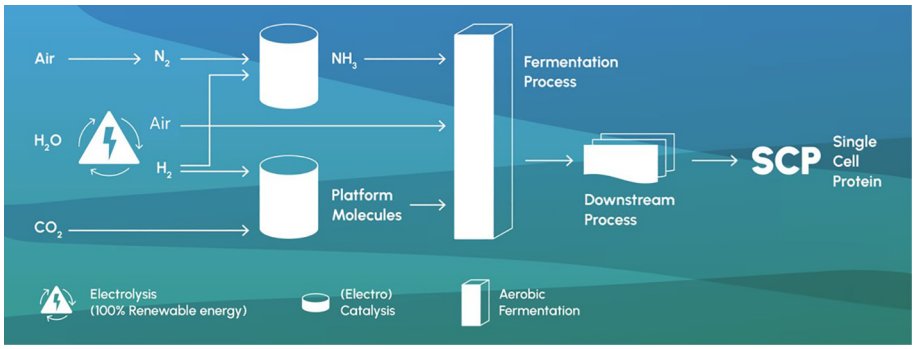

FIGURE 1
Single-cell protein production from air, water, CO_2, and renewable energy (Fackler et al., 2021; Mishra et al., 2020; Molitor et al., 2019).

emissions, and minimized water use make them an attractive option for addressing the challenges. In addition, there is limited impact on biodiversity, which will be a vital sustainability metric going forward.

Scalability and advances in fermentation technologies

SCPs belong to an extensive library of microorganism options that can grow further as fermentation technology improves and evolves to become an industrial, state-of-the-art process. In addition, because microorganisms have extremely short generation times compared to plants and animals, biotechnology research has a key role to play in the selection and improvement of strains with high and digestible protein content and a targeted amino acid profile for precise nutrition.

Companies working in the pathway towards commercial production are in operation. One example is Calysta (www.calysta.com), and through a joint venture with Calysseo, it will produce 20,000 MT per year in its first FeedKind production plant in China. Other ventures, such as UniBio (Uniprotein®, www.unibio.dk) with a unique U-Loop® technology, have also been reported to be commercial. Emerging companies, such as Solar Foods (https://solarfoods.com/) and Deep Branch (www.deepbranch.com), are not yet at commercial scale. Both UniBio and Calysta use gas fermentation platforms of methanotrophic bacteria to produce the protein-rich product, while others use hydrogen-oxidizing bacteria. dsm-firmenich is a world leader in fermentation technologies and is working on the development of SCPs for aquaculture, companion animals, and food products.

Transitioning to commercial scale requires a large capital investment to scale up and reduce the cost of production to deploy the right product specifications at a commercial sales price. Accordingly, there has always been a benchmark in salmon aquafeed, as an example, to compare price/kg with standard raw materials and less appreciation for an investment price needed as companies ramp up production. At the same time, historically there was less emphasis on environmental and biodiversity impacts and a short-term approach to raw material basket availability and feed market conditions. However, today, many companies from different parts of the aquaculture value chain are making commitments on climate and nature (see, for instance, sciencebasedtargets.org). Accordingly, there is a wider perspective on raw materials in aquafeeds with longer-term goals, return on investment, and sustainability targets becoming more relevant as stakeholders take note that conventional protein sources cannot meet the future demand for protein within planetary boundaries.

Success at scale-up is also determined by the potential of the fermentation platform for commercial quantities, and historically, some start-ups with new bioproducts have failed to commercialize because of lack of scale-up knowledge and practical insight or industrial experience. Financing of the ramp up can also be a barrier as large capital is required for fermentation technologies at commercial scale. Government incentives play a role in site selection, where current government policies and growing climate concerns can support the development. A recent example of government focus is the social sustainable feed mission from the Norwegian government (Et samfunnsløft for bærekraftig fôr), recognizing both the urgency around climate change and the low self-sufficiency of Norway in the raw material supply chain (https://www.forskningsradet.no/en/research-policy-strategy/ltp/sustainable-feed/). For example, in 2021, only 8% of the feed raw materials used in the Norwegian salmon industry were sourced from Norway (Aas et al., 2022). In addition, the European Union has over-dependence on protein supply from outside EU and has adopted import restrictions [carbon border adjustment mechanism (CBAM)]. Simultaneously, the EU has also initiated programs to stimulate protein production (examples include EU Protein Strategy and New Green Deal).

A proof-of-concept trial: fish nutrition and performance

The performance of SCP in fish trials is an important screening stage for the development of alternative raw materials for aquaculture. Because previous studies indicated that some SCP products can have adverse effects on protein digestibility with

repercussions on fish growth, health, and welfare (Glencross et al., 2020b), the current trial was designed to go beyond the conventional approach of zootechnical indicators, and therefore also tested the effect of SCP sources in protein digestibility and retention, amino acid digestibility, and health. We showcase two SCP products that were included in rainbow trout (*Oncorhynchus mykiss*) diets up to 20% inclusion over a 12-week trial.

The trial was conducted in CRNA facilities (Village-Neuf, France; Permit no. 26235). Two different non-GM, SCP products (SCP1 and SCP2: DSM Biotechnology Centre, Delft, The Netherlands) were tested. Experimental diets were formulated to be isonitrogenous and isoenergetic. The six experimental diets (SCP1-5, SCP1-10, SCP1-20, SCP2-5, SCP2-10, and SCP2-20) were compared against a control diet formulated with 10% fish meal and 20% soy protein concentrate (Supplementary Table 1). The experimental diets had SCP inclusion of 5% (SCP1 5% and SCP2 5%), 10% (SCP1 10% and SCP2 10%), and 20% (SCP1 20% and SCP2 20%) of both test products (SCP1 and SCP2). In the 5% and 10% SCP feeds, the SCP replaced fish meal, meaning that the 10% SCP feed did not contain any fish meal. In the 20% SCP feeds, all the fish meal was replaced and 10% of the dietary soy protein concentrate was also replaced with the SCP (as % feed inclusion).

Rainbow trout eyed eggs (generation E21SPR; Aqualor, Fénétrange, France) were hatched at CRNA. Fish were individually weighed at the beginning of the trial (IBW 49.7 ± 0.03 g) and allocated to the experimental groups; each group consisted of three replicate tanks with 20 fish per tank. Fish were fed the experimental diet twice a day for 84 days. At the end of the experiment, zootechnical parameters were assessed: survival (%), body weight (FBW, g), weight gain (WG, g), daily weight gain (DWG, g), specific growth rate (SGR, % BW d^{-1}), and feed conversion ratio (FCR). The detailed formulas for calculation of WG, DWG, SGR, and FCR are provided in the Supplementary Materials. Whole fish samples were taken at the beginning and end of the trial to analyze whole-body protein retention. Samples for apparent digestibility coefficient (ADC) calculation and samples from the head kidney for oxidative burst measurements (as an indicator of health status) were also taken (see the Supplementary Materials).

All diets showed similar performance in final weight (267.0 ± 6.56 g; average ± standard deviation) except for the SCP2 20%, which performed significantly lower than the control, although the difference was less than 5% (256.3 ± 4.9 g). The diet with the highest final mean weight was the SCP2 10% (276.5 ± 1.8 g). In addition, no difference in feed intake values was observed across all treatment groups (data not shown). In recent years, there have been many trials assessing the effect of SCP on fish and shrimp performance (Glencross et al., 2020b; Jones et al., 2020; Sharif et al., 2021). However, it is important to note that results are not always consistent and vary with the level of inclusion, trial design, feed design, initial weight, trial duration, and origin of the SCP organism used for the replacement. For example, the final weight of small Atlantic salmon was significantly lower when 40% of crude protein from FM was substituted with SCP from the yeasts *Candida utilis* (34.5% dietary inclusion) or *Kluyveromyces marxianus* (30.2% dietary inclusion) (Øverland et al., 2013). However, at lower levels of inclusion, SCP from the bacterium *Methylococcus capsulatus* induced no changes in growth performance when used at up to 14% inclusion of the feed in spotted seabass (Yu et al., 2023).

In the present trial, protein ADC was significantly improved in relation to the control diet when either SCP was included in the diet at 10% and 20% inclusion (Table 1). Furthermore, multiple comparisons revealed that inclusion levels but not SCP source had a significant effect on protein ADC, with inclusion at 10% producing the highest protein ADC ($p < 0.001$, Table 1). Control, SCP1 5%, and SCP2 5% groups showed a lower total amino acid digestibility, but differences did not clearly correlate to growth performance. Essential amino acid digestibility did not show significant differences. Interestingly, branched-chain amino acid digestibility showed a dose response with higher digestibility with increased inclusion levels of SCP1 and showed less differences across SCP2 treatments.

It has been previously suggested that SCPs in aquafeeds might negatively impact performance due to the lower digestibility of the protein ingredient (e.g., cell walls of microorganisms and non-amino acid protein fraction) and have detrimental impacts on gut health (Glencross et al., 2020b; Jones et al., 2020). However, the results here recorded support the use of SCPs tested because the protein ADC was significantly improved relative to that of the control diet, when SCP1 or SCP2 were included at 10% (Table 1). Moreover, the protein ADCs obtained here (>91%) were higher than those previously recorded for salmonids (80% to 90%) fed SCP diets (Glencross et al., 2023b; Hardy et al., 2018; Kaushik and Luquet, 1980; Lee et al., 2020; Romarheim et al., 2011; Storebakken et al., 2004). Concomitantly, the ADC of amino acids was highest at 10% or 20% inclusion, mainly driven by non-essential and branched-chain amino acids (Table 1). These results are particularly notable for branched-chain amino acids (e.g., leucine, isoleucine, and valine), as these cannot be synthesized by fishes and play significant structural and functional roles (Ahmad et al., 2021). Results here recorded for oxidative burst showed a pattern for an improved dose response for either SCP with increased inclusion levels among experimental diets (no significant differences; Supplementary Table 2). The functional benefits of branched-chain amino acids, as well as the functional components usually present in SCPs that are beneficial for fish health, such as nucleic acids, β-glucans, and microbe-associated molecular patterns, among others (Morales-Lange et al., 2024; Øverland and Skrede, 2017; Øvrum Hansen et al., 2019; Rocha et al., 2023; Romarheim et al., 2011), might warrant the health benefits recorded for fish fed SCP-based diets. This probably explains the nominally positive dose-dependent response found here for oxidative burst, which reflects the increase in cell metabolism and oxygen consumption coupled with the release of reactive oxygen species that serve as the first line of defense against microbial infection. Nevertheless, and considering the non-statistical significance of the oxidative burst pattern here recorded, future studies are needed to confirm the functional benefits of SCP1 and SCP2 under challenging more commercial-like conditions.

In conclusion, digestibility of the amino acids in the finished feed with high inclusion of SCPs showed excellent results, suggesting that the high fish performance observed was related to the high digestibility of the AA in the product. At the same time, feed intake was similar across treatments, demonstrating a high

10.3389/fmars.2024.1384083

TABLE 1 Effect of experimental diet on protein apparent digestibility coefficient (ADC), protein retention, and total, essential, non-essential, and branched-chain amino acid ADC.

	Protein ADC (%)	Protein retention (% intake)	Amino acid ADC (%)			
			Total	Essential	Non-essential	Branched-chain
Control	91.4 ± 0.19bc	53.23 ± 0.52	93.2bc	93.9	92.8bc	93.8ab
SCP1-5	91.3 ± 0.11c	52.63 ± 1.86	92.8c	93.3	92.5c	93.5b
SCP1-10	92.3 ± 0.17a	53.77 ± 4.20	93.7abc	94.0	93.5ab	94.3ab
SCP1-20	91.9 ± 0.09ab	55.90 ± 2.00	93.7ab	94.1	93.5ab	94.9a
SCP2-5	91.2 ± 0.19c	52.72 ± 2.57	93.4abc	93.9	93.0bc	93.9ab
SCP2-10	92.1 ± 0.20a	51.07 ± 4.10	94.2a	94.2	94.1a	94.6ab
SCP2-20	91.8 ± 0.37ab	54.04 ± 1.75	94.0ab	93.8	94.1a	94.9ab
ANOVA						
p-value	<0.0001	0.5228	0.0026	0.2295	<0.0001	0.0412
Main effects						
Protein source						
SCP1	91.1	54.10	93.4	93.8	93.1	94.2
SCP2	91.7	52.61	93.8	94.0	93.8	94.1
p-value	0.2994	0.3026	0.0141	0.4399	0.0013	0.4373
Inclusion level						
5%	91.2c	52.68	93.1	93.6	92.8	93.7
10%	92.2a	52.42	93.9	94.1	93.8	94.3
20%	91.9b	54.97	93.9	94.0	93.8	94.5
p-value	<0.0001	0.2883	0.0012	0.1095	0.0001	0.0228
Interaction *p*-value	0.8561	0.7065	0.6598	0.1698	0.971	0.0576

Values show average ± standard deviation. Different letters among treatments denote significant differences.
Statistical analyses considered each tank as an experimental unit. All percentage data were arcsine transformed. Data were analyzed by two-way analysis of variance (ANOVA), using protein source and inclusion rate as the independent variables (ANOVA main effects), followed by Tukey's honest significant difference (HSD) test for multiple comparisons. All statistical analyses were conducted in JMP software (https://www.jmp.com) considering $p < 0.05$ as significant.

palatability of the ingredient, and indicating that the SCP tested in the current trial had limited negative properties, such as the presence of nucleic acids. Ultimately, the present results successfully demonstrate the potential of incorporating two SCP products in rainbow trout aquafeeds up to 20% dietary inclusion, either as full replacers of FM or as partial replacers of soy protein concentrate.

Future perspectives

SCP products are considered low carbon-intensive microbial-sourced proteins that can help close the impending protein gap without increasing the carbon footprint of the aquaculture food system, as well as that of terrestrial species. Indeed, SCP products do not require the extensive use of arable land, freshwater, or marine resources, and they can utilize waste streams as substrates. In addition, microbial organisms hold a huge potential to integrate circular bioeconomy processes because different biomass sources often classified as residues can be used as energy sources to produce single-cell organisms. This will ensure the sustainability of blue and green systems, particularly in the food sector, by partially decoupling animal production from conventional inputs and associated challenges, such as fertilizer use, deforestation, biodiversity impact, and elevated water consumption. Ultimately, SCPs can be seen as a potential driver for decarbonization and circular economy, given that such microorganisms can be powered by renewable energy sources (i.e., solar, wind, or biogas) and concomitantly capture and convert carbon dioxide into biomass. Success at scale also relies on partnerships along the value chain. Each member of the value chain has a role to play in enabling the industrial production of SCP products, from research on the biology of microbial organisms to industry players committed to invest in large-scale production, and feed formulators and farmers, who must be ready to adopt and willing to pay an investment price in view of a more sustainable industry with a lower environmental footprint. In conclusion, the growing momentum behind SCP products and evolving technologies with an ambitious scale, coupled with

exciting nutritional value, and their benefits in terms of sustainability metrics, will accelerate the use of SCPs in aquaculture in the future.

Data availability statement

The original contributions presented in the study are included in the article/Supplementary Material. Further inquiries can be directed to the corresponding author.

Ethics statement

The animal study was approved by project authorization using animals for scientific purposes N°26235 obtained by the Centre of Animal Nutrition and Health (Village-neuf, France) following the legal EU legislation in force Directive 2010/63. The study was conducted in accordance with the local legislation and institutional requirements.

Author contributions

LB: Writing – original draft, Writing – review & editing. HN: Writing – review & editing; CRE: Writing – review & editing. ES: Conceptualization, Methodology, Data curation, Formal analysis, Writing – review & editing.

Funding

The author(s) declare that financial support was received for the research, authorship, and/or publication of this article. dsm-firmenich entirely funded the production of the test products and the fish study. The funder was not involved in the study design, collection, analysis, interpretation of data, the writing of this article, or the decision to submit it for publication.

Acknowledgments

The authors would like to thank P. Cabo-Valcarce, C. Chatelle, P. Jenn, J. Schmeisser, and E. Bacou for conducting the fish trial.

Conflict of interest

Authors LB, ES, HM, and CE were employed by company dsm-firmenich.

Publisher's note

Supplementary material

The Supplementary Material for this article can be found online at: https://www.frontiersin.org/articles/10.3389/fmars.2024.1384083/full#supplementary-material

References

Aas, T. S., Åsgård, T., and Ytrestøyl, T. (2022). Utilization of feed resources in the production of Atlantic salmon (*Salmo salar*) in Norway: An update for 2020. *Aquacult. Rep.* 26, 101316. doi: 10.1016/j.aqrep.2022.101316

Ahmad, I., Ahmed, I., Fatma, S., and Peres, H. (2021). Role of branched-chain amino acids on growth, physiology and metabolism of different fish species: A review. *Aquac. Nutr.* 27, 1270–1289. doi: 10.1111/anu.13267

Boyd, C. E., and McNevin, A. A. (2024). Resource use and pollution potential in feed-based aquaculture. *Rev. Fish. Sci. Aquac.* 32, 306–33. doi: 10.1080/23308249.2023.2258226

Colombo, S. M., Roy, K., Mraz, J., Wan, A. H. L., Davies, S. J., Tibbetts, S. M., et al. (2023). Towards achieving circularity and sustainability in feeds for farmed blue foods. *Rev. Aquac.* 15, 1115–1141. doi: 10.1111/raq.12766

Fackler, N., Heijstra, B. D., Rasor, B. J., Brown, H., Martin, J., Ni, Z., et al. (2021). Stepping on the gas to a circular economy: Accelerating development of carbon-negative chemical production from gas fermentation. *Annu. Rev. Chem. Biomol. Eng.* 12, 439–470. doi: 10.1146/annurev-chembioeng-120120-021122

FAO. (2022). *The state of World Fisheries and Aquaculture 2022. Towards Blue Transformation* (Rome: FAO). doi: 10.4060/cc0461en

Fry, J. P., Love, D. C., MacDonald, G. K., West, P. C., Engstrom, P. M., Nachman, K. E., et al. (2016). Environmental health impacts of feeding crops to farmed fish. *Environ. Int.* 91, 201–214. doi: 10.1016/j.envint.2016.02.022

Gastaldello, A., Giampieri, F., De Giuseppe, R., Grosso, G., Baroni, L., and Battino, M. (2022). The rise of processed meat alternatives: A narrative review of the manufacturing, composition, nutritional profile and health effects of newer sources of protein, and their place in healthier diets. *Trends Food Sci. Technol.* 127, 263–271. doi: 10.1016/j.tifs.2022.07.005

Glencross, B. D., Baily, J., Berntssen, M. H. G., Hardy, R., MacKenzie, S., and Tocher, D. R. (2020a). Risk assessment of the use of alternative animal and plant raw material resources in aquaculture feeds. *Rev. Aquacult.* 12, 703–758. doi: 10.1111/raq.12347

Glencross, B. D., Fracalossi, D. M., Hua, K., Izquierdo, M., Mai, K., Øverland, M., et al. (2023a). Harvesting the benefits of nutritional research to address global challenges in the 21st century. *J. World Aquacult. Soc.* 54, 343–363. doi: 10.1111/jwas.12948

Glencross, B. D., Huyben, D., and Schrama, J. W. (2020b). The application of single-cell ingredients in aquaculture feeds—A review. *Fish. Sahul.* 5, 22. doi: 10.3390/fishes5030022

Glencross, B., Muñoz-Lopez, P., Matthew, C., MacKenzie, S., Powell, A., Longshaw, M., et al. (2023b). Digestibility of bacterial protein by Atlantic salmon (*Salmo salar*) is affected by both inclusion level and acclimation time. *Aquaculture* 565, 739137. doi: 10.1016/j.aquaculture.2022.739137

Hardy, R. W., Patro, B., Pujol-Baxley, C., Marx, C. J., and Feinberg, L. (2018). Partial replacement of soybean meal with *Methylobacterium extorquens* single-cell protein in feeds for rainbow trout (*Oncorhynchus mykiss* Walbaum). *Aquac. Res.* 49, 2218–2224. doi: 10.1111/are.2018.49.issue-6

Jones, S. W., Karpol, A., Friedman, S., Maru, B. T., and Tracy, B. P. (2020). Recent advances in single cell protein use as a feed ingredient in aquaculture. *Curr. Opin. Biotechnol.* 61, 189–197. doi: 10.1016/j.copbio.2019.12.026

Kaushik, S. J., and Luquet, P. (1980). Influence of bacterial protein incorporation and of sulphur amino acid supplementation to such diets on growth of rainbow trout, *Salmo gairdnerii* Richardson. *Aquaculture* 19, 163–175. doi: 10.1016/0044-8486(80)90017-4

Lee, S., Chowdhury, M. A. K., Hardy, R. W., and Small, B. C. (2020). Apparent digestibility of protein, amino acids and gross energy in rainbow trout fed various feed ingredients with or without protease. *Aquaculture* 524, 735270. doi: 10.1016/j.aquaculture.2020.735270

Mishra, A., Ntihuga, J. N., Molitor, B., and Angenent, L. T. (2020). Power-to-protein: Carbon fixation with renewable electric power to feed the world. *Joule* 4, 1142–1147. doi: 10.1016/j.joule.2020.04.008

Molitor, B., Mishra, A., and Angenent, L. T. (2019). Power-to-protein: converting renewable electric power and carbon dioxide into single cell protein with a two-stage bioprocess. *Energy Environ. Sci.* 12, 3515–3521. doi: 10.1039/C9EE02381J

Morales-Lange, B., Hansen, J.Ø., Djordjevic, B., Mydland, L. T., Castex, M., Mercado, L., et al. (2024). Immunomodulatory effects of hydrolyzed *Debaryomyces hansenii* in Atlantic salmon (*Salmo salar* L): From the *in vitro* model to a natural pathogen challenge after seawater transfer. *Aquaculture* 578, 740035. doi: 10.1016/j.aquaculture.2023.740035

Naylor, R. L., Hardy, R. W., Buschmann, A. H., Bush, S. R., Cao, L., Klinger, D. H., et al. (2021). A 20-year retrospective review of global aquaculture. *Nature* 591, 551–563. doi: 10.1038/s41586-021-03308-6

Øverland, M., Karlsson, A., Mydland, L. T., Romarheim, O. H., and Skrede, A. (2013). Evaluation of Candida utilis, Kluyveromyces marxianus and Saccharomyces cerevisiae yeasts as protein sources in diets for Atlantic salmon (*Salmo salar*). *Aquaculture* 402–403, 1–7. doi: 10.1016/j.aquaculture.2013.03.016

Øverland, M., and Skrede, A. (2017). Yeast derived from lignocellulosic biomass as a sustainable feed resource for use in aquaculture. *J. Sci. Food Agric.* 97, 733–742. doi: 10.1002/jsfa.2017.97.issue-3

Øvrum Hansen, J., Hofossæter, M., Sahlmann, C., Ånestad, R., Reveco-Urzua, F. E., Press, C. M., et al. (2019). Effect of Candida utilis on growth and intestinal health of Atlantic salmon (*Salmo salar*) parr. *Aquaculture* 511, 734239. doi: 10.1016/j.aquaculture.2019.734239

Rocha, S. D. C., Morales-Lange, B., Montero, R., Teklay Okbayohanese, D., Kathiresan, P., Press, C. M., et al. (2023). Norway spruce extracts (NSEs) as bioactive compounds in novel feeds: Effect on intestinal immune-related biomarkers, morphometry and microbiota in Atlantic salmon pre-smolts. *J. Funct. Foods.* 111, 105888. doi: 10.1016/j.jff.2023.105888

Romarheim, O. H., Øverland, M., Mydland, L. T., Skrede, A., and Landsverk, T. (2011). Bacteria grown on natural gas prevent soybean meal-induced enteritis in Atlantic salmon. *J. Nutr.* 141, 124–130. doi: 10.3945/jn.110.128900

Sarker, P. K. (2023). Microorganisms in fish feeds, technological innovations, and key strategies for sustainable aquaculture. *Microorganisms* 11, 439. doi: 10.3390/microorganisms11020439

Sharif, M., Zafar, M. H., Aqib, A. I., Saeed, M., Farag, M. R., and Alagawany, M. (2021). Single cell protein: Sources, mechanism of production, nutritional value and its uses in aquaculture nutrition. *Aquaculture* 531, 735885. doi: 10.1016/j.aquaculture.2020.735885

Skretting Sustainability report (2022). skretting-sustainability-report-2022.pdf.

Soni, R. A., Sudhakar, K., Rana, R. S., and Baredar, P. (2021). Food supplements formulated with Spirulina, in: Algae. *Springer. Singapore. Singapore.* pp, 201–226. doi: 10.1007/978-981-15-7518-1

Storebakken, T., Baeverfjord, G., Skrede, A., Olli, J. J., and Berge, G. M. (2004). Bacterial protein grown on natural gas in diets for Atlantic salmon, *Salmo salar*, in freshwater. *Aquaculture* 241, 413–425. doi: 10.1016/j.aquaculture.2004.07.024

Ulf, H., Nistad, A. ,. A., Aiegler, F., Shraddha, M., Wocken, Y., and Hognes, E. S. (2022). *Greenhouse gas emissions of Norwegian Salmon products, SINTEF rapport; 2022:01198 A, SINTEF Ocean As.* (Norway: SINTEF Ocean AS).

Yu, M.-H., Li, X.-S., Wang, J., Longshaw, M., Song, K., Wang, L., et al. (2023). Substituting fish meal with a bacteria protein (*Methylococcus capsulatus*, Bath) grown on natural gas: Effects on growth non-specific immunity and gut health of spotted seabass (*Lateolabrax maculatus*). *Anim. Feed. Sci. Technol.* 296, 115556. doi: 10.1016/j.anifeedsci.2022.115556

frontiers | Frontiers in Marine Science

TYPE Original Research
PUBLISHED 07 January 2025
DOI 10.3389/fmars.2024.1473319

OPEN ACCESS

EDITED BY
Yngvar Olsen,
Norwegian University of Science and Technology, Norway

REVIEWED BY
Pranaya Kumar Parida,
Central Inland Fisheries Research Institute (ICAR), India
Amit Ranjan,
Tamil Nadu Fisheries University, India

*CORRESPONDENCE
Gyanaranjan Dash
gyanranjandashcmfri@gmail.com;
gyanranjan.dash@icar.org.in

RECEIVED 30 July 2024
ACCEPTED 06 December 2024
PUBLISHED 07 January 2025

CITATION
Ghosh S, Dash G, Dash B, Pradhan RK, Megarajan S, Behera PR, Ranjan R, Sen S, Das M, Suresh VR, Gopalakrishnan A and Jena J (2025) From ocean to cage: evaluating the culture feasibility of Black-spotted croaker (*Protonibea diacanthus*). *Front. Mar. Sci.* 11:1473319. doi: 10.3389/fmars.2024.1473319

From ocean to cage: evaluating the culture feasibility of Black-spotted croaker (*Protonibea diacanthus*)

Shubhadeep Ghosh[1], Gyanaranjan Dash[2]*, Biswajit Dash[2], Rajesh Kumar Pradhan[2], Sekar Megarajan[3], Pralaya Ranjan Behera[3], Ritesh Ranjan[3], Swatipriyanka Sen[2], Madhumita Das[2], Vettath Raghavan Suresh[4], Achamveetil Gopalakrishnan[4] and Joykrushna Jena[5]

[1]Fisheries Science Division (Marine Fisheries), Indian Council of Agricultural Research (ICAR), Krishi Anusandhan Bhawan - II, Pusa, New Delhi, India, [2]Shellfish and Finfish Fisheries Divisions, Puri Field Centre of Indian Council of Agricultural Research-Central Marine Fisheries Research Institute (ICAR-CMFRI), Puri, Odisha, India, [3]Mariculture, Marine Biodiversity and Environment Management Divisions, Visakhapatnam Regional Centre of Indian Council of Agricultural Research-Central Marine Fisheries Research Institute (ICAR-CMFRI), Visakhapatnam, Andhra Pradesh, India, [4]Mariculture and Marine Biotechnology Divisions, Indian Council of Agricultural Research-Central Marine Fisheries Research Institute (ICAR-CMFRI), Kochi, Kerala, India, [5]Fisheries Science Division, Indian Council of Agricultural Research (ICAR), Krishi Anusandhan Bhawan - II, Pusa, New Delhi, India

Introduction: This study evaluates the feasibility of culturing the high-value marine fish *Protonibea diacanthus* in a polyculture system with Indian pompano (*Trachinotus mookalee*) using a marine cage culture setup. The study aims to determine growth performance, feed efficiency, and the potential of *P. diacanthus* as a candidate species for polyculture.

Methods: Wild-caught *P. diacanthus* were reared in six high-density polyethylene sea cages (Inner Diameter: 6 m; Outer Diameter: 7 m; Depth: 4.5 m; Area: 28.29 m^2; Volume: 127.29 m^3). Two experimental groups were established: Group-1 with 90 individuals (average weight: 130.15 ± 6.39 g) and Group-2 with 90 individuals (average weight: 287.80 ± 16.90 g). Each group was divided into three cages (30 fish/cage) and reared in triplicate with *T. mookalee* (2,500 fish/cage, average weight: 31.12 ± 1.17 g). The fish were cultured for 148 days and fed a commercial diet (40% crude protein, 10% crude lipid). Growth indices and feed efficiency indices were analyzed, and growth of the fish was modeled using von Bertalanffy Growth Function (VBGF).

Results: Growth performance indices, including total length gain, body weight gain, and specific growth rate, were significantly higher in Group-1 ($P \leq 0.05$). Feed efficiency indices (feed conversion ratio, feed efficiency ratio, and protein efficiency ratio) did not differ significantly between the groups ($P > 0.05$). VBGF modeling estimated *P. diacanthus* asymptotic length (L_∞) at 164.21 ± 3.58 cm, asymptotic weight (W_∞) at 44,070.19 ± 2811 g, growth coefficient (K) at 0.30 ± 0.01 yr^{-1} and t_0 at -0.005 ± 0.02 yr. The growth performance index (ϕ') was calculated at 1.91, surpassing values reported for wild populations. Polyculture with *P. diacanthus* did not significantly affect the growth or feed utilization of *T. mookalee* ($P > 0.05$).

10.3389/fmars.2024.1473319

Discussion and conclusion: The results indicate that *P. diacanthus* exhibits superior growth under marine cage culture conditions, with a high growth performance and compatibility in polyculture systems. These findings support the potential of *P. diacanthus* as a viable candidate for integration into commercial polyculture systems.

KEYWORDS

captive rearing, growth modeling, feed utilization, cage farming, sustainable aquaculture

1 Introduction

Global aquaculture production has been growing at an average annual rate of 5% and, for the first time in 2022, surpassed capture fisheries production, contributing 51% to global aquatic animal production. Excluding algae, global aquaculture achieved a record production of 94.4 million tonnes in 2022, with an estimated value of 295.7 billion USD. Marine aquaculture, which involves the cultivation of marine organisms for food and other products, accounted for approximately 35.3 million tonnes in 2022, representing about 31% of total marine animal production (FAO, 2024). These findings highlight the pivotal role of aquaculture in meeting the growing global demand for seafood. In order to promote the environmental, ecological and socio-economical sustainability of this important sector, continuous research and innovation for the improvisation of the existing farming techniques, refinement of the feed and disease management strategies and diversification of the production and utilization strategies are some of the fundamental aspects that require focused and dedicated attention (Boyd et al., 2020; Carballeira Braña et al., 2021). Species diversification helps to diversify production, reducing the vulnerability of the aquaculture industry to unforeseen challenges from emerging disease outbreaks, environmental challenges such as rising sea temperatures and/or ocean acidification and market dynamics such as change in consumer preference, market demand, culinary and cultural diversity (Harvey et al., 2017; Cai et al., 2022; Chan et al., 2024). Inclusion of species that can rapidly grow and efficiently convert feed into edible protein can make aquaculture practice more resource-efficient and sustainable.

India, the second largest aquaculture producer (excluding algae) of the world, alone contributed about 10.2 million tonnes of aquatic animal production in 2022 which is about 11% of the global aquaculture production and 27% of Asia's aquaculture production. As far as the marine and coastal aquaculture of aquatic animals is concerned, India ranks the 6th global position with a production of about 1.2 million tonnes against the projected potential of 4–8 million tonnes (FAO, 2024). Nevertheless, marine aquaculture holds significant opportunities in India considering the rapidly increasing demand for seafood, a demand that cannot be satisfied solely by the capture fisheries sector (Parappurathu et al., 2023). Currently, marine aquaculture in India mainly encompasses the cage culture of finfish and shellfish in open seas and internal waters using the hatchery produced and wild collected seeds, bivalve and pearl oyster farming, ornamental fish culture, seaweed cultivation and integrated multi-trophic aquaculture (IMTA) (Parappurathu et al., 2023). Presently, in India, the breeding and seed production techniques have already been standardized for nine marine finfish species (*Rachycentron canadum*, *Epinephelus coioides*, *Trachinotus blochii*, *T. mookalee*, *Lethrinus lentjan*, *Pomadasys furcatus*, *Lutjanus johnii*, *Siganus vermiculatus* and *Acanthopagrus berda*) by ICAR-Central Marine Fisheries Research Institute (Anuraj et al., 2021; Suresh Babu et al., 2022) out of which, many are popularly used for grow-out operation (Aswathy et al., 2020). Apart from this ICAR-CMFRI (India) has also prioritized 76 finfish and shellfish species that could be targeted for future expansion of marine aquaculture production in the country (Ranjan et al., 2017). The Black-spotted croaker, *P. diacanthus* (Lacepède, 1802) is one such prime species that is presently being evaluated for its marine aquaculture potential in India by ICAR-CMFRI.

P. diacanthus, also known as *Ghol* in India, belongs to the family Sciaenidae and is widely distributed in the coastal waters of the Indo-West Pacific region (Barton, 2018). It is a fast-growing and long-lived large predatory fish species that dwells in the epibenthic near-shore waters and feeds mainly on crustaceans and small fishes (Phelan et al., 2008; Barton, 2018). The species has significant market demand for its swimbladder, which is priced at USD 480-600 per kilogram (Dutta et al., 2014). It is also highly regarded as a food fish, with a market price ranging from USD 25-35 per kilogram (Dutta et al., 2014; Li et al., 2020). All these benefits make it one of the highly lucrative marine species. Due to its high market price, the species has been the prime focus of fishers for quite some time and forms an important component of commercial and subsistence fisheries in India and many countries abroad (Phelan et al., 2008; Dutta et al., 2014). However, its catch depends more on chance due to its rare and patchy (non-uniform) distribution (Dutta et al., 2014). Several studies have reported intra-annual changes in the abundance of *P. diacanthus* in inshore waters (Bhatt et al., 1964; Ansari et al., 1995), which indicated a seasonal migratory nature of the species. The fish is believed to perform seasonal migration and

aggregation probably in response to reproduction cycles (Dhawan, 1971) and/or food availability (Thomas and Kunju, 1981). Unfortunately, fish that show aggregation behaviour are typically vulnerable to overfishing and excessive targeting, especially during spawning aggregation, which could be detrimental for such species (Sadovy and Cheung, 2003), as has been the case in Australia with reduction in total length and an abundance of smaller size groups in the catches, and a declining size at maturity (Phelan et al., 2008; Leigh et al., 2022).

Due to its fisheries' significance and vulnerability, the species has drawn the attention of researchers in the past, with global studies focusing mostly on growth, food and feeding habits, reproductive biology and fisheries management (Bibby and McPherson, 1997; McPherson, 1997; Phelan et al., 2008; Ghosh et al., 2010; Leigh et al., 2022). Considering the high demand and the challenges involved in its capture fishery in India, alternate production strategies like captive breeding and farming have been suggested. Farming of *P. diacanthus* in marine cages would not only reduce exploitation pressure on the natural population of this species but also produce a dependable source of production to meet the ever-increasing consumer demand for the species. Due to its fast growth rate, disease resistance, strong adaptability and excellent market value, it is lately being preferred as a lucrative candidate species for commercial aquaculture in China (Li et al., 2016; Rong et al., 2020). Several studies have attempted to understand its ovarian, embryonic and larval development to standardize artificial breeding (Shi et al., 2004; Zhang et al., 2006; Shen et al., 2007). Apart from this, several trials have also been made to study the nutritional requirements of this fish to develop a cost-effective, balanced diet for ensuring better growth under captivity (Li et al., 2017, 2019). Nevertheless, based on the review of accessible literature, it is evident that the aforementioned studies primarily consist of brief trials in which the growth and/or feed utilisation of the species have been assessed within a very short timeframe spanning up to eight weeks. None of the studies presented in the literature portray the growth performance of the species over an adequate timeframe that is necessary for achieving a consumer-acceptable table size (marketable size), which is a crucial factor in determining its suitability as a potential aquaculture species. Therefore, the present study was envisaged (1) To generate *in-situ* growth data for *P. diacanthus* by rearing it in floating marine cages under natural captive conditions, (2) To develop a model that simulates the future growth potential of *P. diacanthus* in floating cages over an extended culture period, and (3) To assess the growth performance of *P. diacanthus* and evaluate its suitability as a candidate species for aquaculture.

2 Materials and methods

2.1 Experimental cages (location and design)

A total of 12 numbers of cages were used for the experiments, and the entire cage units occupied a stretch of approximately 1.5 km

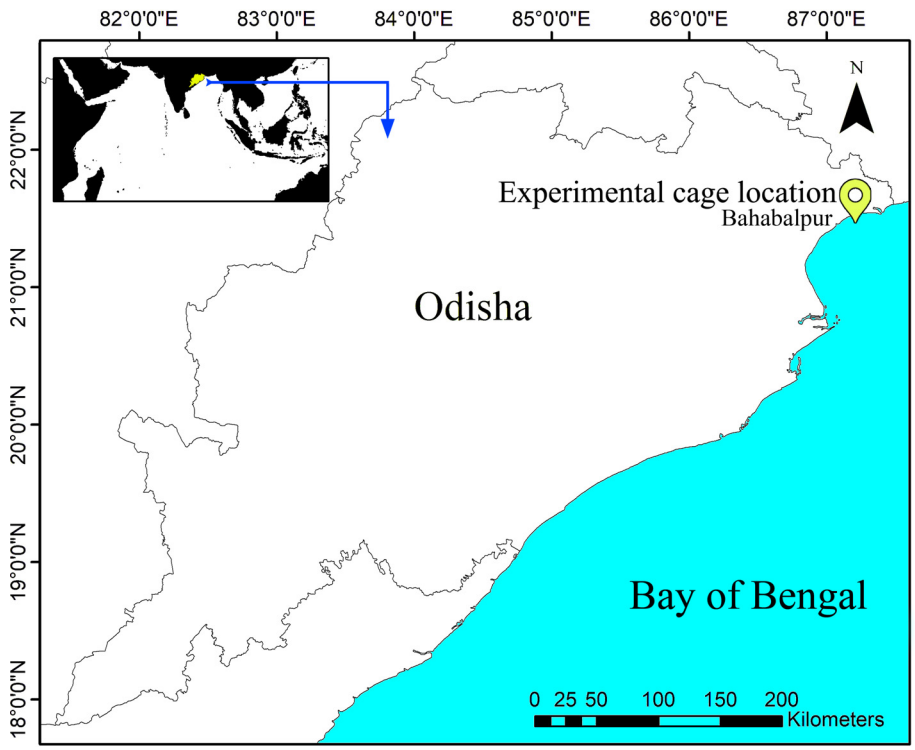

FIGURE 1
Map showing the experimental location of open sea cage farms established at Bahabalpur (Odisha, India) for the experimental rearing of *Protonibea diacanthus*.

neighboring the Bahabalpur Fishing Harbour (21^0 27.441'N and 87^0 9.602'S, Odisha, India) (Figure 1). Circular floating cages of 6.0 m inner diameter and 8.0 m outer diameter with 4.5 m net depth (water holding depth) were used for the experiment (area: 28.29 m^2; volume: 127.29 m^3). The High-Density Polyethylene (HDPE) pipes of Pressure Nominal (PN)-10 and Polyethylene (PE) 100-grade quality were used for the fabrication of the floating cages. HDPE nets were used for better strength; where, inner fish-holding vertical hanging net of 4.5 m water holding depth with 25 mm mesh size was used; outer vertical hanging net of 5.0 m depth with 40.0 mm mesh size was used as predator net; and a horizontal surface net with 80 mm mesh size was used as bird protection net. The inner holding net was supported with two ballast pipes at 2.0 m and 4.0 m below the water surface to maintain the cylindrical shape of the net. The floating cage structure was stabilized in the sea with the help of mooring systems supported by 1.5 t capacity concrete cement blocks (dead weight anchor) and mooring chain (long link alloy steel chain of 13 mm diameter with 22 t shearing strength).

2.2 Experimental fish

The live juveniles of Blackspotted croaker (*P. diacanthus*) were collected from the local fishers fishing in the vicinity of the cage farming demonstration of Indian pompano (*Trachinotus mookalee*), which was underway in the above-mentioned geographical location. The fish were caught in gill nets (mesh size: 50 mm) from a depth of 5-10 m. The fishes were identified as *P. diacanthus* (Figure 2) following the morphological description of Fischer and Bianchi (1984). A total of 193 live specimens were collected from the local fishers over a month as and when they were caught, and were transported in 1,000 l onboard water tanks filled with seawater (32 ppt) with continuous aeration. Due to the scarcity of separate and independent offshore farming facilities, the specimens (n = 180) were stocked in six cages, in which culture of the Indian Pompano, *T. mookalee* of mean total length (TL) 12.29 ± 0.16 cm and mean body weight (BW) of 31.12 ± 1.17 was ongoing at a density of 2,500 individuals per cage. Indian pompano fingerlings, produced in the marine finfish hatchery complex at the Regional Centre of ICAR-CMFRI in Visakhapatnam, India, were transported overnight to the cage farming demonstration site using insulated live-fish carriers. The stocking density used for Indian pompano was determined based on our earlier work (Sekar et al., 2021).

2.3 Experimental design

The study was conducted using a Completely Randomized Design (CRD) with two experimental groups, each replicated three times. The experimental groups, Group-1 and Group-2, were classified based on size variations in *P. diacanthus* specimens.

- Group-1: This group consisted of 90 smaller-sized individuals (n = 90) with a mean total length (TL) of 22.69 ± 0.44 cm (mean ± SE) and a mean body weight (BW) of 130.15 ± 6.39 g (mean ± SE). The fish were distributed across three cages in triplicates, with 30 individuals per cage.
- Group-2: This group included 90 larger-sized individuals (n = 90) with a mean TL of 29.34 ± 0.78 cm and a mean BW of 287.80 ± 16.90 g. These were also distributed across three cages in triplicates, with 30 individuals per cage.

Due to lack of dedicated sea cages for *P. diacanthus*, both the Group-1 and Group-2 were maintained as polyculture setups, where the 30 numbers of *P. diacanthus* were added to the existing 2,500 numbers of *T. mookalee* (a mean TL of 12.18 ± 0.27 cm and a mean BW of 30.90 ± 1.83 g) per cage, resulting in a total stocking density of 2,530 fish per cage in the polyculture setups. Additionally, a monoculture setup comprising six cages stocked only with 2,500 numbers of *T. mookalee* (mean TL of 12.39 ± 0.24 cm and a mean BW of 31.34 ± 1.84 g) per cage was maintained to compare and evaluate any synergistic or antagonistic effects of *P. diacanthus* on *T. mookalee* in the polyculture setups.

2.4 Experimental diet and feeding regime

The feeding regime followed for *T. mookalee* using a commercial diet (Nutrila Marine Fish Feed, Growel, Andhra Pradesh, India; Ingredients: fish meal, soybean meal, wheat products, rice products, fish oil, vegetable oil, soya lecithin, amino acid, vitamins and minerals; Nutritional Composition: 40% crude protein, 10% crude fat, 3% crude fiber, and 12% crude moisture; Pellet size: 1.5 mm, 3.0 mm and 6.0 mm) was continued unchanged in both the experimental groups; and was at 6% of the combined body weight initially, which was gradually reduced to 3% of the combined body weight. The fish were grown for a maximum

FIGURE 2
Black-spotted croaker (*Protonibea diacanthus*) experimentally cultured at Bahabalpur (Odisha, India).

duration of 148 days. Feeding trials with *P. diacanthus* were conducted during the acclimatization phase using the specified feed to evaluate its acceptability by the species. The entire ration was divided into 3 equal portions and broadcasted in early morning (06:00 hr), mid-day (12:00 hr) and evening (18:00 hr) in the middle of the cage to make it available for all the fish. Adequate measures were employed to control feed wastage from the cage, where the inner fish-holding cage net was stitched with a zero-mesh size nylon net at the water and air interface to retain the feed completely inside the cage. The growth was monitored fortnightly and the feeding rate and ration were adjusted accordingly.

2.5 Evaluation of growth performance

The growth performance of the fish (*P. diacanthus*) during the culture duration was evaluated using the indices such as total length gain (TLG%), body weight gain (BWG%), specific growth rate (SGR) and absolute growth rate (AGR) which were assessed using the following formula.

$$Total\ \ length\ \ gain\ \ (TLG\,\%) = \frac{Final\ \ total\ \ length - Initial\ \ total\ \ length}{Initial\ \ total\ \ length} \times 100$$

$$Body\ \ weight\ \ gain\ \ (BWG\,\%) = \frac{Final\ \ body\ \ weight - Initial\ \ body\ \ weight}{Initial\ \ body\ \ weight} \times 100$$

$$Specific\ \ growth\ \ rate\ \ (SGR) = \frac{\ln(Final\ \ body\ \ weight) - \ln(Initial\ \ body\ \ weight)}{Experiment\ \ period} \times 100$$

$$Absolute\ \ growth\ \ rate\ \ (AGR) = \frac{Final\ \ body\ \ weight - Initial\ \ body\ \ weight}{Experiment\ \ period}$$

Fulton's condition factor was calculated according to Htun-Han (1978) equation, as per the formula given below:

$$Condition\ \ factor\ \ (CF) = \frac{BW}{(TL)^3} \times 100$$

Where, BW is the body weight of fish in g; TL is the total length of fish in cm.

2.6 Evaluation of feed utilization performance

The feed utilization performance of the fish (*P. diacanthus*) during the culture duration was evaluated using the indices such as feed conversion ratio (FCR), protein conversion rate (PCR) and protein efficiency rate (PER) which were assessed using the following formula. The average protein content of the commercial feed was used for the calculation of PCR and PER.

$$Feed\ \ conversion\ \ ratio\ \ (FCR) = \frac{Total\ \ feed\ \ intake\ \ (g)}{Total\ \ wet\ \ weight\ \ gain\ \ (g)}$$

$$Feed\ \ efficiency\ \ ratio\ \ (FER) = \frac{Total\ \ wet\ \ weight\ \ gain\ \ (g)}{Total\ \ feed\ \ intake\ \ (g)}$$

$$Protein\ \ efficiency\ \ ratio\ \ (PER) = \frac{Total\ \ wet\ \ weight\ \ gain\ \ (g)}{Crude\ \ protein\ \ fed\ \ (g)}$$

The survival rate (%) was calculated using the following formulae

$$Survival\ \ rate\ \ (\%) = \frac{Final\ \ number\ \ of\ \ surviving\ \ animals}{Initial\ \ number\ \ of\ \ animals} \times 100$$

The above-mentioned indices on growth and feed utilization performances were also assessed for Indian Pompano grown in both the monoculture and polyculture setups and compared to assess any possible impact of *P. diacanthus* on the standalone growth and feed utilization performances of *T. mookalee*.

2.7 Growth modeling and simulation

To simulate and project the growth potential of the fish beyond the actual culture duration of the present study, the available growth data was modeled using the fortnightly collected periodic length (mm) and weight (g) increment data. The growth was modeled using the non-linear von Bertalanffy's growth equation (von Bertalanffy, 1934) using 'nls' routine in the R statistical software package.

$$L_t = L_\infty \times (1 - exp^{-k(t-t_0)}) \quad (1)$$

$$W_t = W_\infty \times (1 - exp^{-k(t-t_0)})^b \quad (2)$$

Where L_t and W_t are the length (cm) and weight (g) of fish, respectively, that can be expected at age t (years); L_∞ and W_∞ are asymptotic length (cm) and weight (g) of the fish, respectively; k is the growth coefficient of the fitted curve; t_0 is the age (year) when the size of the fish was theoretically zero. It is also the point where the fitted growth curve intersects the x-axis and is also used as a proxy for the gestation or incubation period (hatching duration). The weight form of the von Bertalanffy's growth equation (Equation 2) necessitates another parameter, i.e., b, which is the power of the length-weight relationship of the fish. The relationship between length and weight (LWR) was established using the power law suggested by Le Cren (1951).

$$BW = a(TL)^b$$

Where BW is the body weight of fish in g; TL is the total length of fish in cm; 'a' and 'b' are model coefficients. A Wald test was performed to check if the growth is isometric (b=3.0) or allometric (b≠3.0).

2.8 Statistical analysis

The Shapiro-Wilk test (Shapiro and Wilk, 1965) was performed on growth performance and feed utilization performance data to check the normality of the data. An F-test was performed to check the equality or homogeneity of variance (homoscedasticity). When the assumption of normality of the data was not met, the Welch t-test was performed to determine if there were statistically significant differences between the means of the experimental groups. All the statistical analyses in the present study were performed using the R statistical software package (R Core Team, 2021).

3 Results

3.1 Growth performance and feed utilization efficiency of Black-spotted croaker in polyculture setups (Group-1 and Group-2)

The growth performance and feed utilization efficiency indicators and their comparisons between the two experimental groups (Group-1 vs. Group-2) are shown in Figure 3 and Supplementary Table S1. Both the relative growth indicators, i.e., total length gain (TLG%, Figure 3A), body weight gain% (BWG%, Figure 3B) and the instantaneous growth indicator, i.e., specific growth rate (SGR, Figure 3D) were significantly higher ($P \leq 0.05$) in Group-1 compared to the Group-2. Contrary to this a significantly lower ($P \leq 0.05$) absolute growth rate (AGR) (Figure 3F) was recorded in the Group-1 compared to the Group-2. The condition factor (CF) (Figure 3C) did not show any significant difference ($P > 0.05$) among the experimental groups.

The modeled growth in terms of absolute increase in body weight is presented in Figure 3E. None of the feed efficiency indicators, i.e., feed conversion ratio (FCR, Figure 3G), feed efficiency ratio (FER, Figure 3H) as well as the protein efficiency ratio (PER, Figure 3I) showed any signficant difference ($P > 0.05$) among the experimental groups. The survival was 100% in both the experimental groups.

3.2 Growth performance and feed utilization efficiency of Indian pompano (polyculture and monoculture setups)

The growth performance and feed utilization efficiency indicators and their comparisons between the two culture systems (polyculture and monoculture) are shown in Figure 4 and Supplementary Table S2. The relative growth indicators, i.e., TLG % (Figure 4A), BWG% (Figure 4B) and CF (Figure 4C) of *T. mookalee* grown in polyculture mode with *P. diacanthus* did not vary significantly ($P > 0.05$) from that of the fish grown in monoculture mode. Similarly, there was no significant difference ($P > 0.05$) in the SGR (Figure 4D) and AGR (Figure 4F) of *T. mookalee* grown in polyculture and monoculture modes. The von Bertalanffy's growth function (VBGF) parameters derived by fitting the growth model using fortnightly weight increment data of *T. mookalee* is shown in Figure 4E. The asymptotic length (L_∞) and weight (W_∞) for the fish were derived as 95.06 ± 1.24 cm and 11574.49 ± 377.90 g, respectively for polyculture mode and 95.17 ± 1.30 cm and 11850.12 ± 387.80 g, respectively for monoculture mode. The modeled growth coefficient (k) and t_0 were 0.48 ± 0.01 yr^{-1} and -0.004 ± 0.01 yr, respectively for polyculture mode and 0.48 ± 0.01 yr^{-1} and -0.003 ± 0.01 yr, respectively for monoculture mode. The simulated growth trajectories for *T. mookalee* grown in polyculture mode with *P. diacanthus* did not vary significantly ($P > 0.05$) from that of the *T. mookalee* grown alone in monoculture mode. Similarly, none of the feed utilization efficiency indices viz., FCR ('Figure 4G), FER (Figure 4H) and PER (Figure 4I) of *T. mookalee* were significantly different beween the polyculture and monoculture setups.

3.3 Growth modeling of Black spotted croaker in captive conditions (marine cages)

The length-weight relationship (LWR) modeled for the fish is shown in Figure 5. The weight increment appears to be isometric as the exponent (b) is not significantly different from 3 (Wald-test, F-value=0.2292, P=0.6339). The von Bertalanffy's growth function (VBGF) parameters derived by fitting the growth model using fortnightly length and weight increment data are shown in Figure 6 and their comparison with earlier studies is given in Table 1, Supplemetary Table S3 and Figure 7. The asymptotic length (L_∞) and weight (W_∞) for the fish were derived as 164.21 ± 3.58 cm and 44070.19 ± 2811 g, respectively. The modeled growth coefficient (K) and t_0 were 0.30 ± 0.01 yr^{-1} and -0.005 ± 0.02 yr, respectively. The fortnightly and annual growth projections from previously established growth models using samples from the natural feral (wild) condition and the presently fitted growth model using samples from the natural captive (culture) condition are shown in Figure 7 and Supplementary Table S3. The projected age for sexual maturity (TM_{50}) appears to be earlier (approximately 2.5 years) under natural captivity compared to the wild condition (Figure 7), which indicates that the species grows faster and matures earlier when cultured in a natural captive condition. The growth performance index (ϕ'=1.91) was also observed to be higher in the fish cultured in sea cage farms compared to the fish in the wild (Table 1).

4 Discussion

The fast growth and high market price, especially due to the demand for swimbladders and the nutritional quality of its meat make *P. diacanthus* a potential candidate species for marine aquaculture (Li et al., 2016; Rong et al., 2020). The data available in the public domain at present describes the growth of the species over short-duration trials conducted for a maximum of up to 56 days. Furthermore, there is no predictive model available to understand the growth of this species in captive conditions for a longer timeframe, which is essential to assess the culture

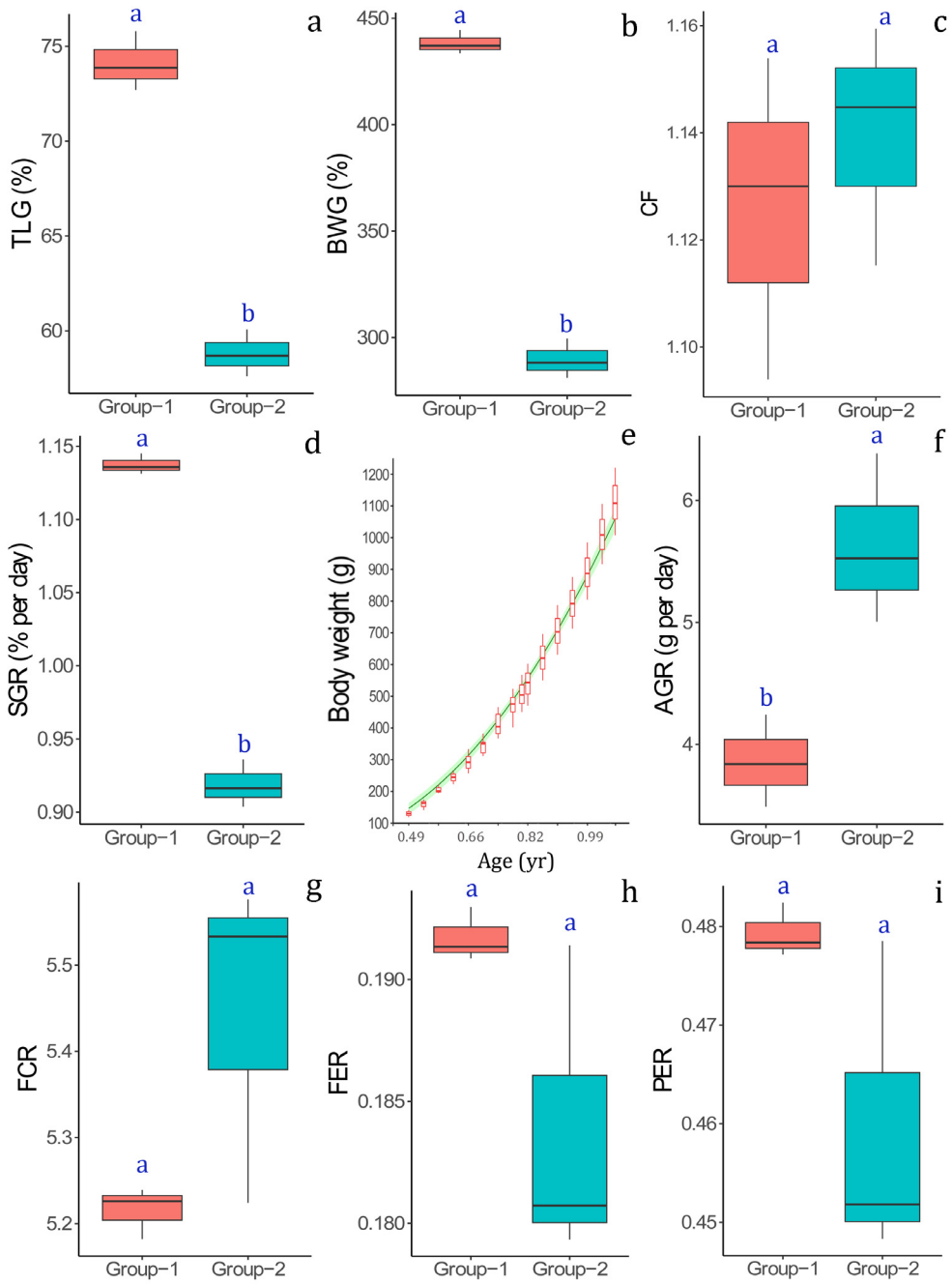

FIGURE 3
Comparison of growth performance indices, **(A)** total length gain (TLG%), **(B)** body weight gain (BWG%), **(C)** condition factor (CF), **(D)** specific growth rate (SGR), **(E)** modeled growth (increment in body weight) during culture, **(F)** absolute growth rate (AGR); and feed utilization indices, **(G)** feed conversion ratio (FCR), **(H)** feed efficiency ratio (FER), and **(I)** protein efficiency ratio (PER) between the fish (*Protonibea diacanthus*) reared in two experimental groups (Group-1 vs. Group-2).

performance of the species for aquaculture. The experiment has generated distinctive *in situ* length increment data, which has been applied to develop models to understand the growth of the species under captive conditions beyond the duration of culture in this study to assess its suitability for aquaculture. The modeled growth performance of the species will pave the way for future research to further refine the technological interventions to develop the species as an ideal candidate species for aquaculture.

From a thorough review of the accessible literature available in the public domain, it appears that in most of the world including India, the breeding and seed production technologies, along with grow-out technology for the species, are yet to be standardized. Therefore, the present study was attempted by using wild-caught juveniles of *P. diacanthus* and integrating it to the culture set-up originally developed for the grow-out of *T. mookalee*. Uniformity in initial stocking size could not be ensured for both the culture groups

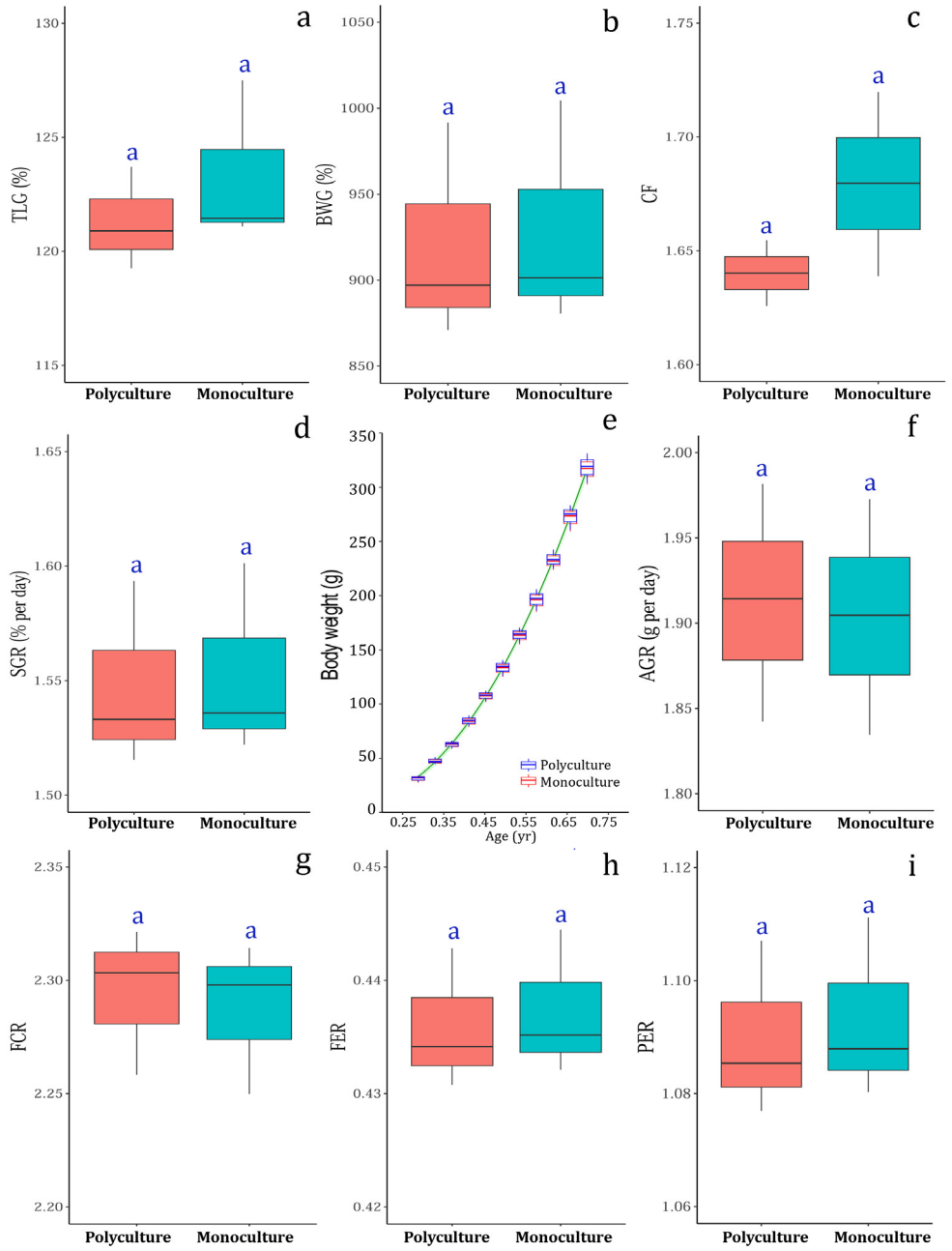

FIGURE 4
Comparison of growth performance indices, **(A)** total length gain (TLG%), **(B)** body weight gain (BWG%), **(C)** condition factor (CF), **(D)** specific growth rate (SGR), **(E)** modeled growth (increment in body weight) during culture, **(F)** absolute growth rate (AGR); and feed utilization indices, **(G)** feed conversion ratio (FCR), **(H)** feed efficiency ratio (FER), and **(I)** protein efficiency ratio (PER) between the fish (*Trachinotus mookalee*) reared in two culture setups (Polyculture vs. Monoculture).

of *P. diacanthus* (Group-1 and Group-2) due to the sole dependency on nature for seed materials. As the *T. mookalee*, the originally mandated species of the ongoing demonstration program, were harvested after a culture period of 5 months (148 days), it was economically not viable to further continue the culture experiment with *P. diacanthus*. Nevertheless, the experiment could generate the much-needed and rarely available length and weight increment data for 148 days necessary to model the growth performance of *P. diacanthus* under natural captive conditions, which is of paramount importance to evaluate the species for its aquaculture potential so that future research for its artificial propagation, seed production and grow-out technology can be envisaged.

The few short-duration (56-day) sea-based *in-situ* culture trials conducted by earlier studies have reported the growth performance

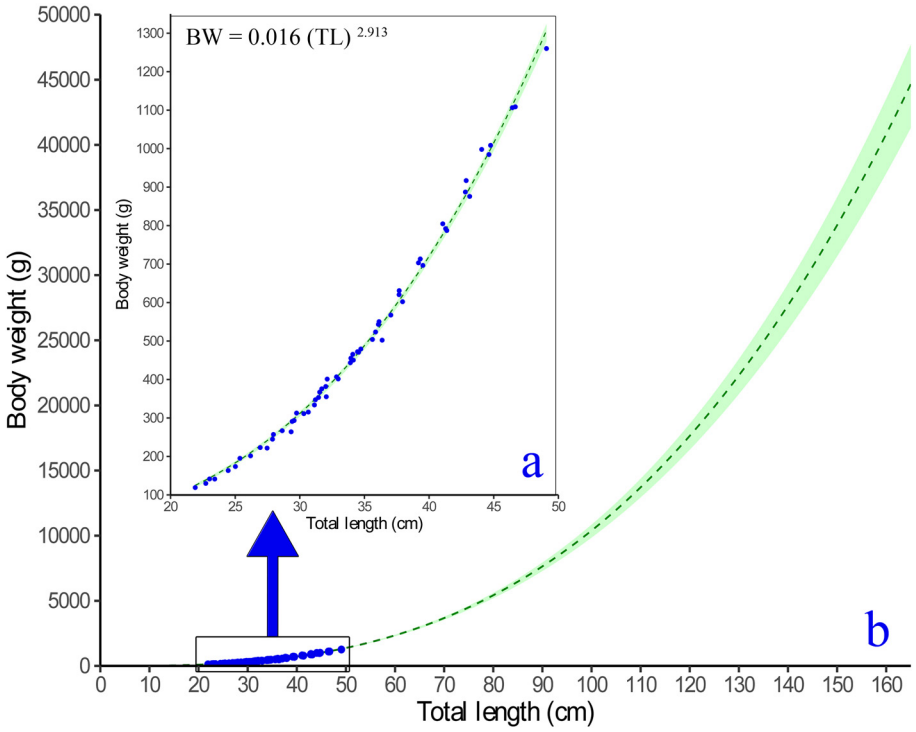

FIGURE 5
Relationship between the total length (cm) and body weight (g) of *Protonibea diacanthus* (**A**: observed data; **B**: modeled projection).

of *P. diacanthus* either in terms of absolute growth rate (length or weight increase) or relative growth rate (length or weight gain percentage compared to initial length or weight, respectively) or as an instantaneous growth rate (specific growth) (Li et al., 2016, 2017, 2019; Rong et al., 2020). However, these indices have certain inherent limitations in their underlying assumptions. For example, the absolute growth rate (AGR) in the present study was observed to be significantly higher ($P < 0.05$) in Group-2 (mean weight ± SE: 287.80 ± 16.90 g) compared to the Group-1 (mean weight ± SE: 130.15 ± 6.39 g). In aquaculture studies, the AGR,

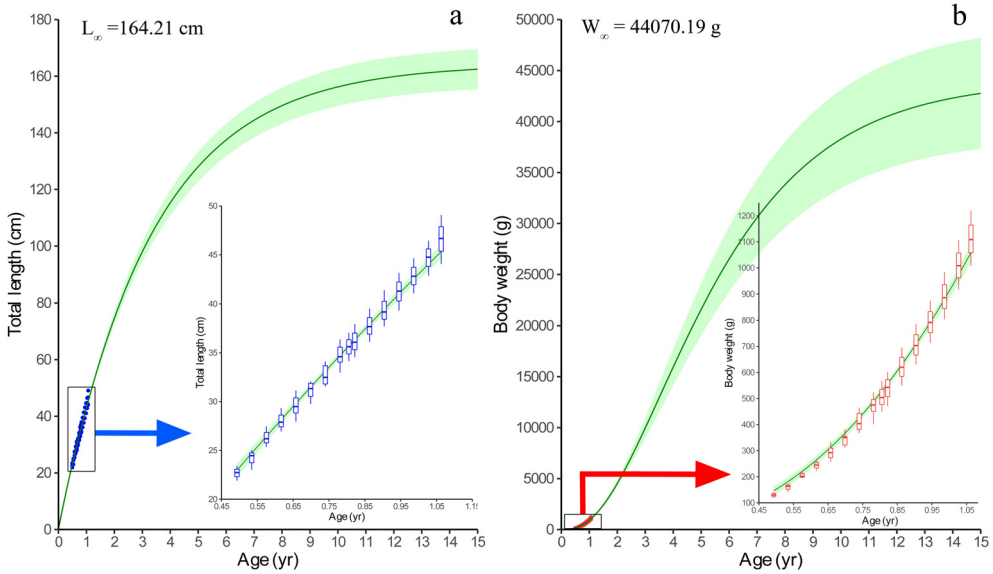

FIGURE 6
Growth modeling of *Protonibea diacanthus* using fortnightly length and weight increment data. **(A)** represents length-based VBGF model, with the blue arrow indicating a zoomed view of the actual length increment data fitted by the model. **(B)** represents weight-based VBGF model, with the red arrow indicating a zoomed view of the actual weight increment data fitted by the model.

TABLE 1 Von Bertalanffy's Growth Function (VBGF) parameters and Length-Weight Relationship (LWR) parameters (Mean ± SE) modeled for *Protonibea diacanthus* reared in sea cage farms at Bahabalpur (Odisha, India), and comparison with earlier studies.

	VBGF parameters				Length-weight relationship	
Parameters	L_∞ (cm)	K (yr^{-1})	ϕ'	t_0 (yr)	a	b
Present study	164.21	0.30	1.91	-0.005	0.016	2.91
Rao, 1966	122.14	0.32	1.67	-0.310		
Rao, 1968	144.72	0.19	1.61	-0.690		
Erzini, 1991	114.00	0.39	1.70			
Bibby and McPherson, 1997	136.60	0.32	1.78	0.180	0.015	2.88
Ghosh et al., 2010	145.30	0.14	1.47	-0.074	0.017	2.86
Leigh et al., 2022	118.50	0.42	1.77			

L_∞, asymptotic length; K, growth coefficient; t_0, age when length was theoretically zero; a & b, length weight relationship parameters.

though considered a standard method or index for expressing and comparing the growth rate, it assumes that growth is linear and constant throughout the entire life history of fish, which is not true (Hopkins, 1992). Furthermore, AGR measures the total change in the mass of cultured animals over a specified time period, but it assumes that the individuals being compared should have the same initial sizes. Otherwise, the periodic increase in absolute mass of a slow growing larger individual could be higher than the fast-growing smaller individuals. Therefore, AGR could give biased results if the cultured animals have different initial sizes. One way to address this issue (different initial stocking size or biomass) is to calculate the growth rate of the cultured animals in terms of relative growth rate index (RGR) that derives the growth as a ratio of final to initial mass. It assumes that the animals grow in equal proportion throughout their entire life stage which is not true. Fish usually grow slower during the initial and late stages and faster during the intermediate stage, which is entirely ignored by the above-mentioned growth performance indices and therefore, could be less informative when such indices are used to compare growth over a longer duration. In the present study, contrary to the AGR, the RGRs (i.e., TLG and BWG), were significantly higher ($P< 0.05$), in the Group-1 (mean weight ± SE: 130.15 ± 6.39 g) compared to the Group-2 (mean weight ± SE: 287.80 ± 16.90 g), which is due to faster growth rate of the smaller individuals compared to the larger. Another way of expressing the growth rate is the instantaneous growth rate, a form of which is expressed as the specific growth rate

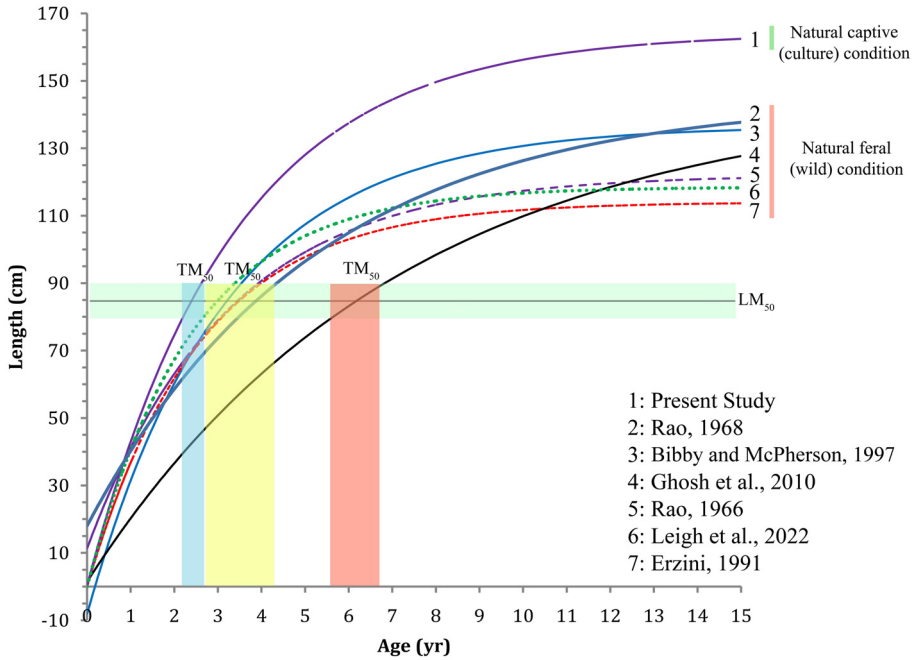

FIGURE 7
Comparison of growth performance of *Protonibea diacanthus* in natural wild conditions, derived from length-at-age keys modeled in earlier studies, with the growth performance of *P. diacanthus* cultured in captive conditions modeled using periodic length increment data from sea cage farms at Bahabalpur (Odisha, India).

(SGR). Since it assumes the weight of fish grows exponentially, it is only valid to compare the growth of fast-growing young fish cultured for a short-duration but not valid for larger fish cultured for a long duration (Hopkins, 1992). In the present study, just like the AGRs, the SGR was found to be higher for smaller sized Group-1 compared to the large sized Group-2. Therefore, all these indices may not always be suitable to compare the growth performance of the fish in experimental set-ups, especially which depends on feral fish as it is difficult to ensure same culture size and duration among the experimental groups due to the sole dependency on wild for seed. Another way of expressing the growth rate is the instantaneous growth rate, a form of which is expressed as the specific growth rate (SGR). Since it assumes the weight of fish grows exponentially, it is only valid for young fish cultured for a short-duration but not valid for larger fish cultured for a long duration (Hopkins, 1992).

Furthermore, the conventional growth indices have very limited applicability as they can only describe the growth that can be observed during a culture experiment, mostly by differentiating the growth at the end by comparing it with the growth at the beginning of the experiment. To visualize what is happening at intermediate points and beyond the observable experimental data and make any predictions about further growth development, it is essential to use complex non-linear models. The von Bertalanffy growth function (VBGF) is one such nonlinear model that is popularly used in fishery biology to describe the growth of fish (Hopkins, 1992; Lugert et al., 2016; Lugert et al., 2017). Furthermore, the majority of the studies conducted to assess the life history parameters of feral populations of *P. diacanthus* have modeled the growth parameters using the non-linear von Bertalanffy growth function (VBGF) and therefore, the same was adopted in the present study so that the results can be compared. The present study is unique in that the growth performance of *P. diacanthus* has been modeled using the length and weight increment data collected over the longest available culture duration of 148 days through the VBGF model, which could be considered scientifically sound and more reliable.

According to Leigh et al. (2022), *P. diacanthus* is a large species which can attain lengths of at least 150 cm in total length and weights of at least 42 kg, and can live up to at least 15 years. The growth performance modeled using von Bertalanffy's growth function (VBGF) revealed an asymptotic length (L_∞) of 164.21 cm and a growth rate of 0.30 yr^{-1} for the species. By comparing the L_∞ derived in the present study with that of the earlier studies mentioned in Table 1, though it appears to be higher, it is reasonable as the back calculated L_{max} (i.e., 156 cm) using the empirical thumb rule of the relationship between L_∞ and L_{max} (i.e., $L_\infty = L_{max}/0.95$) recommended by Pauly (1984) and Taylor (1958), is similar to the observed L_{max} of 156 cm and 152 cm for this species that have previously been reported from Maharashtra and Gujarat states of India (Hotagi, 1994; Mohammed et al., 2009). The present estimate is also similar to the L_{max} of 154 cm (Bibby and McPherson, 1997) reported from the Queensland Gulf (Australia). However, the present estimate of maximum length (L_{max} = 156 cm) and maximum body weight derived using the L_{max} and length-weight relationship (W_{max} = 37925 g) are smaller compared to the L_{max} of 176 cm and W_{max} of 45000 g reported by Grant (1982) from Queensland (Australia), though the latter was almost similar to the asymptotic weight (W_∞=44070 g) modeled in the present study. Similarly, there are studies from India (Rao, 1966, 1968; Ghosh et al., 2010) as well as Australia (Erzini, 1991; Bibby and McPherson, 1997; Leigh et al., 2022) where the derived L_∞ can be observed to be lower compared to the present study. As the L_{max} (and so does the dependent L_∞) depends mostly on the exploitation parameters, it tends to decrease when there is targeted fishery for the species, which is evident in the *P. diacanthus* fishery of Queensland (Australia), where the L_{max} has decreased drastically from 176 cm in 1982 to 92.5 cm in 2000, and then subsequently revived to 103.5 cm in 2002-2003 (Phelan et al., 2008). In the present study, the dissimilarity observed in the derived L_{max} (and therefore the modeled L_∞) with that of earlier studies could be due to the spatiotemporal differences in the fishery-related factors. However, the growth coefficient (K) modeled for the species in the present study appears to be similar or higher compared to most of the earlier studies mentioned in Table 1, except for those conducted by Erzini (1991) and Leigh et al. (2022). However, careful scrutiny reveals that for these studies, the reported L_∞ is very low (L_∞< 120 cm) compared to the present study. Due to its compensatory behaviour, the K increases as the L_∞ decreases and vice versa, so that the overall growth performance remains more or less constant for a species (Pauly and Munro, 1984). Therefore, a merely high K value does not necessarily mean a better growth rate and hence the growth performance index (ϕ) should rather be compared to understand the growth performance of the species. As ϕ' is based on body length rather than body weight, it is less liable to bias. It has the dimensions of both length and time and is usually normally distributed with smaller standard deviations compared to other growth indices and therefore, it has been recommended as the most flexible and precise estimator of growth performance (Mathews and Samuel, 1990). The higher ϕ' (=1.91) observed in the present study illustrates the superior growth performance of the species under natural captive conditions, which can also be seen in Supplementary Table S2 and Figure 7. As the growth of the animals in a culture system is strongly boosted in a time-bound manner by technological interventions like highly proteinaceous feed and augmented environmental conditions, they may outperform their wild counterparts in terms of growth performance. It has been substantiated that fish grown in sea-based cage culture set-up exhibit better growth, probably due to the acquisition of supplementary nutrition (apart from highly proteinaceous feed) from naturally occurring organisms growing in/on the culture system, as well as plankton, invertebrates and other live prey items that move through the culture system (Simon and James, 2007; Perez-Benavente et al., 2010). Furthermore, fish reared in sea-based culture systems with adequate water exchanges are likely to receive environmental (physical) enrichment that attenuates stress and improves overall welfare (Johnsson et al., 2014; Näslund and Johnsson, 2016; Jones et al., 2021).

McPherson (1997) and Phelan et al. (2008) have reported the length at first maturity to be 79 cm TL in Northern Cape York Peninsula waters and 92 cm TL in Queensland waters respectively, that approximately corresponds to the 3 and 4 years age classes using the length/age keys developed by Bibby and McPherson (1997). The findings of Phelan et al. (2008) also match with the observations by Rao (1963) from Indian waters, who found that 5% of the fish were mature in the 75–80 cm TL, 36.8% in 80–85 cm TL,

91% in 85–90 cm TL, and 100% in 90–95 cm TL, in which the first length at maturity is attained at an approximate age of 3 years using the VBGF modeled for the species by Rao (1966). The spatiotemporal variations in the size of maturity observed in these studies could be attributed to fisheries related exploitation factors that influence the maturity of the targeted population, which decreases as the targeted exploitation increases (Phelan et al., 2008). According to the growth model developed in the present study, these lengths of maturity, i.e., 79 cm and 92 cm TL would be attained at about 2.2 years and 2.7 years respectively if the fish are allowed to grow under natural captive conditions. This implies that the fish matures a year earlier in the natural captive condition (which can be verified in Figure 6) as it grows faster compared to the wild ones that grow in natural conditions. The information has great implications as it can be used to design future experiments to standardize artificial breeding and seed production of *P. diacanthus*.

A comparison with previous captive-rearing studies conducted in China provides valuable insights into growth performance. As growth performance indicators (GPIs) like WG% and SGR depend on the initial size or body weight of fish, the indices generated in the present study cannot be compared directly with those from the earlier studies. To enable an unbiased comparison, initial body weight of the present study was simulated to match with the initial body weights of the previous studies and the final body weight after 56 days of culture (which is the culture duration of the previous studies) was derived using the established VBGF growth model. The simulated GPIs, i.e., 160.81 WG% and 1.71 SGR obtained in the present study by feeding the fish a commercial diet containing 40% crude protein were marginally lower compared to the GPIs (171.74 WG% and 1.78 SGR) obtained by Li et al. (2016) when fish were fed a commercial diet having 41% crude protein. The GPIs were also observed to be higher compared to the present study when the fish were fed a commercial diet having higher percentage (≥ 45%) of crude protein (Li et al., 2016, 2017, 2019 and Li et al., 2020). It is well established that carnivorous fish generally exhibit enhanced growth performance when provided with diets containing high levels of good-quality protein (McGoogan and Gatlin, 1999). As a carnivorous species, *P. diacanthus* exhibits a limited ability to utilize non-protein energy sources, and relies primarily on protein oxidation to fulfill its cellular energy requirements (Li et al., 2017).

A comparison of feed utilization indicators across the experimental groups (Group-1 vs. Group-2) revealed no significant differences in FCR, FER, and PER. However, the feed efficiency indicators obtained in this study (i.e., FCR of 5.15, FER of 0.19, and PER of 0.49) were inferior to those reported by Li et al. (2016), who observed an FCR of 1.59, FER of 0.63, and PER of 1.55 by feeding *P. diacanthus* a diet containing 41% crude protein, primarily supplemented with fishmeal. Similarly, better feed utilization indicators were noted in studies where diets with higher protein content (≥45%) were provided (Li et al., 2019, 2020). The considerable deviation in feed efficiency parameters between the present study and earlier investigations could be attributed to the differences in initial stocking size. Additionally, the present study did not specifically focus on evaluating feed utilization efficiency of *P. diacanthus*. This was due to the limited availability of wild-caught *P. diacanthus* seeds, resulting in its rearing alongside *T. mookalee* in small proportions. Consequently, the same feeding regime was applied to both species, making it challenging to monitor and optimize the actual feed intake of *P. diacanthus*. Instead, this experiment served as an opportunity to generate growth data for *P. diacanthus* under natural captive conditions (marine cages). The primary aim was to assess the feasibility of captive rearing for this species rather than to optimize feed utilization.

The condition factor (CF) reported in the present study, i.e., 1.13 g cm^{-3} and 1.14 g cm^{-3} for Group-1 and Group-2, respectively, though not significantly different between the groups, are less compared to the CF of 1.74 g cm^{-3} reported by Li et al. (2016), 1.61 g cm^{-3} reported by Li et al. (2017) and 1.65 g cm^{-3} reported by Li et al. (2020). This indicates that the fish grown in the present study were lean and slender compared to the fishes grown in these above-mentioned earlier studies. As the crude lipid content in most of the previous studies was slightly higher, it might have influenced the fish to become fatty and pulpier. Furthermore, as both the feed utilization indicators and condition factors were lower in the present study, the possibility of growth interference due to the intense competition from the dominant *T. mookalee* for feed and space cannot be entirely ruled out. This also indicates that there is a possibility in which *P. diacanthus* could perform better (both in growth and feed utilization) if allowed to grow in a monoculture setup. Therefore, further studies should be envisaged to optimize the feed efficiency of the species by growing them alone in the laboratory as well as in natural captive conditions. Nevertheless, the study indicates that the species grows faster in natural captive conditions (marine cages) and therefore, can be considered as a probable candidate species for aquaculture.

Interestingly, neither the growth performance indices (TLG, BWG, SGR and AGR) nor the feed utilization indices (FCR, FER and PER) of *T. mookalee* were significantly affected when *P. diacanthus* was introduced. The SGR (≈1.55% day^{-1}), AGR (≈1.91 g day^{-1}) and FCR (2.29) of *T. mookalee* observed in the present study are also found to be in congruence with the earlier reported values of SGR (1.47% day^{-1}), AGR (1.89 g day^{-1}) and FCR (2.19) obtained by growing *T. mookalee* in marine cages off Visakhapatnam coast in India (Sekar et al., 2021). This indicates that in the present study, the inclusion of *P. diacanthus* in the existing monoculture setups of *T. mookalee* has not adversely or synergistically impacted the growth performance and feed utilization of *T. mookalee*. However, as the number of *P. diacanthus* was lower compared to *T. mookalee*, it would be too premature to comment on this aspect of polyculture.

5 Conclusion

The present study assessed the survival and actual growth of *P. diacanthus* and modeled its potential growth in captive conditions within floating marine cages in a polyculture system with *T. mookalee*. The results, based on length and weight increments analyzed and modeled using the von Bertalanffy Growth Function

(VBGF), indicate that *P. diacanthus* exhibits superior growth performance in marine cages compared to wild conditions. Additionally, the study found that co-culturing *P. diacanthus* with Indian Pompano (*T. mookalee*) does not negatively affect the growth or feed utilization efficiency of *T. mookalee*. These findings highlight the potential of *P. diacanthus* to be used as a candidate species in marine cage farming.

Data availability statement

The original contributions presented in the study are included in the article/Supplementary Material. Further inquiries can be directed to the corresponding author.

Ethics statement

The animal study was approved by ICAR-CMFRI, Central Marine Fisheries Research Institute, Kochi, India. The study was conducted in accordance with the local legislation and institutional requirements.

Author contributions

SG: Conceptualization, Methodology, Project administration, Supervision, Writing – original draft. GD: Conceptualization, Methodology, Software, Writing – original draft, Writing – review & editing. BD: Data curation, Methodology, Writing – original draft. RKP: Data curation, Writing – original draft. SM: Data curation, Writing – original draft. PRB: Data curation, Writing – review & editing. RR: Data curation, Writing – review & editing. SS: Formal analysis, Writing – original draft. MD: Data curation, Writing – original draft. SVR: Writing – review & editing. GA: Conceptualization, Supervision, Writing – review & editing. JJ: Conceptualization, Supervision, Writing – review & editing.

Funding

The author(s) declare financial support was received for the research, authorship, and/or publication of this article. In-house Project Research Grant provided by Indian Council of Agricultural Research, New Delhi, India.

Acknowledgments

The authors are thankful to the Director, ICAR-Central Marine Fisheries Research Institute, Kochi for providing the requisite infrastructure and facilities to carry out the work.

Conflict of interest

The authors declare that the research was conducted in the absence of any commercial or financial relationships that could be construed as a potential conflict of interest.

Publisher's note

Supplementary material

The Supplementary Material for this article can be found online at: https://www.frontiersin.org/articles/10.3389/fmars.2024.1473319/full#supplementary-material

References

Ansari, Z. A., Chatterji, A., Ingole, B. S., Sreepada, R. A., Rivonkar, C., and Parulekar, A. H. (1995). Community structure and seasonal variation of an inshore demersal fish community at Goa. West Coast of India. *Estuarine. Coast. Shelf Sci.* 41, 593–610. doi: 10.1016/0272-7714(95)90029-2

Anuraj, A., Suresh Babu, P. P., Loka, J., Ignatius, B., Santhosh, B., Ramudu, K. R., et al. (2021). Induced breeding and larval rearing of vermiculated spinefoot, *Siganus vermiculatus* (Valenciennes 1835) in indoor conditions. *Aquaculture* 539, 736600. doi: 10.1016/j.aquaculture.2021.736600

Aswathy, N., Joseph, I., Ignatius, B., and Joseph, S. (2020). *Economic Viability of Cage Fish Farming in India* Vol. 134 (Kochi: Central Marine Fisheries Research Institute). CMFRI Special Publication.

Barton, D. P. (2018). Notes on the diet of the Black-spotted Croaker (*Protonibea diacanthus*) across northern Australia. *Northern Territory Nat.* 28, 61–69. doi: 10.5962/p.374206

Bhatt, Y. M., Kutty, M. N., Rao, K.V., and Punwani, D. M. (1964). Ghol-Dara" fishery off Bedi port in the Gulf of Kutch. *Indian J. Fisheries* 11A, 135–156. Available online at: https://eprints.cmfri.org.in/2128.

Bibby, J. M., and McPherson, G. R. (1997). "Age and growth of five target fish species in the Gulf of Carpentaria inshore gillnet fishery," in *Biology and Harvest of Tropical Fishes in the Queensland Gulf of Carpentaria Gillnet Fishery*. Ed. R. N. Garrett (Department of Primary Industries, Queensland), 61–85. QI98018.

Boyd, C. E., D'Abramo, L. R., Glencross, B. D., Huyben, D. C., Juarez, L. M., Lockwood, G. S., et al. (2020). Achieving sustainable aquaculture: Historical and current perspectives and future needs and challenges. *J. World Aquaculture Soc.* 51, 578–633. doi: 10.1111/jwas.12714

Cai, J. N., Yan, X., and Leung, P. S. (2022). *Benchmarking species diversification in global aquaculture* (Rome: FAO), 52. doi: 10.4060/cb8335en

Carballeira Braña, C. B., Cerbule, K., Senff, P., and Stolz, I. K. (2021). Towards environmental sustainability in marine finfish aquaculture. *Front. Mar. Sci.* 8. doi: 10.3389/fmars.2021.666662

Chan, H. L., Cai, J., and Leung, P. S. (2024). Aquaculture production and diversification: What causes what? *Aquaculture* 583, 740626. doi: 10.1016/j.aquaculture.2024.740626

Dhawan, R. M. (1971). On an unusual abundance of *Pseudosciaena diacanthus* off Goa. *Indian J. Fisheries* 18, 191–193. Available online at: https://epubs.icar.org.in/index.php/IJF/article/view/13184.

Dutta, S., Giri, S., Dutta, J., and Hazra, S. (2014). Blackspotted Croaker, *Protonibea diacanthus* (Lacepède 1802): A new dimension to the fishing pattern in West Bengal, India. *Croatian J. Fisheries* 72, 41–44. doi: 10.14798/72.1.684

Erzini, K. (1991). *A compilation of data on variability in length-age in marine fishes* (Collaborative Research Support Program, University of Rhode Island), 36. Working Paper 77.

FAO. (2024). *The State of World Fisheries and Aquaculture 2022 – Blue Transformation in action* (FAO: Rome), 236. doi: 10.4060/cc0461en

Fischer, W., and Bianchi, G. (1984). *FAO species identification sheets for fishery purposes* Vol. 4 (Rome, Italy: FAO).

Ghosh, S., Mohanraj, G., Asokan, P. K., Dhokia, H. K., Zala, M. S., Bhint, H. M., et al. (2010). Fishery and population dynamics of *Protonibea diacanthus* (Lacepede) and *Otolithoides biauritus* (Cantor) landed by trawlers at Vanakbara, Diu along the west coast of India'. *Indian J. Fisheries* 57, 15–20. Available online at: https://epubs.icar.org.in/index.php/IJF/article/view/61757.

Grant, E. M. (1982). *Guide to fishes. 5th edition* (Brisbane, Queensland, Australia: Dep. Harbours Mar.), 896.

Harvey, B., Soto, D., Carolsfeld, J., Beveridge, M., and Bartley, D. M. (2017). *Planning for aquaculture diversification: The importance of climate change and other drivers* (Rome: FAO), 50–91.

Hopkins, K. D. (1992). Reporting fish growth: a review of the basics. *J. World Aquaculture Soc.* 23, 173–179. doi: 10.1111/j.1749-7345.1992.tb00766.x

Hotagi, J. S. (1994). Unusual high catch of 'Ghol' at Basein Kolliwada, Thane district, Maharashtra. *Mar. Fisheries Inf. Service Tech. Extension Ser.* 126. pp, 16–17. Available online at: https://eprints.cmfri.org.in/4184.

Htun-Han, M. (1978). The reproductive biology of the dab *Limanda limanada* (L.) in the North Sea: gonadosomatic index, hepatosomatic index and condition factor. *J. Fish Biol.* 13, 351–377. doi: 10.1111/j.1095-8649.1978.tb03445.x

Johnsson, J. I., Brockmark, S., and Näslund, J. (2014). Environmental effects on behavioural development consequences for fitness of captive-reared fishes in the wild. *J. Fish Biol.* 85, 1946–1971. doi: 10.1111/jfb.2014.85.issue-6

Jones, N. A. R., Webster, M. M., and Salvanes, A. G. V. (2021). Physical enrichment research for captive fish: Time to focus on the DETAILS. *J Fish Biol.* 99, 704–725. doi: 10.1111/jfb.14773

Lacepède, B. G. E. (1802). *Histoire naturelle des poissons: IV* Vol. 4 (Paris, France: Chez Plassan), 728. Available at: https://www.biodiversitylibrary.org/page/6705733.

Le Cren, C. D. (1951). The length-weight relationship and seasonal cycle in gonad weight and condition in perch, *Perca fluviatilis*. *J. Anim. Ecol.* 20, 201–219. doi: 10.2307/1540

Leigh, G. M., Janes, R., Williams, S. M., and Martin, T. S. H. (2022). *Stock Assessment of Queensland East Coast black jewfish (*Protonibea diacanthus*), Australia, with data to December 2021* (State of Queensland, Brisbane: Department of Agriculture and Fisheries, Qeensland Government). Technical Report.

Li, W. J., Wen, X. B., Zhao, J., Li, S. K., and Zhu, D. S. (2016). Effects of dietary protein levels on growth, feed utilization, body composition and ammonia–nitrogen excretion in juvenile *Nibea diacanthus*. *Fisheries Sci.* 82, 137–146. doi: 10.1007/s12562-015-0945-9

Li, W., Wen, X., Huang, Y., Zhao, J., Li, S., and Zhu, D. (2017). Effects of varying protein and lipid levels and protein-to-energy ratios on growth, feed utilization and body composition in juvenile *Nibea diacanthus*. *Aquaculture Nutr.* 23, 1035–1047. doi: 10.1111/anu.12471

Li, W., Xu, B., Wei, F., Li, S., Wang, S., and Wen, X. (2020). Effects of partial substitution of dietary fishmeal by fermented soybean meal on growth, amino acid and protein metabolism of juvenile *Nibea diacanthus*. *Aquaculture Nutr.* 26, 2147–2158. doi: 10.1111/anu.13153

Li, Z., Zhang, X., Aweya, J. J., Wang, S., Hu, Z., Li, S., et al. (2019). Formulated diet alters gut microbiota compositions in marine fish *Nibea coibor* and *Nibea diacanthus*. *Aquaculture Res.* 50, 126–138. doi: 10.1111/are.2019.50.issue-1

Lugert, V., Tetens, J., Thaller, G., Schulz, C., and Krieter, J. (2017). Finding suitable growth models for turbot (*Scophthalmus maximus* L.) in aquaculture 1 (length application). *Aquaculture Res.* 48, 24–36. doi: 10.1111/are.12857

Lugert, V., Thaller, G., Tetens, J., Schulz, C., and Krieter, J. (2016). A review on fish growth calculation: multiple functions in fish production and their specific application. *Rev Aquacult.* 8, 30–42. doi: 10.1111/raq.12071

Mathews, C. P., and Samuel, M. (1990). Using the growth performance index Phi to choose species aquaculture: an example from Kuwait. *Aquabyte* 3, 2–4. Available online at: https://hdl.handle.net/20.500.12348/3201.

McGoogan, B. B., and Gatlin, D. M. III. (1999). Dietary manipulations affecting growth and nitrogenous waste production of red drum *Sciaenops ocellatus*: I. Effects of dietary protein and energy levels. *Aquaculture* 178, 333–348. doi: 10.1016/S0044-8486(99)00137-4

McPherson, G. R. (1997). "Reproductive biology of five target fish species in the gulf of Carpentaria inshore gillnet fishery," in *Biology and Harvest of Tropical Fishes in the Queensland Gulf of Carpentaria Gillnet Fishery*. Ed. R. N. Garrett (Department of Primary Industries, Queensland), 86–103. QI98018.

Mohammed, G., Ghosh, S., and Makadia, B. V. (2009). "Unusual heavy landing of otolithoides biauritus and protonibea diacanthus at salaya landing centre, jamnagar, gujarat," in *Marine fisheries information service, technical and extension series (200)* (Kochi, Kerala, India: CMFRI), 22. Available at: https://eprints.cmfri.org.in/8188/1/MFIS_-_200_English.pdf.

Näslund, J., and Johnsson, J. I. (2016). Environmental enrichment for fish in captive environments: effects of physical structures and substrates. *Fish Fisheries* 17, 1–30. doi: 10.1111/faf.2016.17.issue-1

Parappurathu, S., Menon, M., Jeeva, C., Belevendran, J., Anirudhan, A., Lekshmi, P. S. S., et al. (2023). Sustainable intensification of small-scale mariculture systems: Farm-level insights from the coastal regions of India. *Front. Sustain. Food Syst.* 7. doi: 10.3389/fsufs.2023.1078314

Pauly, D. (1984). Fish population dynamics in tropical waters: a manual for use with programmable calculators. *ICLARM Stud. Rev.* 8, 1–325. Available online at: https://hdl.handle.net/20.500.12348/3445.

Pauly, D., and Munro, J. L. (1984). Once more on the comparison of growth in fish and invertebrates. *Fishbyte* 2, 21. Available online at: https://EconPapers.repec.org/RePEc:wfi:wfbyte:38103.

Perez-Benavente, G., Uglem, I., Browne, R., and Mariño-Balsa, C. (2010). Culture of juvenile European lobster (*Homarus gammarus* L.) in submerged cages. *Aquac. Int.* 18, 1177–1189. doi: 10.1007/s10499-010-9332-9

Phelan, M. J., Gribble, N. A., and Garrett, R. N. (2008). Fishery biology and management of *Protonibea diacanthus* (Sciaenidae) aggregations in far northern Cape York Peninsula waters. *Continental Shelf Res.* 28, 2143–2151. doi: 10.1016/j.csr.2008.03.022

Ranjan, R., Muktha, M., Ghosh, S., Gopalakrishnan, A., Gopakumar, G., and Joseph, I. (Eds.) (2017). *Prioritised species for mariculture India* (Kochi: ICAR-Central Marine Fisheries Research Institute), 450.

Rao, K. V. S. (1963). Some aspects of the biology of 'Ghol', *Pseudosciaena diacanthus* (Lacépède). *Indian J. Fisheries* 10, 413–459. Available online at: https://eprints.cmfri.org.in/10402.

Rao, K. V. S. (1966). Age and growth of 'Ghol', *Pseudosciaena diacanthus* (Lacepède) in Bombay and Saurashtra waters. *Indian J. Fisheries* 13, 251–292. Available online at: https://epubs.icar.org.in/index.php/IJF/article/view/13535.

Rao, K. S. (1968). Studies on the scales of *Pseudosciaena diacanthus* (Lacepède) for estimating growth parameters. *Indian J. Fisheries* 15, 127–144. Available online at: https://epubs.icar.org.in/index.php/IJF/article/view/13282.

R Core Team. (2021). *R: A language and environment for statistical computing* (Vienna, Austria: R Foundation for Statistical Computing). Available online at: https://www.R-project.org/ (Accessed December 06, 2022).

Rong, H., Lin, F., Zhang, Y., Bi, B., Dou, T., Wu, X., et al. (2020). The TOR pathway participates in the regulation of growth development in juvenile spotted drum (*Nibea diacanthus*) under different dietary hydroxyproline supplementation. *Fish Physiol. Biochem.* 46, 2085–2099. doi: 10.1007/s10695-020-00863-z

Sadovy, Y., and Cheung, W. L. (2003). Near extinction of a highly fecund fish: the one that nearly got away. *Fish Fisheries* 4, 86–99. doi: 10.1046/j.1467-2979.2003.00104.x

Sekar, M., Ranjan, R., Xavier, B., Ghosh, S., Pankyamma, V., Ignatius, B., et al. (2021). Species validation, growth, reproduction and nutritional perspective of Indian pompano, *Trachinotus mookalee*–A candidate species for diversification in coastal mariculture. *Aquaculture Volume 545* 2021, 737212. doi: 10.1016/j.aquaculture.2021.737212

Shapiro, S. S., and Wilk, M. B. (1965). An analysis of variance test for normality (Complete samples). *Biometrika* 52, 591–611. doi: 10.2307/2333709

Shen, Z., Chen, H., Yao, R., and Zhao, H. (2007). Seasonal cycles of ovary development of *Nibea diacanthus*. *J. Guangdong Ocean Univ.* 27, 7–11. Available online at: https://caod.oriprobe.com/articles/11843330/Seasonal_Cycles_of_Ovary_Development_of_Nibea_diacanthus.html.

Shi, Z. H., Xia, L. J., and Wang, J. G. (2004). A study on artificial propagation technique of *Nibea diacanthus* (Lacepede). *Mar. Sci.* 28, 34–37.

Simon, C. J., and James, P. J. (2007). The effect of different holding systems and diets on the performance of spiny lobster juveniles, Jasus edwardsii (Hutton 1875). *Aquaculture* 266, 166–178. doi: 10.1016/j.aquaculture.2007.02.050

Suresh Babu, P. P., Anuraj, A., Shilta, M. T., Asokan, P. K., Vinod, K., Praveen, N. D., et al. (2022). Broodstock development, breeding and larval rearing of Acanthopagrus berda (Forsskal 1775), a suitable species for farming in tropical waters. *Aquacult. Res.* 53, 6439–6453. doi: 10.1111/are.v53.18

Taylor, C. C. (1958). Cod growth and temperature. *J. du Conseil* 23, 366–370. doi: 10.1093/icesjms/23.3.366

Thomas, P. A., and Kunju, M. M. (1981). On an unusual catch of Ghol *Pseudosciaena diacanthus* off Goa. *Indian J. Fisheries* 25, 266–268. Available online at: https://eprints.cmfri.org.in/789.

von Bertalanffy, K. L. (1934). Untersuchungen Über die gesetzlichkeit des wachstums. *W. Roux' Archiv f. Entwicklungsmechanik* 131, 613–652. doi: 10.1007/BF00650112

Zhang, Y., Hu, S., Xu, S., Xie, Y., and Hu, J. (2006). Study on early development of *Nibea diacanthus*. *J. Jimei Univ.* 11, 13–17. Available online at: https://caod.oriprobe.com/articles/10185936/Study_on_Early_Development_of_Nibea_diacanthus.html.

frontiers | Frontiers in Marine Science

TYPE Original Research
PUBLISHED 19 May 2025
DOI 10.3389/fmars.2025.1526265

OPEN ACCESS

EDITED BY
Xinxin Wang,
Akvaplan niva AS, Norway

REVIEWED BY
Yuwen Dong,
University of Pennsylvania, United States
Yang Jin,
Johns Hopkins University, United States
Gang Wang,
Chinese Academy of Fishery Sciences (CAFS), China

*CORRESPONDENCE
Xu Yang
yangxu@zjou.edu.cn

RECEIVED 11 November 2024
ACCEPTED 23 April 2025
PUBLISHED 19 May 2025

CITATION
Niu S, Wang Z, Guo L, Tang L, Gu T, Cui C, Feng D, Gui F and Yang X (2025) Dynamic motion response of a large-scale steel aquaculture cage during towing. *Front. Mar. Sci.* 12:1526265. doi: 10.3389/fmars.2025.1526265

Dynamic motion response of a large-scale steel aquaculture cage during towing

Shuai Niu[1], Zhi Wang[1], Lianyi Guo[1], Lianghao Tang[1], Tianyu Gu[1], Can Cui[2], Dejun Feng[1], Fukun Gui[1] and Xu Yang[1]*

[1]National Engineering Research Center for Marine Aquaculture, Zhejiang Ocean University, Zhoushan, Zhejiang, China, [2]School of Fisheries, Zhejiang Ocean University, Zhoushan, Zhejiang, China

As global aquaculture ventures further into offshore environments, the safe transport of large-scale aquaculture net cages across varied marine conditions has become a critical technical concern. This study conducts a detailed numerical simulation of the wet towing process for an octagonal aquaculture cage using AQWA software, systematically examining the effects of towline length, towing speed, towing configuration, and environmental factors on the cage's dynamic response and towline load characteristics. The findings reveal that towline length and towing speed are pivotal in determining the pitch amplitude of the cage and the resulting towline tension. Compared to a towline length of 200 m, using a towline length of 150 m combined with a towing speed of 0.5 m/s reduces pitch amplitude by 51.6% and towline tension by 24.8%. Additionally, an interval towing arrangement significantly enhances cage stability while minimizing towline stress. Under conditions of low wave height and longer wave period, the cage's motion response remains stable, contributing to enhanced transport safety. This research offers critical theoretical foundations and optimization strategies for the wet towing design considerations of offshore aquaculture cages, providing valuable insights to advance transport safety in challenging marine environments.

KEYWORDS

net cage, aquaculture, towing system, optimal towing configuration, dynamic response, marine structures

1 Introduction

With rising global living standards and increasing demand for fish protein, nearshore aquaculture is nearing its production capacity. Consequently, offshore aquaculture net cages have emerged as vital marine farming infrastructure, providing an effective solution to spatial constraints and environmental sustainability challenges in coastal areas (Dong et al., 2024). Compared to nearshore farming, offshore aquaculture offers advantages such as improved water quality, larger farming areas, and enhanced seafood quality (Froehlich et al., 2017). However, offshore operations are often located in open ocean environments where aquaculture platforms are vulnerable to typhoons, large waves, and strong currents.

To mitigate these challenges, offshore net cages are typically constructed with steel structures, which increase their resistance to wind and waves, ensuring the safety and productivity of aquaculture activities.

Offshore net cages build on traditional floating net cage designs, integrating technical advancements from floating marine engineering platforms and innovating to meet the specific demands of offshore aquaculture. This approach overcomes the structural limitations faced by traditional aquaculture platforms in offshore environments, representing a significant strategic shift from nearshore to offshore aquaculture (Ding et al., 2023). Since offshore net cages are designed to be positioned far from shore, they are typically constructed on land, where the towing system is first deployed at a designated location before transporting (Figure 1) and securing the cage offshore (Lira et al., 2019). For instance, the 'Deep Blue one' tilting incident, which involved significant damage during towing operations, underscores the importance of ensuring safe towing methods for these platforms. Current research primarily focuses on the dynamic response, structural strength, and fatigue resistance of net cage towing systems, with relatively little attention given to the safety of cage transport. Ensuring safety during towing is crucial for the overall structural integrity of net cages. While studies on the transport of offshore net cages remain limited, existing literature on marine structure dynamics and engineering provides a solid foundation for the design and optimization of net cage transport systems.

Since the 1950s, detailed analyses have been conducted on towing systems for floating structures and the factors affecting towing operations, both domestically and internationally. Wet towing has been widely applied in marine engineering and has been extensively studied as a critical technology. The feasibility of the wet towing method for the offshore substation WSBJF has been confirmed through experimental and numerical studies (Wang et al., 2023). The allowable pressure range for the Composite Bucket Foundation (CBF) during offshore transport has been analyzed using the finite element method, highlighting its potential for offshore applications (Li et al., 2024). Strategies for reducing installation costs in offshore projects have been proposed through investigations into the wet towing transport method for the "jacket + three-bucket foundation" structure in offshore wind farms (Yan et al., 2021). The safety of air-buoyancy structures during transport has been verified through physical experiments, which observed the floating behavior of the CBF under varying speeds, wave heights, and wind conditions (Ding et al., 2020). The air-buoyancy towing behavior of multi-bucket foundation platforms (MBFPs) has been studied using MOSES numerical simulation software, demonstrating that towing stability can be significantly improved by reducing towing speed and selecting appropriate sea conditions (Le et al., 2013). These studies collectively emphasize the essential role of wet towing in ensuring the safe and stable transport of marine structures.

The composition of the towing system is also critical to the safety of net cages. In 1958, (Holmstrom, 1982) studied towing systems based on linear theory and found that adjusting the position of the towline configuration and the length of the towline could improve the stability of the towing system (Yasukawa and Yamada, 2009) enhanced the safety of towing systems for floating wind turbines by adjusting the towline position and length. (Li et al., 2020) used MOSES to examine the static stability of floating wind turbines under different environmental conditions. (Le et al., 2021) conducted model tests and found that towing speed and wave height significantly impact the towing stability and drag of tension-leg platforms. (Fitriadhy et al., 2013) discovered that towline elasticity and the weight of the towed structure play crucial roles in the directional stability of towing systems (Shin, 2011)further analyzed the effect of elastic towlines on towing stability. Through simulation studies (Shi, 2011)investigated the combined effects of towline length, water depth in the towing area, and current speed on the towing system, noting that towing against the current causes greater system drift, with water depth having a more substantial effect than towline length. (Han et al., 2017) used a multibody dynamics approach to analyze the impact of wind, waves, and currents on the towing stability of floating wind turbines, concluding that pitch motion is more affected by wind and waves than roll and heave motions. These studies underscore the importance of towline length and towing speed for the safe transport of net cages, providing essential theoretical support for maintaining stability during the towing process.

In offshore aquaculture, the shape of the net cage plays a critical role in its stability and adaptability. Octagonal cages are commonly

FIGURE 1
The towing process of **(A)** Ocean Farm one and **(B)** Deep Blue one (photo courtesy of www.salmar.no and sd.ifeng.com).

used in offshore farming due to their unique geometric structure. Compared to traditional circular or square cages, octagonal cages offer superior hydrodynamic stability, enabling them to more effectively distribute the forces exerted by ocean currents and waves (Fan et al., 2023). This shape has been widely adopted (e.g., in Ocean Farm one and Deep-Blue one) and not only helps to reduce stress concentrations in dynamic environments but also provides greater internal space, optimizing the growth conditions for fish.

Therefore, this study focuses on an octagonal steel cage, using a combination of physical experiments and numerical simulations to analyze in detail the effects of various towing configurations on cage stability. Key variables, including towline length, towing speed, and marine environmental conditions, are comprehensively considered to explore their impact on the dynamic response characteristics during towing. The structure of this paper is as follows: Section 2 provides an overview of the platform, model, and towline geometry, detailing the geometric structure and physical properties. Based on hydrodynamic theory, the equations of motion and forces acting on the net cage in a marine environment are established. Section 3 verifies the accuracy of the numerical simulations through comparisons with physical model tests. Section 4 discusses the steady-state stability of the net cage under different towing points. The influence of key factors such as towline length, towing speed, wave period, and wave height on towing stability is then examined. The subsequent section presents the main insights of this study, along with a grounded discussion on potential directions for future research. Finally, conclusions are summarized in Section 6.

2 Materials and methods

Numerical simulation and laboratory experiments are employed to investigate the effects of towing position, towing length, towing speed, wave period, and wave height on the dynamic response characteristics of a newly built cage. In this study AQWA is utilized to develop a numerical model for simulating the towing process of a fish farm, focusing on analyzing the effects of towing point position and wave loads on its dynamic response.

2.1 Experimental setup

The net cage is designed an octagonal structure (Figure 2A), primarily consisting of external edge columns, a central column, and supporting trusses. The external frame is divided into two parts: side pontoons and external edge columns. Eight side pontoons are arranged in a regular octagonal layout around the perimeter of the net cage and are connected to the central float by cylindrical trusses. An octagonal ballast tank is installed at the lowest part of the net cage, to lower the center of gravity and enhance its stability. The net cage has an overall height of 11.23 m, a width of 23.57 m, and a draft depth of 2.2 m. The side pontoons have a diameter of 1.6 m and a height of 1.7 m, while the central float has a diameter of 6.7 m and a height of 4.5 m (Figure 2B). The main parameters are provided in Table 1 for reference.

2.1.1 Equations of motion for towed body

The planar motion equations are typically used to describe the behavior of objects moving in a two-dimensional plane. The forces acting on the net cage can be categorized into externally applied forces, damping forces, and restoring forces. The combined effect of these forces determines the motion state of the net cage. When the net cage moves in water, the resultant force can be expressed as:

$$\boldsymbol{F_{total} = F_{ext} + F_{damping} + F_{restoring}}$$

Where F_{ext} represents the externally applied forces, $F_{damping}$ represents the damping forces, and $F_{restoring}$ represents the restoring forces. The damping force is typically proportional to velocity and can be expressed as:

$$\boldsymbol{F_{damping} = -\, c \cdot V}$$

Where $F_{damping}$ *is* the damping force, c is the damping coefficient, and V is the velocity. The restoring moment is related to displacement and is typically expressed as:

$$\boldsymbol{F_{restoring} = -\, k \cdot X}$$

Where $F_{restoring}$ is the elastic force, k is the stiffness coefficient, and X is the displacement. Substituting the above equations into Newton's second law and simplifying yields:

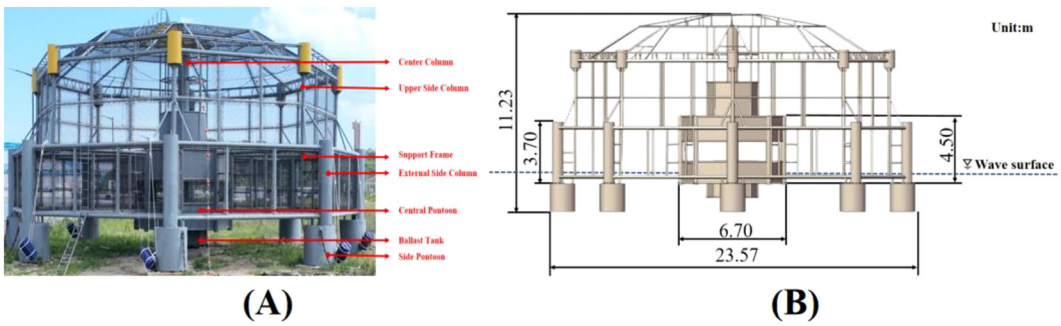

FIGURE 2
Photo: **(A)** Net cage prototype; **(B)** Geometric dimension.

TABLE 1 Principal parameters of the model.

Component	Parameter	Prototype (m)	Model (m)
Cage Size	Height	11.23	0.56
	Diameter	23.57	1.17
Center Column	Height	1.70	0.09
	Diameter	0.70	0.04
Center Pontoon	Height	4.50	0.23
	Diameter	6.70	0.34
Side Pontoon	Height	1.70	0.09
	Diameter	1.60	0.08
Upper Side Column	Height	5.23	0.27
	Diameter	0.20	0.01
External Side Column	Height	3.70	0.19
	Diameter	0.70	0.04

$$M_{trans}\cdot\frac{d^2X}{dt^2}+C_{trans}\cdot\frac{dX}{dt}+D_{trans}(X)+F_{ext,trans}=0$$

Where M_{trans} is the translational mass matrix, D_{trans} is the translational damping matrix, D_{trans} is the translational restoring force, and $F_{ext,trans}$ is the translational external force (wave force). Based on this, the rotational motion equation further describes the behavior of the object during rotation.

During the rotational process, the expression for the resultant moment can be represented as:

$$M_{total}=M_{ext}+M_{damping}+M_{restoring}$$

Where M_{total} is the total moment applied, M_{ext} is the external moment, $M_{damping}$ is the damping moment, and $M_{restoring}$ is the restoring moment. The damping moment is typically proportional to the angular velocity and can be expressed as:

$$M_{damping}=-c_{rot}\cdot\Omega$$

The restoring moment is related to angular displacement and is typically expressed as:

$$M_{restoring}=-k_{rot}\cdot\Theta$$

By substituting the above equations into the rotational equation and simplifying, we obtain:

$$I\cdot\frac{d^2\Theta}{dt^2}+C_{rot}\cdot\frac{d\Theta}{dt}+D_{rot}(\Theta)=0$$

Where I is the rotational inertia, C_{rot} is the rotational damping matrix, Ω is the angular acceleration, k_{rot} is the rotational restoring coefficient, and $\Theta$is the angular displacement of the net cage.

In the practical application of net cages, there exists a coupling relationship between translational and rotational motion. The coupled motion equation can be used to describe the interaction between these two types of motion, as follows:

$$F_{couple}=M_{couple}\cdot A+C_{couple}\cdot V+D_{couple}(X)$$

Where M_{couple} is the coupled mass matrix, A is the acceleration vector, V is the velocity vector, and $D_{couple}(X)$ is the coupled restoring force.

2.2 Towing system

Based on the octagonal structure of the net cage, this experiment adopts two towing configurations: the adjacent fixation configuration and the spaced fixation configuration. In the adjacent fixation configuration, two towlines are symmetrically fixed to two adjacent side pontoons, while in the spaced fixation configuration, two towlines are symmetrically fixed to alternate side pontoons, with the other ends secured to the stern of the tugboat (Figure 3).

2.2.1 Towing length

The towline is an important factor affecting the motion of the net cage. In towing analysis, the dynamic response of the towline can be calculated by considering its stiffness and damping coefficients. The calculation formula for the towline force is as follows:

$$F_{cable}=k_{cable}\Delta L+c_{cable}\frac{d}{dt}(\Delta L)$$

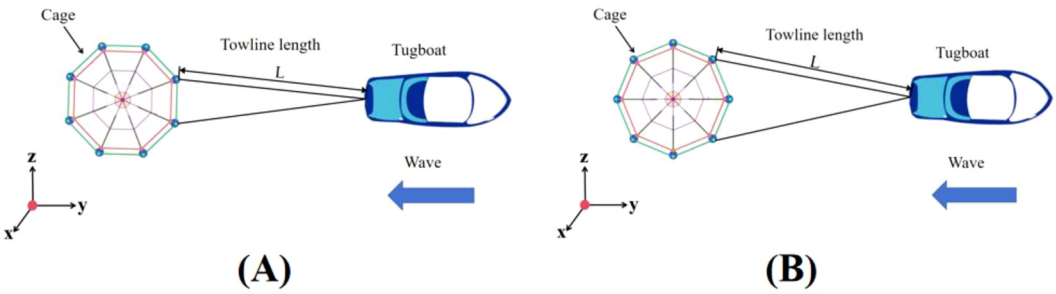

FIGURE 3
Top view of the towing systems with towline fixed on two: **(A)** adjacent pontoons; **(B)** spaced pontoons.

Where F_{cable} is represents the stiffness of the towline, indicating its ability to resist stretching, ΔL is the elongation of the towline, c_{cable} is the damping coefficient of the towline, describing energy dissipation during towing.

According to international maritime regulations, the minimum safe length of the main towline must be calculated (Solas, 2002). The formula for calculating the minimum safe length of the main towline is as follows:

$$L=(L_1+L_2)\cdot K$$

Where L represents the minimum safe length of the main towline, L_1 represents the total length of the tugboat, L_2 represents the total length of the towed vessel, and K is the wind and wave coefficient. Based on weather conditions, the value of K ranges from 2.3 to 3.3, with 2.3 used for favorable weather and 3.3 for rough conditions. In this analysis, the wind and wave coefficient K is set to 2.3, and the length of the tugboat L_1 is 23 m. Therefore, the minimum safe length of the main towline is calculated as 100 m (rounded).

2.3 Numerical simulation analysis

This study uses Airy wave theory to describe wave motion by setting reasonable parameters such as wave height, period, and wavelength to construct a wave environment for simulating the dynamic response of the net cage during towing. The wave model not only effectively reflects the wave motion characteristics under actual sea conditions but also provides a reliable theoretical foundation for analyzing the dynamic behavior of the towing system.

2.3.1 Frequency domain analysis

In the frequency domain, the equations of motion can be transformed into the complex domain for solving. By solving the Frequency Response Function (FRF), the response characteristics of the structure under different wave frequencies can be obtained.

$$\hat{\xi}(\omega)=\frac{\hat{F}(\omega)}{(-\omega^2M+i\omega C+K)}$$

Where $\hat{\xi}(\omega)$ denotes the frequency response, and $\hat{F}(\omega)$ represents the wave force in the frequency domain.

2.3.2 Time domain analysis

Time domain analysis solves the equations of motion using numerical integration methods, which are suitable for simulating complex nonlinear problems, especially under real wave conditions.

$$M\ddot{\xi}(t)+C\dot{\xi}(t)+K\xi(t)=F(t)$$

In the above equation, M represents the mass matrix, describing the system's mass characteristics and its effect on motion; C represents the damping matrix, describing the system's damping characteristics, i.e., friction or energy dissipation; K represents the stiffness matrix, describing the system's stiffness characteristics, i.e., its resistance to deformation; $\xi(t)$ denotes the displacement vector, representing the system's displacement state at time t; $\dot{\xi}(t)$ denotes the velocity vector, which is the derivative of displacement with respect to time, reflecting the system's motion speed; $\ddot{\xi}(t)$ denotes the acceleration vector, which is the second derivative of displacement with respect to time, reflecting the system's acceleration;

In the time domain analysis module of AQWA, the wave propagation time step is set to 0.1 s, and the total simulation time is 1000 s to observe the long-term motion response of the net cage.

2.4 Simulation conditions

To comprehensively evaluate the effects of various factors on the stability of the towing system, this study designs a series of simulation scenarios. Given the significant impact of towing method, towing length, towing speed, and sea state on system stability and efficiency, simulations were conducted under 17 distinct conditions using sea state data provided by the China Oceanic Information Network (COIN). The simulations analyzed the time varying motion response of the net cage across different scenarios, as presented in Table 2. Comparisons were made to assess the effects of varying towing speeds (3 knots, 4 knots, 5 knots), towing lengths, and sea state levels (3, 4, 5) on the motion response.

3 Model validation

The experiments were conducted in a flume tank at Zhejiang Ocean University (Figures 4, 5). This flume tank featured a horizontal, square water channel with flow generated by axial-flow pumps. The test section had dimensions of 6.0 meters in length, 1.5 meters in width, and 1.2 meters in water depth. For model validation, a series of experiments were carried out on an octagonal cage model at a Froude scale of 1:20, with the results compared to numerical simulations conducted under identical environmental conditions. The specific environmental load conditions used in the experiments, including a spaced fixation configuration, a towline length of 100 meters, and a towing speed of 1.5 m/s, are summarized in Table 3. A comparison of the longitudinal pitching motion between the numerical simulations and experimental results is presented in Figure 6.

The experimental results were compared with the simulation results, with the standard deviation for the simulation results being 0.038°, while the standard deviation for the experimental results is 0.041°. The maximum difference remained within 10%, indicating a close agreement between the two sets of data. This close alignment demonstrates that the numerical simulation can accurately predict towing responses.

4 Results

4.1 Effect of the towline configuration

The position of the towing configuration exerts a substantial influence on the motion amplitude of the net cage during towing

TABLE 2 Conditions of the simulation test.

Case	Fixation Methods	Towline Length (m)	Towing Speed (m/s)	Wave Height (m)	Wave Period (s)	Note
Case 1	Adjacent fixation	100	1.5	0.5	8	Effect of towline configuration
Case 2	Spaced fixation					
Case 3	Spaced fixation	100	2.1	0.5	8	Effect of towing length
Case 4		150				
Case 5		200				
Case 6	Spaced fixation	150	1.5	0.5	8	Effect of towing speed
Case 7			2.1			
Case 8			2.6			
Case 9	Spaced fixation	150	2.1	0.5	7	Effect of the marine environment
Case 10					8	
Case 11					9	
Case 12				1.5	7	
Case 13					8	
Case 14					9	
Case 15				2.5	7	
Case 16					8	
Case 17					9	

10.3389/fmars.2025.1526265

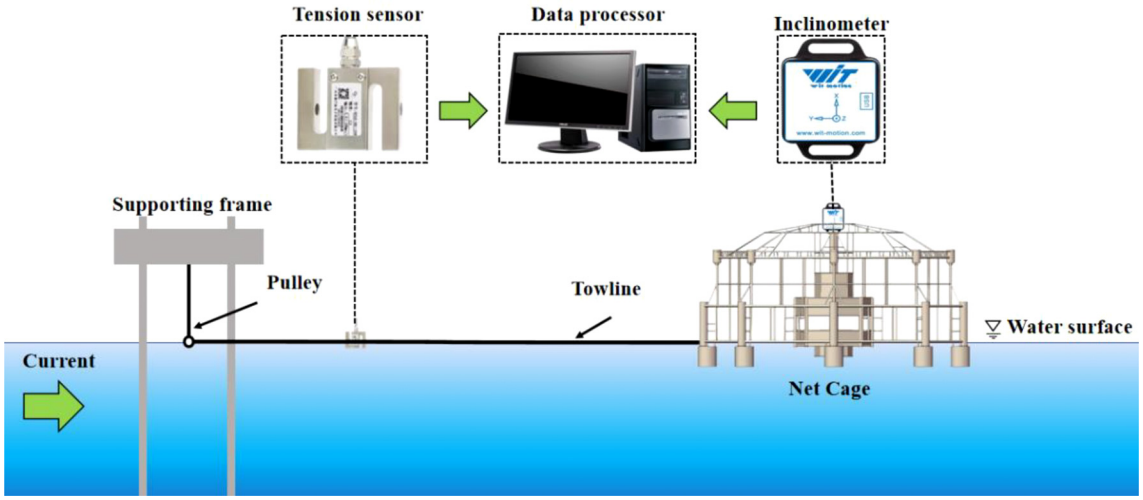

FIGURE 4
Schematic diagram of the towing experiments.

operations. To quantify this effect, a comparative analysis was conducted on two experimental configurations, as outlined in Table 2 (Adjacent fixation and Spaced fixation). Figure 7 presents a statistical comparison of the roll and heave motions of the net cage across the different towing configurations.

The comparison reveals that the towing position has minimal influence on the roll and heave responses of the net cage. Under both configurations, the roll and heave amplitudes remain stable at approximately 5.5° and 0.55 m, respectively. This finding demonstrates that different choices of towing points exert an insignificant effect on roll and heave responses, aligning with the conclusions of (Chen et al., 2024; Huynh and Kim, 2024) study similarly found that variations in towing position during towing have negligible impacts on heave and roll, likely due to the small geometric dimensions and shallow draft of the towed structure, resulting in limited motion differences.

FIGURE 5
Photo of the experiment in the recirculating flume tank.

Comparatively, the pitch motion is markedly influenced by the towing position. Figure 8 presents the pitch time history curves for different towing configurations, showing that the numerical simulation stabilizes after 400 seconds, with Adjacent fixation exhibiting significantly higher pitch values than Spaced fixation. A focused analysis of the pitch amplitude over the 800–1000 second interval indicates that, in Adjacent fixation, the pitch amplitude fluctuates between -0.35° and 0.51°, while in Spaced fixation, the range is notably reduced to -0.16° to 0.24°, representing a 53.49% decrease relative to Adjacent fixation. This reduction is attributed to the optimized towing position in Spaced fixation, where the tow cable's configuration are positioned more laterally, leading to a more uniform force distribution and a corresponding decrease in longitudinal moment impact on the net cage.

Figure 9 provides a detailed illustration of the variation in towline tension under different towing configurations. It is evident from the figure that the towline tension in Adjacent fixation is significantly higher than that in Spaced fixation, with greater fluctuations, indicating more severe load variations in the system under Adjacent fixation, where the maximum tension reaches 37.43 kN. In contrast, Spaced fixation shows a maximum tension of 31.11 kN, with relatively smoother tension fluctuations. A comparison reveals that the towline tension in Spaced fixation is reduced by 16.88% compared to Adjacent fixation, likely due to the smaller towing angle in Adjacent fixation, causing uneven loading on the net cage during towing. Spaced fixation, with a lower towline load, demonstrates higher stability. Under identical sea conditions, the

TABLE 3 Parameters of test conditions for numerical model verification.

Case	Towline Length (m)	Towing Speed (m/s)
Simulation	100	1.5
Experiment	5	0.335

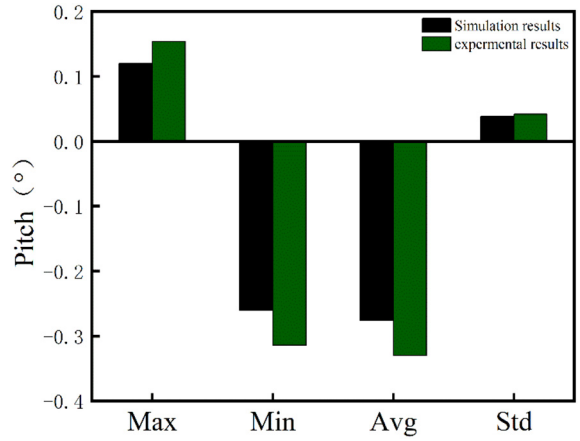

FIGURE 6
Comparisons of the pitch results from simulation and experiment. (Max., Min., Avg., and Std are the abbreviations for maximum, minimum, average, and standard deviation dataset).

towing configuration in Spaced fixation proves safer than that in Adjacent fixation.

4.2 Effect of the towing length

In engineering applications, the towline serves as a critical variable in the towing system, where its length significantly impacts the motion response of the net cage. Consequently, this section considers towing length as the primary variable (Table 2) to examine its effect on the motion behavior of the net cage.

The time history of the pitch angle of the net cage at various towing lengths is illustrated in Figure 10. As the cable length increases, the pitch angle gradually rises, exhibiting periodic fluctuations across all lengths. Generally, towing length is inversely proportional to oscillation frequency. At a cable length of 100 m, the pitch angle exhibits minor fluctuations, around 0.38°, with a relatively high oscillation frequency. When extended to 150 m, the pitch amplitude increases to approximately 0.61°, accompanied by a slight decrease in frequency. At 200 m, the pitch amplitude increases considerably, with fluctuations reaching up to 1.26° and the lowest frequency recorded. Therefore, selecting an optimal towing length can effectively minimize pitch amplitude, allowing the net cage to reach a steady state more rapidly and maintain stability during towing.

Figure 11 provides an illustration of the power spectral density (PSD) variation of pitch motion across three conditions as a function of frequency for different towing lengths. At the resonance frequency of 0.3 Hz and wave frequency of 0.17 Hz, cable length significantly influences the net cage's pitch response. A shorter cable exhibits lower PSD values at these frequencies, indicating a smaller pitch response. As the cable length extends to 150 m, the PSD rises, reflecting an increase in vibration response. At a length of 200 m, the PSD reaches peak values at both resonance and wave frequencies, suggesting that a longer cable intensifies the net cage's response to external disturbances, especially at wave frequency, where the pitch amplitude is greatest. Thus, increasing the cable length leads to stronger low-frequency vibration responses, which impacts the towing system's stability.

Figure 12 shows the effect of towing length on towing tension. The figure indicates that towing tension decreases as cable length increases. At a cable length of 100 m, the tension reaches its peak at approximately 109 kN; when the length extends to 150 m, the tension fluctuations reduce. At 200 m, the tension further declines to 75 kN, representing a 31.19% reduction compared to the 100 m length. This result suggests that shorter towlines are more susceptible to external environmental influences, leading to unstable force distribution and increased system complexity and risk. As the cable length increases, the variation in towing tension diminishes, enhancing the overall safety of the towing system.

4.3 Effect of the towing speed

Given the substantial volume of the aquaculture net cage, its wetted surface and horizontal plane are subject to considerable variation under intense motion. Table 2 provides a comparative

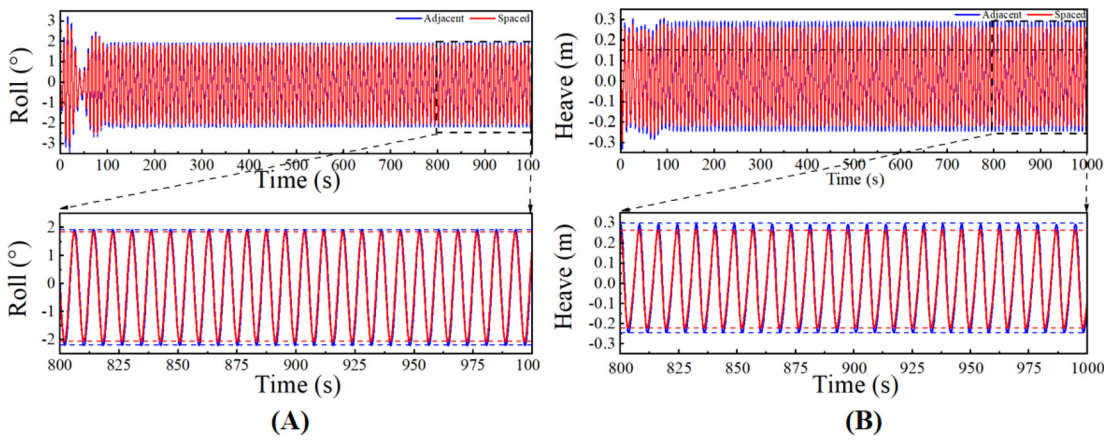

FIGURE 7
Dynamic response of **(A)** Roll and **(B)** Heave of the net cage for different towing configurations.

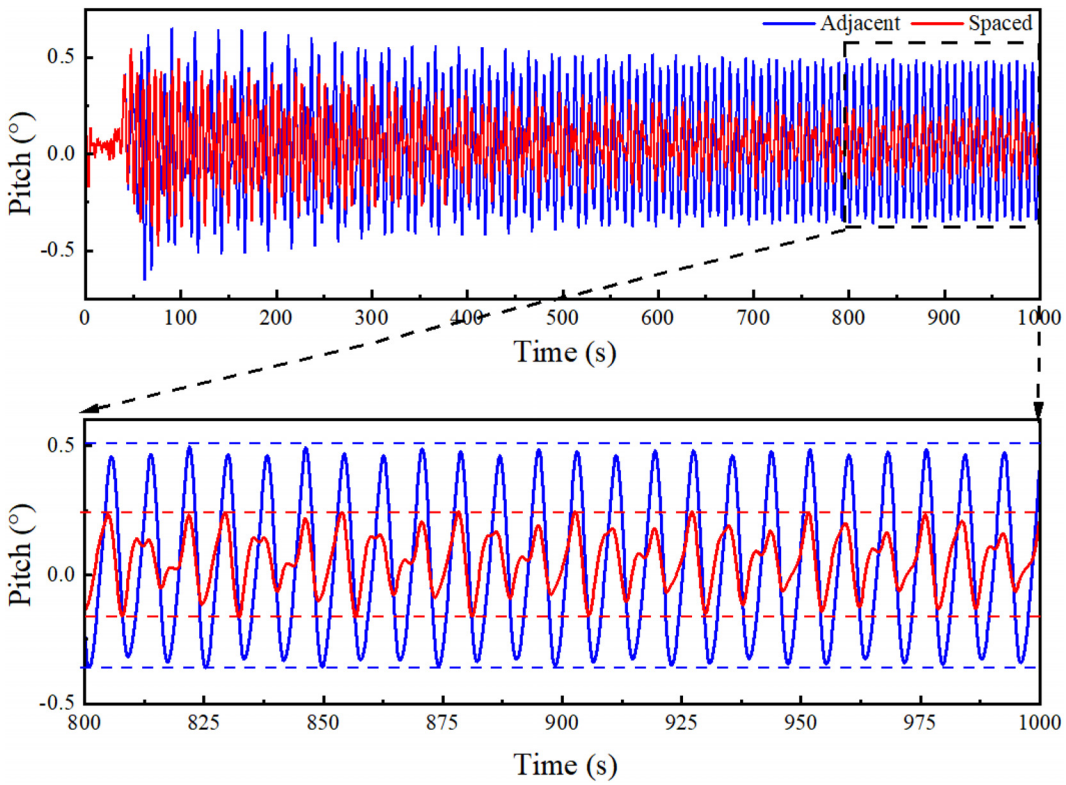

FIGURE 8
Dynamic response of the pitch of the net cage with different towing configurations.

analysis of selected towing speeds (1.5 m/s, 2.1 m/s, and 2.6 m/s) to assess the influence of towing speed on the net cage under representative marine conditions, including a wave height of H=0.5m, wave period of T=8s, towing length of 150 m, and a head on wave direction.

Figure 13 presents the time dependent trend of the vessel's pitch angle under different towing speeds. The pitch amplitude and frequency both increase significantly with higher towing speeds. At 1.5 m/s, the pitch angle displays minor and steady fluctuations, indicating stable vessel motion at lower speeds. At 2.1 m/s, the pitch amplitude and fluctuation range expand. When the towing speed reaches 2.6 m/s, the pitch angle of the net cage shows intense fluctuations in both frequency and amplitude, highlighting the pronounced effect of high towing speeds on vessel motion.

An expanded view between 800 s and 1000 s provides insight into the pitch angle's detailed variations post stabilization under different speeds. At 1.5 m/s, the net cage exhibits small, consistent fluctuations with an amplitude of around 0.51°. With an increase to 2.1 m/s, the fluctuation amplitude rises to 1.22°. At 2.6 m/s, the pitch amplitude peaks at 1.62°, indicating intense motion. These observations reflect a nonlinear increase in pitch amplitude with rising towing speed, especially at higher speeds. It can be inferred that elevated speeds substantially affect net cage stability, intensifying the dynamic response of the system and potentially increasing structural fatigue risks.

The frequency distribution of the power spectral density (PSD) for the vessel's pitch angle under different towing speeds is presented in Figure 14, revealing the vibration response characteristics of the vessel at various frequencies. A prominent resonance frequency is observed around 0.15 Hz, with peaks present across all speeds, and power values increasing progressively with higher towing speeds. At low speed (1.5 m/s), the power at this frequency is minimal, indicating a weaker pitch response; however, at moderate (2.1 m/s) and high speeds (2.6 m/s), the peak power increases significantly, suggesting that the vessel is more prone to resonance at this frequency under higher speeds. Thus, as towing speed increases, the vessel's vibration response at the pitch resonance frequency is markedly enhanced, with the pitch response becoming more intense, especially under high-speed towing conditions.

Figure 15 shows the variation in towline tension across different towing speeds. An increase in towing speed correlates with a rise in cable tension. At lower speeds, the tension remains steady around 48 kN; as the speed increases to 2.6 m/s, the tension reaches a peak of 73 kN. At this speed, the maximum fluctuation in tension is observed at 106 kN. These results suggest that higher towing speeds contribute to increased instability in cable tension, thereby adding complexity to the forces acting on the net cage.

4.4 Effect of the wave conditions

To investigate the effect of various marine environments on the towing of an octagonal cage, nine random sea states were selected through an orthogonal combination of different wave heights (H =

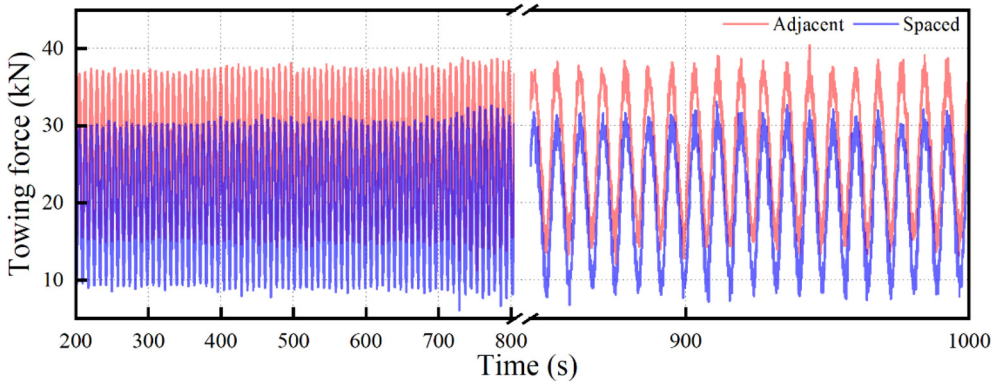

FIGURE 9
Dynamic response of the towing force at different towing configurations.

0.5 m, 1.5 m, and 2.5 m) and periods (T = 7 s, 8 s, and 9 s), Data were compiled to summarize the pitch motion response amplitude and towline tension under different marine conditions, and a comprehensive analysis of the results is provided in Table 4.

Figure 16 shows the time-history curves of the net cage's pitch motion under various conditions, illustrating how pitch motion amplitude fluctuates with changes in wave height and period:

When the wave height is 0.5 m and the wave period is 7 s, the system exhibits large pitch angle fluctuations, with a maximum amplitude of approximately 2.51°, indicating an unstable state. Increasing the wave period to 8 s markedly reduces the pitch angle, with a maximum amplitude of 0.52°, and stabilizes the net cage motion, resulting in decreased fluctuation amplitude and frequency. At a wave period of 9 s, the maximum amplitude further reduces to 0.39°, producing smoother motion;

For a wave height of 1.5 m and a wave period of 7 s, the system reaches a maximum amplitude of 11.49°, which represents a 150.21% increase over the 0.5 m case. Increasing the wave period

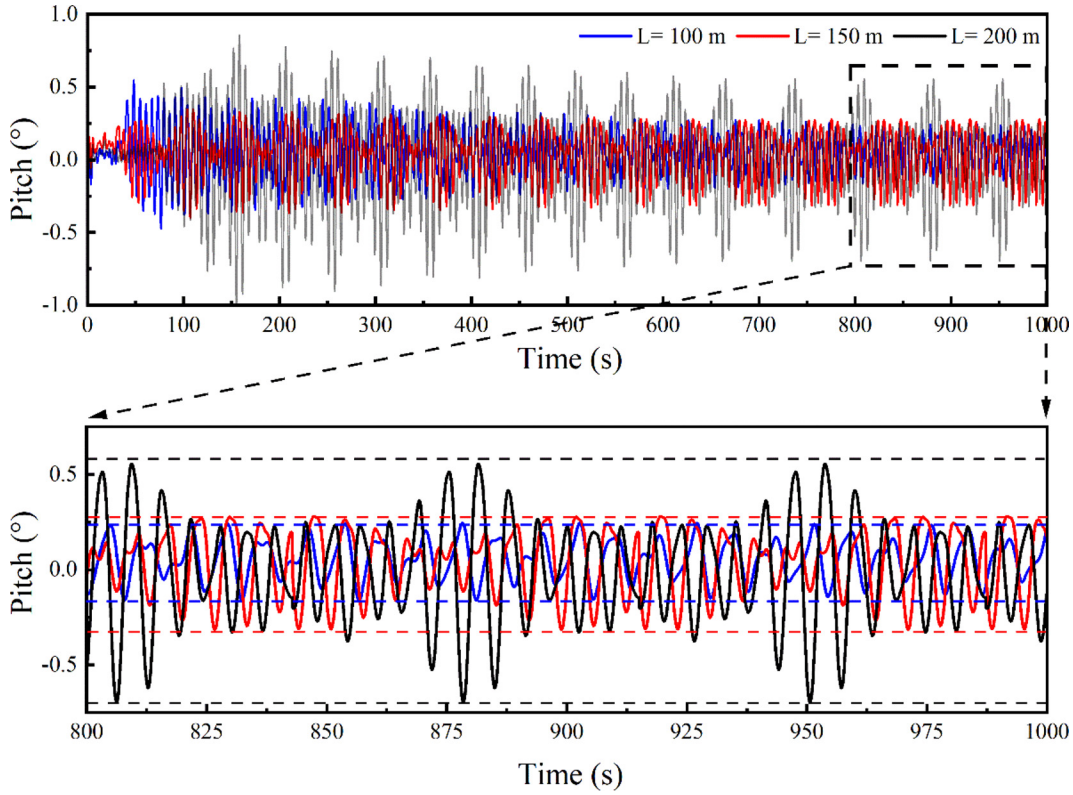

FIGURE 10
Dynamic response of the pitch of the net cage with different towing lengths.

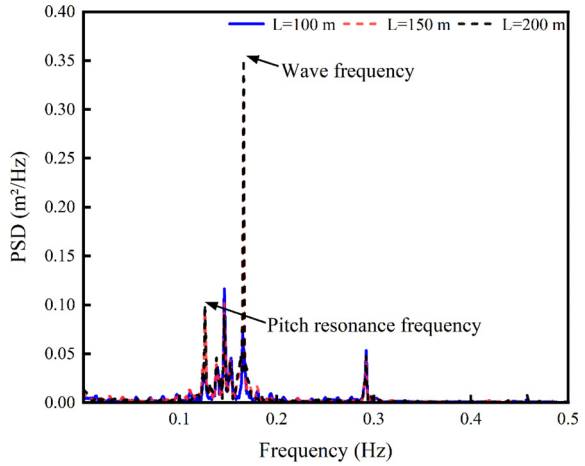

FIGURE 11
Power spectra of net cage pitch motion with different towing lengths.

to 8 s reduces the pitch amplitude significantly to approximately 0.94°. When the period increases to 9 s, the maximum amplitude further declines to about 0.47°, indicating a 20.51% increase compared to the 0.5 m wave height condition;

In cases with a wave height of 2.5 m, the dynamic response of the system becomes even more pronounced. At a wave period of 7 s, the maximum amplitude approaches 13.50°, representing a 17.67% increase over the 1.5 m wave height case, highlighting more severe motion under high-wave conditions. Extending the wave period to 8 s decreases the pitch amplitude to 2.13°, an 81.24% reduction, with some fluctuations persisting. At a wave period of 9 s, the pitch amplitude decreases further, showing pitch angles similar to the 1.5 m wave height case.

Through an analysis of the changes in pitch angles under varying wave heights and periods, it becomes clear that the wave period significantly influences the pitch motion of the net cage. As wave height increases, the motion response of the net cage gradually intensifies; however, at higher wave periods, the system's response appears more stable. Notably, under conditions of high waves and long periods, the net cage demonstrates a more stable dynamic response.

The towline tension curves under various marine environments are presented in Figure 17. A comprehensive analysis reveals that fluctuations in towline tension significantly increase with changes in wave height and wave period.

When the wave height is 0.5 m, the towing force remains relatively stable, with a maximum fluctuation range of approximately 76.3 kN and minimal fluctuation amplitude, indicating that under low wave height conditions, the influence of wave period on towline tension is limited. However, as the wave height increases to 1.5 m, the fluctuation amplitude of the towing force increases significantly, reaching a maximum of 810.4 kN, which represents a 90.48% increase. Particularly at a wave period of 7 s, the fluctuations in towline tension become more intense, indicating that the influence of wave period is more pronounced under higher wave height conditions.

When the wave height increases to 2.5 m, the fluctuation amplitude of the towline tension reaches its maximum value of approximately 1210 kN, representing a 93.7% increase compared to the wave height of 0.5 m. At a wave period of 7 s, the towing force of the system reaches its peak, with extremely intense fluctuations, indicating that the combination of high wave height and short-wave period has the most significant impact on the dynamic stability of the system.

An analysis of towline tension and pitch angle under varying marine conditions indicates that changes in wave height and wave period significantly impact the towline tension and pitch angle of the octagonal cage. In general, a combination of high wave height and short-wave period increases net cage instability, resulting in substantial fluctuations in towline tension and marked intensification of pitch angle. This combination may lead to structural fatigue, thereby increasing the risk of damage. As wave height rises, the system's pitch angle also increases significantly due to stronger hydrodynamic forces exerted by higher waves, which intensifies the system's dynamic response. Conversely, under low wave height conditions, both the pitch angle and towline tension decrease significantly, contributing to greater system stability.

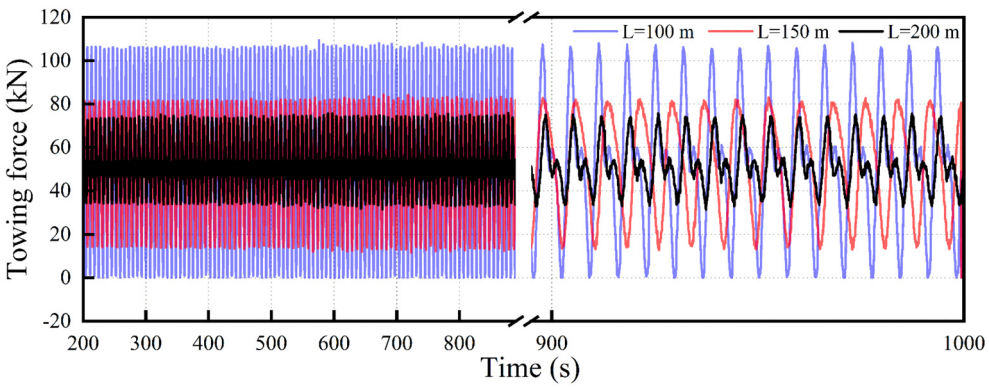

FIGURE 12
Dynamic response of the towing force at different towing lengths.

TABLE 4 Summary of pitch motion response and towing tension.

Case	Wave Height(m)	Wave Period (s)		
		7	8	9
Pitch(°)	0.5	2.31	0.52	0.39
	1.5	11.49	0.94	0.47
	2.5	13.50	2.13	0.72
Towing tension(kN)	0.5	76.30	69.00	62.30
	1.5	833.10	110.00	76.30
	2.5	1210.30	930.60	84.20

Additionally, wave period has a pronounced effect. Under identical wave height conditions, a longer wave period effectively reduces pitch amplitude and towline tension, suggesting that a longer wave period mitigates the system's dynamic response and enhances towing stability.

5 Discussion

Large steel net cages are essential for marine aquaculture. These cages are typically installed on land and then towed by tugboats to the operational sea area. Unlike conventional cylindrical foundation platforms, the large size and high center of gravity of net cage platforms result in a higher water surface elevation under the same draft conditions. This increases the risk of tipping during long-distance towing operations. For example, the Deep Blue one net cage platform experienced two towing tilt incidents, leading to significant economic losses. As a result, the towing safety of large floating net cage platforms is a critical engineering issue (Shi, 2019). During towing, the dynamic performance of the net cage platform is influenced by factors such as towing configuration, towline length, and towing speed. These factors not only determine the platform's motion response but also affect the distribution of towline tension and overall towing stability.

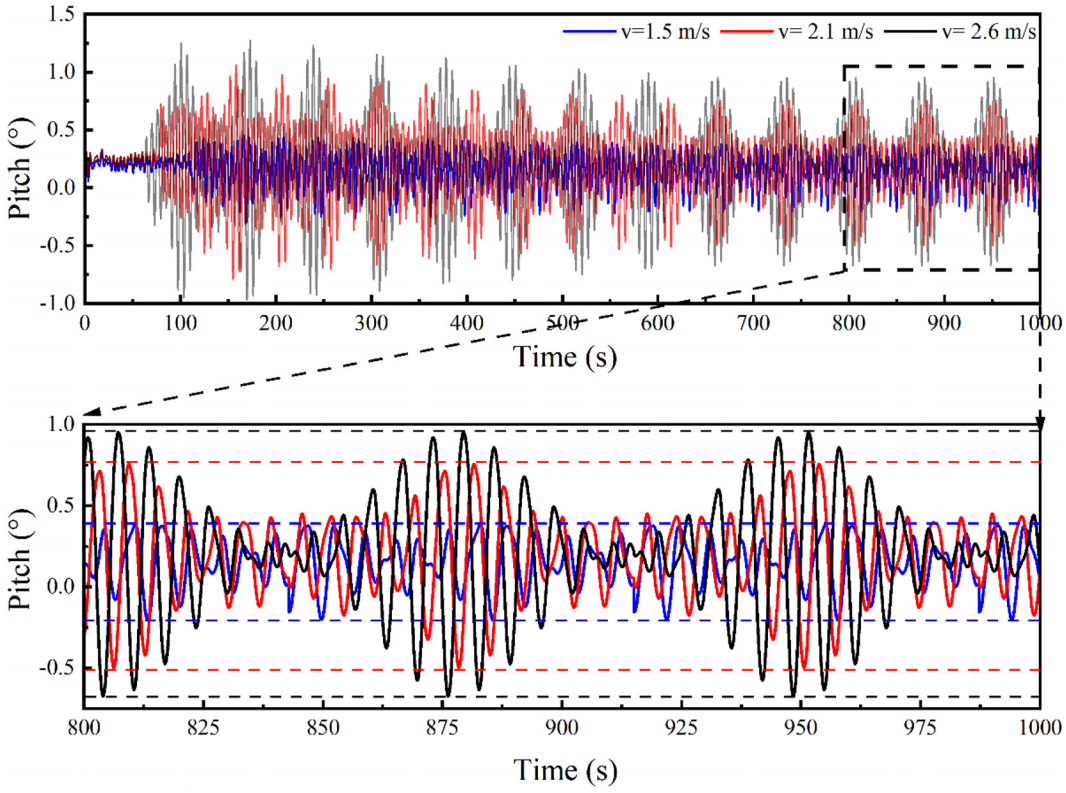

FIGURE 13
Dynamic response of the pitch of the net cage under different towing speeds.

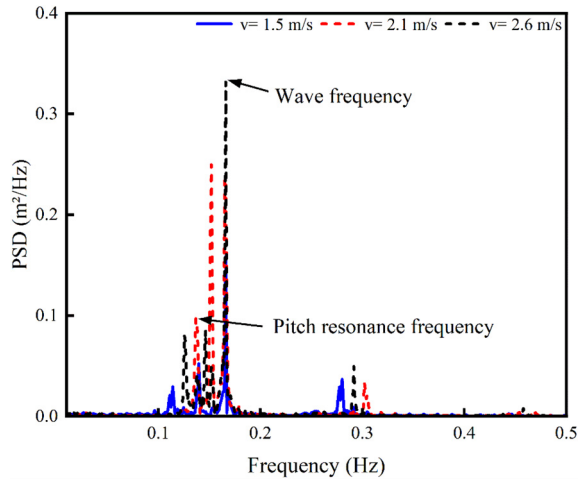

FIGURE 14
Power spectra of net cage pitch motion under different towing speeds.

5.1 The impact of towing method on the towing performance of net cage platforms

The towing position (towline configuration) directly impacts the pitch angle of the net cage platform. The V-shaped towing configuration is commonly used in offshore wet towing operations. The choice of towing points has little effect on roll and heave responses, as noted by Liu et al (2024). Similarly, Huynh and Kim, (2024) found that changes in towing position have minimal effects on heave and roll during towing, likely due to the smaller dimensions and shallow draft of the towed structure, resulting in limited motion differences. However, this study compares two towing configurations: spaced and adjacent. The results show that spaced towing results in smaller motion amplitudes than adjacent towing. This agrees with Wang et al (2024), where the difference is attributed to the larger towline angle in the spaced configuration, which leads to a more balanced force distribution during towing and enhances stability. In contrast, for net cage platforms with large dimensions, the lateral force area is significant, which can cause substantial oscillations and create instability. The V-shaped towing configuration optimizes the towline's distribution and angle, effectively dispersing lateral forces, thus improving resistance to tipping and enhancing overall towing stability.

In towing systems, the net cage platform is connected to the tugboat by a towline, and the length of the towline is a key factor affecting the dynamic performance of the net cage platform. This study demonstrates that increasing the towline length effectively mitigates the impact tension within the towline, a finding that is highly consistent with the conclusions of Fitriadhy and Yasukawa (2011), further validating the positive role of towline length in damping vibrations. However, this study also delves into the low-frequency vibration issues that may arise from excessive towline length. The phenomenon of low-frequency vibrations is consistent with the findings of Shin (2011), who noted that while longer towlines significantly reduce instantaneous stress, they may also increase the risk of system vibrations. Additionally, in tests using a 200-meter towline, an increase in pitch amplitude was observed, which contradicts the theoretical expectation that longer towlines should reduce system fluctuations. Analysis shows that when the towline length exceeds a critical threshold, low-frequency vibrations may be amplified, significantly complicating the system's dynamic response. This finding aligns with the research of Xu et al (2024), further revealing the low-frequency dynamic challenges potentially induced by excessively long towlines and highlighting the importance of properly controlling towline length to ensure the safety and stability of the towing system.

Additionally, towing speed has a direct impact on the wet towing operation of the net cage platform. According to the statistical analysis of the pitch angle and towline tension, as the towing speed increases, the towing resistance of the net cage platform also increases, resulting in higher towline tension. This is consistent with the findings of Neisi et al (2024). regarding floating wind turbines. Furthermore, as the towing speed increases further, the amplitude and frequency of the pitch motion of the net cage platform significantly rise, demonstrating stronger nonlinear dynamic

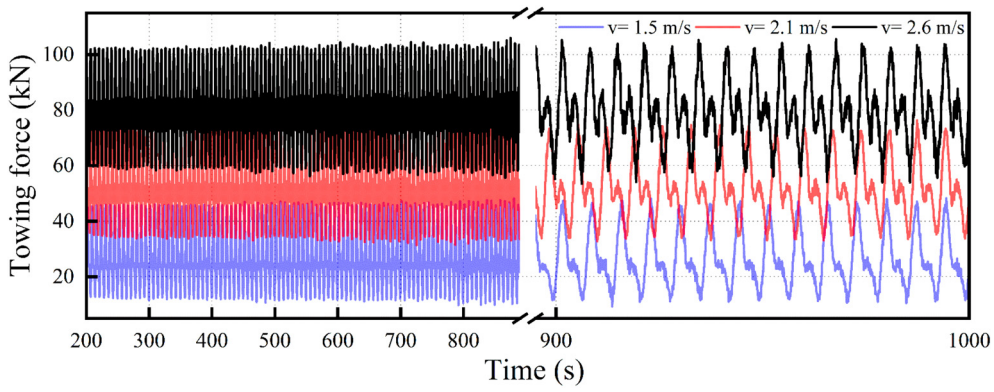

FIGURE 15
Dynamic response of the towing force at different towing speeds.

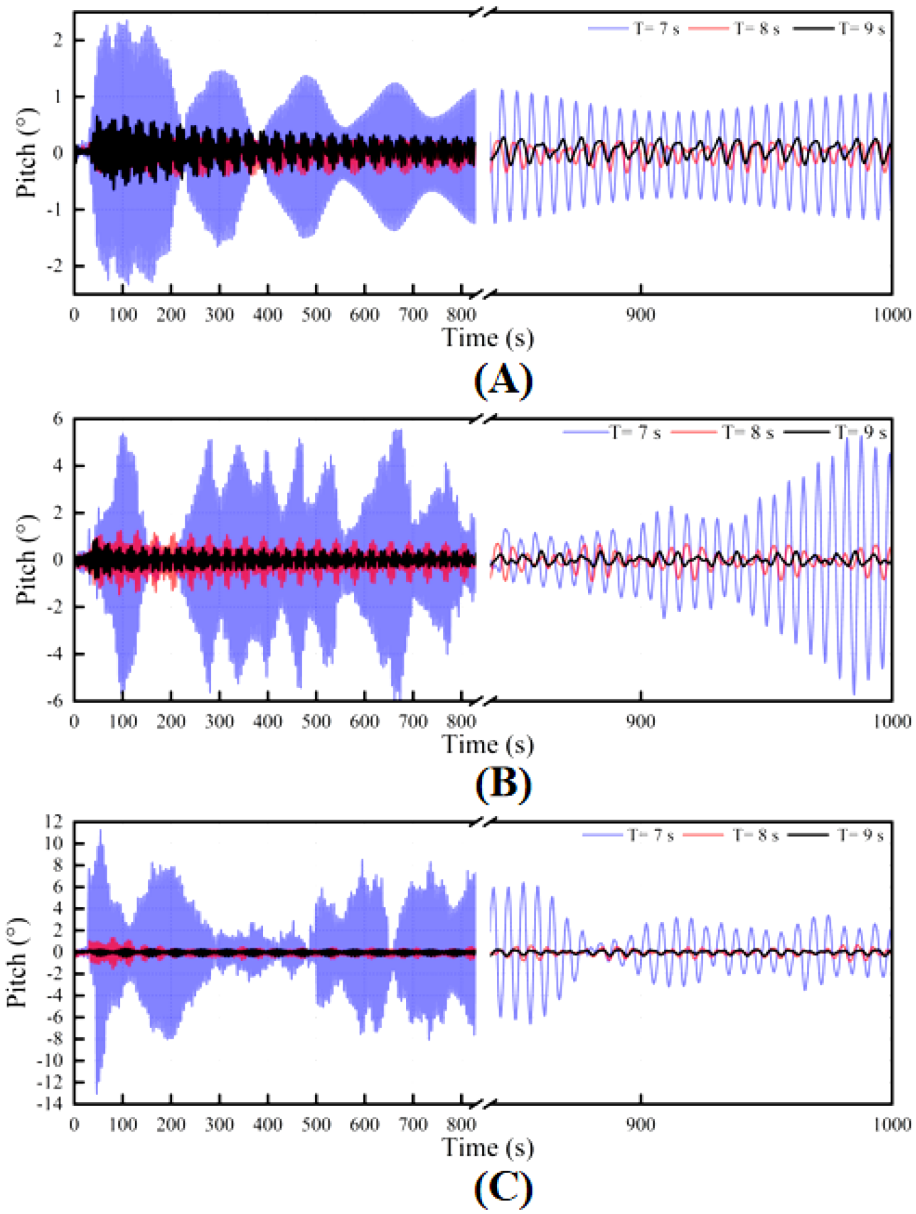

FIGURE 16
Dynamic response of the pitch of the net cage under wave heights: **(A)** 0.5 m; **(B)** 1.5 m; **(C)** 2.5 m.

responses. This phenomenon is in line with the results observed by Zhang et al (2019) under high towing speed conditions, where increased towing speed significantly induces fluctuations in the pitch angle, increasing the dynamic load on the system and placing higher demands on the structural design of the net cage.

5.2 The impact of marine environment on the towing performance of net cage platforms

Wave parameters are key factors influencing the towing performance of net cage platforms, especially under harsh sea conditions, where towing operations can easily result in excessive motion response or even cable failure. According to the statistical analysis of pitch angle and towline tension, the effects of significant wave height and wave period on the towing performance of the net cage platform have been found to be particularly significant. As the effective wave height increases, wave forces are intensified, causing a simultaneous increase in the platform's motion response and towline tension, which significantly reduces the stability of the net cage platform during towing. This finding is consistent with the results reported by Wang et al (2023); Zhang et al (2017), and Soares and Das (2009) regarding the hydrodynamics of cylindrical foundation towing, confirming that wave conditions are considered one of the primary external factors affecting towing stability.

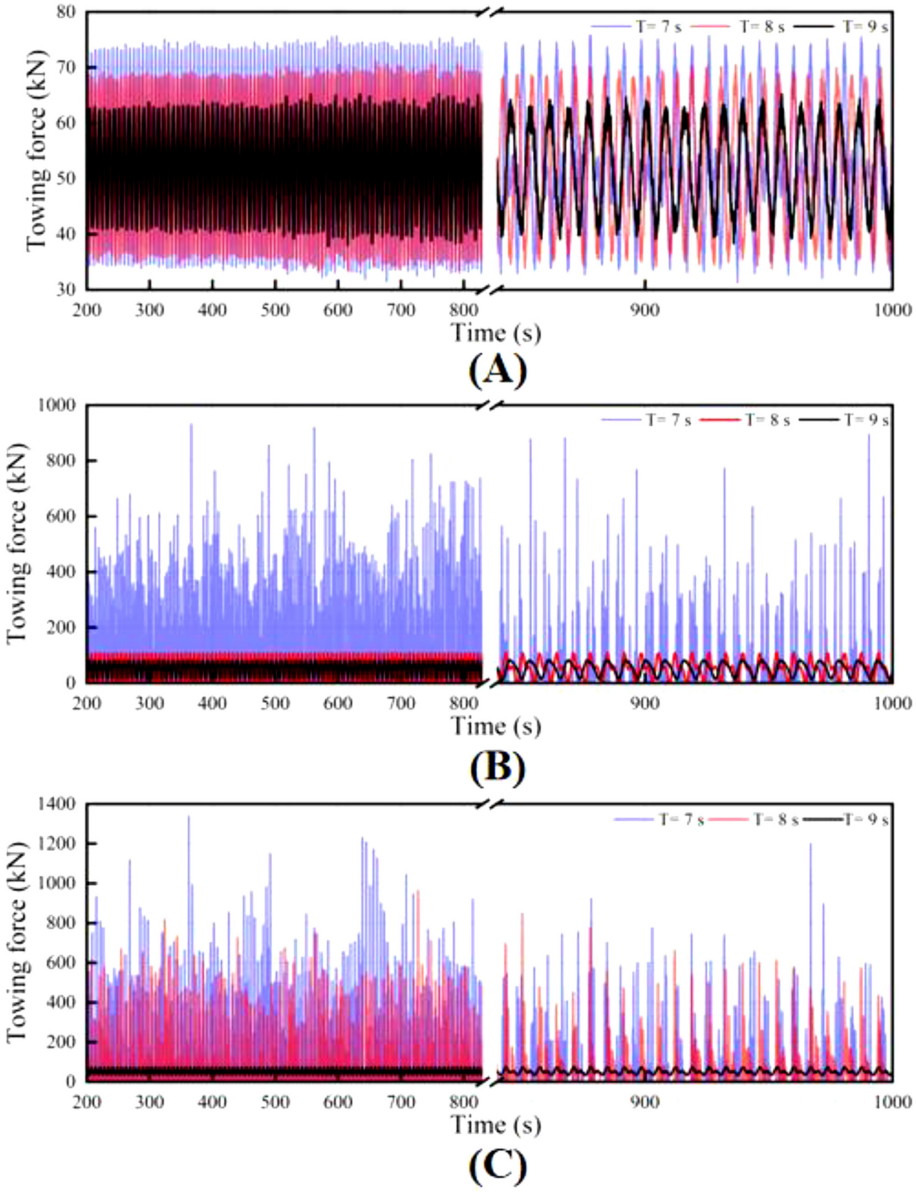

FIGURE 17
Dynamic response of the towing force under different wave heights: **(A)** 0.5 m; **(B)** 1.5 m; **(C)** 2.5 m.

Moreover, the wave period plays a crucial role in the dynamic response characteristics of the net cage platform. Short-period waves are more likely to induce high-frequency vibrations in the platform, resulting in significant fluctuations in both the pitch angle and towline tension during towing. In contrast, long-period waves tend to mitigate the effects of wave loads to some extent, thereby reducing the amplitude of the platform's dynamic response and enhancing system stability. This phenomenon is consistent with the findings of Zhai et al (2023) in their study on large prefabricated sinking boxes, and it has also been further corroborated by the research of Sun et al (2023) on offshore wind turbine jacket foundations. They noted that, under conditions of high wave heights and short-period waves, the hydrodynamic loads on floating structures increase significantly, which can lead to structural risks during towing. Therefore, in order to meet towline tension requirements and ensure towing safety, several studies recommend limiting the sea conditions for towing offshore structures to sea states no higher than level 4.

Although the findings of this study provide valuable guidance for the towing of octagonal cages, certain limitations remain. Firstly, the study primarily focused on the effects of towing length, towing speed, and towing position, while the influence of draft depth on the net cage's motion response under varied sea conditions was not fully explored. Variations in draft depth may significantly affect the interaction between the net cage and the marine environment, particularly in complex wave and towing scenarios, where the coupling between the net cage submerged section and hydrodynamic forces could lead to distinct motion characteristics.

Additionally, the effect of wind-current coupling was not included in the analysis, even though, in practical operations, the interaction between wind forces and ocean currents could substantially impact system stability and towline tension. Future research should incorporate the effects of draft depth and wind-current coupling to conduct a more comprehensive analysis of the towing system, enhancing the understanding of dynamic responses under complex ocean conditions and providing more precise theoretical support for offshore towing operations.

6 Conclusions

Through numerical simulations, the motion response of an octagonal offshore aquaculture net cage during towing was analyzed under various towing lengths, towing speeds, marine conditions, and towing configurations. Key findings show that spaced towing configurations significantly reduce pitch amplitude and towline tension by evenly distributing external forces, thereby enhancing the system's stability. An optimal towing length of 150 m minimizes pitch motion and maintains stable tension, though excessively long cables may introduce complications due to increased sag. The 150 m towline is most effective under moderate sea states, with wave heights ranging from 0.5 to 1.5 meters and wave periods around 7 seconds. In more extreme conditions, a shorter towline may be more suitable for maintaining stability. Towing speed significantly affects the dynamic response, with higher speeds increasing pitch and tension fluctuations, while lower speeds promote greater stability. Additionally, wave height and period play critical roles in the system's behavior; higher wave heights and short-period waves amplify motion and increase towing risks, while long-period waves help stabilize the system by reducing dynamic responses.

Comprehensive analysis shows that optimizing towing length, towing position, and towing speed, along with accurate assessment of wave period and height, is essential for ensuring the safety of wet towing operations for offshore net cages. This study provides theoretical foundations and practical guidelines for enhancing the stability in the transport of marine aquaculture equipment.

Data availability statement

The original contributions presented in the study are included in the article/supplementary material. Further inquiries can be directed to the corresponding authors.

Ethics statement

Informed consent was obtained from all subjects involved in the study.

Author contributions

SN: Conceptualization, Investigation, Writing – original draft, Writing – review & editing. ZW: Conceptualization, Writing – original draft, Writing – review & editing. LG: Methodology, Writing – original draft, Writing – review & editing. LT: Data curation, Writing – original draft, Writing – review & editing. TG: Software, Writing – original draft, Writing – review & editing. CC: Software, Writing – original draft, Writing – review & editing. DF: Project administration, Writing – original draft, Writing – review & editing. FG: Funding acquisition, Project administration, Writing – original draft, Writing – review & editing. XY: Funding acquisition, Resources, Supervision, Writing – original draft, Writing – review & editing.

Funding

The author(s) declare that financial support was received for the research and/or publication of this article. National Key Research and Development Program (Grant No.2020YFE0200100), National Natural Science Foundation of China (Grant No. 42306229), Natural Science Foundation of Zhejiang Province (Grant No. LQ24D060003).

Acknowledgments

The authors would like to thank all the reviewers who participated in the review.

Conflict of interest

The authors declare that the research was conducted in the absence of any commercial or financial relationships that could be construed as a potential conflict of interest.

Generative AI statement

The author(s) declare that no Generative AI was used in the creation of this manuscript.

Publisher's note

References

Chen, M., Chen, Y., Li, T., Tang, Y., Ye, J., Zhou, H., et al. (2024). Analysis of the wet-towing operation of a semi-submersible floating wind turbine using a single tugboat. *Ocean Eng.* 299, 117354. doi: 10.1016/j.oceaneng.2024.117354

Ding, H., Feng, Z., Zhang, P., Le, C., and Guo, Y. (2020). Floating performance of a composite bucket foundation with an offshore wind tower during transportation. *Energies* 13, 882. doi: 10.3390/en13040882

Ding, W. W., Jiang, J. Q., Yue, W. Z., Li, Y. Z., Wang, W. S., Sheng, S. W., et al. (2023). Numerical study on hydrodynamic performance of a new semi-submersible aquaculture platform. *Appl. Sci.* 13, 12652. doi: 10.3390/app132312652

Dong, S. L., Dong, Y. W., Huang, L. Y., Zhou, Y. G., Cao, L., Tian, X. L., et al. (2024). Advancements and hurdles of deeper-offshore aquaculture in China. *Rev. Aquaculture* 16, 644–655. doi: 10.1111/raq.12858

Fan, Z. Q., Liang, Y. H., and Yun-Peng, Z. (2023). Review of the research on the hydrodynamics of fishing cage nets. *Ocean Eng.* 276, 114192. doi: 10.1016/j.oceaneng.2023.114192

Fitriadhy, A., Yasukawa, H., and Koh, K. K. (2013). Course stability of a ship towing system in wind. *Ocean Eng.* 64, 135–145. doi: 10.1016/j.oceaneng.2013.02.001

Fitriadhy, A., and Yasukawa, H. (2011). Course stability of a ship towing system. *Ship Technol.* 58 (1), 4–23. doi: 10.1016/j.oceaneng.2013.02.001

Froehlich, H. E., Gentry, R. R., Rust, M. B., Grimm, D., and Halpern, B. S. (2017). Public perceptions of aquaculture: evaluating spatiotemporal patterns of sentiment around the world. *PLoS One* 12, e0169281. doi: 10.1371/journal.pone.0169281

Han, Y. Q., Ding, H. Y., and Zhang, P. Y. (2017). Environmental impact analysis of floating wind turbine towing based on multibody dynamics. *J. Tianjin Univ.* 50, 1055–1061. doi: 10.1063/1.4982742

Holmstrom, J. T. (1982). Custom designing winches for deep tow survey use. *Sea Technol.* 23, 10–1061.

Huynh, T., and Kim, Y. B. (2024). Control system design for offshore floating platform transportation by combination of towing and pushing tugboats. *J. Marine Sci. Eng.* 12 (3), 459. doi: 10.3390/jmse12030459

Le, C. H., Ding, H. Y., and Zhang, P. Y. (2013). Air-floating towing behaviors of multi-bucket foundation platform. *China ocean Eng.* 27, 645–658. doi: 10.1007/s13344-013-0054-4

Le, C., Ren, J., Wang, K., Zhang, P., and Ding, H. (2021). Towing performance of the submerged floating offshore wind turbine under different wave conditions. *J. Marine Sci. Eng.* 9, 633. doi: 10.3390/jmse9060633

Li, X., Lian, J., Jia, Z., Wu, H., He, S., Zhang, X., et al. (2024). Allowable differential air pressure during offshore transportation of composite bucket foundation. *Ships Offshore Structures* 19, 338–347. doi: 10.1080/17445302.2023.2169064

Li, L., Ruzzo, C., Collu, M., Gao, Y., Failla, G., and Arena, F. (2020). Analysis of the coupled dynamic response of an offshore floating multi-purpose platform for the Blue Economy. *Ocean Eng.* 217, 107943. doi: 10.1016/j.oceaneng.2020.107943

Lira, A. D., Pinheiro, M., Leuwen, J. V., Seij, M., and Goetheer, R. (2019). *P-67: Review of Dry Transportation of FLNG's/FSRU's/FPSO's* (Offshore Technology Conference Brasil), D011S014R001. OTC.

Liu, C., Zhang, Y., Xin, Y., Yin, J., Chen, C., and Hao, J. (2024). Towing hydrodynamic characteristics of semi-submersible cage platform. *China Fisheries Sci.* 31, 1151–1162. doi: 10.12264/JFSC2024-0123

Neisi, A., Ghassemi, H., and Iranmanesh, M. (2024). Dynamic response of three different floating platform (OC4, BSS, GVA) using multi-segment mooring system. *Appl. Ocean Res.* 153, 104301. doi: 10.1016/j.apor.2024.104301

Shi, L. (2011). *Research on Towing Performance of Large Floating Body Based on Aqwa* (Dalian: Dalian University of Technology).

Shi, L. (2019). *Dynamic analysis of semi-submersible offshore fish farm operated in China East Sea*. New York: NTNU.

Shin, S. M. (2011). Simulation of fluid-structure interaction of a towed body using an asymmetric tension model. *J. Comput. fluids Eng.* 16, 7–13. doi: 10.6112/kscfe.2011.16.1.007

Soares, C. G., and Das, P. K. (Eds.) (2009). *Analysis and design of marine structures.* (Boca Raton: CRC).

Solas, I. M. O. (2002). *International convention for the safety of life at sea (solas)* (London: International Maritime Organization).

Sun, K., Xu, Z., Li, S., Jin, J., Wang, P., Yue, M., et al. (2023). Dynamic response analysis of floating wind turbine platform in local fatigue of mooring. *Renewable Energy* 204, 733–749. doi: 10.1016/j.renene.2022.12.117

Wang, H., Liu, C., Guo, Y., Zhao, Y., Li, X., and Lian, J. (2023). Experimental and numerical research on the wet-towing of wide-shallow bucket jacket foundation for offshore substation. *Ocean Eng.* 275, 114126. doi: 10.1016/j.oceaneng.2023.114126

Wang, H., Xiang, G., Xiang, X., and Ahmed, F. (2024). Motion characteristics and T-foil based optimization of marine towed-cage in swell. *Appl. Ocean Res.* 147, 103992. doi: 10.1016/j.apor.2024.103992

Xu, H., Wang, J., Ling-ke, R., Wang, J., Cheng, S., and Liang, X. (2024). Cable length prediction for towing models of reverse towing systems based on the cable deployment process. *Ocean Eng.* 313, 119331. doi: 10.1016/j.oceaneng.2024.119331

Yan, C., Wang, H., Guo, Y., Wang, Z., and Liu, X. (2021). Laboratory study of integrated wet-towing of a triple-bucket jacket foundation for far-offshore applications. *J. Marine Sci. Eng.* 9, 1152. doi: 10.3390/jmse9111152

Yasukawa, H., and Yamada, R. (2009). Course stability and yaw response of tow and towed ships. *Trans. Japan Soc. Naval Architects Ocean Engineers* 9, 167–176. doi: 10.2534/jjasnaoe.9.167

Zhai, Q., Wang, P., Wang, H., Yan, S., Hu, X., and Zhao, H. (2023). Analysis of towing stability and seakeeping of large prefabricated caisson in sea. *Res. Adv. A Ser. Water dynamics* 01), 114–123. doi: 10.16076/j.cnki.cjhd.2023.01.015

Zhang, P., Liang, D., Ding, H., Le, C., and Zhao, X. (2019).). Floating state of a one-step integrated transportation vessel with two composite bucket foundations and offshore wind turbines. *J. Marine Sci. Eng.* 7, 263. doi: 10.3390/en13040882

Zhang, H., Xie, Z., Fang, G., and Kong, L. (2017). Investigation on the impact tension characteristics of taut mooring lines. *Ocean Eng.* 35, 23–32. doi: 10.16483/j.issn.1005-9865.2017.05.003

Frontiers in Marine Science

Explores ocean-based solutions for emerging global challenges

The third most-cited marine and freshwater biology journal, advancing our understanding of marine systems and addressing global challenges including overfishing, pollution, and climate change.

Discover the latest Research Topics

See more →

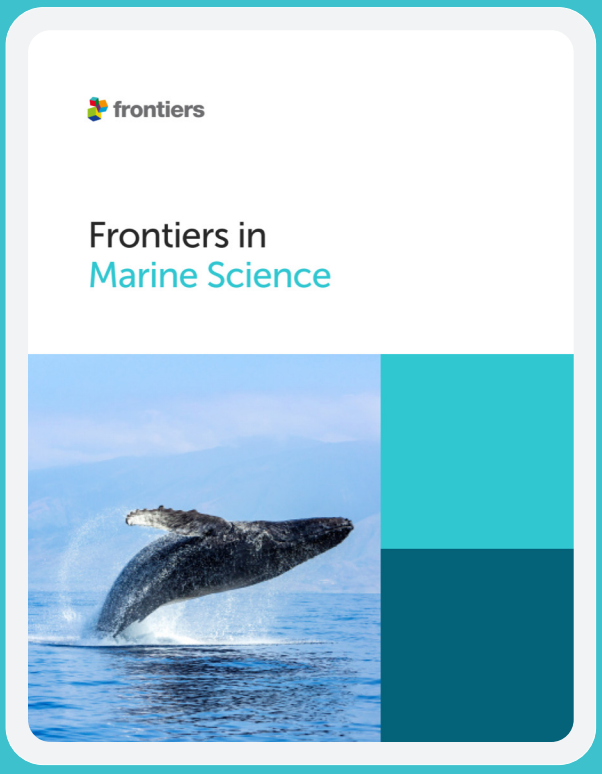

Frontiers

Avenue du Tribunal-Fédéral 34
1005 Lausanne, Switzerland
frontiersin.org

Contact us

+41 (0)21 510 17 00
frontiersin.org/about/contact